Frontispiece: Pilot's View on Approach to USS George Washington
[Source: http://home.pacbell.net/ok3/final.jpg]

Cranfield UNIVERSITY

SCHOOL OF ENGINEERING

DEPARTMENT OF AEROSPACE SCIENCES

DYNAMICS, SIMULATION AND CONTROL GROUP

PHD THESIS

ACADEMIC YEAR 2004-2005

PIO FITZGERALD

FLIGHT CONTROL SYSTEM DESIGN FOR AUTONOMOUS UAV CARRIER LANDING

SUPERVISOR: M V COOK

OCTOBER 2004

ABSTRACT

The challenge of integrating the UAV fleet into the carrier landing operational structure with respect to navigation and control strategies is addressed. A simulation model was developed which includes an aircraft model, an atmosphere model and an aircraft carrier motion model. The six degree of freedom non-linear aircraft model is based on the aerodynamic characteristics of the Mk 4a Jindivik extended to include rudder, spoiler and thrust vectoring controls, and an undercarriage model. The atmosphere model includes a carrier landing atmospheric disturbance model. The six degree of freedom aircraft carrier motion model is based on the ship motion simulation program SEAWAY.

A Navigation System was developed which conforms to current operational procedures and future military navigation goals. This Navigation System continuously predicts the position in space where touchdown on the carrier deck will take place, based on aircraft position, the relative velocity between the aircraft and carrier, and the motion time history of the carrier. A reference flight path to the predicted touchdown point is continuously defined. The aircraft deviation from this flight path is determined and input to the autoland control system. For the purposes of this study perfection prediction is assumed.

Automatic flight control systems were developed to assess three control strategies for suitability to the carrier landing task. The focus of this assessment was on vertical glide path deviation control. Direct Lift Control was compared to conventional control and was found to have superior performance, especially in turbulence. As UAV planforms tend to be tailless, and therefore lateral and pitch control are generated by a common aerodynamic surface, thrust vectoring was investigated as a means of alleviating aerodynamic pitch control requirements in the carrier landing task.

An Adaptive Approach Speed Controller was developed as an extension of the Navigation System. This system synchronises the time that the aircraft passes over the stern, or ramp, of the carrier with the minimum absolute carrier pitch attitude attainable for a given range of approach speeds. This system was shown to be an effective method of minimising the negative effect that carrier motion has on the clearance between the aircraft and the carrier's ramp.

DEDICATION

To Mom and Dad

---------- o0o ----------

ACKNOWLEDGEMENTS

This thesis would not have been possible without the support, encouragement, motivation and advice given to me in abundance by so many. I would like to take this opportunity to sincerely thank everyone who contributed in so many ways. I would especially like to thank the following people.

Mike Cook, my supervisor, for giving so freely of his time and wisdom. This thesis would never have begun if I had not received Mike's encouragement and support. Throughout the duration of this project I received thoughtful advice, support and motivation from Mike which ensured that the project remained on track. I am eternally indebted.

Dr. Robert Stirling, Chairman of Stirling Dynamics Limited. This project was initiated while I was employed by Stirling Dynamics Ltd. and was supported financially for the duration of my employment. I am very grateful to Bob for supporting this project and for his valuable advice.

Professor Johan Journée, the developer of SEAWAY, the ship motion model used in this study. The use of this model adds considerably to the realism of the simulation environment and consequently the confidence in the results achieved. I owe a great deal of thanks to Professor Journée who offered the use of SEAWAY to this study and provided advice and assistance while I integrated this model into the simulation environment.

Anita Beal and the entire staff of Cranfield University's Kings Norton Library. As I was off-campus for the duration of this project I depended very much on the library staff for support and assistance in sourcing references. Throughout the duration of the project the library staff never failed to assist and support me. I am forever grateful and greatly admire the dedication and professionalism of the library staff.

Hisako Yamashiro for her advice and especially her guidance through the frequency domain. Hisako always had time to discuss issues I was struggling with and always provided me with valuable insights.

Dr. Richard Roberts and Alan Shepherd for reading the first draft of the thesis and providing me with the benefit of their wisdom, knowledge, and motivation. I am extremely grateful for this.

Geoff Radmore for introducing me to Simulink's Non-linear Control Design toolbox and for his encouragement throughout the duration of the project.

My friend, and fellow engineer, Tim Condon who endured listening to me talk endlessly about this project. Thanks also to Tim for reviewing the introduction and literature review, but mostly for listening to my many rambles.

To my friends Enrique Herencia, Russell Fleming, Eric Porter, Aidan Dennehy, Hughie Courtney and Alastair Tucker for reviewing the introduction to the thesis and offering their honest thoughts and criticism.

My brother Denis for proof reading the entire thesis and providing endless encouragement and support throughout the project.

My brother Brendan for providing me with two computers to run the many simulations required. Thanks also for driving me to and from the airport on my many visits to Cranfield and for your encouragement.

My brothers John and Kevin for their support, encouragement and motivation throughout the project.

My Mom and Dad for their love, support and encouragement. Thank you for always believing in me. This thesis is dedicated to you.

Sharon Healy for her love, support, encouragement and patience when listening to me drone on and on about this project. Thank you.

TABLE OF CONTENTS

TABLE OF FIGURES

---------- o0o ----------

TABLE OF TABLES

---------- o0o ----------

NOTATION

Roman Alphabet

A	Aspect ratio
a	Acceleration , Speed of sound
$a_{1_{wb}}$	Wing-body combination lift curve slope
a_{1_T}	Tailplane lift curve slope
a_{2_T}	Elevator effectiveness
A_s	Aspect ratio of the wing section defined by the inboard and outboard limit of the spoiler
a_x	Axial acceleration
a_{x_s}	Sensed axial acceleration
a_y	Lateral acceleration
a_{y_s}	Sensed lateral acceleration
a_z	Normal acceleration
a_{z_s}	Sensed normal acceleration
b	Wingspan
c	Wing chord
$\overline{c}$	Mean aerodynamic chord
$c_{1/4_{wl}}$	Height of quarter chord from waterline
C_D	Drag coefficient
C_{D_i}	Induced drag coefficient
$C_{D_{is}}$	Induced drag coefficient increment due to symmetric deflection of spoilers
C_{D_s}	Drag coefficient increment due to symmetric deflection of spoilers
$C_{D_{uc}}$	Drag coefficient increment due to extension of undercarriage
$C_{D_{C_L > C_{L_{crit}}}}$	Drag coefficient increment due to lift coefficient being greater than the critical lift coefficient
C_{D_M}	Coefficient of drag due to Mach effects
$C_{D_{os}}$	Increment in profile drag due to symmetric deflection of spoilers
C_{D_Z}	Profile drag coefficient
c_f	Flap chord
c_{hs}	Spoiler chord aft of hinge
C_l	Rolling moment coefficient
C_{l_p}	Rolling moment coefficient due to roll rate
C_{l_r}	Rolling moment coefficient due to yaw rate
C_{l_v}	Rolling moment coefficient due to lateral velocity
C_{l_ξ}	Rolling moment coefficient due to aileron deflection
C_{l_ς}	Rolling moment coefficient due to rudder deflection
C_L	Lift coefficient
$C_{L_{crit}}$	Critical lift coefficient

C_{L_s}	Spoiler lift increment
$C_{L_{s\,\delta f=1}}$	Lift coefficient due to symmetric spoiler deflection with flaps retracted
$C_{L_{s\,\delta f>1}}$	Lift coefficient due to symmetric spoiler deflection with flaps extended
$C_{L_{s\,\infty}}$	Two dimensional lift coefficient increment due to symmetric spoiler deflection
$C_{L_{wb}}$	Wing-body combination lift coefficient
C_{L_T}	Tail lift coefficient
$C_{m_{1/4}}$	Quarter chord pitching coefficient moment
C_m	Pitching moment coefficient
C_n	Yawing moment coefficient
C_{n_p}	Yawing moment coefficient due to roll rate
C_{n_r}	Yawing moment coefficient due to yaw rate
C_{n_v}	Yawing moment coefficient due to lateral velocity
C_{n_ξ}	Yawing moment coefficient due to aileron deflection
C_{n_ζ}	Yawing moment coefficient due to rudder deflection
c_r	Wing chord at root
c_t	Wing chord at tip
c_{ws}	Wing chord at mid spoiler location
$C_{x_{wb}}$	Wing-body combination coefficient of axial forces
C_Y	Sideforce coefficient
C_{Y_p}	Sideforce coefficient due to roll rate
C_{Y_v}	Sideforce coefficient due to lateral velocity
C_{Y_ζ}	Sideforce coefficient due to rudder deflection
$C_{z_{wb}}$	Wing-body combination coefficient of normal force
D_{BE}	Body from earth axes direction cosine matrix
D_{EB}	Earth from body axes direction cosine matrix
$D_{EB_{ac}}$	Earth from aircraft carrier body axes direction cosine matrix
D_{int}	Engine intake drag
d	Distance between aircraft and desired touchdown point
d_ε	Tail hook deviation from the prescribed track
d_m	Maximum gust length
d_{rd}	Relative distance between the predicted touchdown point and the aircraft projected on to the flat earth
d_x, d_y, d_z	Axial, Lateral and Normal gust length
e_0, e_1, e_2, e_3	Euler parameters (Quaternions)
$e_{0i}, e_{1i}, e_{2i}, e_{3i}$	Initial values of Euler parameters (Quaternions)
F	General force, Force vector
$f_{act\,d}$	Trailing edge flap actuator demand
g	Acceleration due to gravity
H	Effective height of spoiler plus ordinate of wing section at x_s
$H_{1/3}$	Significant wave height

$H_s(\omega)$	Ship motion transfer function
h	Altitude
h_{cg}	Centre of gravity position as a percentage of the mean aerodynamic chord
h_d	Altitude demand
h_ε	Tail hook vertical deviation from desired approach glide path
$h_{\varepsilon f}$	Approach glide path vertical deviation lead signal
h_{eff}	Effective height of spoiler
h_o	Aerodynamic centre position as a percentage of the mean aerodynamic chord
h_r	Ramp crossing height
h_s	Sensed altitude
h_{sp}	Height of spoiler when deflected
h_{te}	Distance from trailing edge of deflected flap to chord line
h_{th}	Perpendicular distance from the axial body axis to the tail hook
H_{th}	Height of the tail hook from the aircrafts centre of gravity
h_{th_d}	Tail hook desired altitude
h_{wl}	Height of cg from waterline
h_ε	Altitude error
I_x	Moment of inertia about *ox* axis
I_{xy}	Product of inertia about *ox* and *oy* axes
I_{xz}	Product of inertia about *ox* and *oz* axes
I_y	Moment of inertia about *oy* axis
I_{yx}	Product of inertia about *oy* and *ox* axes
I_{yz}	Product of inertia about *oy* and *oz* axes
I_z	Moment of inertia about *oz* axis
I_{zx}	Product of inertia about *oz* and *ox* axes
I_{zy}	Product of inertia about *oz* and *oy* axes
k	Gain
k_{de}	Baseline approach glide path controller derivative gain
$k_{d\beta}$	Sideslip controller derivative gain
k_{dlc}	Direct Lift Control proportional gain
$k_{d\lambda}$	Track controller derivative gain
k_{dpa}	Pitch attitude controller derivative gain
$k_{\delta f=1}$	Value of gain at flap deflection of 1 degree
$k_{\delta f=20}$	Value of gain at flap deflection of 20 degrees
k_{fe}	Flap to elevator feedforward gain
k_{fsg}	Flap to Spoiler ratio gain
k_h	Altitude correction factor
k_{hd}	Altitude hold and acquire autopilot derivative gain
k_{hi}	Altitude hold and acquire autopilot integral gain
k_{hp}	Altitude hold and acquire autopilot proportional gain
k_{te}	Baseline approach glide path controller integrator gain

k_{ipa}	Pitch attitude controller integrator gain
k_{iu}	Autothrottle integrator gain
$k_{i\beta}$	Sideslip controller integrator gain
$k_{i\lambda}$	Track controller integrator gain
k_m	Mass flow correction factor
k_p	Roll rate SAS gain
k_{pe}	Baseline approach glide path controller proportional gain
k_{ppa}	Pitch attitude controller proportional gain
$k_{P_{rec}}$	Engine pressure recovery factor
k_{pu}	Autothrottle proportional gain
$k_{p\beta}$	Sideslip controller proportional gain
$k_{p\lambda}$	Track controller proportional gain
k_q	Pitch rate SAS gain
k_r	Yaw rate SAS gain
k_s	Correction factor for flat type spoilers
k_{te}	Reduction in elevator demand gain
k_{sD}	Spoiler induced drag factor
k_{sf}	Flap factor
k_{TG}	Gross thrust factor
k_{uc}	Undercarriage drag calculation coefficient
$k_{uc\delta_{f=1}}$	Undercarriage drag calculation coefficient flaps retracted
$k_{uc\delta_{f=20}}$	Undercarriage drag calculation coefficient flaps fully extended
k_ϕ	Roll attitude SAS gain
k_θ	Pitch attitude SAS gain
k_τ	Throttle SAS gain
$k_{\psi i}$	Heading acquire and hold autopilot integral gain
$k_{\psi p}$	Heading acquire and hold autopilot proportional gain
L	Rolling moment
L_{Aero}	Rolling moment due to aerodynamics
L_{Grav}	Rolling moment due to gravity
l_p	Moment arm of angle of attack probe
L_{Thrust}	Rolling moment due to thrust
l_t	Tail moment arm
l_{th}	Distance from the centre of gravity to the tail hook measured parallel to the axial body axis
l_{thrust}	Thrust moment arm
L_u, L_v, L_w	Axial, lateral and normal turbulence scale length
M	Mach number
M	Pitching moment
	Moment vector
m	Mass
$\dot{m}$	Engine mass flow
m_λ	'Slope' of the prescribed track
M_{Aero}	Pitching moment due to aerodynamics

M_{Grav}	Pitching moment due to gravity
M_s	Sensed Mach number
M_{Thrust}	Pitching moment due to Thrust
m_{mto}	Maximum take-off mass of aircraft
m_{zf}	Zero fuel mass of aircraft
N	Yawing moment
$N1$	Engine speed
$N1_{idle}$	Engine idle speed
$N1_{\max}$	Engine maximum speed
N_{Aero}	Yawing moment due to aerodynamics
N_{Grav}	Yawing moment due to gravity
N_{nd}	Equivalent non dimensional engine speed corrected for temperature
N_{Thrust}	Yawing moment due to thrust
o	Origin of body axes system
o_{ac}	Origin of aircraft carrier body axes system
o_E	Origin of earth axes system
o_0	Earth reference point
o_t	Origin of thrust vectoring axes system
P	Random phase
P	Atmospheric pressure
p	Roll rate
p_i	Initial roll rate
P_{intake}	Engine intake pressure
$P_{int\ ratio}$	Engine intake pressure ratio
P_O	Sea level pressure
P_{ratio}	Engine pressure ratio
P_{rec}	Engine pressure recovery
p_s	Sensed roll rate
P_s	Sensed atmospheric pressure
q	Pitch rate
q_{dyn}	Dynamic pressure
$q_{dyn\ s}$	Sensed dynamic pressure
q_i	Initial pitch rate
q_s	Sensed pitch rate
R	Universal gas constant
r	Yaw rate
r_i	Initial yaw rate
r_s	Sensed yaw rate
S	Wing area
s	Wing semi-span, Laplace operator
s_{act_d}	Spoiler actuator demand
S_s	Area of wing bounded by spoiler
S_T	Tailplane area
$S_T(\omega)$	PSD of ship motion response to a particular wave height
$S_w(\omega)$	Wave height PSD
T	Temperature
t	Time
T_1	Average wave period
t_1	Time to touchdown at maximum approach speed
$t_{1'}$	Time to ramp crossing at maximum approach speed

t_2	Time to touchdown at minimum approach speed
$t_{2'}$	Time to ramp crossing at minimum approach speed
T_G	Gross thrust
$T_{G_{nd}}$	Non dimensional gross thrust
T_{intake}	Engine intake temperature
T_L	Temperature lapse rate
T_O	Sea level temperature
T_τ	Thrust
t_{td}	Time to Touchdown
t_{tr}	Time to ramp
$t_{tr_{\min\theta_c}}$	Minimum absolute aircraft carrier predicted pitch attitude over a defined time range
T_{wl}	Tailplane height from waterline
T_{xy}	Thrust component resolved onto the x_t, y_t plane
U	Axial velocity (body axes) Velocity vector
u	Axial velocity of a point
u_1	Axial component of random free air turbulence (aircraft carrier body axes)
u_2	Axial component of ship-wake disturbance (aircraft carrier body axes)
u_3	Axial component of periodic ship-motion-induced turbulence (aircraft carrier body axes)
u_4	Axial component of random ship-wake disturbance (aircraft carrier body axes)
u_{20}	Wind speed at 20 feet above the ground (earth axes)
u_{aad}	Adaptive approach speed demand
U_{ac}	Aircraft carrier axial velocity (body axes)
$U_{ac_{Trim}}$	Aircraft carrier steady state axial velocity (body axes)
u_c	Carrier disturbance axial velocity (earth axes)
u_d	Velocity demand
U_d	Total axial atmospheric disturbance velocity (earth axes)
u_ε	Speed error
U_E	Axial velocity (earth axes)
$U_{E_{ac}}$	Aircraft carrier axial velocity (earth axes)
$U_{E_{ac(tdp)}}$	Aircraft carrier touchdown point axial velocity (earth axes)
u_g	Gust axial velocity (earth axes)
U_i	Initial axial velocity (body axes)
$u_{\max}$	Maximum approach speed
$u_{\min}$	Minimum approach speed
U_R	Relative axial velocity (body axes)
u_s	Senses axial velocity (Body axes)
u_t	Turbulence axial velocity (earth axes)
u_w	Axial steady wind velocity component (earth axes)
U_w	Absolute magnitude of steady wind (earth axes)
V	Lateral velocity (body axes)

v	Lateral velocity of a point
v_1	Lateral component of random free air turbulence (aircraft carrier body axes)
v_4	Lateral component of random ship-wake disturbance (aircraft carrier body axes)
v_c	Carrier disturbance lateral velocity (earth axes)
V_{ac}	Aircraft carrier lateral velocity (body axes)
$V_{ac_{Trim}}$	Aircraft carrier steady state lateral velocity (body axes)
V_d	Total lateral atmospheric disturbance velocity (earth axes)
V_E	Lateral velocity (earth axes)
$V_{E_{ac}}$	Aircraft carrier lateral velocity (earth axes)
$V_{E_{ac(tdp)}}$	Aircraft carrier touchdown point lateral velocity (earth axes)
v_g	Gust lateral velocity (earth axes)
V_i	Initial lateral velocity (body axes)
v_m	Maximum gust velocity (earth axes)
V_R	Relative lateral velocity (body axes)
V_T	True airspeed
V_{T_s}	Sensed true airspeed
$V_{w/d}$	Wind over deck
v_t	Turbulence lateral velocity (earth axes)
v_w	Lateral steady wind velocity component (earth axes)
V_ε	Speed error
W	Normal velocity (body axes)
w	Normal velocity of a point
w_1	Normal component of random free air turbulence (aircraft carrier body axes)
w_2	Normal component of ship-wake disturbance (aircraft carrier body axes)
w_3	Normal component of periodic ship-motion-induced turbulence (aircraft carrier body axes)
w_4	Normal component of random ship-wake disturbance (aircraft carrier body axes)
w_c	Carrier disturbance normal velocity (earth axes)
W_{ac}	Aircraft carrier normal velocity (body axes)
$W_{ac_{Trim}}$	Aircraft carrier steady state normal velocity (body axes)
W_d	Total normal atmospheric disturbance velocity (earth axes)
W_E	Normal velocity (earth axes)
$W_{E_{ac}}$	Aircraft carrier normal velocity (earth axes)
$W_{E_{ac(tdp)}}$	Aircraft carrier touchdown point normal velocity (earth axes)
w_g	Gust normal velocity (earth axes)
W_i	Initial normal velocity (body axes)
W_R	Relative normal velocity (body axes)
w_t	Turbulence normal velocity (earth axes)

w_{ws}	Wind shear normal velocity (Earth axes)
X	Axial 'drag' force
x	General axial position
X_{Aero}	Axial 'drag' force due to aerodynamics
$x_{ac_{Pert}}$	Aircraft carrier axial position perturbation (body axes)
$x_{ac_{Pert\,(tdp)}}$	Aircraft carrier axial position perturbation at touchdown point (body axes)
x_B	longitudinal coordinate (body axes)
$x_{B_{ac}}$	longitudinal coordinate (Carrier body axes)
X_c	Aircraft range from aircraft carrier centre of pitch
x_E	longitudinal coordinate (earth axes)
$x_{E_{ac}}$	Aircraft carrier longitudinal coordinate (earth axes)
$x_{E_{ac}i}$	Initial aircraft carrier longitudinal coordinate (earth axes)
$x_{E_{ac}i(tdp)}$	Initial Aircraft carrier touchdown point longitudinal coordinate (earth axes)
$x_{E_{ac(tdp)}}$	Aircraft carrier touchdown point longitudinal coordinate (earth axes)
x_{Ei}	Initial longitudinal coordinate (earth axes)
$x_{E_{ptd}}$	Axial coordinate of predicted touchdown point (earth axes)
X_{Grav}	Axial force due to gravity
x_h	Chordwise position of spoiler hinge
x_s	Chordwise position of spoiler trailing edge
x_o	Earth axes system origin coordinate
x_t	Axial thrust vectoring axes system coordinate
X_{Thrust}	Axial force due to thrust
Y	Sideforce
y	General lateral position
Y_{Aero}	Sideforce due to aerodynamics
$y_{ac_{Pert}}$	Aircraft carrier lateral position perturbation (body axes)
$y_{ac_{Pert\,(tdp)}}$	Aircraft carrier lateral position perturbation at touchdown point (body axes)
y_B	Lateral coordinate (body axes)
$y_{B_{ac}}$	Lateral coordinate (Carrier body axes)
y_E	Lateral coordinate (earth axes)
$y_{E_{ac}}$	Aircraft carrier lateral coordinate (earth axes)
$y_{E_{ac}i}$	Initial aircraft carrier lateral coordinate (earth axes)
$y_{E_{ac}i(tdp)}$	Initial Aircraft carrier touchdown point lateral coordinate (earth axes)
$y_{E_{ac(tdp)}}$	Aircraft carrier touchdown point lateral coordinate (earth axes)
y_{Ei}	Initial lateral coordinate (earth axes)
$y_{E_{ptd}}$	Lateral coordinate of predicted touchdown point (earth axes)
Y_{Grav}	Sideforce due to gravity
y_o	Earth axes system origin coordinate

y_t	Lateral thrust vectoring axes system coordinate
Y_{Thrust}	Thrust sideforce
Z	Normal 'lift' force
z	General normal position
z_0	Altitude of zero wind shear
Z_{Aero}	Normal 'lift' force due to aerodynamics
z_{acPert}	Aircraft carrier normal position perturbation (body axes)
$z_{ac_{Pert\ (tdp)}}$	Aircraft carrier normal position perturbation at touchdown point (body axes)
z_B	Normal coordinate (body axes)
$z_{B_{ac}}$	Normal coordinate (Carrier body axes)
z_E	Normal coordinate (earth axes)
$z_{E_{ac}}$	Aircraft carrier normal coordinate (earth axes)
$z_{E_{ac}{}^i}$	Initial aircraft carrier normal coordinate (earth axes)
$z_{E_{ac}\,i\,(tdp)}$	Initial Aircraft carrier touchdown point normal coordinate (earth axes)
$z_{E_{ac\,(tdp)}}$	Aircraft carrier touchdown point normal coordinate (earth axes)
z_{Ei}	Initial normal coordinate (earth axes)
$z_{E_{ptd}}$	Normal coordinate of predicted touchdown point (earth axes)
Z_{Grav}	Normal force due to gravity
z_o	Earth axes system origin coordinate
z_t	Normal thrust vectoring axes system coordinate
z_s	Ordinate of wing section at x_s
Z_{Thrust}	Normal force due to thrust

---------- o0o ----------

Greek Alphabet

α	Angle of attack
α_0	Zero lift angle of attack
$\alpha_{local\ probe}$	Angle of attacked sensed at probe
α_R	Tailplane rigging angle
α_s	Sensed angle of attack
α_T	Tailplane angle of attack
α_{wb}	Wing-body combination angle of attack
β	Sideslip angle
β_d	Sideslip demand
β_ε	Sideslip error
β_s	Sensed sideslip angle
χ	Probability of occurrence
ΔC_{L_f}	Increment in total lift coefficient due to flap deflection
$\Delta C_{L_f\ \delta_{f=20}}$	Increment in total lift coefficient due to full flap deflection
δ_f	Flap angle
δ_m	Incremental mass
δ_s	Spoiler angle
δ_{ϕ_t}	Lateral thrust vectoring paddle deflection
δ_η	Elevator angle
$\delta_{\eta d}$	Elevator demand
$\delta_{\eta\,trim}$	Trim elevator angle
δ_{θ_t}	Longitudinal thrust vectoring paddle deflection
δ_μ	Undercarriage position
δ_τ	Engine speed
δ_ξ	Aileron angle
$\delta_{\xi d}$	Aileron deflection demand
δ_ς	Rudder angle
$\delta_{\varsigma d}$	Rudder deflection demand
ε	Downwash angle
ε_{iw}	Downwash angle in the region of the spoiler
Φ_i	Inboard part span correction factor
Φ_{ie}	Effective inboard part span correction factor
Φ_o	Outboard part span correction factor
Φ_{oe}	Effective outboard part span correction factor
ϕ	Roll attitude
ϕ_{ac}	Aircraft carrier roll attitude
$\phi_{ac_{ptd}}$	Predicted aircraft carrier roll attitude at touchdown
ϕ_d	Roll attitude demand
ϕ_e	Roll attitude error
ϕ_s	Sensed roll attitude
ϕ_τ	Lateral thrust paddle deflection
$\phi_{\tau\ act\ d}$	Lateral thrust paddle actuator demand
$\phi_{u_1}, \phi_{v1}, \phi_{w_1}$	Carrier landing disturbance model free air turbulence axial, lateral and normal velocity spectra

$\phi_{ut}, \phi_{vt}, \phi_{wt}$	Axial, lateral and normal turbulence velocity spectra
γ	Flight path angle, Specific heat ratio of air
$\eta_{act\,d}$	Elevator actuator demand
η_i	Spanwise location of inboard end of spoiler as a percentage of wing semi-span
η_{ie}	Spanwise location of effective inboard end of flap as a percentage of wing semi-span
η_{if}	Spanwise location of inboard end of flap as a percentage of wing semi-span
η_o	Spanwise location of outboard end of spoiler as a percentage of wing semi-span
η_{oe}	Spanwise location of effective outboard end of flap as a percentage of wing semi-span
η_{of}	Spanwise location of outboard end of flap as a percentage of wing semi-span
η_s	Spanwise location of centre of spoiler as a percentage of wing semi-span
κ	Angular rates vector
λ_{ac}	Aircraft carrier track
$\mu_{act\,d}$	Undercarriage actuator demand
θ	Pitch attitude
θ_{ac}	Aircraft carrier pitch attitude
$\theta_{ac_{ptd}}$	Predicted aircraft carrier pitch attitude at touchdown
θ_d	Pitch attitude demand
θ_e	Pitch attitude error
θ_s	Sensed pitch attitude
θ_{trim}	Trim pitch attitude
θ_σ	Aircraft carrier pitch amplitude
θ_τ	Longitudinal thrust paddle deflection
$\theta_{\tau\,act\,d}$	Longitudinal thrust paddle actuator demand
θ_w	Bearing of steady wind
ρ	Air density
ρ_O	Sea level air density
Σ	Summation
σ	Standard deviation, RMS turbulence amplitude
σ_{u4}	RMS amplitude random component of carrier airwake
$\sigma_u, \sigma_v, \sigma_w$	Axial, lateral and normal turbulence intensity
τ	Time constant
τ_d	Throttle demand
Ω	Turbulence spatial frequency
ϖ	Band limited white noise
ϖ_R	White noise
ω	Frequency
ω_p	Aircraft carrier pitch frequency
$\xi_{act\,d}$	Aileron actuator demand
ξ_d	Aileron demand
ψ	Yaw attitude
ψ_{ac}	Aircraft carrier yaw attitude

$\psi_{ac_{ptd}}$	Predicted aircraft carrier yaw attitude at touchdown
ψ_d	Heading demand
ψ_s	Sensed yaw attitude
ψ_ε	Heading error
$\zeta_{act\,d}$	Rudder actuator demand

---------- o0o ----------

ACRONYMS

ACLS	Automatic Carrier Landing System
AFCS	Automatic Flight Control System
AoA	Angle of Attack
APCS	Automatic Power Compensation System
ARMAX	Auto Regressive Moving Average with Exogenous Input
CAP	Control Anticipation Parameter
CLASS	Carrier Landing Aid Stabilisation System
CPAFC	Cross Product Automatic Frequency Control
CSAS	Command and Stability Augmentation System
DCM	Direction Cosine Matrix
DLC	Direct Lift Control
DMC	Deck Motion Compensation
EKF	Extended Kalman Filter
ESDU	Engineering Sciences Data Unit
FCS	Flight Control System
FFT	Fast Fourier Transform
FLOLS	Fresnel Lens Optical Landing System
GPS	Global Positioning System
GUI	Graphical User Interface
HARV	High Alpha Research Vehicle
ICLS	Instrument Carrier Landing System
IFLOLS	Improved Fresnel Lens Optical Landing System
ILS	Instrument Landing System
ISA	International Standard Atmosphere
JPALS	Joint Precision Approach and Landing System
LDGPS	Local Differential Global Positioning System
LSO	Landing Signal Officer
ML	Maximum Likelihood
MNS	Mission Needs Statement
NATO	North Atlantic Treaty Organisation
NCD	Non-Linear Control Design
P-I-D-DD	Proportional-Integral-Derivative-Double Derivative
PLL	Phase-Locked Loop
PSD	Power Spectral Density
RMS	Root Mean Square

SAS	Stability Augmentation System
SI	System Identification
TAFCOS	Total Aircraft Flight Control System
UAV	Unmanned Air Vehicle
UCAV	Unmanned Combat Air Vehicle
USAF	United States Air Force
USN	United States Navy
USS	United States Ship
V/STOL	Vertical/Short Take Off and Landing

1 INTRODUCTION

1.1 OVERVIEW

Ever since January 18th 1911 when Eugene Ely landed a Curtis pusher biplane aboard the armoured cruiser USS Pennsylvania anchored in San Francisco Bay the task of recovering an aircraft aboard a ship has been universally recognised as the most challenging manoeuvre in all of aviation.

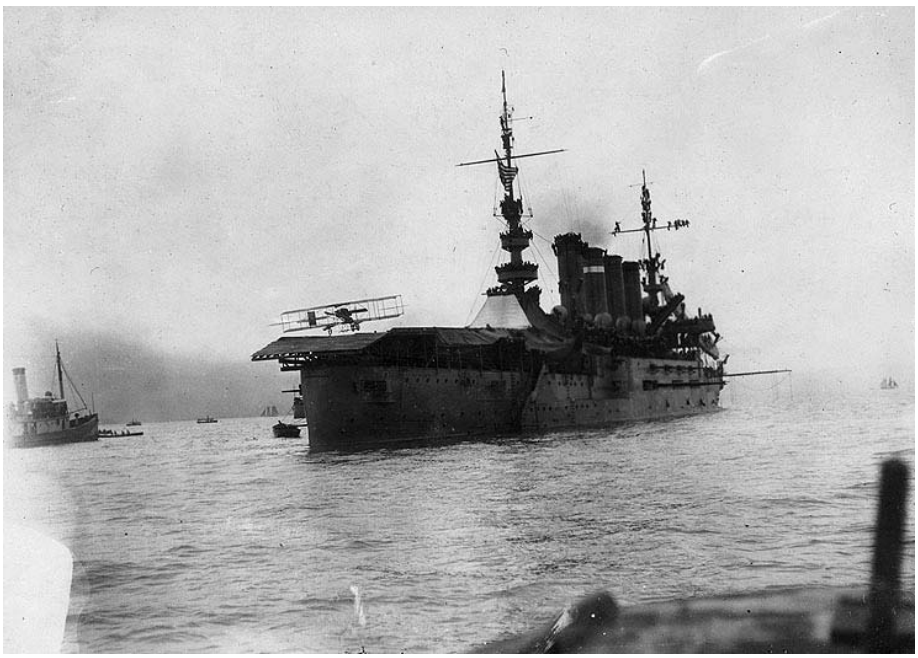

Figure 1-1 Eugene Ely Landing aboard USS Pennsylvania January 18th 1911 [1]

There are a number of factors which set an approach and landing aboard an aircraft carrier apart from an approach and landing to a fixed landing surface in terms of difficulty. These are the diminished size of the landing area, the translation and rotation of the landing area, which is intensified when inclement weather conditions prevail, and the air wake aft of the carrier due to the presence and motion of the carrier.

Procedures and landing aid systems have been developed to assist a pilot in making the recovery of an aircraft aboard a carrier safe in nearly all weather conditions, night or

day. However, even at their most autonomous modes of operation, these systems and procedures require a level of human interaction both aboard the aircraft and the carrier which is inadequate to realise the goal of truly autonomous operations.

Truly autonomous operations are highly desirable for Unmanned Air Vehicle (UAV) applications. The UAV market is currently the predominant growth sector of the aerospace industry. The roles played by the UAV in Kosovo, Afghanistan and Iraq has strengthened its position as a vital combat tool. Unmanned Combat Air Vehicles (UCAV) have been under development for some time and as confidence in the capabilities of, and advantages afforded by, unmanned operation increases, the introduction of these vehicles into frontline service will be accelerated.

The challenge presented to operators of UAVs is how to integrate the UAV fleet with the piloted fleet while adhering to the tried and tested operational procedures already in place without abating the benefits of autonomy afforded by UAVs. This is especially challenging in the carrier landing environment.

With respect to carrier operations this challenge raises two questions. Firstly, what is the most effective navigation method to guide a UAV through the approach and landing phase of a recovery aboard an aircraft carrier considering the systems and procedures currently in place, the future military navigational goals, and the objective of seamlessly integrating the UAV fleet with the piloted fleet while attaining maximum autonomy?

And secondly how best to control a UAV through the approach and landing phase of a recovery aboard an aircraft carrier considering the non-conventional planforms proposed for UCAVs and the precarious nature of the carrier landing environment?

These questions encapsulate the central theme of this study. While these questions are posed with reference to UAVs there is little doubt that the answers to these questions would also be of benefit to piloted carrier operations.

1.1.1 Navigation

A navigation concept has been conceived which responds to the navigation question. When an aircraft is on approach to a carrier, the time until touchdown is determined

based on the distance between the aircraft and the carrier and the rate of change of their relative positions. Ship motion prediction techniques are used to determine the position of the carrier at that time in the future and a standard glide path and track from that point is generated. The lateral and vertical position deviations from the desired approach glide path and track are calculated and form the input to appropriate approach controllers. These deviations could be monitored and compared with predefined limits autonomously during approach.

It is thought that the position and the rate of change of position signals can be determined using Differential Global Positioning System (DGPS). It is proposed that this navigation concept can be implemented using the operating procedures currently in place. This would reduce the number of carrier-based systems required for automatic carrier landings and increase the level of autonomy to the ultimate level for all weather, night or day operations.

1.1.2 Control

Three control strategies have been conceived for development and comparative analysis in order to determine the most suitable strategy for this task. The focus for the control strategy development and assessment is on the pitch axis. As a result all three systems share a common lateral-directional control strategy of standard aileron and rudder control as well as a common autothrottle system.

The first system, or baseline system, controls vertical flight path deviations from the desired glide path via elevators.

The second system controls vertical flight path deviations from the desired glide path via constant pitch attitude Direct lift Control (DLC). This is effected through trailing edge flaps and spoilers with elevators compensating for the pitching moment induced by the trailing edge flaps and spoilers in order to maintain a constant pitch attitude.

The third system comprises of an addition of thrust vectoring capability to the Direct Lift Control system. The thrust vectoring is used in this instance to alleviate the magnitude of elevator pitch control required during the approach. Future UCAV planforms are tending towards a tailless configuration in an effort to reduce the

aircraft's radar signature. This implies that lateral, directional and pitch control is to be effected through common aerodynamic control surfaces. As the tailless planform inherently lacks stability in the lateral and directional senses it is imperative that these common aerodynamic control surfaces never become saturated. In such a case the aircraft's dynamics revert to that of the un-augmented airframe. Reducing the pitch control required from such a surface has the effect of increasing the overall safety of the aircrafts Flight Control System (FCS) design.

A comparative analysis of these three control strategies coupled with the navigation concept over a range of operating conditions, from the most to the least favourable, will be used to assess the control strategies for their suitability to the task as well as determining the feasibility of the navigation system for the task.

1.2 OBJECTIVES

The objectives of this study are defined as:

- To develop and assess the feasibility of the navigation concept which builds on operating procedures currently in place; reduces the number of associated subsystems required; accounts for future military navigational goals; accounts for ship motion through the use of ship motion prediction; facilitates the seamless integration of the UAV fleet with the piloted fleet and allows for truly autonomous carrier landing operations.

- To assess three control strategies applied to the carrier landing task with an emphasis on control strategies suitable for future UCAV planforms and which coupled with the navigation strategy would allow for the expansion of the UAV carrier recovery operations to be genuinely all weather day or night capable.

1.3 LIMITATIONS TO THE SCOPE OF STUDY

The following limitations to the scope of the study have been applied:

- Aircraft Type

From the outset the study is limited to fixed wing non Vertical/Short Take Off and Landing (V/STOL) UAVs.

- Operational Procedures

Due to the availability of material published by the United States Navy (USN), the procedures and systems used by the USN form the basis of the subsequent discussions.

- Definition of Approach

An aircraft approaching an aircraft carrier typically flies at an altitude of 500 feet until capturing the glide path, either visually or through the Instrument Landing System (ILS). This point is known as 'tip over'. For the purpose of this study only the descent phase of the approach is considered, i.e. the segment of the approach after 'tip over'.

- Aircraft Carrier

It is assumed that the subject aircraft carrier's landing area is aligned with the aircraft carrier's velocity vector, i.e. the deck is not angled, and that the arresting wires are spaced as per USN standards. For all simulations involving the aircraft on approach to the aircraft carrier it is assumed that the aircraft carrier is steaming into the wind and is maintaining its track, i.e. not turning.

- Control Strategies Focus

Previous carrier approach related research has concentrated on pitch approach performance. This is reflective of the challenges that the pitch axis presents as well the fact that aircraft carrier motion has a more dominant effect on the desired glide path than on the desired track, assuming that the aircraft carrier is not executing a change in course. Consequently pitch approach control is the focus of the control strategies potion of this study. Flight Control System failure cases and reversion modes are not considered.

- Ship Motion Prediction

Perfect ship motion prediction is assumed. Although ship motion prediction is an intrinsic component of the navigation strategy, the development of a suitable prediction algorithm is considered outside the scope of this study as the magnitude of the task would detract the focus of this study from the stated objectives.

1.4 PROJECT PLAN

The approach to the realisation of the objectives of this study can be broadly summarised by the following task definitions.

1 Literature Review

A literature review is to be completed comprising a critical review of relevant literature pertaining to the areas of (1) carrier landing operations and procedures, (2) flight control research in the area of carrier landings, (3) navigation systems research in the area of carrier landings and (4) ship motion prediction techniques.

2 Simulation Environment Development

A simulation environment of high fidelity is the most essential tool in a study of flight control and associated systems. In order to increase confidence in the results and subsequently the conclusions derived from the results it is sought to develop a simulation environment which rigorously represents the physics of its constituent components.

3 Development and Assessment of Navigation Strategy

The navigation concept is to be developed to allow truly autonomous UAV carrier landings and to facilitate the seamless integration of the UAV fleet with the piloted fleet. This concept is to be developed and assessed in light of current carrier landing operations and procedures, future military navigation goals and research in the area of carrier landing navigation systems.

4 Development and Assessment of Control Strategies

Control strategies employing Direct Lift Control (DLC) and vectored thrust are to be developed along with a conventional Flight Control System. These systems are to be assessed relative to each other using suitable approach and landing performance metrics.

The results of the completion of these tasks are presented in the following chapters.

---------- o0o ----------

2 BACKGROUND AND LITERATURE REVIEW

2.1 INTRODUCTION

There are two objectives in reviewing carrier landing operating procedures and research related to the objectives of this study. The first is to gain a better understanding of operating procedures and the current state of the art. The second is to provide a context for this current study in relation to that state of the art.

In the absence of publications on carrier based UAV operations and related research the review has focused on piloted operations and related research. In general, there exists a distinct lack of publications in the area of carrier landing flight control systems and associated navigation systems. As a result many of the publications reviewed were found not to be directly relevant to this study but did serve to increase the understanding of the carrier landing environment.

2.2 CARRIER LANDINGS

On 26 October 1922, Lieutenant Commander Godfrey deC. Chevalier, flying an Aeromarine 39B biplane, made the first arrested carrier landing aboard the United States Navy's first dedicated aircraft carrier, the USS Langley [2]. The arrested carrier landing has become the standard method of recovering non-vertical landing aircraft aboard a carrier.

As an introduction to an analysis of an augmentation of the Fresnel Lens Optical Landing System (FLOLS) Durand and Wasicko [3] present a very useful discussion on the carrier landing environment and its inherent challenges. Their short but thorough discussion provides valuable insights into the carrier landing environment from an engineering point of view, or more specifically from the point of view of navigation

system development. In addition to this a discussion on optical landing aids and air wake characteristics is also presented along with the actual intent of the study. These areas will be reviewed in the appropriate sections that follow.

The landing area on an average carrier is approximately 600 ft long and 90 ft wide, and aircraft touchdown should occur 160 ft from the ramp. Four arrestment wires for tail-hook engagement are located about the nominal touchdown point and spaced 40 ft apart. With a realistic approach speed, and a 3.5^{o} glide slope projected by the optical landing system, under no ship motion conditions an aircraft nominally will clear the carrier's ramp by 8.4 ft and touch down 1 second later with an impact velocity of 12.36 ft/sec.

The glide slope projected by the optical landing system can be varied, depending on the closure rate of the aircraft to the carrier, to provide an effective glide slope of 3^{o} [4]. A decrease in closure rate, caused by the carrier's speed and wind over the deck, has the effect of reducing the actual glideslope flown [4]. As the navigation strategy proposed aims to provide guidance to a fixed point in space, as opposed to a moving point in the current navigation strategy, a glide slope of 3^{o} will be used in this study.

The moving carrier deck is one of the most significant obstacles to safe aircraft recovery, and can by itself render catastrophic terminal landing conditions. When the aircraft's inertial path is precisely controlled, ship heave motion directly alters the ramp clearance by a 1:1 ratio and changes the touchdown point by a 14:1 ratio. Likewise, $\pm 1^{o}$ of ship pitch produces a motion of ±9 ft at the ramp and a ±80 ft range in the touchdown position. The heave and pitch motions also cause large vertical deck velocities and thus drastically reduce the available impact velocity margin [3].

The motion of the aircraft carrier and the presence of obstacles on the deck create major air disturbances in the wake of the carrier. The magnitude of this disturbance is greatest just aft of the carrier's ramp, close to the point where the pilot has to decide whether to commit to landing or abort the approach [5]. Considering that the response of an aircraft in the approach configuration tends to be sluggish, the consequences of the air disturbances on precise flight path control can be detrimental.

As with the approach and landing of an aircraft on a conventional runway, the prevailing atmospheric conditions affect the precision with which the desired approach glide path and track are followed. The difference in this case is that the greater the atmospheric disturbances, the greater the ship motion and, consequently, the greater the carrier air-wake disturbances.

On approach to an aircraft carrier a pilot is largely dependent on visual cues for judgement of the aircrafts deviation from the desired glide path and track. These cues take the form of the carrier's visual approach aids, the horizon and the observed motion of the carrier's deck. In conditions of poor visibility, such as night time, these cues are either significantly reduced or absent.

Although poor visibility does not present a problem to UAV carrier operation, the tight confines of the landing area, the motion of the carrier, the air disturbances in the carrier air-wake and the probability of inclement atmospheric conditions remain factors.

With the aim of facilitating seamless integration of UAVs into the present piloted aircraft fleet it is necessary to understand the procedures and systems currently utilised. While some of these systems are exclusively designed for piloted operations, knowledge of such allows better comprehension of the problem.

2.2.1 Overview

The approach to land on a carrier begins when the aircraft is cleared from a holding pattern by the carrier air traffic control centre, located below deck on the carrier. Depending on the type of approach required the aircraft is required to be configured for landing at a specified altitude and distance from the carrier prior to acquisition of glideslope and the commencement of the final approach phase.

The exact USN air traffic control procedures employed are presented in the United States Navy Aircraft Carrier Operations Manual [6]. This comprehensive document presents standard, non-standard and emergency operating procedures for pre-flight, launch and recovery of aircraft. Much of this document is of no relevance to this study; however the section on recovery of aircraft provides an insight into the systems and

procedures used as well as some anecdotal information on the process which serves to better understand the environment.

Having configured the aircraft for landing and acquired the glideslope the pilot tightly controls angle of attack and the aircraft's speed while correcting for any deviations from the required approach glide path and track. Approach cues are available to the pilot from the Improved Fresnel Lens Optical Landing System (IFLOLS), the Instrument Carrier Landing System (ICLS), and the Automatic Carrier Landing System (ACLS). These systems are discussed in sections 2.2.3, 2.2.4 and 2.2.5 respectively.

Aboard the carrier, the Landing Signal Officer (LSO) monitors the aircraft's approach visually as well as the carrier's motion, while also having reference to glideslope and track deviation data. The LSO decides whether the aircraft will continue its approach to a landing or whether the aircraft is to be waved-off based on this information as well as knowledge of the pilot's ability. The role of the LSO is discussed in section 2.2.2.

On approach the target is to catch the third arresting wire with the tail-hook which extends below the rear of the aircraft. The presence of multiple arresting wires has the effect of extending the target area. The third wire provides the safest target; if the first wire were aimed for, and the aircraft approached too low, a collision with the stern of the ship is likely. If the fourth wire were aimed for, and the aircraft landed long, a go around is inevitable. The arresting wires are visible in the Frontispiece of this document.

It is the procedure of the United States Navy that full power is selected upon touchdown on the carrier deck, idle power is selected only when the aircraft has been brought to a full stop. In the event that the aircraft lands beyond the fourth arresting wire, which results in a go-around, having full power already selected mitigates the time delay due to recognition of the situation, selecting full power and the associated engine spool time. A go-around due to landing beyond the fourth arresting wire is known as a 'bolter'.

2.2.2 Landing Signal Officer

The LSO's primary responsibility is the safe and expeditious recovery of non Vertical/Short Take Off and Landing fixed-wing aircraft aboard the carrier. Through training and experience the LSO is capable of correlating factors of wind, weather,

aircraft capabilities, ship configuration and pilot experience in order to provide optimum control and assistance in aircraft landings. The LSO is also directly responsible for training pilots in carrier landing techniques [7].

The pilot of an aircraft on approach to a carrier and the LSO, who is also a pilot, operate as a team to ensure the safe recovery of the aircraft. The LSO communicates with the pilot through a radio link and through light signals. As previously stated, the LSO has the responsibility of making the final decision as to whether an approach is to be continued to landing or whether the aircraft is to be waved-off.

The LSO grades each approach and debriefs the pilots on their performance to ensure that the highest standards are maintained. The LSO's function is not minimised in the event that an aircraft makes an automatic approach to a carrier. A full description of the responsibilities and a detailed description of LSO procedures can be found in the United States Navy Landing Signal Operators Manual [7], United States Navy Landing Signal Officers Reference Manual [4], and a memo from the Chief of Staff of the Department of the Navy (USN) entitled Landing Signal Officers [8].

These documents provide invaluable insights into the problem of safely recovering an aircraft aboard a carrier. Much of the detailed information presented in these manuals is not relevant to this study as it pertains to LSO selection, training and qualification. However the anecdotal information presented in each is invaluable in increasing familiarity with the problem and understanding both the risks involved and the level of human interaction required, even in the most autonomous recovery mode.

Detailed descriptions on carrier landing aid systems are also presented in these manuals. These descriptions, while lacking in engineering design detail, help bridge the gap in knowledge created by the lack of publications on this subject.

2.2.3 Improved Fresnel Lens Optical Landing System

The Improved Fresnel Lens Optical Landing System is a derivative of the Fresnel Lens Optical Landing System. The Fresnel Lens Optical Landing System is an electro-optical landing aid which projects glide slope data to the pilot of an aircraft on approach to the

carrier. The Fresnel Lens Optical Landing System incorporates the Carrier Landing Aid Stabilisation System (CLASS) which provides stabilisation to compensate for carrier motion.

A Fresnel lens is a lens designed to minimise astigmatism and the loss of light projected from a light source and as such allows a powerful focused beam of light. The Fresnel Lens Optical Landing System uses this lens to project a set of different coloured light beams which represent the desired glide slope and deviation data. Because of the ability of the lens to focus the beam of light with precision the pilot will be able to judge if the aircraft is above, below or tracking the desired glide path. The Fresnel Lens Optical Landing System is normally positioned on the left hand side of the carrier deck, from the pilot's perspective, about 10 ft from the edge of the carrier and 750 ft from the stern of the carrier [9]. The Fresnel Lens Optical Landing System is clearly visible in the Frontispiece of this document.

In its primary mode of operation the Carrier Landing Aid Stabilisation System provides stabilisation of the lens for the carrier's pitch, roll and heave motions. This provides a stabilised glide slope from the point of visual contact with the light plane to the hook touchdown point, as long as the pilot is lined up with the centreline of the angled deck, and the carrier's pitch motion is within $\pm 6^{o}$, the carrier's roll motion is within $\pm 10^{o}$ and the carrier's heave motion is within ±15ft. There are two backup modes of operation which offer reduced stabilisation. A comprehensive description of Carrier Landing Aid Stabilisation System is presented in the United States Navy Landing Signal Officers Reference Manual [4].

As the aircraft approaches, the pilot will see different colour lights depending on the aircraft position relative to the desired glide path. If the aircraft is on the glide path, the pilot will see an amber light, dubbed the meatball, in line with a row of green lights. If the amber light appears above the green light, the aircraft is above the glide path; if the amber light appears below the green lights, the aircraft is below the glide path. If the aircraft is significantly below the glide path the pilot will see red lights. Four red wave-off lights are located on either side of the lens. These are illuminated by the LSO in the event that a wave-off is required. The Fresnel Lens Optical Landing System also

has a pair of green lights located either side of the lens known as cut in lights. These lights are used by the LSO to communicate with the pilot. Illumination of the cut in lights may mean 'add power' or 'roger ball', a concurrence with the pilot's interpretation of the aircraft's position relative to the glide path when asked by the LSO to 'call the ball'. The arrangement of the Fresnel Lens Optical Landing System is presented in Figure 2-1.

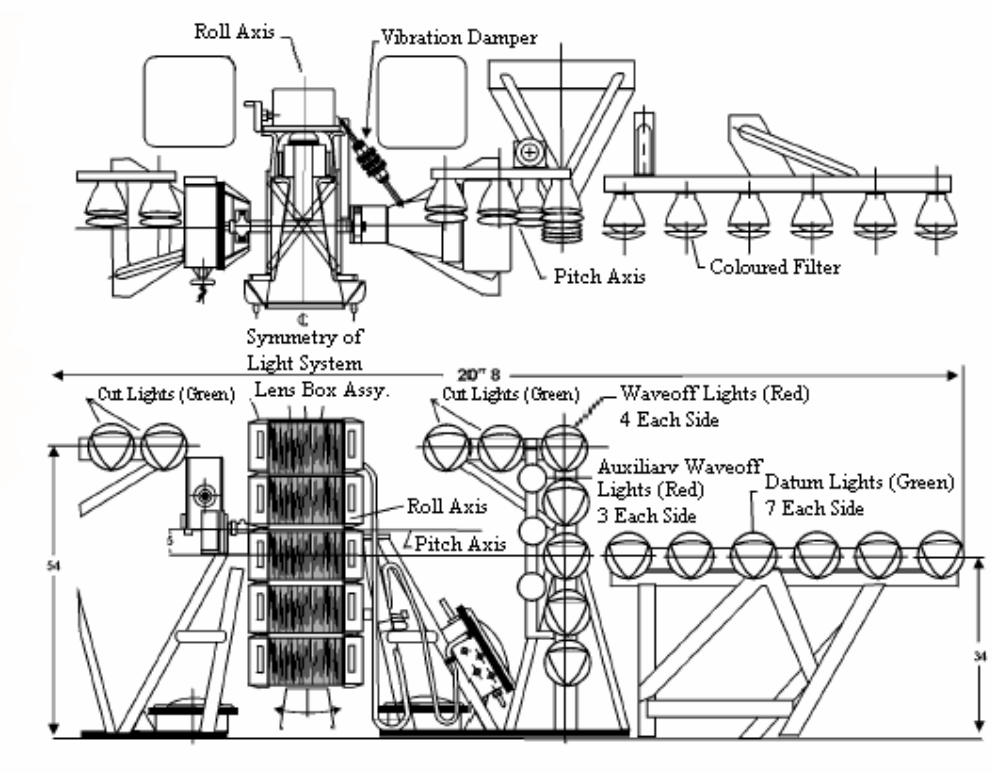

Figure 2-1 Fresnel Lens Optical Landing System [4]

The improvement of the Fresnel Lens Optical Landing System which resulted in the Improved Fresnel Lens Optical Landing System allows the pilot to receive more accurate glide path information from one mile out to touchdown. This has been accomplished by increasing the length of the assembly to accommodate 12 light cells as opposed to 5, while presenting the same range of glide path information as the Fresnel Lens Optical Landing System thus increasing sensitivity. This gives the pilot a more accurate and earlier visual cue of ball movement, allowing the pilot to correct quicker

since the ball movement is amplified compared to the Fresnel lens optical landing system.

A more complete explanation of the Fresnel Lens Optical Landing System and Improved Fresnel Lens Optical Landing System is presented in the United States Navy Landing Signal Officers Reference Manual [4], while the United States Navy Training Manual: Construction Electrician, Intermediate [9] provides some supplemental information. Durand and Wasicko [3] present a succinct overview of the Fresnel Lens Optical Landing System and its stabilisation.

As the aim of this study is to provide complete autonomy to a UAV landing aboard a carrier the Improved Fresnel Lens Optical Landing System does not provide any means of achieving this aim, nor does it present a point from which development of an autonomous system can begin. It does however represent the state of the art with respect to visual carrier landing aids.

2.2.4 Instrument Carrier Landing System

The Instrument Carrier Landing System (ICLS) operates in a similar manner as the conventional land based Instrument Landing System (ILS). A manual precision approach is flown to appropriate minimums based on precise and continuous position error and range information displayed to the pilot. As with an ILS system this information is conveyed to the pilot through a set of needles on the appropriate display. Operational details are presented in the United States Navy Aircraft Carrier Operations Manual [6].

The azimuth and elevation signals transmitted from the carrier are stabilised with reference to a co-ordinate system referenced to the desired touchdown point on the carrier's flight deck.

This system, as with a conventional ILS system, is not an automatic approach controller but a source of guidance cues which can be coupled with an automatic approach controller as will be presented in the following section.

In contrast with the navigation strategy proposed in this study the Instrument Carrier Landing System provides navigation cues from a moving point, albeit with a degree of stabilisation with respect to ship pitch and heave motions, whereas the strategy proposed provides navigation cues from a point at which touchdown is predicted to occur.

The relative merits of these navigation strategies rest in how well the Instrument Carrier Landing System can be stabilised with respect to the carrier's motion and for the strategy proposed, how well the carrier's motion can be predicted. While these facts may negate each other it is in their implementation that the proposed system may prove to be superior.

As will be discussed in section 2.3.1, the noise induced into the Instrument Carrier Landing System by the radar, which is used to determine the aircraft's position, has a negative effect on the precision of control when the system is coupled with an automatic approach controller. In addition, the Instrument Carrier Landing System does not fulfil the future military navigation requirement, which will also be discussed in section 2.3.1, and as such may become obsolete as early as 2009 [10].

However, the proposed navigation strategy, which uses digital Differential Global Positioning System signals, will not have that noise induced into the system and also adheres to future military navigation requirements.

2.2.5 Automatic Carrier Landing System

The Automatic Carrier Landing System is designed to provide control of an aircraft during the final approach and landing sequence. It consists of two operating channels, each capable of controlling the approach and landing sequence of a returning aircraft to touchdown on the carrier's flight deck. Each channel is capable of landing one suitably equipped aircraft per minute, allowing for multiple simultaneous approaches. Each channel has three primary modes of operation [4].

(1) Mode I – Fully automatic to touchdown.

Mode IA – Fully automatic to minimums of 200 ft and one-half mile.

(2) Mode II – Semi automatic approach providing glide path and track deviation data in a similar manner as a Flight Director.

(3) Mode III – Manual approach with the system providing aural cues only (talk down).

In all of these modes there is communication between the pilot and the LSO to ensure the accuracy of the system. As with a manual approach the LSO is responsible for making the decision as to whether or not the aircraft will complete the approach to touchdown or be waved-off.

Durand and Wasicko [3] discuss the fact that what the LSO and the pilot see during an approach is not the same and that problematic situations can arise because of these differing views. This manifests itself in the LSO giving the wave-off command to an approaching aircraft which is stabilised relative to the pilot's visual reference but appears unstabilised relative to the LSO's visual reference because the LSO is standing on the pitching and heaving deck of the carrier.

In the navigation strategy proposed an automatic wave-off mode can be easily implemented, which would not suffer from the problem identified by Durand and Wasicko [3] and as such would prevent successful approaches from being misinterpreted and being waved-off.

A comprehensive presentation of the components that constitute Automatic Carrier Landing System and associated operating procedure are presented in the United States Navy Aircraft Carrier Operations Manual [6], the United States Navy Landing Signal Officers Reference Manual [4] and the United States Navy Training Manual: Aviation Electronics Technician 1 (Organizational), Intermediate [11], and the United States Navy Training Manual: Aviation Electronics Technician 4 – Radar Systems [12].

These manuals provide much information not relevant to this study. A lot of the information on pertinent systems lacks engineering design detail and is intentionally presented for an operator of a system rather than as a detail design document. However, the anecdotal information presented is invaluable in understanding the related operating procedures and as an overview of how the aforementioned systems operates.

The Automatic Carrier Landing System is presented in detail by Davies and Noury [13] and a review of this is presented in section 2.3.1.

2.3 CARRIER LANDING RELATED RESEARCH

2.3.1 Navigation System

Davies and Noury [13] of Bell Aerospace, the manufacturer of the Automatic Carrier Landing System currently in service, present a detailed technical description of the AN/SPN-42 system. This system is a carrier-based controller. A radar tracks the aircraft to determine its actual position and the system computes the aircraft's distance from a stable horizontal coordinate system with origin at the average position of the intended touchdown point. This coordinate system is computed using the ship's Euler angles, thus removing the effects of the ship's motion on the measurement of the aircraft's position in inertial space.

Altitude and lateral position errors are generated based on the aircraft's range, altitude and desired glide slope. These error estimates are amplified and sent to an α-β filter which estimates the aircrafts acceleration, velocity and position errors. These estimates are then passed through a Proportional-Integral-Derivative-Double Derivative (P-I-D-DD) controller, which produce corrective pitch and roll commands required to direct the aircraft to and along the desired flight path. These commands are transmitted to the aircraft and implemented through the aircraft's Automatic Flight Control System (AFCS). The use of the Automatic Carrier Landing System requires that the Automatic Power Compensation System (APCS), or autothrottle, is used to maintain a reference angle of attack and to improve phugoid damping.

Prior to 12 seconds to go to touchdown the aircraft is directed to the average, rather than the actual, position of the touchdown point. This is done to reduce aircraft manoeuvring. However, if satisfactory landings are to be accomplished, the aircraft must be directed to the actual touchdown point during the last few seconds. At the 12 second to go mark the target is faded from the average position to the actual position of the touchdown point over a 2 second period. A phase lead of about 2 seconds is applied to this new target, in effect predicting the position of the desired touchdown point; this is to compensate for

the dynamic response lag inherent in altitude command control systems. This is known Deck Motion Compensation (DMC).

Descriptions of the design procedure, the associated hardware, safety features and control laws are included in this report. Problems encountered during the design of the system and the solutions developed to overcome these are presented. Only the operation of the system in Mode I (fully automatic) is considered. Throughout the report the emphasis is on using well-known conventional control techniques coupled with sound engineering knowledge in the design process.

Currently the AN/SPN-46 version of the automatic carrier landing system is in operational service. This system incorporates some upgrades from the AN/SPN-42, the most notable of which is the systems ability to control two aircraft on approach.

The system described by Davies and Noury [13] is the benchmark against which the performance of the navigation system proposed in this study is to be measured against. An equivalent to the deck motion compensation mode is not necessary for the proposed navigation strategy as the aircraft will be guided to the predicted touchdown point from the initiation of the approach, although this predicted touchdown point may vary through the approach.

Durand and Wasicko [3] single out for detailed study a stabilisation mode of the Fresnel Lens Optical Landing System. This system has been shown to not be of direct relevance to this study and as a result the analysis of this stabilisation mode is of no consequence.

Urnes and Hess [14] in the development of the F/A-18A Automatic Carrier Landing System acknowledge the fact that the radar tracking system introduces noise into the control loop. Mook et al. [15] and Crassidis et al. [16] present, at different stages of development, a flight dynamics-based tracking filter to greatly reduce the noise introduced into the system by reducing or eliminating the need for the numerical differentiation associated with the Automatic Carrier Landing System radar tracking system. This study is limited to the pitch axis. Traditionally the addition of a noise rejection feedback loop lowers the sensitivity of the pitch command to noise. This occurs at the expense of an increased turbulence response A primary objective of the

Automatic Carrier Landing System is to limit the aircraft response to turbulence. Consequently, motivation existed to explore new methods of lowering the noise content of the pitch command without simultaneously increasing the response of the aircraft to turbulence.

The filter presented uses airspeed and angle of attack measurements from the aircraft to synthesis a normal acceleration signal using a simplified lift model. A comparative study is presented based on the current α-β filter and the flight dynamics based filter and as a result a definition of both filters is presented. The F-4 aircraft was used as the subject aircraft for this study due to the availability of data. The F-4 pitch autopilot and autothrottle system are briefly discussed, and an informative discussion on the coupling of these systems is also presented. The optimisation techniques employed in the development of the filter are discussed in both papers. The results of this study were that the flight dynamics based filter rejected nearly 100% of the noise content in the pitch demand during the simulation study.

As a follow on from the filter design, Crassidis and Mook [17] present a robust controller, utilising H^{∞} control design techniques which is designed to replace the P-I-D-DD controller in the Automatic Carrier Landing System. As only position measurements are required to develop the H^{∞} control signal the α-β tracking filter is not required. A comparison of the Automatic Carrier Landing System with the flight dynamics based tracking filter and the robust controller with a noise rejection loop is presented. The results show an increased system bandwidth when utilising the robust controller. The system attenuates the turbulence response by a factor of 2 in comparison to the Automatic Carrier Landing System with the flight dynamics based tracking filter.

It has already been stated that the navigation system proposed will not be dependent on radar for aircraft position determination. As a result, the consequent control loops will not be subject to the noise induced by such a radar system. These studies however are important in highlighting a negative aspect of the current state of the art Automatic Carrier Landing System. The fact that the contributors to this study are based at the State University of New York at Buffalo and the manufacturer of the Automatic Carrier

Landing System, Bell Aerospace, are also based at Buffalo indicates possible collaboration.

Costes et al. [18] and Le Moing [19] present a French study which proposes a new carrier landing procedure, for both manual and automatic approaches, using deck motion prediction to determine an updated flight path angle and approach airspeed during the final seconds of the approach in order to adhere to ramp clearance, sink rate and touchdown dispersion constraints. A fully integrated airborne system is proposed which includes the aircraft Flight Control System and the landing aid system.

The new procedure effects approximately the final 10 seconds of the approach, a time frame where cited ship motion prediction studies indicate accuracy of the prediction is greatest. Results of automatic approaches in the presence of ship air wake are presented in which deck motion prediction is initiated five seconds prior to touchdown. At this point the desired flight path angle and airspeed are abruptly changed. The flight path angle is changed in order to maintain ramp clearance and the airspeed is changed correspondingly so that the sink rate at touchdown remains constant regardless of flight path angle. The results presented indicate that a reduction in touchdown dispersion and sink rate and an increase in ramp clearance can be achieved.

This French study is forward thinking and represents a departure from the standard approach navigation strategy in that a variable flight path angle strategy is proposed. It shares the use of ship motion prediction with the navigation strategy proposed in this study, however in this study it is proposed to use ship motion prediction through the complete approach phase.

The variable flight path angle approach strategy aims to substitute for the deck motion compensation mode currently in use. As a consequence of the proposed navigation strategy providing navigation guidance to a fixed point in space, which represents the predicted touchdown point, a variable flight path angle strategy is not necessary.

McPeak [20] in a joint United States Air Force (USAF) and USN Mission Need Statement (MNS) defines the need to provide a rapidly deployable, adverse weather, adverse terrain, day-night, survivable, and mobile precision approach and landing

capability for world wide deployment and interoperability between the services. This system should allow aircraft to land on any suitable land or sea based surface. The development program resulted in what is known as the Joint Precision Approach and Landing System (JPALS). A Differential Global Positioning System was found to satisfy all the requirements of the study.

Wallace [10] presents the results of a limited flight test program of an F/A-18A completing 10 fully automatic approaches to a carrier using Differential Global Positioning System. The system was shown to meet the certification criteria. A schedule presented by Wallace [10] shows the Joint Precision Approach and Landing System being phased into operation by the USN as early as 2009.

The Joint Precision Approach and Landing System is important to this study as it states the future military navigation requirements over a time period where UAV carrier based operation can expect to become a reality and as a consequence any UAV carrier landing navigation system should address these requirements. In addition, it has been demonstrated that Differential Global Positioning System meets the requirements and as a result validates the use of Differential Global Positioning System in the proposed navigation strategy.

What isn't clear from Wallace [10] is the exact architecture of the navigation and flight control system combination used by the F/A-18A during these 10 fully automatic approaches. It is assumed that the aircraft relative position normally determined via radar is replaced with the Local Differential Global Positioning System and aspects such as the navigation strategy and flight control system remain unchanged.

Fitzgibbon and Parkinson [21] present a study of using Global Positioning System (GPS) for use in automatic landing systems. Their study considered commercial applications as opposed to military applications. It should be noted that a position bias is introduced into the GPS signal for civil users by the military custodians of the system.

A comparison between Differential Global Positioning System and standard Global Positioning System is presented. It was concluded that Differential Global Positioning System may satisfy the civil aircraft operations regulatory authorities' criteria for fully

automatic approach and landing guidance but that the bias in the GPS signal makes it unsuitable when used in isolation. The fact that GPS provides direct velocity measurement and that no other landing aid has this capability is highlighted.

The significance of the study completed Fitzgibbon and Parkinson [21] is superseded by the results presented by Wallace [10]. However Fitzgibbon and Parkinson [21] draw attention to the very useful fact that GPS provides direct velocity measurement, which is relevant to the proposed navigation strategy.

2.3.2 Flight Control System

Hess and Urnes [14] of the McDonnell Aircraft Company, manufacturer of the F/A-18A aircraft, present the design criteria and analysis methods used to develop the Automatic Carrier Landing System for the F/A-18A. Both the Stability Augmentation System (SAS) and autothrottle subsystem were configured with optimised control gains different from those gains considered optimum for manual flight approaches. The control strategy used is comparable to the baseline control strategy proposed in this study

Discussions are included on sources of time delay in the complete system, which can be up to 250 ms, air turbulence as the dominant source of approach glide path and touchdown errors, radar tracking noise attenuation, structural mode and Automatic Carrier Landing System flight control system coupling avoidance. A discussion on the use of quad redundant command limiters to minimise the transient aircraft response due to failure of non redundant system components is also included, but this is of little relevance to this study as failure cases and Flight Control System reversion modes are not considered.

Of particular interest to this study is the determination that air turbulence is the dominant source of glide path and touchdown errors. Attenuation of atmospheric disturbances is thus deemed a major design consideration in the design of the control strategies in this study. As previously stated radar noise is highlighted as a problem for the control loops.

Results from land and shipboard flight trials are included which show the system to have better touchdown dispersion characteristics to the F-4 aircraft's equivalent system to which it is compared.

This paper is significant in that it presents the development of an Automatic Carrier Landing System which is in operational service. The touchdown performance results from sea trials presented provide a limited source of data for comparison with the performance of the control strategies developed in this study.

Fortenbaugh [22] presents a discussion of the practical integration of Direct Lift Control in the F-14A and associated Automatic Carrier Landing System. At the time that Direct Lift Control was added to the F-14A the aircraft was at an advanced stage of development and as a consequence design constraints were imposed. Direct Lift Control was implemented through the use of the aircraft's spoilers and flaps. These constraints along with some lessons learned during the F-14A Direct Lift Control design study are presented. A preceding feasibility study indicated the superiority of altitude error as a variable for controlling the Direct Lift Control. As a result this method was used in this study.

It is proposed that attributes of a good Automatic Carrier Landing System should be insensitivity to wide variations in trim conditions and insensitivity to widely varying sea states and atmospheric turbulence levels. This proposition is of direct relevance to this study and has been incorporated in the design of the flight control systems that follow. A statistical comparison of the baseline F-14A flight control system and that with Direct Lift Control shows that the Direct Lift Control system provides better flight path control, and consequently better ramp clearance and touchdown dispersion. This finding has direct relevance to this study and clearly sets a goal in relation to the relative performance of the baseline and Direct lift Control strategies developed .

The results of a piloted study showed that the baseline system performed well up until the point where Deck Motion Compensation was introduced; at that point the aircraft made large attitude, angle of attack, and glideslope excursions with large touchdown dispersion while attempting to follow deck motions. The Direct Lift Control system was

superior during the approach before introduction of Deck Motion Compensation; however the ride was rougher due to the rapidly alternating Direct Lift Control motion.

After the point where Deck Motion Compensation was introduced the Direct Lift Control was much tighter, a more constant attitude, near optimum sink rate and closer glideslope control were evident. Large throttle motions, activated by the autothrottle, were evident with the Direct Lift Control system, but no accompanying unsatisfactory flight path control characteristics were noted.

The main conclusion of this study, which is supported by statistical comparison results and pilot qualitative assessment, is that Direct Lift Control integration into the existing Automatic Carrier Landing System greatly enhances the approach and landing performance of the Automatic Carrier Landing System. This finding is significant to this study as it is demonstrated that Direct Lift Control has the potential for increasing the approach and landing performance when applied to the carrier landing task.

The system presented by Fortenbaugh [22] uses Direct Lift Control to augment the existing F-14A Automatic Carrier Landing System which is comparable to the baseline control system of this study. The use of Direct Lift Control by Fortenbaugh [22] is different to that proposed in this study which proposes to couple Direct Lift Control with a constant pitch attitude control system. Fortenbaugh's [22] system presents an alternative design which the Direct Lift Control system proposed in this study should be compared to.

Martorella et al. [23] present a study on precision flight path control in carrier landing approach and put forth the opinion that this is a case for integrated system design. Their opinion is that the aircraft's dynamic characteristics are augmented through the use of Command and Stability Augmentation Systems (CSAS), Autothrottle and Direct Lift Control in order to aid the pilot in maintaining precise flight path control. However, current specifications provide independent design criteria for each of these systems that do not specifically address interaction in terms of total flight path control.

The purpose of the study was to improve approach flight path control quality for a high performance fighter using the full potential of its control capability by means of an

integrated system design. The study focused on the pitch axis. Qualitative design criteria are defined to reduce pilot workload relative to a baseline aircraft and provide acceptable transient excursions. These criteria are intuitive, such as “minimise aircraft flight path deviations caused by atmospheric disturbances”, but provide a useful design brief for the flight control systems to be developed in this study.

A design based on the F-14A is presented, as the F-14 has all the control effectors and flight control elements needed. The authors are employees of the aircraft’s manufacturers, Grumman Aerospace Corporation, and thus have access to an extensive aircraft database. Simulation results are presented which show that the system developed meets the qualitative criteria; however, a comparison with the original system is not included but it is concluded that by complying with the criteria presented, a more effective flight path controller resulted.

The focus of the study presented by Martorella et al. [23] is on piloted applications and as such much of what is presented is not directly applicable to this study. However, the use of Direct Lift Control is affirmation of the potential of this control strategy when applied to the carrier landing task.

Huff et al. [24] present a follow up to the study presented by Martorella et al. [23]. In their study, the system presented by Martorella et al. [23] is the subject of a manned simulation study for both manual and automatically controlled carrier landings. A pilot comparison to the baseline F-14A flight control system shows that the new system reduces pilot workload and also facilitates more precise tracking and consequently better touchdown dispersion characteristics. A similar comparison is presented where the system is coupled with the Automatic Carrier Landing System in which the new system was shown to significantly reduce touchdown dispersion. All simulations were conducted without carrier pitch and heave motions. These results support the opinion set forth by Martorella et al. [23] that carrier landing is a case for integrated system design procedure. This fact is noted and applied in the development of the flight control systems that follows.

Clark and Miller [25] present an investigation of the use of vectored thrust during carrier landings. The aircraft considered is the F-8A with thrust being vectored from underneath the aircraft at a point forward of the exhaust nozzle and slightly aft of the centre of gravity. The study was limited to the aircraft's pitch axis. Piloted fixed base flight simulator studies were conducted to obtain information on the effects of thrust vector angle, pitching moment due to thrust line offset from the centre of gravity, and thrust available for flight path control on performance of the landing task. The use of an Autothrottle in combination with vectored thrust was also investigated. Thrust vector angles of up to 76.5^{o} were considered.

The results show that vectored thrust offers substantial reductions in approach airspeed and sink rate, improvements in flight path control, and improvements in wave-off performance. However, these advantages are offset by a reduction in the thrust margin available for wave-off and as approach speed is reduced by increasing the thrust vector angle the elevator angle required to trim the aircraft is large; this is due to the large vectored thrust induced pitching moment and is compounded by the reduction in elevator effectiveness due to reduced airspeed.

The manner is which Clark and Miller [25] apply the concept of vectored thrust is not similar to the manner proposed in this study. Clark and Miller [25] reduce the requirement of lift generated by forward speed by vectoring thrust downward at large angles to balance the forces and trim the induced moments using elevator angle. It is proposed in this case to use vectored thrust to supplement elevator pitch control by vectoring thrust through relatively small angles and to maintain a constant approach speed. Nonetheless Clark and Miller [25] present a novel, and arguably precarious, use of vectored thrust.

Crassidis and Mook [26] present a simulation of an F-4A aircraft with pitch autopilot and autothrottle for use in investigations of aircraft tracking and control performance in an Automatic Carrier Landing System. The discussion presented is limited to the pitch axis. Both the pitch autopilot and the autothrottle are presented in detail and an informative discussion on the coupling of these systems is included. The pitch autopilot maintains a desired pitch attitude, while the autothrottle maintains the desired angle of

attack and minimises vertical acceleration changes in the aircraft. It is shown that the autothrottle reduces the aircraft's response to atmospheric turbulence.

The autothrottle does not respond to a pitch command, but rather to a change in angle of attack or vertical acceleration. These changes are delayed with respect to elevator movement based upon the aircraft's response time. As a result the autothrottle control loops include an elevator feedback loop, which leads the aircraft's response, in order to ensure tight control of angle of attack.

After some consideration it was decided to implement a standard autothrottle in the control strategies developed in this study as opposed to that suggested by Crassidis and Mook [26]. The reason for this decision is that a standard autothrottle is used in aircraft in service for which there is published touchdown performance data available e.g. F-14A and F-4A. If the autothrottle system proposed by Crassidis and Mook [26] were implemented the baseline flight control system would not be directly comparable to these in service aircraft.

Gerdes et al. [27] present the results of a piloted simulation study of a novel trajectory control system implemented to provide manual control of an A-7E during carrier approaches. The concept, called Total Aircraft Flight Control System (TAFCOS), utilises an inverse model of the aerodynamic and propulsion characteristics and employs feedforward control to provide the required acceleration command.

Total Aircraft Flight Control System uses a balance of open loop feedforward control and closed loop feedback control. The presence of detailed models of aircraft force, moment and thrust characteristics in the feedforward path enable it to provide most of the control. Feedback is needed only to compensate for external disturbances and for differences between the models and the actual aircraft.

Two control modes were studied, a vertical velocity command mode and a vertical acceleration command mode. The results of the studies show superior performance of this system when compared to the conventionally controlled aircraft. This, however, was less apparent for the cases where ship motion was included. The study shows that the Total Aircraft Flight Control System concept is feasible as an addition to a pre-

existing Command and Stability Augmentation System and that it has potential as an improved mode of control over conventional control for the carrier approach task. However, it was concluded that further optimisation and development studies are needed to explore the full potential of the system and to determine what degree of improvement can be realistically expected.

Meyer and Smith [28] in a paper published prior to Gerdes et al [27] present a detailed mathematical definition of the Total Aircraft Flight Control System based trajectory system and a comprehensive set of simulation results.

The findings of Gerdes et al. [27] and by inference the paper by Meyer and Smith [28] is of little relevance to this study as their focus is entirely piloted control oriented. However, the discussion of the control problems associated with carrier landings and the pilot comments from the piloted simulations presented by Gerdes et al. [27] is of interest and help further the understanding of the carrier landing environment.

Bannett [29] presents a detailed description of the theory of optimal control and the application of such on the design of an Automatic Carrier Landing System for an F-8C. The single command input of the longitudinal channel of the AN/SPN-42, elevator deflection, and autothrottle are employed to control airspeed, altitude and pitch attitude response for both deterministic and stochastic input. Bannett proposes that this system lacks independence in specifying the various responses for both inputs. In order to alleviate this problem and obtain good response characteristics for the critical variables, a multicontroller, multivariable design is employed.

A longitudinal controller system incorporating command inputs of elevator, thrust and Direct Lift Control flaps is presented. The control system configuration is a 12 parameter feedback system. The design procedure and its subsequent application to the F-8C is presented in detail. An assessment of the system design shows that the glide path tracking is very precise, and variations in aircraft position from the nominal glide path in the presence of carrier air-wake and carrier motion is held to a tight tolerance.

While the optimal control aspect presented by Bannett [29] is not directly relevant to the flight control systems which are to be developed using classical control techniques in

this study, the inclusion of Direct Lift Control is relevant. The performance of the system indicates that Direct Lift Control coupled with elevator and thrust control provides very precise glide path tracking. This again supports the use of Direct Lift Control in this study.

It is interesting to note that the majority of publications reviewed concentrated on control of the pitch axis. Durand and Wasicko [3] present a statistic to explain this. In 1964 80% of all carrier landing accidents were vertical flight path control related, e.g. ramp strikes and hard landings [3]. This affirms the decision for this study to focus on pitch axis control strategies.

2.3.3 Supplementary Research

Bihrle [30] presents a study on aircraft characteristics that influence longitudinal handling qualities during a carrier approach. Approximately 7000 manual approaches were completed using a moving base simulator to evaluate the influence of short period frequency, damping ratio, load factor attainable per unit of angle of attack, tail length, operation on the backside of the trimmed power required versus speed curve, and engine thrust response on handling qualities. In addition, the influences of both an autothrottle and a Direct Lift Control system on the longitudinal handling qualities were investigated.

It was found that the two most important quantities that affect the longitudinal handling qualities are the frequency of the short period mode and the magnitude of the load factor attainable per unit of angle of attack. The effectiveness of the pilot in the precision control loop is determined by the specific relationship between these two parameters known as the Control Anticipation Parameter (CAP). Upper and lower limits of Control Anticipation Parameter are presented.

It was found that damping ratio per se does not affect the precision control task. An influence of tail length on handling qualities was not detected. It was found that pilots operated well on the back side of the trimmed power required versus speed curve; however, beyond a certain point, performance was seen to degrade. This point was identified as where the slope of the curve is equal to -100 lbs per knot.

With respect to the operation of an Autothrottle and a Direct Lift Control system it was found that a poorly rated airframe, with respect to longitudinal handling qualities, can be appreciably upgraded by activating an Autothrottle system. The benefits to be realised from a Direct Lift Control system are most apparent for airframes that have both low CAP and load factor attainable per unit of angle of attack values. It is proposed that to realise the potential of a Direct Lift Control an effective Autothrottle system must be operating.

The findings of Bihrle [30] with respect to the Control Anticipation Parameter and piloted operation on the back side of the power required versus speed curve are not directly relevant to this study. The findings with respect to Autothrottle and Direct Lift Control systems are directly applicable and are applied in the development of the flight control systems. Much of the discussion presented by Bihrle [30] serves to increase the understanding of the carrier landing environment from the point of view of Flight Control System development.

Ebers et al. [31] present a study on ship motion effects on landing impact loads. A simulation study is discussed which considered V/STOL aircraft landing impact onto a moving deck. Surge, sway, heave, roll, pitch and yaw deck motions were considered for a selected ship hull, sea state, heading and ship speed. The results presented show that deck motions increase landing loads significantly. Three point, tail down and drift landing conditions were examined. In order to comply with landing loads criteria it is suggested that a maximum aircraft sink rate of 6.7 ft/sec be imposed in heavy sea conditions. The paper presents an interesting discussion on the effects of ship motion on landing impact loads; however the suggested maximum sink rate seems to be very restrictive and is not considered in the design and analysis of the flight control systems developed in this study but this should not preclude the findings of Ebers et al. [31] from being considered in follow on work from this study.

Connelly [32] presents the development of a method of measuring the performance of an aircraft carrier approach and landing. The previous measure used, the Root Mean Square (RMS) of deviations from the desired glide path, can provide identical scores for both satisfactory and unsatisfactory flight paths. The method presented constructs a

second order performance model that measures performance according to how well the pilot controls the second derivative given the error and its first derivative. The results of the study were inconclusive with respect to the feasibility of the performance measurement method presented and as a consequence is not used in this study.

As a result of the observation made by Connelly [32] with respect to the Root Mean Square of glide path deviations, and the lack of published carrier approach and landing performance criteria, it was decided to develop a set of dedicated performance metrics to be used in the analysis of a carrier approach and landing.

Durand [33] presents a study on piloted longitudinal control during a carrier approach, focusing on the difficulty described by pilots as an inability to arrest sink rate or control altitude. It is suggested that this problem is theoretically traceable to a speed sensitive performance reversal associated with pilot control of attitude with elevator and altitude with throttle. The term performance reversal refers to a decreased altitude tracking bandwidth when the pilot is attempting to increase this bandwidth by tightening control with either stick or throttle. The speed at which this occurs closely corresponds to the minimum approach speed.

A piloted simulation and subsequently a computer simulation study were conducted. An informative discussion is presented concerning the piloting techniques used during the different phases of an approach. It was found that a reduction in the static margin of the aircraft theoretically eliminated the reversal problem and experimentally received pronounced improvement in pilot ratings. It was also found that performance reversal was eliminated with pilot control of altitude with elevator, providing there is adequate means for holding constant airspeed. It was proposed that lower approach speeds are attainable for the pitch attitude and altitude controlled by elevator and speed controlled by throttle piloting technique compared with the pitch attitude controlled by elevator and height controlled by throttle method. It was found during the piloted simulation phase of this study that a gradual switchover to elevator control of altitude was noted when within 5 to 10 seconds from the ramp. Elevator control of altitude is used to make small precise height adjustments while all gross corrections are made with throttle irrespective of the approach phase.

Much of the study presented by Durand [33] is of little relevance to this study as the focus is entirely piloted control oriented; however, some insights into the control problems associated with carrier landings can be gleaned. The finding with respect to the use of elevator control for making precise height adjustments is of some interest as this method of control has been selected for the baseline control strategy.

Brictson [34] presents a synopsis of a five-year program of human factors research on carrier landing performance. Empirical measures of day and night final approach to landing were recorded and used to describe differences in landing performance across a wide variety of aircraft, ship, pilot, LSO and environmental conditions. The empirical data were used to develop carrier landing performance criteria which were applied to evaluate and assess the relative influence of system components on carrier landing system effectiveness. However, these criteria were not presented.

With respect to carrier landing accidents it was found that slow response, high approach speed aircraft accounted for the majority of aircraft involved and that pitching deck was found to be the most significant contributory factor in carrier landing accidents. As a result of this finding with respect to the pitching deck, and along with findings during the analysis of the performance of the control strategies developed as part of this study which concurred with this, a Variable Approach Speed Controller was developed. This system is presented in chapter 8.

2.3.4 Ship Motion and Ship Motion Prediction

Johnson [35] presents an analysis of aircraft carrier motions in high sea states as part of a program aimed at providing an analytical base useful in the development of improved carrier landing methods and systems. Pitch, roll and touchdown point displacement motion data for this study was recorded aboard the USS Independence. Characteristics of ship motion were observed and a short discussion on this is presented. Power Spectral Density (PSD) plots over appropriate time intervals were generated and these form the basis for the discussion presented by Johnson.

It was found that for pitch and heave motions the centre frequency was typically between 0.5 and 0.7 rad/sec and the bandwidth was typically between 0.1 and 0.2 rad/sec, characterising these motions as being essentially narrowband processes. The

general shapes of the PSD plots that show the roll spectra are more broad and flat in a head wave condition while in a beam wave conditions the spectra was found to have a very narrow band and highly peaked PSD profile. These results correlated well with prior studies and as a result it is suggested that these results be used in future analyses that require knowledge of large carrier motion characteristics. These results provide a useful means of evaluating the accuracy of a ship motion model at representing the motion of an aircraft carrier.

Kaplan [36] presents a study of prediction techniques for aircraft carrier motions at sea. The focus of his study is a deterministic technique which uses wave height measured forward of the bow of the carrier as its input. A second method known as the Wiener prediction method is presented. This method is a statistical technique, where the predictor is derived on the basis of knowledge of the spectral characteristics of the stochastic variable under consideration. However, the implementation of this method requires a complete knowledge of the power spectrum of the signals to be predicted. The deterministic technique was found to have a prediction time of about 6 seconds. It is suggested that a Kalman filter applied to the wave motion input would have the effect of smoothing some of the prediction errors inherent in the technique; this would have the effect of extending the prediction time by up to an additional 3 seconds. With respect to the prediction time required by the proposed navigation strategy, this prediction method is not suitable for this study.

Doolin and Sidar [37] present a study on the feasibility of real time prediction of aircraft carrier motion at sea. A predictor was designed on the basis of Kalman's optimum filtering theory for the discrete time case, adapted for real time digital computer operation. A full derivation of this system is presented. The predictor uses power density spectrum function data for pitch and heave measured for various ships and sea conditions as its reference model.

It was shown that motion can be predicted well for up to 15 seconds. An adaptive predictor scheme is suggested whereby ship motion variables are measured in real time and through the use of Fast Fourier Transform (FFT) algorithms a power density spectrum of the ships motion is calculated for use by the predictor. Again, with respect

to the prediction time required by the proposed navigation, this prediction method is not suitable for this study.

Hess and Judd [38] present a study on improved Automatic Carrier Landing System using deck motion prediction. The study focused on the A-7E. Its slow response characteristics makes it a suitable aircraft to assess the benefits of deck motion prediction. A method of prediction is not presented; instead the Deck Motion Compensation mode of the Automatic Carrier Landing System was augmented to lead the actual ship motion and prediction was assumed to be exact. The results of this study show that deck motion prediction reduces touchdown dispersion. This study indicates that ship motion prediction has a positive effect on touchdown performance; however a method of ship motion prediction is not presented.

Broome and Pittaras [39] present an adaptive ship motion predictor. The advantages of an adaptive solution is that no previous knowledge about the ship and the mathematical model describing its response to sea waves is necessary as a mathematical model is formulated on-line using System Identification (SI) techniques. The SI method is used and an Auto Regressive Moving Average with eXogenous Input (ARMAX) model is formulated and arranged so as to predict a selected variable. Real ship roll motion is used in the simulation of this technique. Results for prediction periods of 1, 5 and 10 seconds are presented. The 1 second prediction period results compared very well with the actual motion while the 5 and 10 second prediction period results showed some deterioration. However, the prediction error did not increase in proportion to the prediction period. The predictor successfully predicted regular periodic motions, but performed less well in predicting sudden sharp motions. The predictor presented by Broome and Pittaras [39] is a follow on to that presented by Jefferys and Samra [40]

In a subsequent PhD thesis Pittaras [41] fully developed the ideas introduced by Broome and Pittaras [39]. Background information into the system identification technique and the mathematical methods employed with the prediction technique are fully presented along with three case studies. One of the case studies includes comparison with an Extended Kalman Filter predictor. The results of this show that while the Extended

Kalman Filter successfully predicts the low frequency component of the motion the overall performance was marginally worse than the SI method.

Broome and Hall [42] present an application of the prediction technique introduced by Broome and Pittaras [39]. The application presented is a display system that uses measured ship motion to predict and subsequently display actual and predicted ship motions and is used as a helicopter landing aid. Results of sea trials are presented which show that roll prediction reduced the number of landings where the ship roll angle would have been greater than a prescribed operating limit, in this case 5^{o}, significantly.

Broome [43] presents an extension to the previous work by examining the variation of ship motion due to ship heading changes relative to the dominant wave direction. Of particular interest was the variation in the coefficients of the Auto Regressive Moving Average with Exogenous Input model. The result of a ship changing heading was shown to cause a significant change on these coefficients. Considerable cross coupling of motion was evident in the data collected at sea between roll and heading. These changes to the coefficients of the model have the effect of reducing the accuracy of the prediction until a new model has been identified. A method was employed whereby the model was varied according to pre-calculated values of the coefficients as a function of heading; this had the effect of updating the model as the heading was changed reducing the time taken for the model to adapt to the new operating conditions.

An adaptive predictor seems to address the shortfalls of the other available methods. In adaptive prediction there is no need to include any prior knowledge about the ship response in the algorithm. The ship mathematical model is formed on-line and is conveniently updated whenever it is necessary, due to changes in operating or weather conditions.

Adaptive prediction promises to be the most suitable method for the purposes under consideration in this study, and in particular the research undertaken at the Department of Mechanical Engineering at University College London [39,40,41,42,43].

The main limitation of these adaptive prediction methods [39,40,41,42,43] is that no knowledge of the ship dynamics are assumed. The online model identification increases

the phase lags of the prediction scheme and hence reduces the bandwidth and associated prediction accuracy and accurate horizon times. Additional measurements of the sea state could also be incorporated with the effect of increasing the prediction horizon.

In terms of predicting the three dimensional position of the touchdown point the latitude and longitude coordinates are relatively straightforward as the motion which has the greatest effect on these is essentially linear, i.e. aircraft carrier forward speed and direction. The vertical position of the predicted touchdown point is effected by two non-linear aircraft carrier motions, pitch and heave, and as such represent the greatest challenge to prediction accuracy.

2.4 FLIGHT CONTROL SYSTEM DESIGN

A review of Flight Control System design literature directly associated with carrier landings has been presented in section 2.3.2. However, some more general Flight Control System design literature has been reviewed and is presented in this section.

Flight Control System design is a multidiscipline activity. Knowledge of control theory, aerodynamics, aircraft flight dynamics and handling qualities, aero-servo-elasticity, aircraft loads, weight and balance, and simulation and modelling methods are required. A very accessible paper by Fielding [44] presents an overview of Flight Control System design and how these disciplines relate.

The Research and Technology Organisation of the North Atlantic Treaty Organisation (NATO) present a report on 'best practices' of Flight Control System design [45]. The first part of this report presents examples of flight control design problems and lessons learned from these problems. These examples span the history of powered flight, from the Wright Flyer to the F-22. A series of recommended best practise are presented in relation to the design of flight control system based on lessons learned. Where appropriate these best practices have been applied.

The second part of this report presents an extensive review of flying qualities, Pilot Induced Oscillations (PIO), and Modelling. This section provides an excellent reference source on these areas. A comprehensive reference list is also provided. This report,

especially the first part, is essential reading for anyone involved in the design and development of Flight Control Systems

Throughout the course of this study two main reference texts were used. Cook [46] provides an invaluable reference for modelling, flight dynamics and basic Flight Control System design issues. McLean [47] provides an excellent reference text for more advanced Flight Control System design issues.

In order to augment the available literature on Direct Lift Control and Thrust Vectoring techniques applied to carrier landing related Flight Control Systems literature relevant to other applications of these techniques were reviewed. A brief review of such literature is presented in the following sections.

2.4.1 Direct Lift Control

Prilliman et al. [48] and Henry et al. [49] present studies based on an F-8C aircraft modified to include Direct Lift Control. Neither paper presents a detailed description of the control system implementation. However, discussions are included on the aerodynamic implementation of Direct Lift Control and the benefits afforded by such a system during approach and landing.

Although the same aircraft was used for both studies, some modification of the Direct Lift Control system was instigated as a result of the results presented by Prilliman et al. Both studies are concerned with manual operation of the Direct Lift Control system.

The ailerons of the F-8C aircraft are positioned considerable inboard of the conventional aileron position and are drooped in the landing configuration. For the purposes of these studies the symmetric aileron deflection provided the means of aerodynamically effecting Direct Lift Control.

An interconnect between aileron deflection and elevator was used to trim the Direct Lift Control induced pitching moment. For the study presented by Prilliman et al. [48] the neutral aileron droop deflection was reduced from the standard landing configuration.

The use of ailerons for Direct Lift Control had the effect of compromising lateral control authority, especially when the Direct Lift Control system deflected the ailerons to its maximum allowable deflection. This was found not to be a problem during the simulator and flight test trials presented by Prilliman et al. [48]. However the pilots expressed a desire for more lateral control authority.

For the NASA study presented by Henry et al. [49] the neutral aileron position was reduced further and total aileron travel was increased. This had the dual effect of providing more lateral control authority and provided more 'up-lift' control for arresting excessive sink rates prior to touchdown.

The inboard trailing edge flap deflection for landing was increased from 20 degrees to 40 degrees. This had the effect of providing a linear relationship between Direct Lift Control induced pitching moment and symmetric aileron deflection. It also had the effect of recovering the lift lost due to the reduction in aileron droop.

Two methods of activating the Direct Lift Control were provided. A bang-bang, or full authority only, and proportional control of the symmetric aileron deflection. A thumb wheel mounted on the centre stick was used as the pilot interface. It was noted that pilot's preferred the proportional control method for small adjustments to aircraft approach glide path.

Simulator and flight test results are presented by Prilliman et al. [48] of a comparison of the Direct Lift Control system and the standard aircraft controls. The intent was to augment the standard aircraft control mechanisms through the use of Direct Lift Control and so pilots used Direct Lift Control to correct small altitude errors and gross errors using standard aircraft controls.

For the tests conducted it was found that there was significantly less dispersion in altitude error when using bang-bang or proportional Direct Lift Control as compared to standard aircraft controls alone. The flight test portion of this study conducted approaches to conventional runways as well as aircraft carriers.

Henry et al. [49] presents the results of a flight test program of the F-8C Direct Lift Control aircraft augmented, as previously described. All approaches were flown to a

conventional runway. The conclusions of Henry et al. [49] concur with the conclusions of Prilliman et al. [48].

2.4.2 Thrust Vectoring

The area of thrust vectoring has received considerable attention over the past two decades. There are many benefits to be afforded by the use of vectored thrust. These benefits include: low airspeed manoeuvring and agility; high angle of attack operations; recovery from deep stall or departure; backup for aerodynamic control surface in the case of damage or malfunction; reduction in trim drag; reduced tail size for reduced weight, drag and radar signature.

The intent of this section is not to present a rigorous review all available related literature, but to briefly summarise the state of the art and to provide a context for the use of thrust vectoring in this study.

Thrust vectoring is the capability to vector or point the thrust of an aircraft engine so as to control the aircraft. The thrust may be vectored by paddles located aft of the engine nozzle [50], by a gimballed engine nozzle [51] or by fluidic injected flow inside a fixed position engine nozzle [52].

Single engine aircraft employing thrust vectoring can use the vectored thrust as a means of pitch and yaw control. Twin engine aircraft employing thrust vectoring can use the vectored thrust for roll control as well as pitch and yaw control. Intuitively the control power of the vectored thrust is a function of thrust.

Bowers et al. [53] present an overview of the High Alpha Research Vehicle (HARV) and the associated High Alpha Technology Program (HATP). An F-18 modified with three thrust vectoring paddles located aft of both engine nozzles was used to investigate control in the post-stall region of the high alpha envelope. Later in the research program forebody strakes were added to the aircraft.

The research program consisted of three main phases. The first phase consisted mostly of aerodynamic research. The aerodynamic characteristics of the aircraft without thrust vectoring in the high alpha region were characterised. The second phase was dominated

by control research. The use of thrust vectoring increased the highest attainable alpha from 55 degrees for the basic aircraft to 70 degrees for the aircraft with thrust vectoring. The emphasis of the third phase was on forebody vortex control. A series of flight trials were conducted investigating the use of forebody strakes with and without thrust vectoring for enhanced roll control at high alpha.

While the emphasis of the research presented by Bowers et al. [53] was on thrust vectoring at high angle of attack the inference is that thrust vectoring is a viable means of aircraft control.

Bosworth and Stoliker [54] present a summary of flight test results of the X-31A Quasi-Tailless aircraft. The X-31A research aircraft has a thrust vectoring system similar to that of the F-18 HARV. In flight simulations were used to assess the effect of partial or total vertical tail removal. The rudder control surface was used to cancel the stabilising effects of the vertical tail, and yaw thrust vector commands were used to restabilise and control the aircraft. The desire to reduce or remove the vertical fin is driven by the desire to reduce an aircraft's radar signature.

A set of manoeuvres were flown to assess the effectiveness of yaw thrust vectoring to stabilise a tailless or reduced tail aircraft. These manoeuvres included a landing approach. This is significant in that a landing approach is flown at a low power setting, and hence reduced thrust vectoring control power. In order to increase the control power, speed brakes were deployed to increase the aircraft drag. A higher than normal power setting was thus used while the approach was flown at the normal speed. This had the effect of increasing the thrust vectoring control power.

The flight test experiment presented by Bosworth and Stoliker [54] successfully demonstrated the ability to use thrust vectoring to replace the functions of stabilisation and turn coordination usually required of a rudder and vertical tail. Limitations were found when more control power was demanded than was available.

In the context of this study, the use of thrust vectoring for stabilisation and control at approach power settings demonstrated by Bosworth and Stoliker [54] validate the use of thrust vectoring in this study.

3 DEVELOPMENT OF THE SIMULATION MODEL

3.1 INTRODUCTION

A simulation model is the most significant tool used in any Flight Control System design exercise. The confidence with which conclusions and recommendations can be made is directly proportional to the fidelity of the simulation model used. For this reason great attention was applied in the development of this simulation model.

It was apparent from the literature survey that the simulation model necessary for this study required three main components: an aircraft model, an atmosphere model and an aircraft carrier dynamics model. The aim, with respect to all three components, was to develop a model that accurately describes reality and is appropriate to the carrier landing task.

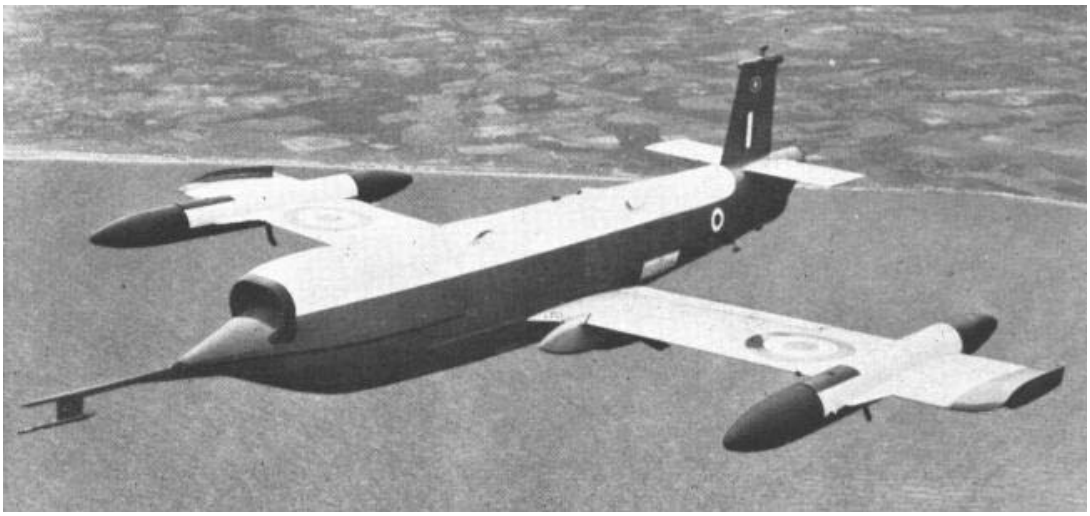

Figure 3-1 A Jindivik with Wing Tip Extensions

The first component to be developed was the aircraft model. An aerodynamic and thrust model representative of a likely carrier based UCAV was sought. Factors such as physical size, weight, and performance were considered. Fortuitously such an aircraft model existed within Cranfield University [55]. Cranfield Aerospace Ltd. is the design

authority for the Jindivik UAV and previous flight dynamics investigations have been conducted on the aircraft by the staff of the College of Aeronautics. In addition, personal experience with the aircraft was gained through a previous study [56].

The Jindivik is a low/mid straight wing monoplane, controlled in pitch via elevators and trailing edge flaps, and in roll via ailerons alone, this aircraft does not have a rudder. A picture of a Jindivik is presented in Figure 3-1. The aircraft presented in Figure 3-1 has wing tip extensions, outboard of the wing pods, which are not included in the aerodynamic model used in this study. The Jindivik provides a suitable platform for this study owing to its physical size (length 23.25 ft, wingspan 21 ft), weight and performance. The aircraft's flight envelope is presented in Figure 3-2.

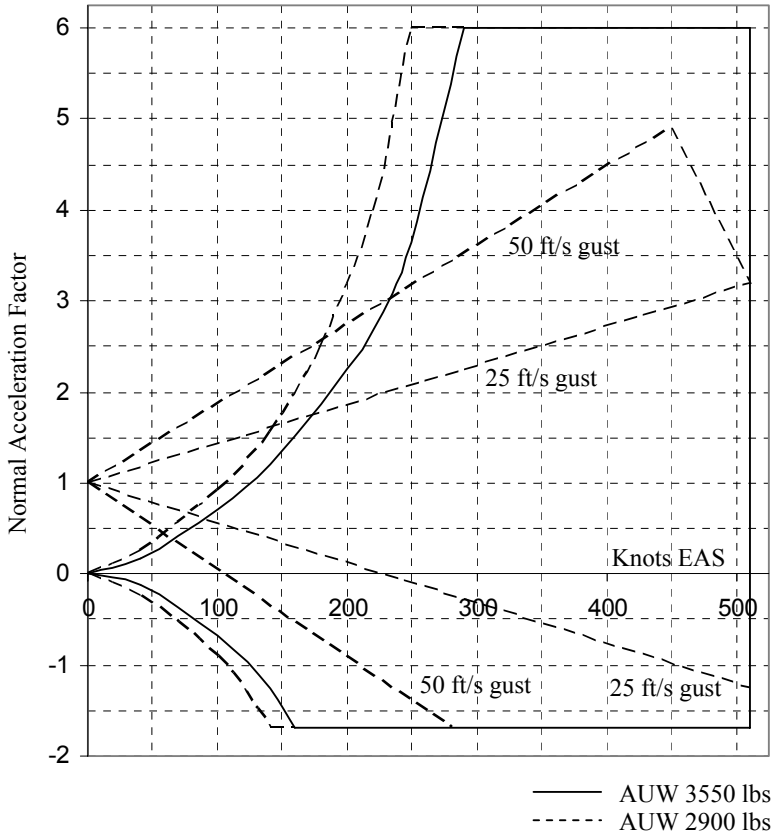

Figure 3-2 Flight Envelope of the Mk 4A Jindivik [57]

The aerodynamic model of the Mk 4A Jindivik presented by Gautrey and Cook [55] is based on manufacturer's wind tunnel data and subsequent flight trial validation. This model includes correction factors due to aircraft flexibility applied to the rigid body

aerodynamic data; although at the speeds of interest to this study flexibility is not a factor.

The thrust model of the Jindivik's engine, a Rolls-Royce Viper Mk 201 Turbojet, presented by Gautrey and Cook [55] is based on the model used in the Jindivik Procedural Trainer.

Some modifications to the aerodynamic and thrust models were necessary in order to achieve the objectives of this study. Firstly a rudder model developed by Fitzgerald [56] was added to the basic model to allow independent control about all three axes. As Direct Lift Control is required, a spoiler model was developed using a method presented by ESDU [58,59,60]. Spoilers provide a means of dumping lift, while the aircraft's trailing edge flaps can be used to increase lift. In addition, a conventional undercarriage model was added as the Jindivik uses a landing skid in place of standard undercarriage [61]. In order to facilitate thrust vectoring a simple thrust vectoring system was added to the thrust model.

The aircraft model was completed with the addition of a Flight Control System developed by Fitzgerald [56]. A three axis Stability Augmentation System provides the airframe with consistent flying qualities characteristics across the entire flight envelope. Three basic autopilot modes were implemented, Altitude, Heading and an Autothrottle, to provide a means of controlling the aircraft. Associated sensor and actuator models were also included.

The model developed by Gautrey and Cook [55] and subsequently used by Fitzgerald [56] was achieved using the Dymola simulation program. For this study Matlab and its associated graphical interface, Simulink, was chosen as the simulation platform. This choice was based on familiarity with the program, extensive use of this program in industry and the functionality which the program provides.

The aircraft model was constructed in a modular manner to allow ease of reconfiguration and further development. The model was validated against the model presented by Gautrey and Cook [55] and also against the stability and control analysis of the basic airframe and augmented airframe presented by Fitzgerald [56].

The second component of the simulation model to be developed was the atmosphere model. The underlying element of this is the International Standard Atmosphere [62] model which describes the atmospheric properties with respect to temperature, density and pressure from sea level to 65,617 ft i.e. the Troposphere and lower Stratosphere. While the altitudes of interest to this study are below 1000 ft the model was implemented in its entirety for completeness.

From the literature review it was clear that atmospheric disturbance attenuation is a major consideration in the design of a Flight Control System for carrier based aircraft. Therefore it is crucial to model turbulence to a known and exacting standard. It was discerned from the literature review that it is necessary that the atmospheric disturbance model include atmospheric disturbances due to the motion and proximity of the aircraft carrier as well as inherent atmospheric disturbances [3,5].

The Flying Qualities of Piloted Airplanes Military Specification document, MIL-F-8785C [63], presents such an atmospheric disturbance model. As this model is defined in the Military Specification document it is of a suitable standard and satisfies the objective of accurately modelling reality and it is appropriate to the carrier landing task.

The MIL-F-8785C [63] atmospheric disturbance has four main elements: a turbulence model, a discrete gust model, a low altitude wind shear model and a carrier landing disturbance model. The model is defined from sea level to 80,000 ft. As with the International Standard Atmosphere the atmospheric disturbance was implemented in its entirety for completeness.

A continuous time domain implementation of the MIL-F-8785C [63] atmospheric disturbance model was developed and integrated with the aircraft model. The atmospheric disturbance model outputs disturbance velocity components. These velocity components are summed to the aircraft velocity components with reference to the appropriate axes system. In effect, the disturbances defined by the MIL-F-8785C [63] atmospheric disturbance model are implemented as instantaneous aircraft velocity changes.

The final component of the simulation model to be developed was the aircraft carrier dynamics model. This model proved to be the most challenging with respect to the objectives of the simulation model development. A search was conducted for an appropriate model. Approximate models were found, such as summing sine waves of appropriate frequency and magnitude to represent pitch and heave motions. Such models, while adequate for approximating the motion of the aircraft carrier, would have the effect of reducing the fidelity of the entire model, and hence reducing the confidence in the conclusions and recommendations resulting from this study.

The author of a commercially available ship motion model, SEAWAY [64,65,66], was contacted and a dialogue ensued which resulted in a copy of SEAWAY being made available for this study without charge. SEAWAY is a frequency domain ship motion Fortran simulation, based on linear strip theory, to calculate wave induced loads, motions, added resistance and internal loads for six degree of freedom displacements. The model was limited to a hull form most similar to that of an aircraft carrier. This model satisfies the objectives of the simulation model development.

In order to integrate the aircraft carrier dynamics model into the complete model it was necessary to run the model off-line and store the aircraft carrier motion time history. When the complete model was executed the aircraft carrier time history was input to the simulation at each time step. This method of integration has the advantage of facilitating perfect ship motion prediction in an uncomplicated manner.

A data flow diagram of the simulation model is presented in Figure 3-3. The simulation model is defined in the following sections and this definition is supplemented by Appendix A. The aerodynamic data from which the model is developed is not presented here; however, these are presented by Fitzgerald in a Cranfield University College of Aeronautics report [67].

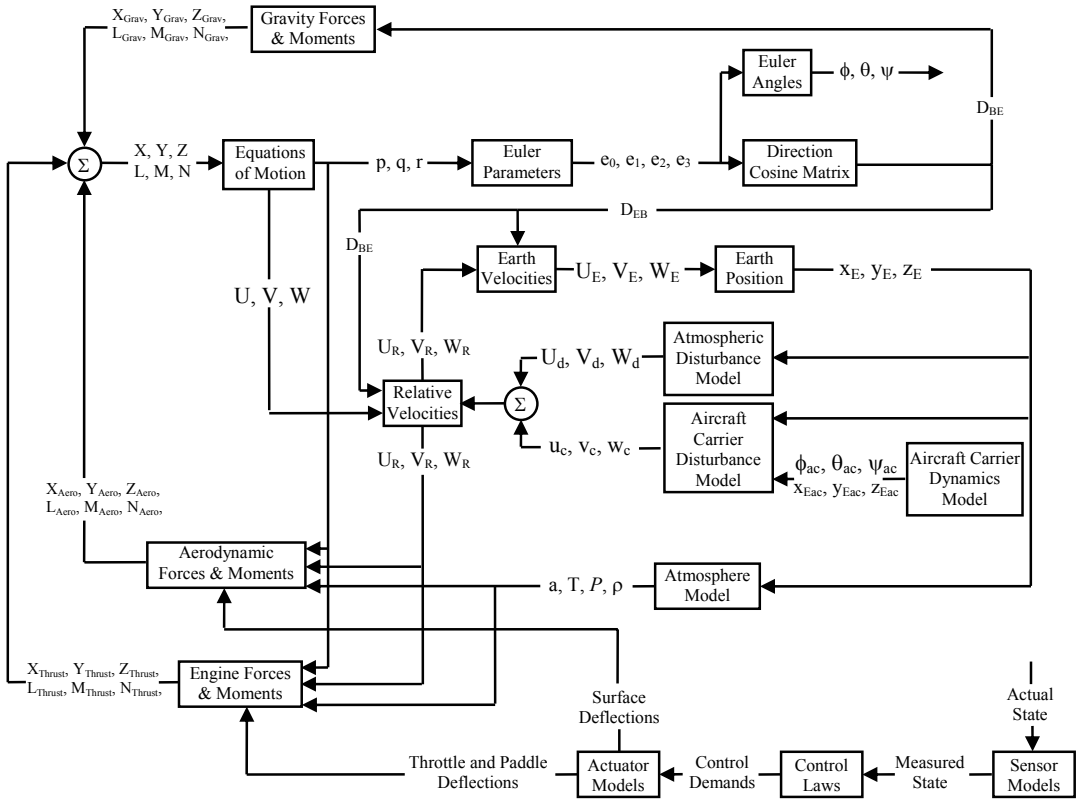

Figure 3-3 Simulation Model Data Flow Diagram

3.2 AXES SYSTEM AND NOTATION

Three axes systems are used in the development of this simulation model. A fixed axes system relative to a point on the surface of the earth, referred to as the 'Earth Axes', a fixed axes system relative to the aircraft's centre of gravity, referred to as the 'Body Axes' and a fixed axes system relative to the aircraft carrier's centre of gravity, referred to as the 'Carrier Body Axes'.

The Earth and Body axes systems follow the convention and notation defined by Cook [46]. This convention has been applied to the Carrier Body Axes system.

3.2.1 EARTH AXES

The earth axes system, (o_E, x_E, y_E, z_E), used in this simulation is defined relative to a reference point o_0 on the surface of the earth which is the origin of a right-handed orthogonal system of axes (o_0, x_0, y_0, z_0), where o_0x_0 points to the north, o_0y_0 points to the east and o_0z_0 points vertically down along the gravity vector, as illustrated in Figure 3-4. As the distance travelled by both the aircraft and aircraft carrier in the simulation are relatively small when compared to the dimensions of the earth, the earth's curvature is ignored and the earth's surface is assumed to be flat.

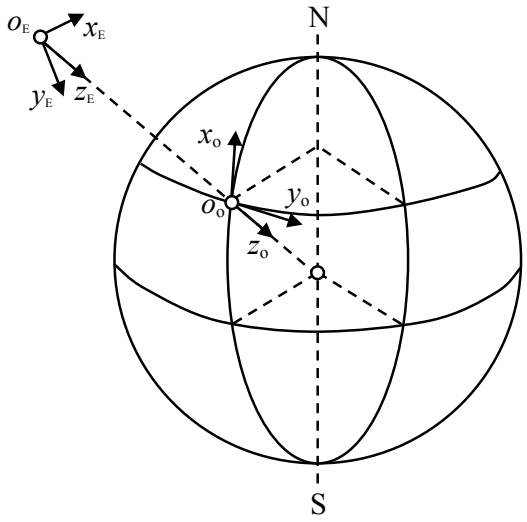

Figure 3-4 Earth Axes [46]

3.2.2 AIRCRAFT BODY AXES

The aircraft body axes system (o, x_B, y_B, z_B) is defined as a right handed orthogonal axes system which is fixed in the aircraft and constrained to move with it. The origin o of the axes is fixed coincident with the centre of gravity of the aircraft. The aircraft body axes system is presented in Figure 3-5.

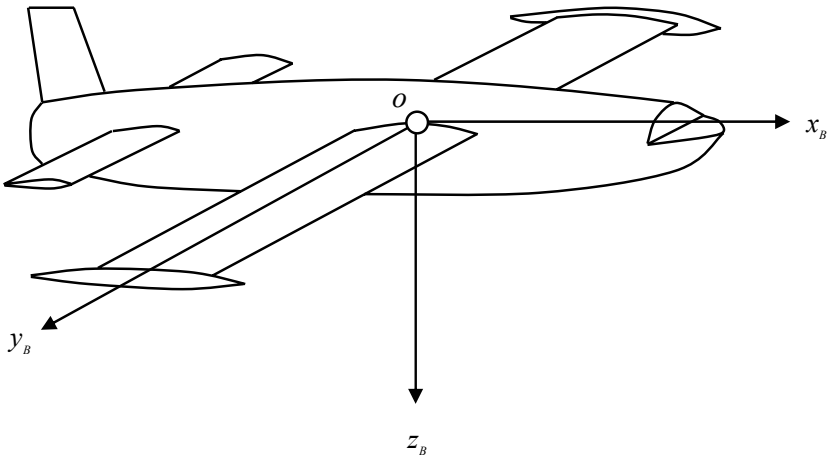

Figure 3-5 Aircraft Body Axes [46]

3.2.3 AIRCRAFT CARRIER BODY AXES

The aircraft carrier body axes system $\left(o_{ac}, x_{B_{ac}}, y_{B_{ac}}, z_{B_{ac}}\right)$ is defined as a right handed orthogonal axes system which is fixed in the aircraft carrier and constrained to move with it. The origin of the axes system, o_{ac}, is fixed coincident with the centre of gravity of the aircraft carrier. All motion variables outputted by the carrier dynamics model are referenced to the aircraft carriers body axis system. The aircraft carrier body axes system is presented in Figure 3-6.

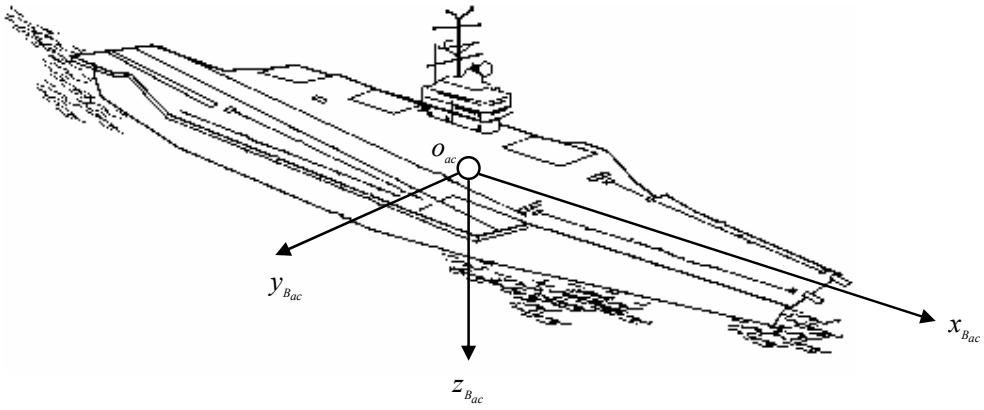

Figure 3-6 Aircraft Carrier Body Axes

3.2.4 AIRCRAFT NOTATION

The motion of the aircraft is described in terms of force, moment, linear and angular velocities and attitude resolved into components with respect to the aircraft body axes system. These variables are presented in Figure 3-7 and summarised in Table 3-1.

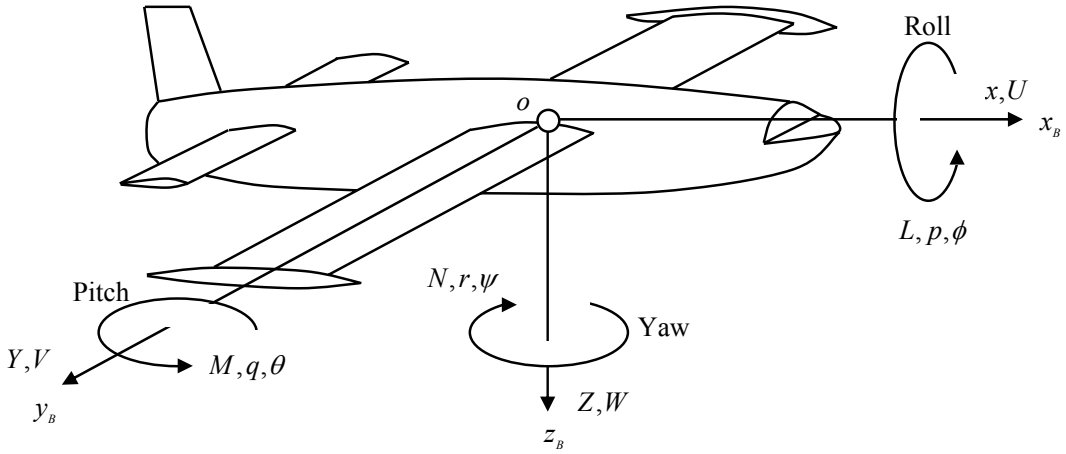

Figure 3-7 Aircraft Motion Variables Notation [46]

X	Axial 'drag' force	Sum of the components of aerodynamic, thrust and gravitational forces.
Y	Sideforce	
Z	Normal 'lift' force	
L	Rolling moment	Sum of the components of aerodynamic, thrust and gravitational moments.
M	Pitching moment	
N	Yawing moment	
p	Roll rate	Components of angular velocity.
q	Pitch rate	
r	Yaw rate	
U	Axial velocity	Total linear velocity components of the centre of gravity.
V	Lateral velocity	
W	Normal velocity	
ϕ	Roll attitude	Components of angular attitude.
θ	Pitch attitude	
ψ	Yaw attitude	

Table 3-1 Aircraft Motion Variables Notation [46]

3.2.5 AIRCRAFT CARRIER NOTATION

The motion of the aircraft carrier is described in terms of linear velocities and attitude resolved into components with respect to the aircraft carrier's body axes system. These variables are presented in Figure 3-8 and summarised in Table 3-2.

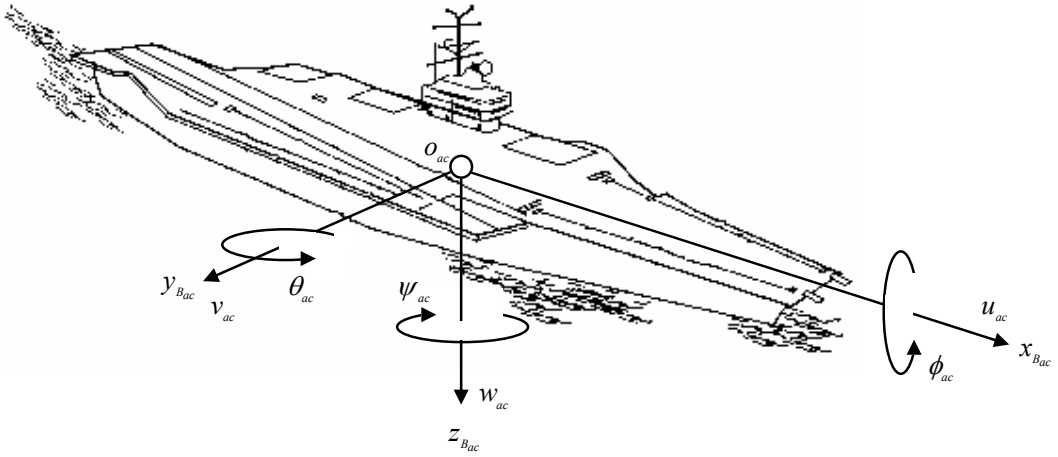

Figure 3-8 Aircraft Carrier Motion Variables Notation

U_{ac}	Axial velocity	Total linear velocity components of the centre of gravity.
V_{ac}	Lateral velocity	
W_{ac}	Normal velocity	
ϕ_{ac}	Roll attitude	Components of angular attitude.
θ_{ac}	Pitch attitude	
ψ_{ac}	Yaw attitude	

Table 3-2 Aircraft Carrier Motion Variables Notation

3.2.6 CONTROL ANGLE DEFINITIONS

The elevator, aileron and rudder control angle deflections are defined so that a positive control surface displacement gives rise to a negative aircraft response. Spoiler deflection is limited to travel in one direction and consequently this direction is defined as positive.

The sign convention employed in the implementation of vectored thrust defines the longitudinal thrust vectoring angle, θ_r, as being positive when deflected downwards, or

in the positive body axes z axis direction, and the lateral thrust vectoring angle, ϕ_r, as being positive when deflected starboard. The definition of lateral thrust vectoring angle is opposite to the standard convention applied to aircraft control angle.

3.3 AIRCRAFT MODEL

The generic UCAV modelled is based on the aerodynamic properties of the Mk 4a Jindivik UAV and the engine characteristics of the Rolls-Royce Viper Mk 201 turbojet. The Mk 4a Jindivik UAV has elevator, aileron and trailing edge flap aerodynamic control surfaces and uses a skid as undercarriage. In this implementation the aerodynamic model has been augmented to include a rudder, spoilers and conventional undercarriage using methods presented by the ESDU [58,59,60,61,68]. Details of these modifications are presented in the following sections. The full definition of the aerodynamic model is presented by Fitzgerald in a Cranfield University College of Aeronautics report [67]. A three view drawing of the Mk 4a Jindivik is presented in Figure 3-9.

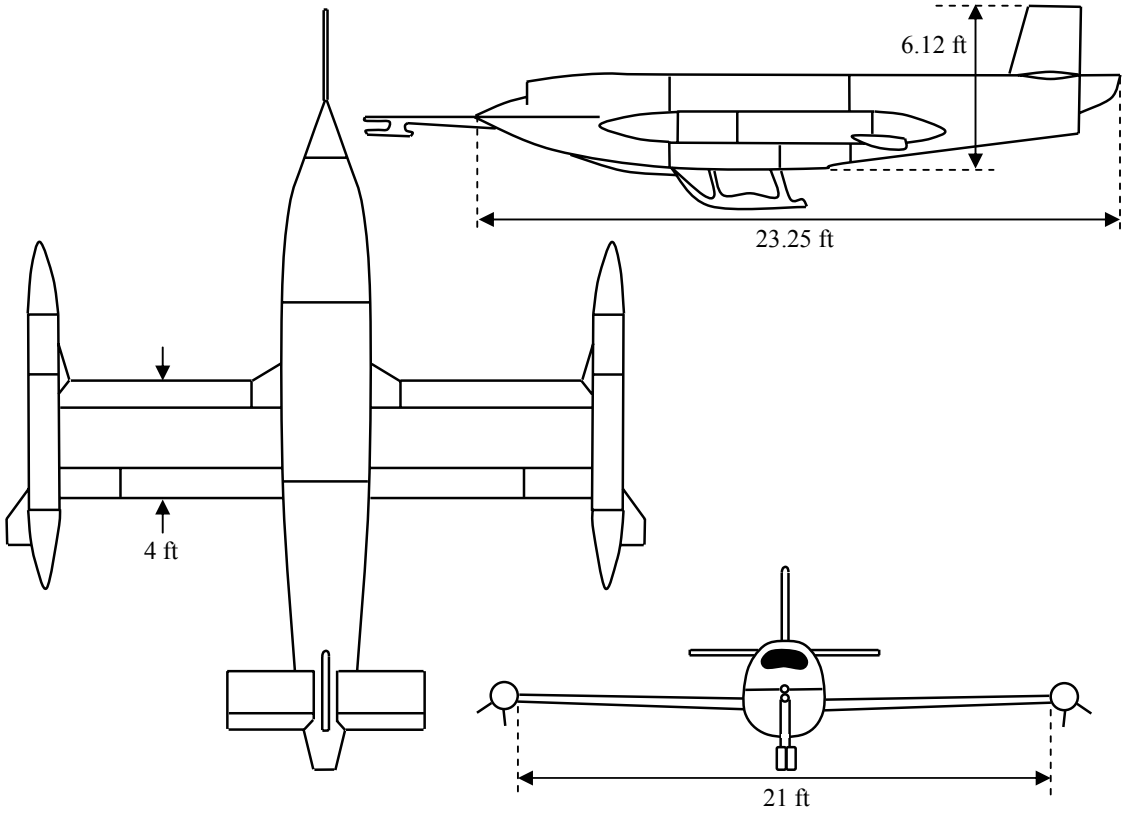

Figure 3-9 Mk 4a Jindivik Three View Drawing

The aircraft model is presented in the form of a data flow diagram in Figure 3-10. The principle element of the aircraft model is the equations of motion. The equations of motion describe the motion of the aircraft in terms of its body axes velocity components and angular rates as a function of the disturbing forces and moments. The equations of motion are presented in section 3.3.2.

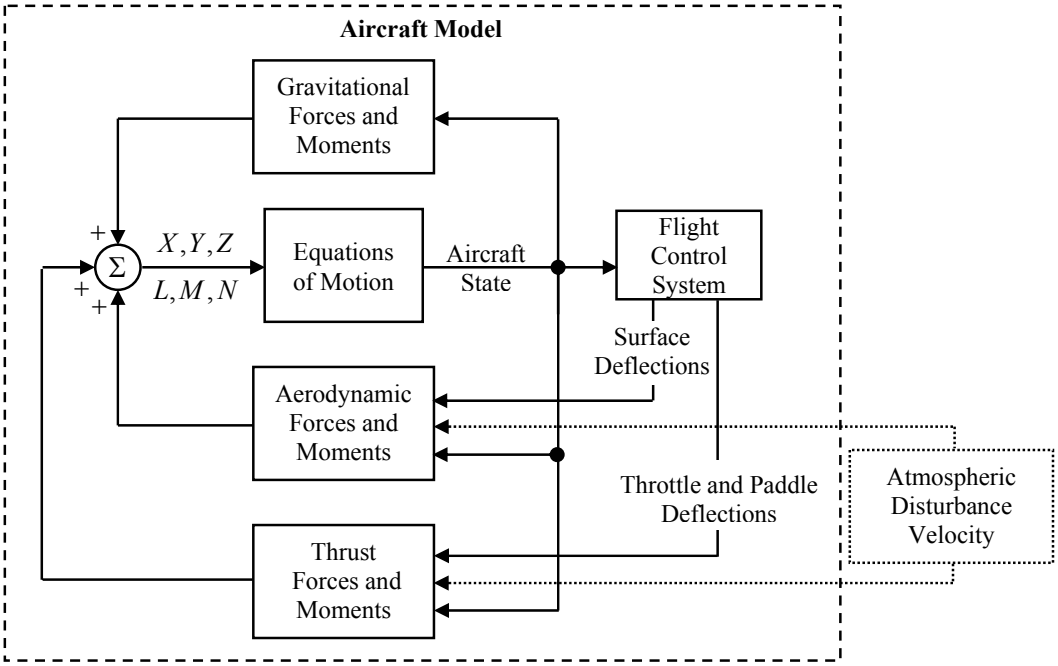

Figure 3-10 Aircraft Model Data Flow Diagram

In this case the disturbing forces and moments are defined as aerodynamic, thrust and gravitational. These forces and moments are defined in sections 3.3.3, 3.3.4 and 3.3.5 respectively.

The velocity components of the aircraft relative to the airflow are calculated by summing the aircraft body axes velocity components with the atmospheric disturbance velocity components referred to the aircraft's body axes system. The aerodynamic and thrust moments and forces are calculated using the velocity components of the aircraft relative to the airflow. In this manner the effects of atmospheric disturbances on the aircraft motion is determined.

The aircraft's Flight Control System controls the aerodynamic and thrust forces and moments via the aerodynamic control surfaces, the throttle and thrust vectoring paddles

to attain the desired aircraft response. The Flight Control System, presented in section 3.3.7, contains sensors, actuators, a three axis Stability Augmentation System and autopilot modes.

3.3.1 LIMITATION OF MODEL

The flight envelope limitations assumed for the aerodynamic model are as follows [55]:

- Altitude between sea level and 20,000 ft.
- True airspeed between 180 and 530 knots.
- Bank angles up to 80 degrees.
- Normal acceleration in the range –2g to +8g.
- Maximum Mach number 0.86.

The limitations are defined by the range in which aerodynamic data are available. The landing airspeed of the aircraft 140 knots. This is outside of the limits of the model. However, extrapolation of the aerodynamic data is acceptable as the aerodynamic properties of the aircraft are essentially linear in this region.

There are two trailing edge flap positions of the Jindivik. When the trailing edge flap is fully retracted it is actually deflected 1 degree and when fully extended it is deflected 20 degrees. Aerodynamic data for both flap positions has been included in the aerodynamic model. The aerodynamic properties are assumed to vary linearly when the trailing edge flap is in motion.

For the purposes of the Direct Lift Control investigation the maximum deflection of the trailing edge flaps has been increased to 35 degrees and the aerodynamic properties have been linearly extrapolated accordingly.

3.3.1.1 RUDDER

The method of estimating the rudder control derivatives is applicable to low speed applications where the fin is reasonably well aft of the wing [68]. Low speed is not defined by ESDU nor is what is considered a reasonable distance of the fin from the wing. However, the speed considered in this study is considered to be acceptable as

being low speed. Also, the fin is not located close to the wing relative to the overall dimensions of the planform.

Rudder characteristics generally depart slowly from linearity as rudder deflection increases beyond 10 or 20 degrees depending on the rudder nose shape. As the rudder modelled is hypothetical, and it has been modelled for the purposes of investigating yaw control on the aircraft, rather than the effects of a particular rudder design, the non-linear characteristics have been ignored.

3.3.1.2 SPOILERS

The method of estimating spoiler aerodynamic effects is applicable to wing and flap geometry of the Jindivik. The airspeed and angle of attack range of the landing approach are within the applicability envelope of the estimation method. The spoiler geometry and position on the wing are in accordance with the method used. The increment of lift and drag coefficient estimated are accurate to within ± 10% [59,58,60]. This level of accuracy is acceptable as the spoilers modelled are hypothetical and adequately represent the effects of symmetric spoiler deflection.

When a spoiler is suddenly extended at high rotational speed, the flow over the upper surface of the wing separates from the spoiler tip because of surface discontinuity. Because of the intensive shear flow near the tip, the resulting shear layer rolls up to form a strong starting vortex behind the spoiler. This starting vortex induces an initial increase in lift; this is referred to as adverse lift. Once the spoiler reaches its maximum deflection, the vortex stops growing and detaches from the spoiler tip to convect downstream. As the vortex moves farther downstream, the lift will decrease and eventually attain its steady state value. The effects of adverse lift are short in duration [69, 70].

The effects of transient adverse lift induced by spoilers can be reduced by suitably positioning the spoiler on the wing and by introducing a gap between the spoiler and the wing [69]. In this implementation the transient adverse effects of spoilers is assumed negligible as it is assumed that if spoilers were to be designed so as to effect Direct Lift Control the design would be such as to minimise the adverse lift effects and the associated Direct Lift Control system would be tuned accordingly.

3.3.1.3 UNDERCARRIAGE

The method of estimating the increment of total drag due to undercarriage deflection is accurate to within ± 30% [61]. This level of accuracy is acceptable as the undercarriage modelled is hypothetical and it has been included in the simulation model to approximate the drag effects due to the presence of conventional undercarriage.

3.3.2 EQUATIONS OF MOTION

The generalised six degree of freedom equations of motion of a rigid symmetric airframe having uniform mass distribution are presented in equation 3-1 [46]. By calculating the disturbing forces and moments, and knowing the initial values of the body axes velocities, U_i, V_i, W_i, and body axes rotational rates, p_i, q_i, r_i, the equations of motion can be solved for the body axes velocities, U, V, W, and body axes rotational rates, p, q, r.

$$
\begin{aligned}
m\left(\dot{U} - rV + qW\right) &= X_{Aero} + X_{Thrust} + X_{Grav} \\
m\left(\dot{V} - pW + rU\right) &= Y_{Aero} + Y_{Thrust} + Y_{Grav} \\
m\left(\dot{W} - qU + pV\right) &= Z_{Aero} + Z_{Thrust} + Z_{Grav} \\
I_x\dot{p} - \left(I_y - I_x\right)qr - I_{xz}\left(pq + \dot{r}\right) &= L_{Aero} + L_{Thrust} + L_{Grav} \\
I_x\dot{q} + \left(I_x - I_z\right)pr + I_{xz}\left(p^2 + r^2\right) &= M_{Aero} + M_{Thrust} + M_{Grav} \\
I_x\dot{r} - \left(I_x - I_y\right)qr + I_{xz}\left(qr - \dot{p}\right) &= N_{Aero} + N_{Thrust} + N_{Grav}
\end{aligned}
\qquad (3\text{-}1)
$$

The generalised equations of motion derived from first principles and the subsequent derivation of the aircrafts attitude, relative velocity, earth velocity and earth position are presented in Appendix A and the formulation of the aerodynamic, gravitational and thrust moments and forces are presented in the following section.

3.3.3 AERODYNAMIC FORCES AND MOMENTS

All equations defining the aerodynamic forces and moments have been extracted from Gautrey and Cook [55]. These equations have been augmented to include the aerodynamic effects of a rudder, spoilers and conventional undercarriage. The aerodynamic effects of symmetric spoiler deflection and the effects of conventional undercarriage are defined in Appendix A.

The aerodynamic effects of a rudder design for the Jindivik are presented by Fitzgerald [56]. In this MSc thesis Fitzgerald defines the geometry of a rudder design for the Jindivik and using methods presented by ESDU calculates the coefficients of sideforce, rolling moment and yawing moment due to deflection of that rudder.

The body axes aerodynamic forces are defined as [55]

$$X_{Aero} = \frac{1}{2}\rho V_T^2 S\left(C_{L_{wb}}\sin(\alpha) - C_D\cos(\alpha)\right) + \frac{1}{2}\rho V_T^2 S_T\left(C_{L_T}\sin(\alpha_T - \alpha_R)\right)$$

$$Y_{Aero} = \rho V_T S C_Y \tag{3-2}$$

$$Z_{Aero} = -\frac{1}{2}\rho V_T^2 S\left(C_{L_{wb}}\cos(\alpha) + C_D\sin(\alpha)\right) - \frac{1}{2}\rho V_T^2 S_T\left(C_{L_T}\sin(\alpha_T - \alpha_R)\right)$$

The body axes aerodynamic moments are defined as [55]

$$L_{Aero} = \rho S V_T s C_l$$

$$M_{Aero} = \frac{1}{2}\rho V_T^2 S C_m + \frac{1}{2}\rho V_T^2 S_T\begin{pmatrix} -\left(l_T + \left(0.25 - h_o\right)\bar{c}\right)\left(C_{L_T}\cos(\alpha_T - \alpha_R)\right) \\ -\left(T_{wl} - h_{wl}\right)C_{L_T}\sin\left(\alpha_T - \alpha_R\right)\end{pmatrix} \tag{3-3}$$

$$N_{Aero} = \rho S V_T s C_n$$

The lift coefficient, C_L, is defined as [55]

$$C_L = \left(C_{L_{wb}} + \frac{S_T}{S}C_{L_T}\right) \tag{3-4}$$

The wing-body lift coefficient, $C_{L_{wb}}$, is defined as [55]

$$C_{L_{wb}} = a_{1_{wb}}\left(\alpha_{wb} - \alpha_0\right) + C_{L_s} \tag{3-5}$$

Where C_{L_s} is lift coefficient increment due to the symmetric deflection of spoilers and is defined in Appendix A.

The tailplane lift coefficient, C_{L_T}, is defined as [55]

$$C_{L_T} = a_{1_T}\alpha_T + a_{2_T}\delta_\eta \tag{3-6}$$

The drag coefficient, C_D, is defined as [55]

$$C_D = C_{D_i} + C_{D_Z} + C_{D_M} + C_{D_{C_L > C_{L_{crit}}}} + C_{D_s} + C_{D_{uc}} \tag{3-7}$$

where C_{D_s} is the drag coefficient increment due to symmetric spoiler deflection and $C_{D_{uc}}$ is the drag coefficient increment due to the extension of undercarriage. C_{D_s} and $C_{D_{uc}}$ are defined Appendix A.

The sideforce coefficient, C_Y, is defined as [55]

$$C_Y = C_{Y_p}ps + C_{Y_v}V_R + C_{Y_\varsigma}\frac{1}{2}V_T\delta_\varsigma \tag{3-8}$$

The derivation of the coefficient of sideforce due to deflection of rudder, C_{Y_ς}, is presented by Fitzgerald [56].

The pitching moment coefficient, C_m, is defined as [55]

$$C_m = C_{m_{1/4}} + C_{Z_{wb}}\left(0.25 - h_{cg}\right) + C_{X_{wb}}\left(\frac{h_{wl} - c_{1/4_{wl}}}{\bar{c}}\right) \tag{3-9}$$

The wing-body combination coefficient of normal force, $C_{z_{wb}}$, is defined as [55]

$$C_{z_{wb}} = -1\left(C_{L_{wb}}\cos\alpha + C_D\sin\alpha\right) \tag{3-10}$$

The wing-body combination coefficient of axial force, $C_{x_{wb}}$, is defined as [55]

$$C_{x_{wb}} = C_{L_{wb}} \sin\alpha - C_D \cos\alpha \tag{3-11}$$

The rolling moment coefficient, C_l, is defined as [55]

$$C_l = \left(C_{l_r} r + C_{l_p} p\right) s + C_{l_\xi} V_T \delta_\xi + C_{l_v} V_T \beta + C_{l_\varsigma} V_T \delta_\varsigma \tag{3-12}$$

The derivation of the coefficient of rolling moment due to deflection of rudder, C_{l_ς}, is presented by Fitzgerald [56].

The yawing moment coefficient, C_n, is defined as [55]

$$C_n = \left(C_{n_r} r + C_{n_p} p\right) s + C_{n_\xi} V_T \delta_\xi + C_{n_v} V_T \beta + C_{n_\varsigma} V_T \delta_\varsigma \tag{3-13}$$

The derivation of the coefficient of yawing moment due to deflection of rudder, C_{n_ς}, is presented by Fitzgerald [56].

3.3.4 THRUST MODEL

The Thrust characteristics of the Rolls-Royce Viper Mk 201 turbojet engine are implemented in the simulation model. The thrust model is presented in Appendix A.

A simple thrust vectoring representation is implemented in the simulation. This implementation assumes perfect thrust vectoring, i.e. no loss of thrust due to vectoring. It also assumes that the thrust line is coincident with the body axes x axis.

Consider the thrust force, T_τ, deflected vertically at some angle, θ_τ, and laterally at some angle, ϕ_τ, from an axes system $\left(o_t, x_t, y_t, z_t\right)$, where $\left(o_t\, x_t\right)$ is coincident with the body axes x axis and the plane $\left(o_t\, y_t\, z_t\right)$ is aligned with the engine exhaust nozzle.

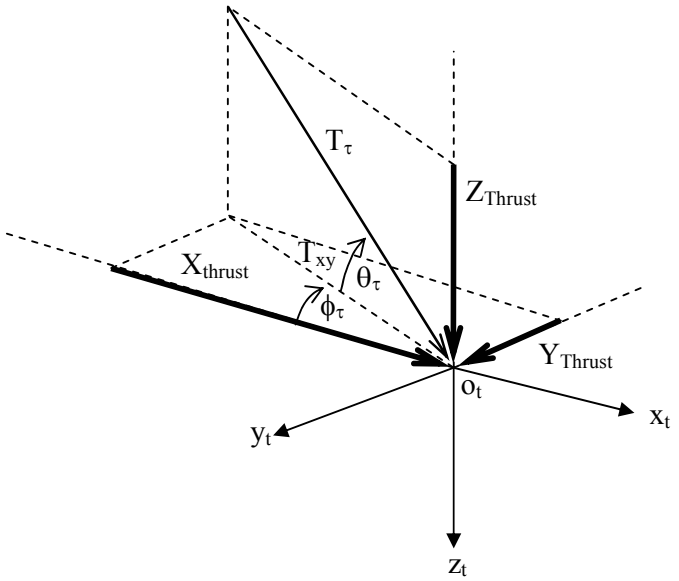

Figure 3-11 Thrust Vectoring Force Components

The axial and lateral components of thrust, X_{Thrust} and Y_{Thrust}, are defined as

$$X_{Thrust} = T_\tau Cos\theta_\tau Cos\phi_\tau$$
$$Y_{Thrust} = T_\tau Cos\theta_\tau \sin\phi_\tau \quad (3\text{-}14)$$

The normal component of thrust, Z_{Thrust}, is defined as

$$Z_{Thrust} = T_\tau \sin\theta_t \quad (3\text{-}15)$$

The moments about the x, y and z aircraft body axes due to vectored thrust are defined as

$$L_{Thrust} = 0$$
$$M_{Thrust} = Z_{Thrust} l_{thrust} \quad (3\text{-}16)$$
$$N_{Thrust} = Y_{Thrust} l_{thrust}$$

where the axial distance from the aircraft's centre of gravity to the engine exhaust nozzle, l_{thrust}, in this case is defined as

$$l_{thrust} = 13.37 - h_{cg}\bar{c} \ \ (\text{ft}) \quad (3\text{-}17)$$

3.3.5 GRAVITY MODEL

As the body axes origin is coincident with the centre of gravity the gravitational forces and moments referred to the body axes may be defined as

$$\begin{bmatrix} X_{Grav} \\ Y_{Grav} \\ Z_{Grav} \end{bmatrix} = D_{BE} \begin{bmatrix} 0 \\ 0 \\ mg \end{bmatrix} \tag{3-18}$$

$$\begin{bmatrix} L_{Grav} \\ M_{Grav} \\ N_{Grav} \end{bmatrix} = \begin{bmatrix} 0 \\ 0 \\ 0 \end{bmatrix} \tag{3-19}$$

where the direction cosine matrix, D_{BE}, is defined in Appendix A.

3.3.6 MASS AND INERTIA PROPERTIES

The zero fuel mass of the aircraft, $m_{zf} = 2716$ lbs [55], the aircraft's maximum fuel capacity is 153 gals (the mass of one gallon of fuel is 7.8 lbs). The movement of the position of the centre of gravity as a percentage of wing chord, h_{cg}, and the aircrafts mass, m, with fuel burn is presented in Figure 3-12. The aircraft's mass is hence defined as [55]

$$m = m_{zf} + 7.8f \tag{3-20}$$

The moments of inertia about the ox, oy and oz axes are presented in Appendix A as a function of aircraft mass, m. All products of inertia are defined as

$$I_{xy} = I_{xz} = I_{yx} = I_{yz} = I_{zx} = I_{zy} = 0 \tag{3-21}$$

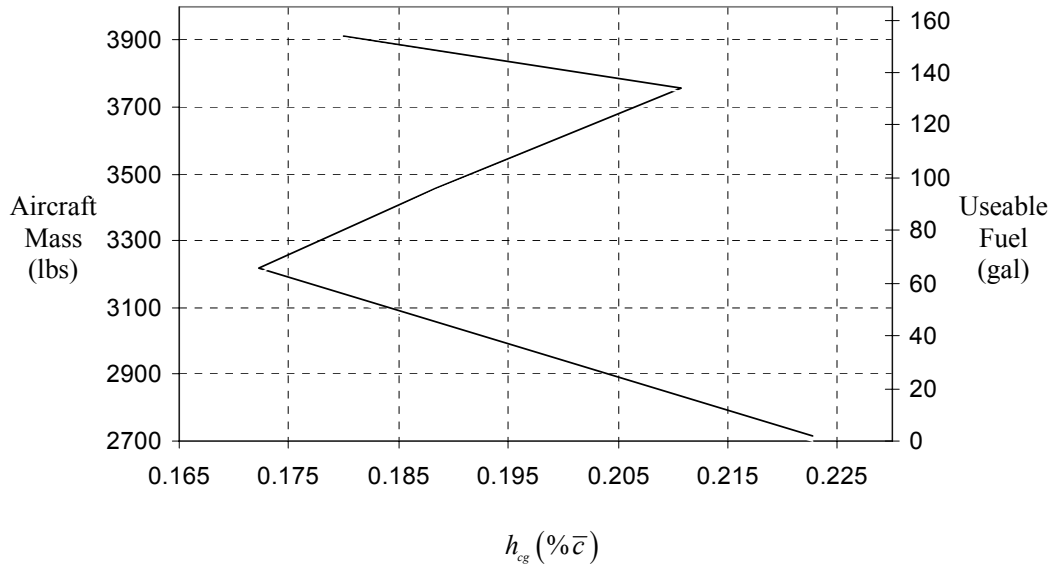

Figure 3-12 Centre of Gravity, h_{cg}, and Aircraft Mass, m, as a Function of Useable Fuel [55]

3.3.7 FLIGHT CONTROL SYSTEM

A flight control system consisting of a sensor suite, actuators a three axis full authority Stability Augmentation System, and autopilot modes have been implemented in the simulation model to provide a means of controlling the aircraft and as a baseline for further flight control development studies.

The general arrangement of the Flight Control System is presented in Figure 3-13. Variables which describe the aircraft's state are passed through the sensor suite. The outputs of the sensor suite are measured variables describing the aircraft's state. The sensor suite is discussed in section 3.3.7.1.

The inputs to the actuator models are control surface demands and the outputs are control surface positions. The control surface demands are a sum of the autopilot and Stability Augmentation System control surface demands. The actuator models are discussed in section 3.3.7.2.

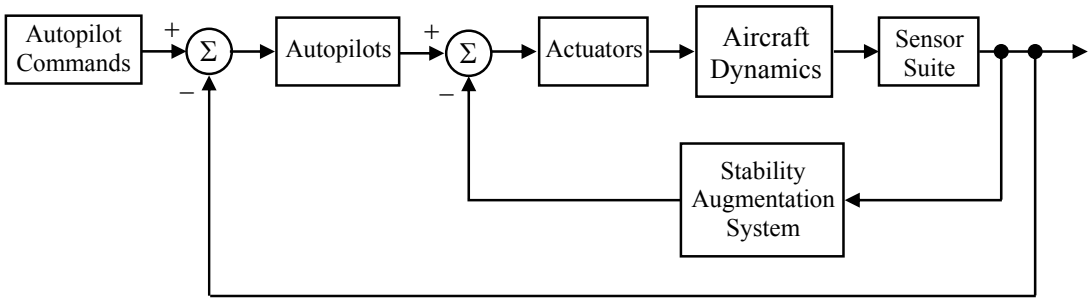

Figure 3-13 Flight Control System Data Flow Diagram

The Stability Augmentation System consists of proportional control of feedback and feedforward signals for the purposes of augmenting the stability and control characteristics of the basic airframe. For illustration purposes the feedforward element of the Stability Augmentation System is not presented in Figure 3-13. The Stability augmentation system is discussed in section 3.3.7.3.

The Autopilots consists of a combination of proportional, integral, and derivative control of an error signal in the feedforward path. The error signal is defined as the difference between the autopilot command and the appropriate aircraft state. The autopilot modes implemented in this model are discussed in section 3.3.7.4.

3.3.7.1 SENSORS

The sensor suite implemented in the simulation model includes an angle of attack probe, sideslip vane, accelerometers, rate gyros, attitude gyros, static and dynamic pressure sensors, Mach meter, altimeter and velocity meter. The majority of the sensor dynamics models have been extracted from Messina et al [71]. These models are defined in Appendix A.

3.3.7.2 ACTUATORS

Second order, no load, elevator, aileron, rudder, trailing edge flap, spoiler and thrust vectoring paddles actuator models presented by Messina et al[71] have been implemented in the simulation model. A first order undercarriage actuator model has also been implemented. These models are defined in Appendix A.

It is accepted that the no load assumption will result in optimistic performance with respect to actuator rate limiting. However this is sufficient for the purposes of this study.

3.3.7.3 STABILITY AUGMENTATION SYSTEM

A three axis stability augmentation system developed by Fitzgerald [56] has been implemented in the simulation model. The architecture, control laws and control system gains for the pitch, roll and yaw Stability Augmentation Systems are presented in the following sections.

The stability augmentation system presented provides the aircraft with stability and control characteristics consistent to level 1 flying qualities characteristics, defined by the MIL-F-8785C [63], across the flight envelope. The approach controllers developed as part of this study has incorporated this system. A full stability and control analysis of the aircraft, with and without stability augmentation, as well as the design of the Stability Augmentation System is presented by Fitzgerald [56].

3.3.7.3.1 PITCH STABILITY AUGMENTATION SYSTEM

The pitch SAS architecture is presented in Figure 3-14 and the associated control laws are defined by equations 3-22 and 3-23 [56].

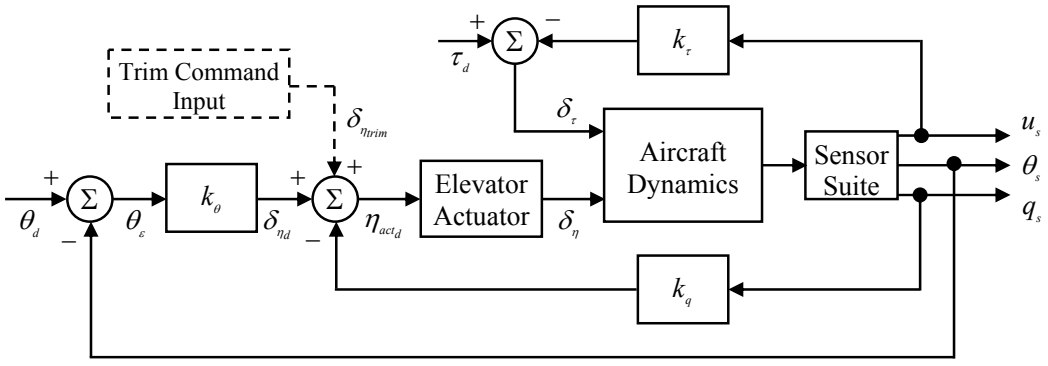

Figure 3-14 Pitch Stability Augmentation System [56]

$$\eta_{act_d} = k_\theta \theta_\varepsilon - k_q q_s + \delta_{\eta\, trim} \tag{3-22}$$

$$\delta_\tau = \tau_d - k_\tau V_{T_s} \tag{3-23}$$

The pitch SAS gains, k_q, k_θ and k_τ are scheduled with dynamic pressure, q_{dyn}, and trailing edge flap position, δ_f, to provide consistent stability and control properties across the flight envelope and configuration. k_q, k_θ and k_τ are defined in figures 3-15,

3-16 and 3-17. It should be noted that the trailing edge flap deflection is limited from 1 to 20 degrees.

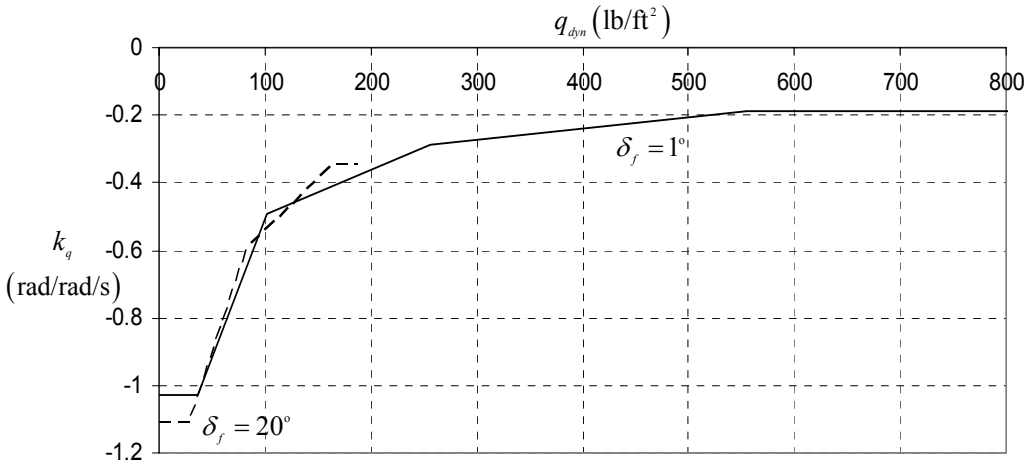

Figure 3-15 k_q as a Function of Dynamic Pressure and Flap Position[56]

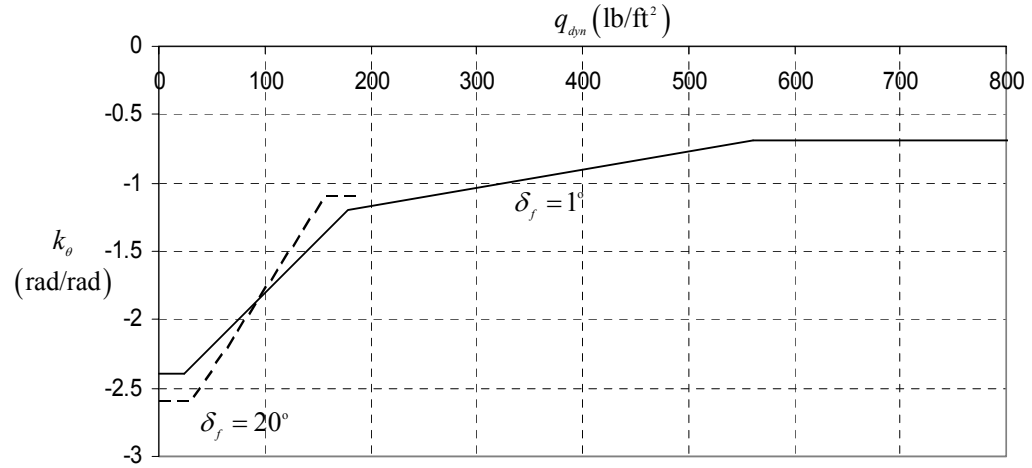

Figure 3-16 k_θ as a Function of Dynamic Pressure and Flap Position[56]

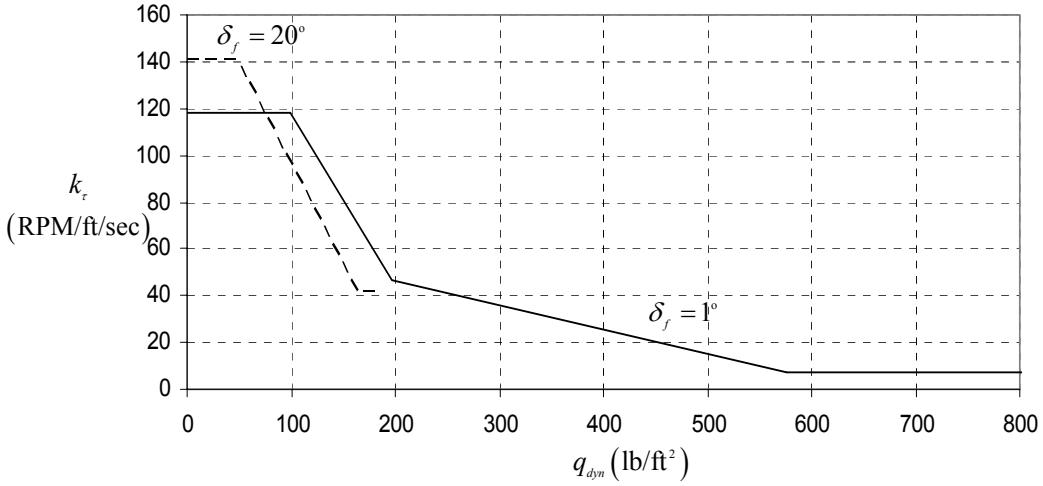

Figure 3-17 k_τ as a Function of Dynamic Pressure and Flap Position[56]

The control system gains k_q, k_θ and k_τ vary linearly with flap position, this may be expressed as[56]

$$k = k_{\delta_{f=1}} + \left(\frac{k_{\delta_{f=20}} - k_{\delta_{f=1}}}{19} \right) \left(\delta_f - 1 \right) \tag{3-24}$$

3.3.7.3.2 ROLL STABILITY AUGMENTATION SYSTEM

The roll SAS architecture is presented in Figure 3-18 and the associated control law is defined by equation 3-25 [56].

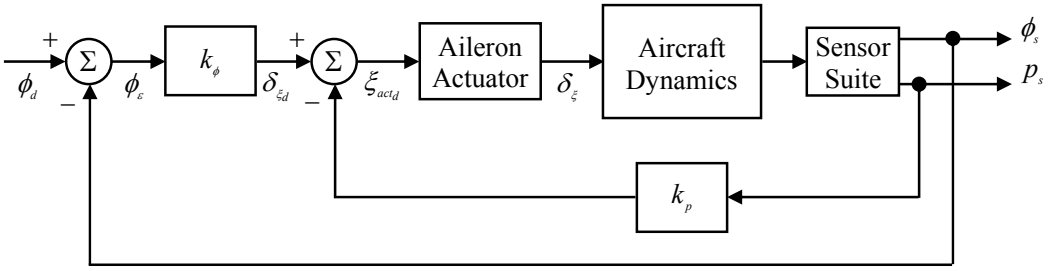

Figure 3-18 Roll Stability Augmentation System [56]

$$\xi_{act_d} = k_\phi \phi_\varepsilon - k_p p_s \tag{3-25}$$

The control system gains k_p and k_ϕ are selected as[56]

$$k_p = -2.5\,\text{rad/rad/sec} \qquad k_\phi = -2.2\,\text{rad/rad} \tag{3-26}$$

3.3.7.3.3 YAW STABILITY AUGMENTATION SYSTEM

The yaw SAS architecture is presented in Figure 3-19 and the associated control law is defined by equation 3-27[56].

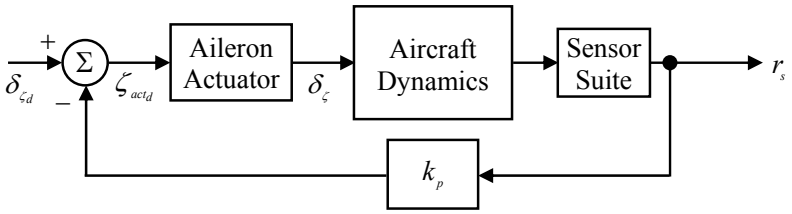

Figure 3-19 Yaw Stability Augmentation System[56]

$$\zeta_{act_d} = \delta_{\zeta_d} - k_r r_s \tag{3-27}$$

The control system gain k_r is selected as

$$k_r = -4.63\,\text{rad/rad/sec} \tag{3-28}$$

3.3.7.4 AUTOPILOTS

An altitude acquire and hold autopilot, heading acquire and hold autopilot, and an autothrottle developed by Fitzgerald[56] have been implemented in the simulation model. These autopilots were implemented to provide a baseline Flight Control System and to facilitate investigation of control properties of the aircraft during the design of the approach controllers. These autopilots are defined in Appendix A.

3.4 ATMOSPHERE MODEL

The aerodynamic and thrust models presented are for an aircraft in atmospheric flight; hence a model of the International Standard Atmosphere [62], an atmospheric disturbance model [63] including a carrier airwake disturbance model[63] have been implemented.

The aerodynamic and thrust forces and moments are calculated using the local temperature, pressure and density determined by the International Standard Atmosphere.

The output of the atmospheric disturbance model are disturbance velocity components relative to the earth axes system. The velocity of the aircraft relative to the airflow is calculated by summing the aircraft body axes velocity components to the disturbance velocity components suitably transformed relative to the body axes system. These relative velocity components are used in the calculation of the aerodynamic and thrust forces and moments; hence the atmospheric disturbance effects on the aircraft motion are determined.

3.4.1 INTERNATIONAL STANDARD ATMOSPHERE

The ISA implementation in the simulation model defines the atmospheric properties with respect to pressure, P, temperature, T, and density, ρ, from sea level to 65,617 ft, i.e. the Troposphere and the lower Stratosphere.

The ISA is based on the assumption that the air consists of a perfect gas which obeys the equation of state

$$P = \rho RT \tag{3-29}$$

where the universal gas constant is defined as

$$R = 8.31436x10^{7}\ \text{ergs mol}^{-1}\left(^{\circ}\text{K}\right)^{-1} \tag{3-30}$$

Sea level pressure, P_o, sea level temperature, T_o, and sea level density, ρ_o, are defined as

$$P_o = 1013.25\,\text{mb}$$

$$\text{T}_\text{o} = 288.15\,^{\circ}\text{K} \tag{3-31}$$

$$\rho_\text{o} = 0.07647425\ \text{lb/ft}^3$$

Temperature is defined to vary linearly from sea level with altitude, i.e.

$$T = T_o + T_L(h) \tag{3-32}$$

where the temperature lapse rate, T_L, is defined as

$$T_L = -0.00198\ ^{o}\text{K/ft} \qquad 0 < h \geq 36,089\ \text{ft}$$
$$T_L = 0\ ^{o}\text{K/ft} \qquad 36,089 < h \geq 65,617\ \text{ft} \tag{3-33}$$

By applying the equation of state, equation 3-29, at sea level and by combining this with the equation of state at any point in the atmosphere an equation of relative properties can be derived

$$\frac{P}{P_o} = \frac{\rho}{\rho_o}\frac{T}{T_o} \tag{3-34}$$

Pressure, P, and density, ρ, may be calculated at any altitude in the ISA by simultaneous use of equations 3-29 and 3-34 using the definition of the universal gas constant, R, the sea level definition of pressure, P_o, temperature, T_o, and density, ρ_o, and the temperature, T, calculated using the appropriate lapse rate, T_L.

The local speed of sound in air, a, a function of local temperature, T, is defined as

$$a = \sqrt{\gamma RT} \tag{3-35}$$

where the specific heat ratio of air $\gamma = 1.4$.

3.4.2 ATMOSPHERIC DISTURBANCE MODEL

The atmospheric disturbance model implemented is that as presented in MIL-F-8785C [63]. There are three main components to this model: a turbulence model, a discrete gust model and a low altitude windshear model. Two turbulence models are presented in MIL-F-8785C, the von Karman form and the Dryden form. The Dryden form has been implemented in this instance due to ease of implementation in the time domain. In addition a steady wind model is also implemented. The method of integrating the disturbance models with the aircraft dynamics model is presented in Appendix A.

3.4.2.1 TURBULENCE MODEL

The Dryden form of the spectra for the turbulence velocities is

$$\phi_{u_t}(\Omega) = \sigma_u^2 \frac{2L_u}{\pi} \frac{1}{1+(L_u\Omega)^2} \qquad \text{per rad/ft}$$

$$\phi_{v_t}(\Omega) = \phi_{w_t}(\Omega) = \sigma_{v,w}^2 \frac{L_{v,w}}{\pi} \frac{1+3(L_{v,w}\Omega)^2}{\left[1+(L_{v,w}\Omega)^2\right]^2} \qquad \text{per rad/ft} \tag{3-36}$$

where L_u, L_v, L_w are the axial, lateral and normal turbulence scale lengths respectively and $\sigma_u, \sigma_v, \sigma_w$ are the axial, lateral and normal turbulence intensities. Turbulence scales and intensities are defined in Appendix A for low altitude and medium/high altitude cases.

Equation 3-36 can be rewritten as a transfer function as presented in equations 3-37[72], which represents filters through which band limited white noise, ϖ, is passed to obtain the appropriate turbulence velocities.

$$\frac{u_t}{\varpi} = \sigma_u \sqrt{\frac{2V_T}{\pi L_u}} \left(\frac{1}{s + \frac{V_T}{L_u}} \right)$$

$$\frac{v_t}{\varpi} = \frac{w_t}{\varpi} = \sigma_{v,w} \sqrt{\frac{3V_T}{\pi L_{v,w}}} \left(\frac{s + \frac{V_T}{\sqrt{3}L_{v,w}}}{\left(s + \frac{V_T}{L_{v,w}} \right)^2} \right) \tag{3-37}$$

where u_t, v_t, w_t are the resulting axial, lateral and normal turbulence velocities and are defined with reference to the earth axes system.

An example of turbulence at an altitude of 1000 feet generated in the aforementioned manner is presented in Figure 3-20. The turbulence intensities used here, and for all further instances involving turbulence are calculated using the following probabilities of exceedance: Light = 1, Moderate = $1x10^{-2}$ and Severe = $1x10^{-3}$.

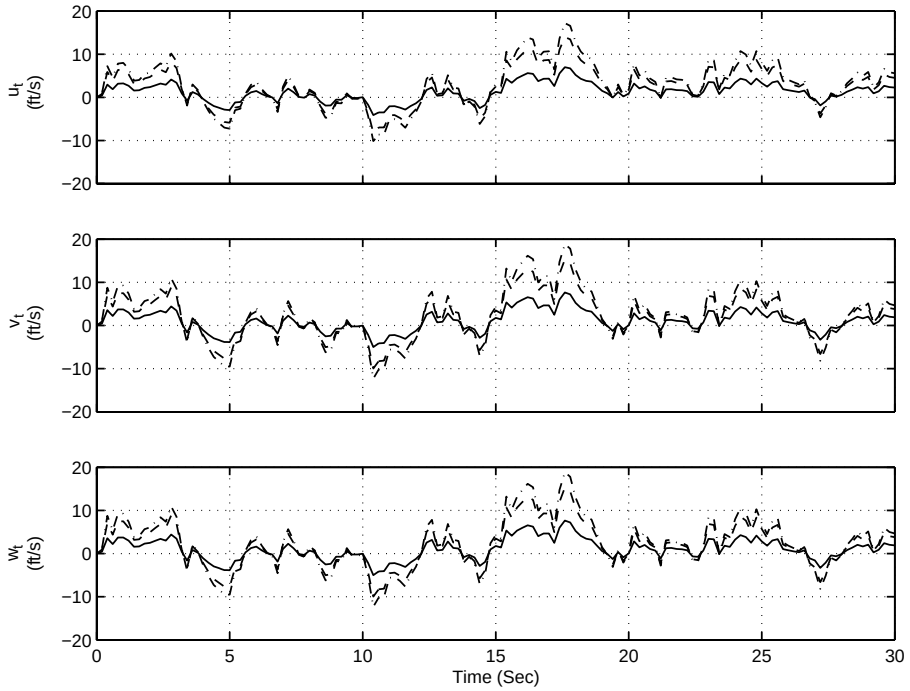

Figure 3-20 Sample Turbulence Time History
Light [——] Moderate [- - -] Severe [- · -]

3.4.2.2 DISCRETE GUST MODEL

The discrete gust as defined by MIL-F-8785C [63] has the "1 – Cosine" shape given by equation 3-38 and illustrated in Figure 3-21.

$$\begin{aligned} u_g, v_g, w_g &= 0 && x < 0 \\ u_g, v_g, w_g &= \frac{v_m}{2}\left(1 - \cos\frac{\pi x}{d_{x,y,z}}\right) && 0 \le x \le d_m \\ u_g, v_g, w_g &= v_m && x > d_m \end{aligned} \qquad (3\text{-}38)$$

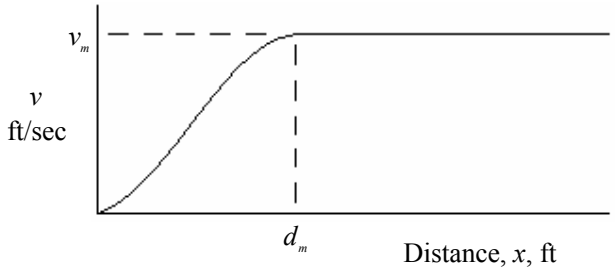

Figure 3-21 Discrete Gust Profile [63]

Where gust magnitudes, u_g, v_g, w_g, are defined in Appendix A and gust lengths, d_x, d_y, d_z, are user defined so that the gust can be tuned to each of the natural frequencies of the aircraft and its FCS. Gust magnitudes are defined with reference to the earth axes system.

An example of a two sided gust, i.e. dissipation of the gust defined as the negative of the onset, is presented in Figure 3-22. The gust lengths used in each case are $d_x, d_y, d_z = 1110$ feet.

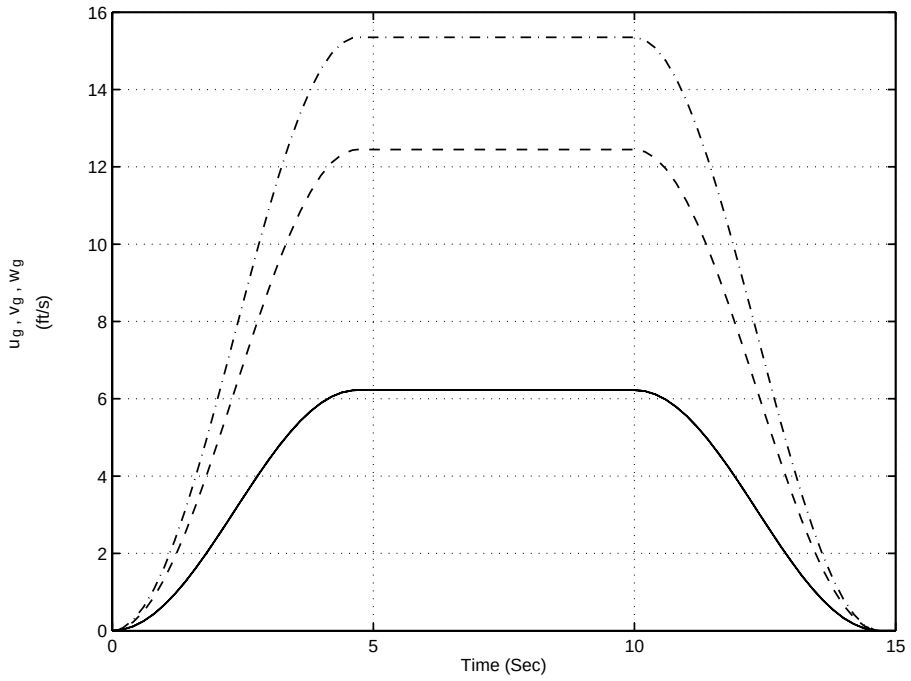

Figure 3-22 Sample Discrete Gusts
Light [——] Moderate [- - -] Severe [- · -]

3.4.2.3 WIND SHEAR

The magnitude of the wind scalar shear, w_w, is defined by equation 3-39, which expresses the mean wind profile as a function of altitude, h, and the wind speed at an altitude of 20 feet, u_{20}. In this application only vertical wind shear is considered. Wind shear is defined with reference to the earth axes system.

$$w_{ws} = u_{20} \frac{\ln(h/z_0)}{\ln(20/z_0)} \tag{3-39}$$

where the altitude of zero wind shear $z_0 = 0.15$ feet for Category C flight phase and 2.0 feet for other flight phases. Category C flight phase, as defined by MIL-F-8785C [63], are terminal flight phases that are normally accomplished using gradual manoeuvres and usually require accurate flight path control. Wind speed at an altitude of 20 feet, u_{20}, is defined in Appendix A.

The wind shear at an altitude of 1000 feet as a function of probability of occurrence, χ, is presented in Figure 3-23.

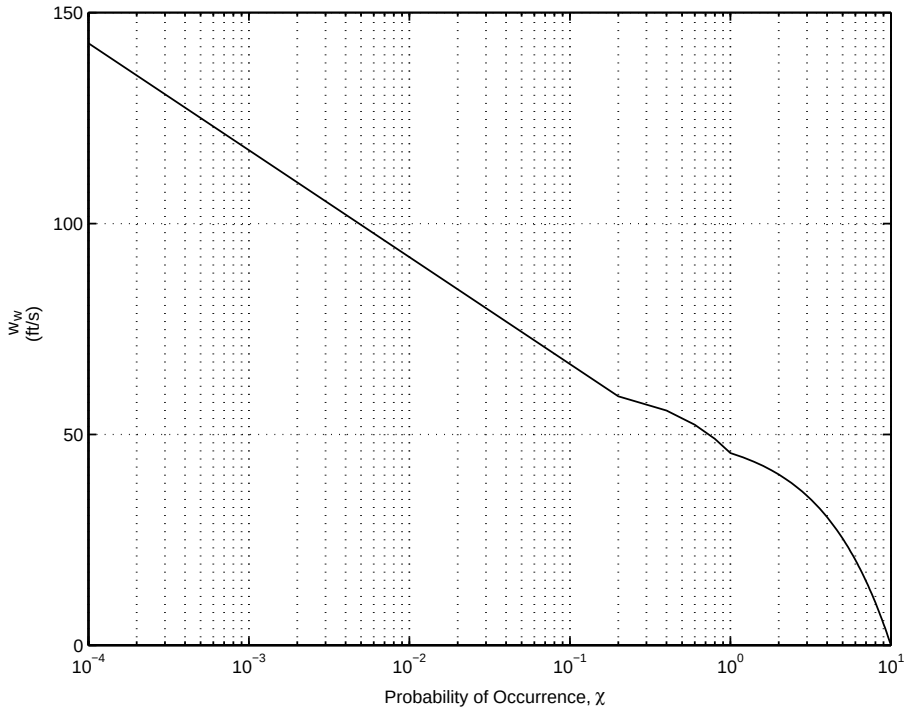

Figure 3-23 Wind Shear at 1000 Feet as a Function of Probability of Occurrence

3.4.2.4 STEADY WIND

The axial and lateral steady wind components with reference to the earth axes system are defined as per equation 3-40.

$$u_w = U_w\left(\sin\theta_w\right)$$
$$v_w = U_w\left(\cos\theta_w\right) \tag{3-40}$$

where U_w is the absolute magnitude of the steady wind and θ_w is the bearing of the steady wind.

3.4.3 CARRIER LANDING DISTURBANCE MODEL

This model, defined in MIL-F-8785C, supplements but does not replace the low altitude model presented in section 3.4.2. The terminal approach carrier landing disturbance model is used during simulation of the last half mile of the carrier approach. The carrier landing disturbance model velocity components are defined relative to the aircraft carrier body axes system. Total disturbance velocities are computed by adding components caused by random free-air turbulence, u_1, v_1, w_1; steady carrier-wake disturbance, u_2, w_2; periodic ship-motion-induced turbulence, u_3, w_3; and random ship-wake disturbance, u_4, v_4, w_4. The total air disturbance components u_c, v_c and w_c are then computed as:

$$\begin{aligned} u_c &= u_1 + u_2 + u_3 + u_4 \\ v_c &= v_1 + v_4 \\ w_c &= w_1 + w_2 + w_3 + w_4 \end{aligned} \tag{3-41}$$

3.4.3.1 FREE AIR TURBULENCE COMPONENTS

The free air turbulence components, which are independent of aircraft relative position, are calculated by filtering the output of white noise generators to produce the following spectra:

$$\phi_{u_1}(\Omega) = \frac{200}{1+(100\Omega)^2} \quad \text{per radian/foot}$$

$$\phi_{v_1}(\Omega) = \frac{5900\left[1+(400\Omega)^2\right]}{\left[1+(1000\Omega)^2\right]\left[1+\left(\frac{400}{3}\Omega\right)^2\right]} \quad \text{per radian/foot} \tag{3-42}$$

$$\phi_{w_1}(\Omega) = \frac{71.6}{1+(100\Omega)^2} \quad \text{per radian/foot}$$

Equations 3-42 can be rewritten as a transfer function as presented in equations 3-43 which represent filters through which band limited white noise, ϖ, is passed to obtain the appropriate turbulence velocities.

$$\frac{u_1(s)}{\varpi} = \sqrt{\frac{200}{V_T}} \frac{1}{1+\frac{100}{V_T}s}$$

$$\frac{v_1(s)}{\varpi} = \sqrt{\frac{5900}{V_T}} \frac{1+\frac{400}{V_T}s}{\left(1+\frac{1000}{V_T}s\right)\left(1+\frac{400}{3V_T}s\right)} \qquad (3\text{-}43)$$

$$\frac{w_1(s)}{\varpi} = \sqrt{\frac{71.6}{V_T}} \frac{1}{1+\frac{100}{V_T}s}$$

3.4.3.2 STEADY COMPONENT OF CARRIER AIR WAKE

The steady components of the carrier airwake consist of a reduction in the steady wind and a predominant upwash aft of the carrier which are functions of aircraft relative position. Figure 3-24 illustrates the steady wind functions $u_2/V_{w/d}$ and $w_2/V_{w/d}$ as functions of aircraft position aft of the carrier's centre of pitch, where $V_{w/d}$ is steady wind over the deck. For the purposes of this study it was assumed that the carrier's centre of pitch is coincident with the carrier's centre of gravity.

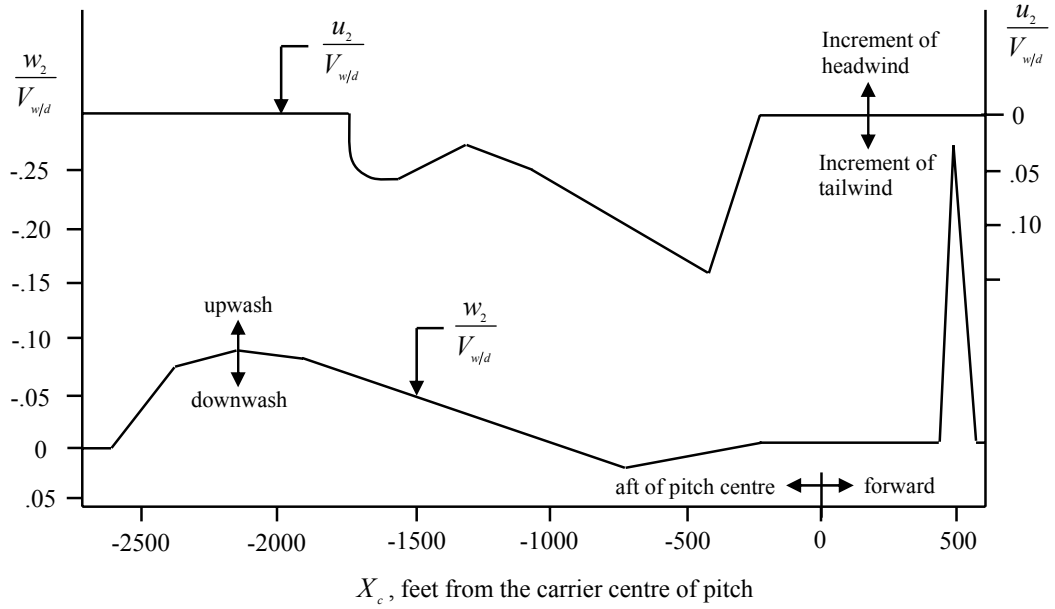

Figure 3-24 Carrier Burble Steady Wind Ratios as a Function of Aircraft Relative Position, X_c [63]

3.4.3.3 PERIODIC COMPONENT OF CARRIER AIR WAKE

The periodic component of the airwake varies with carrier pitching frequency, ω_p pitch magnitude, θ_{ac}, wind over deck, $V_{w/d}$, and aircraft relative position, X_c. These components are computed as per equation 3-44.

$$
\begin{aligned}
u_3 &= \theta_{ac} V_{w/d} \left(2.22 + 0.0009 X_c\right) C \\
w_3 &= \theta_{ac} V_{w/d} \left(4.98 + 0.0018 X_c\right) C \\
C &= cosine\left\{ \omega_p \left[t\left(1 + \frac{V_T - V_{w/d}}{0.85 V_{w/d}}\right) + \frac{X_c}{0.85 V_{w/d}} \right] + \mathrm{P} \right\}
\end{aligned}
\tag{3-44}
$$

where carrier pitch frequency, ω_p, is in units of radians/sec, carrier pitch amplitude, θ_{ac}, in units of radians, random phase, P, in units of radians and aircraft relative position, X_c, in units of feet. The u component is set to zero for $X_c < -2236$ feet, and the w component is set to zero for $X_c < -2536$ feet.

In the actual implementation, carrier pitching frequency is not readily available; instead the dominant frequency of the PSD of carrier pitching motion is used.

3.4.3.4 RANDOM COMPONENT OF CARRIER AIR WAKE

The carrier related random velocity components are computed by filtering white noise, ϖ_R, as per equation 3-45.

$$
\begin{aligned}
\frac{u_4}{\varpi_R} &= \frac{\sigma_{u4}\left(X_c\right)\sqrt{2\tau\left(X_c\right)}}{\tau\left(X_c\right)s + 1} \\
\frac{w_4}{\varpi_R} &= \frac{v_4}{\varpi_R} = \frac{0.035 V_{w/d}\sqrt{6.66}}{3.33s + 1}
\end{aligned}
\tag{3-45}
$$

where the rms amplitude, $\sigma_{u4}\left(X_c\right)$, in units of feet/sec is presented in Figure 3-25, and the time constant, $\tau\left(X_c\right)$, is also presented in Figure 3-25. The white noise, ϖ_R, is calculated as per equation 3-46.

$$
\varpi_R = \begin{bmatrix} \text{random number} \\ \text{output} \end{bmatrix} \left[\frac{j\omega}{j\omega + 0.1} \right] \sin\left(10\pi t\right) \tag{3-46}
$$

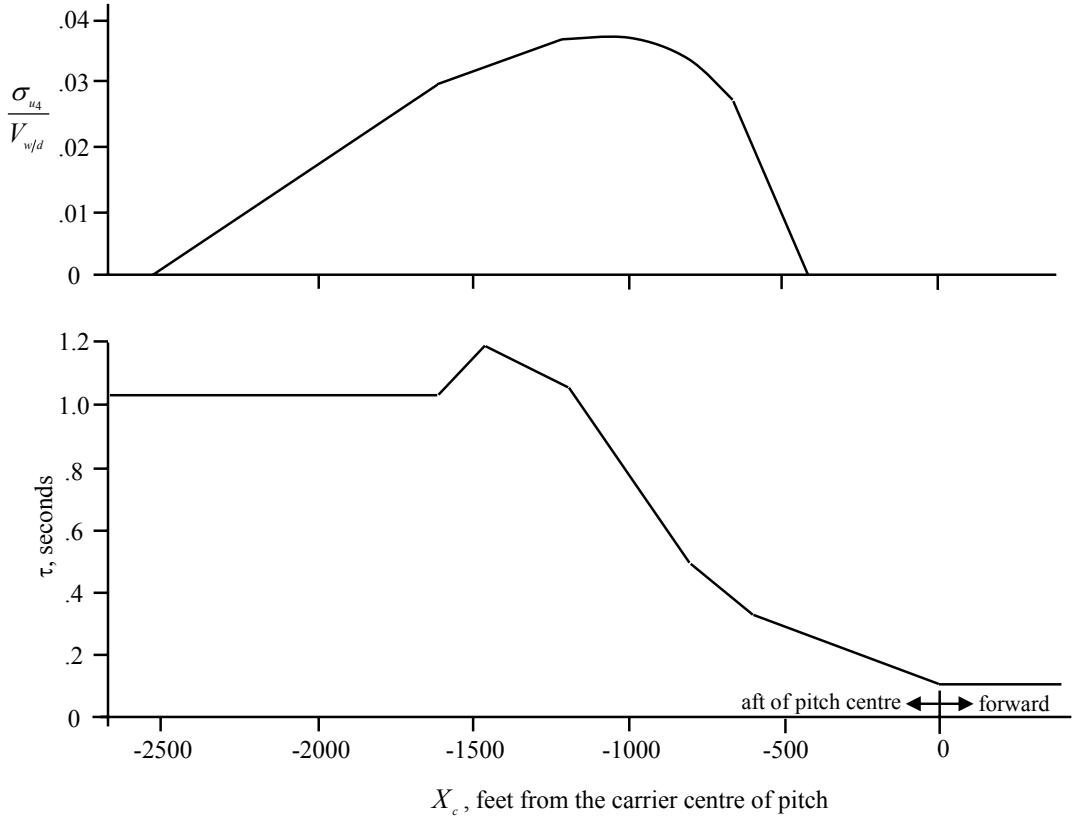

Figure 3-25 u-component Burble Time Constant and Variance of Random Carrier Airwake [63]

3.4.3.5 CARRIER DISTURBANCE MODEL EXAMPLE

An example of the disturbance velocities generated using the carrier disturbance model is presented in Figure 3-26. In this case, the carrier dynamics are defined by a speed of 33 knots and a steady wind speed of 24.5 knots.

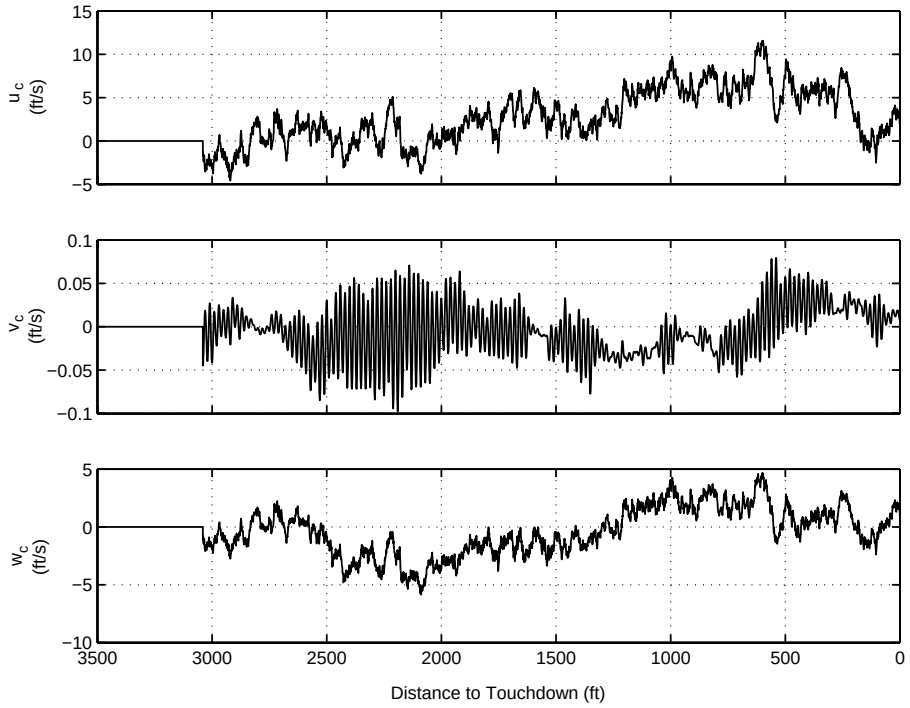

Figure 3-26 Carrier Disturbance Model Example

3.5 AIRCRAFT CARRIER DYNAMICS MODEL

A six degree of freedom ship motion simulation program called SEAWAY[64,65] has been integrated into the modelling environment. SEAWAY has been developed and validated through many years of industry and academic cooperation by Professor Johan Journée formerly of the ship hydromechanics laboratory at Delft University in The Netherlands. The extensive validation of this program is presented by Journée [66].

As previously stated SEAWAY is a frequency domain ship motion Fortran simulation, based on linear strip theory, to calculate wave induced loads, motions, added resistance and internal loads for six degree of freedom displacements.

A hull form, Figure 3-27, which most resembled that of a typical modern aircraft carrier, was selected from the SEAWAY Users Manual [65] and dimensions of a typical modern aircraft carrier were extracted from public domain sources [73]. A sample copy of SEAWAY limited to the hull form and dimensions selected was supplied for the sole use of this study. Bilge keels which provide roll damping are included in this model. The bilge keels are not indicated in Figure 3-27.

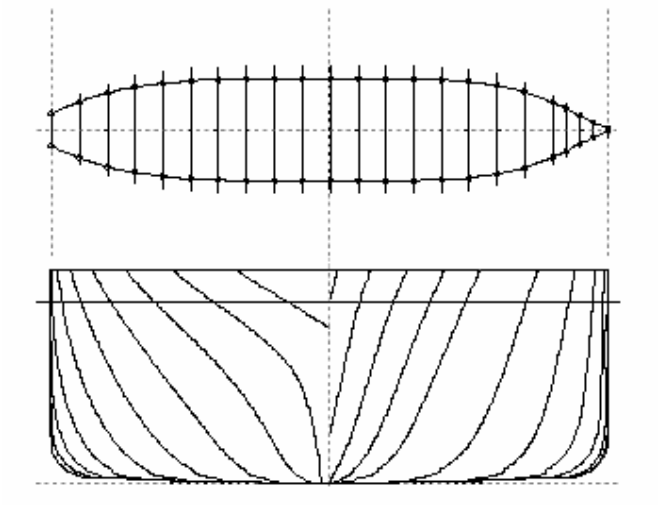

Length at waterline: 317m Draught: 10m Breadth 40m

Figure 3-27 Aircraft Carrier Hull Form [65]

SEAWAY outputs frequency domain transfer functions due to wave height for the following variables: surge, heave and sway position perturbations referred to the aircraft carriers centre of gravity; pitch(θ_{ac}), roll(ϕ_{ac}) and yaw(ψ_{ac}) attitudes referred to the aircraft carriers centre of gravity; and surge, heave and sway position perturbations at the touchdown point of the aircraft carriers flight deck, for a particular ship speed and relative direction between the wave and the bow of the ship.

Surge is linear motion along the aircraft carrier body axes x axis direction. Sway is linear motion along the aircraft carrier body axes y direction. Heave is linear motion along the aircraft carrier body axes z axis.

The first step to integrate the frequency domain transfer functions into the time domain simulation environment was to generate transfer functions using SEAWAY for a range of ship speeds (0-33 knots in 3 knot increments) and wave directions (0-360 degrees in 5 degree increments). These transfer functions were arranged in a structure and a routine was developed which interpolates between data available in the structure in order to generate transfer functions for all ship speeds and wave directions within the stated speed and wave direction ranges.

A time domain simulation of these transfer functions is realised through the process presented in Figure 3-28. A Power Spectral Density (PSD) representation of the ship

motion is generated by multiplying the square of the frequency domain transfer function, $H_s(\omega)^2$, by wave height over the same frequency range as per equation 3-47. The wave model used is the open ocean area Bretschneider model [65] as defined by equation 3-48. The appropriate values for significant wave height, $H_{1/3}$, and average wave period, T_1, as functions of wind speed at a height of 19.5m above the sea are listed in Table 3-3.

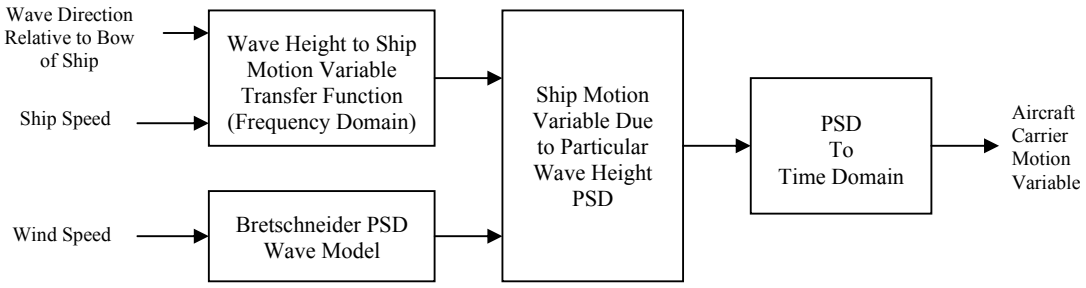

Figure 3-28 Aircraft Carrier Motion Data Flow Diagram

$$S_T(\omega) = \left|H_s(\omega)^2\right| S_w(\omega) \tag{3-47}$$

$$S_w(\omega) = \frac{172.8 H_{1/3}^2}{T_1^4}\omega^{-5}\exp\left\{\frac{-691.2}{T_1^4}\omega^{-4}\right\} \tag{3-48}$$

Beaufort Scale	1	2	3	4	5	6	7	8	9	10	11	12
Wind Speed at 19.5m Above Sea (knots)	2.0	5.0	8.5	13.5	19.0	24.5	30.5	37.0	44.0	51.5	59.5	>64.0
$H_{1/3}$ (m)	1.10	1.20	1.40	1.70	2.15	2.90	3.75	4.90	6.10	7.45	8.70	10.25
T_1 (s)	5.8	5.9	6.0	6.1	6.5	7.2	7.8	8.4	9.0	9.6	10.1	10.5

Table 3-3 Bretschneider Wave Spectrum Parameters as a Function of Wind speed

A time domain representation of a PSD is achieved by superpositioning of the sinusoids according to equation 3-49 [74].

$$y(t) = \sum_{m=1}^{\infty} \sqrt{S_T(\omega_m)\Delta\omega} \cos(\omega_m t + \psi_m) \qquad (3\text{-}49)$$

In practice, the aircraft carrier motion is calculated prior to execution of the simulation. The carrier motion variables are then input to the simulation at each time step. The position variables, which are referred to the aircraft carrier's body axes when generated, are transformed to the earth axes system when input to the simulation. The angular motion variables remain referred to the aircraft carrier's body axes.

The duration of the time history a particular motion variable generated in this manner is a function of the frequency range of the ship motion transfer function and the frequency increment by which it is defined. In this case, a time history of 623.3 seconds is generated for each motion variable. This time period is significantly greater than the time required to fly an approach from 500 feet to the aircraft carrier's deck.

In the case of the batch simulations, presented in Chapter 5, this 623.3 second period was divided into 5 sets as defined in Table 3-4. As the dominant frequency varies across the 623.3 period each of these five sets is unique. By simulating an approach using all five sets of motion variables a more accurate judgement can be made of the system under consideration for that set of carrier operating conditions.

Set	Start Time (seconds)	End Time (Seconds)
1	0	188.4
2	125.6	314.1
3	251.3	439.8
4	376.9	565.4
5	439.8	628.3

Table 3-4 Carrier Motion Variables Time History Subsets

The output of PSD to time domain calculations are perturbations about the steady state motion of the aircraft carrier. Hence it is necessary to add the steady state motion to perturbations to realise a model of the aircraft carrier's true motion.

Figure 3-29 presents the longitudinal motion variables of the touchdown point on the aircraft carrier's deck for a headwind 13.5 knots for aircraft carrier speeds of 0, 10 and 33 knots. Figure 3-30 presents the same motion variables describing the touchdown point on the carrier's deck for a constant aircraft carrier speed of 10 knots and headwinds of 2, 24.5 and 37 knots. Note that the touchdown point is 45 feet above the surface of the water.

The output of the aircraft carrier dynamics model is used in the calculation of atmospheric disturbance due to the proximity and motion of the carrier as presented in section 3.4.3. The trajectory of the aircraft carrier is also used by the navigation system presented in Chapter 4.

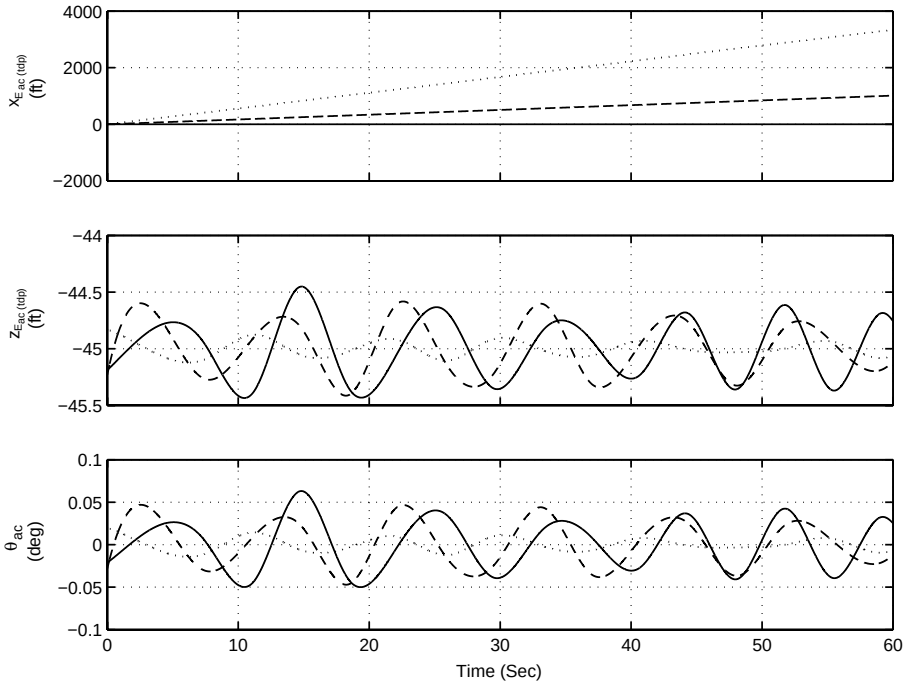

Figure 3-29 Aircraft Carrier Motion Example: Wind Speed = 13.5 knots
Variable Carrier speed: 0 knots [——] 10 knots [- - -] 33 knots [·····]

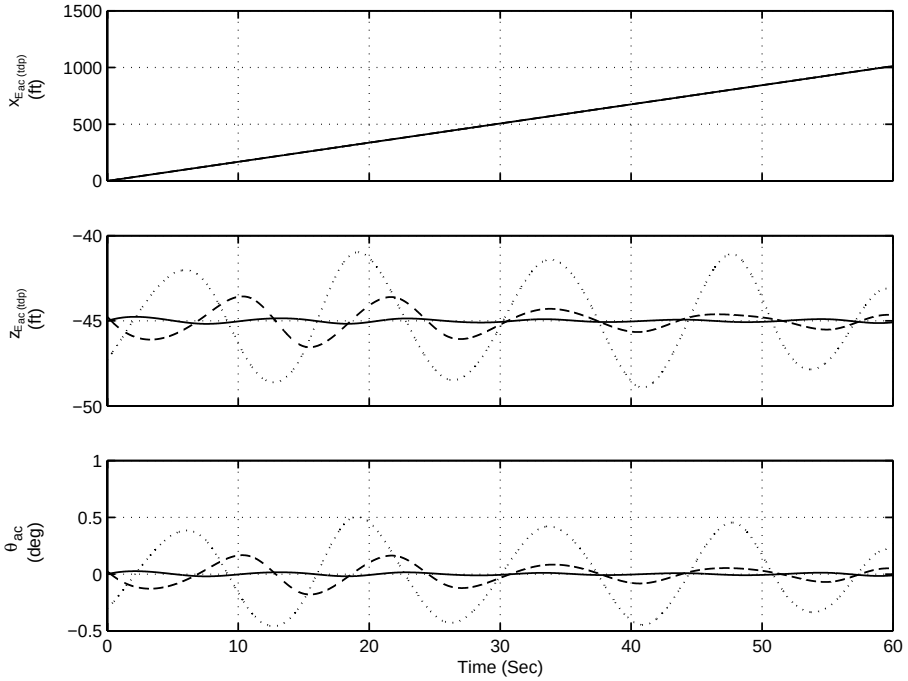

Figure 3-30 Aircraft Carrier Motion Example: Aircraft Carrier Speed = 10 knots
Wind Speed: 2 knots [——] 24.5 knots [- - -] 37 knots [·····]

The trends presented in figures 3-29 and 3-30 are worth noting. The carrier motion is most stable at high speed and light wind conditions. Any departure from this condition, either by reducing the carrier's speed or an increase in wind speed, has the effect of reducing the stability of the carrier.

3.6 AIRCRAFT MODEL VALIDATION

The aircraft model was validated against response time histories presented by Gautrey and Cook [55] and the stability and control analysis and autopilot response time histories presented by Fitzgerald [56].

The design point used for the development of the approach controllers is steady level flight at 140 knots, 1000 ft, flaps 20 degrees, undercarriage extended and 20 gallons of useable fuel aboard.

The stability and control parameters of the augmented airframe at the design point are presented in section 3.6.1. The aircraft's response to control inputs at the design point are presented in section 3.6.2.

3.6.1 STABILITY AND CONTROL PROPERTIES OF DESIGN POINT

Two three degree of freedom linear models of the basic airframe were extracted from the non linear model at the design point representing the longitudinal and lateral-directional dynamics. All control effectors were included with the exception of lateral vectored thrust as it is not used in this study.

The appropriate Stability Augmentation System presented in section 3.3.7.3 was implemented in these linear models. This implementation included appropriate actuator and sensor models. The longitudinal and lateral-directional stability and control characteristics of the augmented airframe were then extracted and are presented in tables 3-5 and 3-6 respectively.

Short Period Damping Ratio	0.76
Short Period Frequency	5.5 rad/s
Speed Subsidence Time Constant	3.44 seconds
Pitch Subsidence Time Constant	0.98 seconds

Table 3-5 Longitudinal Stability and Control Properties of Design Point

Dutch Roll Damping Ratio	0.69
Dutch Roll Frequency	4.87 rad/s
Roll Mode Time Constant	0.11 seconds
Spiral Mode Time Constant	0.96 seconds

Table 3-6 Lateral-Directional Stability and Control Properties of Design Point

The transfer function describing the pitch attitude response to pitch attitude demand is presented in equation 3-50. Elevator actuator and appropriate sensor dynamics are included in this transfer function. The sensors included are velocity, pitch attitude and pitch rate. This applies to all longitudinal transfer functions presented.

$$\frac{\theta_s(s)}{\theta_d(s)} = \frac{\begin{matrix}(s^2 - 46228s + 1.0672\text{x}10^9)(s + 0.2801)(s + 1.23)(s + 33.11)(s^2 + 356s + 40000)\\ (s^2 + 46117s + 1.0647\text{x}10^9)(s^2 + 46228s + 1.0672\text{x}10^9)\end{matrix}}{\begin{matrix}(s + 0.2906)(s + 1.02)(s^2 + 8.3705s + 30.1979)(s^2 + 23.6383s + 691.47)(s + 33.11)\\ (s + 40.4)(s^2 + 355.6s + 39927)\end{matrix}} \text{ (rad/rad)} \tag{3-50}$$

The transfer function describing the body axes axial velocity response to throttle demand is presented in equation 3-51.

$$\frac{u_s(s)}{\tau_d(s)} = \frac{(s+1.0559)(s^2+8.3706s+30.1955)(s^2+23.6383s+691.4813)(s-40.4063)}{(s+0.2906)(s+1.02)(s^2+8.3705s+30.1979)(s^2+23.6383s+691.47)(s+33.11)} \frac{(s^2+355.6s+39927)(s+1.1808\text{x}10^{11})}{(s+40.4)(s^2+355.6s+39927)} \text{ (ft/s/RPM)} \tag{3-51}$$

The transfer function describing the pitch attitude response to trailing edge flap deflection is presented in equation 3-52. It should be noted that the trailing edge flap actuator is not included in this transfer function.

$$\frac{\theta_s(s)}{\delta_f(s)} = \frac{(s^2-63.5125s+2.4123\text{x}10^{13})(s+0.2808)(s+1.2282)(s^2+31.2933s+944.94)}{(s+0.2906)(s+1.02)(s^2+8.3705s+30.1979)(s^2+23.6383s+691.47)(s+33.11)} \frac{(s+33.1102)(s^2+356s+40000)}{(s+40.4)(s^2+355.6s+39927)} \text{ (rad/deg)} \tag{3-52}$$

The transfer function describing the pitch attitude response to symmetric spoiler deflection is presented in equation 3-53. It should be noted that the spoiler actuator is not included in this transfer function.

$$\frac{\theta_s(s)}{\delta_s(s)} = \frac{(s^2+7.4718s+22.0175)(s+5.7656)(s^2+23.443s+697.98)(s+40.4119)}{(s+0.2906)(s+1.02)(s^2+8.3705s+30.1979)(s^2+23.6383s+691.47)(s+33.11)} \frac{(s^2+355.6128s+39928)}{(s+40.4)(s^2+355.6s+39927)} \text{ (rad/deg)} \tag{3-53}$$

The transfer function describing the pitch attitude response to longitudinal thrust vectoring paddle deflection is presented in equation 3-53. It should be noted that the thrust vectoring actuator is not included in this transfer function.

$$\frac{\theta_s(s)}{\theta_r(s)} = \frac{(s-1.7644\text{x}10^{7})(s+0.2801)(s+1.2278)(s^2+31.2933s+944.9476)(s+33.11)}{(s+0.2906)(s+1.02)(s^2+8.3705s+30.1979)(s^2+23.6383s+691.47)(s+33.11)} \frac{(s^2+356s+40000)(s+1.7644\text{x}10^{7})}{(s+40.4)(s^2+355.6s+39927)} \text{ (rad/rad)} \tag{3-54}$$

The transfer function describing the roll attitude response to roll attitude demand is presented in equation 3-55. In this case the aileron and rudder actuator dynamics are included as well as the yaw rate, roll rate and roll attitude sensor dynamics. This applies to all lateral-directional transfer functions presented.

$$\frac{\phi_s(s)}{\phi_d(s)} = \frac{(s-47743)(s^2-65.2874s+2.2764\text{x}10^9)(s^2+6.16s+11.9838)(s^2+96s+4466.9)}{(s+1.0408)(s^2+6.7967s+23.7288)(s+8.5048)(s+41.2834)(s^2+90.039s+4147.5)} \frac{(s^2+144s+8100)(s^2+354s+39621)(s+47678)}{(s^2+101.3431s+4463)(s^2+127.3435s+8106.4)(s^2+354s+39656)} \text{ (rad/rad)} \tag{3-55}$$

The transfer function describing the yaw rate response to yaw rate demand is presented in equation 3-56.

$$\frac{r_s(s)}{r_d(s)} = \frac{(s-1.04\text{x}10^5)(s+0.105)(s+3.4935)(s+9.8342)(s-41.7764)(s^2+92.0177s+3722.5)}{(s+1.0408)(s^2+6.7967s+23.7288)(s+8.5048)(s+41.2834)(s^2+90.039s+4147.5)} \frac{(s^2+127.8175s+8249.1)(s^2+101.4115s+1.0825\text{x}10^{10})(s+104090)}{(s^2+101.3431s+4463)(s^2+127.3435s+8106.4)(s^2+354s+39656)} \text{ (rad/sec/rad)} \tag{3-56}$$

3.6.2 CONTROL RESPONSES

In the following sections the aircraft's response to the various control effectors at the design point are presented. For each response a step input is injected into the system at the input to the applicable actuator at a time of 1 second and held for the duration of the response. For each response the three axis Stability Augmentation System is engaged. The input to each channel of the Stability Augmentation System is the steady state trim values before the control input is applied. Each response is initiated from trimmed flight at the design point flight condition.

3.6.2.1 ELEVATOR

The aircraft response to a 1 degree step input to the elevator actuator at 1 second and held for the duration of the response is presented in Figure 3-31. The damping of this disturbance by the Stability Augmentation System is clearly evident. From the elevator angle time history it can be seen that the actuator dynamics are fast when compared to the aircraft's response.

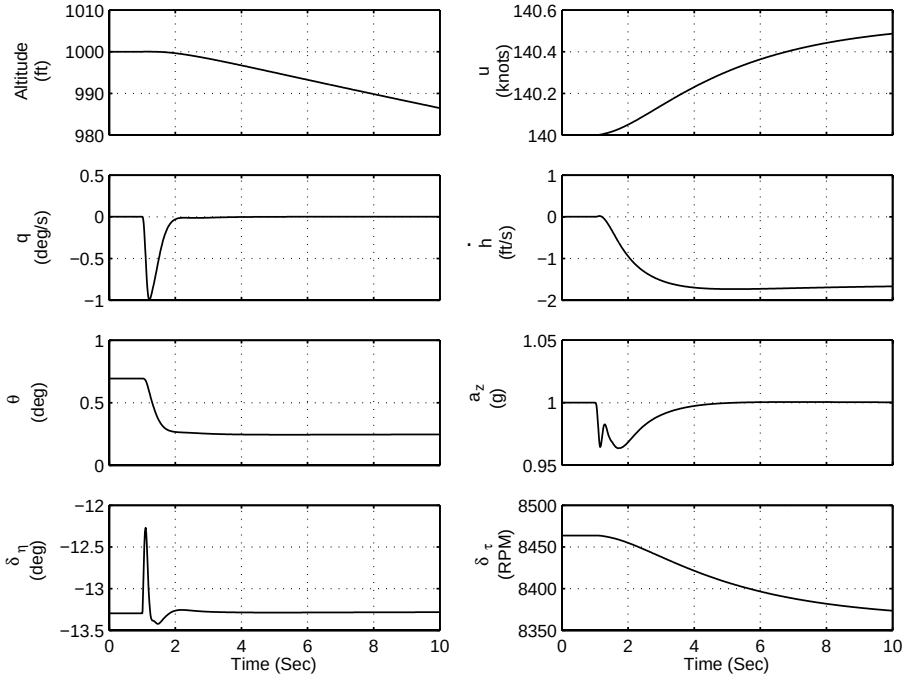

Figure 3-31 Aircraft Response to 1 Degree elevator Step

3.6.2.2 AILERONS

The aircraft response to a 1 degree step input to the aileron actuator at 1 second and held for the duration of the response is presented in Figure 3-32. The damping of this disturbance by the Stability Augmentation System is clearly evident as is the effects of adverse aileron yaw.

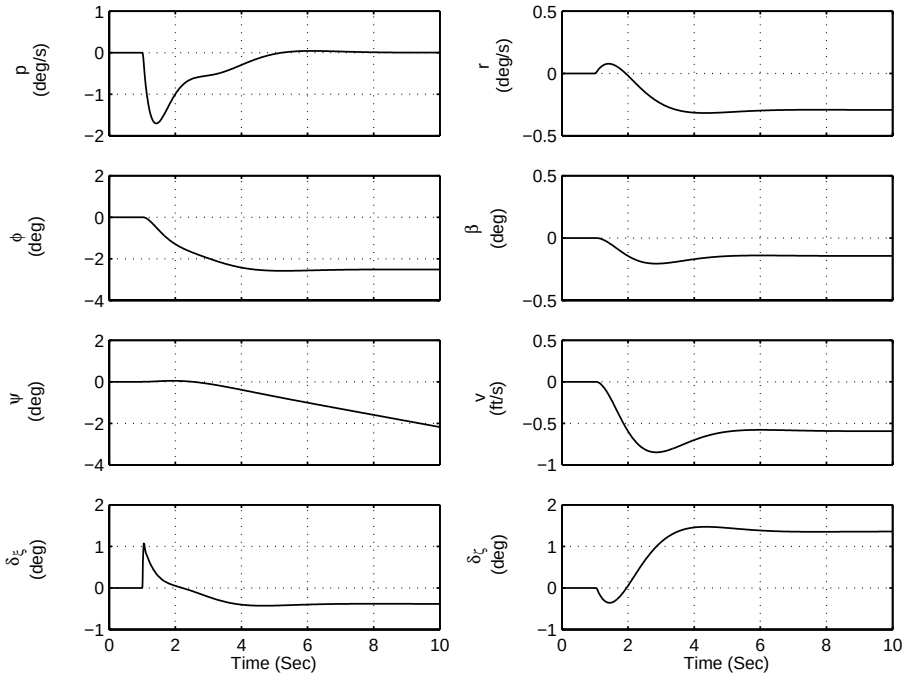

Figure 3-32 Aircraft Response to 1 Degree Aileron Step

3.6.2.3 RUDDER

The aircraft response to a 1 degree step input to the rudder actuator at 1 second and held for the duration of the response is presented in Figure 3-33. The damping of this disturbance by the Stability Augmentation System is clearly evident as is the coupling between the lateral and directional dynamics of the aircraft.

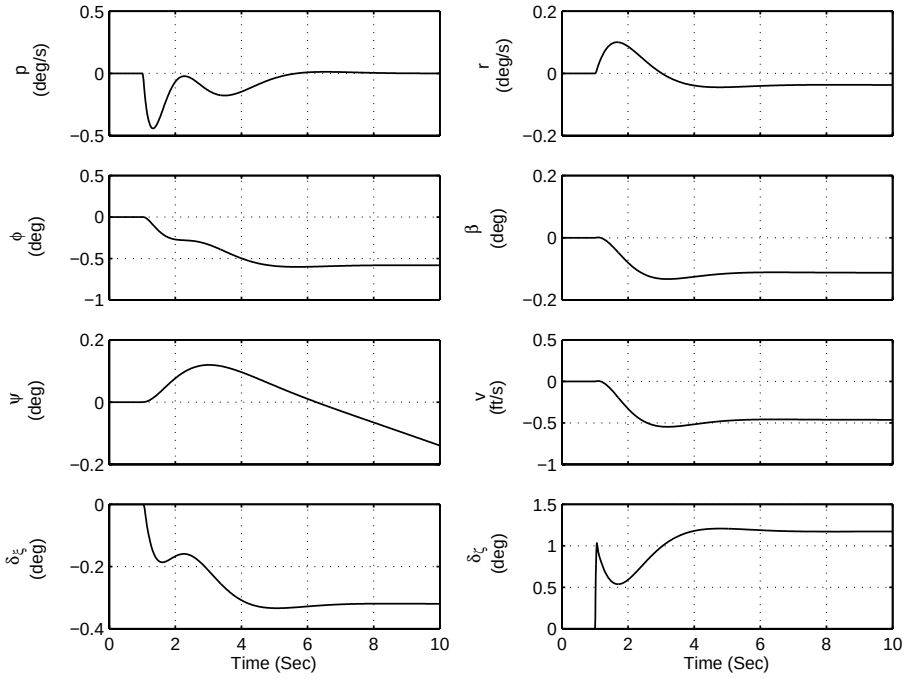

Figure 3-33 Aircraft Response to 1 Degree Rudder Step

3.6.2.4 THROTTLE

The aircraft response to a 1000 RPM step input to the engine at 1 second and held for the duration of the response is presented in Figure 3-34. The Phugoid mode which would normally be excited by such a disturbance is clearly damped by the Stability Augmentation System.

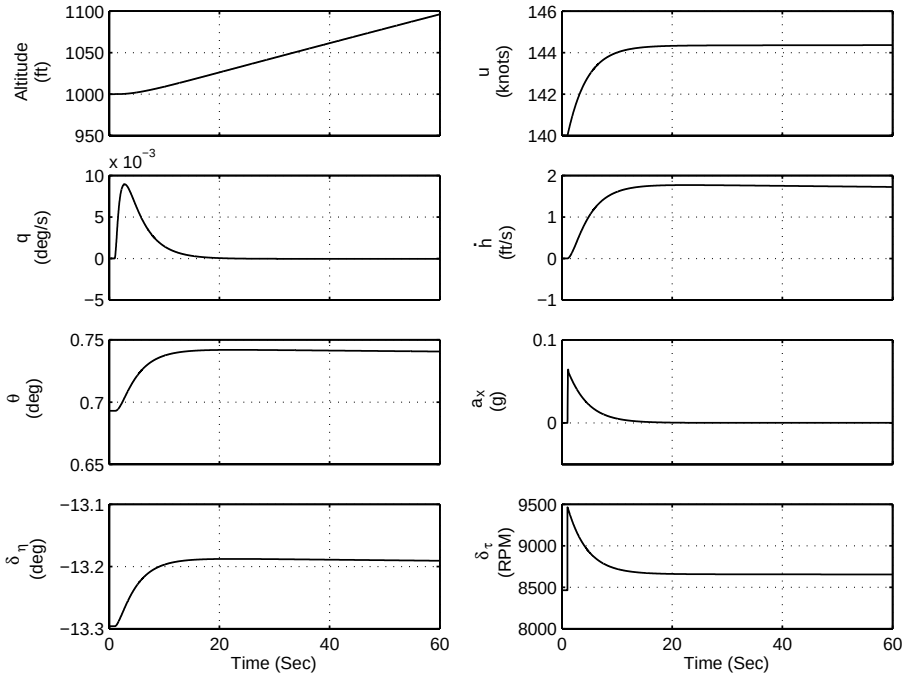

Figure 3-34 Aircraft Response to 1000 RPM Throttle Step

3.6.2.5 LONGITUDINAL THRUST VECTORING

The aircraft response to a 1 degree step input to the longitudinal thrust vectoring paddle actuator at 1 second and held for the duration of the response is presented in Figure 3-35. The damping of this disturbance by the Stability Augmentation System is clearly evident.

An appreciation of the relative control powers of the elevator and longitudinal thrust vectoring at this operating point can be extracted from this response. It can be seen that the effect of 1 degree of longitudinal thrust vectoring paddle deflection is trimmed by an additional -0.25 degrees of elevator deflection. This infers that at this operating point the elevator has four times the control power of vectored thrust.

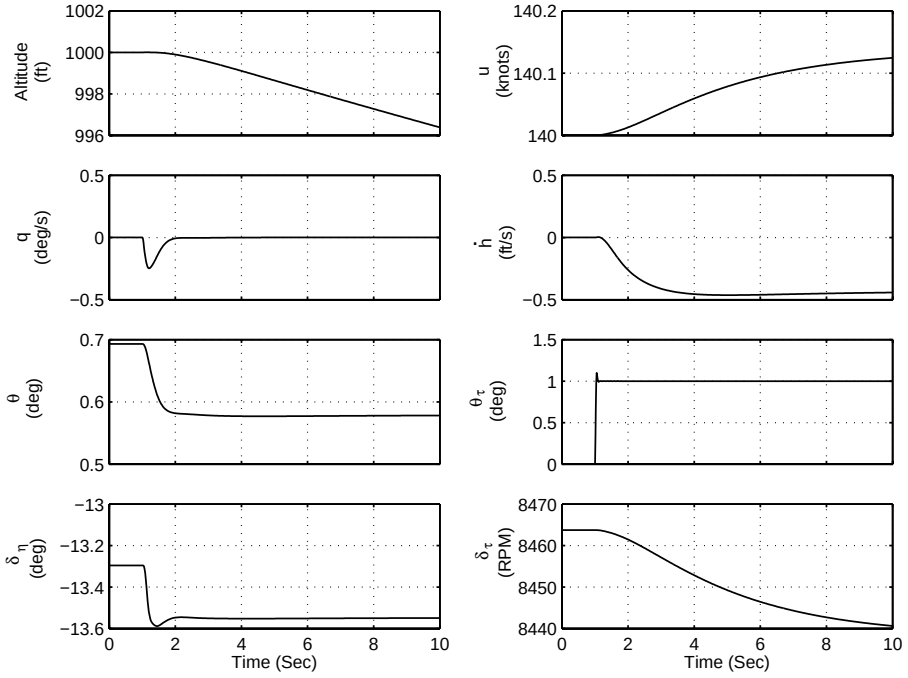

Figure 3-35 Aircraft Response to 1 Degree longitudinal Thrust Paddle Step

3.6.2.6 TRAILING EDGE FLAPS

The aircraft response to a 1 degree step input to the trailing edge flap actuator at 1 second and held for the duration of the response is presented in Figure 3-36. The damping of this disturbance by the Stability Augmentation System is clearly evident. It can be seen that the extension of trailing edge flap has the effect of inducing a nose down pitching moment.

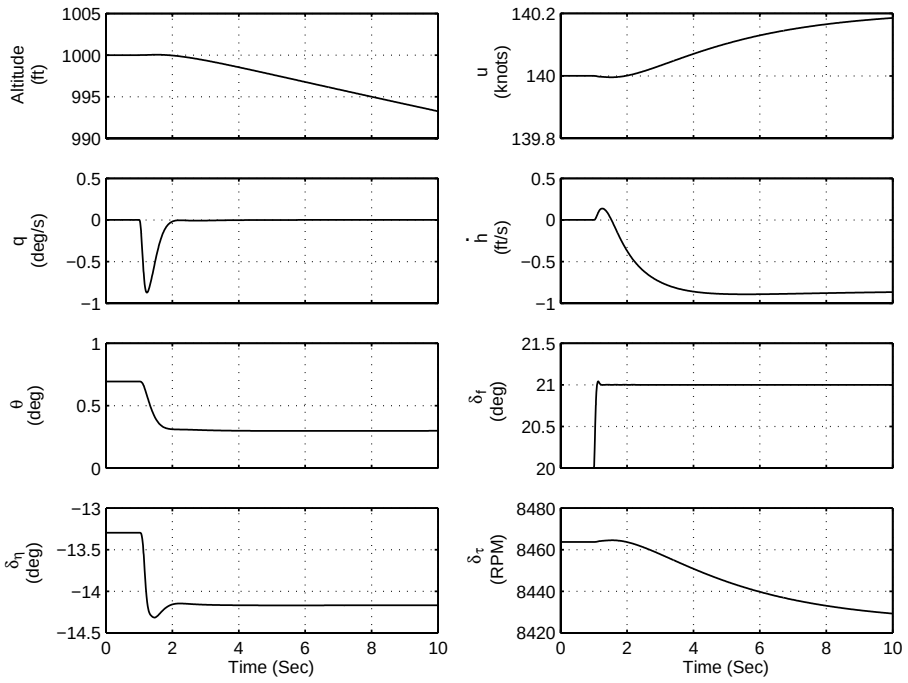

Figure 3-36 Aircraft Response to 1 Degree Trailing Edge Flap Step

3.6.2.7 SPOILER

The aircraft response to a 1 degree step input to the spoiler actuator at 1 second and held for the duration of the response is presented in Figure 3-37. The spoiler induced pitching moment can be seen to be small when compared to that of the trailing edge flap. The spoiler induced pitching moment is in the same sense as the trailing edge flap induced pitching moment, i.e. nose down.

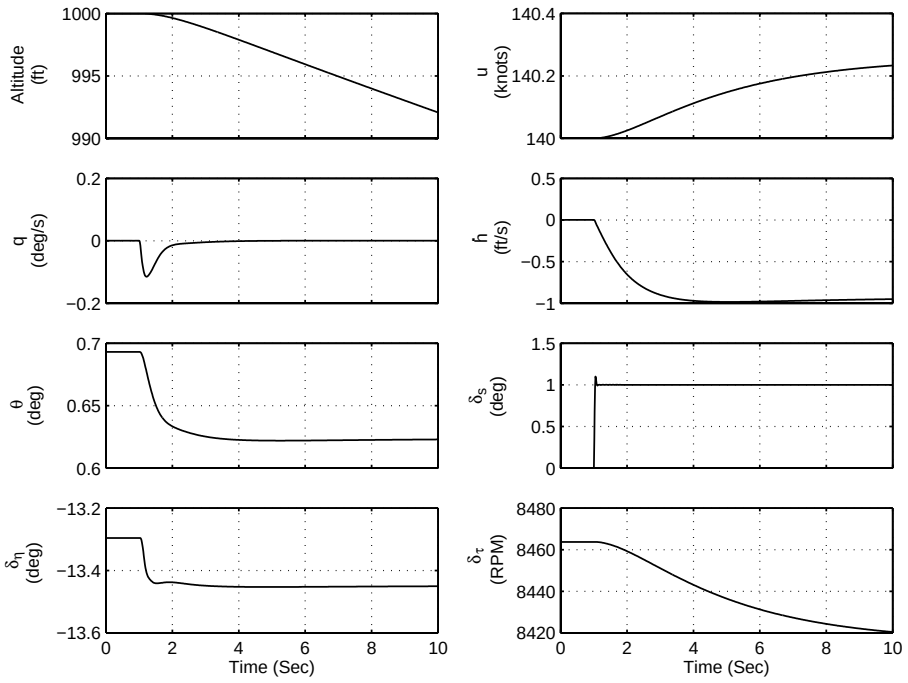

Figure 3-37 Aircraft Response to 1 Degree Spoiler Step

3.6.2.8 UNDERCARRIAGE

The aircraft response to the retraction of the aircraft's undercarriage is presented in Figure 3-38. The reduction in drag is evident from the increase in speed. The damping of this disturbance by the Stability Augmentation System is clearly evident. Typically the retraction or extension of undercarriage could excite the phugoid mode if not compensated by the Stability Augmentation System or the pilot.

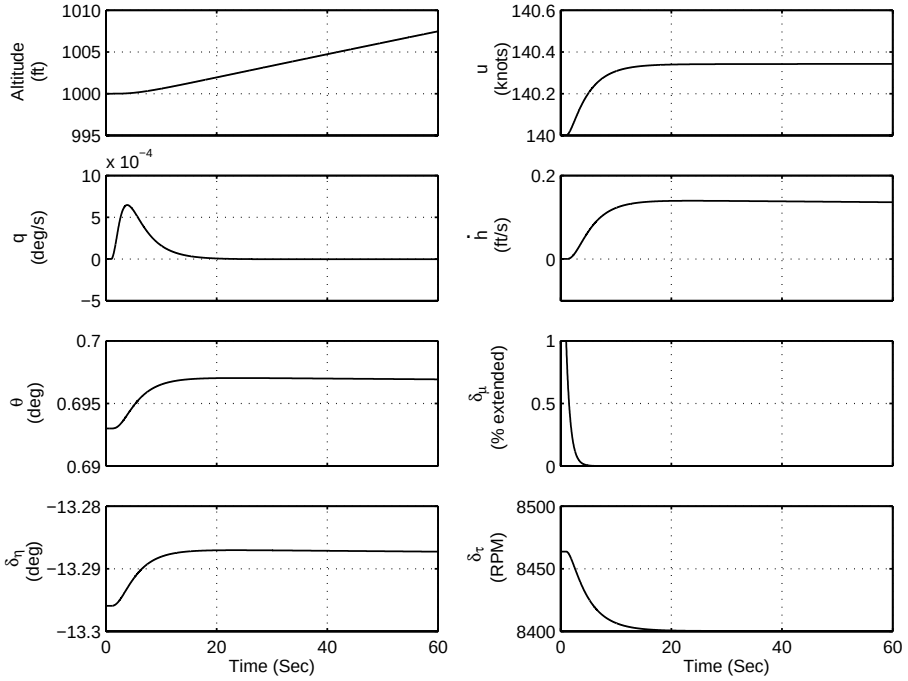

Figure 3-38 Aircraft Response to Retraction of Undercarriage

---------- o0o ----------

4 NAVIGATION SYSTEM

4.1 INTRODUCTION

A navigation system is a central element of any automatic landing approach system. The purpose of a navigation system is to provide guidance cues to the approach controllers. The approach controllers developed in this study are discussed in the following chapters.

At present during a landing approach to a carrier an approach glide path is originated from a point on the carrier's deck. A track approach path is generated similarly. As such the aircraft flies an approach to a moving point. Stabilisation systems are used to negate the effects of ship motion on the approach path; however, these systems have limitations. The current state of the art of carrier landing navigation systems does not meet the requirements of the Joint Precision Approach and Landing systems (JPALS) discussed in Chapter 2.

As stated in the objectives in Chapter 1, the navigation concept developed in this study aims to build on the systems and procedures currently in place, account for future navigation requirements, account for ship motion through the use of ship motion prediction, facilitate the seamless integration of the UAV fleet with the piloted fleet and allow for truly autonomous carrier landing operations. In keeping with the limitations of the scope of this study, the Navigation System presented does not account for any pre 'tip-over' navigation requirements.

The concept developed is presented schematically in Figure 4-1. Carrier and aircraft positions are used to calculate the relative distance and velocity. The time to touchdown is computed using the relative distance and velocity. The position of the nominal touchdown point is predicted at that time in the future using ship motion prediction techniques. A 3 degree approach glide path is generated from that point and the aircraft's vertical deviation from that approach glide path is calculated. Likewise, an approach track path is generated coincident with the carrier's track and the aircraft's

lateral deviation from that approach track path is calculated. The vertical and lateral deviations are the input to the approach controllers.

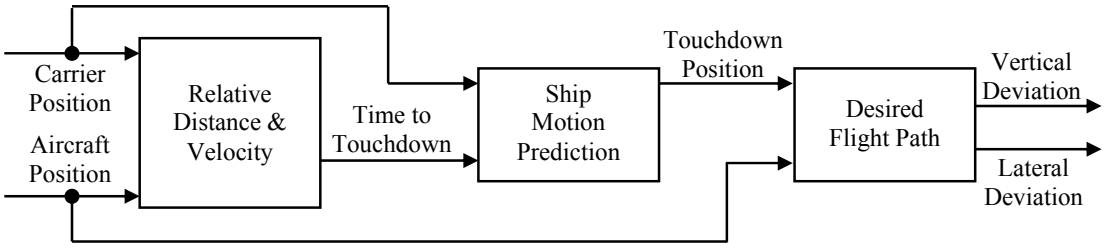

Figure 4-1 Navigation System Data Flow Diagram

Each component of the Navigation System is described in the following sections. Example approaches to landing using this system are presented. This chapter concludes with a critical assessment of this Navigation System.

4.2 TIME TO TOUCHDOWN

The Navigation System uses the aircraft's and carrier's earth axes position. This is to emulate the GPS reference system, and as such the system is conceptually compliant with JPALS requirements.

The Navigation System is based on predicting the position of the touchdown point at a time in the future, which corresponds to that time at which the aircraft touches down on the aircraft carrier's deck. This time is a function of distance between the aircraft and the aircraft carrier and their relative velocity.

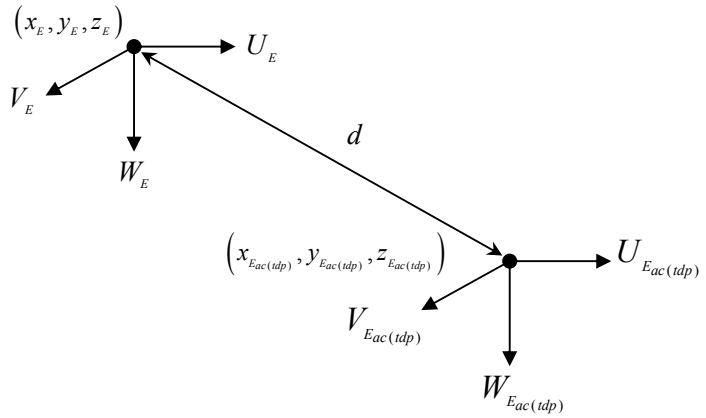

Figure 4-2 Time to Touchdown Geometry

Time to touchdown, t_{td}, is defined as

$$t_{td} = \frac{d}{\dot{d}} \tag{4-1}$$

where the distance between the aircraft and the touchdown point on the aircraft carrier's deck, d, is defined as

$$d = \sqrt{\left(x_E - x_{E_{ac(tdp)}}\right)^2 + \left(y_E - y_{E_{ac(tdp)}}\right)^2 + \left(z_E - z_{E_{ac(tdp)}}\right)^2} \tag{4-2}$$

In this implementation, the rate of change of distance between the aircraft and the touchdown point, $\dot{d}$, is averaged over a period of a half a second. This is to reduce the time to touchdown estimate's sensitivity to atmospheric disturbances. The period of half a second was determined through experiment performed with the simulation.

4.3 SHIP MOTION PREDICTION

As introduced in Chapter 2, various methods exist for predicting ship motion and, consequently, the position of the desired touchdown point. While it is beyond the scope of this research project to refine or adapt the methods of prediction that exist, a discussion of these methods is appropriate.

The Kalman-Bucy filter in predictor form is used by Doolin and Sidar [37]. Mathematical models for ship motion in state-space form are obtained by fitting second-order transfer functions to experimentally derived power spectral densities for aircraft carrier heave and pitch motions. By arguing that heave and pitch motions are in fact narrow band processes, the Kalman filter is shown to give similar results to that of a predictor for the state of a harmonic oscillator.

Any approach for ship motion prediction based on the Kalman-Bucy filter has to assume a mathematical model for the ship's response. However, since the wave spectrum is not constant but changing, and especially so for a vessel manoeuvring in a seaway, the mathematical model on which the filter is based should be changing too. An Extended Kalman Filter could be used to improve predictions, as demonstrated by

Hinedi et al. [75]. However, extended Kalman filters are complex and sometimes encounter convergence problems.

An adaptive predictor seems to address the shortfalls of the other available methods. In adaptive prediction there is no need to include any prior knowledge about the ship response in the algorithm. The ship mathematical model is formed on-line and is conveniently updated whenever necessary due to changes in operating or weather conditions.

As adaptive prediction promises to be the most suitable method for the purposes under consideration in this research project. This discussion is focused on such and, in particular, the research undertaken by the Department of Mechanical Engineering at University College London [39,40,41,42,43].

4.3.1 ADAPTIVE PREDICTION

Adaptive prediction is conceptually composed of two computational steps. Firstly, a model of the system is derived using a suitable System Identification method and, secondly, the identified model is used to predict ahead in time.

This section on predictor theory outlines the methodology used in adaptive prediction and is extracted from Broome and Pittaras [39]. It should be noted that the notation is as presented by Broome and Pittaras [39] and care should be used so as to avoid confusion with the same notation used elsewhere in this thesis. From a notation point of view this section should be treated in isolation.

Consider the following discrete-time mathematical model of a system with an input u (e.g. rudder and stabilisers) and output y (e.g. heave and pitch angle)

$$A\left(z^{-1}\right)y(t) = B\left(z^{-1}\right)u(t) + C\left(z^{-1}\right)e(t) \qquad (4\text{-}3)$$

In general y, u and e are vector signals of dimensions m, n and m respectively. A, B and C are polynomial matrices in the unit delay operator z^{-1}, of the form

$$A(z^{-1}) = I + A_1 z^{-1} + ... + A_{na} z^{-na}$$

$$B(z^{-1}) = B_1 z^{-1} + B_2 z^{-2} + ... + B_{nb} z^{-nb} \quad (4\text{-}4)$$

$$C(z^{-1}) = I + C_1 z^{-1} + ... + C_{nc} z^{-nc}$$

where A_i, B_i and C_i are real matrices of dimensions $A_i, C_i, \in R^{m \times m}$, $B_i \in R^{m \times n}$. $e(t)$ is a noise term and is assumed to be a zero-mean stochastic process with Gaussian distribution. t is a discrete time index and the unit delay operator operating on a discrete time signal $x(t)$ has the effect that: $x(t-1) = z^{-1}x(t)$

Models of the form of equation 4-3 are called Auto Regressive Moving Average with eXogenous input (ARMAX). Given an ARMAX model a *k*-step ahead predictor of the system output, $\hat{y}(t+k/t)$ based on available input/output measurements up to and including time t is given by

$$C(z^{-1})\hat{y}(t+k/t) = \alpha(z^{-1})y(t) + \beta(z^{-1})u(t+k) \quad (4\text{-}5)$$

where $\alpha(z^{-1})$ and $\beta(z^{-1})$ are polynomial matrices which are solutions to equations involving $A_i\ (z^{-1})$, $B_i(z^{-1})$ and $C_i(z^{-1})$.

It is noted in equation 4-5 that to predict the output, $y(t)$, of a system *k* steps ahead, the future input strategy must also be known k steps ahead. In practice, several different strategies may be considered depending on whether the system operates in open or closed loop mode. However the method favoured is that of a restricted complexity predictor of the form

$$\hat{y}(t+k/t) = P(z^{-1})y(t) + Q(z^{-1})u(t) \quad (4\text{-}6)$$

where $P(z^{-1})$ and $Q(z^{-1})$ are polynomial matrices of the form

$$P(z^{-1}) = P_0 + P_1 z^{-1} + ... + P_{np} z^{-np}$$

$$Q(z^{-1}) = Q_0 + Q_1 z^{-1} + ... + Q_{np} z^{-np} \quad (4\text{-}7)$$

and $P_i \in R^{m \times m}$, $Q_i \in R^{m \times n}$

Equation 4-6 can be justified because normally the predictor equation can be expressed equivalently as an infinite sum of past system inputs and outputs

$$\hat{y}(t+k/t) = \sum_{i=0}^{\infty} P_i y(t-i) + \sum_{i=0}^{\infty} Q_i u(t-i) \tag{4-8}$$

where the terms of the infinite series $\{P_i\}$ and $\{Q_i\}$ diminish as $i \to \infty$. In most practical cases, only the first few terms in the series are non-zero and hence the orders n_p and n_q of the polynomial matrices $P(z^{-1})$ and $Q(z^{-1})$ can be chosen accordingly.

System Identification techniques are employed to obtain a model of the system in the form of equation 4-3. In System Identification a mathematical model giving an internal system description is not required. Instead, the system is treated as a black box with input and output signals sampled at discrete time intervals. When using System Identification methods it is algorithmically convenient to assume models as in equation 4-3, because it can be written equivalently as

$$y(t) = \theta^T(t-1)\phi(t-1) + e(t) \tag{4-9}$$

where

$$\theta^T(t-1) = [A_1 ... A_{na}\ B_1 ... B_{nb}\ C_1 ... C_{nc}]$$

$$\begin{aligned} \phi^T(t-1) = [&-y^T(t-1) ... -y^T(t-na) \\ &u^T(t-1) ... u^T(t-nb) \\ &e^T(t-1) ... e^T(t-nc)] \end{aligned} \tag{4-10}$$

If $e(t)$ in equation 4-9 is a zero-mean Gaussian random process then it is shown that the best one-step-ahead predictor for equation 4-9 is

$$\hat{y}\left(t/t-1;\theta\left(t-1\right)\right)=E\left[y\left(t\right)\right]$$

$$=E\left\{\theta^{T}\left(t-1\right)\phi\left(t-1\right)\right\}+E\left\{e\left(t\right)\right\} \quad (4\text{-}11)$$

$$=\theta^{T}\left(t-1\right)\phi\left(t-1\right)$$

If the one-step-ahead prediction error is denoted by $\varepsilon\left(t,\theta\left(t-1\right)\right)$ then

$$\varepsilon\left(t,\theta\left(t-1\right)\right)\triangleq y\left(t\right)-\hat{y}\left(t/t-1;\theta\left(t-1\right)\right) \quad (4\text{-}12)$$

A frequently selected criterion of how well the model $\theta\left(t\right)$ performs in the long run is the sum of the squares of the prediction errors, or their Euclidean norms in the multivariable case

$$V_{N}\left(\theta\right)=\frac{1}{2}\sum_{t=1}^{N}\varepsilon^{T}\left(t,\theta\left(t-1\right)\right) \quad (4\text{-}13)$$

In System Identification the algorithms used are designed to minimise $V_{N}\left(\theta\right)$. The general form of the basic algorithm is always

$$\theta\left(t\right)=\theta\left(t-1\right)+\gamma\left(t\right)P\left(t\right)n\left(t\right)\left[y\left(t\right)-\hat{y}\left(t\right)\right] \quad (4\text{-}14)$$

where $\gamma\left(t\right)$ is a time varying scalar gain, $P\left(t\right)$ is a matrix related to the covariance matrix of estimates and $n\left(t\right)$ is a matrix related to the gradient of $y\left(t\right)$ with respect to $\theta\left(t\right)$.

Although prediction of system outputs can be effected in two steps, i.e. by first using a suitable identification method to derive a model as in equation 4-3 and then transforming it to arrive at a predictor equation as in equation 4-5, the advantage of the restricted complexity predictor is that it can be preparameterised in the form of equation 4-11 so that the identification algorithm gives parameter estimates of the polynomial matrices $P\left(z^{-1}\right)$ and $Q\left(z^{-1}\right)$ directly. This can simply be accomplished by rewriting equation 4-11 as

$$\hat{y}\left(t+k/t;\theta\left(t\right)\right)=\theta^{T}\left(t\right)\phi\left(t\right) \quad (4\text{-}15)$$

where

$$\theta^T(t) = \left[P_0 \ldots P_{np}\, Q_0 \ldots Q_{nq} \right]$$
$$\phi(t) = \left[y^T(t) \ldots y^T(t-np)\, u^T(t) \ldots u^T(t-nq) \right] \tag{4-16}$$

At time t prediction k steps ahead is calculated using equation 4-15, while for the parameter estimation the same equation is used but with shifted past system inputs and outputs as

$$\hat{y}\left(t/t-k;\theta(t-k)\right) = \theta^T(t-k)\phi(t-k) \tag{4-17}$$

This method when used without augmentation yields accurate predictions for up to 15 seconds ahead. This time horizon is sufficient to allow flight path changes to be made safely, assuming a reasonable offset from the desired flight path when entering into that timeframe, owing to the aircrafts response time. However, this time horizon is not sufficient for the purposes of the system under investigation in this study which requires reasonably accurate predictions of the touchdown position from the initiation of the approach phase, approximately 70 seconds.

Work has been conducted on methods of augmentation that would extend the accurate time horizon [43]. Such methods include feeding forward changes to the model which reflect changes in operating conditions, thus reducing the model adaptation time and similarly anticipating the slow changes in the sea state.

4.3.2 SIMULATION IMPLEMENTATION

As refinement of prediction methods is beyond the scope of this study, it was decided that accurately modelling a prediction method would not add any value to the study. Instead, the prediction method, is simulated using a simple look-up table.

In order to assess the maximum potential performance enhancement to the autonomous approach and landing task derived from integrating touchdown point position prediction into the approach controllers, it is necessary to assume perfect prediction. In this case, as aircraft carrier motion is calculated prior to simulation of the approach, perfect

prediction is achieved by simply looking ahead on the time 'history' of the aircraft carriers motion variables.

Time to touchdown, t_{td}, is input to look-up tables of the aircraft carriers motion variables and the predicted touchdown position, $\left(x_{E_{ptd}}, y_{E_{ptd}}, z_{E_{ptd}}\right)$, and orientation, $\left(\phi_{ac_{ptd}}, \theta_{ac_{ptd}}, \psi_{ac_{ptd}}\right)$, are output.

At one second to touchdown, approximately the point at which the aircraft passes over the aircraft carriers ramp, the predicted touchdown point is held constant.

4.4 FLIGHT PATH DEVIATIONS

Vertical and lateral flight path deviations of the aircraft's tail hook are calculated based on the aircraft's position, $\left(x_E, y_E, z_E\right)$, the position of the predicted touchdown position, $\left(x_{E_{ptd}}, y_{E_{ptd}}, z_{E_{ptd}}\right)$, and the track of the aircraft carrier, λ_{ac}. These deviations are the approach controller inputs.

4.4.1 VERTICAL DEVIATION

With reference to Figure 4-2 the relative distance between the predicted touchdown point and the aircraft projected on to the flat earth is defined as

$$d_{rd} = \sqrt{\left(x_{E_{ptd}} - x_E\right)^2 + \left(y_{E_{ptd}} - y_E\right)^2} \tag{4-18}$$

At distance d_{rd} from the aircraft carrier the aircraft tail hook desired altitude is defined as

$$h_{th_d} = d_{rd} \tan\gamma \tag{4-19}$$

where the approach flight path angle, γ, is defined as 3^o for this study.

Figure 4-3 presents an illustration of the longitudinal plane geometry used in defining the deviation of the tail hook from the prescribed glide path.

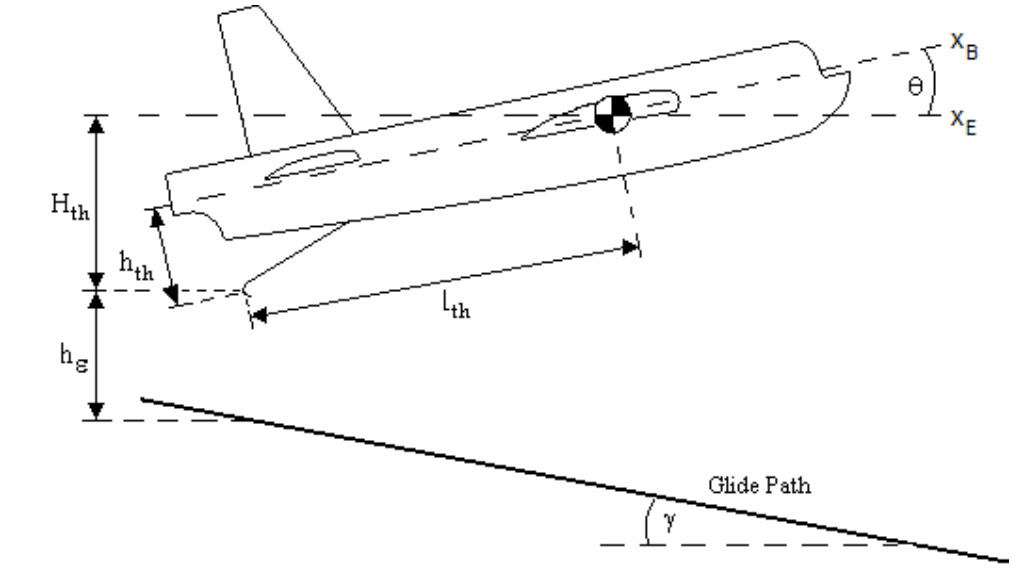

Figure 4-3 Approach Glide Path Deviation Geometry

Noting that the aircraft altitude, h, is defined as

$$h = -z_E \tag{4-20}$$

The tail hook altitude deviation from the prescribed glide path, h_ε, is defined as

$$h_\varepsilon = h - H_{th} - h_{th_d} \tag{4-21}$$

where the height of the tail hook from the aircraft centre of gravity, H_{th}, is defined as

$$H_{th} = l_{th} \sin\theta + h_{th} \cos\theta \tag{4-22}$$

where the perpendicular distance from the axial body axis to the tail hook, h_{th}, is defined as

$$h_{th} = 3.2 \text{ ft} \tag{4-23}$$

and the distance from the centre of gravity to the tail hook measured parallel to the axial body axis, l_{th}, is defined as

$$l_{th} = 10.85 - h_{cg}\bar{c} \quad (\text{ft}) \tag{4-24}$$

4.4.2 LATERAL DEVIATION

Figure 4-4 presents the relevant geometry for calculating the lateral deviation from the tail hook to the prescribed track.

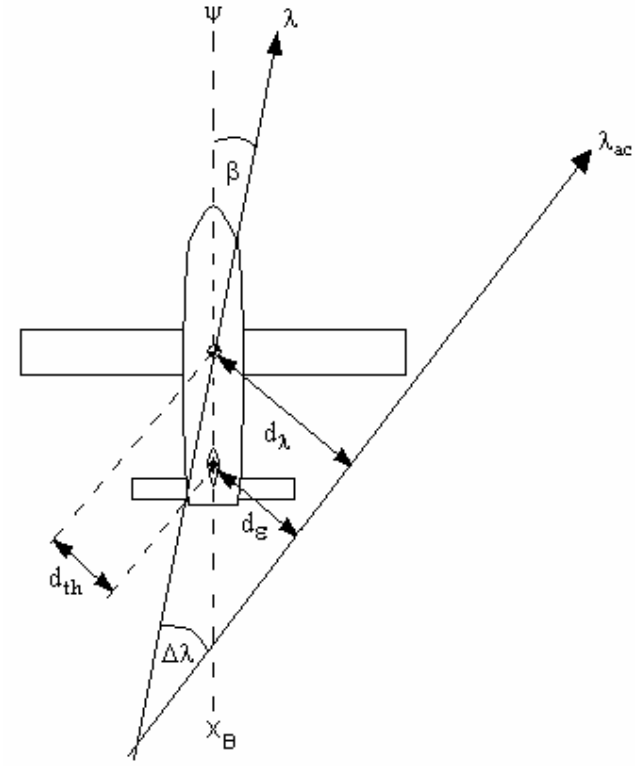

Figure 4-4 Track Deviation Geometry

The distance from the aircraft centre of gravity to the prescribed track is defined as

$$d_{\lambda} = \frac{\mathrm{m}_{\lambda} x_E + (-1)(y_E) + (y_{ptd} - \mathrm{m}_{\lambda} x_{ptd})}{\sqrt{\mathrm{m}_{\lambda}^{\,2} + 1}} \tag{4-25}$$

where the 'slope' of the prescribed track, m_{λ}, expressed in degrees, is defined as

$$\mathrm{m}_{\lambda} = \tan(90 - \lambda_{ac}) \tag{4-26}$$

except in the case that the prescribed track is due north or due south. In such a case the slope of the prescribed track is defined as

$$m_{\lambda}=0 \tag{4-27}$$

The tail hook deviation from the prescribed track, d_{ε}, measured in feet, is defined as

$$d_{\varepsilon} = d_{\lambda} - l_{th}\sin\left(\lambda_{ac} - \psi\right) \tag{4-28}$$

This definition results in a negative value for lateral deviation when the tail hook is to the left of the prescribed track, and similarly a positive value for lateral deviation when the tail hook is to the right of the prescribed path.

4.5 SIMULATED APPROACHES

The Navigation System was implemented in the simulation environment and simulations were conducted to validate the systems response. In instances where signals would be transmitted from the carrier to the aircraft perfect transmission has been assumed, i.e. no time delay or signal degradation has been modeled.

Two example approaches are presented here to demonstrate the concept presented. The aircraft is controlled during these approaches by an autothrottle, a track controller and the baseline longitudinal approach controller. These systems are presented in full in chapters 5 and 6.

The first approach has no atmospheric disturbances other than the steady wind associated with the aircraft carrier dynamics. The second approach includes moderate turbulence and aircraft carrier induced turbulence. The steady wind over the deck is 37.5 knots and the aircraft carrier is steaming into the wind at 10 knots.

4.5.1 NO ATMOSPHERIC DISTURBANCE APPROACH

The positions of the aircraft and aircraft carrier during the no atmospheric disturbance approach are presented in Figure 4-5. All position variables are plotted against time to touchdown, t_{td}, which is calculated by the Navigation System as presented in section 4.2. The predicted position of the touchdown point, $\left(x_{E_{ptd}}, y_{E_{ptd}}, z_{E_{ptd}}\right)$, the vertical deviation from the prescribed glide path, h_{ε}, and lateral deviation from the prescribed track, d_{ε}, are presented in Figure 4-6.

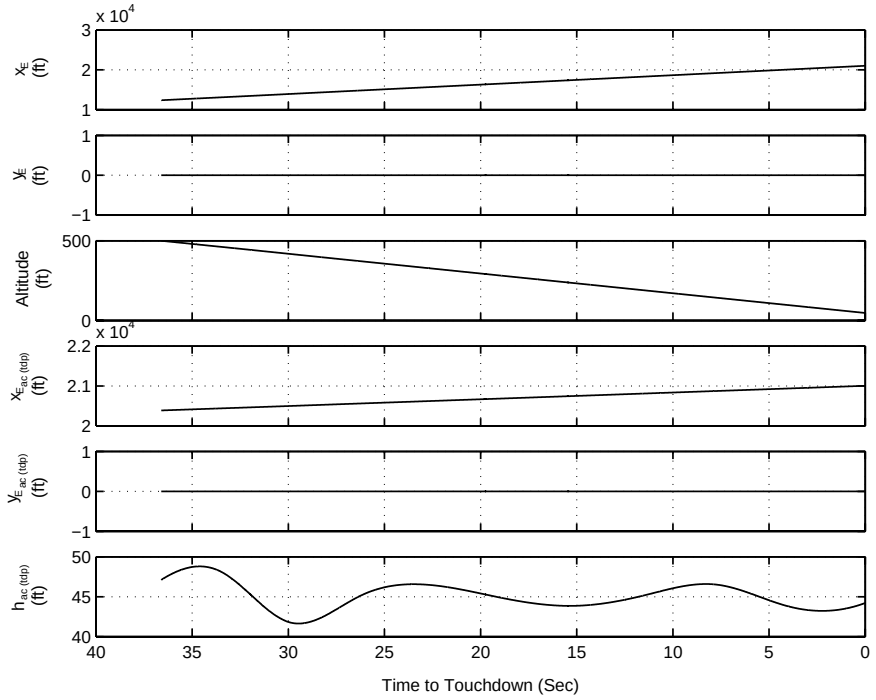

Figure 4-5 Aircraft and Aircraft Carrier Position

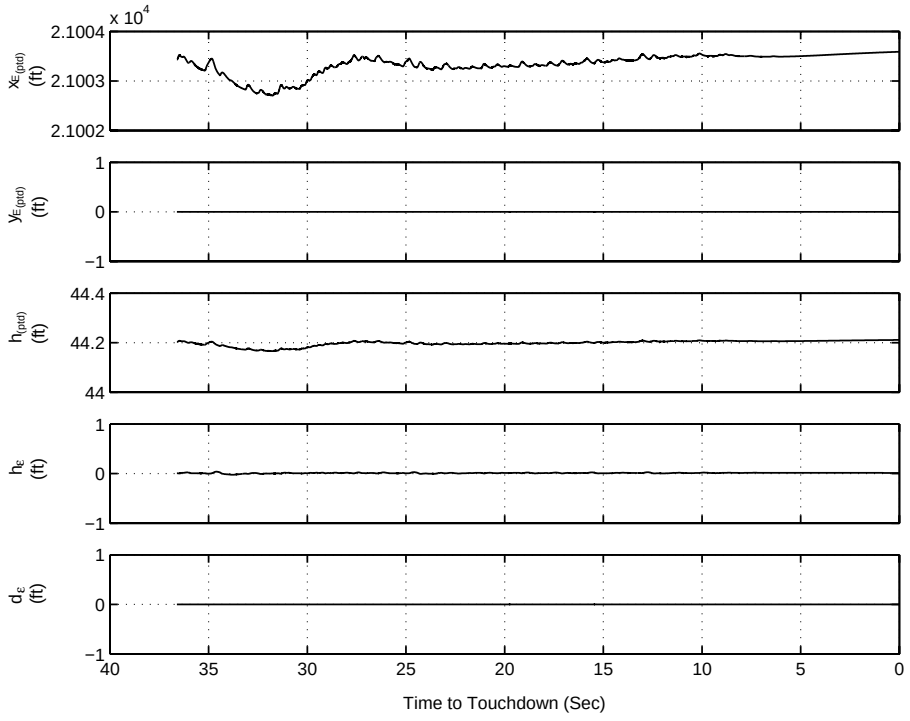

Figure 4-6 Predicted Touchdown Position, Longitudinal and Lateral Deviations

4.5.2 ATMOSPHERIC DISTURBANCE APPROACH

The positions of the aircraft and aircraft carrier during the approach are presented in Figure 4-7. Again, all position variables are plotted against time to touchdown, t_{td}, which is calculated by the Navigation System as presented in section 4.2. The predicted position of the touchdown point, $\left(x_{E_{ptd}}, y_{E_{ptd}}, z_{E_{ptd}}\right)$, the vertical deviation from the prescribed glide path, h_ε, and lateral deviation from the prescribed track, d_ε, are presented in Figure 4-8. The moderate turbulence and carrier induced turbulence velocities are presented in figures 4-9 and 4-10 respectively.

The effect that the turbulence has on the prediction of the position of the touchdown point is evident when this approach is compared with the no turbulence case. As the aircraft progress along the prescribed glide path and track is altered by turbulence, the time to touchdown changes, and hence the predicted position of the touchdown point changes, which in turn leads to a change in prescribed glide path and track. In order to avoid unfavourable coupling, the time to touchdown is averaged over one half of a second as presented in section 4.2.

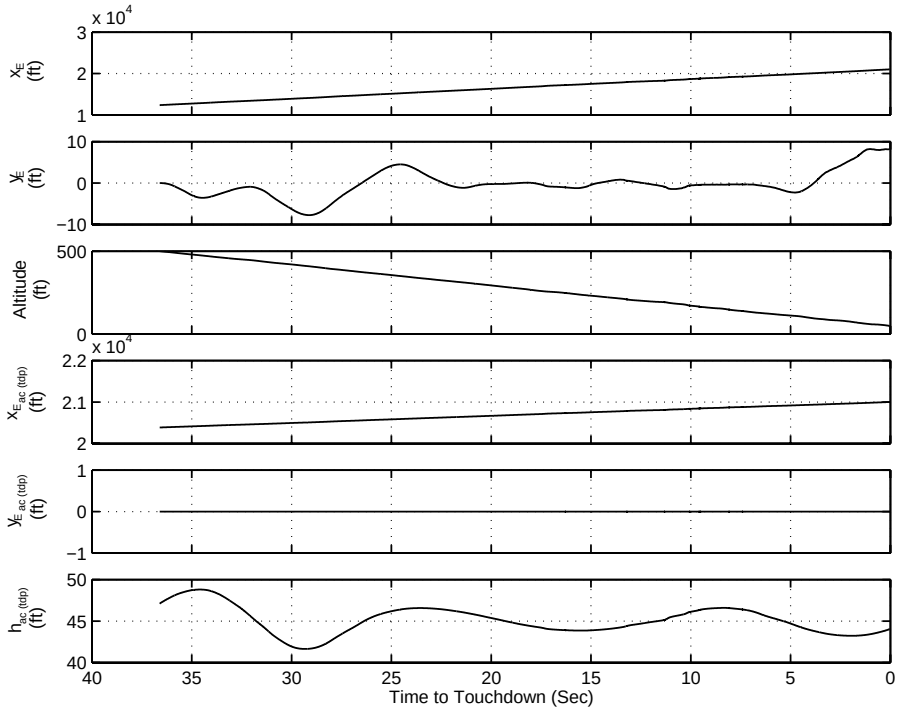

Figure 4-7 Aircraft and Aircraft Carrier Position

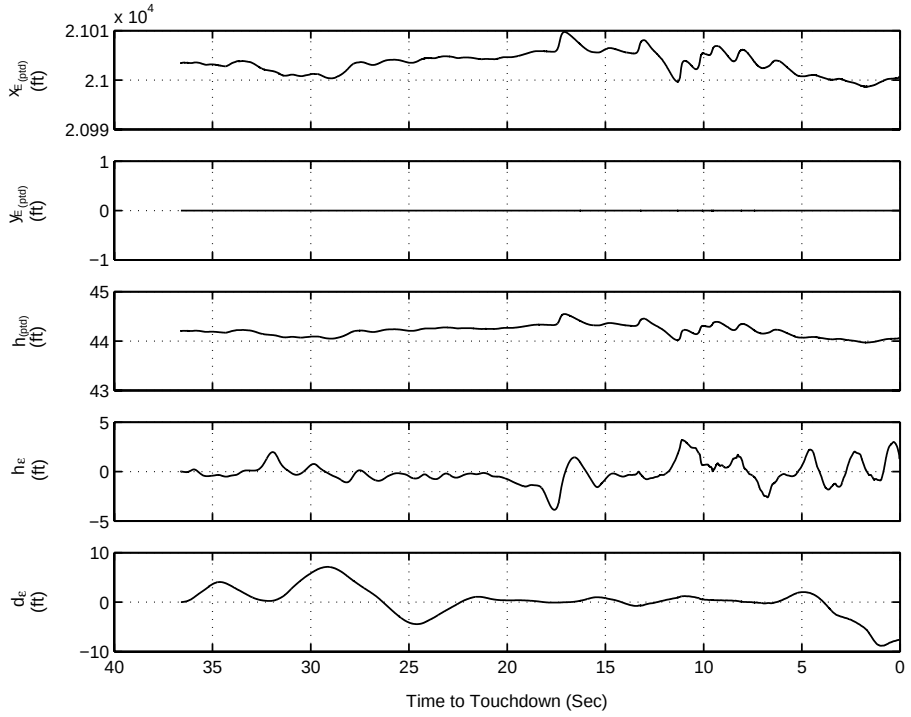

Figure 4-8 Predicted Touchdown Position, Longitudinal and Lateral Deviations

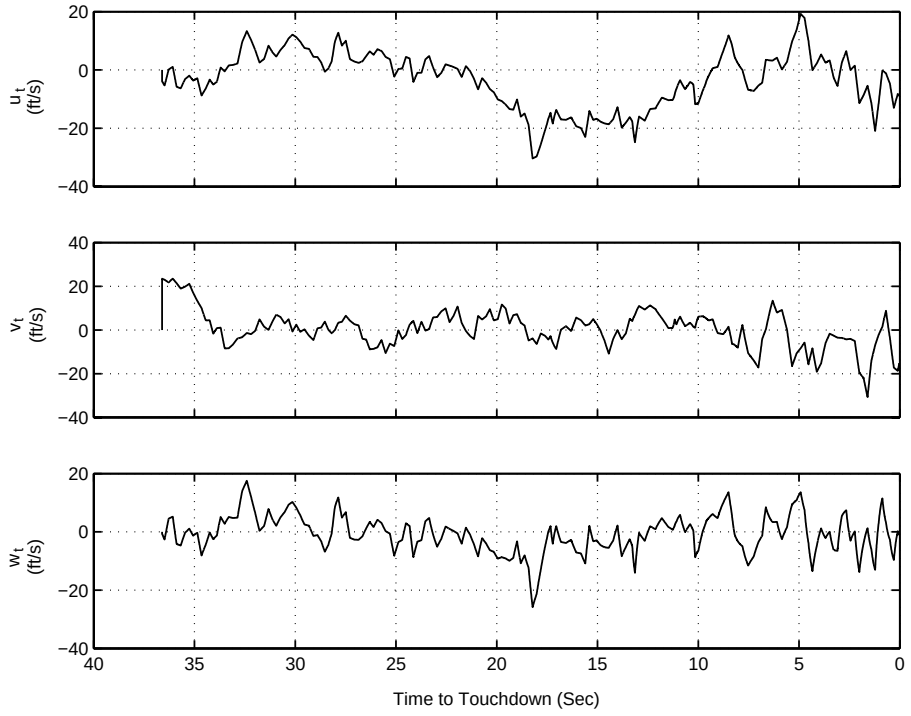

Figure 4-9 Atmospheric Turbulence

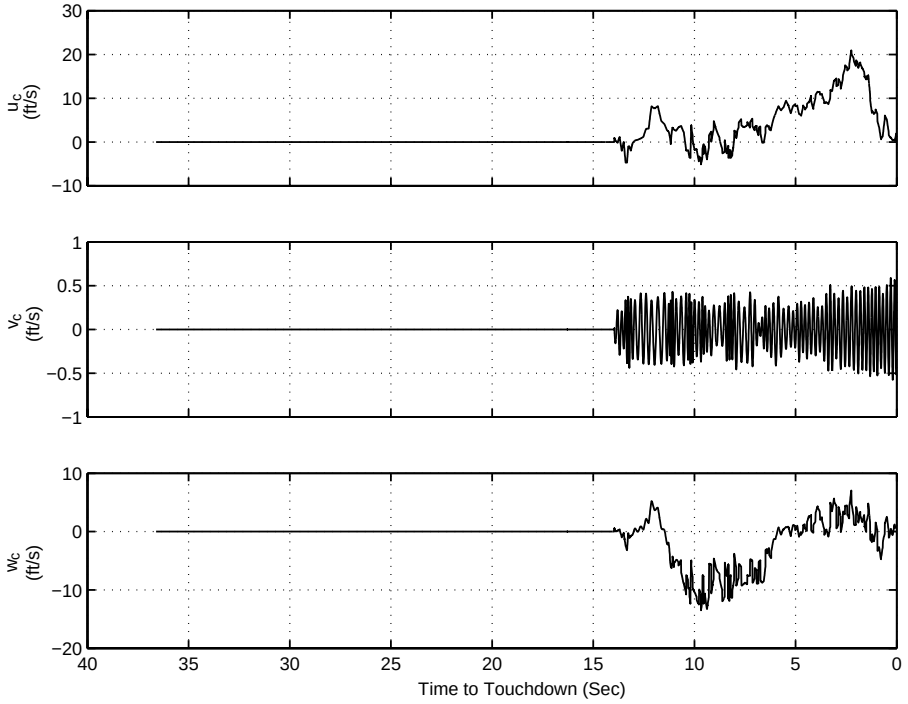

Figure 4-10 Carrier Induced Atmospheric Turbulence

4.6 DISCUSSION

The Navigation System presented here is a central element of this study. Assuming that GPS is used for position and velocity measurement, this system conceptually satisfies the Joint Precision Approach and Landing System requirements, and the systems operation, as applied in this instance, is compatible with current United States Navy operational procedures. The system can be used by piloted aircraft as well and UAVs and facilitates autonomous approaches to landing. In this regard, the system satisfies the constraints imposed upon it from the outset of this study and achieves the associated objectives of this study.

Automatic wave-off monitoring can be provided by the Navigation System based on distance from the aircraft carrier and the vertical and lateral deviations from the desired approach flight path. This facilitates truly autonomous carrier operations and avoids the LSO perspective problem identified by Durand and Wasicko [3].

The most significant contrast between this system and the system currently in use is that this system guides the aircraft to a pseudo-fixed point in space as opposed to a moving point. The system currently in use requires a stabilisation system in order to negate the effects of ship motion on the resulting guidance cues. This adds significantly to the complexity of the system. The system developed in this study does not need such stabilisation systems.

In practice, the prediction of the touchdown point will not be perfect; hence the predicted touchdown point is pseudo-fixed. Assuming that ship motion prediction techniques are suitably tailored for this task it is extremely unlikely that predicted touchdown point will vary significantly during an approach. This will result in more stable approaches, especially in inclement atmospheric conditions as the instability due to ship motion will be effectively removed.

In section 4.5, the concept is shown to operate successfully in the simulated environment. In Chapter 8, this system is extended to allow the aircraft to touchdown when the carrier's pitch attitude is at an optimum condition for landing. The significance of this is that the detrimental effect of pitch attitude on the height that the aircraft passes over the carrier's stern can be minimised, hence increasing the safety level of an approach to landing. This extension is not possible with the current state of the art Navigation System, and, even with less than perfect prediction techniques, provides a step forward in carrier landing navigation strategies.

It is hoped that the demonstration of this concept will provide stimulus to refine the current adaptive prediction methods, or indeed provide motivation to develop a new prediction method specifically for this purpose.

As previously stated, the research undertaken by the Department of Mechanical Engineering at University College London [39,40,41,42,43] is encouraging with regard to the prediction problem. The methods presented by this group appear to be very pure in a mathematical sense. It is thought that if these methods were coupled with prior knowledge of the ship's operating conditions and characteristics, in a sense sacrificing

some of the mathematical purity, that the time horizon of accurate prediction could be extended to a more practical level for this application.

Another approach would be to use several different prediction techniques in parallel. The results of these techniques could be synthesized so as to extract the maximum benefit from each method.

5 AUTOTTHROTTLE AND APPROACH TRACK CONTROLLER

5.1 INTRODUCTION

Three approach controllers have been developed which control the aircraft's approach flight path, as generated by the Navigation System, and approach speed during a carrier landing approach.

The general form of an approach controller is presented in Figure 5-1. The approach controllers' consist of three components (1) An autothrottle, (2) An approach track controller and (3) an approach glide path controller. An autothrottle controls the aircraft's speed via the throttle. A track controller controls lateral deviation from the approach track via ailerons and rudder. These two components are common to all three approach controllers developed. Each of the three approach controllers differs by the manner in which vertical deviation from the approach glide path is controlled. The approach glide path controllers are presented in Chapter 6. A comparative performance analysis of all three approach controllers is presented in Chapter 7.

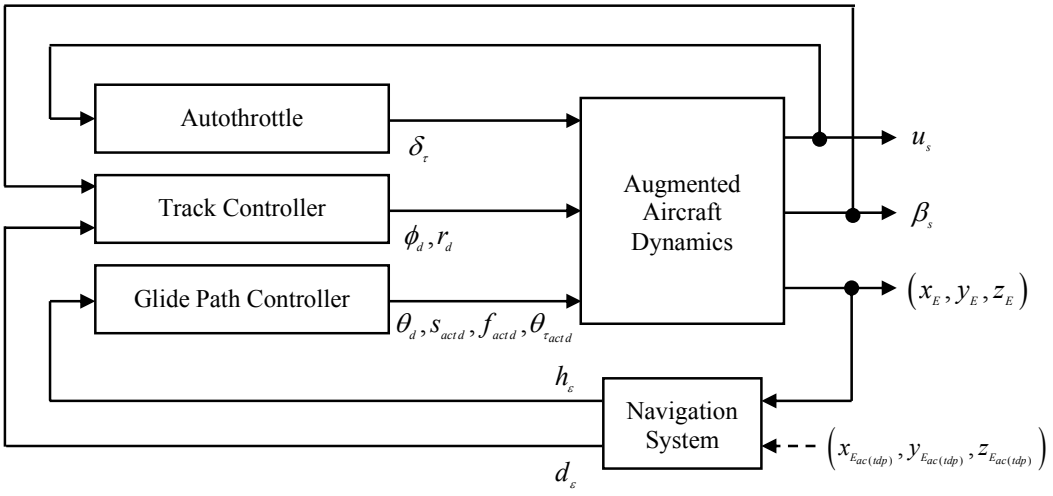

Figure 5-1 Approach Controller

The design and performance of the autothrottle and track controller are presented in the following sections of this chapter. Before reviewing these systems an overview of the design process employed in the development of all controllers is presented.

5.2 DESIGN METHODOLOGY

The design approach is based on standard design methods for classical control systems. Classical control systems have been used as they provide a high level of visibility in the design stage.

The design began with an examination of the performance requirements of each controller along with the constraints on the systems. Published requirements for Automatic Carrier Landing Systems are not available in the public domain and as a result, performance requirements were defined for the performance of the track and approach glide path controllers. These requirements and constraints are presented in the following sections.

From the non-linear simulation model, linearised longitudinal and lateral-directional decoupled models were extracted at the design point. The stability and control characteristics of the linear models were validated against those characteristics presented by Fitzgerald [56].

The appropriate Stability Augmentation System was implemented in the respective linear models. The stability and control characteristics of the augmented aircraft were validated against those characteristics presented by Fitzgerald [56]. The response of the linear models to small control inputs were validated against the response of the non-linear model to the same inputs.

The architecture of the autothrottle, track controller and the three approach glide path controllers were defined using knowledge of the aircraft's behaviour, the requirements and constraints of each system and the knowledge gained through the literature review. Having defined the architecture the control system gains were tuned using Simulink's Non-linear Control Design (NCD) tool.

The NCD tool is an interactive Graphical User Interface (GUI). This tool can be placed in a Simulink model and the signal which is being controlled attached to it. The NCD tool takes the form of a response plot which presents the signal being controlled against time. Performance constrains are presented on this response plot. These constraints are user defined.

During this design process, step inputs to the system being developed were used as inputs to the model. The tool requires that initial values of the controller gains are defined. The NCD tool then runs the simulation using the initial controller gain values and compares the response against the constraints. If the response is outside the defined constraints, the controller gains are varied and the new response is plotted. This process iterates until the response is within the performance constraints.

This tool is very efficient when tuning controller gains, however care has to be exercised in its use as this tool does not replace good engineering judgement. This tool is a mathematical process and the response characteristics are limited to the time period defined in the simulation model. Therefore the long term performances of the resultant controller gains were examined before proceeding with the design process.

The controllers used are Proportional Plus Integral (P+I) and Proportional Plus Integral Plus Derivative (PID) controllers. The proportional control provides feedback of the error signal. The integral term will drive the error to zero and the derivative term will smooth the transient response. The disadvantage of using a proportional controller is that if used in isolation it will have some error in its performance accuracy. The main disadvantage of an integral controller is that it introduces a pole at the origin on the s-plane together with 90 degree phase lag and is therefore destabilising. The main disadvantage of the derivative controller is that it is insensitive to slow varying error signals which results in drift and it can introduce noise.

Having selected the control system gains in this manner, the frequency response characteristics of the controller were examined. For all controllers, the minimum acceptable gain margin was defined as 6 db and the minimum acceptable phase margin was defined as 30 degrees. These minimums are suggested by McLean [47].

The Military Specification document for Flight Control Systems Design, Installation and Test of Piloted Aircraft, Mil-F-9490 [76] was not available for reference; however Kanade et al. [77] quote Mil-F-9490 as requiring a minimum phase margin of 45 degrees and minimum gain margin of 6 db. This came to light after the controllers were designed and it was decided not to amend the design as a 30 degree phase margin minimum is adequate for the purposes of this study.

The performance of the controllers was then assessed in the non-linear simulation model. This performance assessment consisted of step responses and the response to atmospheric disturbances. The final assessment consisted of testing the autothrottle, track controller and each of the approach glide path controllers in the non-linear simulation environment during approaches to landing using varying degrees of atmospheric disturbance and ship motion.

This process is an iterative process and several iterations between the linear and the non-linear simulation environments were required until satisfactory performance was achieved.

5.3 AUTOTHROTTLE

Accurate control of airspeed during any approach to landing is paramount to a safe and efficient approach. This is especially true in the aircraft carrier landing environment which is dominated by atmospheric disturbances. It should be noted that the speed loop of the pitch stability augmentation system presented in Chapter 3 is disengaged when an autothrottle is engaged.

5.3.1 PERFORMANCE CRITERIA

Definitive performance requirements for carrier based UAVs were unable to be sourced during the course of this study. Similarly, performance requirements for Automatic Carrier Landing Systems were unable to be sourced due to security clearance restrictions. As a result, existing public domain performance requirements for piloted aircraft and UAVs have been used in addition to sound engineering judgement.

Prosser and Wiler [78] present a first attempt at defining flying qualities requirement for Remotely Piloted Vehicles (RPV), based largely on military specifications for flying qualities of piloted aircraft, Mil-F-8785B [79]. Prosser and Wiler suggest that an Autothrottle system should maintain airspeed within ±5 knots or ±2%, whichever is greater, and that any periodic oscillations within this limit shall not interfere with mission performance.

5.3.2 SYSTEM ARCHITECTURE

The Autothrottle system architecture is presented in Figure 5-2. While the Proportional-Plus-Integral (P+I) control of the error signal is as developed by Fitzgerald [56], the control system gains were optimised using the Simulink NCD tool.

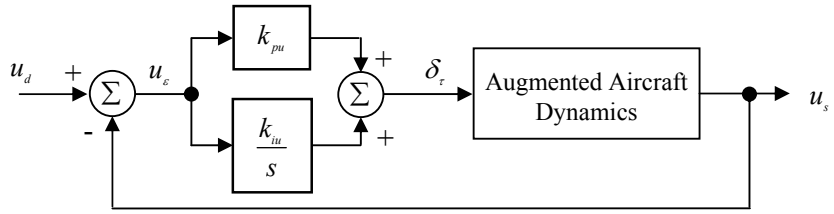

Figure 5-2 Autothrottle Architecture

The control law for the autothrottle controller is defined as

$$\delta_\tau = k_{pu} u_\varepsilon + k_{iu} \int u_\varepsilon dt \tag{5-1}$$

The control system gains are selected as

$$\begin{aligned} k_{pu} &= 659 \text{ RPM/ft/s} \\ k_{iu} &= 15.64 \text{ RPM/ft/s} \end{aligned} \tag{5-2}$$

5.3.3 PERFORMANCE ASSESSMENT USING THE LINEAR MODEL

The open loop frequency response characteristics of the autothrottle are presented in the form of a Bode diagram in Figure 5-3. The autothrottle control loop is broken along the feedback path. The phase margin is 98 degrees at 1.42 rad/s and the gain margin is infinite.

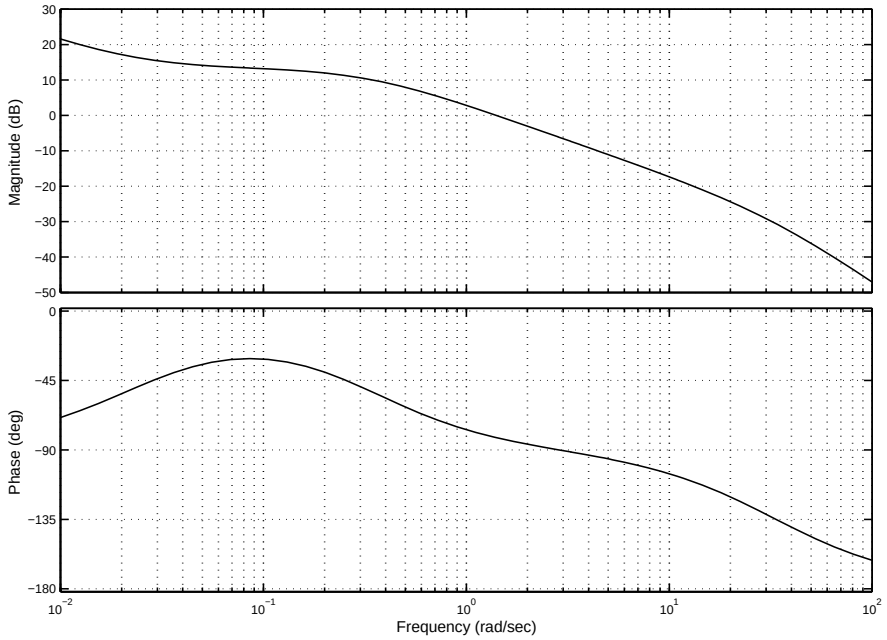

Figure 5-3 Autothrottle Open Loop Bode Diagram

The closed loop frequency response characteristics are presented in the form of a Bode diagram in Figure 5-4. The closed loop bandwidth is 1.15 rad/s. No other loops are active for this response.

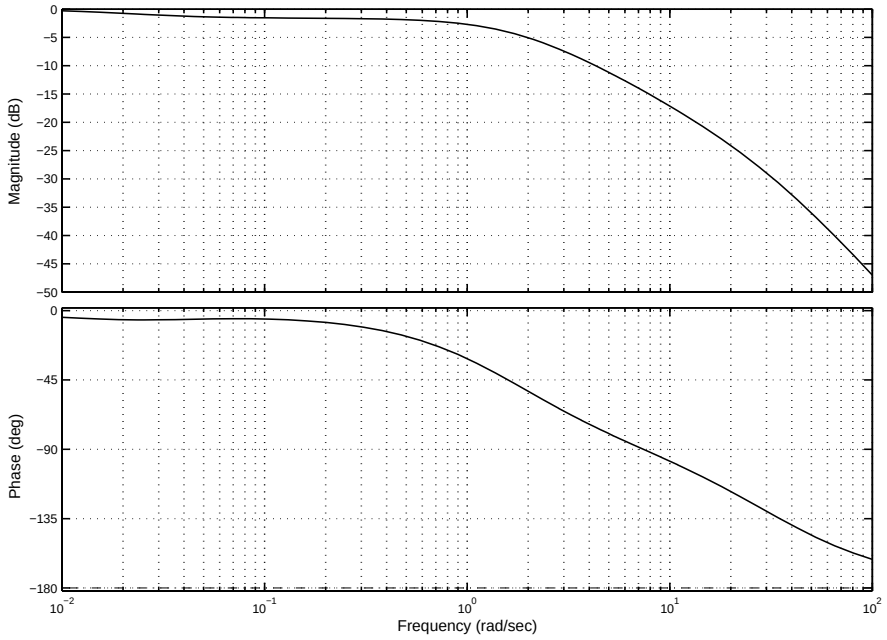

Figure 5-4 Autothrottle Closed Loop Bode Diagram

The aircraft and autothrottle response to a unit step airspeed demand is presented in Figure 5-5. All variables presented in Figure 5-5 are perturbations around the trim flight condition, except for altitude and normal acceleration which are presented in true form. The rise time of the response is 1.14 seconds and the settling time is 2.45 seconds with no overshoot.

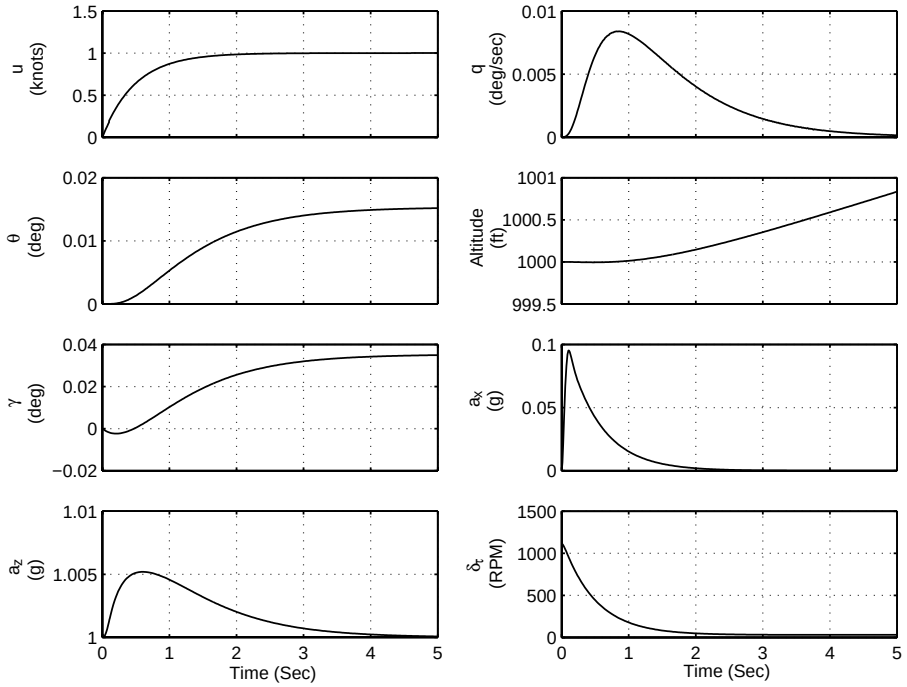

Figure 5-5 Autothrottle Response to Unit Step Demand

5.3.4 PERFORMANCE ASSESSMENT USING THE NON-LINEAR MODEL

The Autothrottle response to a rectangular pulse speed demand is presented in Figure 5-6. It should be noted that the baseline glide path controller, which is presented in Chapter 6, is actively controlling altitude deviations due to velocity change. It can be seen that the performance criteria presented in section 5.3.1 are achieved.

The Autothrottle response to continuous moderate turbulence, as defined by Mil-8785C [63] and generated as presented in Chapter 3, with the baseline glide path controller controlling altitude deviations is presented in Figure 5-7. In this case, the airspeed is controlled to within ±0.1 knots, achieving the performance criteria presented

in section 5.3.1. It should be noted that engine speed is presented as a perturbation about the trim value, while all other variables are presented in true form.

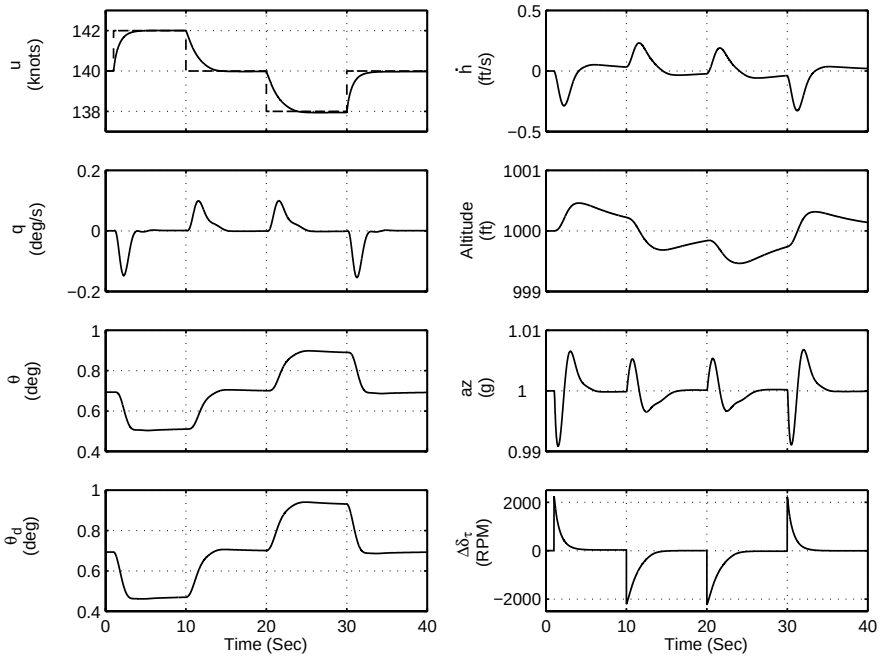

Figure 5-6 Autothrottle Response to Rectangular Pulse Speed Demand

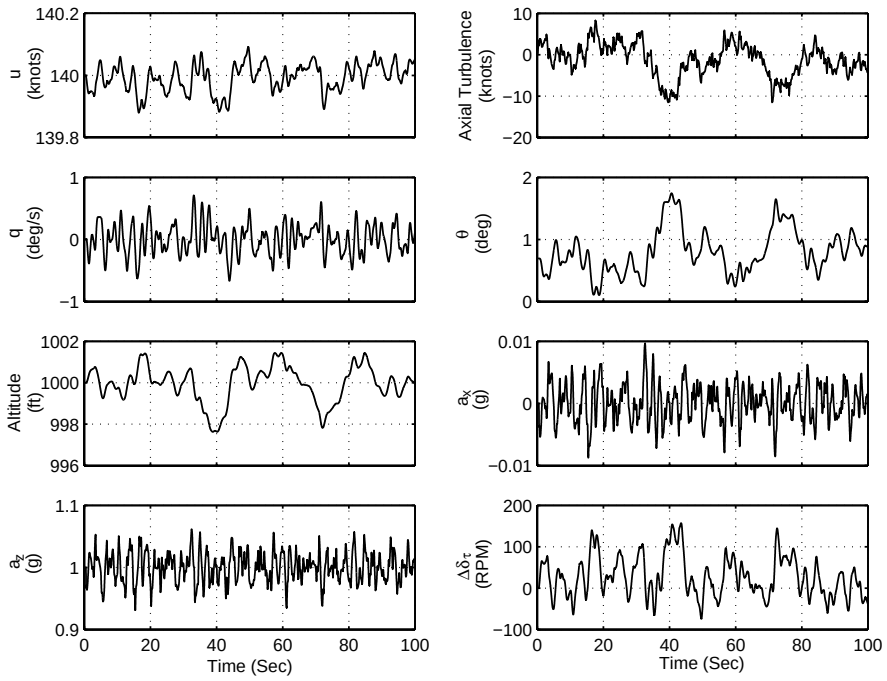

Figure 5-7 Autothrottle Response to Continuous Moderate Axial Turbulence

5.4 TRACK CONTROLLER

Flying an approach onto the tight confines of the landing area of an aircraft carrier deck dictates precise control of the aircraft's lateral position. A track controller has been developed which controls the aircraft with respect to lateral position deviation from the desired track.

5.4.1 PERFORMANCE CRITERIA

Prosser and Wiler [78] suggest that a heading hold autopilot should maintain the aircraft in its existing heading when engaged within a static accuracy of ±0.5 degrees in smooth air. When a heading autopilot is used to change heading, the system shall automatically turn through the smallest angle to achieve the heading change, and the bank angle while turning to the selected heading shall provide satisfactory turn rates and preclude impending stall. The aircraft shall not roll in a direction other than the direction required for the aircraft to assume its proper bank angle. In addition, the roll-in and roll-out shall be accomplished smoothly with no disturbing variation in roll rate.

Many of these points are relevant to the operation of the track controller, however further performance requirements were imposed. In calm air a lateral position error of 4 feet shall be corrected within five seconds with minimal sideslip during correction within ± 0.5 feet. The value of 4 feet was selected through investigation of the effects of varying lateral turbulence levels on aircraft lateral position. Atmospheric disturbances shall be attenuated. For steady state operation, track error shall not be greater than ± 0.5 feet and sideslip angle should be zero.

5.4.2 SYSTEM ARCHITECTURE

The track controller system architecture is presented in Figure 5-8. This controller contains two components. The aircraft's lateral position is controlled via ailerons while the aircraft's sideslip is controlled via the rudder. The input to the lateral position controller is lateral position error as defined in Chapter 4. The input to the sideslip controller is measured sideslip angle.

The sideslip controller ensures that the aircraft aligns itself with the approach track. This ensures that the aircraft does not drift, especially important when close to the carrier deck. Ideally the aircraft should touchdown on the deck with zero sideslip. Any lateral velocity at touchdown has the effect of inducing a side load on the landing gear. The sideslip controller also provides turn coordination.

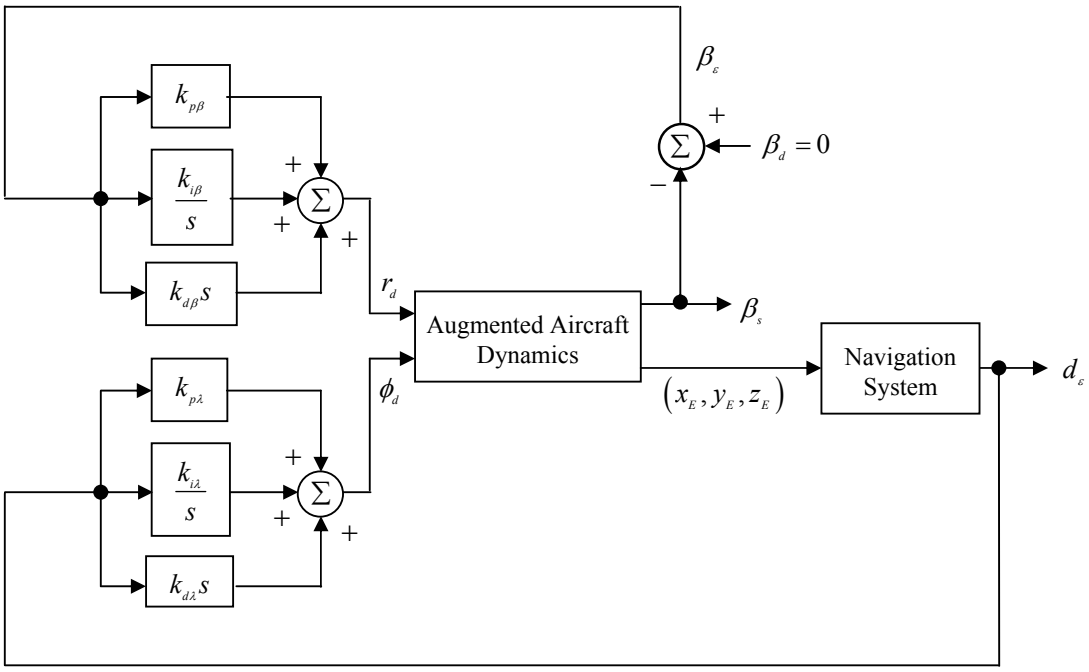

Figure 5-8 Track Controller System Architecture

The control law for the track controller is defined as

$$\phi_d = k_{p\lambda}\lambda_\varepsilon + k_{i\lambda}\int \lambda_\varepsilon dt + k_{d\lambda}\frac{d\lambda_\varepsilon}{dt} \tag{5-3}$$

where the control system gains are selected as

$$k_{p\lambda} = -0.1253 \text{ rad/ft}$$

$$k_{i\lambda} = -0.00022 \text{ rad/ft} \tag{5-4}$$

$$k_{d\lambda} = -0.255 \text{ rad/ft}$$

The control law for the sideslip controller is defined as

$$r_d = k_{p\beta}\beta_\varepsilon + k_{i\beta}\int \beta_\varepsilon dt + k_{d\beta}\frac{d\beta_\varepsilon}{dt} \tag{5-5}$$

The control system gains are selected as

$$k_{p\beta} = -3.72 \quad \text{rad/rad}$$

$$k_{i\beta} = -4.49 \quad \text{rad/rad} \tag{5-6}$$

$$k_{d\beta} = -0.49 \quad \text{rad/rad}$$

It was found through testing that in order to optimise the systems performance for both steady wind and atmospheric disturbance operation, the bank angle demand, ϕ_d, should be limited to 6 degrees. This is implemented for the responses presented in section 5.4.4.

5.4.3 PERFORMANCE ASSESSMENT USING THE LINEAR MODEL

The open loop frequency response characteristics of the sideslip controller are presented in the form of a Bode diagram in Figure 5-9. The control loop is broken at the output of the sideslip sensor. The roll Stability Augmentation System loops are closed. The phase margin is 88.5 degrees at 0.56 rad/s and the gain margin is 18.4 db at 6.28 rad/s.

The closed loop frequency response characteristics of the sideslip controller are presented in the form of a Bode diagram in Figure 5-10. The roll Stability Augmentation System loops are closed. The closed loop bandwidth is 0.58 rad/s. This bandwidth is consistent with the fact that the aircraft's directional dynamics are slower than pitch and roll.

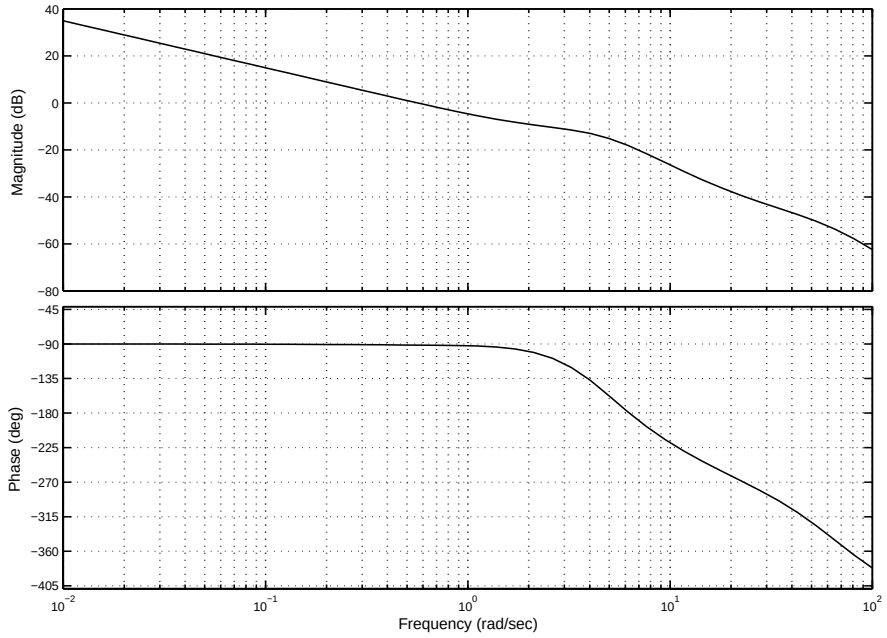

Figure 5-9 Sideslip Controller Open Loop Bode Diagram

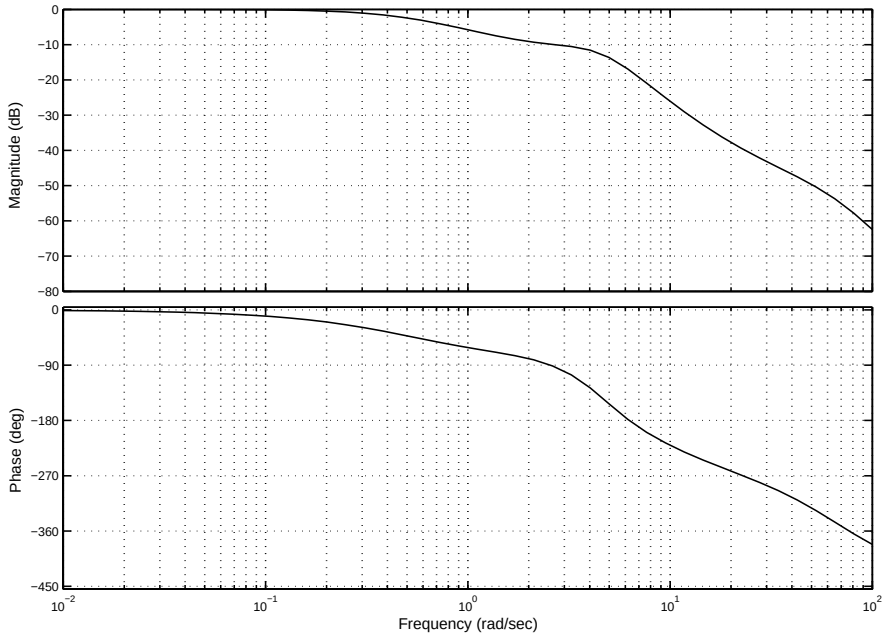

Figure 5-10 Sideslip Controller Closed Loop Bode Diagram

The open loop frequency response characteristics of the lateral position controller are presented in the form of a Bode diagram in Figure 5-11. The Navigation System is not included in this response. Lateral position feedback was used to emulate the Navigation

System in the linear simulation model. The control loop is broken along the lateral position feedback loop. The sideslip control loop and yaw Stability Augmentation System loops are closed. The phase margin is 144 degrees at 1.76 rad/s and the gain margin is 49 db at 12.6 rad/s.

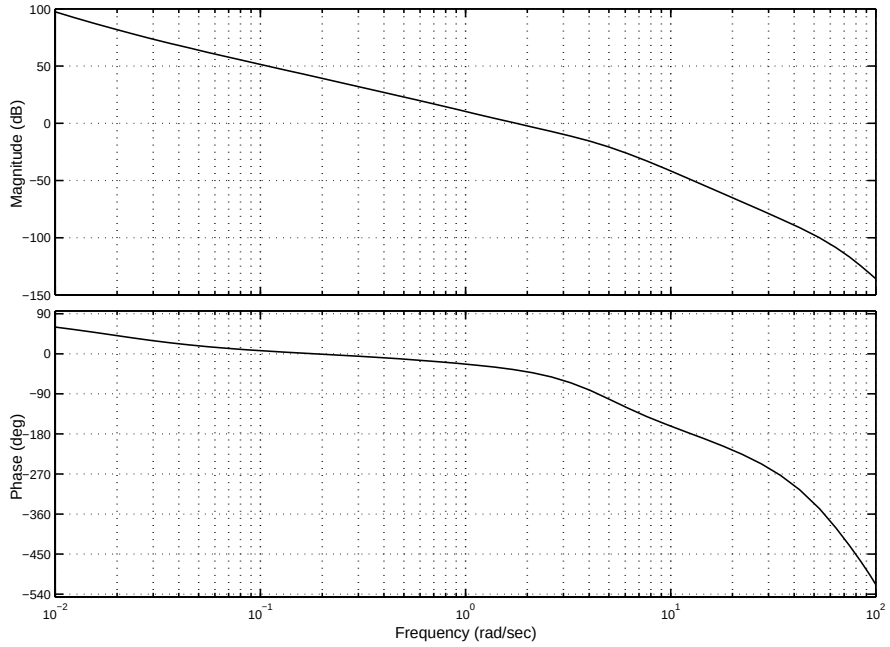

Figure 5-11 Lateral Position Controller Open Loop Bode Diagram

The closed loop frequency response characteristics of lateral position controller are presented in the form of a Bode diagram in Figure 5-12. The sideslip control loop and yaw Stability Augmentation System loops are closed. The closed loop bandwidth is 1.21 rad/s.

The aircraft's response to a unit step sideslip demand is presented in Figure 5-13. The rise time is 6.5 seconds and the settling time is 8 seconds. The roll Stability Augmentation System loops are closed for this response.

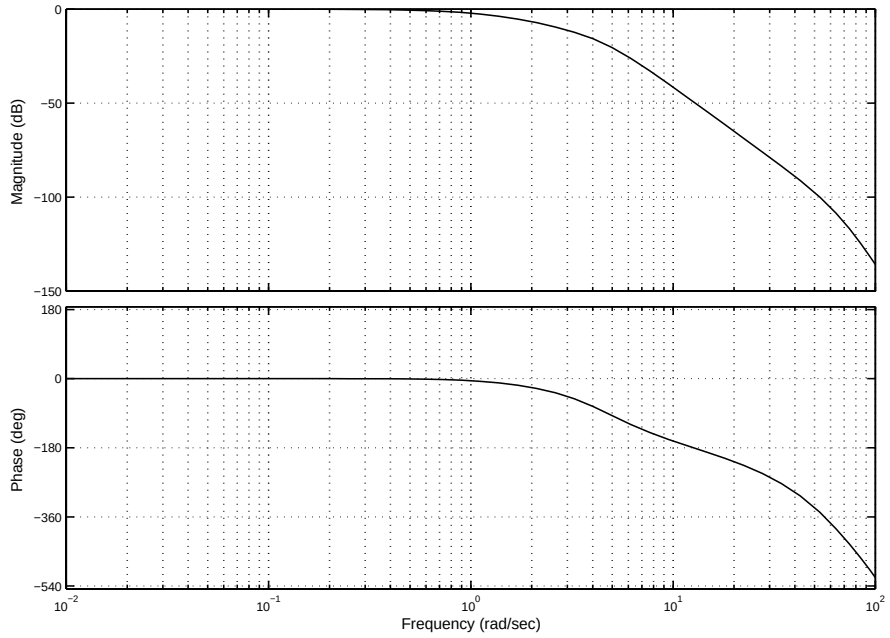

Figure 5-12 Lateral Position Controller Closed Loop Bode Diagram

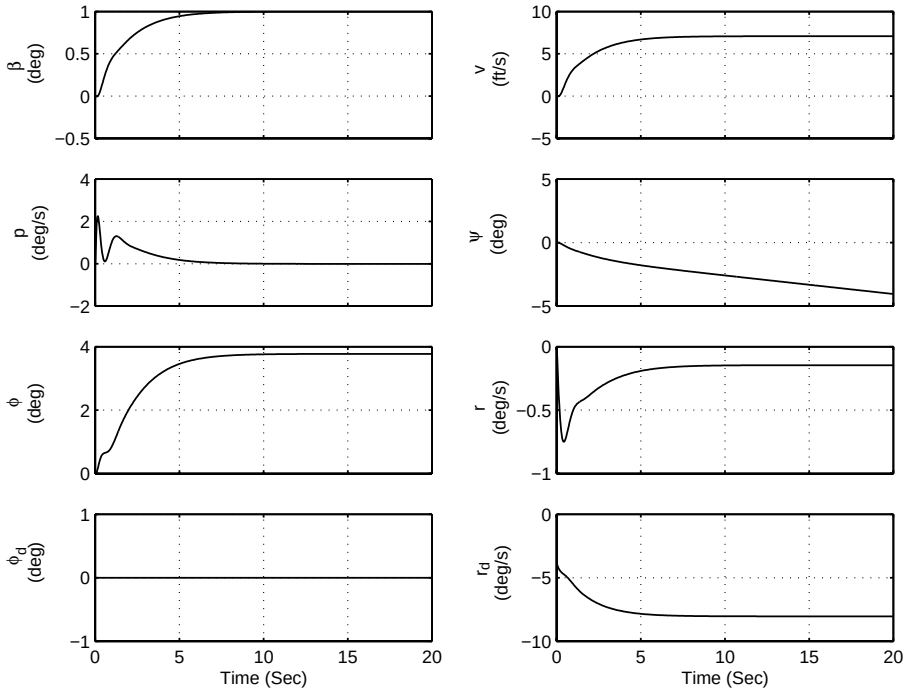

Figure 5-13 Sideslip Controller Response to a Unit Step Demand

The aircraft's response to a unit lateral position demand is presented in Figure 5-14. The rise time is 7.2 seconds and the settling time is 13.5 seconds. The effects of adverse

aileron yaw are evident in this response plot. As with the closed loop frequency response, the Navigation System is not included and the control loop is closed using lateral position. The sideslip and yaw Stability Augmentation System loops are closed.

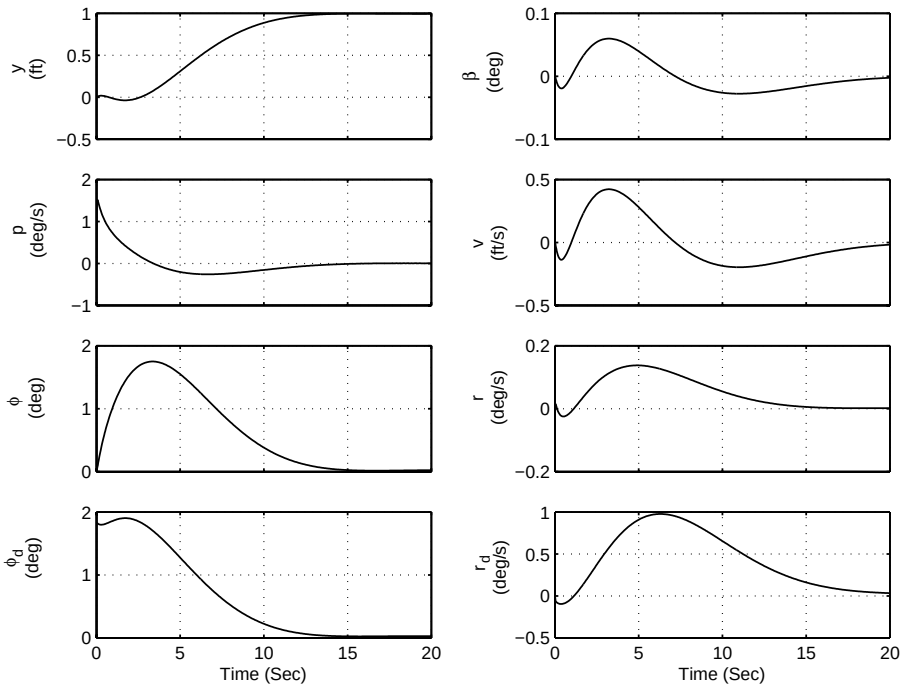

Figure 5-14 Lateral Position Controller Response to a Unit Step Demand

5.4.4 PERFORMANCE ASSESSMENT USING THE NON-LINEAR MODEL

The track controller response to a rectangular pulse lateral position demand is presented in Figure 5-15. The track controller response to continuous moderate lateral turbulence is presented in Figure 5-16. The autothrottle and baseline approach glide path controllers are active for both scenarios. The baseline approach glide path controller is presented in Chapter 6. The performance criteria presented in section 5.4.1 can be seen to be achieved. Considering the inherent atmospheric conditions of the carrier landing environment control of lateral position deviation in turbulence is an important design factor.

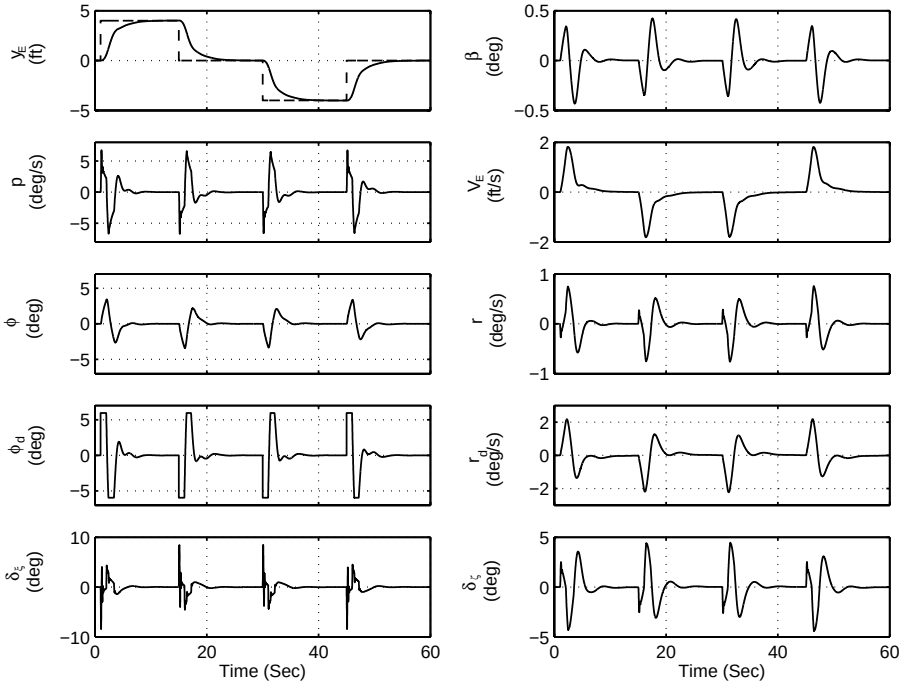

Figure 5-15 Track Controller Response to Rectangular Pulse Lateral Position Demand

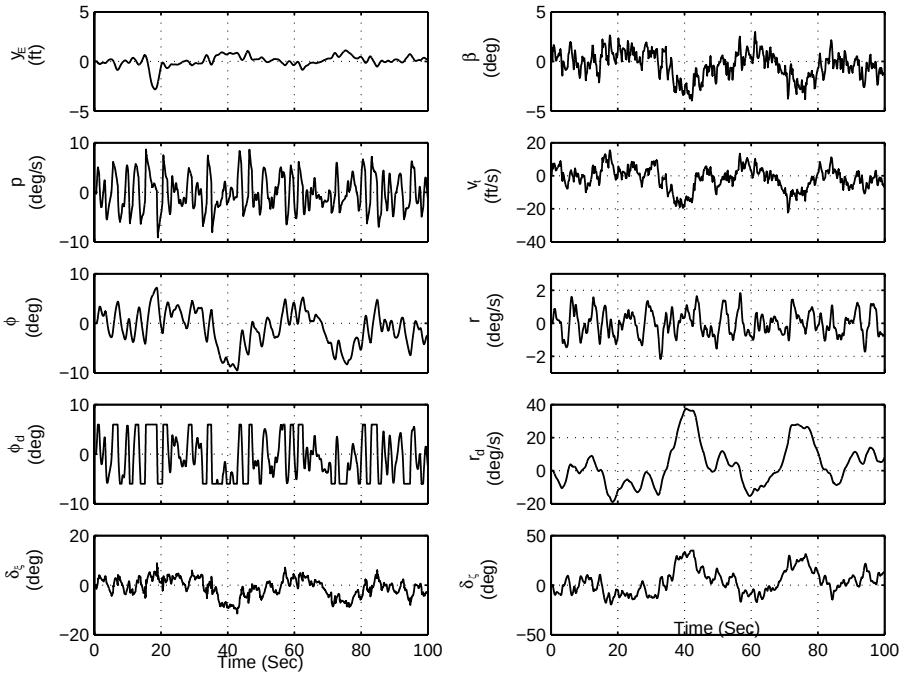

Figure 5-16 Track Controller Response to Continuous Moderate Turbulence

6 APPROACH GLIDE PATH CONTROLLERS

6.1 INTRODUCTION

Three different approach glide path controllers have been developed to assess three different control strategies for suitability to the carrier landing task. The first, or baseline, approach glide path controller controls vertical deviation from the approach glide path using elevator control.

The second approach glide path controller controls vertical deviation from the approach glide path using Direct Lift Control effected through trailing edge flaps and spoilers. The original intention was to develop a controller which responded to vertical deviations from the approach glide path with pure vertical translation of the aircraft. This required a constant pitch attitude to be maintained throughout the approach. A controller was developed which maintained a constant pitch attitude through trailing edge flap feedforward to elevator, to compensate for trailing edge flap induced pitching moment and active control of pitch attitude using elevator control.

This approach glide path controller was found to be unsuitable for approach glide path control due to its slow response to large turbulence induced vertical deviations. A second Direct Lift Control strategy was examined. In this case the baseline approach glide path controller was augmented to include Direct Lift Control. This strategy was found to have acceptable performance in the presence of atmospheric turbulence.

The third approach glide path controller comprises an addition of thrust vectoring to the Direct Lift Control system. In this instance, thrust vectoring is used to alleviate the magnitude of elevator pitch control required during the approach. The motivation for this has been presented in Chapter 1 and is concurred with by Friehmelt [81].

6.2 BASELINE APPROACH GLIDE PATH CONTROLLER

The baseline approach glide path controller controls vertical deviation via elevator. Tight control of vertical deviation is especially critical as the aircraft passes over the aircraft carriers ramp, a point on the approach which approximately coincides with the peak atmospheric disturbances due to the presence of the carrier. Therefore the approach glide path controller has been optimised for maximum attenuation of atmospheric disturbances.

6.2.1 PERFORMANCE CRITERIA

In the absence of available published requirements, the baseline approach glide path controller was designed to provide tracking of ±0.5 feet in steady wind conditions, attenuation of atmospheric disturbances and shall be capable of correcting a 4 foot deviation within 2 seconds to within ±0.75 feet.

As motion of the touchdown point directly alters the vertical deviation from the desired glide path, the design deviation of 4 feet was chosen as it is representative of a sudden displacement of the desired touchdown point in a heavy sea state.

6.2.2 SYSTEM ARCHITECTURE

The baseline approach glide path controller architecture is presented in Figure 6-1. The input to the system is vertical deviation, h_ε, calculated by the Navigation System as presented in Chapter 4. A pitch attitude demand, θ_d, is calculated based on Proportional-Plus-Integral-Plus-Derivative (PID) control of vertical deviation.

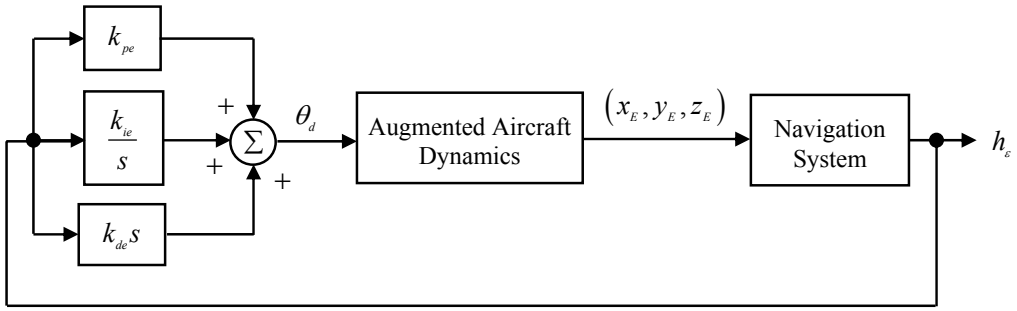

Figure 6-1 Baseline Glide Path Controller Architecture

The control law for the baseline approach glide path controller is defined as

$$\theta_d = k_{pe} h_\varepsilon + k_{ie} \int h_\varepsilon dt + k_{de} \frac{dh_\varepsilon}{dt} \tag{6-1}$$

The control system gains are selected as

$$k_{pe} = 0.00731 \text{ rad/ft}$$

$$k_{ie} = 0.000869 \text{ rad/ft} \tag{6-2}$$

$$k_{de} = 0.00515 \text{ rad/ft}$$

Pitch attitude demand, θ_d, is limited to ± 10 degrees.

6.2.3 PERFORMANCE ASSESSMENT USING THE LINEAR MODEL

Frequency response characteristics and step response of the baseline approach glide path controller presented do not have the Navigation System included. Essentially the Navigation System is a comparator, with the altitude demand a function of predicted touchdown point. The system from which the frequency response characteristics and step response have been extracted is presented in Figure 6-2 where it can be seen that the Navigation System has been replaced by a comparator.

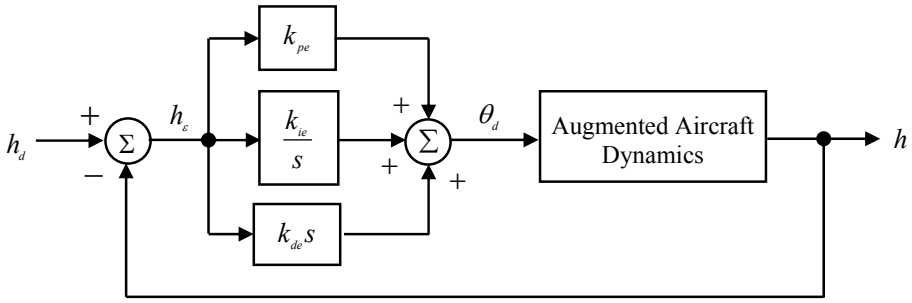

Figure 6-2 Baseline Glide Path Controller Architecture for Linear Model

The open loop frequency response characteristics of the approach glide path controller are presented in the form of a Bode diagram in Figure 6-3. The control loop is broken along the feedback path. The autothrottle loop is closed for this response. The phase margin is 30.2 degrees at 1.05rad/s and the gain margin is 6.89 db at 1.23 rad/s.

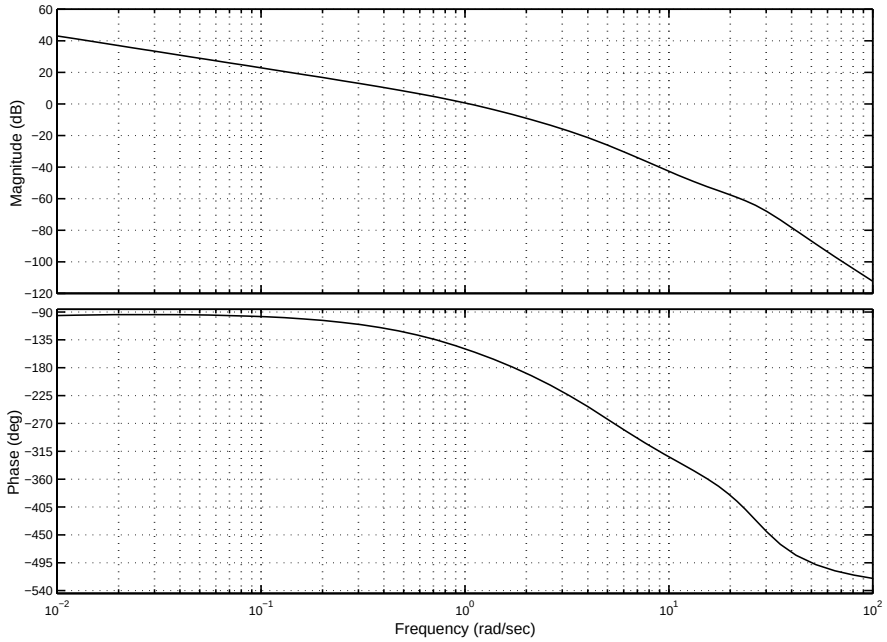

Figure 6-3 Baseline Glide Path Controller Open Loop Bode Diagram

The closed loop frequency response characteristics of the baseline approach glide path controller are presented in the form of a Bode diagram in Figure 6-4. The closed loop bandwidth is 1.83 rad/s. The same additional loops are active for the closed loop response as in the open loop response.

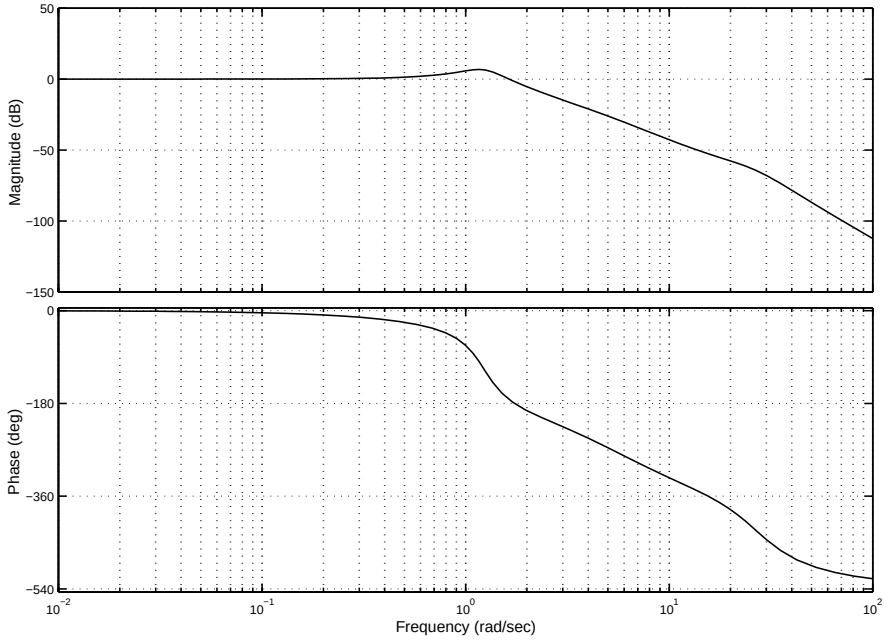

Figure 6-4 Baseline Glide Path Controller Closed Loop Bode Diagram

The aircraft response to a unit step altitude demand is presented in Figure 6-5. All variables are presented as perturbations about their trim value except for normal acceleration and altitude which are presented in their true form. The rise time of the response is 1.3 seconds and the settling time is 2.8 seconds with no overshoot. The autothrottle control loop was closed for this response.

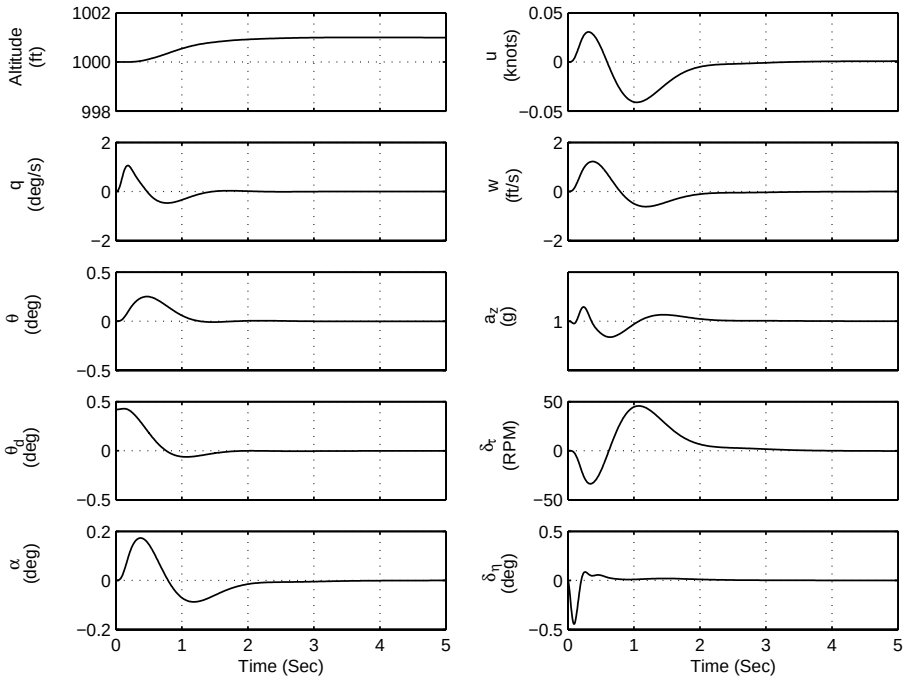

Figure 6-5 Baseline Glide Path Controller Response to Unit Step Demand

6.2.4 PERFORMANCE ASSESSMENT USING THE NON-LINEAR MODEL

The baseline approach glide path controller response to a rectangular pulse altitude demand is presented in Figure 6-6 along with the associated autothrottle response. Both systems can be seen to meet their respective performance criteria. The response of the baseline approach glide path controller and autothrottle to continued moderate vertical turbulence over a time period of 100 seconds is presented in Figure 6-7.

The vertical turbulence velocity presented in Figure 6-7 is implemented as an instantaneous velocity increment of the aircraft measured at the centre of gravity of the aircraft. It can be seen that the aircraft's response to turbulence is attenuated and the

aircraft's axial velocity is maintained to within the autothrottle performance specification.

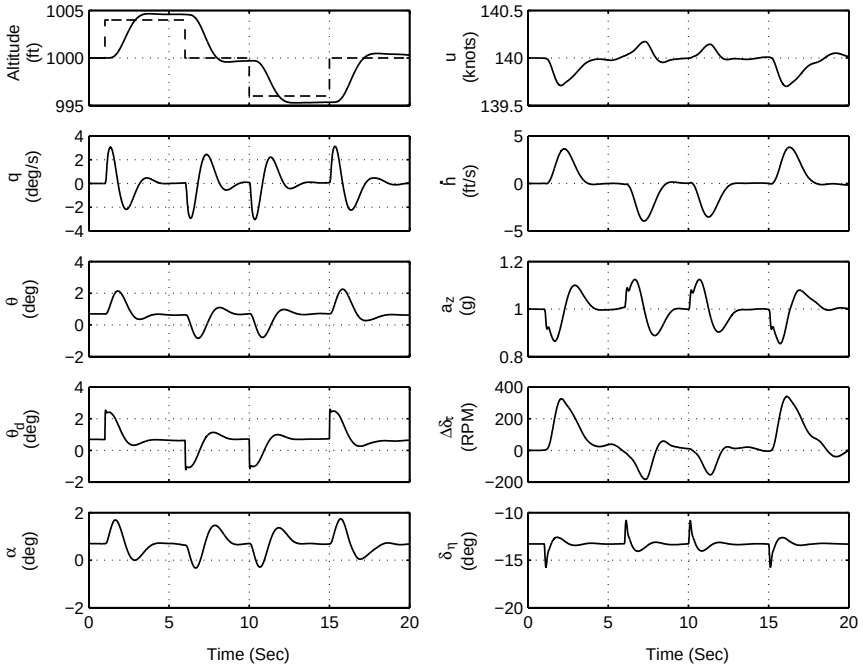

Figure 6-6 Baseline Glide Path Controller Response to Rectangular Pulse Altitude Demand

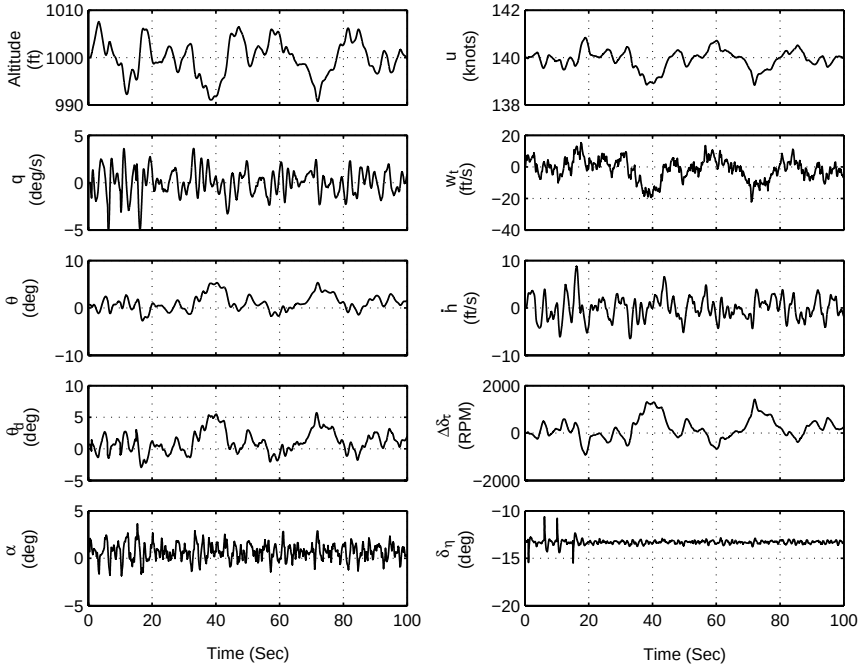

Figure 6-7 Baseline Glide Path Controller Response to Continuous Moderate Vertical Turbulence

6.3 DIRECT LIFT CONTROL APPROACH GLIDE PATH CONTROLLER

A Direct Lift Control system employing trailing edge flaps and spoilers was developed. In order to attain pure vertical translation, it was necessary to develop a constant pitch attitude controller which negates the pitching moment induced by the trailing edge flaps and spoilers. When this system was tested for attenuation of atmospheric disturbances it was found that it responded slowly to non-zero mean disturbances, i.e. a disturbance which is concentrated in one sense, such as wind shear or non-zero mean turbulence. As a result, it was decided that this controller was not suitable for the carrier approach task.

Following the work of Fortenbaugh [22] it was decided to investigate the performance of the baseline approach glide path controller augmented with Direct Lift Control. The Direct Lift Control system and the baseline approach glide path controller were integrated and it was found that no further tuning of the systems were required. The performance of this system was found to be suitable for the carrier approach task.

It should be noted that several iterations of the design procedure presented in Chapter 5 were completed before the decision on the suitability of the constant pitch attitude system for the carrier approach task was made.

6.3.1 CONSTANT PITCH ATTITUDE DIRECT LIFT CONTROL SYSTEM

The philosophy of this control strategy is to provide pure vertical translation of the aircraft with no pitching moment. This is attained by controlling lift through the use of trailing edge flaps and spoilers and negating the associated pitching moment by controlling the pitch attitude through the elevators.

6.3.1.1 PERFORMANCE CRITERIA

The performance criteria for this system are the same as presented in section 6.2.1.

6.3.1.2 SYSTEM ARCHITECTURE

The control system architecture for the constant attitude Direct Lift Control system is presented in Figure 6-8.

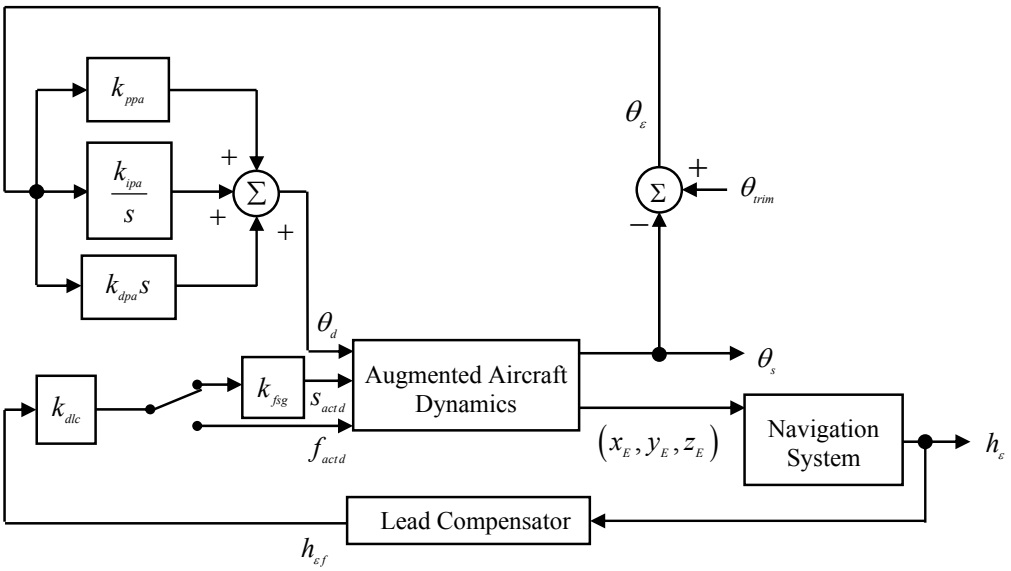

Figure 6-8 Constant Pitch Attitude Direct Lift Control System Architecture

The Direct Lift Control loop consists of a lead compensator filter acting on vertical deviation from the approach glide path. The purpose of this filter is to essentially provide proportional and derivative control of the error signal. The filtered error signal is acted upon by a proportional gain, k_{dlc}. The proportional gain of the filter and the proportional gain k_{dlc} provides a large proportional gain, as suggested by Fortenbaugh [22], which ensures the systems full authority on-off command for gross error control.

Depending on whether the vertical deviation is positive or negative a switch routes the control signal to either the flap or the spoiler actuators. This ensures that only one Direct Lift Control aerodynamic effector is active at any instant. It should also be noted that the Direct Lift Control system's trailing edge flap authority is limited to the range of 20-35 degrees, i.e. the Direct Lift Control system cannot retract the flaps to a deflection angle less than that of the approach configuration.

As the control power of the flaps and spoilers are not identical and they are both being effected by the same controller it is necessary to have a gearing ratio in one of the control paths, hence the gain k_{fsg} represents the ratio of flap to spoiler control power.

The lead compensator was tuned so as to provide the feedback signal with sufficient lead to minimise overshoot. The lead filer has the effect of retracting the active Direct Lift Control effector as the vertical deviation from the approach glide path approaches zero. The lead compensator was tuned to suit the dynamics of the spoiler and trailing edge flap dynamics. The centre frequency of the filter is 3 rad/sec. The large lead ratio of the lead compensator has the drawback of being sensitive to noise.

The transfer function of the filter is defined as

$$\frac{h_{\varepsilon f}}{h_{\varepsilon}} = \frac{1.2s+1}{0.1s+1} \tag{6-3}$$

The Direct Lift Control gains are selected as

$$\begin{aligned} k_{dlc} &= 5 \ \text{deg/ft} \\ \mathrm{k_{fsg}} &= 2 \ \text{deg/deg} \end{aligned} \tag{6-4}$$

A pitching moment is induced due to the deflection of trailing edge flaps, and to a lesser degree the deflection of the spoilers. In order to attain pure vertical translation of the aircraft it is necessary to compensate for this. This is achieved in two ways. A flap to elevator feed forward gain, k_{fe}, is implemented as presented in Figure 6-9. This serves to adjust the elevator angle to negate the pitching moment induced by the trailing edge flap deflection. A pitch attitude PID controller is also implemented, thus providing closed loop control of pitch attitude, as presented in Figure 6-8.

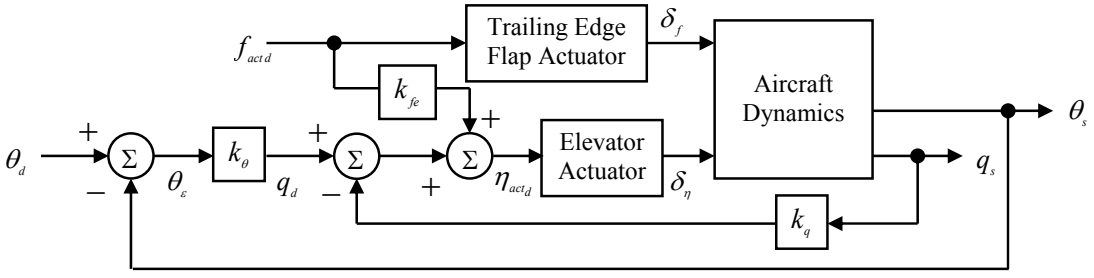

Figure 6-9 Flap to Elevator Feed Forward System

The control law for the pitch attitude controller is defined as

$$\theta_d = k_{ppa}\theta_\varepsilon + k_{ipa}\int\theta_\varepsilon + k_{dpa}\frac{d\theta_\varepsilon}{dt} \tag{6-5}$$

The pitch attitude control system gains and the flap to elevator feed forward gain are selected as

$$\begin{aligned} k_{ppa} &= 3.057 \text{ rad/rad} \\ k_{ipa} &= 1.288 \text{ rad/rad} \\ k_{dpa} &= 1.364 \text{ rad/rad} \\ k_{fe} &= \text{-}0.00955 \text{ rad/deg} \end{aligned} \tag{6-6}$$

6.3.1.3 PERFORMANCE ASSESSMENT USING THE LINEAR MODEL

The open loop frequency response characteristics of the pitch attitude controller are presented in the form of a Bode diagram in Figure 6-10. The control loop is broken along the feedback path. The autothrottle loop is closed for this response. The phase margin is 41.8 degrees at 8.02 rad/s and the gain margin is 7.98 db at 14.3 rad/s.

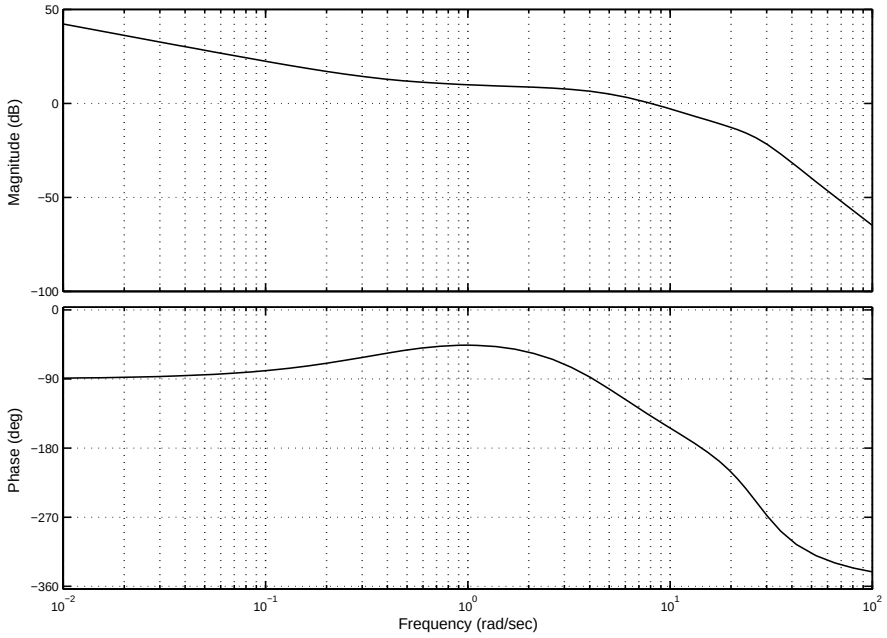

Figure 6-10 Pitch Attitude Controller Open Loop Bode Diagram

The closed loop frequency response characteristics of the pitch attitude controller are presented in Figure 6-11. The closed loop bandwidth is 14 rad/s. The same additional loops are active for the closed loop response as in the open loop response.

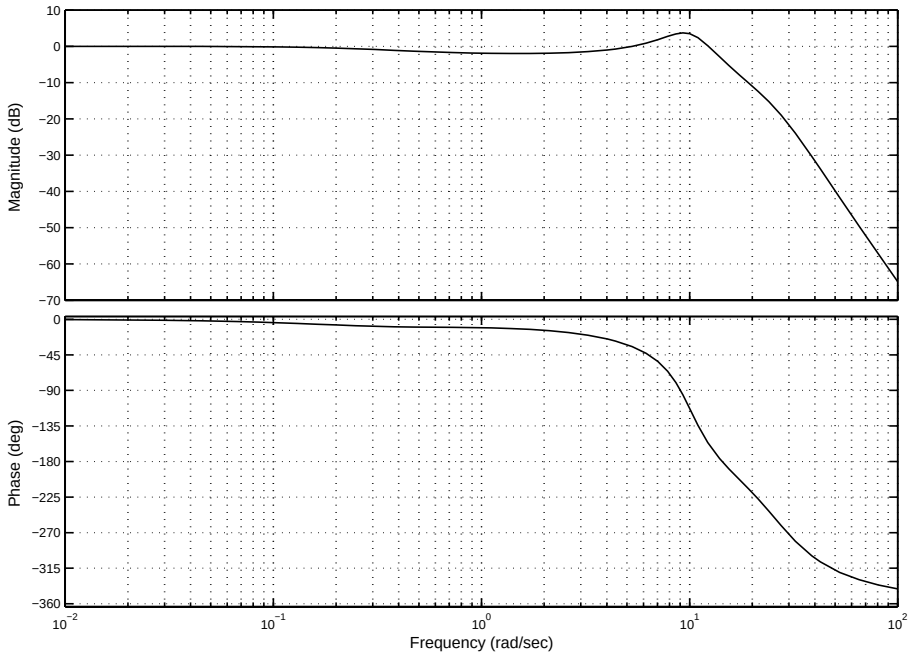

Figure 6-11 Pitch Attitude Controller Closed Loop Bode Diagram

The pitch attitude controller's response to a unit step pitch attitude demand is presented in Figure 6-12. The rise time of the response is 1.47 seconds and the settling time is 6 seconds with no overshoot. The autothrottle control loop was closed for this response. No other loops were active.

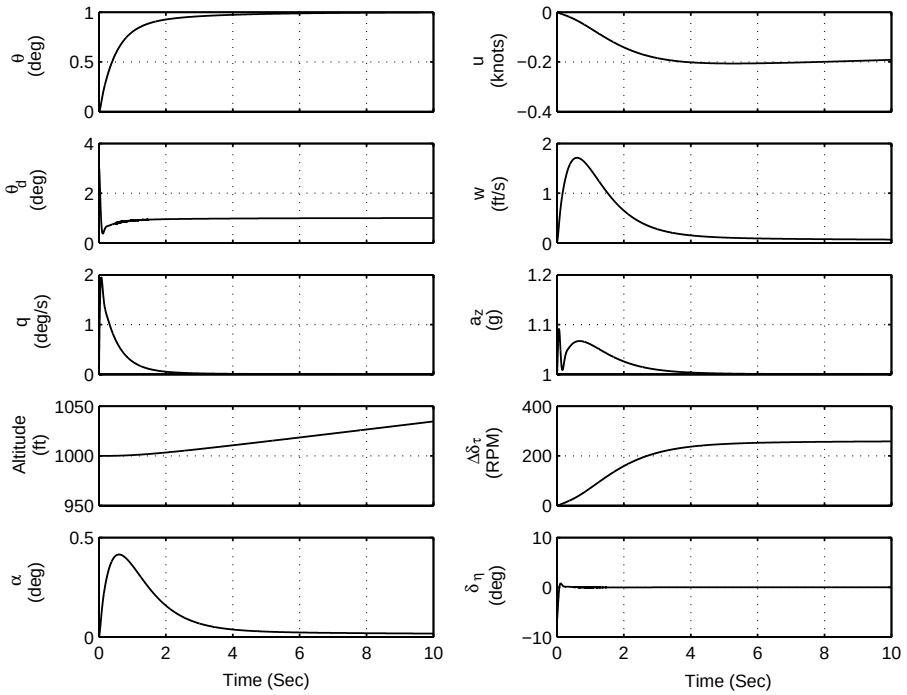

Figure 6-12 Pitch Attitude Controller Response to Unit Step Demand

The open loop frequency response characteristics of the trailing edge flap controller loop are presented in the form of a Bode diagram in Figure 6-13. The autothrottle, pitch attitude and flap to elevator feed forward loops are closed for this response and the spoiler loop is isolated. The Navigation System is again replaced with a comparator and the system is used essentially as an altitude autopilot. The control loop is broken along the altitude feedback path. The phase margin is 51 degrees at 5 rad/s and the gain margin is 10.2 db at 11 rad/s.

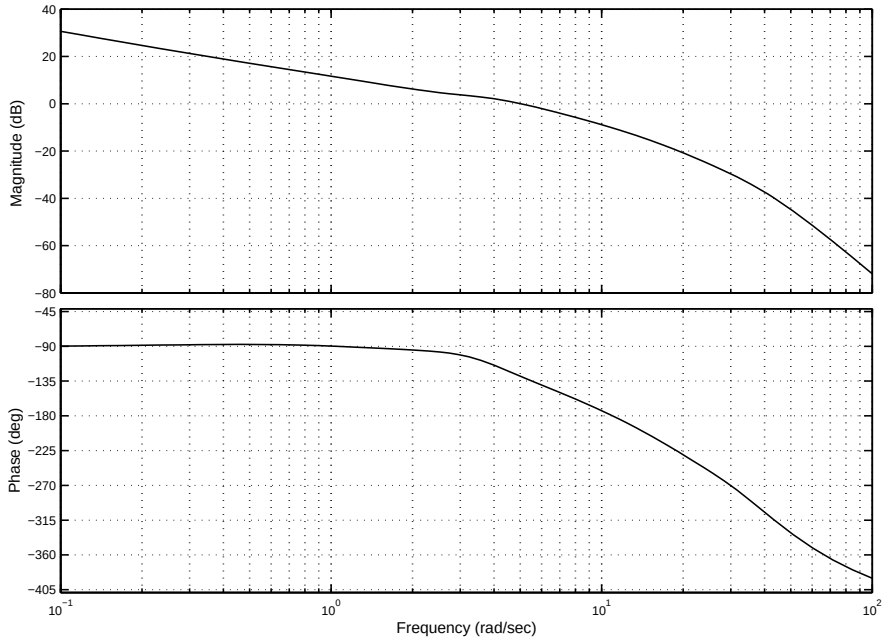

Figure 6-13 Flap Controller Open Loop Bode Diagram

The closed loop frequency response characteristics of the trailing edge flap controller are presented in Figure 6-14. The closed loop bandwidth is 9 rad/s. The same additional loops are active for the closed loop response as in the open loop response.

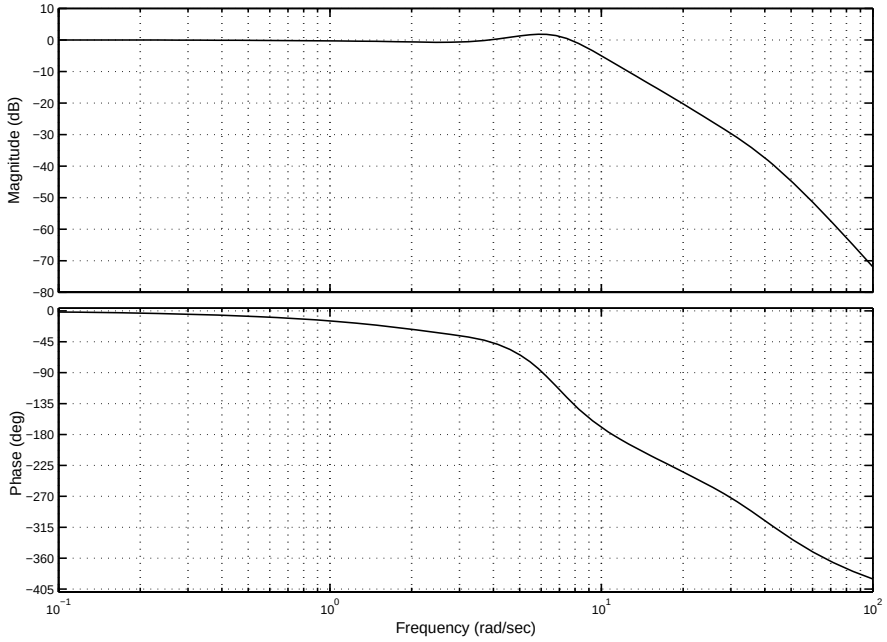

Figure 6-14 Flap Controller Closed Loop Bode Diagram

The open loop frequency response characteristics of the Spoiler controller loop are presented in the form of a Bode diagram in Figure 6-15. The autothrottle and pitch attitude loops are closed for this response and the trailing edge flap loop is isolated. The Navigation System is again replaced with a comparator as previously described. The control loop is broken along the altitude feedback path. The phase margin is 37.9 degrees at 4.7 rad/s and the gain margin is 13.8 db at 15.1 rad/s.

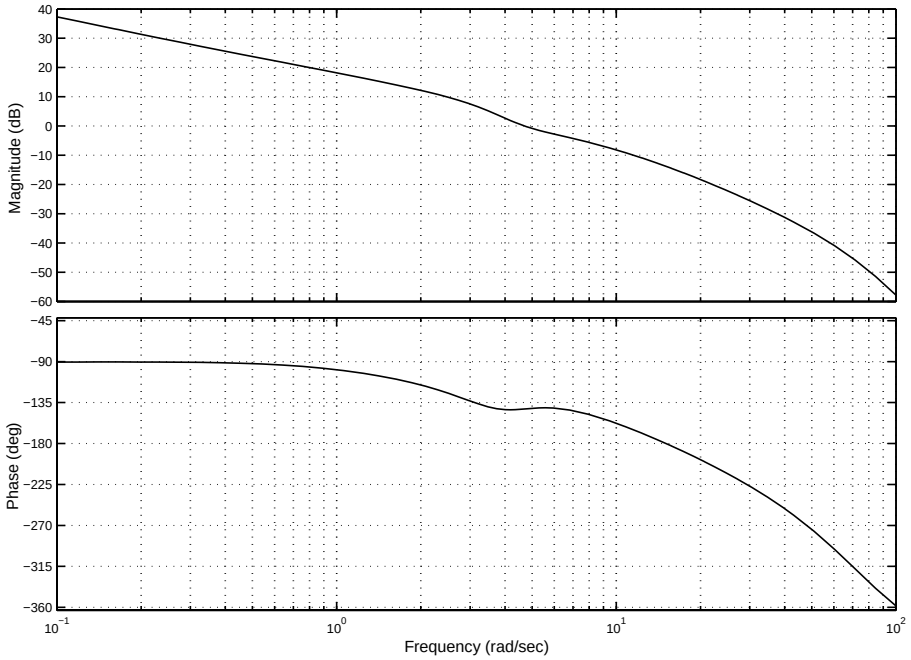

Figure 6-15 Spoiler Controller Open Loop Bode Diagram

The closed loop frequency response characteristics of the spoiler controller are presented in Figure 6-16. The closed loop bandwidth is 9 rad/s. The same additional loops are active for the closed loop response as in the open loop response.

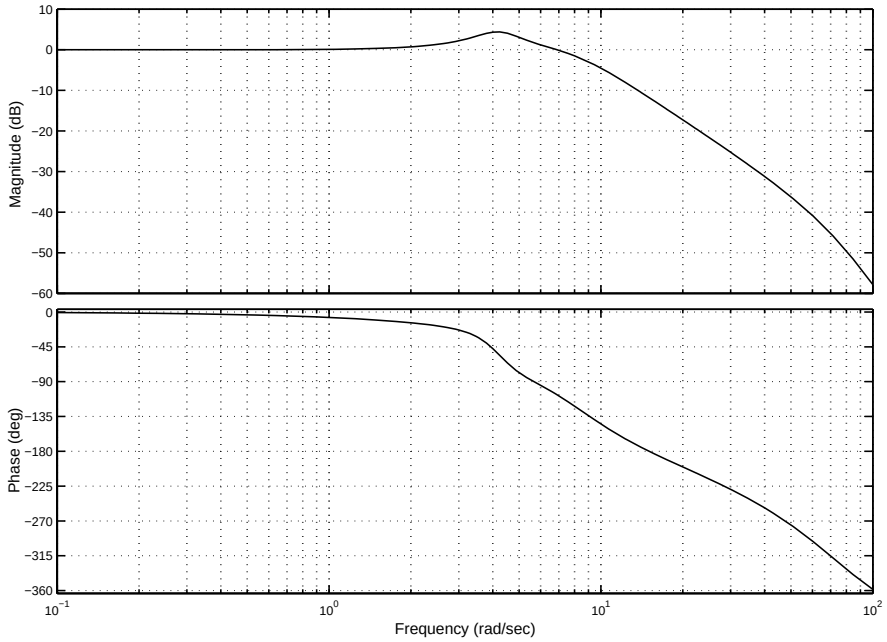

Figure 6-16 Spoiler Controller Closed Loop Bode Diagram

The constant attitude Direct Lift Control system's response to a unit step altitude demand is presented in Figure 6-17. The rise time of the response is 2.2 seconds and the settling time is 5.9 seconds.

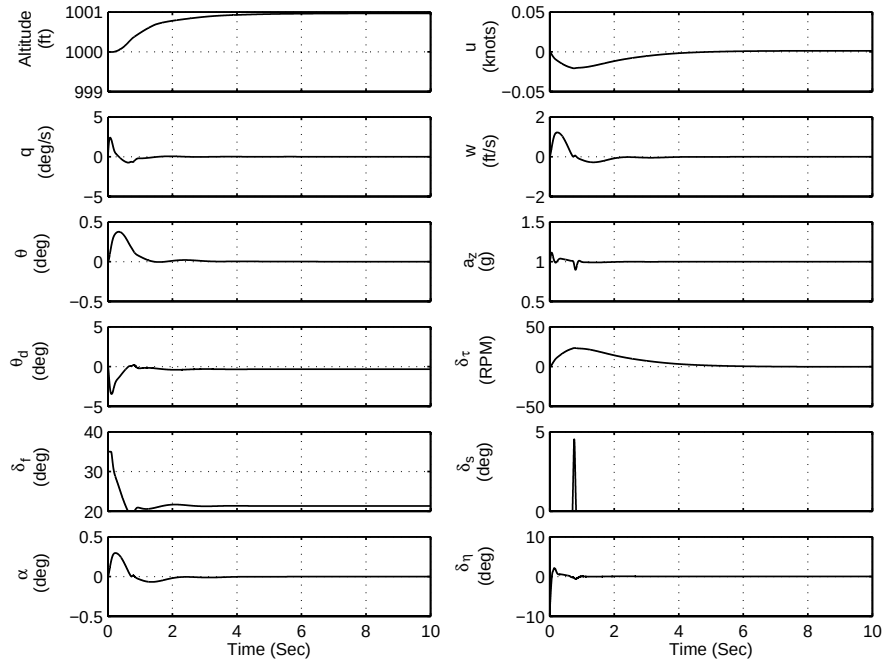

Figure 6-17 Constant Attitude Direct Lift Control System Response to a Unit Step Altitude Demand

6.3.1.4 PERFORMANCE ASSESSMENT USING THE NON-LINEAR MODEL

The response of the constant pitch attitude Direct Lift Control system to a rectangular pulse altitude demand is presented in Figure 6-18. The system's response to continuous moderate vertical turbulence over a time period of 100 seconds is presented in Figure 6-19.

The response to the rectangular pulse altitude demand is not as fast as the baseline approach glide path controller to the same demand, however the change in pitch attitude is much less. When the response of this system to continuous vertical turbulence is compared to the response of the baseline approach glide path controller to the same disturbance, Figure 6-7, it can be seen that while Direct Lift Control system attenuates the disturbance of approximately zero-mean disturbances better, e.g. 0 to 20 seconds, it is slow in responding to disturbances concentrated in one sense, e.g. 30 to 45 seconds. As a result of this it was decided that this system is not suitable for the carrier approach task.

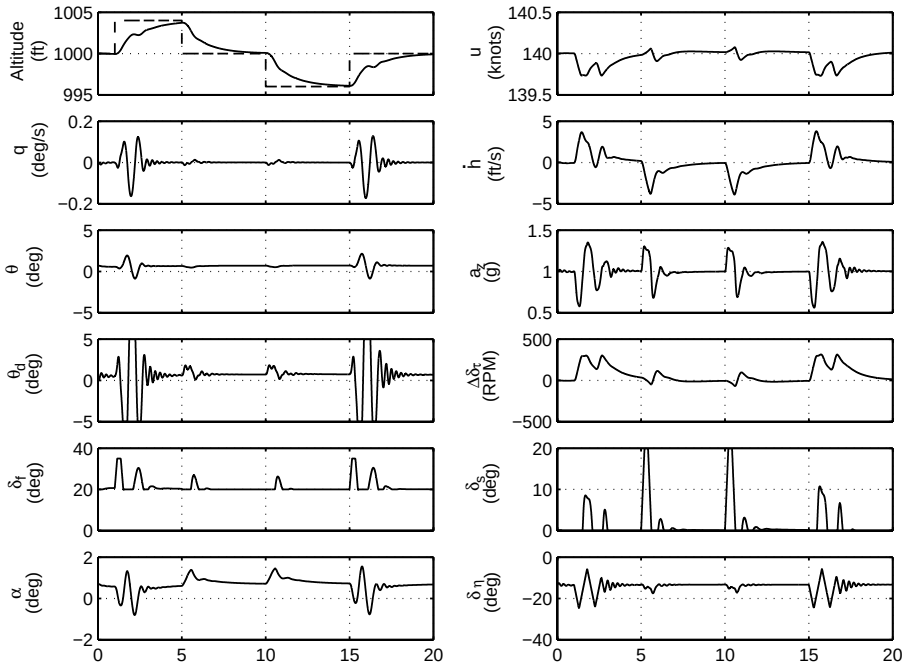

Figure 6-18 Constant Attitude Direct Lift Control System Response to Rectangular Pulse Altitude Demand

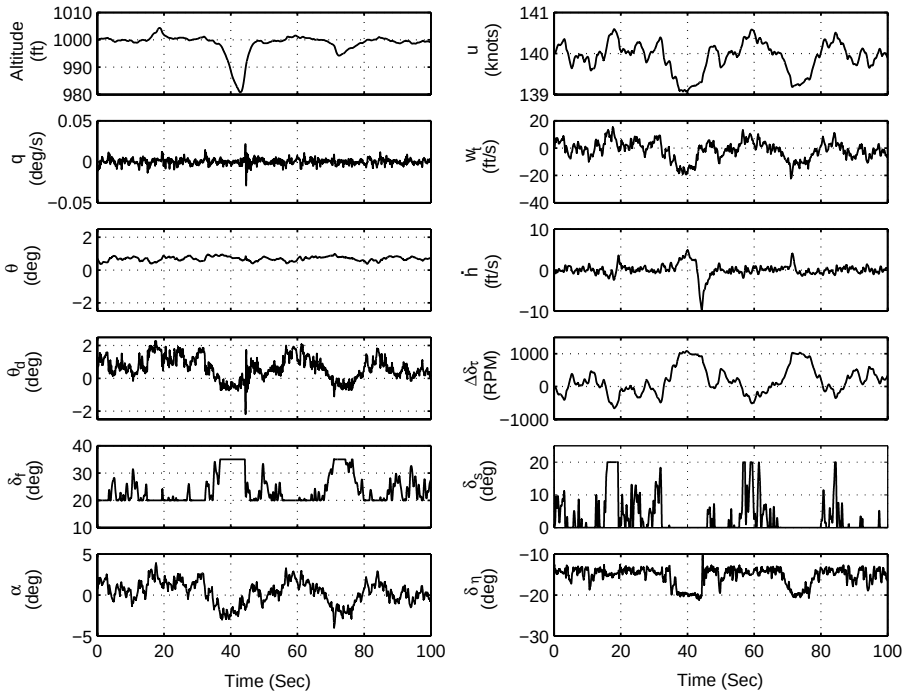

Figure 6-19 Constant Attitude Direct Lift Control System Response to Continuous Moderate Turbulence

6.3.2 DIRECT LIFT CONTROL AIDED BASELINE SYSTEM

Fortenbaugh presents a report on the integration of a Direct Lift Control system to the F-14A, a carrier based fighter aircraft [22]. In this instance Direct Lift Control is used to augment the existing longitudinal controller, which controls the aircraft's horizontal stabilisers. It was therefore decided to investigate the use of Direct Lift Control to augment the baseline approach glide path controller.

6.3.2.1 PERFORMANCE CRITERIA

The performance criteria for this system are the same as presented in section 6.2.1.

6.3.2.2 SYSTEM ARCHITECTURE

The Direct Lift Control aided baseline approach glide path controller system architecture is presented in Figure 6-20. The PID control of vertical deviation from the approach glide path is as presented in section 6.2 and the Direct Lift Control loops are as presented in section 6.3.1. All control laws and control system gains are as previously

defined. A flap to elevator feed forward gain is implemented as presented in section 6.3.1.2.

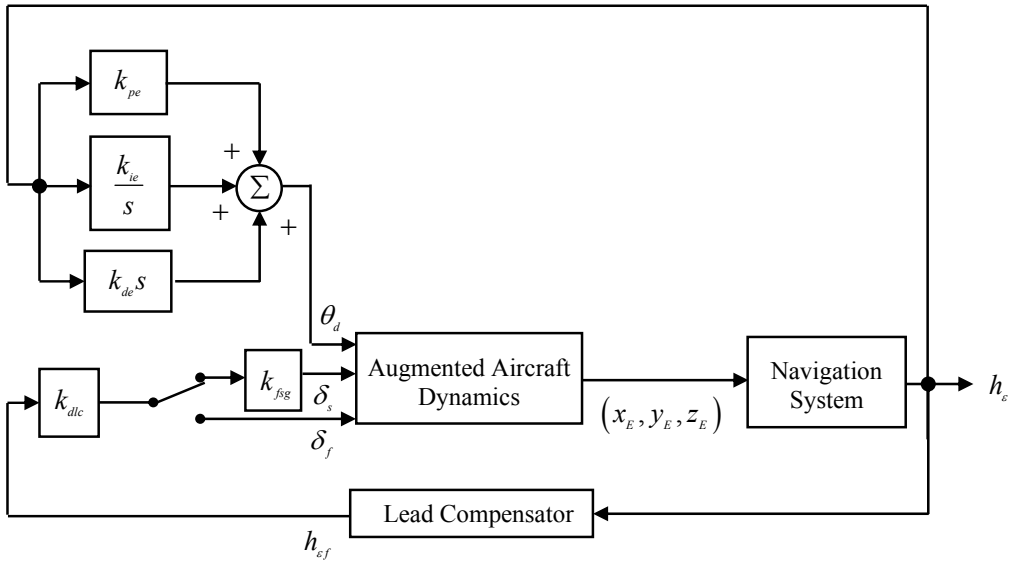

Figure 6-20 Direct Lift Control Aided Baseline Glide Path Controller System Architecture

6.3.2.3 PERFORMANCE ASSESSMENT USING THE LINEAR MODEL

When the Direct Lift Control system and the Baseline approach glide path controller were merged and their performance investigated it was found that no further tuning of the systems were necessary. As a result the Bode diagrams presented in this section were extracted from the non-linear simulation model using Simulink's Linear Time Invariant (LTI) viewer and no step response from the linear environment is presented.

For the extraction of Bode plots from the non-linear simulation model the Navigation system is replaced with a comparator as presented in Figure 6-21. For open loop responses the control loop is broken at the negative input to the comparator. The open loop frequency response characteristics of this system with the spoiler loop isolated are presented in the form of a Bode diagram in Figure 6-22. The autothrottle, baseline approach glide path controller and flap to elevator feed forwards loops are closed for this response. The gain margin is 10.4 db at 11 rad/s and the phase margin is 53.8 degrees at 4.8 rad/s.

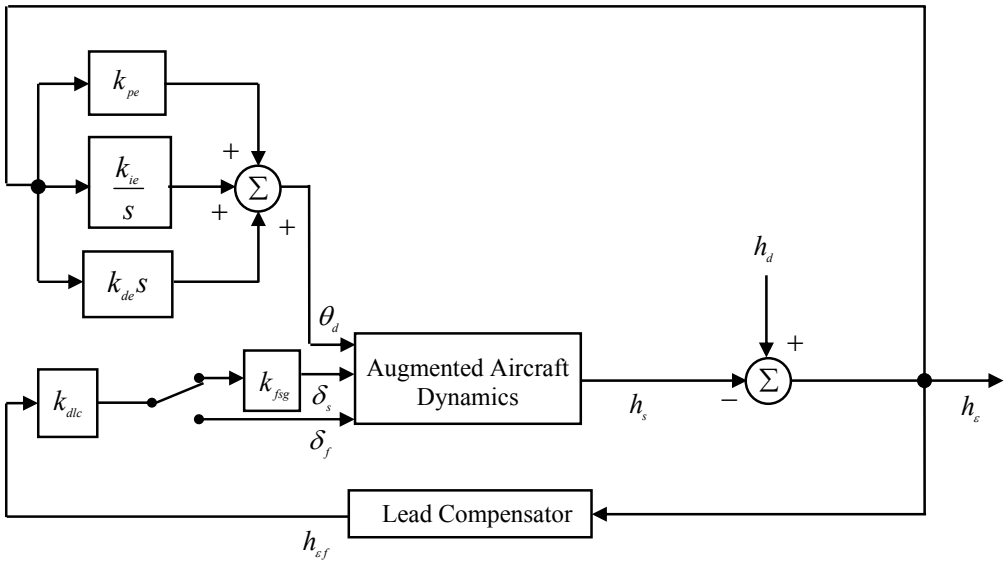

Figure 6-21 Direct Lift Control Aided Baseline Glide Path Controller System Architecture for Bode Plot Extraction from Non-Linear Model

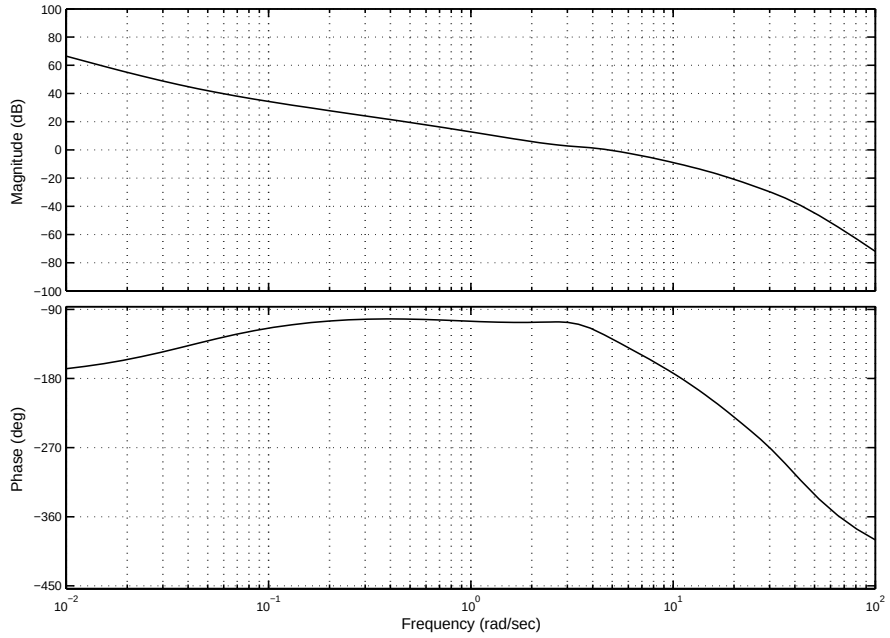

Figure 6-22 Flap Controller and Elevator Controller Open Loop Bode Diagram

The closed loop frequency response characteristics of the trailing edge flap controller are presented in Figure 6-23. The closed loop bandwidth is 8.97 rad/s. The same additional loops are active for the closed loop response as in the open loop response.

Recalling that the closed loop bandwidth of the baseline approach glide path controller is 1.83 rad/s it can be seen that the addition of Direct Lift Control has the effect of substantially increasing the bandwidth of the controller.

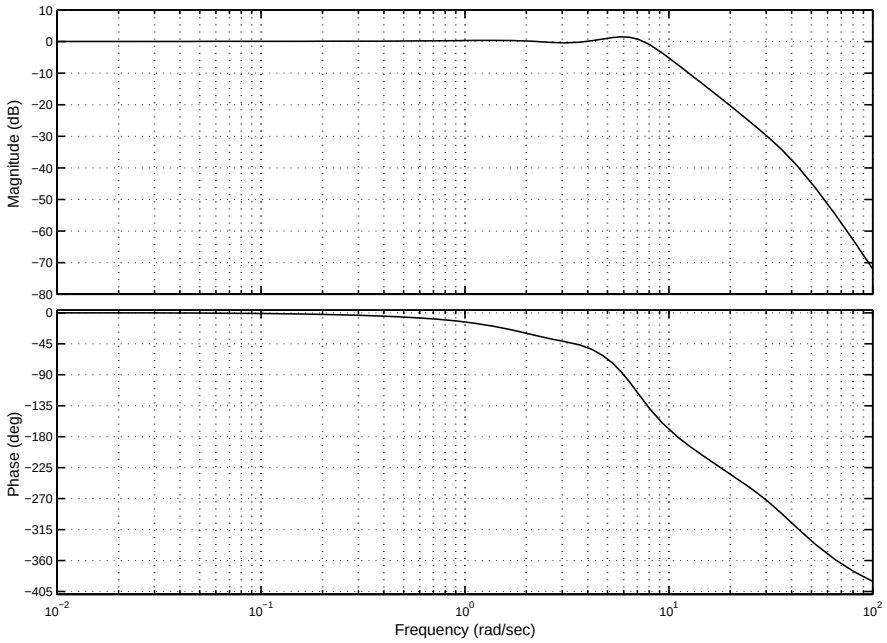

Figure 6-23 Flap Controller and Elevator Controller Closed Loop Bode Diagram

The open loop frequency response characteristics of this system with the trailing edge flap control loop isolated are presented in the form of a Bode diagram in Figure 6-24. The control loop is broken in the same manner as above. The autothrottle and baseline approach glide path controller are closed for this response. The phase margin is 35.7 degrees at 4.54 rad/s and the gain margin is 13.9 db at 15.11 rad/s.

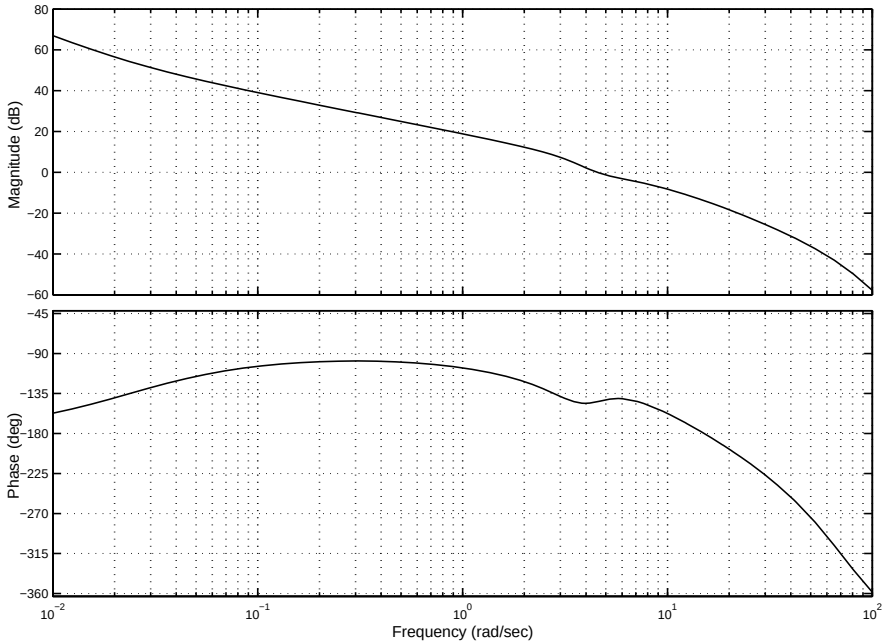

Figure 6-24 Spoiler Controller and Elevator Controller Open Loop Bode Diagram

The closed loop frequency response characteristics of this system with the trailing edge flap control loop isolated are presented in the form of a Bode diagram in Figure 6-25. The closed loop bandwidth is 8.84 rad/s. The same additional loops are active for the closed loop response as in the open loop response.

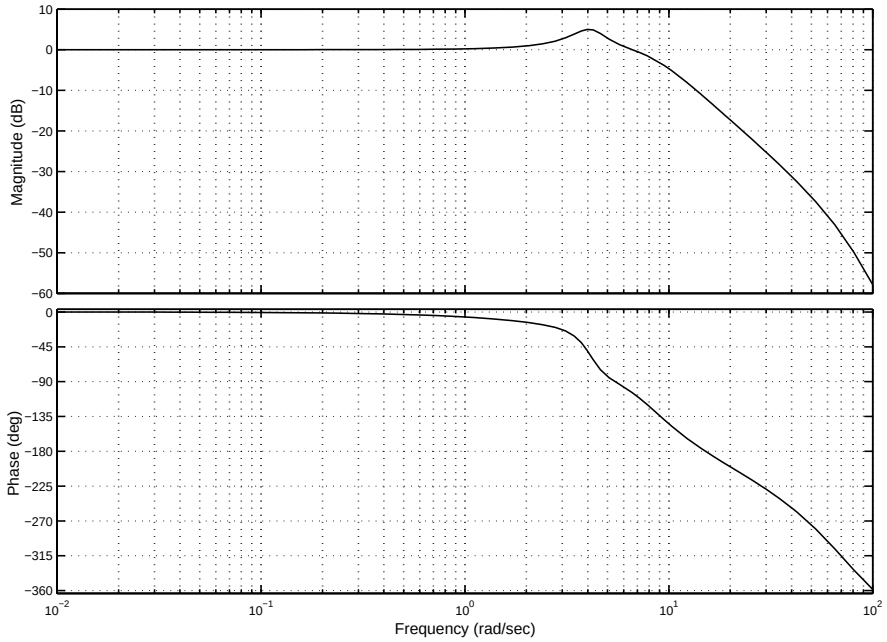

Figure 6-25 Spoiler Controller and Elevator Controller Closed Loop Bode Diagram

6.3.2.4 PERFORMANCE ASSESSMENT USING THE NON-LINEAR MODEL

The response of the Direct Lift Control aided baseline approach glide path controller to a rectangular pulse altitude demand is presented in Figure 6-26. The system's response to continuous moderate vertical turbulence over a time period of 100 seconds is presented in Figure 6-27. The response of the system to the rectangular pulse altitude demand can be seen to meet the performance criteria. When the system's response to continuous moderate vertical turbulence to the response of the baseline system to the same disturbance, Figure 6-7, the benefits of Direct Lift Control are readily apparent.

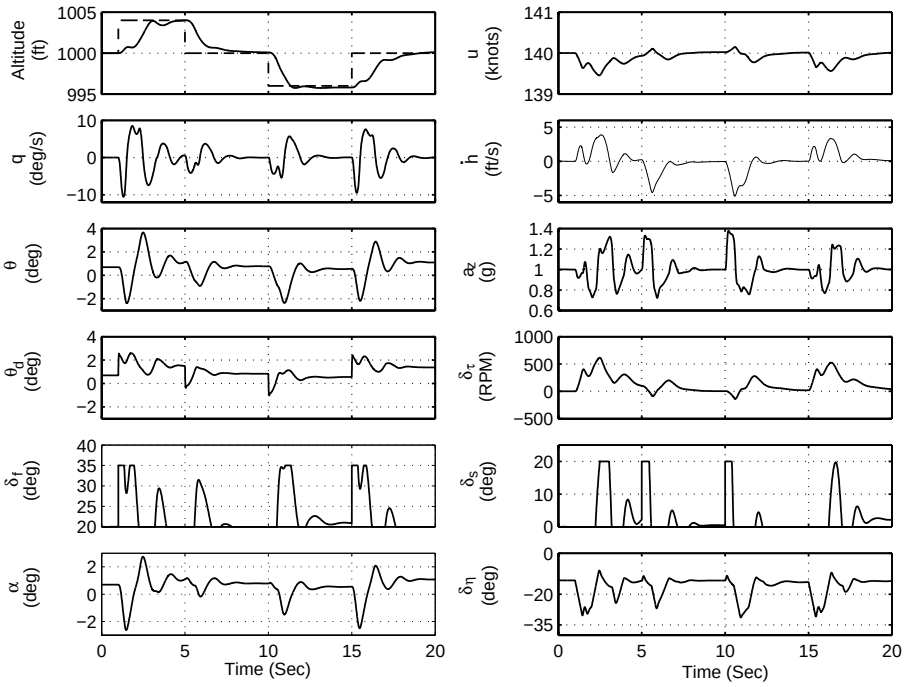

Figure 6-26 Direct Lift Control Aided Baseline System Response to Rectangular Pulse Altitude Demand

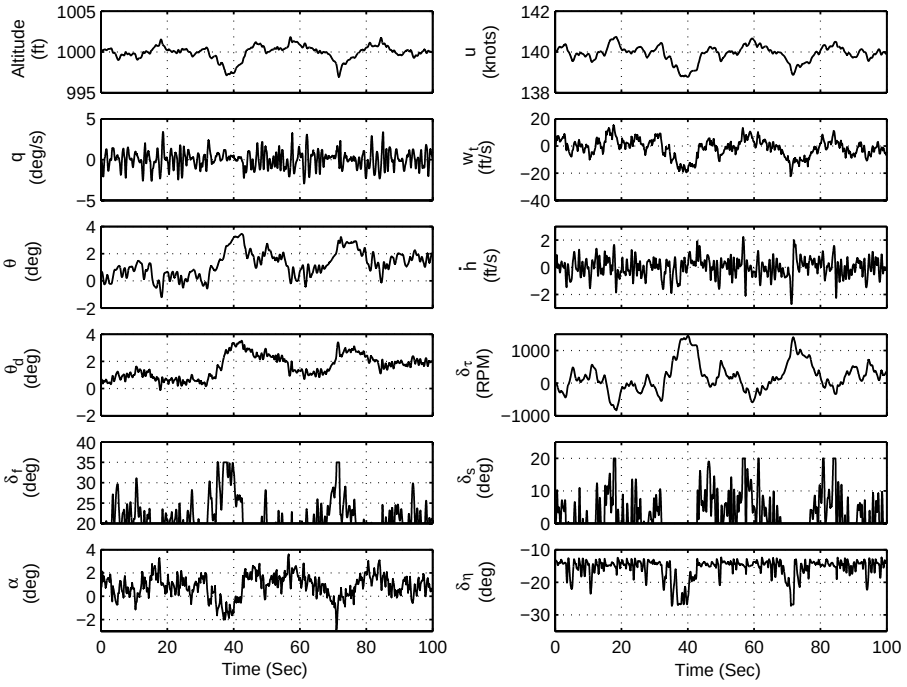

Figure 6-27 Direct Lift Control Aided Baseline System Response to Continuous Moderate Turbulence

6.4 THRUST VECTORING SYSTEM

The third system comprises of the addition of thrust vectoring to augment elevator pitch control to the Direct Lift Control aided baseline approach glide path controller. This system was developed to allow investigation of the feasibility of using vectored thrust to augment pitch control during a carrier approach.

Due to reduced radar signatures, tailless aircraft are preferable for many operations. These aircraft present a challenge to flight control engineers. This planform is generally inherently unstable in roll and yaw. This infers that a Stability Augmentation System is required. The challenge presents itself in the limited number of aerodynamic control effectors on a tailless aircraft. It is typical that pitch, roll and yaw control is achieved through the same aerodynamic control effector.

In order to maintain effectiveness of the Stability Augmentation System, it is imperative that the associated control effectors never become saturated. Such a situation would result in the aircraft's stability and control properties reverting to those of the un-augmented airframe. Certain phases of flight require more control activity than others. The carrier landing environment is such a case. This is the motivation for this aspect of this study. The aim is to demonstrate the feasibility of using vectored thrust to augment elevator pitch control, and hence alleviate the demand on aerodynamic pitch control effector, during a carrier approach.

In this instance vectored thrust is used to alleviate the required pitch control from the elevators while the aileron and rudders are controlled as normal, i.e. the aircraft simulated is not a tailless aircraft. The pitch control power of vectored thrust is a function of engine thrust. During a landing approach the engine thrust is relatively low, and similarly the pitch control power is also relatively low. Bosworth and Stoliker [54] suggest that drag increasing devices, such as spoilers, be deployed on approach in order to facilitate higher engine thrust while maintaining a constant approach speed in order to increase vectored thrust control power. As the spoilers are being used for Direct Lift Control purposes this has not been implemented here.

6.4.1 PERFORMANCE CRITERIA

The performance criteria for this system are the same as presented in section 6.2.1.

6.4.2 SYSTEM ARCHITECTURE

The architecture of the vectored thrust loop control loop is presented in Figure 6-28 which illustrates how the vectored thrust loop is integrated with the Direct Lift Control aided baseline approach glide path control system. The addition of the vectored thrust loop is effectively an augmentation to the Stability Augmentation System elevator loop, presented in Chapter 3.

In this implementation thrust vectoring is used to alleviate elevator deflection about the trim elevator angle. This ensures that thrust vectoring deflection angles are kept at a minimum.

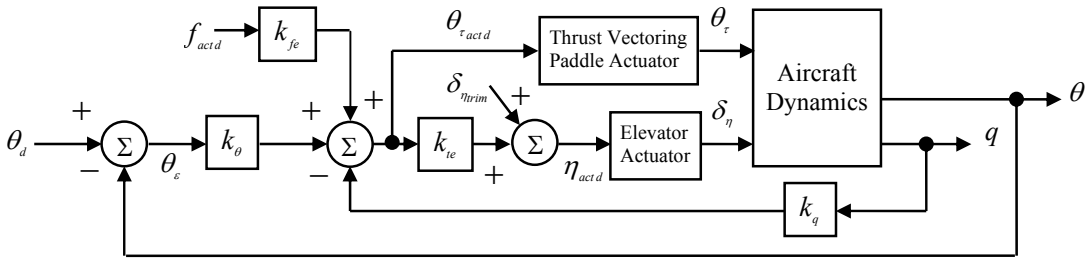

Figure 6-28 Thrust Vectoring System Architecture

The control law for the vectored thrust loop is defined as

$$\theta_{\tau act\,d} = k_\theta \theta_\varepsilon - k_q q + k_{fe} \delta_f \tag{6-7}$$

The control law for the elevator loop now becomes

$$\eta_{act\,d} = k_{te} \theta_{\tau act\,d} + \delta_{\eta trim} \tag{6-8}$$

The reduction in elevator demand gain, k_{te}, is calculated as a function of relative control powers and for the design point is selected as:

$$k_{te} = 0.76 \text{ rad/rad} \tag{6-9}$$

For the nominal approach engine thrust the reduction in elevator demand gain, k_{te}, is selected as

$$k_{te} = 0.81 \text{ rad/rad} \qquad (6\text{-}10)$$

These gains were selected so as to provide the equivalent total pitch control power of the elevators when $k_{te} = 1$ and the vectored thrust is disengaged. This ensures that the effectiveness of the Stability Augmentation System is preserved when pitch control is shared between the elevators and vectored thrust. It should be noted that thrust vectoring and elevator actuators have the same dynamic properties.

At both thrust settings the gains selected resulted in a slight increase in the Short Period damping ratio. The damping ratio of the standard augmented aircraft is 0.76. The damping ratio with the addition of thrust vectoring is 0.80 for both thrust settings.

6.4.3 PERFORMANCE ASSESSMENT USING THE LINEAR MODEL

Bode plots are generated in the same manner as described for the Direct Lift Control aided baseline approach glide path controller. The open loop frequency response characteristics of this system with the spoiler loop isolated are presented in the form of a Bode diagram in Figure 6-29. The autothrottle, baseline approach glide path controller, trailing edge flap and trailing edge flap to elevator feed forwards loops are closed for this response. The gain margin is 7.62 db at 10.3 rad/s and the phase margin is 32.9 degrees at 5.68 rad/s.

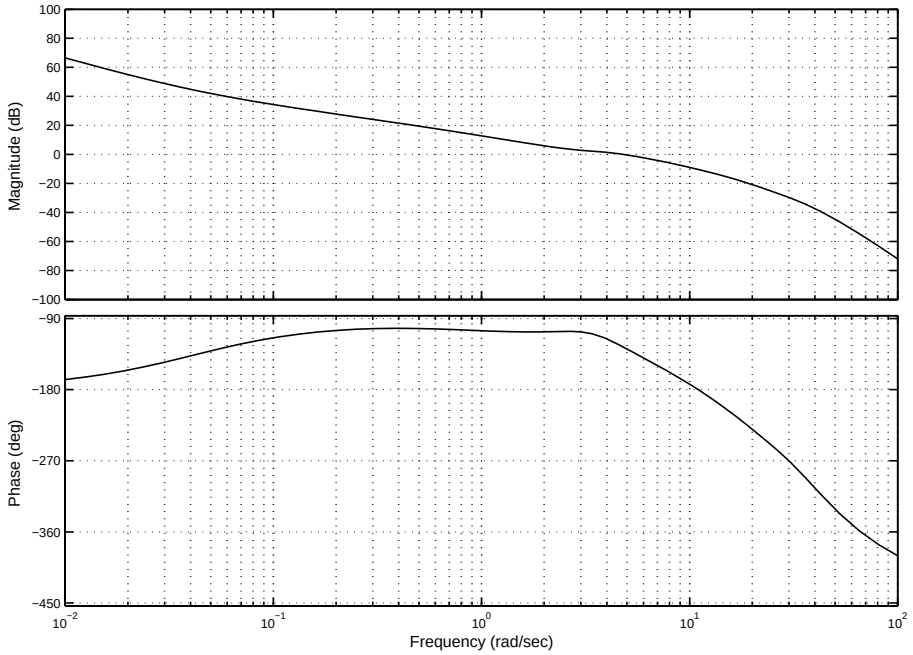

Figure 6-29 Open Loop Thrust Vectoring Approach Glide Path Controller Bode Diagram with Spoiler Loops Isolated

The closed loop frequency response characteristics of this system with the spoiler control loops isolated are presented in the form of a Bode diagram in Figure 6-30. The same loops are active as for the open loop response. The closed loop bandwidth is 10.3 rad/s. When this is compared with the bandwidth of the Direct Lift Control aided baseline approach glide path controller, which is 8.97 rad/s, it can be seen that the addition of thrust vectoring has increased the bandwidth of the system.

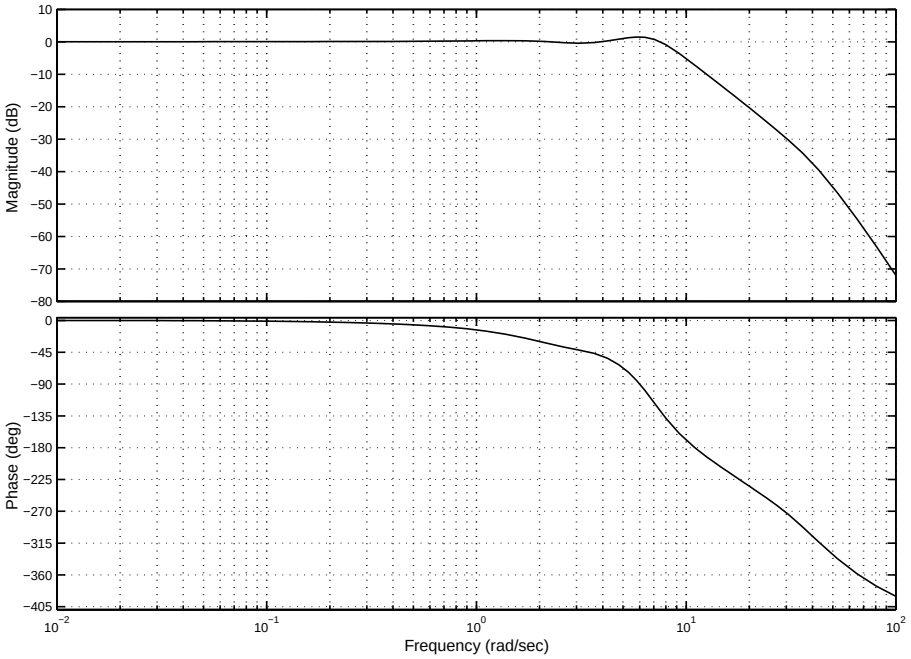

Figure 6-30 Closed Loop Thrust Vectoring Approach Glide Path Controller Bode Diagram with Spoiler Loops Isolated Bode Diagram

The open loop frequency response characteristics of this system with the trailing edge flap loop isolated are presented in the form of a Bode diagram in Figure 6-31. The autothrottle, baseline approach glide path controller and spoiler control loops are closed for this response. The gain margin is 13.5 db at 15.2 rad/s and the phase margin is 53.2 degrees at 5.28 rad/s.

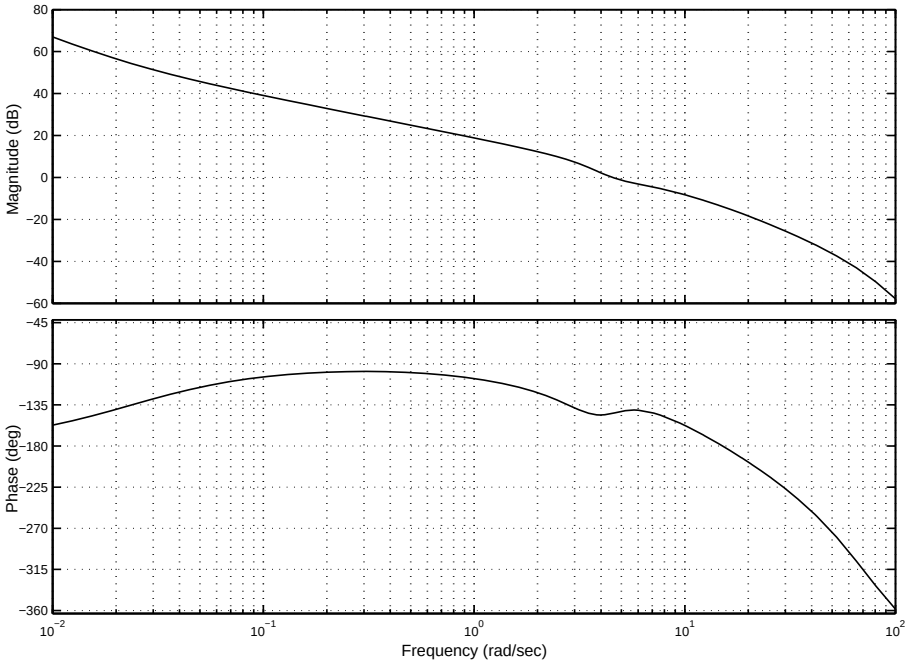

Figure 6-31 Open Loop Thrust Vectoring Approach Glide Path Controller Bode Diagram with Trailing Edge Flap Loops Isolated

The closed loop frequency response characteristics of this system with the trailing edge flap control loops isolated are presented in the form of a Bode diagram in Figure 6-32. The same loops are active as for the open loop response. The closed loop bandwidth is 9.67 rad/s. Recalling that the closed loop bandwidth of the Direct Lift Control aided baseline approach glide path controller with trailing edge flaps isolated is 8.84 rad/s it can be seen again that thrust vectoring has had the effect of increasing the bandwidth of the system.

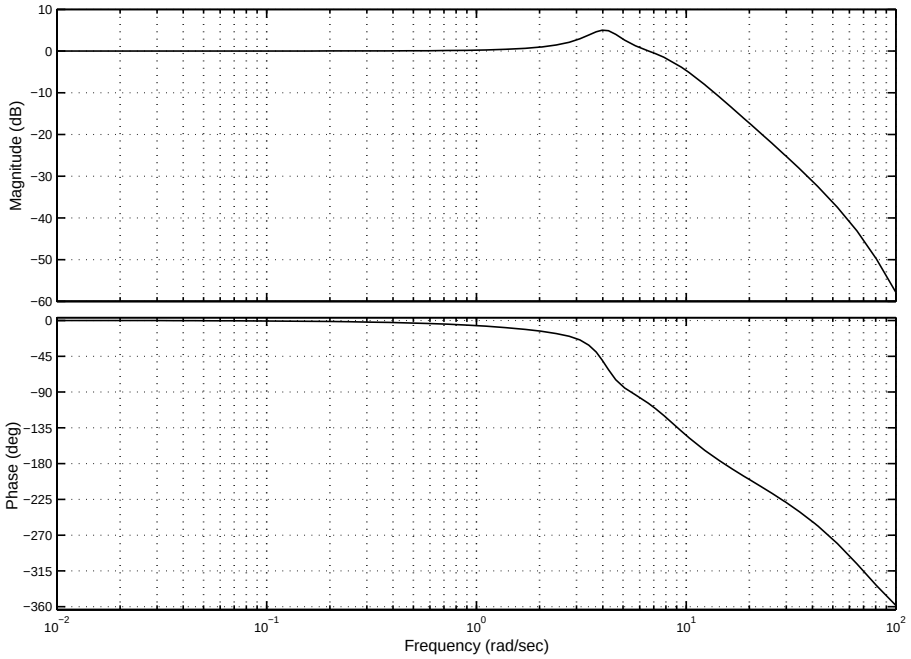

Figure 6-32 Closed Loop Thrust Vectoring Approach Glide Path Controller Bode Diagram with Trailing Edge Flap Loops Isolated

The system's response to a unit step altitude demand with elevator and vectored thrust loops closed is presented in Figure 6-33. The trailing edge flap and spoiler loops are not active for this response. This can be compared to the baseline approach glide path controller response to a unit step altitude demand, Figure 6-5. All response variables are very similar with the exception of axial velocity, u, which is showing a larger perturbation in this case as a result of the rotation of the thrust line.

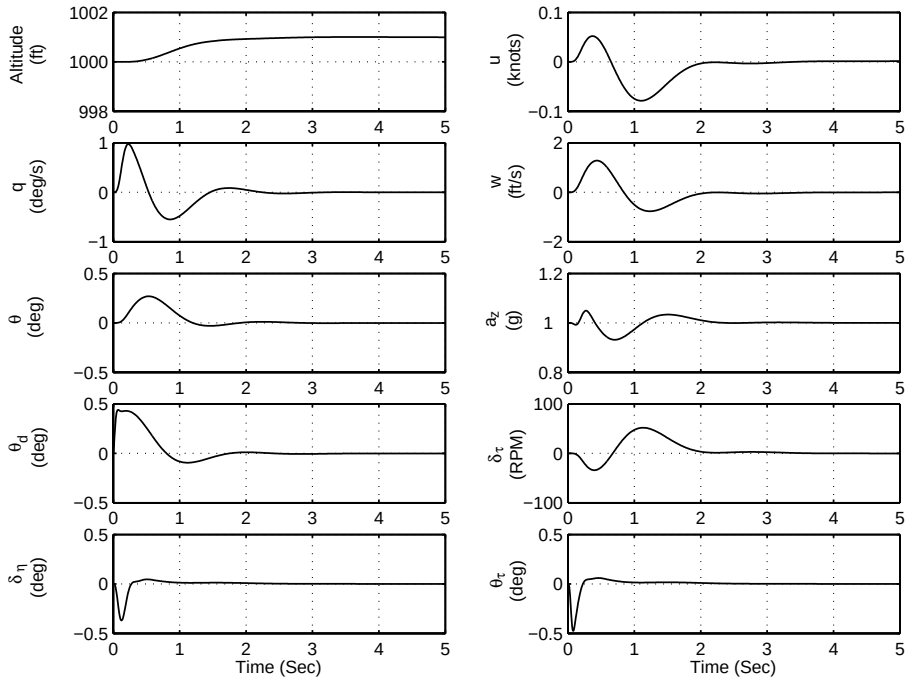

Figure 6-33 Thrust Vectoring System Response to a Unit Step Demand

6.4.4 PERFORMANCE ASSESSMENT USING THE NON-LINEAR MODEL

The system's response to a rectangular pulse altitude demand is presented in Figure 6-34. All control loops are closed for this response, i.e. autothrottle, elevator, trailing edge flaps and spoilers. The response can be seen to meet the applicable performance criteria. The response of the system to continuous moderate vertical turbulence over a time period of 100 seconds is presented in Figure 6-35. When this response is compared to that of the Direct Lift Control aided baseline approach glide path controller, Figure 6-27, it can be seen that the response to atmospheric turbulence has been further attenuated due to the increased short period damping afforded by vectored thrust.

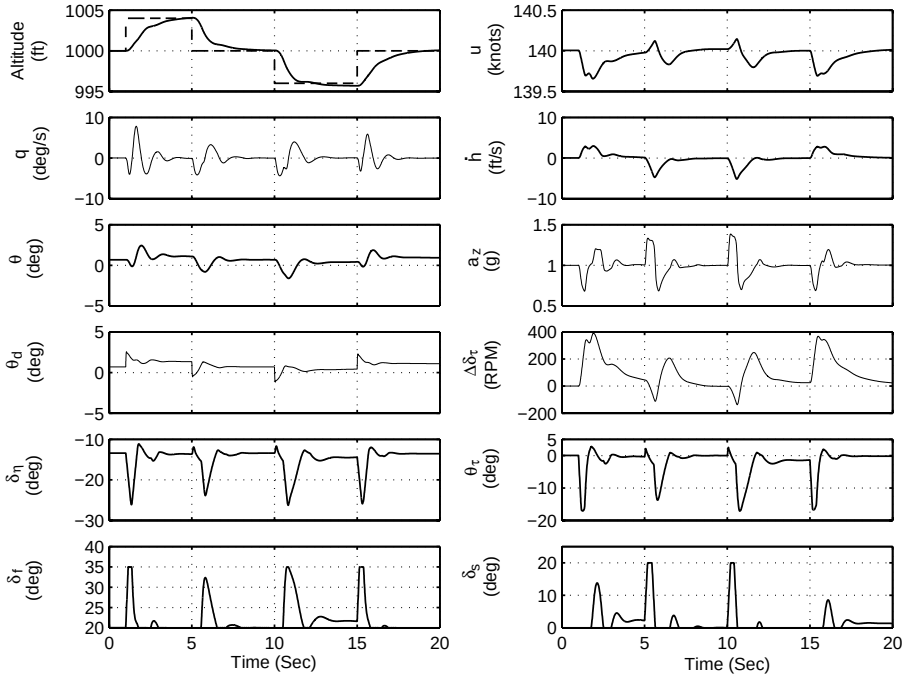

Figure 6-34 Thrust Vectoring System Response to Boxcar Altitude Demand

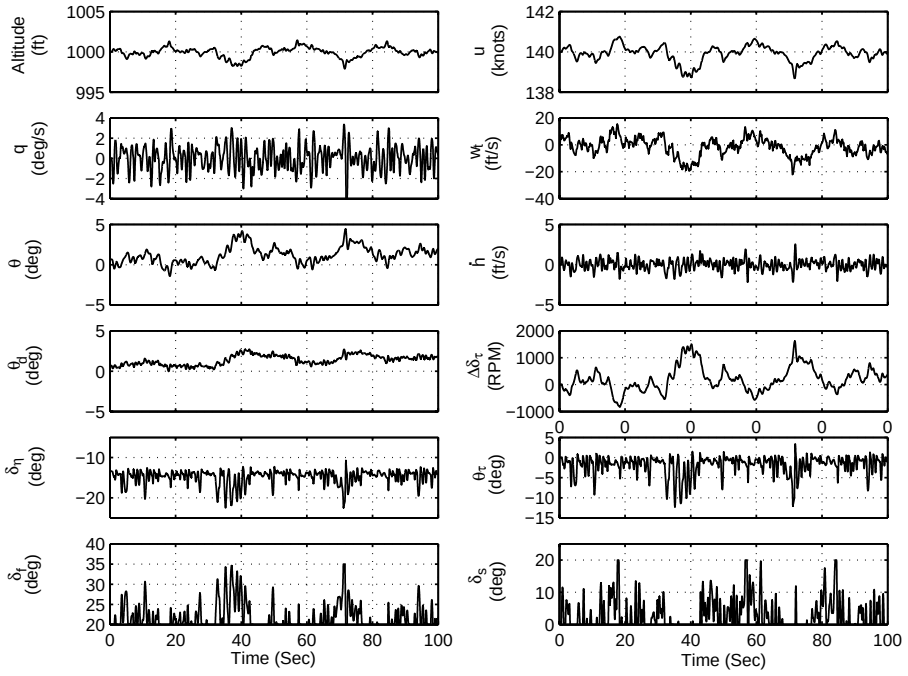

Figure 6-35 Thrust Vectoring System Response to Continuous Moderate Turbulence

7 COMPARATIVE ANALYSIS AND DISCUSSION OF APPROACH CONTROLLER DESIGNS

7.1 INTRODUCTION

To assess the performance of the approach controllers developed, a series of simulations with varying operating conditions were conducted. The objective of this simulation exercise was to characterise the performance of each controller with respect to its approach and touchdown performance in order to facilitate a comparison of all three controllers. Each approach controller was simulated operating in the same conditions. This allowed a direct comparison between each approach controller.

In this and subsequent Chapters 'baseline approach controller' refers to the Autothrottle; baseline approach glide path controller; track controller and Navigation System combination. 'Direct Lift Control approach controller' refers to the Autothrottle, Direct Lift Control aided baseline approach glide path controller, track controller and Navigation System combination. 'Thrust vectoring approach controller' refers to the Autothrottle, Direct Lift Control aided baseline approach glide path controller with thrust vectoring, track controller and Navigation System combination.

Operating parameters, such as turbulence intensity and wind speed, were varied and may exceed actual operating conditions. This was done to allow the limits of the approach controllers and Navigation System combinations to be determined and hence a more comprehensive comparison of the control strategies and associated flight control systems is achieved. Two sets of results are presented.

(i) Approach Performance

Three approach cases are presented to illustrate the approach performance of the approach controllers and Navigation System combination with respect to response to discrete atmospheric disturbances. The first case considered is a no disturbance case

which characterises the approach controllers steady state response. The second case introduces windshear, discrete gusts and carrier induced turbulence. The third case involves continuous atmospheric turbulence and carrier induced turbulence.

(ii) Statistical Performance Analysis

A statistical analysis of the approach controllers is presented: In the statistical analysis atmospheric turbulence, intensity and direction are varied for a set of carrier motion cases. In total, 1440 approaches, 480 per approach controller, are assessed in this analysis.

In the absence of published Automatic Carrier Landing System's performance requirements in the public domain, the relative performance of each system is determined and discussed.

In total the results of 1449 approach simulations are presented representing various operating conditions which assess the limits of the system and characterise the approach performance and touchdown dispersion characteristics of each approach controller and Navigation System combination. These data are presented in a manner consistent with publications that quote the USN Automatic Carrier Landing System performance requirements [80] and allow for a direct comparison of these systems to systems in service.

In order to assess the performance of each simulated approach, a set of performance metrics were defined. These are presented in section 7.2 and form the basis of the subsequent discussions. A discussion on the simulation procedures used precedes the results of the comparative analysis. This Chapter is concluded with a discussion on the findings of the comparative analysis.

7.2 PERFORMANCE METRICS

In order to assess and compare each simulated approach and touchdown on the carrier it was necessary to define quantitative performance metrics. No previous published study reviewed presented a set of performance metrics for the complete approach and landing

scenario. As a result, the following method of assessing the carrier approach and landing task was developed.

An overview of the success criteria applied to the approach and landing task is presented in Figure 7-1. This is similar to the criteria presented by Durand and Wasicko [3] who concentrated on the segment of the approach from crossing the stern of the carrier to touchdown.

A successful approach and landing is required to satisfy three conditions according to these criteria. During the approach phase, prior to passing the stern of the ship, the aircraft is required to remain within defined maximum allowable lateral and vertical deviations from the approach path. If the aircraft exceeds either of these maximum allowable deviations, the approach is 'waved-off'. The second success criterion is that the aircraft has the pass over the stern, or ramp, of the carrier with adequate clearance. If the aircraft does not pass over with adequate clearance, the aircraft will strike the ramp. Finally, the aircraft is required to touchdown at least before the fourth and final arresting wire and within the lateral confines of the landing area. If the aircraft does not touchdown accordingly, the approach is terminated in a go-around. In naval aviation parlance a go around resulting from landing beyond the fourth arresting wire is known as a 'bolter'. These criteria are fully defined in the following sections

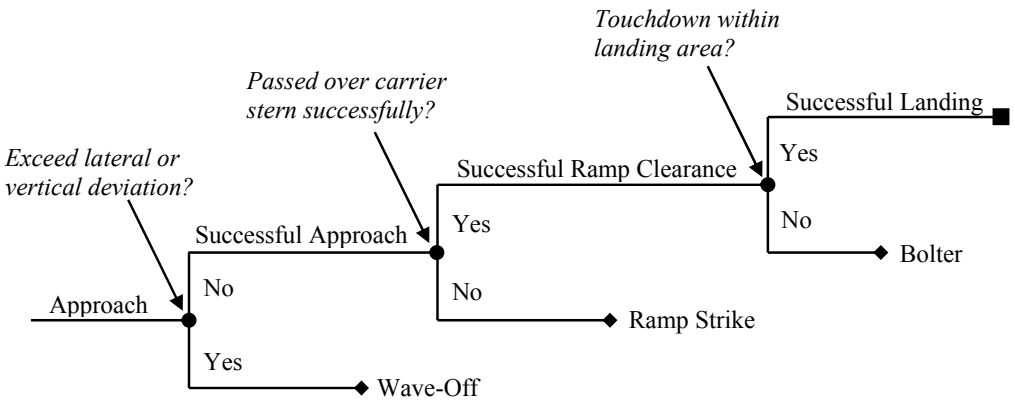

Figure 7-1 Approach and Landing Success Criteria

7.2.1 APPROACH DEVIATION PERFORMANCE

Connelly [32] suggests that the Root Mean Square (RMS) of deviations from the desired approach glide path and approach track can provide identical scores for both satisfactory and unsatisfactory flight paths and, as such, is not a suitable performance metric for the assessment of the approach task. For example a low approach which results in an aircraft landing short of the runway, which is unacceptable, could have the same RMS deviation as a high approach which would result in an aircraft landing beyond the desired touchdown point but still acceptable from a safety standpoint. However, if used in conjunction with another performance metric, which ensures that satisfactory and unsatisfactory approaches are distinguishable, then the RMS of approach glide path and approach track deviations does provide a useful means of comparing different systems tracking performance.

The method of assessing a satisfactory approach is achieved by applying the criteria that the Landing Signal Officers use in determining when to wave-off an automated approach.

Figure 7-2 presents the vertical flight path control wave-off boundaries for both Mode I and II automatic approach modes [4]. Recalling from Chapter 2 that a Mode I approach is a full automatic approach to touchdown, and a Mode II approach is a semi automatic approach providing the pilot with approach glide path and approach track deviation data similar to a flight director. As Mode I is the mode with the most demanding level of autonomy those boundaries are applied.

The illustration in the Landing Signal Officers Reference Manual [4] was not accompanied with a numerical definition of the boundaries; hence some speculation is necessary to extract numerical boundaries. The boundary applied in this case is defined as a maximum allowable vertical deviation from the desired approach glide path of ±50 ft at 8,600 ft from touchdown reducing linearly to +10 ft, -5 ft at 1000 ft from touchdown. No maximum allowable vertical deviation is defined for a range of less than 1000 ft. Past this point, the pilot is committed to landing on the carrier. This logic is adopted here.

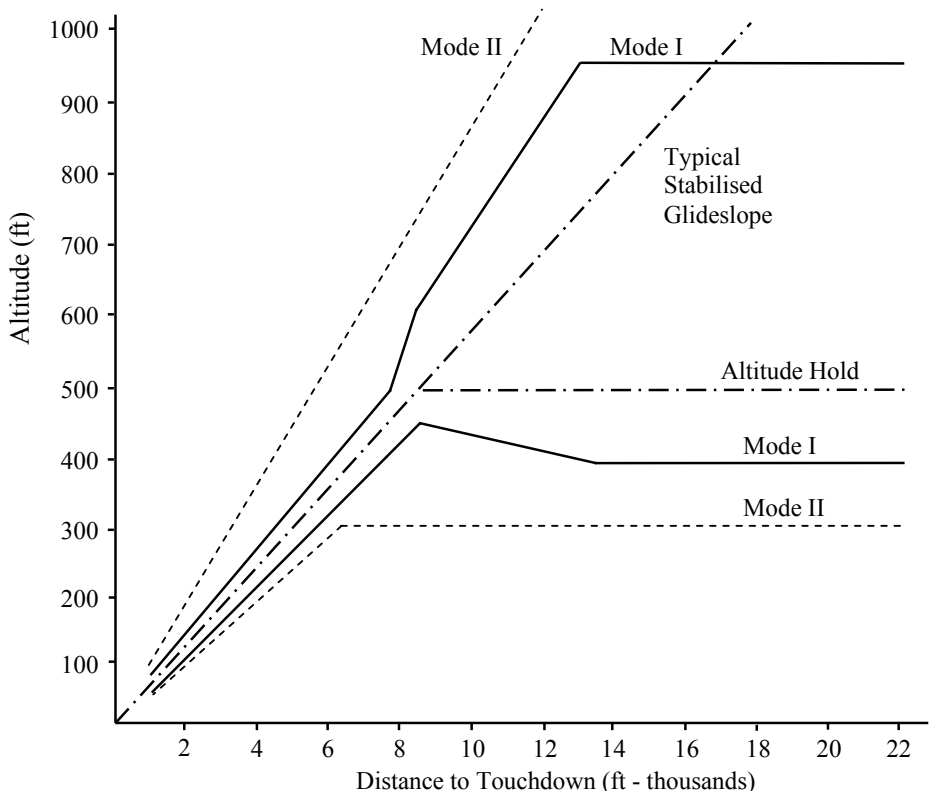

Figure 7-2 Vertical Flight Path Control Wave-Off Boundaries [4]

Figure 7-3 presents the lateral flight path control wave-off boundaries for both Mode I and II automatic approach modes [4]. In this case, the Mode I boundaries are also applied. The boundaries applied are defined as ± 22 ft at 2,250 ft from touchdown reducing linearly to ± 14 ft at 800 ft from touchdown. It is assumed that at a distance closer that 800 ft to touchdown, the aircraft will arrive safely on the landing area of the deck.

For each simulated approach these boundaries are applied as part of the post processing of the simulation results. If the approach trajectory of the aircraft's tail hook breaches these boundaries, the approach is classified as a 'wave-off' and none of the metrics defined in the following section are calculated. If the approach is classified as a wave-off, the time to touchdown at which the approach failed is recorded, along with the RMS value for deviation from the desired approach glide path, approach track, and approach speed, and whether the approach failed in a vertical or lateral sense.

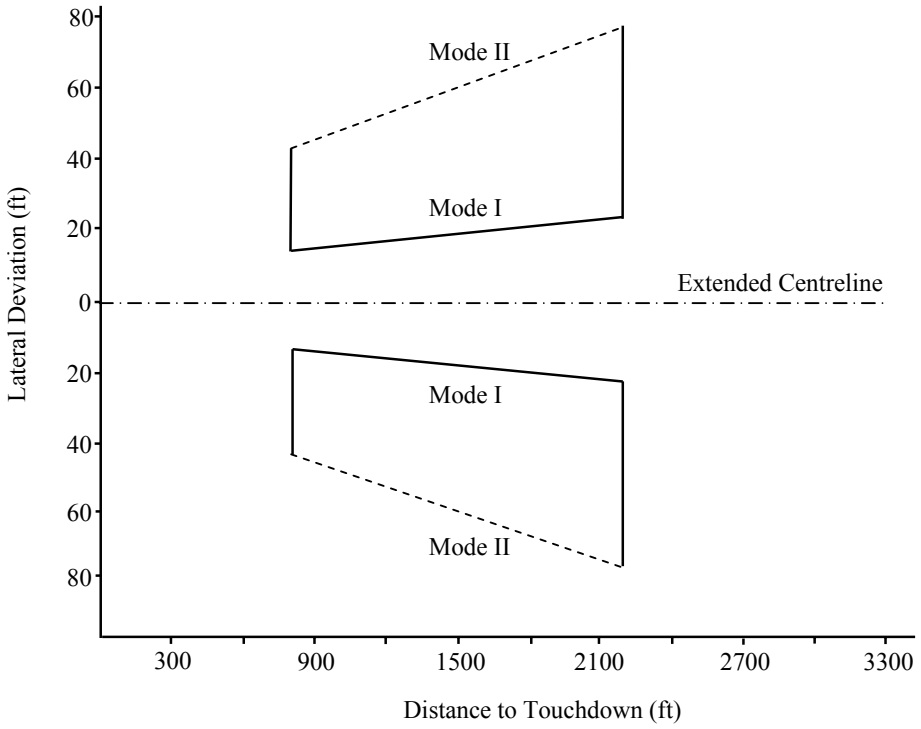

Figure 7-3 Lateral Flight Path Control Wave-Off Boundaries [4]

If the approach does not fail, and if a ramp strike does not occur, it is classified as a successful approach and the RMS value for deviation from the desired approach glide path, approach track, and approach speed are recorded.

7.2.2 RAMP CROSSING HEIGHT

The height of the tail hook over the ramp is an important metric in assessing the approach to a carrier deck as it represents the precision of control at the most critical phase of the approach - when the aircraft is committed to landing. The aircraft passes over the ramp with, nominally, one second of flight time to touchdown remaining. If the aircraft is too high at this point in the approach, the aircraft will land beyond the desired touchdown point and the approach may be terminated by a bolter. If the aircraft is too low, it will land short of the desired touchdown point and, if critically low, a ramp strike may occur, i.e. the aircraft may impact the stern of the carrier.

With reference to Figure 7-4: During the simulated approach the trajectory of the desired touchdown point, as well as three other points, are recorded. These three points, A, B and C, represent the starboard and port extremities of the ramp and a point above the centreline located on a plane perpendicular to the flat earth surface.

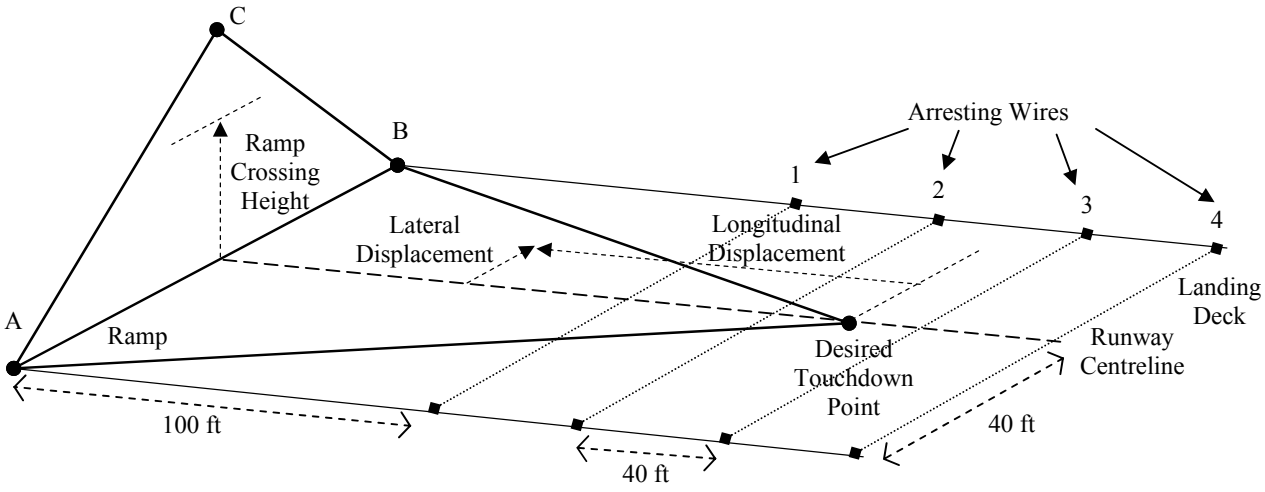

Figure 7-4 Touchdown Geometry Definition

The ramp crossing height is determined by the perpendicular distance, relative to the flat earth, between the point at which the trajectory of the tail hook intersects the plane defined by the points A, B and C and the line joining the points A and B.

If the ramp crossing height is negative, the approach is defined as a ramp strike and no further metrics are calculated.

Ramp crossing height is determined by two main factors: (1) the approach glide path deviation at the instant that the aircraft crosses over the ramp and (2) the aircraft carrier's pitch attitude at that instant. For this reason, it is necessary to consider both contributions when analysing ramp crossing height performance. Each of the approach controllers presented control approach glide path vertical deviation and do not account for the aircraft carrier's pitch attitude. The contribution of the aircraft carrier's pitch attitude to ramp crossing height is defined as

$$\Delta h_r = 160 \tan \theta_{cr} \tag{7-1}$$

A ± 1 degree variation in aircraft carrier pitch attitude results in a vertical displacement of the ramp by ± 2.79 feet, or 33% of the clearance between the aircraft carrier's ramp and the desired 3 degree approach glide path.

7.2.3 TOUCHDOWN DISPERSION

Ultimately, the task of any automatic landing system is to deliver the aircraft safely to a desired point on the landing surface. Hence, the most revealing performance metric of an automatic landing system is a measure of how close the system delivers the aircraft to the desired touchdown point.

With reference to Figure 7-4, the touchdown point is determined by calculating the point at which the trajectory of the tail hook intersects the carrier's deck, which is the plane defined by the points A, B and the desired touchdown point. The longitudinal and lateral displacements of the touchdown point from the desired touchdown point are determined by calculating the appropriate two-dimensional distance between the actual touchdown point and the desired touchdown point.

If touchdown occurs more than 60 ft forward of the desired touchdown point, the approached is defined as a bolter.

Landing forward of the desired touchdown point is defined as being positive longitudinal displacement, and landing to the port side of the centreline is defined as being positive lateral displacement.

Fortenbaugh [22] quotes the USN Automatic Carrier Landing System requirements document [80] as specifying that the dispersion of longitudinal displacement at touchdown should be less than 40 feet during Mode 1 operation. No atmospheric disturbance properties are defined for this dispersion requirement. Fortenbaugh calculates the standard deviation for a set of longitudinal touchdown dispersions and compares with the 40 feet requirement. The same approach has been adopted in this study.

For the statistical analysis where multiple approaches are simulated for a given carrier motion case for approaches that terminate with a successful touchdown, the mean

longitudinal and mean lateral touchdown displacements are calculated, along with the standard deviation of the touchdown displacements. This provides a means of comparing the performance of the systems with the only known Automatic Carrier Landing System requirement.

7.2.4 VERTICAL RATES

A useful set of performance metrics are the aircraft and aircraft carrier vertical rates. When the aircraft sink rate is compared to that of the nominal sink rate, the effects of atmospheric disturbances are evident.

7.2.4.1 AIRCRAFT SINK RATE

With reference to Figure 7-4, the aircraft sink rate at touchdown is defined as the instantaneous height rate referred to earth axes when the tail hook trajectory hook intersects the plane defined by the points A, B and the desired touchdown point. For the purposes of this study, sink rate is defined as being positive in the same direction as height rate, i.e. climb is positive and descent is negative.

7.2.4.2 AIRCRAFT CARRIER HEIGHT RATE

With reference to Figure 7-4. The aircraft carrier vertical rate at touchdown is defined as the instantaneous height rate referred to earth axes when the aircraft's tail hook trajectory hook intersects the plane defined by the points A, B and the desired touchdown point. For the purposes of this study, aircraft carrier vertical rate is defined as being positive in the same direction as aircraft sink rate.

7.3 METHOD OF SIMULATION

The method that was found to maximise efficiency of the batch simulations, and which also allowed the data to be stored for post simulation inspection, without imposing large virtual memory requirements that would slow the simulation process down, or even halt the process, was to write data to a file upon completion of each simulated approach, and then post process these data files upon completion of the entire batch.

For each simulation the aircraft is flown through the simulated aircraft carrier's deck, which is notionally at an altitude of 45 feet, to an altitude of 10 feet. This is to ensure that sufficient data is recorded to accurately define the point at which touchdown occurred during post processing of the data. Data is extracted from the simulation environment for the period of interest, from an altitude of 500 feet to an altitude of 10 feet, and written to a unique data file identified by the approach controller in use, turbulence conditions, wind speed and aircraft carrier speed.

During post processing, the approach performance metrics were calculated and written to a Matlab data structure. Also, it is during post processing that the trajectories of the points A, B and C are calculated. Each simulation takes between 8 and 10 minutes to process and the subsequent post processing takes between 4 and 6 minutes. The majority of the post processing time is due to time taken to read in the data files to the workspace.

While there are 1449 simulation results presented in this Chapter, many more simulations were conducted in the design phase. Three sets of batch simulations of 300 approaches and three sets of 180 approaches were conducted using two computers in an effort to increase time efficiency.

Depending on the relative velocities of the aircraft and the aircraft carrier under consideration, the simulated approach is initiated at an appropriate distance from the aircraft carrier. All simulated approaches are initiated at an altitude of 1200 feet, but only data from an altitude of 500 feet to touchdown is considered in this analysis, i.e. from tip over to touch down. For approaches in atmospheric turbulence, the turbulence velocities are held at zero until the aircraft reaches an altitude of 500 feet. In the case of carrier induced turbulence, the turbulence velocities are held at zero until the aircraft is within half a nautical mile of the aircraft carrier. As turbulence velocities are time variable they are calculated from initiation of the simulation.

The purpose of initiating the simulated approaches at an attitude of 1200 feet is to ensure that the vertical, track and approach speed deviations are zero at an altitude of 500 feet. As the relative distance between the aircraft and the aircraft carrier at initiation does not account for effects of steady wind on ground speed the initial vertical deviation

varies depending on the combination of wind speed and aircraft carrier dynamics. By experiment 1200 feet was found to be an appropriate altitude to initiate a simulated approach to ensure that these deviations were zero at an altitude of 500 feet.

The duration of each approach from an altitude of 1200 feet is dependent on the relative velocities of the aircraft and aircraft carrier. The duration of a particular approach will vary slightly depending on which approach controller is being used. The difference in duration between the baseline approach controller and the Direct Lift Control approach controller has been found to be in the region of 0.3 seconds, with the Direct Lift Control approach controller approach being longer in duration. The difference between the Direct Lift Control approach controller and the thrust vectoring approach controller is in the region of 0.02 seconds and is considered negligible. The differences in the duration of the approach is due to the manner in which each system responds to the position error at the initiation of the simulation. This initial position error is identical for all three systems as a function of aircraft carrier speed and wind speed.

As turbulence is time variable and it is generated from initiation of the simulation, albeit the velocities are held to zero until an altitude of 500 feet, for identical turbulence cases, depending on the approach controller in use at a particular time to touchdown, the turbulence velocities at that instant will be different as a function of approach controller. Essentially, the turbulence velocities are shifted in time by up to 0.3 seconds between the baseline approach controller and the Direct Lift Control approach controller or the thrust vectoring approach controller, i.e. Direct Lift Control approach controller or the thrust vectoring approach controller will experience the same turbulence profile but at a time to touchdown approximately 0.3 seconds closer to zero than baseline approach controller. This has a slight effect on touchdown performance and needs to be considered when comparing each systems performance.

7.4 APPROACH PERFORMANCE TEST CASES

The following three Test Cases are presented in order to illustrate the approach performance of the approach controllers and Navigation System. The metrics described in section 7.2 are used to assess the performance of each approach controller.

7.4.1 TEST CASE 1: NO ATMOSPHERIC DISTURBANCE

The purpose of this Test Case is to determine the steady state, or nominal, performance of the system with respect to the performance metrics defined in section 7.2. This Test Case considered omits atmospheric disturbance other than the steady wind associated with the aircraft carrier dynamics. The ship motion for this case is the most stable case, i.e. 2 knot headwind with a ship speed of 33 knots.

The vertical and lateral deviations from the approach path are presented in Figure 7-5. All parameters are plotted against time to touchdown, t_{td}, generated by the Navigation System. The pitch attitude and pitch attitude demand from the approach controllers are also presented. The pitch attitude of the Direct Lift Control approach controller and the thrust vectoring approach controller are both generally slightly greater than that of the baseline approach controller.

Despite the fact that there is no external disturbances the Direct Lift Control approach controller and the thrust vectoring approach controller demand small but relatively high frequency activity from both the trailing edge flap and spoiler presented in Figure 7-6. This is due to the large lead ratio of the lead compensator in the Direct Lift Control system.

The roll angle demanded by the approach controllers and the aircraft roll angle are also presented in Figure 7-5. Both of these are static at zero for all three approach controllers, reflecting the fact that there are no lateral disturbances. Similarly the rudder and aileron angle are zero as presented in Figure 7-6. The altitude and axial Earth position of both the aircraft and aircraft carrier are also presented in Figure 7-5.

The approach speed is held constant at 140 knots by all three approach controllers, however it is interesting to note that the engine speed is higher and reduces slightly as the aircraft approaches touchdown for the Direct Lift Control approach controller and the thrust vectoring approach controller when compared with the baseline approach controller. This reduction in engine speed coincides with a reduction of pitch attitude for both approach controllers.

With reference to Figure 7-6 it can be seen that the Direct Lift Control approach controller and the thrust vectoring approach controller require more elevator movement than the baseline approach controller, as expected due to the feedforward flap to elevator gain. It was commented by Fortenbaugh [22] that Direct Lift Control increases actuator wear of both the Direct Lift Control surfaces and the elevator, the increased actuator activity is readily apparent in Figure 7-6. It can be seen that thrust vectoring approach controller demands less activity from the elevator than the Direct Lift Control approach controller.

The performance metrics are presented in presented in Table 7-1. The RMS value of approach glide path, approach track and approach speed deviation for an ideal approach is zero. The ideal aircraft height over the ramp is 8.39 ft, assuming that the aircraft carrier has a pitch attitude of zero at the time that the aircraft passes over its ramp. Intuitively the ideal longitudinal and lateral touchdown dispersions are 0 feet in both instances. Based on an approach speed of 140 knots and a headwind of 2 knots the ideal aircraft sink rate at touchdown is -12.20 ft/s.

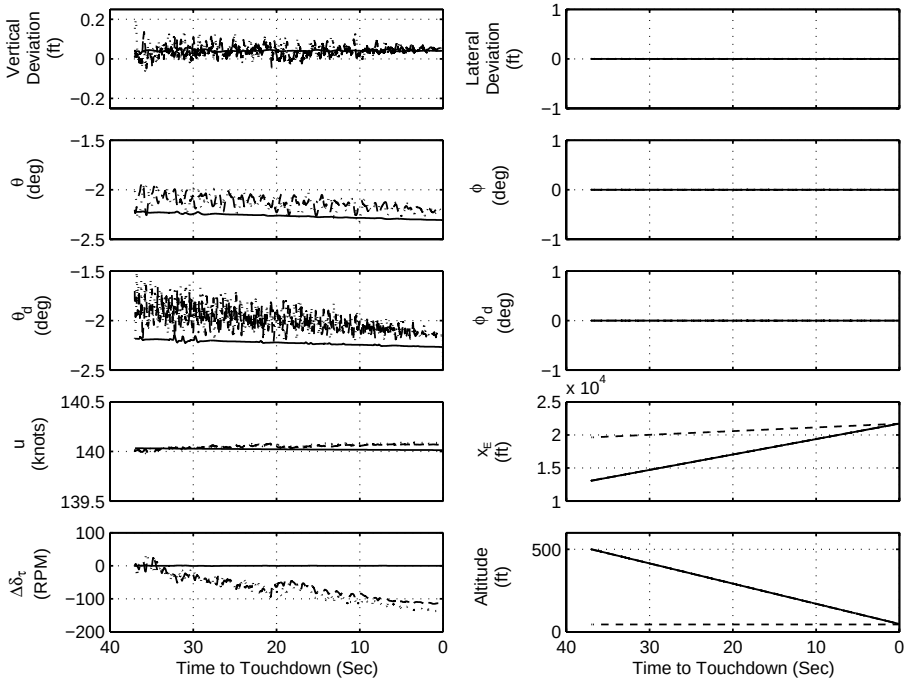

Figure 7-5 Selected Aircraft Parameters for No Atmospheric Disturbance Approach Baseline [——] Direct Lift Control [- - -] Thrust Vectoring [·····] Aircraft Carrier [- · -]

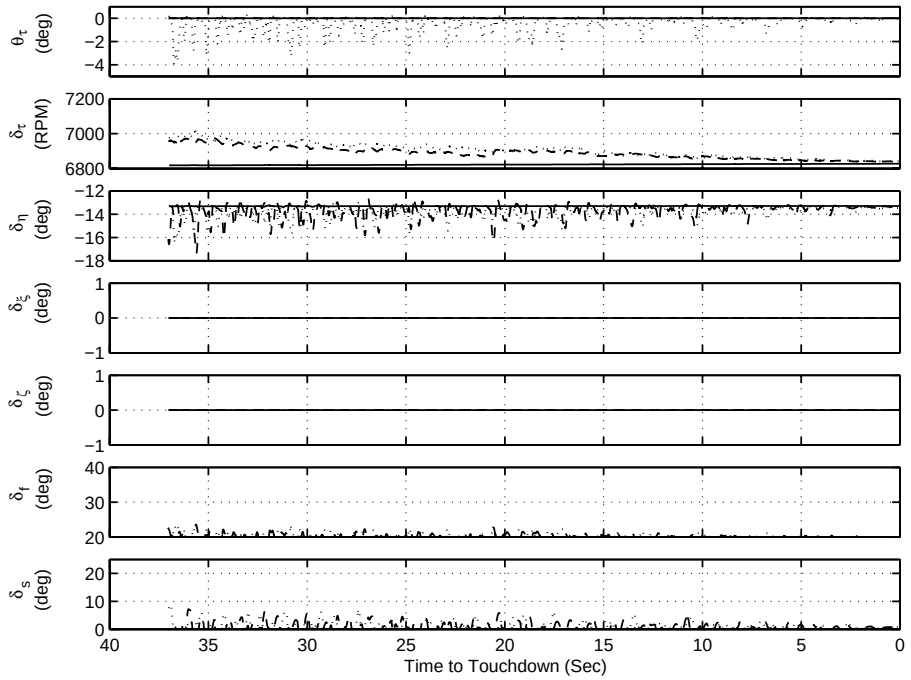

Figure 7-6 Control Effectors Positions for No Atmospheric Disturbance Approach
Baseline [——] Direct Lift Control [- - - -] Thrust Vectoring [·····]

	Baseline	Direct Lift Control	Thrust Vectoring
Approach Success	Yes	Yes	Yes
Approach Glide Path Deviation RMS	0.03 ft	0.03 ft	0.03 ft
Approach Track Deviation RMS	0 ft	0 ft	0 ft
Approach Speed Deviation RMS	0.01 kts	0.03 kts	0.04 kts
Ramp Crossing Height	8.40 ft	8.40 ft	8.40 ft
Aircraft Carrier Pitch Attitude at Ramp Crossing	-0.01 deg	-0.01 deg	-0.01 deg
Approach Glide Path Deviation at Ramp Crossing	0.04 ft	0.04 ft	0.04 ft
Ramp Strike	No	No	No
Longitudinal Displacement at Touchdown	0.59 ft	0.91 ft	1.15 ft
Lateral Displacement at Touchdown	0 ft	0 ft	0 ft
Aircraft Sink Rate at Touchdown	-12.18 ft/s	-12.20 ft/s	-12.22 ft/s
Aircraft Carrier Vertical Rate at Touchdown	-0.08 ft/s	-0.06 ft/s	0 ft/s
Bolter	No	No	No

Table 7-1 Test Case 1 Performance Summary

7.4.2 TEST CASE 2: INTRODUCTION OF WINDSHEAR, DISCRETE GUST AND CARRIER INDUCED TURBULENCE

The second Test Case includes vertical wind shear, an axial discrete gust, steady wind associated with the carrier dynamics and carrier induced turbulence. The carrier dynamics are the same as for Test Case 1. The purpose of this Test Case is to assess and compare the approach controllers' response to discrete atmospheric disturbances.

Longitudinal aircraft, approach controller and navigation parameters are presented in Figure 7-7, lateral parameters are presented in Figure 7-8, and the associated control effectors positions in Figure 7-10.

The velocity components of each of the constituent disturbances, atmospheric disturbances velocities, (u_a, v_a, w_a), which includes wind shear, discrete gusts and atmospheric turbulence, carrier induced turbulence velocities, (u_c, v_c, w_c), and steady wind velocities, (u_w, v_w, w_w), are presented in Figure 7-9 with reference to the earth axis system. The total disturbance velocity components, (U_d, V_d, W_d), are presented with reference to the body axis system.

All parameters are plotted against the Navigation System generated time to touchdown, t_{td}. Time to touchdown, t_{td}, is defined in Chapter 4. Time to touchdown generally decreases as the aircraft approaches the carrier; however, in the presence of an atmospheric disturbance that impedes the aircraft's progress, time to touchdown can be seen to increase. This manifests itself in what resembles a loop in the plot of a particular variable. This is evident in Figure 7-7 at the onset of the vertical wind shear. The associated performance summary is presented in Table 7-2.

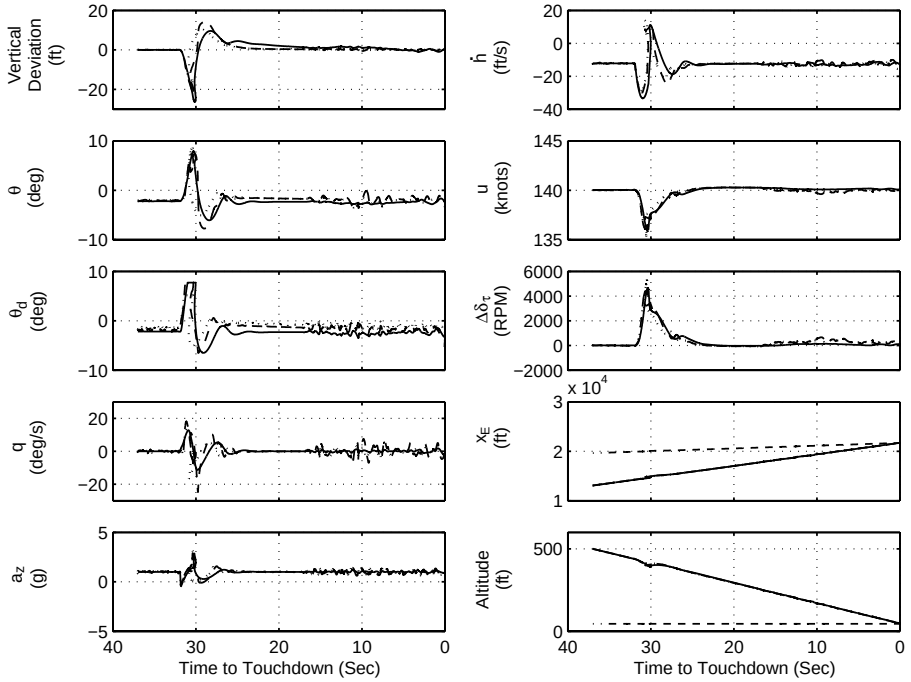

Figure 7-7 Longitudinal Aircraft Variables for Test Case 2
Baseline [——] Direct Lift Control [– – –] Thrust Vectoring [·····] Aircraft Carrier [– · –]

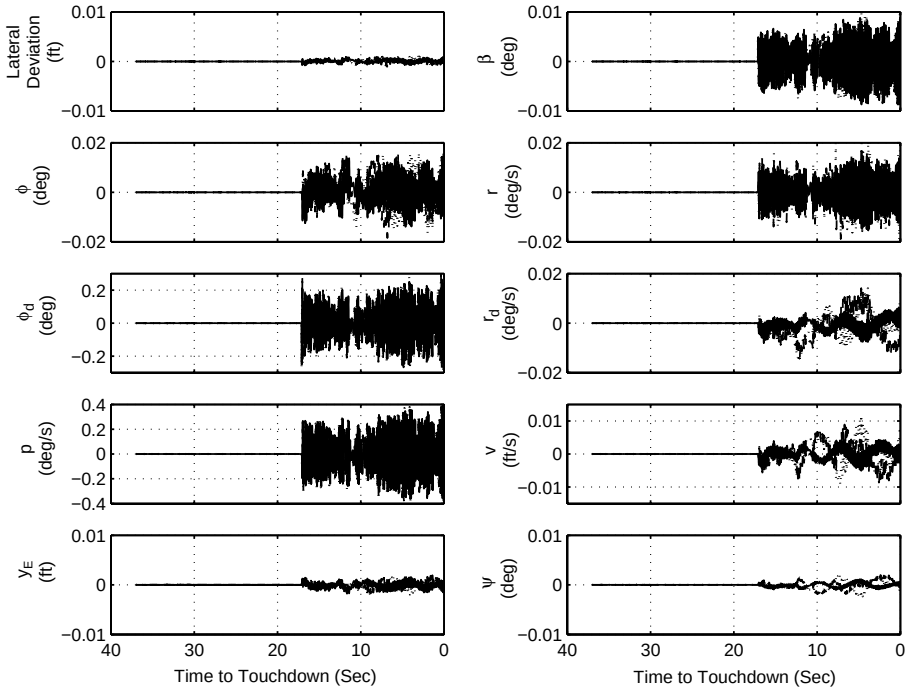

Figure 7-8 Lateral Aircraft Variables for Test Case 2
Baseline [——] Direct Lift Control [- - - -] Thrust Vectoring [·····]

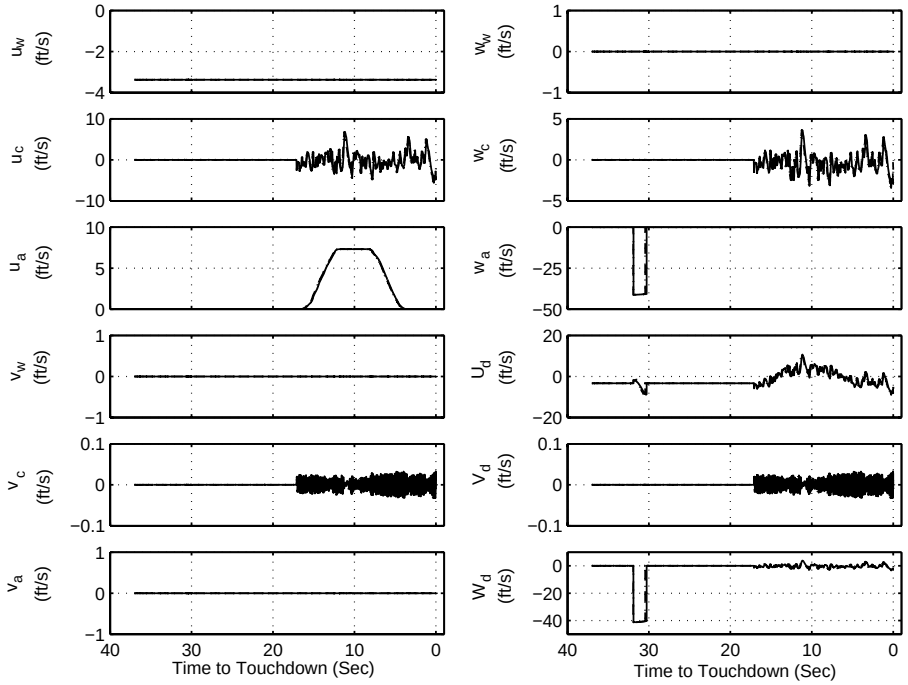

Figure 7-9 Atmospheric Disturbances for Test Case 2
Baseline [——] Direct Lift Control [- - - -] Thrust Vectoring [·····]

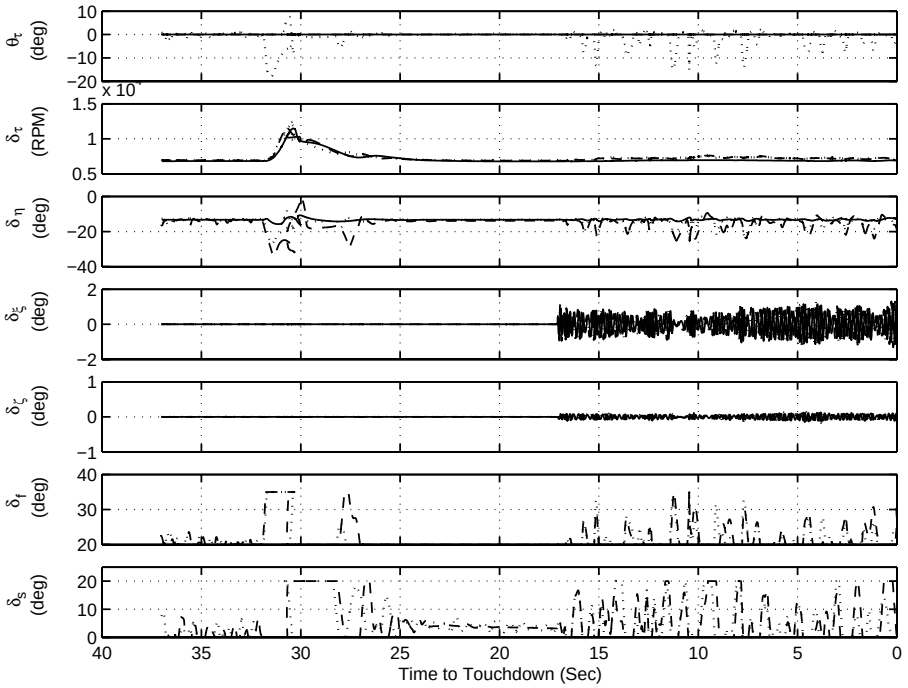

Figure 7-10 Control Positions Effectors for Test Case 2
Baseline [——] Direct Lift Control [- - - -] Thrust Vectoring [·····]

	Baseline	Direct Lift Control	Thrust Vectoring
Approach Success	Yes	Yes	Yes
Approach Glide Path Deviation RMS	3.53 ft	2.89 ft	2.42 ft
Approach Track Deviation RMS	0 ft	0 ft	0 ft
Approach Speed Deviation RMS	0.53 kts	0.56 kts	0.58 kts
Ramp Crossing Height	7.47 ft	8.07 ft	8.4 ft
Aircraft Carrier Pitch Attitude at Ramp Crossing	-0.01 deg	-0.01 deg	-0.01 deg
Approach Glide Path Deviation at Ramp Crossing	-0.89 ft	-0.28 ft	0.04 ft
Ramp Strike	No	No	No
Longitudinal Displacement at Touchdown	11.69 ft	6.20 ft	0.54 ft
Lateral Displacement at Touchdown	0 ft	0 ft	0 ft
Aircraft Sink Rate at Touchdown	-13.06 ft/s	-17.12 ft/s	-14.63 ft/s
Aircraft Carrier Vertical Rate at Touchdown	-0.04 ft/s	-0.04 ft/s	-0.1 ft/s
Bolter	No	No	No

Table 7-2 Test Case 2 Performance Summary

With reference to Figure 7-7, it can be seen that both the Direct Lift Control approach controller and the thrust vectoring approach controller respond quicker to the wind shear and as a result deviate less below the desired approach glide path, with the thrust vectoring approach controller responding best in this regard. However, during recovery of the desired approach glide path both the Direct Lift Control approach controller and the thrust vectoring approach controller overshoot the zero deviation point to a greater degree than the baseline approach controller, with the thrust vectoring approach controller responding better than the Direct Lift Control approach controller in this regard. It is interesting to note that the vertical wind shear velocity reduced to zero at a point that all three approach controller's height rate is at a maximum and acting in the opposite direction to the wind shear velocity, hence such a pronounced overshoot by all three approach controllers.

The Direct Lift Control approach controller and the thrust vectoring approach controller return to a steady state zero approach glide path deviation condition quicker than the

baseline approach controller, reflected in the approach glide path deviation RMS values presented in Table 7-2.

Under the wind shear condition it can be seen that all three approach controllers responded very similarly with respect to approach speed deviations. The cause of the deviation in all three cases is the sudden change in pitch attitude, which is identical for all three approach controllers, i.e. a maximum commanded pitch attitude change of 10 degrees.

The response of all three approach controllers to the axial gust are very similar. The direction of the gust is the reciprocal of the aircraft's heading, i.e. a tail wind. Tail winds are not favourable during an approach for landing as they have the effect of lowering airspeed. An inspection of the engine speed shows a slight increase at the onset of the gust and a corresponding decrease as the gust dissipates for all three systems. This is to compensate for the loss of airspeed due to the tailwind.

It is interesting to note that for all three approach controllers aircraft velocity was slightly high, 140.25 knots, at the onset of the discrete gust. For all three approach controllers the engine speed at the onset of the gust was at idle (idle engine speed is a function of altitude and Mach number). This is evident by the fact that the autothrottle is demanding a reduction in engine speed and the engine speed is static for this period. This aircraft is known for its lack of drag, even in the landing configuration, providing little aerodynamic braking during such an approach, hence the slight overspeed.

When inspecting the time history of aircraft velocity for the Direct Lift Control approach controller and the thrust vectoring approach controller, care has to be paid in separating the response due to the gust and that due to the aircraft's pitch attitude, recalling that u is body axis velocity. During the last 15 seconds of the approach, the trailing edge flaps become quite active due to aircraft carrier induced turbulence, and hence trailing edge flap induced pitching moment. The velocity oscillations correlate to the pitch attitude oscillations. The pitch attitude, and as a result velocity, oscillations are less pronounced for the thrust vectoring approach controllers when compared to the

Direct Lift Control approach controllers. The baseline approach controller is immune from this phenomenon as the trailing edge flaps are static.

There is a single lateral disturbance of almost negligible magnitude, carrier induced lateral velocity. The response of all three approach controllers to this disturbance is similar. While this disturbance is of almost negligible magnitude, and of zero mean, it is of high frequency, hence the high frequency roll rate and roll attitude demand signals. It should be noted that all three approach controller responses are plotted on the same axes, perhaps giving the impression of an even higher frequency response.

With reference to Table 7-2 it can be seen that the thrust vectoring approach controller performs best in terms of approach glide path deviation RMS; however, the baseline approach controller performs marginally better with respect to approach speed deviation for reasons already discussed.

With respect to ramp crossing height, it is readily apparent that the thrust vectoring approach controller performs best. The aircraft carrier's pitch attitude at that instant is equal for all three systems. The approach glide path deviation of the baseline system at that instant is 10.5% of the ideal ramp crossing height, or 10.5% of the ideal safety margin at that instant. In this instance, it does not pose a threat to the safety of the approach. It is indicative of the systems' performance.

The thrust vectoring approach controller has the least longitudinal displacement at touchdown from the desired touchdown point with the baseline approach controller showing the least accurate performance. However, the sink rate at touchdown is significantly higher than the ideal sink rate for both the Direct Lift Control approach controller and the thrust vectoring approach controller, while the sink rate of the baseline approach controllers is also greater than ideal.

As expected there is a finite lag between a given atmospheric disturbance event and an approach controller response, the duration of which is defined by the combination of the control system and aircraft dynamics. In this case, just before touchdown, the total vertical turbulence velocity changes from +3 ft/s at 1.25 seconds to touchdown to -3.5 ft/s at 0.4 seconds to touchdown.

The effects of this sudden change in vertical velocity are reflected in the higher than ideal sink rates. This change in total vertical turbulence velocity was preceded by a similar sudden change vertical turbulence velocity but in the opposite direction. The approach controllers were responding to this first change while the second vertical velocity change was occurring and had begun to respond to the second change as touchdown occurred. The fact that the approach controllers had begun to respond to the second change of total vertical velocity is evident by the fact that spoilers are retracted and the trailing edge flap extended at the touchdown instant.

The fact that the Direct Lift Control approach controller and the thrust vectoring approach controller responds quicker to disturbances is manifest by greater changes in height rate. The result of this, coupled with the finite lag between the atmospheric disturbance event and the approach controller response, is a higher sink rate at touchdown due to the approach controller response to the first change in vertical turbulence velocity. This is compounded by the actual vertical turbulence velocity at the instant of touchdown.

The higher sink rates of the Direct Lift Control approach controller and the thrust vectoring approach controller should not be correlated with the better longitudinal touchdown dispersion of these systems. The fact that the Direct Lift Control approach controller and the thrust vectoring approach controller have lower approach glide path deviation values indicate that the better longitudinal touchdown performance is due to the approach controllers better approach glide path tracking performance.

Laterally there is no significant performance difference between all three systems, as expected, considering the lack of lateral disturbances.

As with Test Case 1, the level of elevator actuator activity required for the Direct Lift Control approach controller and the thrust vectoring approach controller is greater than the baseline approach controller.

7.4.3 TEST CASE 3: CONTINUOUS THREE DIMENSIONAL TURBULENCE AND CARRIER INDUCED TURBULENCE

The third Test Case includes three dimensional continuous moderate turbulence, steady wind associated with the carrier dynamics and carrier induced turbulence. The carrier dynamics are the same as Test Case 1. Longitudinal aircraft, approach controllers and navigation parameters are presented in Figure 7-11, lateral parameters are presented in Figure 7-12, the disturbance velocities are presented in Figure 7-13 and the associated control effectors positions are presented in Figure 7-14. The disturbance velocities are presented similarly to Test Case 2 and again all parameters are plotted against the Navigation System generated time to touchdown, t_{td}. The associated performance metrics are presented in Table 7-3.

With reference to Figure 7-11 it can clearly be seen that the Direct Lift Control approach controller and the thrust vectoring approach controller outperform the baseline approach controller with respect to attenuating the effects of vertical turbulence during the approach. This is reflected in the systems respective approach glide path deviation RMS values, which show that the thrust vectoring approach controller performs the best of the three systems.

It is interesting to note that the thrust vectoring approach controller commands less trailing edge flap and spoiler activity in the latter stages of the approach, presented in Figure 7-14. This has the effect of introducing less trailing edge flap induced pitching moment, which is evident in Figure 7-11.

Each of the three approach controllers has the same approach track controller. It is interesting to note that as the approach glide path deviation performance improves from the baseline approach controller to the thrust vectoring approach controller, the track deviation performance degrades, although the magnitude of degradation is insignificant, approximately 1.9 inches.

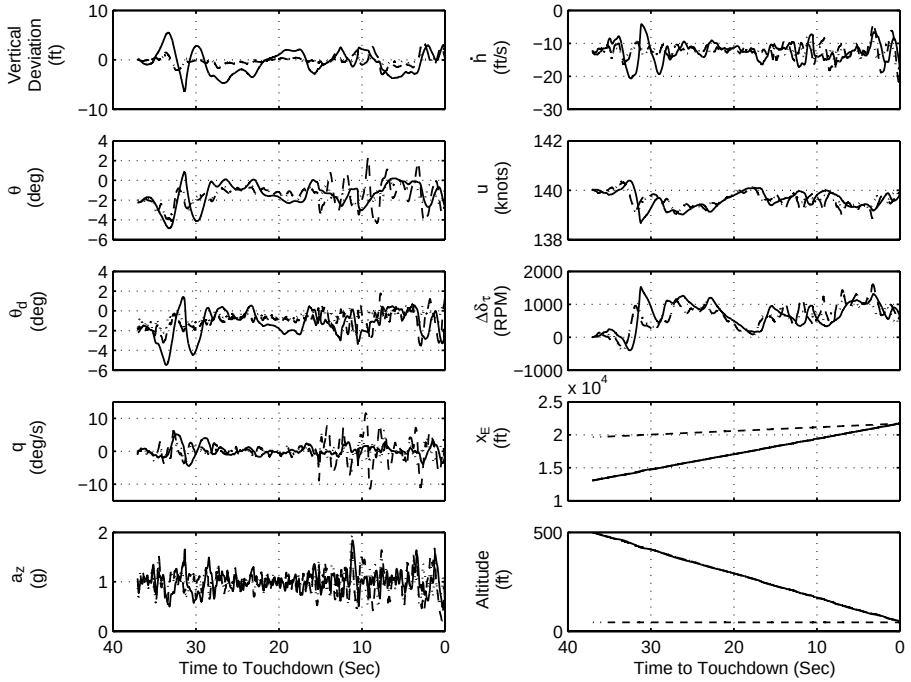

Figure 7-11 Longitudinal Aircraft Variables for Test Case 3
Baseline [——] Direct Lift Control [- - -] Thrust Vectoring [·····] Aircraft Carrier [- · -]

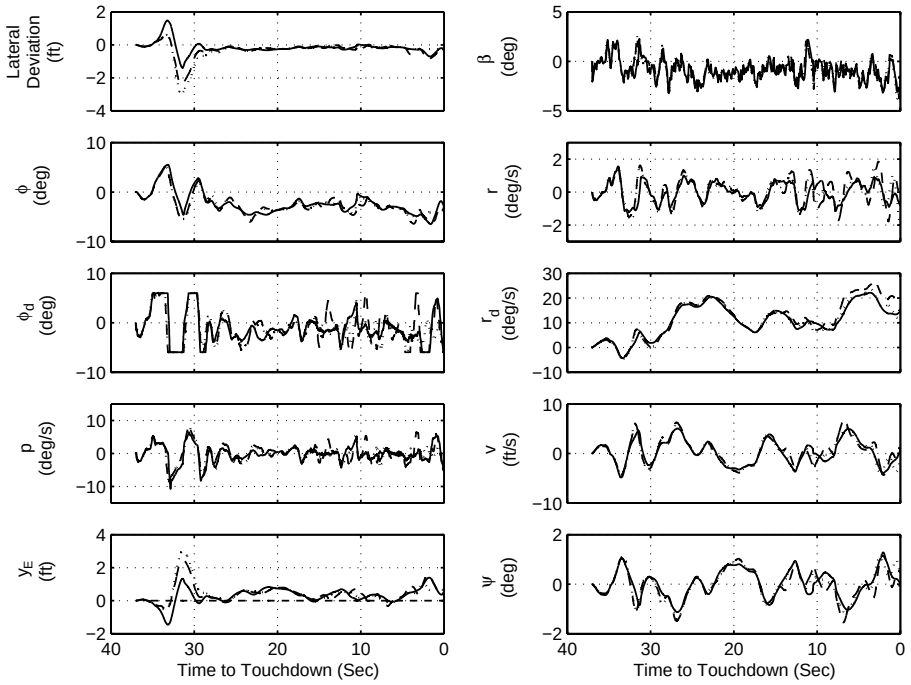

Figure 7-12 Lateral Aircraft Variables for Test Case 3
Baseline [——] Direct Lift Control [- - -] Thrust Vectoring [·····] Aircraft Carrier [- · -]

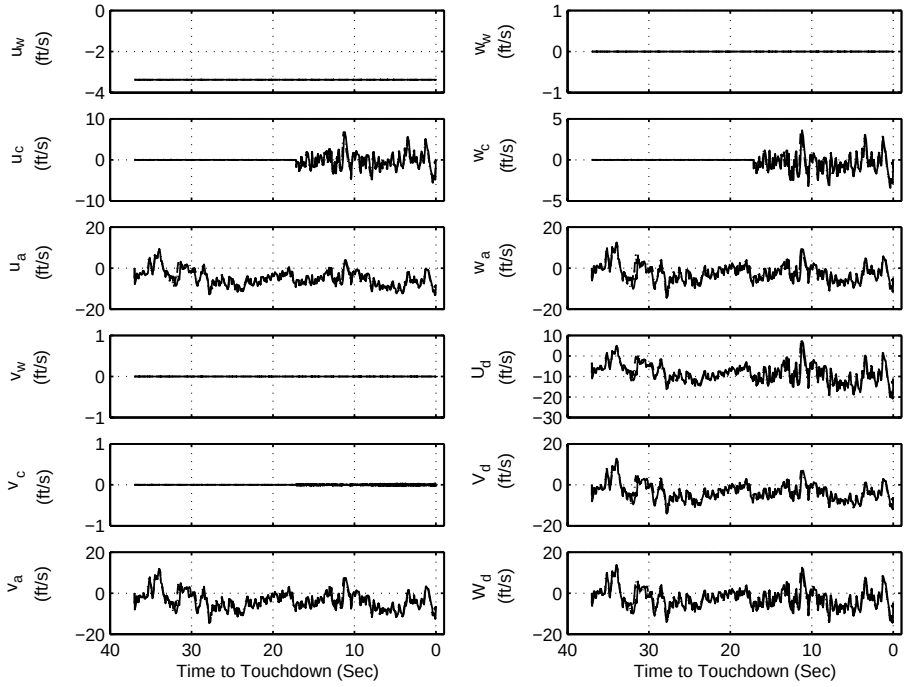

Figure 7-13 Atmospheric Disturbances for Test Case 3
Baseline [——] Direct Lift Control [- - - -] Thrust Vectoring [·····]

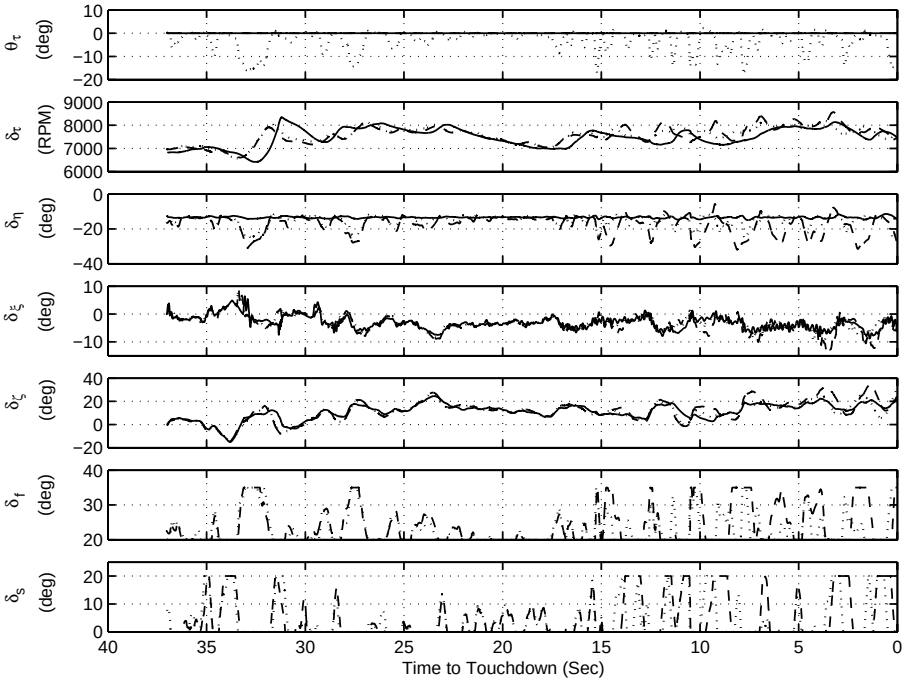

Figure 7-14 Control Effectors Positions for Test Case 3
Baseline [——] Direct Lift Control [- - - -] Thrust Vectoring [·····]

	Baseline	Direct Lift Control	Thrust Vectoring
Approach Success	Yes	Yes	Yes
Approach Glide Path Deviation RMS	1.57 ft	0.68 ft	0.36 ft
Approach Track Deviation RMS	0.26 ft	0.35 ft	0.42 ft
Approach Speed Deviation RMS	0.33 kts	0.31 kts	0.29 kts
Ramp Crossing Height	8.44 ft	8.99 ft	9.08 ft
Aircraft Carrier Pitch Attitude at Ramp Crossing	-0.01 deg	-0.01 deg	-0.01 deg
Approach Glide Path Deviation at Ramp Crossing	0.08 ft	0.64 ft	0.73 ft
Ramp Strike	No	No	No
Longitudinal Displacement at Touchdown	28.62 ft	1.58 ft	-10.3 ft
Lateral Displacement at Touchdown	0.72 ft	0.95 ft	0.77 ft
Aircraft Sink Rate at Touchdown	-17.87 ft/s	-21.0 ft/s	-16.58 ft/s
Aircraft Carrier Vertical Rate at Touchdown	-0.05 ft/s	-0.05 ft/s	-0.04 ft/s
Bolter	No	No	No

Table 7-3 Test Case 3 Performance Summary

At the initiation of the approach, the atmospheric turbulence velocity profiles for all three axes is rectangular pulse-like. This turbulence profile has the effect of causing relatively large approach glide path and approach track deviations. With respect to approach glide path deviation the baseline approach controller responds less well in comparison to the Direct Lift Control approach controller and the thrust vectoring approach controller. However, with respect to lateral position deviation the baseline approach controller responded better than the Direct Lift Control approach controller and the thrust vectoring approach controller. The overshoot seen in the time history of lateral deviation of the baseline approach controller is increased for the Direct Lift Control approach controller and the thrust vectoring approach controller due to the extension of trailing edge flaps. The extension of the flaps while the aircraft was banked had the effect of compounding the effects of the lateral turbulence.

In this case, the approach speed deviation performance improves from the baseline approach controller to the thrust vectoring approach controller, although the difference between approach speed deviation RMS values of these approach controllers is

practically negligible, 0.04 kts. From Figure 7-11 it can be seen that the autothrottle performance criteria specified in Chapter 5 is maintained.

For all three approach controllers the aircraft passes over the ramp at heights greater than ideal. At that instance it can be seen that the baseline approach controller is closest to the ideal height while the Direct Lift Control approach controller is furthest from the ideal height. In the case of atmospheric turbulence ramp crossing, height should be analysed in conjunction with approach glide path deviation RMS in order to assess an approach controllers ramp crossing height characteristics. The lower the approach glide path deviation RMS, the more likely an aircraft controlled by that approach controller will consistently pass over the ramp at the height indicated. In this case, the aircraft when controlled by the baseline approach controller passes over the ramp at a height closest to ideal, but has the largest approach glide path vertical deviation RMS value, indicating that it is less likely to consistently pass over the ramp at its indicated height than the aircraft controlled by the thrust vectoring approach controller which has the lowest approach glide path vertical deviation RMS value.

With reference to Table 7-3, the longitudinal displacement at touchdown for the baseline approach controller is greater than 20 ft, but less than 60 ft, indicating that the aircraft landed beyond the third arresting wire, but before the fourth arresting wire. Both the Direct Lift Control approach controller and the thrust vectoring approach controller landed before the third wire. The higher than ideal sink rates at touchdown produced by all three approach controllers is explained similarly to Test Case 2.

The lateral displacements at touchdown are all relatively small and within 2.76 inches of each other, and together with the track deviation RMS values indicate very precise track control in the presence of continuous moderate turbulence.

The same conclusions can be drawn here as with Test Case 1 with respect to the level of actuator activity required for the Direct Lift Control approach controller and the thrust vectoring approach controller.

In general, it can be seen that the thrust vectoring approach controller has the best performance with respect to attenuating the atmospheric disturbance effects on the flight

path. In this case, the only parameter in which the performance of the Direct Lift Control approach controller was better than the thrust vectoring approach controller is longitudinal displacement at touchdown. The baseline approach controller consistently performed least well.

7.5 STATISTICAL ANALYSIS

In order to investigate the limits of each approach controller, and to characterise its performance in a general sense, a series of simulations were conducted for varying atmospheric and aircraft carrier motion conditions for each of the three approach controllers.

Aircraft carrier motion is defined by wind speed and aircraft carrier speed and the relative direction of the aircraft carrier and wind velocity vectors. As this study is limited to head wind conditions only, wind speed and aircraft carrier speed were varied. The combination of four wind speeds and three aircraft carrier speeds, giving a total of 12 aircraft carrier motion cases, were considered. These speeds are listed in Table 7-4. As discussed in Chapter 3, five sets of aircraft carrier motion time histories are considered for each carrier motion case.

Wind Speed (kts) [Beaufort Scale]	Aircraft Carrier Speed (kts)
2 [1]	0
13.5 [4]	10
24.5 [6]	33
37 [8]	

Table 7-4 Aircraft Carrier Speeds and Wind Speeds Considered for Statistical Analysis

For each of these sixty unique aircraft carrier motion conditions, a total of eight atmospheric disturbance conditions were considered as listed in Table 7-5. The purpose of turbulence cases 4, 6 and 8 is to allow any trends relating to the interaction between the approach glide path controller and the approach track controller to be identified. The

turbulence parameters used to define light, moderate and severe turbulence are defined in Chapter 3.

	Turbulence Case							
	1	2	3	4	5	6	7	8
Carrier Induced Turbulence	No	Yes	Yes	Yes	Yes	Yes	Yes	Yes
Vertical Turbulence	No	No	Light	Light	Moderate	Moderate	Severe	Severe
Axial Turbulence	No	No	Light	Light	Moderate	Moderate	Severe	Severe
Lateral Turbulence	No	No	Light	No	Moderate	No	Severe	No

Table 7-5 Atmospheric Disturbance Conditions Considered for Statistical Analysis

For each of these 1440 simulated approaches, the performance metrics presented in section 7.2 have been calculated. For each set of five aircraft carrier motion time histories defined by wind speed and aircraft carrier speed, the mean and standard deviation of these metrics have been calculated. This statistical data forms the basis of the following sections and are tabulated in full in Appendix B. The following discussion concerns the mean data only, the standard deviation of the data is only discussed in the event that it indicates a large spread in performance.

The discussion is presented in two sections. Firstly, the approach performance of each system, including ramp crossing height, is discussed per atmospheric disturbance case, and secondly, the touchdown performance of each system is discussed per atmospheric disturbance case.

7.5.1 APPROACH PERFORMANCE

7.5.1.1 NO ATMOSPHERIC DISTURBANCE

The purpose of this atmospheric disturbance case is to provide a measure of how well the systems perform in ideal conditions. Any peculiarities associated with aircraft carrier motion will be evident in this case. The associated statistical data is presented in Appendix B, Tables B-1 to B-4.

A summary of the approach performance with respect to the success criteria is presented in Figure 7-15. Every approach for each approach controller for this atmospheric disturbance case is presented in Figure 7-15. Successful approaches are presented along with wave-offs due to exceeding lateral and vertical approach path deviations if applicable. Ramp strikes are not presented in Figure 7-15, or any subsequent similar Figure as no ramp strikes occurred in any of the 1440 simulated approaches.

The 180 simulated approaches for the no atmospheric disturbance case are presented in Figure 7-15 with respect to the approach performance criteria in twelve sub-figures. The sub-figures are defined by a unique combination of wind speed and aircraft carrier speed. The five simulated approaches for each of the three approach controllers are presented for that combination of wind speed and aircraft carrier speed in each of the sub-figures. With reference to the legend accompanying Figure 7-15 the approach controllers are labelled along the horizontal axis and each of the five simulated approaches along the vertical axis for each sub-figure. Each simulated approach is represented by a block the colour of which is determined by the approach success criteria. In the case of Figure 7-15 all approaches were successful and as a result each simulated approach is presented in white. In similar figures for the remaining atmospheric disturbance cases, failed approaches are presented in grey and black as appropriate. These figures allow a large quantity of data to be accurately interpreted visually.

As expected, all approaches for this atmospheric disturbance case were completed successfully. The largest mean approach glide path vertical deviation RMS value is 0.35 ft recorded for the baseline approach controller for a wind speed of 37 knots and an aircraft carrier speed of 33 knots, while the majority of mean approach glide path vertical deviation RMS values were less than 0.05 ft. All approach track lateral deviation RMS values were zero. The largest approach speed deviation is 0.15 knots recorded for the Direct Lift Control approach controller for a wind speed of 13.5 knots and an aircraft carrier speed of 33 knots, while the majority of mean approach speed deviation RMS values were less than 0.05 knots.

The mean approach glide path vertical deviation at ramp crossing for all three approach controllers are all in the range of 0.05 to 0.01 ft, or 0.6 inches to 0.1 inches. The thrust vectoring approach controller consistently demonstrates the most precise tracking of the approach glide path, with the baseline controller being the least precise. However, considering the relative errors and the fact that the Test Case is extremely clinical, it has to be concluded that all three approach controllers demonstrate very precise approach glide path control from the initiation of the approach to touchdown.

Any variations in mean ramp crossing height are solely due to the effects of aircraft carrier pitch attitude. This effect is greatest for the Direct Lift Control approach controller and the thrust vectoring approach when the aircraft carrier speed is 0 knots and the steady wind speed is 37 knots. The aircraft carrier pitch attitude at ramp crossing is -0.18 degrees, eroding the ramp crossing height by 0.5 feet.

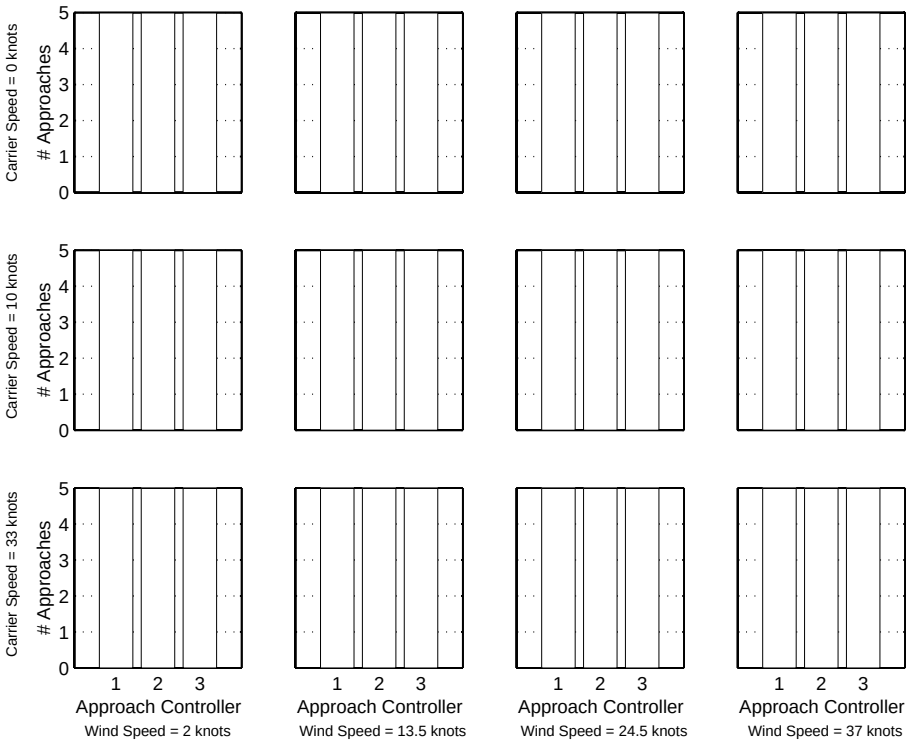

Figure 7-15 Approach Performance – No Atmospheric Disturbance
1= Baseline; 2 = Direct lift Control; 3 = Thrust Vectoring
Success □, Exceeded Vertical Deviation ■, Exceeded Lateral Deviation ▭

7.5.1.2 NO ATMOSPHERIC DISTURBANCE AND CARRIER INDUCED TURBULENCE

The purpose of this atmospheric disturbance case is to assess the performance of the approach controllers in an atmospheric disturbance case that is most representative of normal operating conditions.

The associated statistical data is presented in Appendix B, Tables B-5 to B-8. A summary of the approach performance with respect to the success criteria is presented in Figure 7-16. Before reviewing the performance it should be recalled that the steady, periodic, and random components of the carrier induced turbulence are defined as functions of steady wind.

All approaches are successful for this atmospheric disturbance case. As expected the mean approach glide path deviation RMS values increase as the wind speed increases regardless of the system. The thrust vectoring approach controller consistently performs best with the baseline approach controller performing the least well, with the notable exception of the 33 knots aircraft carrier speed, 2 knot steady wind case where the baseline approach controller outperforms both the Direct Lift Control approach controller and the thrust vectoring approach controller, with the Direct Lift Control approach controller performing the least well.

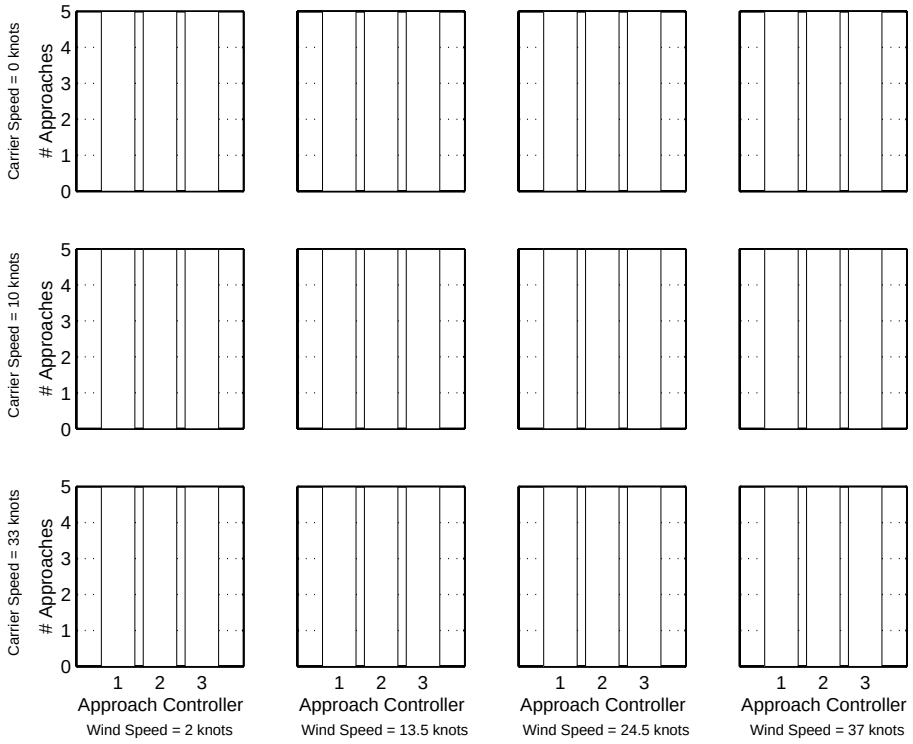

Figure 7-16 Approach Performance – No Atmospheric Disturbance and Carrier Induced Turbulence
1= Baseline; 2 = Direct lift Control; 3 = Thrust Vectoring
Success □, Exceeded Vertical Deviation ■, Exceeded Lateral Deviation ▭

With regard to mean approach glide path vertical deviation at ramp crossing, the absolute magnitudes for the thrust vectoring approach controller are consistently lower than both the Direct Lift Control approach controller and the baseline approach controller with the exception being the 10 knot aircraft carrier speed, 13.5 knot steady wind case where the baseline approach controller is of a lower absolute magnitude. However, when the mean approach glide path vertical deviation RMS values are inspected, it can be seen that the thrust vectoring approach controller provides more precise control over the duration of the approach and the baseline approach controller is the least precise. This case highlights the effects that the random nature of turbulence has on a point analysis and that in order to fully appreciate an approach controller's performance, metrics should not be assessed in isolation.

For the more precise approach glide path controllers, the contribution of aircraft carrier pitch attitude can be seen to be greater than the glide path deviation contribution to deviation from the ideal ramp crossing height.

The mean approach track lateral deviation RMS values are of the order of 0.07 feet to 0 feet. With regard to mean approach speed deviation RMS, the trend indicates that the Direct Lift Control approach controller performs the least well with the baseline approach controller performing slightly better than the thrust vectoring approach controller.

7.5.1.3 LIGHT TURBULENCE AND CARRIER INDUCED TURBULENCE

The purpose of this atmospheric disturbance case is to assess the performance of the approach controller in an atmospheric disturbance environment representative of a challenging but realistic operating condition

In order to decouple the lateral and vertical performance of each system, two Test Cases are presented for light, moderate and severe atmospheric turbulence. In the first case, axial and vertical turbulence are applied as normal and the lateral turbulence velocity is fixed at zero. In the second case, all three turbulence velocities are applied as normal. The data discussed in this section are presented in Appendix B, Tables B-9 to B-16. A summary of the approach performance with respect to the success criteria for the two dimensional turbulence case is presented in Figure 7-17 and similarly for the three dimensional turbulence case in Figure 7-18.

As with the preceding atmospheric turbulence case, the thrust vectoring approach controller more precisely controls approach glide path deviation, with the baseline approach controller performing the least well. In both the two and three dimensional cases, all five approaches for the 10 knot aircraft carrier speed, 24.5 knot wind speed case breach the approach glide path vertical deviation limits presented in Figure 7-2 for the baseline approach controller, while the Direct Lift Control approach controller and thrust vectoring approach controller continue to landing.

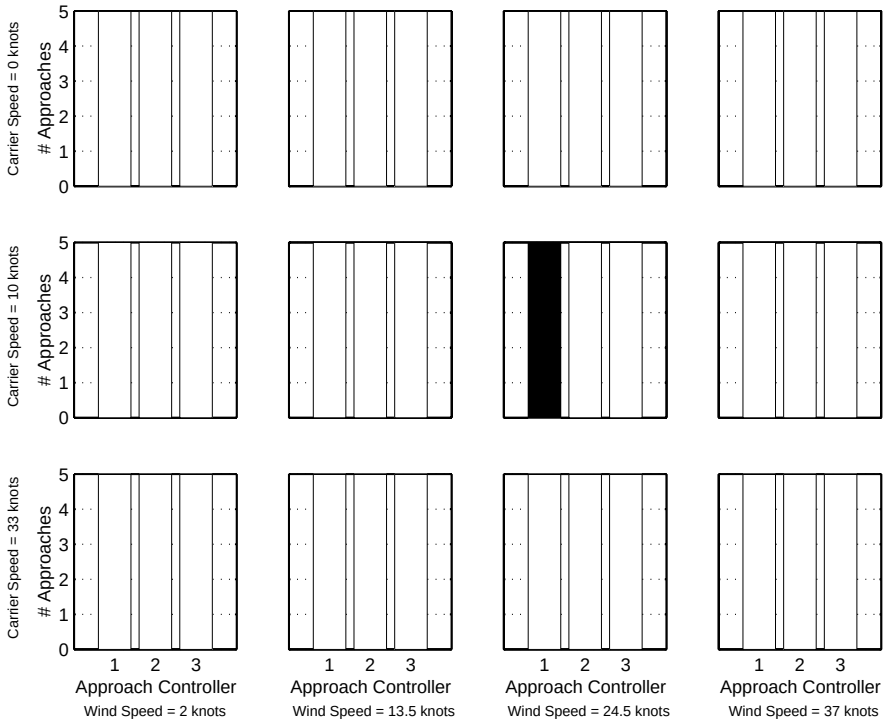

Figure 7-17 Approach Performance – Light Two Dimensional Turbulence and Carrier Induced Turbulence
1= Baseline; 2 = Direct lift Control; 3 = Thrust Vectoring
Success □ , Exceeded Vertical Deviation ■ , Exceeded Lateral Deviation ▭

When the mean approach glide path vertical deviation RMS values are compared for the two and three dimensional turbulence cases, it can be seen that the lateral turbulence slightly degrades the approach glide path controller's tracking performance. However, this is more evident for the baseline approach controller and less so for the thrust vectoring approach controller.

The trend with respect to mean lateral deviation RMS for the three dimensional turbulence case indicates that at lower wind speeds the baseline approach controller controls approach track performance more precisely, while the thrust vectoring approach controller controls approach track performance the least well. However, at the maximum wind speed case, 37 knots, the lateral track control performance of the baseline approach controller degrades to such an extent that all five approaches for the cases of aircraft carrier speeds of 10 knots and 33 knots breach the lateral wave-off boundaries presented in Figure 7-3, while the corresponding approaches for the Direct

Lift Control approach controller and the thrust vectoring approach controller are successful with the exception of two approaches by the Direct Lift Control approach controller at an aircraft carrier speed of 10 knots. This indicates that more precise approach glide path deviation control benefits lateral track deviation control.

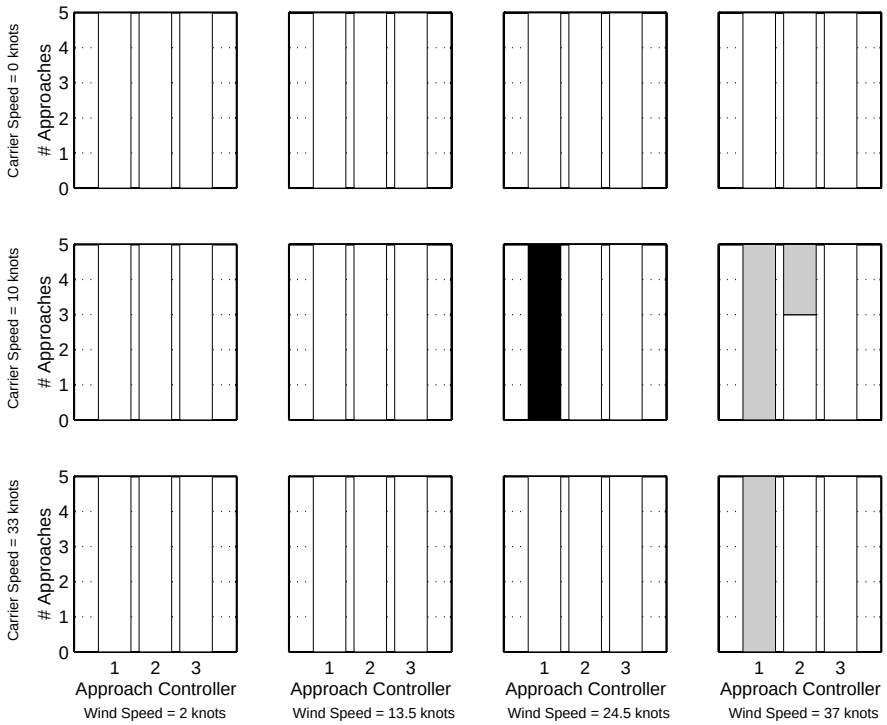

Figure 7-18 Approach Performance – Light Three Dimensional Turbulence and Carrier Induced Turbulence
1= Baseline; 2 = Direct lift Control; 3 = Thrust Vectoring
Success □, Exceeded Vertical Deviation ■, Exceeded Lateral Deviation ▭

With regard to mean approach speed RMS deviation, the Direct Lift Control approach controller consistently performs least well. At lower wind speeds, the baseline approach controller performs better than the thrust vectoring approach controller; however, this trend is reversed for the 24.5 knots and 37 knots wind speed cases. The maximum approach speed deviation RMS is 0.87 knots indicating that, in general, approach speed is controlled tightly by all approach controllers.

The trend in mean ramp crossing heights is the same as the preceding case. The mean values of approach glide path vertical deviation RMS at ramp crossing are, in general, correlated to the overall approach glide path vertical deviation performance. There is no

appreciable difference in ramp crossing height performance between the two and three dimensional turbulence cases.

7.5.1.4 MODERATE TURBULENCE AND CARRIER INDUCED TURBULENCE

The purpose of this atmospheric disturbance environment is to assess the performance of the approach controllers in an atmospheric disturbance environment representative of a very challenging operating condition.

The data discussed in this section are presented in Appendix B, Tables B-17 to B-24. A summary of the approach performance with respect to the success criteria for the two dimensional turbulence case is presented in Figure 7-19 and similarly for the three dimensional turbulence case in Figure 7-20. The trends discussed in the previous section in relation to each systems' approach glide path vertical deviation, lateral approach track deviation, approach speed deviation and ramp crossing height performance are evident in this atmospheric case. However, in this case, the magnitudes of the turbulence velocities are greater and hence the frequency of wave-offs increases.

All approaches for the 2 knot steady wind case for all aircraft carrier speeds are successful, albeit with higher vertical and lateral deviation RMS values that for the light turbulence case.

For both the two dimensional and three dimensional turbulence cases in the 13.5 knots steady wind case at a carrier speed of 0 knots, all five baseline approach controller approaches exceed the approach glide path vertical deviation limits defined in Figure 7-2. The corresponding Direct Lift Control approach controller and thrust vectoring approach controller approaches continue successfully to touchdown.

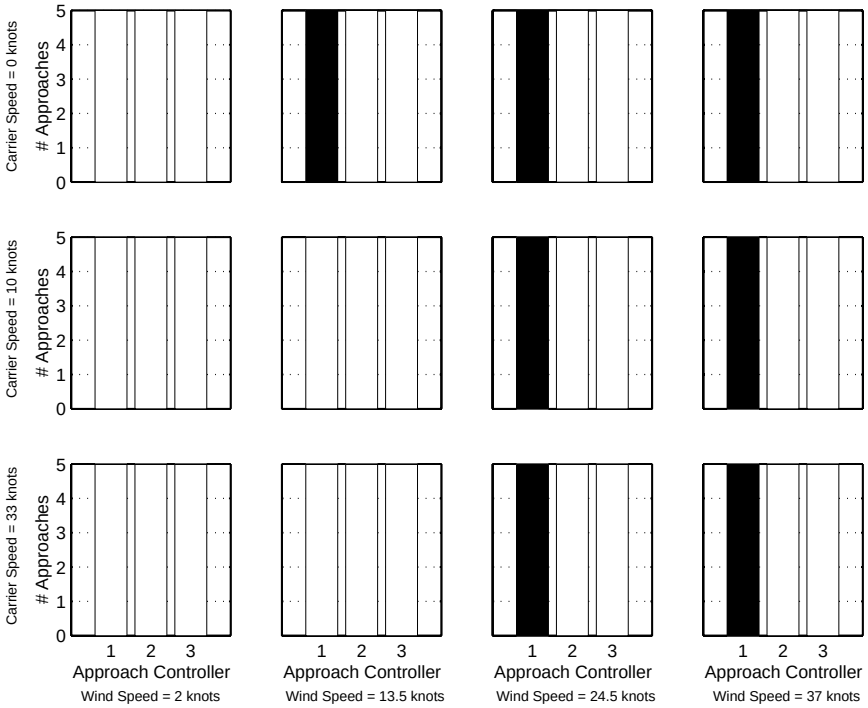

Figure 7-19 Approach Performance – Moderate Two Dimensional Turbulence and Carrier Induced Turbulence
1= Baseline; 2 = Direct lift Control; 3 = Thrust Vectoring
Success □ , Exceeded Vertical Deviation ■ , Exceeded Lateral Deviation ▭

For both the two dimensional and three dimensional turbulence cases at a wind speed of 24.5 knots for all aircraft carrier speeds, all baseline approach controller approaches are terminated with a wave-off due to breaching the approach glide path vertical deviation limits defined in Figure 7-2. Again, all corresponding Direct Lift Control approach controller and thrust vectoring approach controller approaches continue successfully to touchdown.

For the three dimensional turbulence case at the 37 knot wind speed case, all baseline approach controller approaches are terminated with a wave-off due to breaching the lateral approach track deviation limits defined in Figure 7-3. These wave-offs occur at a greater distance from intended touchdown than any of the previous wave-offs, indicating a very poor performance with respect to the precision of approach track deviation control.

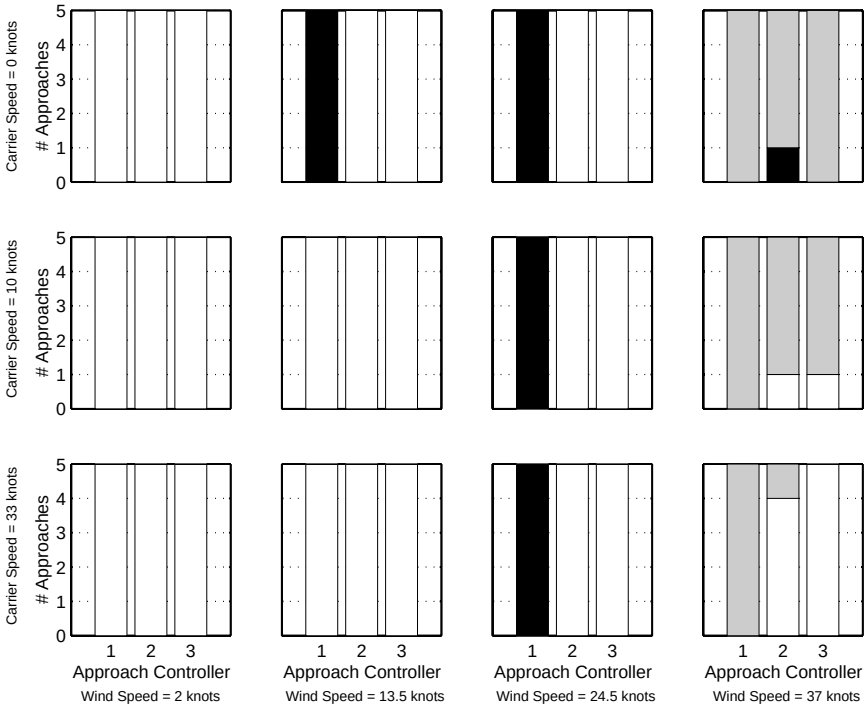

Figure 7-20 Approach Performance – Moderate Three Dimensional Turbulence and Carrier Induced Turbulence
1= Baseline; 2 = Direct lift Control; 3 = Thrust Vectoring
Success □ , Exceeded Vertical Deviation ■ , Exceeded Lateral Deviation ▭

At the ship speed of 0 knots, at a wind speed of 37 knots, four Direct Lift Control approach controller and five thrust vectoring approach controller approaches are terminated with a wave-off for the same reasons, while the remaining Direct Lift Control approach controller approach is terminated in a wave-off for breaching the approach glide path vertical deviation limits presented in Figure 7-2. The mean time to touchdown of the Direct Lift Control approach controller and thrust vectoring approach controller lateral failures is approximately half of the baseline approach controller failure, indicating greater lateral deviation control but ultimately not precise enough.

For the 10 knot aircraft carrier speed case, at a wind speed of 37 knots, four approaches of both the Direct Lift Control approach controller and thrust vectoring approach controller are terminated in a wave-off due to breaching the lateral deviation limits defined in Figure 7-3. Once again the failure occurs closer to touchdown, which is indicative of better lateral deviation control when compared to the baseline approach

controller. The remaining approach from both the Direct Lift Control approach controller and thrust vectoring approach controller continue to touchdown.

For the aircraft carrier speed of 33 knots one Direct Lift Control approach controller approach terminates in a wave-off for breaching the lateral deviation wave-off limits defined in Figure 7-3. Again, this failure occurs closer to touchdown than the corresponding baseline approach controller failures. The remaining approaches continue to touchdown.

For the two dimensional case at the 37 knots wind speed case, all baseline approach controller approaches are terminated with a wave-off for breaching the approach glide path vertical deviation limits defined in Figure 7-2 for all aircraft carrier speeds. The corresponding Direct Lift Control approach controller and thrust vectoring approach controller approaches continue to touchdown.

At the 37 knot wind speed case, it can be seen that while the approach glide path vertical deviation performance of the Direct Lift Control approach controller and the thrust vectoring approach controller was acceptable in some instances the lack of attenuation of the lateral turbulence caused the majority of these approach controllers approaches to be terminated with a wave-off. Whether or not this atmospheric disturbance case is representative of a deteriorated operational condition, the fact remains that a successful approach controller requires both precise approach glide path deviation and approach track deviation control.

7.5.1.5 SEVERE TURBULENCE AND CARRIER INDUCED TURBULENCE

The purpose of this atmospheric disturbance case is to assess the performance of the approach controllers in an atmospheric disturbance environment representative of the worst case operational scenario.

The data discussed in this section are presented in Appendix B, tables B-25 to B-32. A summary of the approach performance with respect to the success criteria for the two dimensional turbulence case is presented in Figure 7-21 and similarly for the three dimensional turbulence case in Figure 7-22.

For both the two and three dimensional turbulence cases, at a wind speed of 2 knots and all aircraft carrier speeds, all approaches flown by all three approach controllers are successful and the same trends are evident in relation to their relative performance. The trends discussed in the previous sections, in relation to each approach controllers approach glide path vertical deviation, approach track deviation, approach speed deviation and ramp crossing height performance, are evident in this atmospheric case.

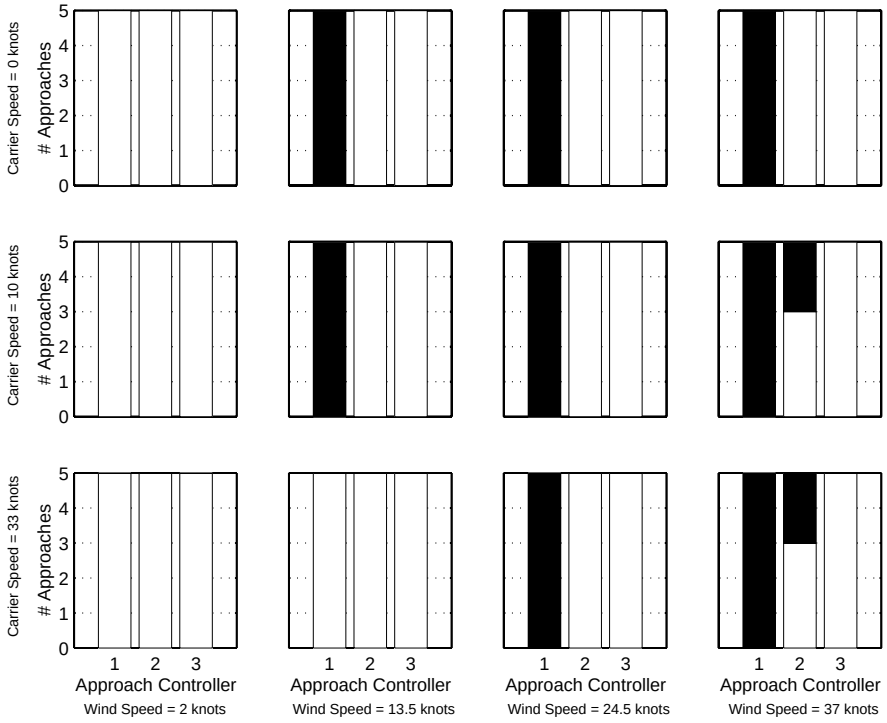

Figure 7-21 Approach Performance – Severe Two Dimensional Turbulence and Carrier Induced Turbulence
1= Baseline; 2 = Direct lift Control; 3 = Thrust Vectoring
Success ☐, Exceeded Vertical Deviation ■, Exceeded Lateral Deviation ▭

For both the two and three dimensional turbulence cases, at a wind speed of 13.5 knots and at aircraft carrier speeds of 0 knots and 10 knots all baseline approach controller approaches are terminated with a wave-off due to breaching the approach glide path vertical deviation limits defined in Figure 7-2. All corresponding Direct Lift Control approach controller and thrust vectoring approach controller approaches continue to touchdown. For the three dimensional turbulence case at the same wind speed but at an aircraft carrier speed of 33 knots all approaches for all approach controllers execute a successful approach, with one exception. A single Direct Lift Control approach

controller approach is terminated with a wave-off due to breaching the lateral deviation limits defined in Figure 7-3. This failure occurs at a time to touchdown of 23.7 seconds, approximately 0.85 nautical miles from the touchdown point at an approximate altitude of 300 feet. With regard to the successful approaches at this wind speed, the same trends can be seen with respect to the systems relative performance.

For both the two and three dimensional turbulence cases at a wind speed of 24.5 knots and for all aircraft carrier speeds all baseline approach controller approaches are terminated in a wave-off due to breaching the approach glide path vertical deviation limits defined in Figure 7-2. All corresponding Direct Lift Control approach controller and thrust vectoring approach controller approaches continue to touchdown, with the exception of two thrust vectoring approach controller approaches in the three dimensional turbulence case which are terminated due to breaching the lateral deviation limits defined in Figure 7-3.

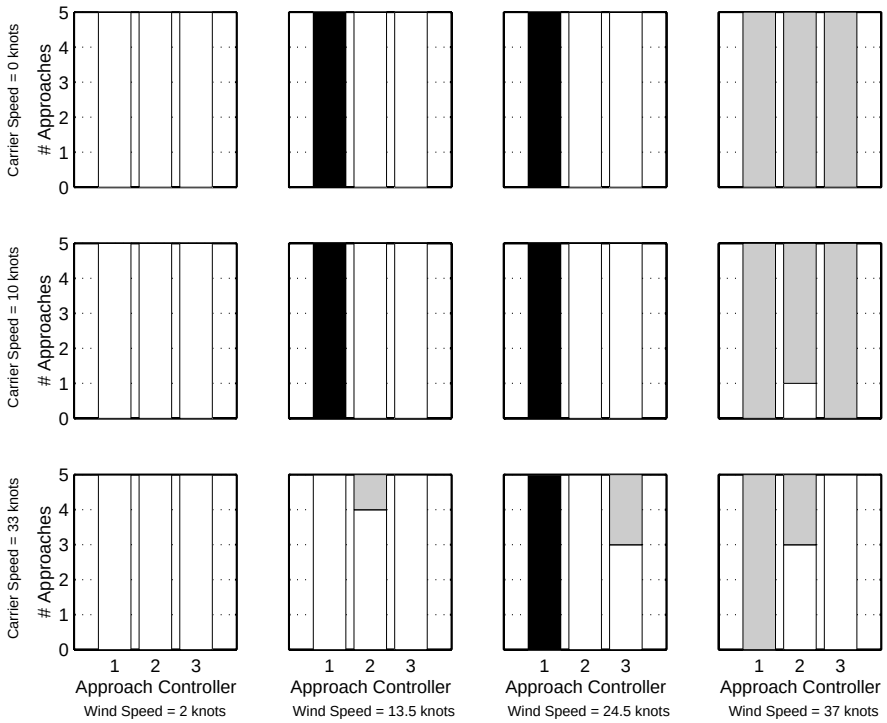

Figure 7-22 Approach Performance – Severe Three Dimensional Turbulence and Carrier Induced Turbulence
1= Baseline; 2 = Direct lift Control; 3 = Thrust Vectoring
Success □, Exceeded Vertical Deviation ■, Exceeded Lateral Deviation ▭

For the three dimensional turbulence cases at a wind speed of 37 knots and for all aircraft carrier speeds all baseline approach controller approaches are terminated in a wave-off due to breaching the lateral deviation limits defined in Figure 7-3 for all aircraft carrier speeds. For the 0 knot aircraft carrier speed case, all Direct Lift Control approach controller and thrust vectoring approach controller approaches are terminated for the same reason. For the 10 knots aircraft carrier case all Direct Lift Control approach controller and thrust vectoring approach controller approaches are also terminated for the same reason, with the exception of a single Direct Lift Control approach which continues to touchdown. For the 33 knots aircraft carrier case only two Direct Lift Control approach controller approaches are terminated for this reason while all other Direct Lift Control approach controller and thrust vectoring approach controller approaches continue to touchdown.

For the two dimensional turbulence case at this wind speed, all baseline approaches are terminated with a wave-off due to breaching the approach glide path vertical deviation limits defined in Figure 7-2 for all aircraft carrier speeds. With the exception of two Direct Lift Control approach controller approaches being terminated for the same reasons at aircraft carrier speed of 10 knots and 33 knots, all other Direct Lift Control approach controller and thrust vectoring approach controller approaches continue to touchdown.

7.5.2 TOUCHDOWN PERFORMANCE

7.5.2.1 NO ATMOSPHERIC DISTURBANCE

The purpose of this atmospheric disturbance case is to provide a measure of how well the systems' perform in ideal conditions. The touchdown performance with respect to the success criteria for touchdown is presented in Figure 7-23 for all successful approaches for this atmospheric disturbance case. The touchdown dispersion of successful approaches is presented in Figure 7-24. The mean lateral and longitudinal touchdown displacements for each set of five approaches per aircraft carrier speed, wind speed and approach controller are presented in Appendix B Tables B-1 to B-4.

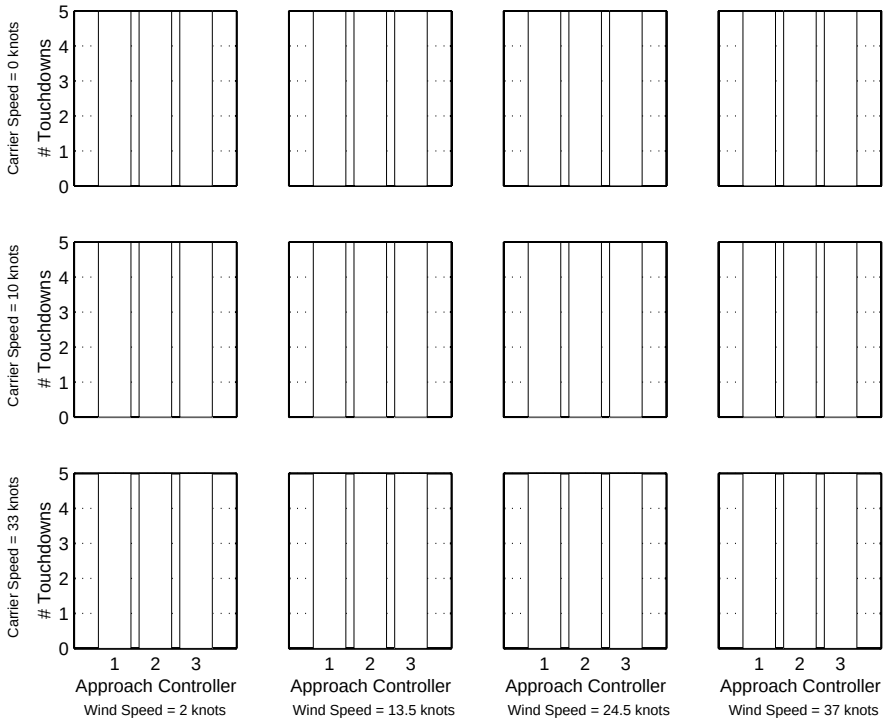

Figure 7-23 Touchdown Performance – No Atmospheric Disturbance
1= Baseline; 2 = Direct lift Control; 3 = Thrust Vectoring
Success □ , Bolter ■

As expected the touchdown dispersion are centred on the desired touchdown point with a maximum longitudinal displacement of 1.7 feet. All lateral displacements are 0.01 feet of centre. The positions of the four arresting wires are indicated in each of the plots in Figure 7-24.

The standard deviations, or dispersion, of all longitudinal displacements of all touchdowns per approach controller for this atmospheric disturbance case are presented in Table 7-6. As is expected, the touchdown dispersions are very low and adhere to the 40 foot minimum dispersion requirement.

Approach Controller	Touchdown Dispersion
Baseline	0.32 ft
Direct Lift Control	0.38 ft
Thrust Vectoring	0.42 ft

Table 7-6 Touchdown Dispersion of all Touchdowns per System – No Atmospheric Disturbance

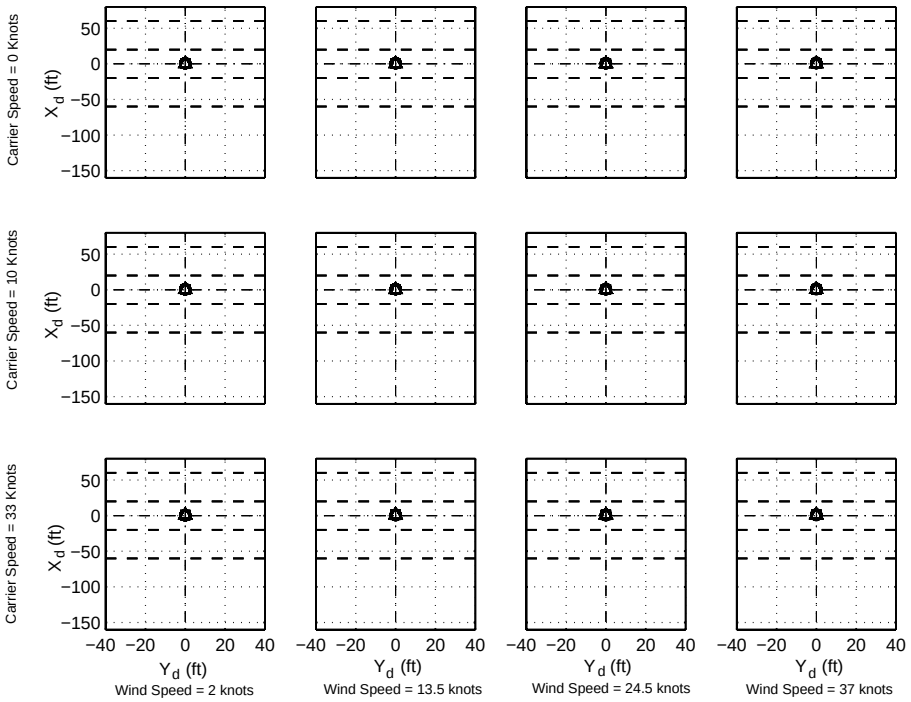

Figure 7-24 Touchdown Dispersion – No Atmospheric Disturbance
Baseline [○], Direct Lift Control [□], Thrust Vectoring [△]

The mean aircraft sink rate at touchdown for successful touchdowns per aircraft carrier motion defined by wind speed and aircraft carrier speed is presented in Table 7-7 per approach controller.

	Aircraft Carrier Speed (kts)								
	0			10			33		
	Approach Controller			Approach Controller			Approach Controller		
Wind Speed (kts)	1	2	3	1	2	3	1	2	3
2	-12.19	-12.19	-12.19	-12.19	-12.19	-12.19	-12.18	-12.19	-12.19
13.5	-11.18	-11.17	-11.17	-11.18	-11.17	-11.17	-11.17	-11.14	-11.17
24.5	-10.22	-10.20	-10.20	-10.22	-10.20	-10.20	-10.21	-10.17	-10.18
37	-9.14	-9.10	-9.10	-9.15	-9.10	-9.10	-9.13	-9.06	-9.07

Table 7-7 Aircraft Mean Sink Rate at Touchdown (ft/s) – No Atmospheric Disturbance
1= Baseline; 2 = Direct lift Control; 3 = Thrust Vectoring

From Table 7-7 it can be seen that sink rate reduces as the magnitude of the headwind increases, reflecting the fact that the magnitude of sink rate is equal to the magnitude of the component of normal the velocity resolved into earth axes.

7.5.2.2 NO ATMOSPHERIC DISTURBANCE AND CARRIER INDUCED TURBULENCE

The purpose of this atmospheric disturbance case is to assess the performance of the approach controllers in an atmospheric disturbance case that is most representative of normal operating conditions.

The touchdown performance with respect to the success criteria for touchdown is presented in Figure 7-25 for all successful approaches for the no atmospheric disturbance and carrier induced turbulence case. The touchdown dispersion of approaches for this atmospheric disturbance case are presented in Figure 7-26. The mean lateral and longitudinal touchdown displacements for each set of five approaches per aircraft carrier speed, wind speed and approach controller are presented in Appendix B Tables B-5 to B-8.

A single bolter occurred for this atmospheric disturbance case. This occurred at a wind speed of 37 knots and a ship speed of 0 knots, the worst case aircraft carrier motion case, for the Direct Lift Control approach controller.

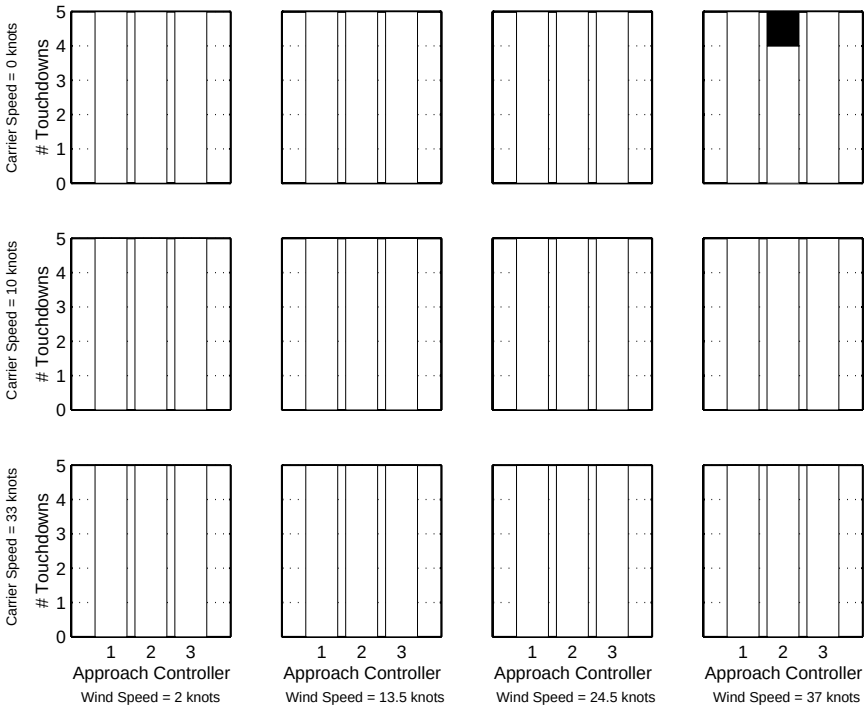

Figure 7-25 Touchdown Performance – No Atmospheric Disturbance and Carrier Induced Turbulence
1= Baseline; 2 = Direct lift Control; 3 = Thrust Vectoring
Success ☐ , Bolter ■

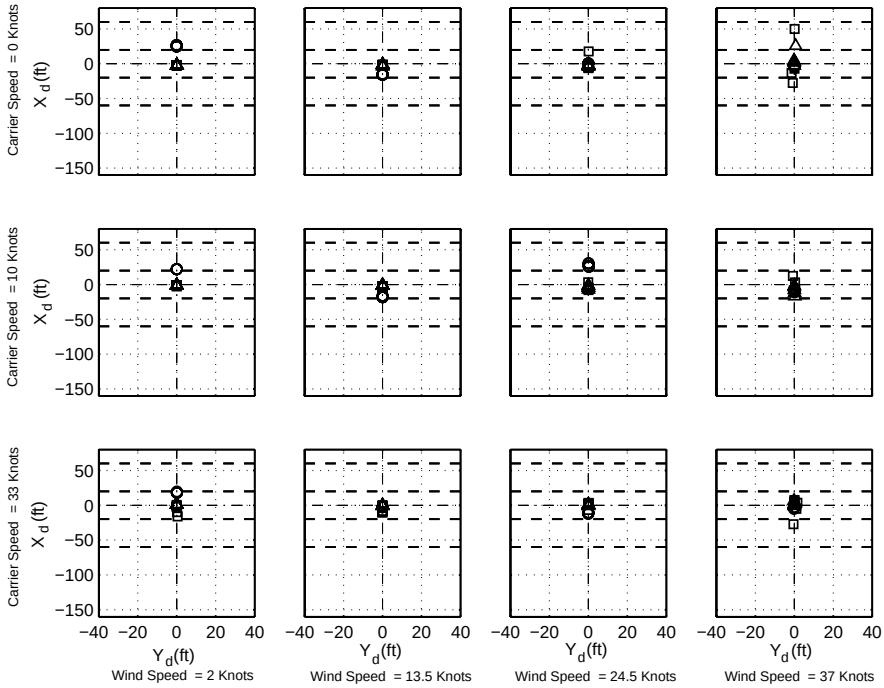

Figure 7-26 Touchdown Dispersion – No Atmospheric Disturbance and Carrier Induced Turbulence
Baseline [○], Direct Lift Control [□], Thrust Vectoring [△]

The dispersion of all touchdowns per approach controller for this atmospheric disturbance case are presented in Table 7-8. The total dispersion of the baseline approach controller is the least relative to the Direct Lift Control approach controller and the thrust vectoring approach controller which is reflective of the approach glide path vertical deviation RMS performance of the Direct Lift Control approach controller. Similarly the Direct Lift Control approach controller outperforms the baseline approach controller as it did in general with respect to its approach performance.

Approach Controller	Touchdown Dispersion
Baseline	15.88 ft
Direct Lift Control	9.93 ft
Thrust Vectoring	4.88 ft

Table 7-8 Touchdown Dispersion of all Touchdowns per System – No Atmospheric Disturbance and Carrier Induced Turbulence

The mean aircraft sink rate at touchdown for successful touchdowns per aircraft carrier motion defined by wind speed and aircraft carrier speed is presented in Table 7-9 per approach controller. The deviation from the ideal sink rates, presented in Table 7-7, is evidence of the effects of turbulence and manoeuvring as a result of that turbulence.

	Aircraft Carrier Speed (kts)								
	0			10			33		
	Approach Controller			Approach Controller			Approach Controller		
Wind Speed (kts)	1	2	3	1	2	3	1	2	3
2	-14.33	-10.27	-10.63	-13.27	-11.41	-11.79	-14.02	-12.82	-11.58
13.5	-11.27	-9.67	-10.13	-7.70	-10.48	-10.82	-14.02	-10.04	-10.46
24.5	-11.62	-10.09	-9.30	-13.83	-9.63	-10.26	-11.57	-11.57	-10.10
37	-10.83	-11.80	-8.19	-9.99	-9.75	-9.33	-13.71	-13.39	-10.90

Table 7-9 Aircraft Mean Sink Rate at Touchdown (ft/s) – No Atmospheric Disturbance and Carrier Induced Turbulence
1= Baseline; 2 = Direct lift Control; 3 = Thrust Vectoring

7.5.2.3 LIGHT TURBULENCE AND CARRIER INDUCED TURBULENCE

The purpose of this atmospheric disturbance case is to assess the performance of the approach controller in an atmospheric disturbance environment representative of a challenging but realistic operating condition.

The touchdown performance with respect to the success criteria for touchdown is presented in Figure 7-27 for all successful approaches for the light three dimensional turbulence and carrier induced turbulence case. A total of 6 bolters occurred for this atmospheric disturbance case. The touchdown dispersion of successful touchdowns for this atmospheric disturbance case are presented in Figure 7-28. The mean lateral and longitudinal touchdown displacements for each set of five approaches per aircraft carrier speed, wind speed and approach controller are presented in Appendix B Tables B-9 to B-12. The lateral touchdown dispersions can be seen to be very limited in range

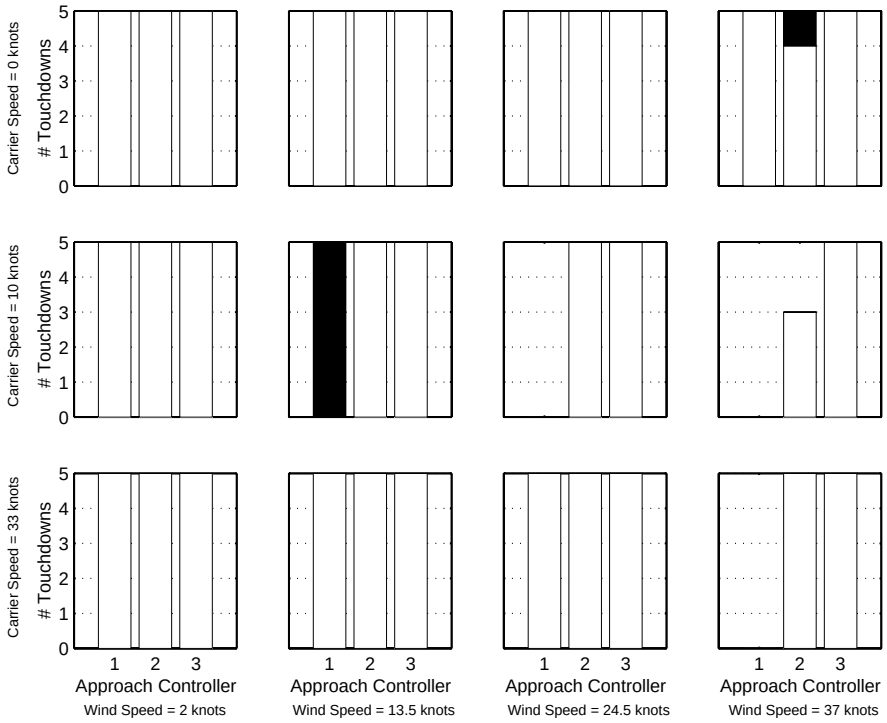

Figure 7-27 Touchdown Performance – Light Three Dimensional Turbulence and Carrier Induced Turbulence
1= Baseline; 2 = Direct lift Control; 3 = Thrust Vectoring
Success ☐ , Bolter ■

	Aircraft Carrier Speed (kts)								
	0			10			33		
	Approach Controller			Approach Controller			Approach Controller		
Wind Speed (kts)	1	2	3	1	2	3	1	2	3
2	-17	-9.99	-11.36	-16.46	-12.16	-12.32	-16.74	-12.66	-12.42
13.5	-9.27	-9.37	-11.21	-	-11.21	-11.54	-17.42	-10.68	-8.74
24.5	-12.06	-9.34	-10	-	-15.81	-10.71	-12.4	-10.55	-9.27
37	-12.26	-11.68	-7.59	-	-8.75	-8.95	-	-12.34	-9.34

Table 7-10 Aircraft Mean Sink Rate at Touchdown (ft/s) – Light Three Dimensional Turbulence and Carrier Induced Turbulence
1= Baseline; 2 = Direct lift Control; 3 = Thrust Vectoring

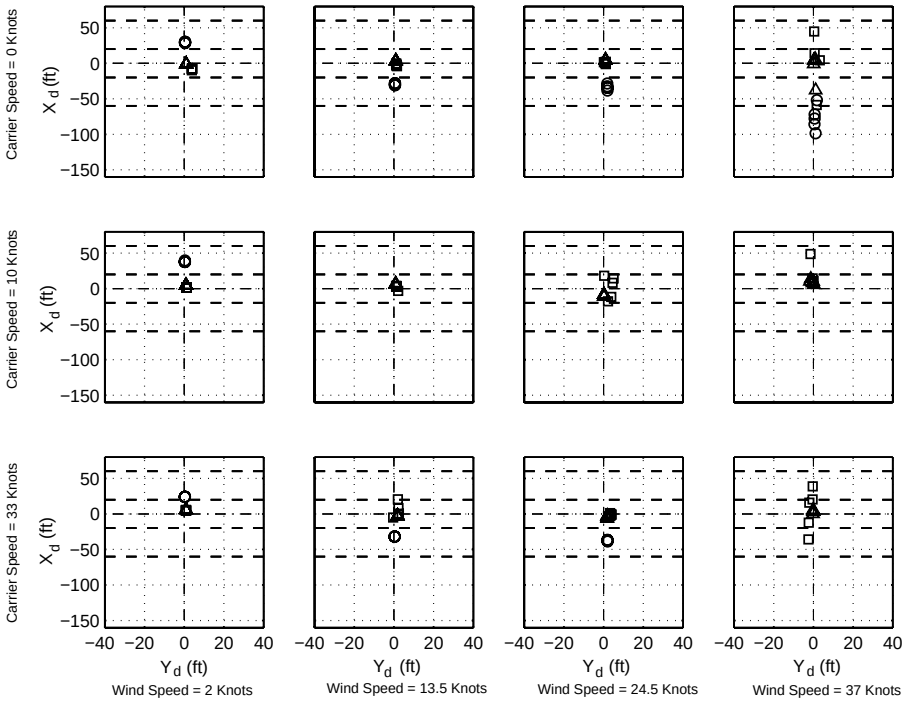

Figure 7-28 Touchdown Dispersion – Light Three Dimensional Turbulence and Carrier Induced Turbulence
Baseline [○], Direct Lift Control [□], Thrust Vectoring [△]

The mean aircraft sink rate at touchdown for successful touchdowns per aircraft carrier motion defined by wind speed and aircraft carrier speed is presented in Table 7-10 per approach controller for the three dimensional turbulence case and in Table 7-11 for the two dimensional turbulence case.

As with the previous atmospheric disturbance case, the mean touchdown sink rates are seen to deviate from the ideal sink rate. As touchdown sink rate is not being controlled by a flare manoeuvre, this data serves only as an indicator of the level of turbulence and manoeuvring as a result of that turbulence. The fact that sink rates are seen to be very high provides motivation for a further study to investigate the feasibility of using a navigation strategy similar to that presented in Chapter 4 to project a non-linear flight path which would allow the sink rate to be arrested prior to touchdown. It is also interesting to note that there is little difference between the mean sink rates for the two and three dimensional turbulence cases, except for some carrier motion cases where there is a disparity in the number of successful approaches between the two and three

dimensional turbulence cases. This indicates that lateral turbulence and associated corrective manoeuvring does not have a significant effect on sink rate.

	Aircraft Carrier Speed (kts)								
	0			10			33		
	Approach Controller			Approach Controller			Approach Controller		
Wind Speed (kts)	1	2	3	1	2	3	1	2	3
2	-17.05	-9.73	-11.38	-16.51	-12.16	-12.37	-16.77	-12.64	-12.37
13.5	-9.16	-9.41	-11.22	-	-11.38	-11.54	-17.50	-10.38	-8.73
24.5	-11.84	-9.5	-9.95	-	-14.58	-10.72	-12.12	-9.27	-9.15
37	-11.07	-11.50	-7.46	-9.54	-11.14	-10.49	-17.51	-14.59	-9.25

Table 7-11 Aircraft Mean Sink Rate at Touchdown (ft/s) – Light Two Dimensional Turbulence and Carrier Induced Turbulence
1= Baseline; 2 = Direct lift Control; 3 = Thrust Vectoring

The touchdown performance with respect to the success criteria for touchdown is presented in Figure 7-29 for all successful approaches for the light two dimensional turbulence and carrier induced turbulence case. As with the three dimensional turbulence case, a total of six bolters occurred for this atmospheric disturbance case.

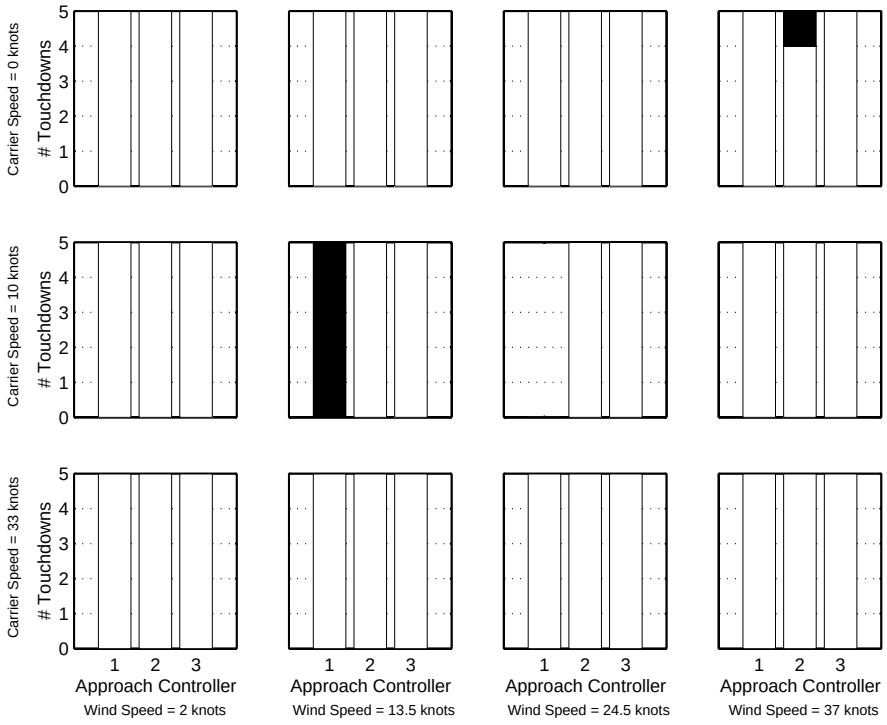

Figure 7-29 Touchdown Performance – Light Two Dimensional Turbulence and Carrier Induced Turbulence
1= Baseline; 2 = Direct lift Control; 3 = Thrust Vectoring
Success □ , Bolter ■

The touchdown dispersion of successful touchdowns for this atmospheric disturbance case are presented in Figure 7-30. The mean lateral and longitudinal touchdown displacements for each set of five approaches per aircraft carrier speed, wind speed and approach controller are presented in Appendix B Tables B-13 to B-16.

Apart from the inclusion of approaches that were terminated in a wave-off due to lateral deviation during the three dimensional case, there is very little difference between the two dimensional turbulence and three dimensional turbulence touchdown dispersions.

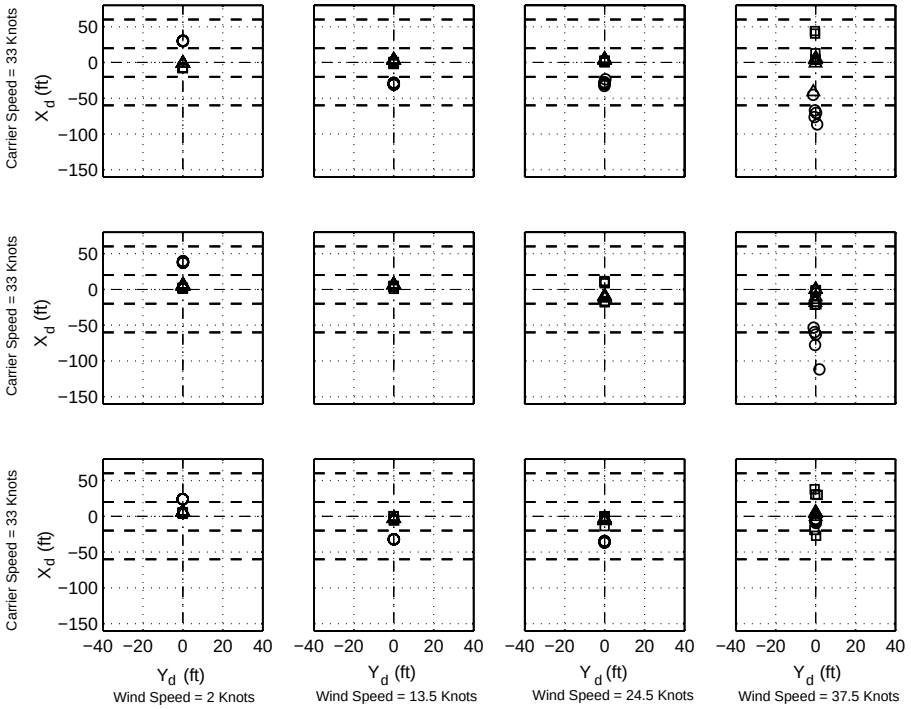

Figure 7-30 Touchdown Dispersion – Light Two Dimensional Turbulence and Carrier Induced Turbulence
Baseline [○], Direct Lift Control [□], Thrust Vectoring [△]

The dispersion of all touchdowns per approach controller for the two dimensional turbulence case are presented in Table 7-12. The first set of touchdown dispersions are for successful touchdowns only, i.e. bolters are not included. The second set of touchdown dispersions are for all touchdowns. As the longitudinal touchdown dispersion is predominantly a function of approach glide path vertical deviation control, the two dimensional turbulence case data are used in determining the total longitudinal touchdown dispersions as this set of data contains more successful approaches and is

essentially a test of the approach glide path vertical deviation control isolated from the approach track controller.

Approach Controller	Longitudinal Touchdown Dispersion (Successful Touchdowns)	Longitudinal Touchdown Dispersion (All Touchdowns)
Baseline	15.87 ft	38.32 ft
Direct Lift Control	9.93 ft	13.52 ft
Thrust Vectoring	4.88 ft	4.88 ft

Table 7-12 Touchdown Dispersions per Approach Controller – Light Turbulence and Carrier Induced Turbulence

As the bolters are defined by the fact that the touchdown occurs at a distance of greater than 60 feet from the desired touchdown point, they have a noticeable effect on the total touchdown dispersions. It is not apparent from the limited data in the public domain whether or not to include the bolters when determining touchdown dispersion. In this case, regardless of whether or not bolters are included, all approach controllers conform to the 40 foot touchdown dispersion requirement. The trend continues to show that the thrust vectoring approach controller performs the best with the baseline approach controller performing the least well.

7.5.2.4 MODERATE TURBULENCE AND CARRIER INDUCED TURBULENCE

The purpose of this atmospheric disturbance environment is to assess the performance of the approach controllers in an atmospheric disturbance environment representative of a very challenging operating condition.

The touchdown performance with respect to the success criteria for touchdown is presented in Figure 7-31 for all successful approaches for the moderate three dimensional turbulence and carrier induced turbulence case. The touchdown dispersion of successful touchdowns for this atmospheric disturbance case are presented in Figure 7-32. The mean lateral and longitudinal touchdown displacements for each set of five approaches per aircraft carrier speed, wind speed and system are presented in Appendix B Tables B-17 to B-20.

The mean aircraft sink rate at touchdown for successful touchdowns per aircraft carrier motion defined by wind speed and aircraft carrier speed is presented in Table 7-13 per approach controller for the three dimensional turbulence case.

As with the light three dimensional turbulence case the lateral touchdown dispersion can be seen to be consistently very close to the centreline.

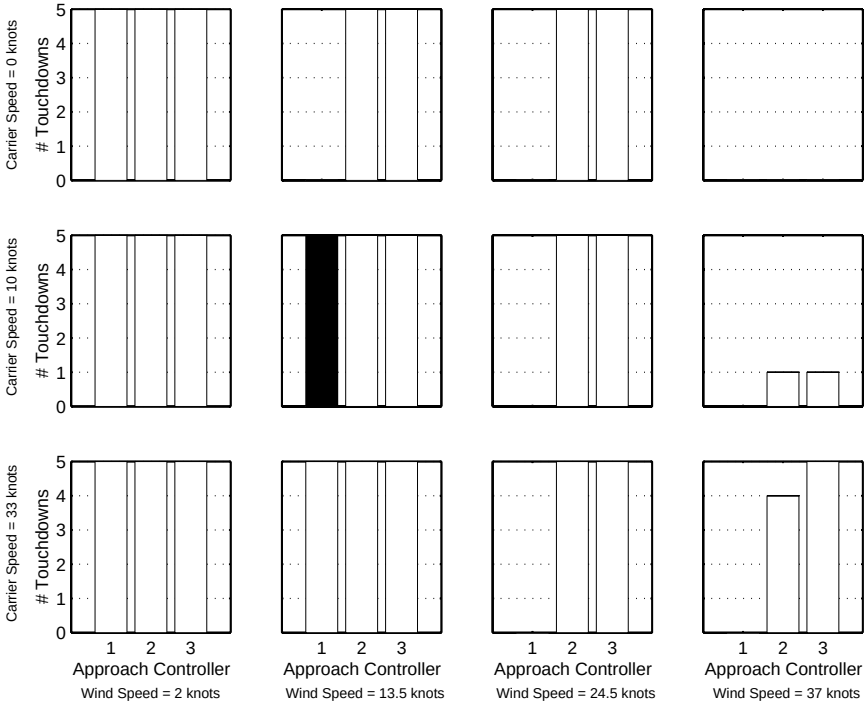

Figure 7-31 Touchdown Performance – Moderate Three Dimensional Turbulence and Carrier Induced Turbulence
1= Baseline; 2 = Direct lift Control; 3 = Thrust Vectoring
Success □ , Bolter ■

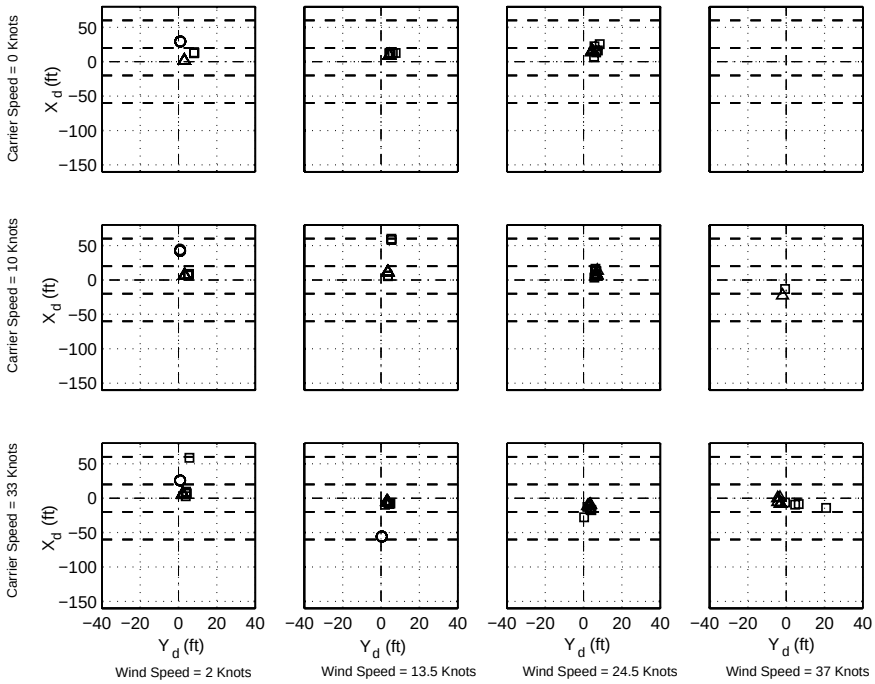

Figure 7-32 Touchdown Dispersion – Moderate Three Dimensional Turbulence and Carrier Induced Turbulence
Baseline [○], Direct Lift Control [□], Thrust Vectoring [△]

	Aircraft Carrier Speed (kts)								
	0			10			33		
	Approach Controller			Approach Controller			Approach Controller		
Wind Speed (kts)	1	2	3	1	2	3	1	2	3
2	-19.38	-10.88	-11.07	-19.03	-12.77	-11.8	-19.21	-12.99	-11.91
13.5	-	-9.7	-12.1	-	-12.98	-11.32	-20.64	-8.7	-7.22
24.5	-	-10.19	-12.02	-	-11.22	-13.53	-	-13	-8.25
37	-	-	-	-	-7.67	-4.87	-	-12.23	-12.97

Table 7-13 Aircraft Mean Sink Rate at Touchdown (ft/s) – Moderate Three Dimensional Turbulence and Carrier Induced Turbulence
1= Baseline; 2 = Direct lift Control; 3 = Thrust Vectoring

The touchdown performance with respect to the success criteria for touchdown is presented in Figure 7-33 for all successful approaches for the moderate two dimensional turbulence and carrier induced turbulence case. The touchdown dispersion of successful touchdowns for this atmospheric disturbance case are presented in Figure 7-34. The mean lateral and longitudinal touchdown displacements for each set of five approaches per aircraft carrier speed, wind speed and system are presented in Appendix B Tables B-21 to B-24.

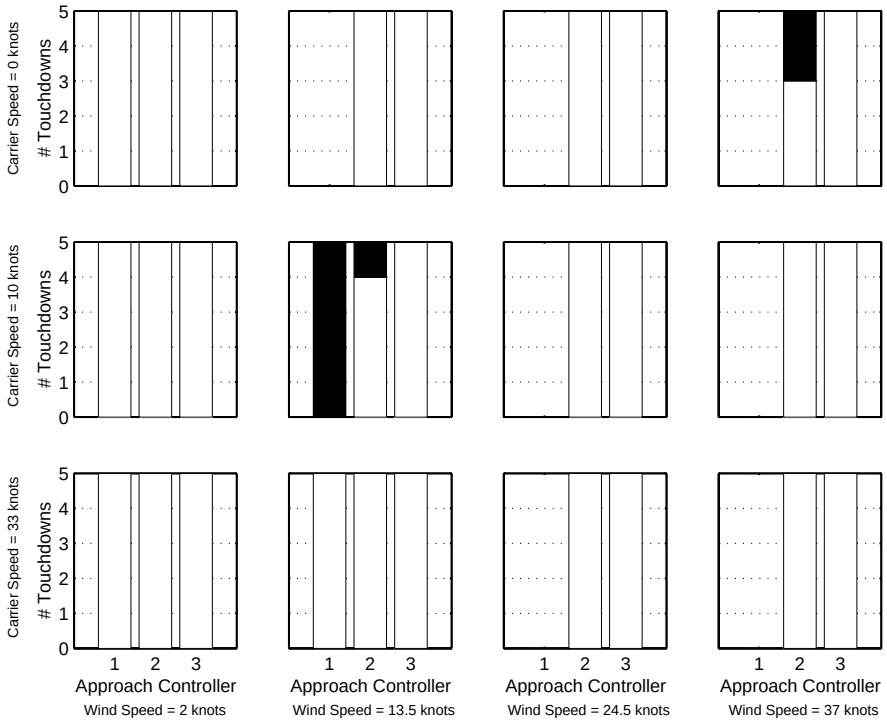

Figure 7-33 Touchdown Performance – Moderate Three Dimensional Turbulence and Carrier Induced Turbulence

1= Baseline; 2 = Direct lift Control; 3 = Thrust Vectoring

Success □ , Bolter ■

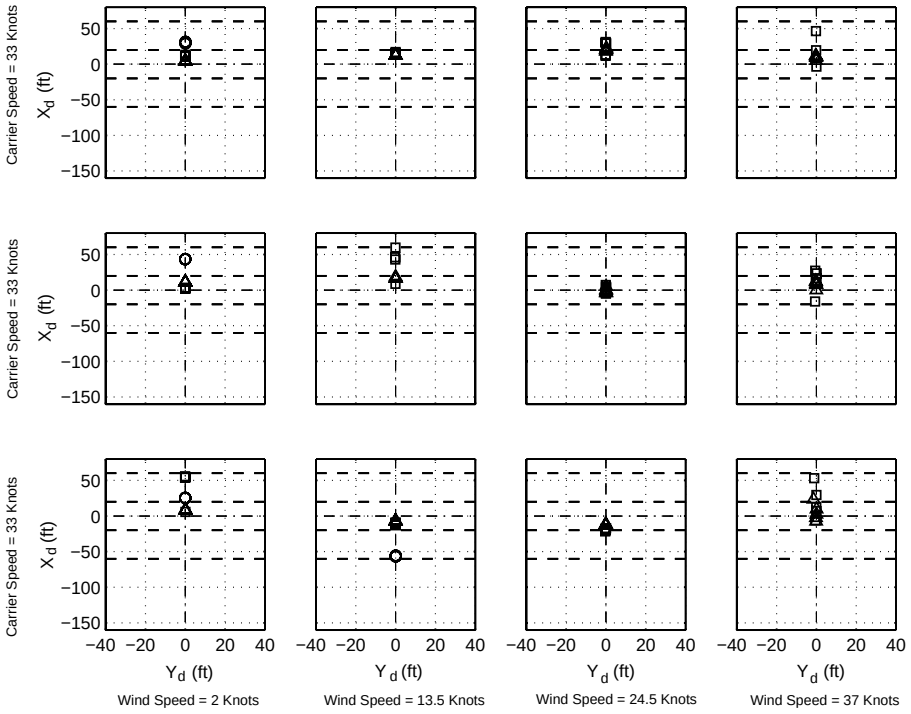

Figure 7-34 Touchdown Dispersion – Moderate Two Dimensional Turbulence and Carrier Induced Turbulence
Baseline [○], Direct Lift Control [□], Thrust Vectoring [△]

The mean aircraft sink rate at touchdown for successful touchdowns per aircraft carrier motion defined by wind speed and aircraft carrier speed is presented in Table 7-14 per approach controller for the two dimensional turbulence case. The same conclusions can be made with respect to the mean sink rates at touchdown for this atmospheric disturbance case as with the previous case. Again there is little significant difference in mean sink rates at touchdown between the two and three dimensional turbulence cases, except for some carrier motion cases where there is a disparity in the number of successful approaches between the two and three dimensional turbulence cases.

	Aircraft Carrier Speed (kts)								
	0			10			33		
	Approach Controller			Approach Controller			Approach Controller		
Wind Speed (kts)	1	2	3	1	2	3	1	2	3
2	-19.55	-10.3	-11.38	-19.24	-10.61	-12.46	-19.4	-14.06	-11.92
13.5	-	-9.92	-12.7	-	-14.71	-11.3	-20.8	-8.67	-7.15
24.5	-	-12.25	-12.53	-	-11.04	-13.63	-	-13.76	-8.19
37	-	-7.59	-6.85	-	-11.28	-12.8	-	-11.11	-9.34

Table 7-14 Aircraft Mean Sink Rate at Touchdown (ft/s) – Moderate Two Dimensional Turbulence and Carrier Induced Turbulence
1= Baseline; 2 = Direct lift Control; 3 = Thrust Vectoring

The dispersion of all touchdowns per approach controller for two dimensional turbulence case are presented in Table 7-15. As there are relatively few baseline approach controller successful touchdowns, the inclusion of the bolters have a very large effect on the total dispersion of the baseline approach controller.

Approach Controller	Longitudinal Touchdown Dispersion (Successful Touchdowns)	Longitudinal Touchdown Dispersion (All Touchdowns)
Baseline	40.26 ft	94.76 ft
Direct Lift Control	21.67 ft	29.24 ft
Thrust Vectoring	9.69 ft	9.69 ft

Table 7-15 Touchdown Dispersions per System – Moderate Turbulence and Carrier Induced Turbulence

The Direct Lift Control approach controller and the thrust vectoring approach controller meet the minimum touchdown dispersion requirement of 40 feet, with the thrust vectoring approach controller demonstrating very tight control. The baseline approach controller falls outside the 40 feet dispersion requirement, especially if all touchdowns are counted.

Fortenbaugh [22] presents touchdown dispersions values for the F-4 and F-14A Automatic Carrier Landing Systems as being 39.7 ft and 40.53 feet respectively. In the case where only successful touchdowns are counted towards the total touchdown dispersion, the baseline approach controller can be seen to perform marginally better than the F-14A. The values for both the F-4 and F-14A were generated in a moderate disturbance environment. The F-4 data was collected during carrier trials with comparable atmospheric disturbances while the F-14A data was the result of simulation with comparable atmospheric disturbances.

The touchdown dispersion value quoted by Fortenbaugh [22] for the Direct Lift Control aided F-14A is 20.58 ft, which is very similar to that value for the Direct Lift Control approach controller developed here when only successful touchdowns are included. This increases the confidence in the realism of these systems and also the benefit demonstrated by the thrust vectoring approach control system.

7.5.2.5 SEVERE TURBULENCE AND CARRIER INDUCED TURBULENCE

The purpose of this atmospheric disturbance case is to assess the performance of the approach controllers in an atmospheric disturbance environment representative of the worst case operational scenario.

The touchdown performance with respect to the success criteria for touchdown is presented in Figure 7-35 for all successful approaches for the severe three dimensional turbulence and carrier induced turbulence case. The mean lateral and longitudinal touchdown displacements for each set of five approaches per aircraft carrier speed, wind speed and system are presented in Appendix B Tables B-25 to B-28.

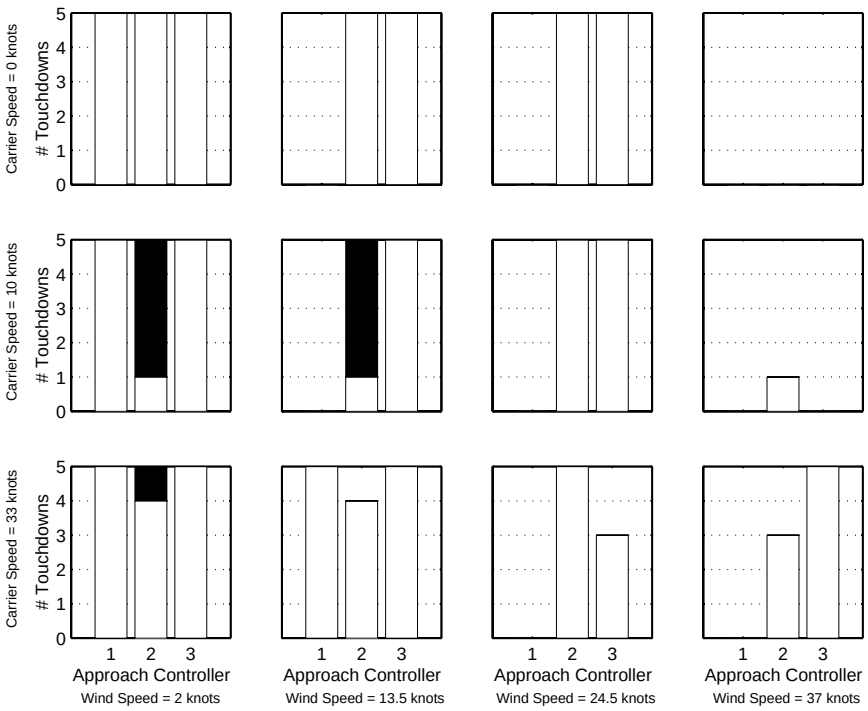

Figure 7-35 Touchdown Performance – Severe Three Dimensional Turbulence and Carrier Induced Turbulence
1= Baseline; 2 = Direct lift Control; 3 = Thrust Vectoring
Success □ , Bolter ■

The touchdown dispersion of successful touchdowns for this atmospheric disturbance case are presented in Figure 7-36. In this case, the lateral dispersions is seen to increase when compared to the moderate turbulence case but however remains at a very acceptable level.

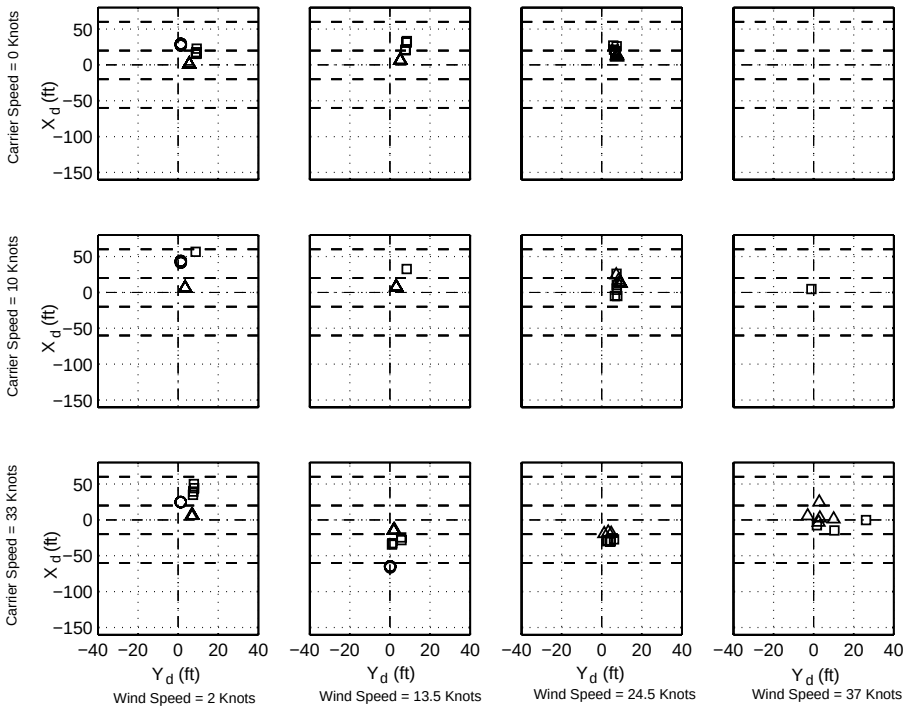

Figure 7-36 Touchdown Dispersion – Severe Three Dimensional Turbulence and Carrier Induced Turbulence
Baseline [○], Direct Lift Control [□], Thrust Vectoring [△]

The mean aircraft sink rate at touchdown for successful touchdowns per aircraft carrier motion defined by wind speed and aircraft carrier speed is presented in Table 7-16 per approach controller for the three dimensional turbulence case. The touchdown sink rates are again seen to deviate from the ideal, again an indication of the turbulence activity and the aircraft's response to this turbulence. The mean touchdown sink rate is seen to increase to over -20 ft/s on occasion, and similarly decrease to as low as -7.15 ft/s.

	Aircraft Carrier Speed (kts)								
	0			10			33		
	Approach Controller			Approach Controller			Approach Controller		
Wind Speed (kts)	1	2	3	1	2	3	1	2	3
2	-20.37	-9.44	-10.67	-20.11	-17.68	-11.31	-20.27	-13.95	-10.99
13.5	-	-14.13	-11.6	-	-14	-10.63	-21.88	-10.77	-7.15
24.5	-	-10.78	-11.03	-	-10.71	-14.46	-	-12.13	-8.68
37	-	-	-	-	-7.25	-	-	-11.82	-13.8

Table 7-16 Aircraft Mean Sink Rate at Touchdown (ft/s) – Severe Three Dimensional Turbulence and Carrier Induced Turbulence
1= Baseline; 2 = Direct lift Control; 3 = Thrust Vectoring

The touchdown performance with respect to the success criteria for touchdown is presented in Figure 7-37 for all successful approaches for the severe two dimensional turbulence and carrier induced turbulence case. The mean lateral and longitudinal touchdown displacements for each set of five approaches per aircraft carrier speed, wind speed and system are presented in Appendix B Tables B-29 to B-32.

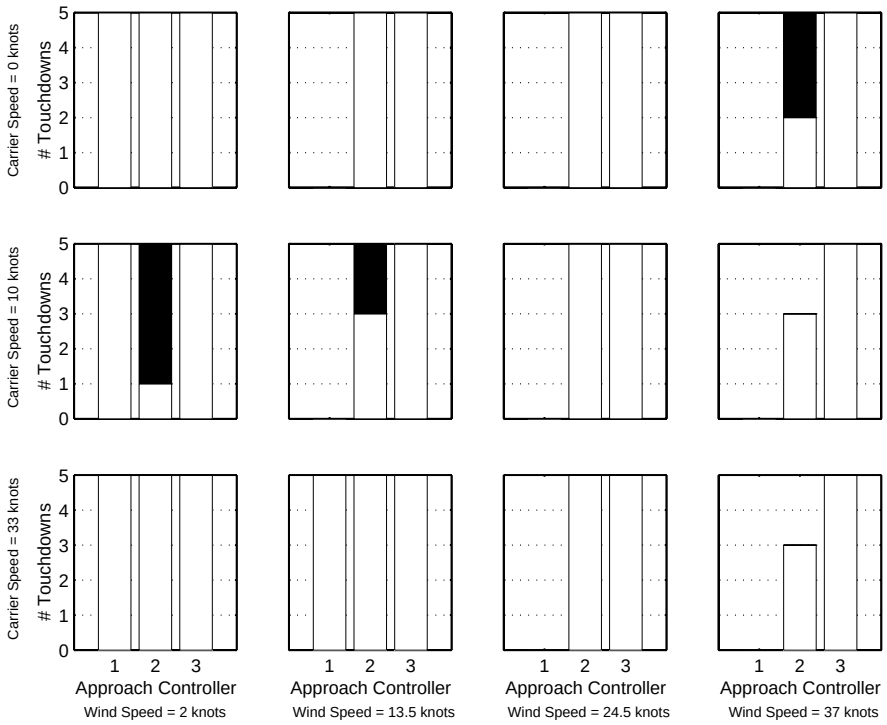

Figure 7-37 Touchdown Performance – Severe Three Dimensional Turbulence and Carrier Induced Turbulence
1= Baseline; 2 = Direct lift Control; 3 = Thrust Vectoring
Success □ , Bolter ■

The touchdown dispersion of successful touchdowns for the severe two dimensional turbulence and carrier induced turbulence are presented in Figure 7-38. As with the moderate turbulence case there is a noticeable difference in the mean lateral touchdown dispersion between the two dimensional and three dimensional turbulence cases.

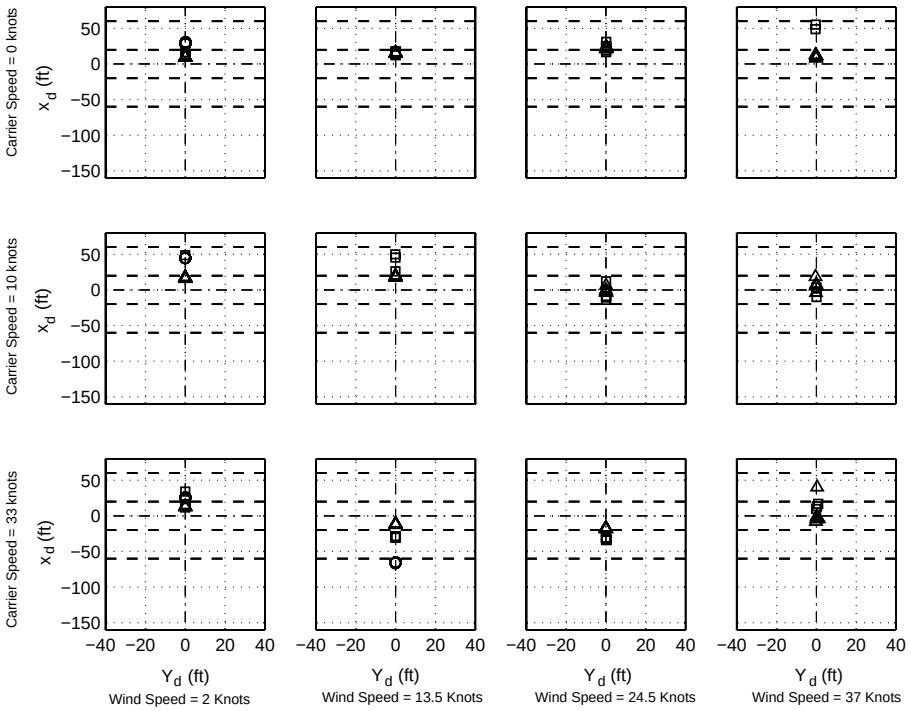

Figure 7-38 Touchdown Dispersion – Severe Two Dimensional Turbulence and Carrier Induced Turbulence
Baseline [○], Direct Lift Control [□], Thrust Vectoring [△]

The mean aircraft sink rate at touchdown for successful touchdowns per aircraft carrier motion defined by wind speed and aircraft carrier speed is presented in Table 7-17 per approach controller for the three dimensional turbulence case. Again there is little significant difference in mean sink rates at touchdown between the two and three dimensional turbulence cases, except for some carrier motion cases where there is a disparity in the number of successful approaches between the two and three dimensional turbulence cases.

	Aircraft Carrier Speed (kts)								
	0			10			33		
	Approach Controller			Approach Controller			Approach Controller		
Wind Speed (kts)	1	2	3	1	2	3	1	2	3
2	-20.62	-9.63	-11.63	-20.46	-17.13	-13.02	-20.53	-12.18	-11.26
13.5	-	-10.23	-13.21	-	-14.4	-11.43	-22.16	-9.81	-6.7
24.5	-	-10.43	-13.04	-	-10.95	-14.02	-	-12.11	-8.04
37	-	-9.1	-6.86	-	-9.44	-13.1	-	-8.9	-8.5

Table 7-17 Aircraft Mean Sink Rate at Touchdown (ft/s) – Severe Two Dimensional Turbulence and Carrier Induced Turbulence
1= Baseline; 2 = Direct lift Control; 3 = Thrust Vectoring

The dispersion of all touchdowns per system for two dimensional turbulence case are presented in Table 7-18. As there are some Direct Lift Control approach controller bolters of large magnitude the inclusion of these is seen to have a large effect on the total longitudinal dispersion.

System	Longitudinal Touchdown Dispersion (Successful Touchdowns)	Longitudinal Touchdown Dispersion (All Touchdowns)
1	44.55 ft	44.55 ft
2	25.03 ft	37.51 ft
3	13.08 ft	13.08 ft

Table 7-18 Touchdown Dispersions per System – Severe Turbulence and Carrier Induced Turbulence

In this case, the baseline approach controller is outside of the touchdown dispersion requirement range; however, not by a large amount. The Direct Lift Control approach controller is within the requirement in either case but comfortably within the requirement if only successful touchdowns are counted. As with the other cases, the thrust vectoring approach controller performs the best being within the requirement by a large margin.

7.6 DISCUSSION

The purpose of the preceding analysis was to assess the performance of each of the three approach controllers developed relative to each other. Two methods of analysis were used in order to achieve this comparative assessment.

The first method consisted of simulating the aircraft executing carrier landing approaches under the control of each of the three approach controllers and subject to discrete atmospheric disturbance events. This allowed the approach controllers' response to a discrete event to be directly compared. The differences in response are directly related to the control strategies and implementation.

The second method of assessment consisted of a statistical analysis comprising of 480 simulated carrier landing approaches for each of the three approach controllers subject to varying ship motion and turbulence characteristics. This method allowed trends in the performance of each approach controller to be identified.

In order to quantitatively analyse each of the simulated approaches a set of performance metrics were defined. These performance metrics fully define the approach and touchdown performance based on operational procedures and desired performance irrespective of approach controller used.

Implicit in each of the simulated approaches is the active guidance cues generated by the Navigation System. The navigation strategy has been demonstrated as being feasible through the preceding simulated approaches. Ship motion prediction underpins the navigation strategy, and for the purposes of this study perfect prediction has been assumed. In reality, this level of accuracy is not achievable.

The effect that non-perfect prediction would have on the results presented is that some corrective manoeuvring would be required during the approach to reflect the fact that the predicted touchdown point is converging on the actual touchdown point. The magnitude of this corrective manoeuvring is a function of prediction accuracy. However, as current accurate prediction horizons are in the region of 10 to 15 seconds, the amount of corrective manoeuvring required would diminish to insignificance over the last half nautical mile of the approach, especially when compared with the manoeuvring required as a result of carrier induced turbulence over this period. Hence, while the results presented should be assessed with the fact that perfect ship motion prediction has been assumed, the overall performance of each approach controller

would not be appreciably adversely affected, and the trends presented in the results with regard to the approach controller's relative performance would not be affected.

The results presented demonstrate that each of the three approach controllers developed are capable of controlling the aircraft through a carrier approach and landing, albeit with varying levels of precision in turbulent conditions.

The benefits of the addition of Direct Lift Control to the baseline approach controller are evident in the enhanced approach glide path tracking precision and resulting touchdown dispersion accuracy. The increased approach glide path tracking is due to the faster reaction to a vertical displacement from the desired approach glide path due to an atmospheric disturbance or navigation cue. This faster reaction is due to the direct control of the lift vector afforded by Direct Lift Control in addition to the response of the baseline approach controller.

The significance of the addition of thrust vectoring to the Direct Lift Control aided approach controller is the demonstration of the use of thrust vectoring as a means to alleviate the magnitude of elevator pitch control required during approach. As described in Chapter 6, the short period damping ratio has been increased slightly as a result of the thrust vectoring control system gain. The increased short period damping ratio has had the effect of augmenting the aircraft's attenuation of atmospheric disturbances. The control loop bandwidth was also increased as a result of the addition of thrust vectoring. Care should be exercised not to associate the increased atmospheric disturbance attenuation of the thrust vectoring approach controller with the addition of the thrust vectoring itself, but with the augmentation of the aircraft's dynamic characteristics.

The implication of this use of thrust vectoring is that it could be used as a means to augment a conventional aircraft's longitudinal stability and control properties at different phases of flight independently to augmentation provided by the elevator. As vectored thrust is most efficient over small angles of deflection auxiliary stability augmentation is possible with little impact on the resultant axial thrust. A possible flight phase requiring auxiliary stability augmentation is a carrier landing approach in turbulence.

With respect to the approach track performance, it was found that increased approach glide path precision benefits the precision with which the approach track is maintained. In general, approach track control is less problematic than approach glide path control.

While turbulence in the Earth's boundary layer is modelled in the simulation the change in steady wind speed due to the proximity of the Earth's surface is not. In the carrier landing environment the dominant atmospheric effect, and hence the atmospheric effect of most importance in the design of an approach controller is that of total turbulence, i.e. the sum of atmospheric and carrier induced turbulence. The slow moving change of wind speed as a function of altitude due to the presence of the Earth's surface would have little, if any, effect on the approach controllers performance when compared with the effects of the faster rate of change of wind velocity due to turbulence.

The correlation of the touchdown dispersion characteristics of the F-14A baseline aircraft and the F-14A Direct Lift Control aided aircraft to the baseline approach controller and the Direct Lift Control aided baseline approach controller provides a sense of confidence in the results obtained in this study.

The potentially adverse effect that the aircraft carrier's pitch attitude can have on the aircraft's ramp crossing height is clearly evident in the preceding analysis. The erosion of ramp crossing height due to aircraft carrier pitch attitude is irrespective of how precisely the approach glide patch is maintained. The navigation strategy developed in Chapter 4 accounts for the position trajectory of the desired touchdown point but does not account for the motion of the aircraft carrier as a whole. As a result of this a brief study was undertaken to examine the feasibility of extending the Navigation System to account for the pitching motion of the aircraft carrier. This is presented in Chapter 8.

---------- o0o ----------

8 VARIABLE APPROACH SPEED CONTROLLER

8.1 INTRODUCTION

From the results presented in Chapter 7 it is clear that, regardless of how well an approach controller maintains the desired approach glide path, the pitch motion of the aircraft carrier can have a detrimental effect on the ramp crossing height. In the instance where an aircraft is below the approach glide path a negative aircraft carrier pitch attitude could have catastrophic consequences. Brictson [34] also presents, in the findings of a five-year study of human factors research on carrier landing performance, that the pitching deck is a major contributory factor in carrier landing accidents.

Current operational procedures rely on the judgement of the Land Signal Officer and the pilot to avoid such a situation. For UAV operations, the pilot is removed from this scenario, and as a consequence the pilot's judgement is removed.

A Variable Approach Speed Controller was developed to synchronise the time at which the aircraft crosses the ramp with the minimum absolute carrier pitch attitude attainable. This strategy is based on defining an approach speed range instead of a single approach speed. This Variable Approach speed strategy was developed to augment the navigation strategy presented in Chapter 4. The Variable Approach Speed Controller is presented schematically in Figure 8-1.

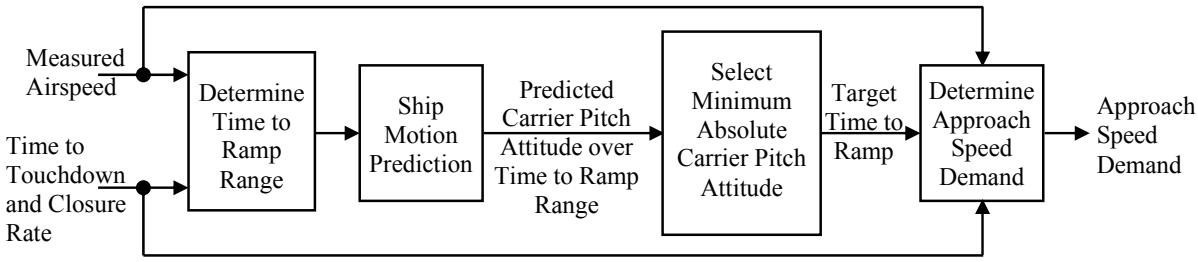

Figure 8-1 Variable Approach Speed Controller Data Flow Diagram

Using the aircraft's current airspeed, the Time to Touchdown and closure rate, both generated by the Navigation System presented in Chapter 4, the distance of the desired touchdown point from the ramp, and the approach speed range, a Time to Ramp range is determined.

Using ship motion prediction techniques, the predicted aircraft carrier pitch attitude over the Time to Ramp range is determined. The minimum absolute predicted aircraft carrier pitch attitude is selected from that range. It is important to note that it is the minimum of the absolute values that is selected. This ensures that the predicted carrier pitch attitude closest to zero is selected. The Time to Ramp, corresponding to the minimum absolute predicted aircraft carrier pitch attitude, is used to determine the approach speed. This will result in the aircraft passing over the ramp at that predicted aircraft carrier pitch attitude. This approach speed is then used as the approach speed demand by the autothrottle presented in Chapter 5.

There is no indication in the literature reviewed that such a strategy has been investigated. Research has been undertaken involving updating approach speed but differences exist. Research undertaken as part of the French Future Nuclear Carrier program [18,19] proposed a control strategy that uses ship motion prediction. This strategy involves continually updating the desired flight path angle to compensate for the aircraft carrier pitch attitude during the last 10-15 seconds of the approach. In addition, the strategy also involves continually updating the aircraft approach speed as appropriate, in order to maintain a constant vertical rate.

The French study aimed to augment the current navigation strategy, which is a landing approach to a moving point as opposed to the navigation strategy presented in this study. The navigation strategy presented in Chapter 4 determines the position of the desired touchdown point using ship motion prediction techniques and then defines an approach flight path to that pseudo-fixed point.

Under the strategy proposed in the French study, the approach speed is not updated throughout the duration of the approach, but only in the last 10-15 seconds and it is updated as a function of flight path angle in order to maintain a constant vertical rate.

As approach speed is aircraft dependent, it is thought that the variable approach speed strategy does not violate the constraints of adhering to the USN operational procedures, although in practice the spacing requirements for multiple aircraft approaches may need refinement to allow for situations where the second aircraft on approach is flying a faster approach than the first aircraft. It is thought that given the mixed fleet of carrier based fixed wing non V/STOL that such a situation is already accounted for.

The Variable Approach Speed strategy was developed to compliment the Navigation System presented in Chapter 4 and the Approach Controllers presented in Chapters 5 and 6. Figure 8-2 shows how the Variable Approach Speed Controller is integrated with the Navigation System and the Approach Controllers.

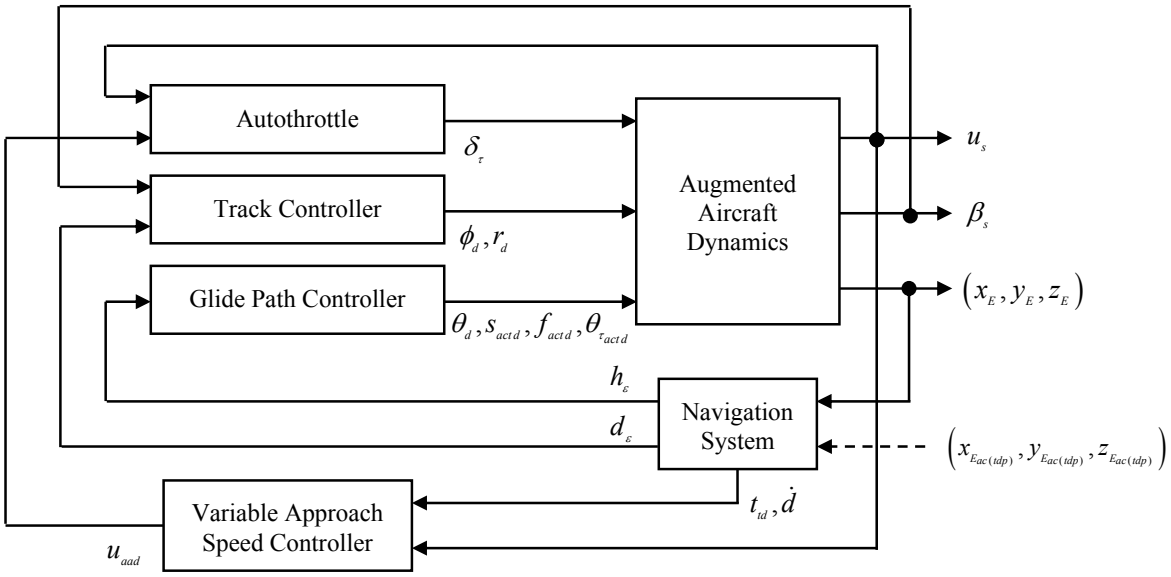

Figure 8-2 Variable Approach Speed Controller Integrated with Navigation System and Approach Controllers

8.2 CONTROL STRATEGY

Given an approach speed range defined by a minimum approach speed $u_{\min}$ and a maximum approach speed $u_{\max}$. At any instant during a landing approach, the corresponding range of Time to Touchdown is defined by a minimum Time to Touchdown t_1 and a maximum Time to Touchdown t_2.

The minimum Time to Touchdown, t_1, corresponding to the maximum approach speed, $u_{\max}$, is defined in equation 8-1.

$$t_1 = t_{td}\left[\frac{u_s + \left(\dot{d} - u_s\right)}{u_{\max} + \left(\dot{d} - u_s\right)}\right] \tag{8-1}$$

The bracketed expression in equation 8-1 expresses the current ground speed as a percentage of ground speed if the aircraft were at the maximum approach speed. The inclusion of the rate of change of distance between the aircraft and the desired touchdown point, $\dot{d}$, allows for the effect of wind on ground speed to be accounted for without need for direct measurement of wind.

The maximum Time to Touchdown, t_2, is determined similarly

$$t_2 = t_{td}\left[\frac{u_s + \left(\dot{d} - u_s\right)}{u_{\min} + \left(\dot{d} - u_s\right)}\right] \tag{8-2}$$

As the Variable Approach Speed control strategy aims to synchronise aircraft carrier pitch motion with the time the aircraft passes over the ramp rather than at touchdown it is necessary to adjust the range of Time to Touchdown accordingly. The minimum Time to Ramp, $t_{1'}$, and the maximum Time to Ramp, $t_{2'}$, is defined as

$$\begin{aligned} t_{1'} &= t_1 - \left[\frac{160}{\dot{d}}\right] \\ t_{2'} &= t_2 - \left[\frac{160}{\dot{d}}\right] \end{aligned} \tag{8-3}$$

The distance between the desired touchdown point and the ramp, when projected on to the flat earth when the aircraft carrier pitch attitude, is zero is 160 ft. The small effect that a non-zero aircraft carrier pitch attitude has on the distance between the desired touchdown point and the ramp when projected onto the flat earth is neglected in light of the groundspeed and the magnitude of aircraft carrier pitch attitude involved. Similarly, the Time to Ramp at any instant is determined by the Time to Touchdown at that instant as per equation 8-4.

$$t_{tr} = t_{td} - \left[\frac{160}{\dot{d}}\right] \tag{8-4}$$

Using ship motion prediction techniques, the aircraft carrier pitch attitude over the time range defined by $t_{1'}$ and $t_{2'}$ is predicted. The ability to predict the aircraft carrier pitch attitude is the key element to this control strategy. A discussion of ship motion prediction techniques is presented in Chapter 4 and a review of related research is presented in Chapter 2.

The minimum absolute aircraft carrier predicted pitch attitude over the time range defined by $t_{1'}$ and $t_{2'}$ is determined. The absolute value is used in order to ensure that the aircraft carrier pitch attitude closest to zero is selected as aircraft carrier pitch attitude can be positive or negative. The Time to Ramp corresponding to the minimum absolute aircraft carrier predicted pitch attitude, $t_{tr_{\min\theta_C}}$, is then used to calculate the approach speed required to synchronise the aircraft passing over the ramp with the aircraft carrier pitch attitude according to equation 8-5.

$$u_{aad} = \frac{t_{tr}\left(u_s + \left(\dot{d} - u_s\right)\right)}{t_{tr_{\min\theta_C}}} - \left(\dot{d} - u_s\right) \tag{8-5}$$

This Variable Approach Speed demand is then used as the airspeed demand by the Autothrottle as presented in Figure 8-3.

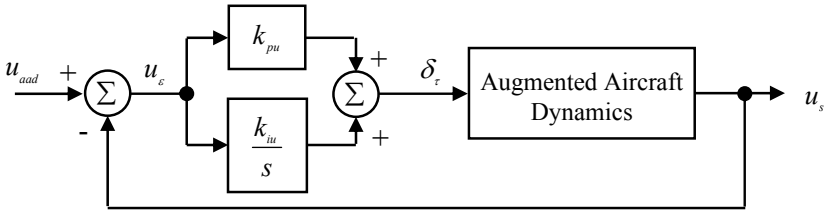

Figure 8-3 Variable Approach Speed Controller Data Flow Diagram

The Autothrottle control law is defined as

$$\delta_\tau = k_{pu}\left(u_{aad} - u_s\right) + k_{iu}\int\left(u_{aad} - u_s\right)dt \tag{8-6}$$

The control system gains are as presented in Chapter 5

$$k_{pu} = 659 \text{ RPM/ft/s}$$
$$k_{iu} = 15.64 \text{ RPM/ft/s} \quad (8\text{-}7)$$

8.2.1 IMPLEMENTATION

For the purposes of this investigation, an approach speed range has been defined as 135-140 knots. This range is not selected based on aerodynamic characteristics of the aircraft, but is chosen to provide a sufficient corresponding Time to Ramp range to allow a proper assessment of the benefits that Variable Approach Speed may afford.

In the simulation Test Cases presented in the following section, the Variable Approach Speed control strategy is implemented from an altitude of 500 ft at which point the aircraft is stabilised on the approach flight path. All navigation parameters prior to this are identical to that of the system presented in Chapter 4.

As with the Navigation System, perfect prediction is assumed. As aircraft carrier motion is calculated prior to simulation of the approach, perfect prediction is achieved by looking ahead on the time 'history' of the aircraft carrier pitch attitude for the Time to Ramp range. The Time to Ramp range was divided into 21 equally spaced times, and the aircraft carrier pitch attitude was predicted at each of those times. The minimum absolute aircraft carrier pitch attitude was determined and the Variable Approach Speed demand was determined as presented in section 8.2.

8.3 COMPARISON TEST CASE

In order to evaluate the benefits of the Variable Approach Speed control strategy, a comparison between the Baseline Approach Controller with a fixed approach speed and the Baseline Approach Controller with the Variable Approach Speed Controller was conducted.

The worst-case aircraft carrier motion the provided the largest aircraft carrier pitch attitude variation was selected. This aircraft carrier motion is defined by a steady wind of 37 knots and an aircraft carrier speed of 0 knots. No atmospheric disturbances other than the steady wind associated with the aircraft carrier motion were simulated. Selected

aircraft and aircraft carrier variables along are presented in Figure 8-4. The approach performance metrics calculated for each system are presented in Table 8-1.

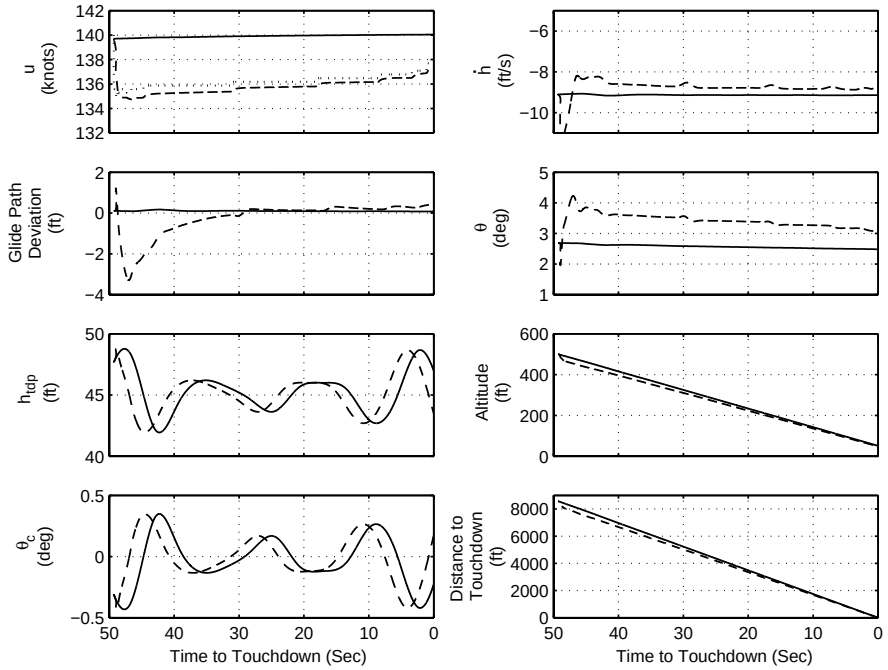

Figure 8-4 Variable Approach Speed Test Case 1
Baseline Approach Controller [—], Baseline Approach Controller with Variable Approach Speed Controller [- -], Speed Demand [·····]

It should be noted that the variables presented in Figure 8-4 are plotted against Time to Touchdown. The aircraft passes over the ramp approximately 1 second prior to touchdown. Based on the flight deck geometry, and an approach glide path of 3 degrees, the ideal ramp crossing height is 8.39 ft.

From the data presented in Table 8-1 it is clear that the Variable Approach Speed Controller successfully controls speed so as to cross the ramp at the minimum absolute aircraft carrier pitch attitude. Using the Variable Approach Speed Controller, the aircraft passed over the ramp when the aircraft carrier pitch attitude was -0.03 deg as opposed to -0.36 deg when flying at the fixed approach speed of 140 knots. This difference in aircraft carrier pitch attitude is equivalent to a difference in ramp crossing height of 0.92 ft.

	Standard Approach Speed Controller	Variable Approach Speed Controller
Approach Success	Yes	Yes
Approach Glide Path Deviation RMS	0.06 ft	0.55 ft
Approach Track Deviation RMS	0 ft	0 ft
Approach Speed Deviation RMS	0.08 kts	0.44 kts
Ramp Crossing Height	7.47 ft	8.68 ft
Aircraft Carrier Pitch Attitude at Ramp Crossing	-0.36 deg	-0.03 deg
Approach Glide Path Deviation at Ramp Crossing	0.075 ft	0.39 ft
Ramp Strike	No	No
Longitudinal Displacement at Touchdown	1.64 ft	-11.52 ft
Lateral Displacement at Touchdown	0 ft	0 ft
Aircraft Sink Rate at Touchdown	-9.14 ft/s	-8.75 ft/s
Aircraft Carrier Vertical Rate at Touchdown	-1.46 ft/s	-2.16 ft/s
Bolter	No	No

Table 8-1 Variable Approach Speed Test Case Performance Summary

As the aircraft's approach speed is reduced, the time to touchdown is increased, thus the predicted position of the touchdown point updates accordingly. It can be seen from time history of the altitude of the desired touchdown point on the aircraft carriers deck, h_{tdp}, that the rate of change of this parameter is greatest around the time of touchdown. As a result of this, small changes in time to touchdown due to changes in aircraft speed correspond to large changes in vertical position of the predicted touchdown point. Changes in the vertical position of the predicted touchdown point have a 1:1 effect on the vertical position of the approach glide slope. This has a large effect on the approach glide path deviation performance.

It should be noted that as with all previous approaches analysed, ramp crossing height is determined by two main components, approach glide path deviation at ramp crossing and the aircraft carrier pitch attitude at ramp crossing. In the case of the Variable Approach Speed Controller the aircraft passes the ramp with a greater positive approach glide path deviation than when flying at the fixed approach speed of 140 knots. This is

due to the motion of the predicted vertical position of the desired touchdown point, which is due to the change in approach speed.

In Chapter 7 the approach glide path deviation performance of the Direct Lift Control Approach Controller and the Thrust Vectoring Approach Controller were shown to be superior to the Baseline Approach controller. The inference is that either of these systems coupled with the Variable Approach Speed Controller would result in less approach glide path deviation at ramp crossing.

The reduced approach speed selected by the Variable Approach Speed Controller also has the effect of reducing the rate of descent and, as a consequence, the aircraft sink rate at touchdown is reduced when compared to the standard approach speed case.

8.3.1 TURBULENCE AND ENGINE SPOOL TIME EFFECTS

In order to assess the effects of turbulence and engine spool time on the performance of the Variable Approach Speed Controller a series of simulations were conducted with varying turbulence intensity and engine spool times.

For the same aircraft carrier speed and wind speed as considered in section 8.3 the approach performance metrics were calculated for the variable approach speed controller operating in axial atmospheric turbulence intensities of light, moderate and severe. The approach performance metrics are presented in Table 8-2. In this case the engine dynamics are ideal, i.e. engine spool time is not considered as in all other cases.

For the same aircraft carrier speed, wind speed and turbulence cases the approach performance metrics were calculated with the engine dynamics modeled as a first order lag with a time constant of 1.2 seconds. This set of approach performance metrics are presented in Table 8-3.

Turbulence Intensity	Light	Moderate	Severe
Approach Success	Yes	Yes	Yes
Approach Glide Path Deviation RMS	0.78 ft	1.14 ft	1.32 ft
Approach Track Deviation RMS	0 ft	0 ft	0 ft
Approach Speed Deviation RMS	0.45 kts	0.45 kts	0.45 kts
Ramp Crossing Height	8.36 ft	8.09 ft	7.95ft
Aircraft Carrier Pitch Attitude at Ramp Crossing	-0.034 deg	-0.036 deg	-0.036 deg
Approach Glide Path Deviation at Ramp Crossing	0.07 ft	-0.19 ft	-0.33 ft
Ramp Strike	No	No	No
Longitudinal Displacement at Touchdown	32.3 ft	34.85 ft	35 ft
Lateral Displacement at Touchdown	-0.1 ft	-0.1 ft	-0.1 ft
Aircraft Sink Rate at Touchdown	-7.82 ft/s	-7.76 ft/s	-7.69 ft/s
Aircraft Carrier Vertical Rate at Touchdown	-2.05 ft/s	-2 ft/s	-1.98 ft/s
Bolter	No	No	No

Table 8-2 Variable Approach Speed Turbulence Performance Summary – Ideal Spool

Turbulence Intensity	Light	Moderate	Severe
Approach Success	Yes	Yes	Yes
Approach Glide Path Deviation RMS	0.86 ft	1.8 ft	1.34 ft
Approach Track Deviation RMS	0 ft	0 ft	0 ft
Approach Speed Deviation RMS	0.58 kts	0.67 kts	0.72 kts
Ramp Crossing Height	8.25 ft	7.75 ft	7.43 ft
Aircraft Carrier Pitch Attitude at Ramp Crossing	-0.034 deg	-0.034 deg	-0.034 deg
Approach Glide Path Deviation at Ramp Crossing	-0.03 ft	-0.54 ft	-0.86 ft
Ramp Strike	No	No	No
Longitudinal Displacement at Touchdown	6.21 ft	3.09 ft	-1 ft
Lateral Displacement at Touchdown	0 ft	0 ft	0 ft
Aircraft Sink Rate at Touchdown	-8.32 ft/s	-7.8 ft/s	-7.62 ft/s
Aircraft Carrier Vertical Rate at Touchdown	-2.36 ft/s	-1.98 ft/s	-1.93 ft/s
Bolter	No	No	No

Table 8-3 Variable Approach Speed Turbulence Performance Summary – Non Ideal Spool

It can be seen from Tables 8-1 and 8-2 that the effects of the axial turbulence have very little effect on the performance of the Variable Approach Speed Controller. As the intensity of the turbulence is increased the vertical glide path deviation increases, however the magnitude is small.

By comparing the data presented in Tables 8-2 and 8-3 it can be seen that the effects of engine spool time, for the range considered, are negligible with respect to the performance of the Variable Approach Speed Controller. As expected the approach speed RMS values increase as turbulence intensity increases.

8.4 SUMMARY

The motivation to develop a Variable Approach Speed Controller to synchronise the aircraft's approach with the aircraft carriers pitching motion came from the results of the approach controllers' comparative analysis. It was shown in Chapter 7 that aircraft carrier pitch attitude can have a significant effect on the clearance between the aircraft and the aircraft carrier's ramp regardless of how well approach glide path is maintained. In addition, Brictson [34] presents findings from a study of human factors on carrier landing performance which state that carrier pitching motion is a major contribution to carrier landing accidents.

The strategy investigated involves defining an approach speed range for an aircraft rather than a single approach speed. For an aircraft on approach to a carrier, ship motion prediction techniques are used to determine the carrier's pitch attitude when the aircraft is predicted to pass over the carrier's ramp over a time range corresponding to that approach speed range. The aircraft's approach speed is then adjusted so that the aircraft passes over the ramp at a time when the aircraft carrier's pitch attitude is at the absolute minimum attainable over that approach speed range.

The Variable Approach Speed Controller was developed to augment the Navigation System presented in Chapter 4. There is no indication that a Variable Approach Speed Controller has previously been investigated in the literature reviewed during the course of this study.

A performance comparison between the Baseline Approach Controller approaching an aircraft carrier at a fixed approach speed and the Baseline Approach Controller using the Variable Approach Speed Controller was presented in section 8.3. The results show that the Variable Approach Speed Controller successfully synchronised the aircrafts approach with the pitching motion of the aircraft carrier.

As the ramp of the aircraft carrier is located 160 feet aft of the desired touchdown point a pitch attitude of -1 degree results in a vertical displacement of 2.79 feet of the ramp, or one third of the ideal ramp crossing height. In heavy sea conditions, which give rise to large ship pitch motion, the Variable Approach Speed Controller has the potential to increase the level of approach safety with respect to ramp crossing height. This is significant as heavy seas are generally accompanied by atmospheric turbulence which has a degrading effect on approach glide path vertical deviation control.

The Variable Approach Speed Controller uses ship motion prediction in the same way as the Navigation System presented in Chapter 4. Both of these systems are limited by the current state of the art of ship motion techniques. As previously stated the research undertaken at the Department of Mechanical Engineering at University College London [39,40,41,42,43] is encouraging with regard to the prediction problem. The benefits of using ship motion prediction techniques as an integral part of a carrier landing navigation system are apparent when the results of the Variable Approach Speed Controller and the benefits afforded by the Navigation System presented in Chapter 4 are considered. It is hoped that these findings will provide stimulus for further ship motion prediction research.

9 CONCLUSIONS AND RECOMMENDATIONS

9.1 INTRODUCTION

The preceding research demonstrated how ship motion prediction can be used as an integral part of a navigation aid to increase the level of safety associated with aircraft carrier landing operations and hence expand the operational envelope for aircraft carrier landings.

Three flight control strategies applied to the carrier landing task were assessed for suitability for application to future carrier based UAV planforms. The results presented demonstrated that autonomous UAV carrier landing operations is feasible, even in inclement atmospheric conditions.

An Adaptive Approach Speed Controller was developed which, using ship motion prediction, controls the aircraft's approach speed so as to synchronise the aircraft's approach with the carrier's pitching motion. This strategy has the potential to increase the level of safety of a carrier landing approach by mitigating the possibility of a ramp strike. This strategy also has the potential to increase the carrier operational envelope.

9.2 CONCLUSIONS

From the analysis and discussions in the preceding chapters the following conclusions can be made with regard to the Navigation System:

- A Navigation System was developed conceptually which (1) adheres to the current operating procedures, (2) requires less associated systems than the current Instrument Carrier Landing System, (3) accounts for future military navigational goals, (4) facilitates the seamless integration of the UAV fleet with the piloted fleets and (5) allows for truly autonomous carrier landing operations.

- The Navigation System, which uses ship motion prediction, has been demonstrated within the scope of this study as being a feasible option for a future carrier landing navigation system.

- An Adaptive Approach Speed Controller, which uses ship motion prediction, was developed and was demonstrated as a feasible means of synchronising an aircraft's approach with the pitching motion of the carrier.

- The Adaptive Approach Speed Controller was developed to augment the Navigation System. Together these systems have the potential to increase the level of safety associated with carrier landings and potentially increase the carrier landing operational envelope.

From the analysis and discussions in the preceding chapters the following conclusions can be made with regard to the control systems:

- Direct Lift Control can be used to augment the performance of a standard glide path controller with respect to glide path tracking and touchdown dispersion performance. The benefits afforded by Direct Lift Control are more apparent in the presence of atmospheric disturbances.

- A constant attitude DLC system is not suitable for the aircraft carrier approach task given the nature of the likely atmospheric disturbances.

- Thrust vectoring can be used to alleviate the demand on an aircraft's aerodynamic pitch control effector. This may be particularly useful to future tailless aircraft carrier based UCAVs where longitudinal and lateral directional control share aerodynamic control effectors; especially so considering the likely atmospheric disturbance conditions and resulting increased demand for pitch control, coupled with the inherently directional unstable planform of a tailless aircraft.

- Thrust vectoring provides a means of providing auxiliary stability augmentation during phases of flight which may require increased stability. Such a situation is

a carrier landing approach where increased pitch stability results in increased attenuation of atmospheric disturbances.

9.3 RECOMMENDATIONS FOR FURTHER WORK

To realise the potential of the Navigation System and Adaptive Approach Speed Controller, a ship motion prediction algorithm is required with a suitable time horizon. It is thought that the research undertaken at University College London [39,40,41,42,43] would provide the most promising starting point for such an endeavour.

Lateral and Directional control during aircraft carrier landing approaches will become more challenging for future UCAV planforms. While the method of alleviating the demand on a shared aerodynamic control effector, as used on tailless aircraft, has been demonstrated, further work should assess the full potential of vectored thrust as both a secondary lateral directional and pitch control effector.

Based on the work presented, an investigation into the feasibility of extending the Navigation System to generate a non-linear, flare-like, flight path prior to touchdown with the aim of arresting sink rate at touchdown is proposed. Such a situation would have operational benefits allowing aircraft to be lighter as less structural reinforcement would be needed. The reduction in weight would allow aircraft to carry more fuel or payload increasing the aircraft's range or effectiveness.

---------- o0o ----------

10 REFERENCES

1 Anon, *Wikipedia http://en.wikipedia.org/wiki/Image:Ely-landing.jpg* Accessed September 6th 2004.

2 Harbaugh, P.M. *Where stands the LSO.* Naval Aviation News, NavWeps No. 00-75R-3, page 16, January 1962.

3 Durand, T. S., Wasicko, R. J. *Carrier landing analysis*. Systems Technology, Inc STI-TR-137-2, Feb 1967.

4 Anon. *Landing Signal Officer Reference Manual*. The United States Navy Landing Signal Officer School, Revision B, June 1999.

5 Lehman, A. F. An experimental study of the dynamic and steady state flow disturbances encountered by aircraft during a carrier landing approach. American Institute of Aeronautics and Astronautics, Annual Meeting, 2nd, San Francisco, California, July 26-29 1965, AIAA Paper 65-332, Jul 1965.

6 Anon. *CV NATOPS manual*. The United States Navy, NAVAIR 00-80T-105, 21st October 1999.

7 Anon. *NATOPS Landing Signal Officer Manual*. The United States Navy, NAVAIR 00-80T-104, 15th December 2001.

8 Casey, R. L., Leitzel, R.L. *Landing Signal Officers*. Memo from Chief of Staff, Department of the Navy, United States Navy, July 29 1996.

9 Anon. *United States Navy Training Manual: Construction Electrician, Intermediate*. http://www.tpub.com/content/construction/14027, accessed May 11th 2004.

10 Wallace, K. *Joint Precision Approach and Landing System*. Presentation given to the landing signal officer's operational advisory group March 13th 2002.

11 Anon. *United States Navy Training Manual: Aviation Electronics Technician 1 (Organizational)*. http://www.tpub.com/content/construction/14027, accessed May 11th 2004.

12 Anon. *United States Navy Training Manual: Aviation Electronics Technician 4 – Radar Systems*. http://www.tpub.com/content/construction/14027, accessed May 11th 2004.

13 Davies, W. D. T., Noury, R. *AN/SPN-42 Automatic Carrier Landing System*. Bell Aerospace Report, February 1982.

14 Hess, R. K., Urnes, J. M. *Development of the F/A-18A automatic carrier landing system*. Journal of Guidance, Control, and Dynamics (ISSN 0731-5090), vol. 8, pp 289-295, May-June 1985.

15 Mook, D. J., Noury, R., Roemer, M. J., Swanson, D. A., *Improved Noise Rejection in Automatic Carrier Landing Systems.* AIAA Guidance, Navigation and Control Conference, Portland, Or., August 20-22, 1990. AIAA-90/3374, August 1990.

16 Crassidis, J. L., Mook, D. J., McGrath, J. M. *Automatic carrier landing system utilizing aircraft sensors* Journal of Guidance, Control, and Dynamics vol. 16, no. 5 pp 914-921. Sept.-Oct. 1993.

17 Crassidis, J. L., Mook, D. J. *Robust Control Design of an Automatic Carrier Landing System* Paper presented at: AIAA Guidance, Navigation and Control Conference, Hilton Head Island, SC., August 10-12, 1992. AIAA-92-4619, August 1992.

18 Costes, P., Le Moing, T., Vu, B. D. *Integration of flight and carrier landing aid systems for shipboard operations.* NATO, AGARD, Symposium on Aircraft/Ship Operations, Seville, Spain, May 20-23, 1991.

19 Le Moing, T. *Integration of flight control and carrier landing aid system*. ICAS, Congress, 18th, Beijing, China, Sept. 20-25, 1992, Proceedings. Vol. 1 (A93-14151 03-01), pp 242-251. Jan 1992.

20 McPeak, M. A. Joint USAF – USN Mission Need Statement for Precision Approach and Landing Capability. USAF 002-94 Aug 1994.

21 Fitzgibbon, K. T., Parkinson, B. W. *Aircraft automatic landing systems using GPS*. Journal of Navigation (ISSN 0373-4633), Vol. 42, pp 47-59, Jan. 1989.

22 Fortenbaugh, R.L. *Practical Integration of Direct Lift Control into an Automatic Carrier Landing System.* American Institute of Aeronautics and Astronautics, Guidance and Control Conference, Stanford, California, August 14-16, 1972, AIAA Paper 72-873, August 1972.

23 Martorella, P. Kelly, C. P. Nastasi, R. *Precision flight path control in carrier landing approach - A case for integrated system design.* American Institute of Aeronautics and Astronautics, Aircraft Systems and Technology Conference, Dayton, OH, Aug. 11-13, 1981, Aug 1981.

24 Huff, R. Martorella, P. McNeill, W. Nastasi, R. Zalesak, T. *Carrier landing simulation results of precision flight path controllers in manual and automatic approach*. American Institute of Aeronautics and Astronautics, Atmospheric Flight Mechanics Conference, Gatlinburg, TN, Aug. 15-17, 1983. AIAA Paper 83-2072, Aug 1983.

25 Clark, J. W. Miller, D. P. *Investigation of the use of vectored thrust during carrier landings*. AIAA/RAeS/JSASS Aircraft Design and Technology Meeting, Los Angeles, CA., Nov 14-18, 1965. AIAA Paper 65-792, Nov 1965.

26 Crassidis, John L. Mook, D. J. *Modeling an autopilot and thrust compensator in an automatic carrier landing system.* AIAA Flight Simulation Technologies Conference, New Orleans, LA., Aug. 12-14, 1991, AIAA Paper 91-2956, Jan 1991.

27 Gerdes, R. M., McNeill, W. E., Smith, G. A., Jr. *Evaluation of a trajectory command concept for manual control of carrier approaches and landings*. NASA Report N82-34060, 1982.

28 Meyer, G., Smith, G. A. *Application of the concept of dynamic trim control to automatic landing of carrier aircraft*. NASA Report NASA-TP-1512 , 1980.

29 Bannett, R. J. Optimal control of the F-8C in a fully automatic carrier approach. AD-753010, Nov 1972.

30 Bihrle, W., Jr. *Aircraft characteristics that influence the longitudinal handling qualities during a carrier approach.* American Institute of Aeronautics and Astronautics, Guidance, control and flight mechanics conference, Princeton, N.J., August 18-20, 1969.

31 Ebers, R. S., Black, R., Sandlin, N. H. *Ship motion effects on landing impact loads.* Structures, Structural Dynamics, and Materials Conference, 20th, St. Louis, Mo., April 4-6, 1979. AIAA Paper 79-0742 Jan 1979.

32 Connelly, E. M. *Performance measures for aircraft landings as a function of aircraft dynamics*. Performance Measurement Associates, Inc. Report N85-14565, 1985.

33 Durand, T. S., *Theory and simulation of piloted longitudinal control in carrier approach*. Systems Technology, Inc. Report No. 130-1, Mar 1965.

34 Brictson, C. A. *Human factors research on carrier landing system performance.* Dunlap and Associates, Inc. AD-733703 July 1971.

35 Johnson, W. A. *Analysis of Aircraft Carrier Motions in a High Sea State*. Systems Technology, Inc. Report No. 137-3, Mar 1969.

36 Kaplan, P. *A study of Prediction Techniques for Aircraft Carrier Motions at Sea*. Journal of Hydronautics, Vol. 3, No. 3, pp 121-131, July 1969.

37 Doolin, B. F., Sidar, M. *On the Feasibility of Real-Time Prediction of Aircraft Carrier Motion at Sea*. NASA Report NASA-TM-X-62,454, June 1975.

38 Hess, R. A., Judd, T. M. *Improved Automatic Carrier Landing Using Deck Motion Prediction*. Journal of Aircraft, Vol. 13, No. 2, pp 153-155, Feb 1976.

39 Broome, D. R., Pittaras, A. *Ship Motion Prediction*. Offshore technology conference, Houston, TX. May 6-9 1990.

40 Jefferys, E. R., Samra, B. S. *Adaptive Prediction of the Motion of Marine Vehicles*. Journal of Energy Resources Technology, Vol. 107, December 1985.

41 Pittaras, A. *Adaptive Signal Prediction with Applications to Ship Motion*. PhD Thesis, University College London, June 1992.

42 Broome, D. R., Hall, M. S. *Application of Ship Motion Prediction I*. Trans IMarE, Vol. 110, Part 1, pp 77-93, July 1997.

43 Broome, D. R. *Application of Ship Motion Prediction II*. Trans IMarE Vol. 110, Part 2, pp 135-153, October 1997.

44 Fielding, C. *The Design of Fly-By-Wire Flight Control Systems.* BAE Systems Limited, 2000.

45 Anon. *Flight Control Design – Best Practices*. NATO RTO-TR-029, December 2000.

46 Cook, M.V. *Flight Dynamics Principles*. Edward Arnold, 1997.

47 McLean, D. *Automatic Flight Control Systems.* Prentice Hall, 1990.

48 Prilliman, F. W., Slingerland, R. D., Smith, L. R. *Direct Lift Control as a Landing Approach Aid.* AIAA Paper 66-14 January 1968.

49 Henry, R. C., Patton, J. M., Stickle, J. W. *Flight Tests of a Direct Lift Control System During Approach and Landing.* NASA TN-D-4854, November 1968

50 Messina, M. D., Strickland, M. E., Hoffler, K. D., Carzoo, S. W., Bundick, W.T, Yeager, C., Beissner Jr., F. L. *Simulation model of the F/A-18 High Angle-of-Attack Research Vehicle Utilized for the Design of Advanced Control Laws.* TM-110216, May 1996, pp. 161.

51 Gerzanics, M. A., Sweeney, J. E. *F-16 Multi-Axis Thrust Vectoring: A Pilots Perspective*. AIAA Paper 94-3364 June 1994.

52 Deere, K. A. *Summary of Fluidic Thrust Vectoring Research Conducted at NASA Langley Research Centre.* AIAA Paper 2002-3800 June 2003.

53 Bowers, A. H., Pahle, J. W., Wilson, R. J., Flick, B. C., Rood, R. L. *An Overview of the NASA F-18 High Alpha Research Vehicle.* NASA-TM-4772, October 1996.

54 Bosworth, J. T., Stoliker, P. C. *The X-31A Quasi-Tailless Flight Test Results*. NASA TP-3624, June 1996.

55 Gautrey, J. E., Cook, M. V. *A "Dymola" Simulation Model of the Mk 4A Jindivik Aircraft for Flight Dynamics Applications* College of Aeronautics Report NFP 0007, Cranfield University, July 2000.

56 Fitzgerald, P. *Modern Flight Control System Design for the Jindivik UAV*. College of Aeronautics MSc Thesis, Cranfield University, September 2000.

57 Anon. *Jindivik Mk. 4A Design summary.* Project report B4A-C00-051, Issue 9, Aerospace Technologies of Australia, April 1991.

58 Anon. Engineering Sciences Data Unit (ESDU) data item 90030: *Lift and Rolling Moment Due to Spoilers on Wings with Flaps Undeflected at Subsonic Speeds.* Amendment B, Nov 1999.

59 Anon. Engineering Sciences Data Unit (ESDU) data item 92002: *Lift and Rolling Moment Due to Spoilers on Wings with Trailing-Edge Flaps Deflected at Subsonic Speeds.* Amendment B, Nov 1999.

60 Anon. Engineering Sciences Data Unit (ESDU) data item 96026: *Drag and Yawing Moment Due to Spoilers.* Amendment B, Nov 1999

61 Anon. Engineering Sciences Data Unit (ESDU) data item 79015: *Undercarriage Drag Prediction Methods*. Amendment A, Mar 1987.

62 Anon. *Standard Atmosphere – Tables and Data for Altitudes to 65,800 Feet.* NACA Report 1235. International Civil Aeronautical Organisation, Montreal, Canada, December 1952 & NACA Langley Aeronautical Laboratory, Langley Field, Va., U.S.A., February 1954.

63 Anon.: *Military Specifications - Flying qualities of piloted airplanes.* MIL-F-8785C. Department of Defence, USA. Notice 2, 28th August 1996.

64 Journée, J. M. J. *Theoretical Manual of SEAWAY.* Delft University Report Number 1216a, release 4.19, February 2001.

65 Journée, J. M. J. *User Manual of SEAWAY.* Delft University Report Number 1212a, release 4.19, February 2001.

66 Journée, J. M. J. *Verification and Validation of Ship Motions Program SEAWAY.* Delft University Report Number 1213a, February 2001.

67 Fitzgerald, P. *Unmanned Combat Air Vehicle Technology Demonstrator Six Degree of Freedom Flight Dynamics Simulation Model*. College of Aeronautics Report NFP 0401, Cranfield University, April 2004.

68 Anon. Engineering Sciences Data unit (ESDU) data item No. 87008: *Rudder sideforce, Yawing Moment and Rolling Moment Control Derivatives at Low Speeds:* Y_ζ, N_ζ *and* L_ζ, June 1987.

69 Yeung, W. W. H,, Xu, C., Gu, W. *Reduction of Transient Adverse Effects of Spoilers*. Journal of Aircraft, Vol. 34, No. 4, 1997, pp 479-484.

70 Choi, S. W., Chang, K. S., Ok, H. *Parametric Study of Transient Spoiler Aerodynamics with Two-Equation Turbulence Models.* Journal of Aircraft, Vol. 38, No. 5, 2001, pp 888-894.

71 Messina, M.D., Strickland, M.E., Hoffler, K.D., Carzoo, S.W., Bundick, W.T, Yeager, C., Beissner Jr., F.L. *Simulation model of the F/A-18 High Angle-of-Attack Research Vehicle Utilized for the Design of Advanced Control Laws.* TM-110216, May 1996, pp. 161.

72 McMinn, John D.: *Extension of a Kolmogorov Atmospheric Turbulence Model for Time -Based Simulation Implementation*. AIAA Guidance Navigation and Control Conference Paper No. 97-3532, New Orleans, La, August 11-13, 1997.

73 Anon. *Jane's Fighting Ship 2003-2004.* Jane's publishing company, London, 2003.

74 Hoblit, F.M., *Gust Loads on Aircraft: Concepts and Applications*, AIAA Education Series, 1988.

75 Hinedi, S., Kumar, F., Vilnrotter, V. A. *A Comparison of Frequency Estimation Techniques for High-Dynamic Trajectories*. NASA Report NASA-CR-184865, Sept 1988.

76 Anon.: *Flight Control System Design, Installation and Test of Piloted Aircraft, General Specification for.* MIL-F-9490. Department of Defence, 5th October 1992.

77 Kanade, T., Messner, W., Mettler, B., Tischler., M. *Attitude control optimization for a small-scale unmanned helicopter.* AIAA-2000-4059, A Guidance, Navigation, and Control Conference and Exhibit, Denver, CO, Aug. 14-17, 2000.

78 Prosser, C. F., Wiler, C. D. *RPV flying qualities criteria*. USAF Flight Dynamics Laboratory Technical Report AFFDL-TR-76-125, December 1976.

79 Anon.: *Military Specifications - Flying qualities of piloted airplanes.* MIL-F-8785B. Department of Defence, USA. 7th August 1969.

80 Anon.: *Automatic Carrier Landing System, Airborne Subsystem, General Requirements for*. Naval Air Systems Command, Washington, D.C., AR-40A, May 1975.

81 Friehmelt, H. *Thrust Vectoring and Tailless Aircraft Design – Review and Outlook.* AIAA Paper 96-3412-CP July 1996.

82 Kuipers J. B.: Quaternions and Rotation Sequences: A Primer with Applications to Orbits, Aerospace, and Virtual Reality. Princeton University Press, October 2002.

---------- o0o ----------

APPENDIX A SIMULATION MODEL DEVELOPMENT

A.1 DYNAMICS MODULE

A.1.1 EQUATIONS OF MOTION OF A RIGID SYMMETRIC AIRCRAFT

Newton's second law of motion states that the acceleration of a body as produced by a force is directly proportional to the magnitude of the force, in the same direction of the force and inversely proportional to the mass of the body. This is presented in equation A-1.

$$F = ma \tag{A-1}$$

In the development of the equations of motion of a rigid symmetric aircraft the objective is to realise Newton's second law of motion for each of the six degrees of motion. The subsequent derivation is based on that presented by Cook[46].

A.1.1.1 THE COMPONENTS OF INERTIAL ACCELERATION

Consider the point p(x, y, z) of the not necessarily rigid body presented in Figure A-1 whose acceleration components are (a_x, a_y, a_z) and velocity components are (u, v, w). The velocity components at p(x, y, z) relative to o are given by

$$\begin{aligned} u &= \dot{x} - ry + qz \\ v &= \dot{y} - pz + rx \\ w &= \dot{z} - qx + py \end{aligned} \tag{A-2}$$

The corresponding components of acceleration at p(x, y, z) relative to o are given by

$$a_x = \dot{u} - rv + qw$$

$$a_y = \dot{v} - pw + ru \qquad \text{(A-3)}$$

$$a_z = \dot{w} - qu + pv$$

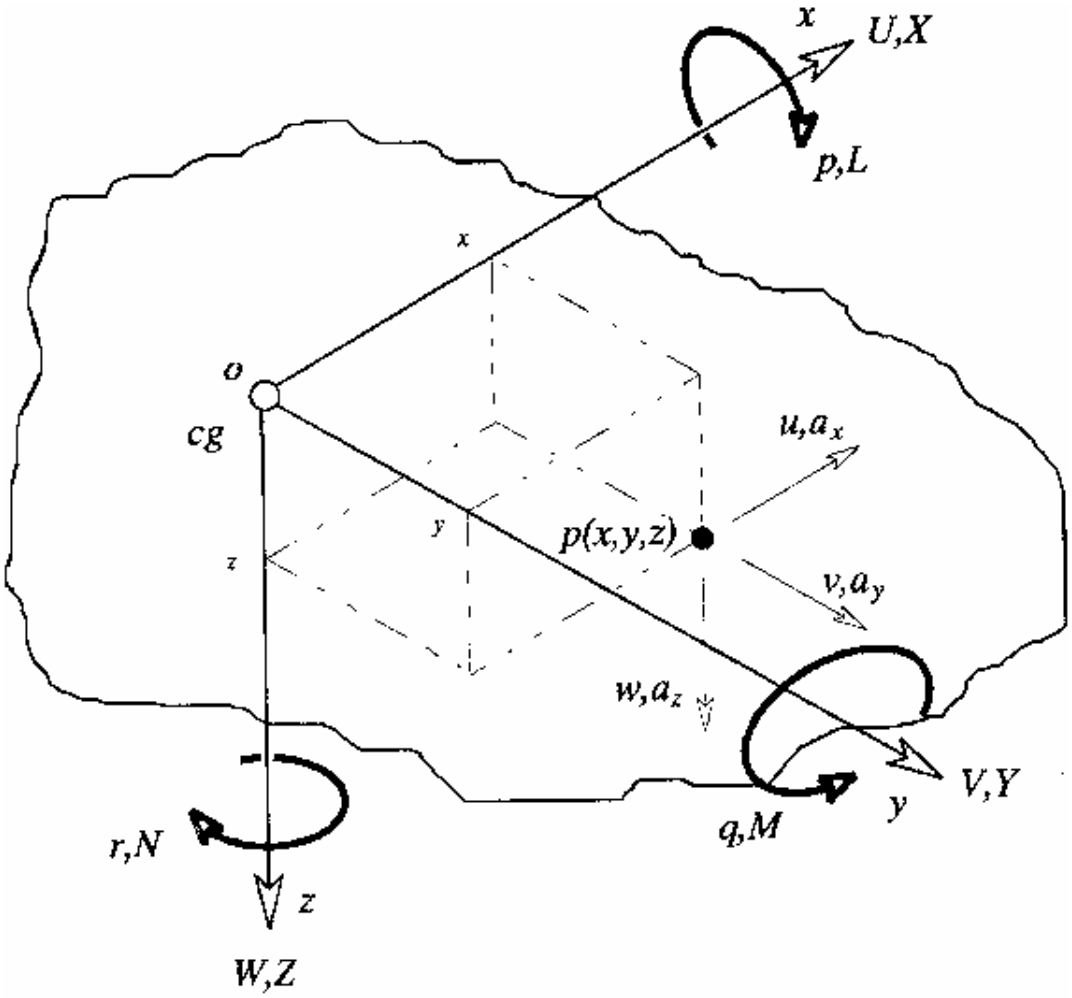

Figure A-1 Motion Referred to Generalized Body Axes[46]

By superimposing the velocity components of the *cg* (*U, V, W*) on to the local velocity components (*u, v, w*) the absolute, or inertial, velocity components (u', v', w') of the point p(*x, y z*) are obtained. Where the expressions for (*u, v, w*) are substituted from equation A-2, this becomes

$$u' = U + u = U + \dot{x} - ry + qz$$

$$v' = V + v = V + \dot{y} - pz + rx \qquad \text{(A-4)}$$

$$w' = W + w = W + \dot{z} - qx + py$$

In this case we assume that the body is rigid, hence

$$\dot{x} = \dot{y} = \dot{z} = 0 \qquad \text{(A-5)}$$

Similarly, the components of inertial acceleration (a'_x, a'_y, a'_z) at the point p(*x, y z*) are obtained by substituting the expressions for (u', v', w'), equations A-4, in place of (*u,v,w*) in equations A-3. Thus

$$a'_x = \dot{u}' - rv' + qw'$$

$$a'_y = \dot{v}' - pw' + ru' \qquad \text{(A-6)}$$

$$a_z' = \dot{w}' - qu' + pv'$$

Differentiating equations A-4 with respect to time and noting that since a rigid body is being considered equation A-5 applies, then

$$\dot{u}' = \dot{U} - \dot{r}y + \dot{q}z$$

$$\dot{v}' = \dot{V} - \dot{p}z + \dot{r}x \qquad \text{(A-7)}$$

$$\dot{w}' = \dot{W} - \dot{q}x + \dot{p}y$$

Thus, by substituting equations A-4 and A-7 into equations A-6 the inertial acceleration components of the point p(*x, y z*) in the rigid body are obtained which, after some rearrangement, may be written

$$a'_x = \dot{U} - rV + qW - x(q^2 + r^2) + y(pq - \dot{r}) + z(pr + \dot{q})$$

$$a'_y = \dot{V} - pW + rU + x(pq + \dot{r}) - y(p^2 + r^2) + z(qr - \dot{p}) \qquad \text{(A-8)}$$

$$a'_z = \dot{W} - qU + pV + x(pr - \dot{q}) + y(qr + \dot{p}) - z(p^2 + q^2)$$

A.1.1.2 THE GENERALIZED FORCE EQUATIONS

Consider an incremental mass δm at point p($x, y\, z$) in the rigid body. Applying Newton's second law, equation A-1, to the incremental mass, the incremental components of force acting on the mass are given by ($\delta m a'_x, \delta m a'_y, \delta m a'_z$). Thus the total force components *(X,Y,Z)* acting on the body are given by summing the force increments over the whole body, whence

$$\begin{aligned} \Sigma \delta m a'_x &= X \\ \Sigma \delta m a'_y &= Y \\ \Sigma \delta m a'_z &= Z \end{aligned} \qquad \text{(A-9)}$$

Substituting the expressions for the components of inertial acceleration (a'_x, a'_y, a'_z) from equations A-8 and A-6 into equations A-9 and since the origin of the axes coincide with the *cg*

$$\Sigma \delta m x = \Sigma \delta m y = \Sigma \delta m z = 0 \qquad \text{(A-10)}$$

Therefore, the resultant components of total force acting on the rigid body are given by

$$\begin{aligned} m\left(\dot{U} - rV + qW\right) &= X \\ m\left(\dot{V} - pW + rU\right) &= Y \\ m\left(\dot{W} - qU + pV\right) &= Z \end{aligned} \qquad \text{(A-11)}$$

where m is the total mass of the body.

A.1.1.3 THE GENERALIZED MOMENT EQUATIONS

Consider the moments produced by the forces acting on the incremental mass δm at point p($x, y\, z$) in the rigid body. The incremental force components create an incremental moment component about each of the three body axes. By summing these over the whole body the moment equations are obtained. The moment equations are the realisation of the rotational form of Newton's second law of motion.

For example, the total moment L about the *ox* axis is given by summing the incremental moments over the whole body.

$$\Sigma\delta m\left(ya'_z - za'_z\right) = L \qquad \text{(A-12)}$$

Substituting in equation A-12 for a'_y and a'_z obtained from equations A-8 and noting that equation A-10 applies then, after some rearrangement, equation A-12 may be written

$$\left.\begin{array}{l} \dot{p}\Sigma\delta m\left(y^2+z^2\right)+qr\Sigma\delta m\left(y^2-z^2\right)+ \\ \left(r^2-q^2\right)\Sigma\delta myz-\left(pq+\dot{r}\right)\Sigma\delta mxz+\left(pr-\dot{q}\right)\Sigma\delta mxy \end{array}\right) = L \qquad \text{(A-13)}$$

Terms under the summation sign Σ in equation A-13 have the units of moment of inertia; thus, it is convenient to define the moments and products of inertia as set out in Table A-1.

$I_x = \Sigma\delta m\left(y^2+z^2\right)$	Moment of inertia about *ox* axis
$I_y = \Sigma\delta m\left(x^2+z^2\right)$	Moment of inertia about *oy* axis
$I_z = \Sigma\delta m\left(x^2+y^2\right)$	Moment of inertia about *oz* axis
$I_{xy} = \Sigma\delta mxy$	Product of inertia about the *ox* and *oy* axes
$I_{xz} = \Sigma\delta mxz$	Product of inertia about the *ox* and *oz* axes
$I_{yz} = \Sigma\delta myz$	Product of inertia about the *oy* and *oz* axes

Table A-1 Moments and Products of Inertia

In a similar way the total moments M and N about the *oy* and *oz* axes respectively are given by summing the incremental moment components over the whole body

$$\begin{array}{l} \Sigma\delta m\left(za'_x - xa'_z\right) = M \\ \\ \Sigma\delta m\left(xa'_y - ya'_x\right) = N \end{array} \qquad \text{(A-14)}$$

Substituting a'_x, a'_y and a'_z obtained from equations A-8, in equations A-14, noting that equation A-10 applies and making use of the inertia definitions expressed in Table A-1,

then the total moment L about the *ox* axis , the total moment M about the *oy* axis and the total moment N about the *oz* axis are given by equations A-15. These represent the moment equations of a generalized rigid body and describe the rotational motion about the orthogonal axes through its *cg* since the origin of the axes system is coincident with the cg of the body.

$$I_x\dot{p} - \left(I_y - I_z\right)qr + I_{xy}\left(pr - \dot{q}\right) - I_{xz}\left(pq + \dot{r}\right) + I_{yz}\left(r^2 - q^2\right) = L$$

$$I_y\dot{q} + \left(I_x - I_z\right)pr + I_{yz}\left(pq - \dot{r}\right) + I_{xz}\left(p^2 - r^2\right) - I_{xy}\left(qr + \dot{p}\right) = M \qquad \text{(A-15)}$$

$$I_z\dot{r} + \left(I_x - I_y\right)pq + I_{yz}\left(pr - \dot{q}\right) + I_{xz}\left(qr - \dot{p}\right) - I_{xy}\left(q^2 + p^2\right) = N$$

A.1.1.4 THE GENERALIZED EQUATIONS OF MOTION

Together, equations A-11 and A-15 comprise the generalized six degrees of freedom equations of motion of a rigid symmetric airframe having a uniform mass distribution.

By calculating the disturbing forces and moments, and knowing the initial values of the body axes velocities, U_i, V_i, W_i, and body axes rotational rates, p_i, q_i, r_i, the equations of motion can be solved for the body axes velocities, *U, V, W*, and body axes rotational rates, *p, q, r*.

The disturbing forces *(X,Y,Z)* and moments *(L,M,N)* are due to aerodynamics, thrust and gravity and are defined in Chapter 3.

A.1.2 ROTATION IN SPACE

The Euler angles, ϕ, θ and ψ, which describe the angular orientation of the body axes system relative to the earth axes system are derived from the rotation rates, *p*, *q* and *r*, through the use of Euler parameter quaternions. The Euler parameter equations are well behaved and have no singularities, unlike the method of calculating the Euler angles directly from the rotational rates. The direction cosine matrix relating the earth axes system to the body axes system can also be calculated using the Euler parameters.

The equations implemented in the simulation model are presented in the following sections. The derivation from first principles of the Euler parameters from rotational

rates, and subsequently the Euler angles and direction cosine matrix, is presented by Kuipers[82].

A.1.2.1 EULER PARAMETERS

The rate of change of the Euler parameters, e_0, e_1, e_2, and e_3, with respect to the rotational rates, p, q and r, is presented in equation A-16.

$$\begin{bmatrix} \dot{e}_0 \\ \dot{e}_1 \\ \dot{e}_2 \\ \dot{e}_3 \end{bmatrix} = \frac{1}{2} \begin{bmatrix} 0 & -p & -q & -r \\ p & 0 & r & -q \\ q & -r & 0 & p \\ r & q & -p & 0 \end{bmatrix} \begin{bmatrix} e_0 \\ e_1 \\ e_2 \\ e_3 \end{bmatrix} \tag{A-16}$$

Where the initial values of the Euler parameters e_0, e_1, e_2, and e_3 are calculated from the initial Euler angles ϕ_i, θ_i and ψ_i, as in equations A-17.

$$\begin{aligned} e_0 &= \cos\frac{\psi_i}{2}\cos\frac{\theta_i}{2}\cos\frac{\phi_i}{2} + \sin\frac{\psi_i}{2}\sin\frac{\theta_i}{2}\sin\frac{\phi_i}{2} \\ e_1 &= \cos\frac{\psi_i}{2}\cos\frac{\theta_i}{2}\sin\frac{\phi_i}{2} - \sin\frac{\psi_i}{2}\sin\frac{\theta_i}{2}\cos\frac{\phi_i}{2} \\ e_2 &= \cos\frac{\psi_i}{2}\sin\frac{\theta_i}{2}\cos\frac{\phi_i}{2} + \sin\frac{\psi_i}{2}\cos\frac{\theta_i}{2}\sin\frac{\phi_i}{2} \\ e_3 &= \sin\frac{\psi_i}{2}\cos\frac{\theta_i}{2}\cos\frac{\phi}{2} - \cos\frac{\psi_i}{2}\sin\frac{\theta_i}{2}\sin\frac{\phi_i}{2} \end{aligned} \tag{A-17}$$

A.1.2.2 EULER ANGLES

The Euler Angles, ϕ, θ and ψ, are defined as functions of Euler parameters, e_0, e_1, e_2, and e_3, as in equations A-18.

$$\phi = \tan^{-1}\left(\frac{2\left(e_0 e_1 + e_2 e_3\right)}{e_0^2 - e_1^2 - e_2^2 + e_3^2}\right)$$

$$\theta = \sin^{-1}\left(-2\left(e_1 e_3 - e_0 e_3\right)\right) \qquad \text{(A-18)}$$

$$\psi = \tan^{-1}\left(\frac{2\left(e_0 e_3 + e_1 e_2\right)}{e_0^2 + e_1^2 - e_2^2 - e_3^2}\right)$$

A.1.2.3 DIRECTION COSINE MATRIX

The earth axes from aircraft body axes direction cosine matrix, D_{EB}, is defined as a function of Euler parameters, e_0, e_1, e_2, and e_3, as presented in equation A-19.

$$D_{EB} = \begin{bmatrix} e_0^2 + e_1^2 - e_2^2 - e_3^2 & 2\left(e_1 e_2 - e_0 e_3\right) & 2\left(e_0 e_2 + e_1 e_3\right) \\ 2\left(e_0 e_3 + e_1 e_2\right) & e_0^2 - e_1^2 + e_2^2 - e_3^2 & 2\left(e_2 e_3 - e_0 e_1\right) \\ 2\left(e_1 e_3 - e_0 e_2\right) & 2\left(e_0 e_1 + e_2 e_3\right) & e_0^2 - e_1^2 - e_2^2 + e_3^2 \end{bmatrix} \qquad \text{(A-19)}$$

Having calculated the earth axes from aircraft body axes direction cosine matrix, D_{EB}, the body axes from earth axes direction cosine matrix, D_{BE}, may be calculated as per equation A-20.

$$D_{BE} = D_{EB}^{-1} \qquad \text{(A-20)}$$

A.1.3 AIRCRAFT RELATIVE VELOCITIES

The relative velocity components of the aircraft relative to the airflow are defined as

$$\begin{bmatrix} U_R \\ V_R \\ W_R \end{bmatrix} = \begin{bmatrix} U \\ V \\ W \end{bmatrix} - D_{BE}\begin{bmatrix} U_d \\ V_d \\ W_d \end{bmatrix} - D_{BE}\begin{bmatrix} u_{cE} \\ v_{cE} \\ w_{cE} \end{bmatrix} \qquad \text{(A-21)}$$

where the disturbance velocities, U_d, V_d, W_d, are defined as

$$U_d = u_t + u_g + u_w$$

$$V_d = v_t + v_g + u_w \qquad \text{(A-22)}$$

$$W_d = w_t + w_g + w_{ws}$$

The carrier landing disturbance model velocity components relative to the earth axes system, $u_{c_E}, v_{c_E}, w_{c_E}$, are defined as

$$\begin{bmatrix} u_{c_E} \\ v_{c_E} \\ w_{c_E} \end{bmatrix} = D_{EB_{ac}} \begin{bmatrix} u_c \\ v_c \\ w_c \end{bmatrix} \tag{A-23}$$

Where the earth axes from aircraft carrier body axes direction cosine matrix is defined in terms of the aircraft carriers Euler angles, $\phi_{ac}, \psi_{ac}, \theta_{ac}$, as presented in equation A-24

$$D_{EB_{ac}} = \begin{bmatrix} \cos\psi_{ac}\cos\theta_{ac} & \cos\psi_{ac}\sin\theta_{ac}\sin\phi_{ac} & \cos\psi_{ac}\sin\theta_{ac}\cos\phi_{ac} \\ & -\sin\psi_{ac}\cos\phi_{ac} & +\sin\psi_{ac}\sin\phi_{ac} \\ \sin\psi_{ac}\cos\theta_{ac} & \sin\psi_{ac}\sin\theta_{ac}\sin\phi_{ac} & \sin\psi_{ac}\sin\theta_{ac}\cos\phi_{ac} \\ & +\cos\psi_{ac}\cos\phi_{ac} & -\cos\psi_{ac}\sin\phi_{ac} \\ -\sin\theta_{ac} & \cos\theta_{ac}\sin\phi_{ac} & \cos\theta_{ac}\cos\phi_{ac} \end{bmatrix} \tag{A-24}$$

Atmospheric disturbance velocity components due to turbulence, u_t, v_t, w_t, gusts, u_g, v_g, w_g, wind shear, w_w, and proximity to an aircraft carrier, u_c, v_c, w_c, are defined in Chapter 3.

A.1.4 AIRCRAFT EARTH VELOCITIES

The aircraft's true velocity components relative to the earth axes system are calculated by multiplying the earth from body axes direction cosine matrix by the relative velocity vector.

$$\begin{bmatrix} U_E \\ V_E \\ W_E \end{bmatrix} = D_{EB} \begin{bmatrix} U_R \\ V_R \\ W_R \end{bmatrix} \tag{A-25}$$

A.1.5 AIRCRAFT EARTH POSITION

The aircraft's position relative the earth axes system is calculated by integrating the aircraft's earth axes velocities with respect to time relative to the aircraft's initial position as per equation A-26.

$$\begin{aligned} x_E &= x_{Ei} + \int U_E \\ y_E &= y_{Ei} + \int V_E \\ z_E &= z_{Ei} + \int W_E \end{aligned} \tag{A-26}$$

where $\left(x_{E_i}, y_{E_i}, z_{E_i}\right)$ is the aircrafts initial earth axes position.

A.1.6 AIRCRAFT CARRIER EARTH VELOCITIES

The aircraft carrier's true velocity components relative to the earth axes system are calculated by multiplying the earth from aircraft carrier body axes direction cosine matrix by the aircraft carrier body axis velocity vector.

$$\begin{bmatrix} U_{E_{ac}} \\ V_{E_{ac}} \\ W_{E_{ac}} \end{bmatrix} = D_{EB_{ac}} \begin{bmatrix} U_{ac} \\ V_{ac} \\ W_{ac} \end{bmatrix} \tag{A-27}$$

where the aircraft carrier body axis velocities are defined as

$$\begin{bmatrix} U_{ac} \\ V_{ac} \\ W_{ac} \end{bmatrix} = \begin{bmatrix} U_{ac_{Trim}} \\ V_{ac_{Trim}} \\ W_{ac_{Trim}} \end{bmatrix} + \begin{bmatrix} \dot{x}_{ac_{Pert}} \\ \dot{y}_{ac_{Pert}} \\ \dot{z}_{ac_{Pert}} \end{bmatrix} \tag{A-28}$$

where $U_{ac_{Trim}}$, $V_{ac_{Trim}}$ and $W_{ac_{Trim}}$ are the steady state axial, lateral and normal aircraft carrier velocities and where $U_{ac_{Pert}}$, $V_{ac_{Pert}}$ and $W_{ac_{Pert}}$ are the axial, lateral and normal position perturbations outputted by the carrier dynamics model. Similarly, the body axis velocities of the touchdown point on the carrier's deck is defined as

$$\begin{bmatrix} U_{ac(tdp)} \\ V_{ac(tdp)} \\ W_{ac(tdp)} \end{bmatrix} = \begin{bmatrix} U_{ac_{Trim}} \\ V_{ac_{Trim}} \\ W_{ac_{Trim}} \end{bmatrix} + \begin{bmatrix} \dot{x}_{ac_{Pert(tdp)}} \\ \dot{y}_{ac_{Pert(tdp)}} \\ \dot{z}_{ac_{Pert(tdp)}} \end{bmatrix} \quad \text{(A-29)}$$

where $x_{ac_{Pert(tdp)}}$, $y_{ac_{Pert(tdp)}}$ and $z_{ac_{Pert(tdp)}}$ are the axial, lateral and normal position perturbations of the touchdown point outputted by the carrier dynamics model.

A.1.7 AIRCRAFT CARRIER EARTH POSITION

The aircraft carrier's centre of gravity position relative the earth axes system is calculated by integrating the aircraft carrier's earth axes velocities with respect to time relative to the aircraft carrier's initial position as per equation A-30.

$$\begin{aligned} x_{E_{ac}} &= x_{E_{ac}i} + \int U_{E_{ac}} \\ y_{E_{ac}} &= y_{E_{ac}i} + \int V_{E_{ac}} \\ z_{E_{ac}} &= z_{E_{ac}i} + \int W_{E_{ac}} \end{aligned} \quad \text{(A-30)}$$

where $\left(x_{E_{ac}i}, y_{E_{ac}i}, z_{E_{ac}i}\right)$ is the aircraft carrier's initial earth axes position

Similarly the touchdown position on the aircraft carrier's deck relative to the earth axes system is defined as

$$\begin{aligned} x_{E_{ac(tdp)}} &= x_{E_{ac}i(tdp)} + \int U_{E_{ac(tdp)}} \\ y_{E_{ac(tdp)}} &= y_{E_{ac}i(tdp)} + \int V_{E_{ac(tdp)}} \\ z_{E_{ac(tdp)}} &= z_{E_{ac}i(tdp)} + \int W_{E_{ac(tdp)}} \end{aligned} \quad \text{(A-31)}$$

where $\left(x_{E_i(tdp)}, y_{E_i(tdp)}, z_{E_i(tdp)}\right)$ is the aircraft carrier's initial earth axes position.

A.2 AERODYNAMICS MODEL

A.2.1 SPOILER AERODYNAMICS

Symmetric deflection of flat type spoilers with no porosity has been modelled using methods presented in the appropriate ESDU documents[58,59,60]. A 'spoiler' attached to the upper surface of the wing will cause the flow to separate, literally 'spoiling' the flow, and usually resulting in a loss of lift and increase in drag. The increment in lift coefficient and the increment in drag coefficient due to symmetric deflection of the spoilers are presented in sections A.2.1.1 and A.2.1.2 respectively. Note that asymmetric deflection of spoilers is not considered in this instance.

The necessary spoiler geometry definitions are presented in Figure A-2. The aerodynamic effects due to symmetric spoiler deflection are implemented so as to allow the user to define the spoiler geometry.

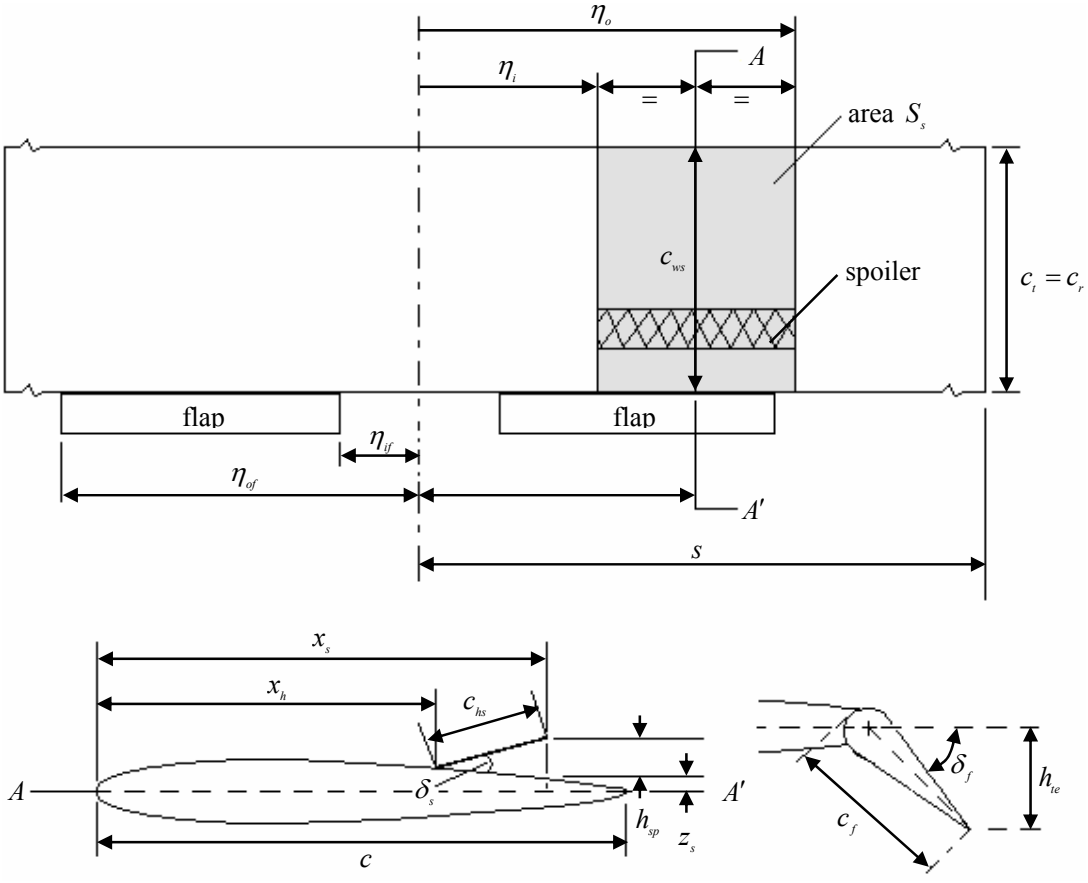

Figure A-2 Spoiler Geometry Definition[58,59,60]

A.2.1.1 SPOILER LIFT COEFFICIENT INCREMENT

The total lift coefficient increment (usually negative, i.e. a decrement) due to symmetric spoiler deflection, C_{L_s}, is defined as[59]

$$C_{L_s} = C_{L_{s\,\delta f=1}} + C_{L_{s\,\delta f>1}} \tag{A-32}$$

where the lift coefficient increment due to symmetric spoiler deflection with trailing edge flaps retracted, $C_{L_{s\,\delta f=1}}$, is defined as[58]

$$C_{L_{s\,\delta f=1}} = \frac{C_{L_{s\,\infty}}}{2\pi} a_{1_{wb}} \left(\Phi_o - \Phi_i\right) \tag{A-33}$$

The two dimensional lift coefficient decrement due to symmetric spoiler deflection, $C_{L_{s\,\infty}}$, is presented in Figures A-4 and A-5 for $\alpha = 0^{\circ}$ and $\alpha = 10^{\circ}$ respectively as a function of spoiler chordwise position, x_s/c, and the parameter H/c, where[58]

$$H = h_{eff} + z_s \tag{A-34}$$

where z_s is the section ordinate at the spoiler position and h_{eff} is an effective spoiler height, which for a flat-type spoiler with no porosity[58] and is defined as

$$h_{eff} = h_{sp} k_s \tag{A-35}$$

where k_s is a function of spoiler deflection angle, δ_s, and is presented in Figure A-3 and the height of the deflected spoiler, h_{sp}, is defined as

$$h_{sp} = c_{hs} \sin \delta_s \tag{A-36}$$

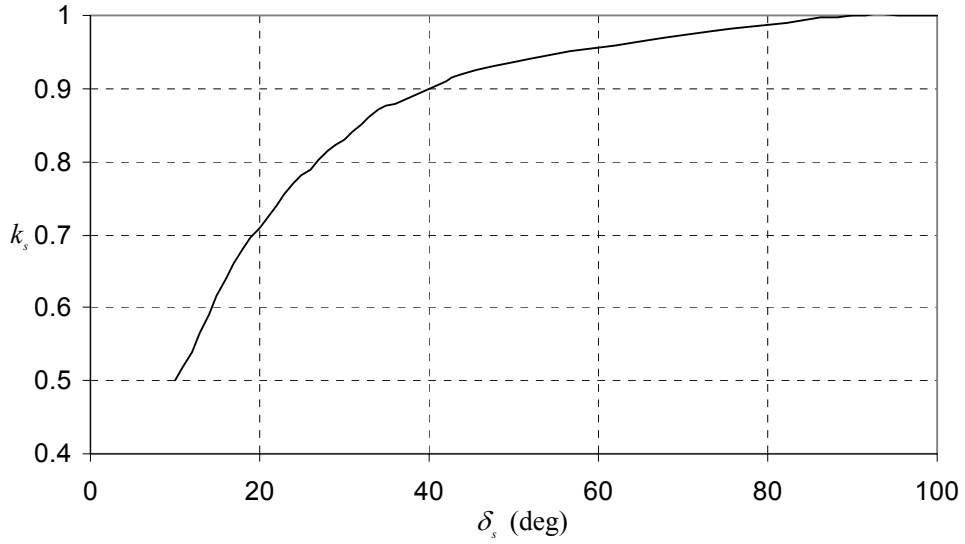

Figure A-3 k_s as a Function of Spoiler Deflection Angle, δ_s [58]

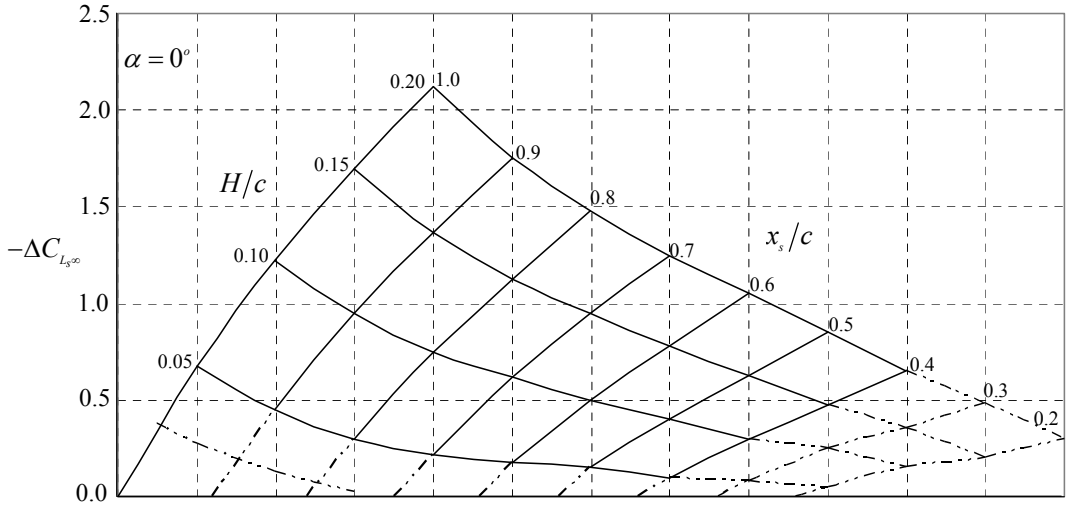

Figure A-4 $-\Delta C_{L_{s\infty}}$ as a Function of x_s/c and H/c for $\alpha = 0^o$ [58]

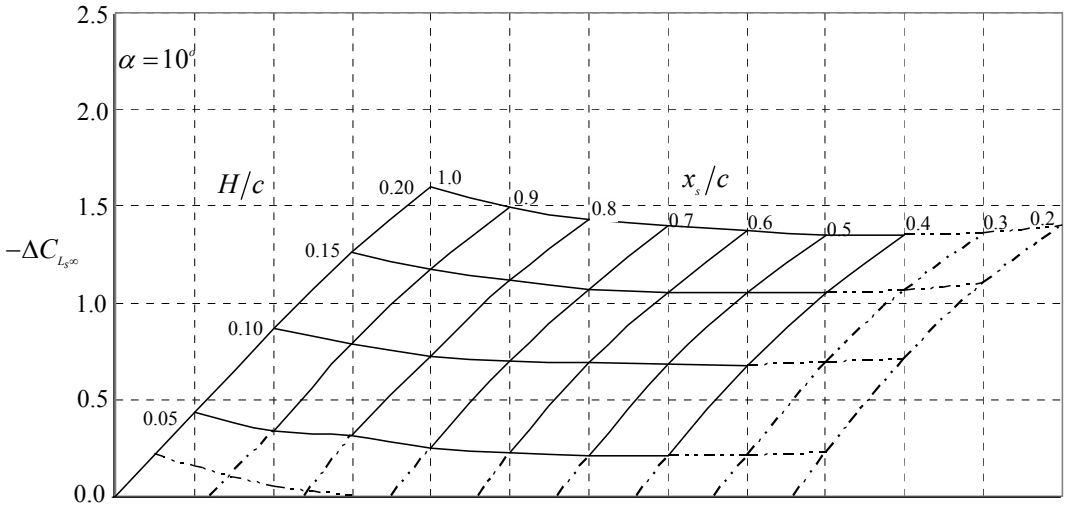

Figure A-5 $-\Delta C_{L_{s\infty}}$ as a Function of x_s/c and H/c for $\alpha = 10^o$ [58]

A linear variation of $C_{L_{s\infty}}$ with angle of attack is assumed. The wing-body combination lift curve slope, $a_{1_{wb}}$, is defined by Fitzgerald in a Cranfield University College of Aeronautics report [67]. The part-span correction factors, Φ_o and Φ_i are functions of η_o and η_i respectively expressed as a percentage of the semi-span, s, and are presented in Figure A-6.

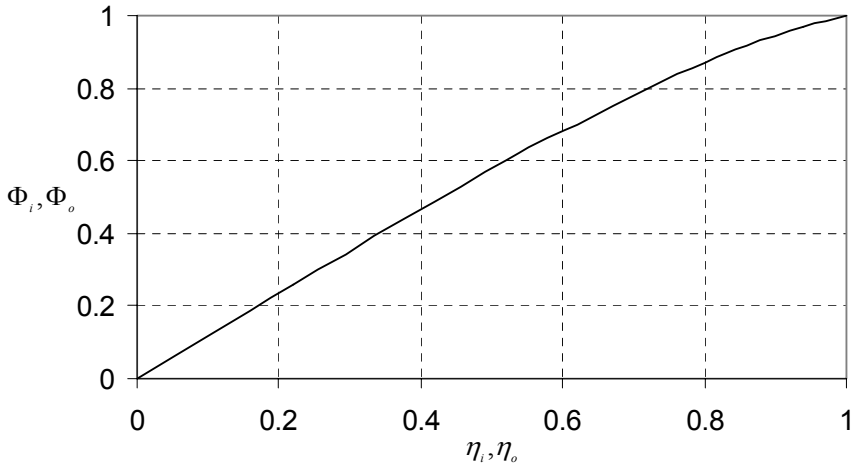

Figure A-6 Part-Span Correction Factor[58]

The lift coefficient increment due to symmetric spoiler deflection with trailing edge flaps deflected, $C_{L_{s\delta f>1}}$, is defined as[59]

$$C_{L_{s\,\delta f>1}} = -\left(k_{s_f}\frac{h_{te}}{c}\right)\left(\frac{1}{2\pi}a_{l_{wb}}\right)\left(\Phi_{oe}-\Phi_{ie}\right) \tag{A-37}$$

where k_{s_f}, presented in Figure A-7, is a function of trailing edge flap deflection, δ_f, and is assumed to vary linearly with angle of attack.

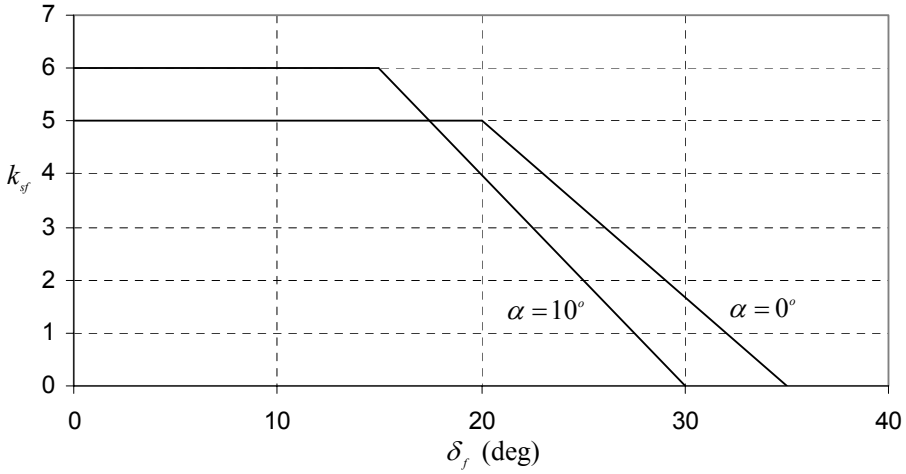

Figure A-7 k_{s_f} as a Function of Trailing Edge Flap Deflection, δ_f [59]

The distance from the trailing edge of the deflected trailing edge flap to the wing chord line, h_{te}, is defined as[59]

$$h_{te} = c_f \sin\delta_f \tag{A-38}$$

where c_f is the trailing edge flap chord length.

The inboard and outboard extremities are η_i and η_o for the spoiler, and η_{if} and η_{of} for the trailing edge flap, expressed as a percentage of the wing semi-span s. The spoiler is assumed to separate the flow over any portion of the trailing edge flap behind the spoiler or within $0.15\bar{c}$ of the ends of the spoiler, thus giving an effective spanwise extent for the separated flow over the trailing edge flap, defined by η_{ie} and η_{oe}.

The effective inboard limit, η_{ie}, is defined as[59]

$$\eta_{ie} = \eta_{if} \text{ when } \eta_{if} \geq \eta_i - \frac{0.3}{A}$$

and (A-39)

$$\eta_{ie} = \eta_i - \frac{0.3}{A} \text{ when } \eta_{if} < \eta_i - \frac{0.3}{A}$$

Similarly, the effective outboard limit, η_{oe}, is defined as[59]

$$\eta_{oe} = \eta_{of} \text{ when } \eta_{of} \leq \eta_o + \frac{0.3}{A}$$

and (A-40)

$$\eta_{oe} = \eta_o + \frac{0.3}{A} \text{ when } \eta_{of} > \eta_o + \frac{0.3}{A}$$

where the aspect ratio, A, is defined as

$$A = \frac{b^2}{S} \tag{A-41}$$

The functions Φ_{ie} and Φ_{oe} are obtained from Figure A-6 for the effective spanwise limits η_{ie} and η_{oe}.

A.2.1.2 SPOILER DRAG COEFFICIENT INCREMENT

The total drag coefficient increment due to symmetric spoiler deflection is defined as[60]

$$C_{D_s} = C_{D_{is}} + C_{D_{os}} \tag{A-42}$$

The increment in induced drag coefficient due to symmetric spoiler deflection, $C_{D_{is}}$, is defined as[60]

$$C_{D_{is}} = \varepsilon_{iw} C_{L_s} + 2k_{s_D}\left(\frac{c}{c_{ws}}\right)\left(\frac{C_{Ls}^2}{\eta_o - \eta_i}\right) \tag{A-43}$$

where the wing downwash in the region of the spoiler, ε_{iw}, is defined as[60

$$\varepsilon_{iw} = 1.2\left(\frac{C_L - \Delta C_{L_f}}{\pi A}\right) + \frac{\Delta C_{L_f}}{\left(\pi A \eta_{of}^2\right)} \tag{A-44}$$

where η_{of} is expressed as a percentage of the semi-span, s. The increment in total lift coefficient due to trailing edge flap deflection, ΔC_{L_f}, is defined as

$$\Delta C_{L_f} = \left(\frac{\Delta C_{L_f\ \delta_{f=20}}}{19} \right) \left(\delta_f - 1 \right) \tag{A-45}$$

where the increment in total lift coefficient due to full trailing edge flap deflection, $\Delta C_{L_f\ \delta_{f=20}}$, was derived using the definition of lift coefficient presented by Fitzgerald in a Cranfield University College of Aeronautics report [67] and is presented in Figure A-8 as a function of dynamic pressure.

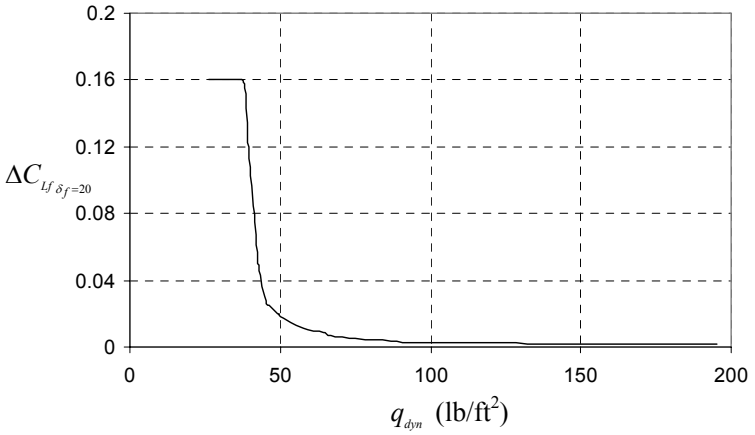

Figure A-8 ΔC_{L_f} as a Function of Dynamic Pressure

The total lift coefficient increment due to symmetric spoiler deflection, C_{L_s}, is as defined by equation A-32. The spoiler induced drag factor, k_{s_D}, presented in Figure A-9 as a function of the aspect ratio of the shaded area of wing in Figure A-2, A_s.

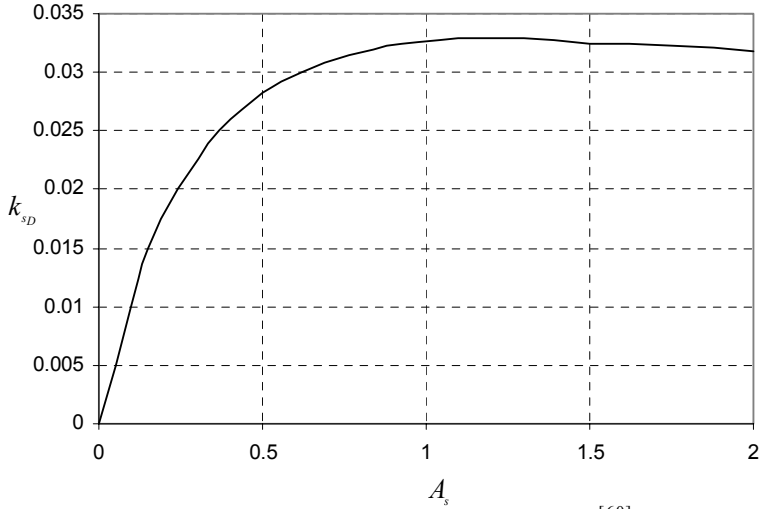

Figure A-9 k_{s_D} as a Function of A_s [60]

where A_s is defined as[60]

$$A_s = \frac{(\eta_o - \eta_i)s}{c_{ws}} \tag{A-46}$$

where η_o and η_i are expressed as a percentage of the wing semi-span, s.

The increment in profile drag coefficient due to symmetric spoiler deflection, $C_{D_{os}}$, in equation A-42 is defined as[60]

$$C_{D_{os}} = \frac{1.2(\sin^2 \delta_s)(\eta_o - \eta_i)sc_{hs}}{S} \tag{A-47}$$

where η_o and η_i are expressed as a percentage of the wing semi-span, s. Spoiler chord length, c_{hs}, as defined in Figure A-2.

A.2.1.3 IMPLEMENTATION

The geometrical definition of the spoiler implemented for the purposes of this study is presented in Table A-2. An assessment in terms the lift and drag increments sensitivity to geometrical variations was conducted before the geometry was fixed. Apart from increasing the area of the spoiler, which intuitively increases its effectiveness, the chordwise position of the spoiler and the relative position of the trailing edge flap had the greatest effect on increasing the spoiler effectiveness. The further aft that the spoiler was position in a chordwise sense increased the lift decrement and drag increment. The greater the overlap between the spoiler and the trailing edge flap had the same effect.

$\eta_o = 4.125\text{ft}$	$\eta_{if} = 1.33\text{ft}$
$\eta_i = 2.125\text{ft}$	$x_h = 2.5\text{ft}$
$s = 76\text{ft}^2$	$c_{hs} = 0.5\text{ft}$
$c_{ws} = c_t = c_r = c = 4\text{ft}$	$z_s = 0.086\text{ft}$
$s = 9.4\text{ft}$	$c_f = 1\text{ft}$
$\eta_{of} = 7.13\text{ft}$	

Table A-2 Spoiler Geometry

The method of calculating the lift and drag increments due to spoiler deflection presented in sections A.2.1.1 and A.2.1.2 is not formulated for implementation in a

simulation environment. As a result, the lift and drag coefficient increments at zero spoiler deflection are non zero. To avoid this situation the effects of the spoiler is faded in linearly from zero over the first two degrees of spoiler deflection. This ensures that when the spoilers are stowed there are no induced aerodynamic effects.

In this instance, the spoiler deflection has been limited to 20 degrees. Over this range, the lift and drag coefficient increments due to spoiler deflection are approximately linear. The lift and drag coefficient increments over this range for the spoiler defined by the geometry in Table A-2 is presented in Figures A-10 and A-11 respectively.

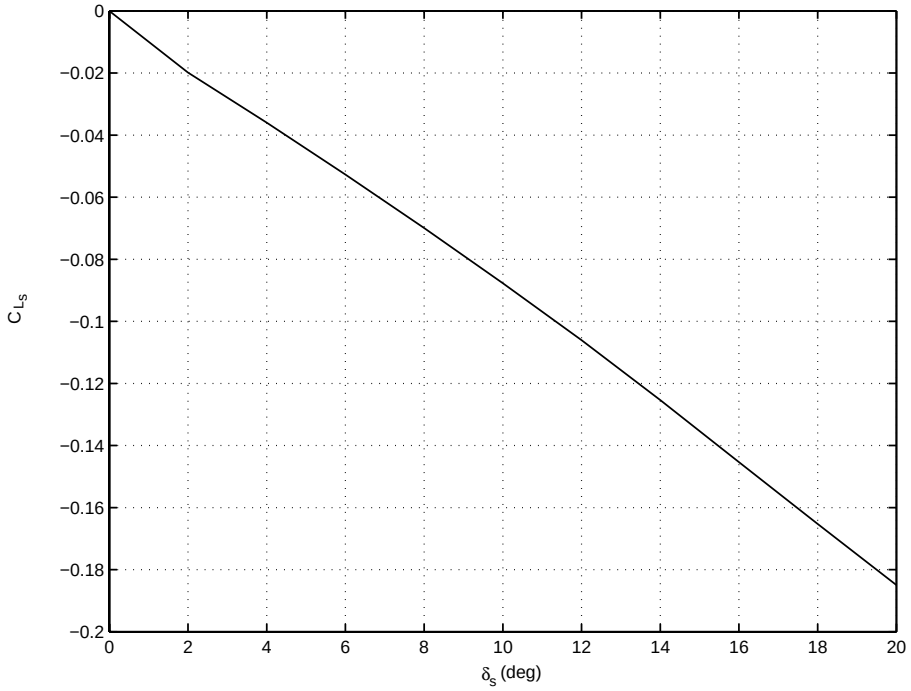

Figure A-10 Lift Coefficient Increment due to Symmetric Spoiler Deflection

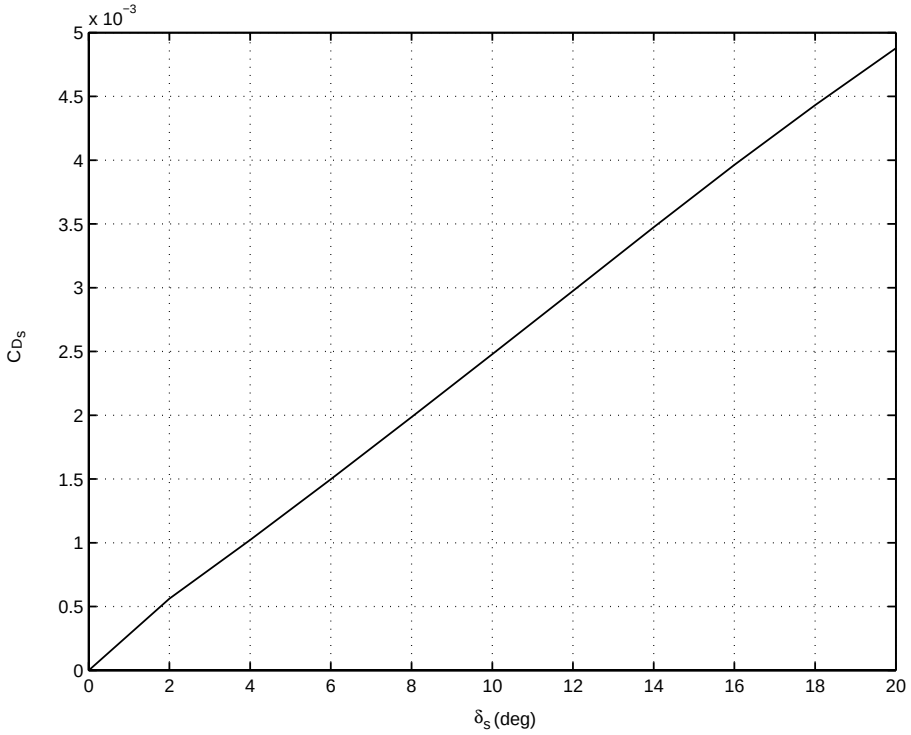

Figure A-11 Drag Coefficient Increment due to Symmetric Spoiler Deflection

A.2.2 UNDERCARRIAGE AERODYNAMICS

The primary aerodynamic effect that the aircraft undercarriage has on the total aircraft aerodynamics is an increment in total drag; all other effects are neglected in this instance. A simple method for the estimation of the increment in aircraft drag due to the extension of undercarriage presented by ESDU has been implemented [61]. The drag coefficient increment due to undercarriage fully extended, $C_{D_{uc}}$, is defined as

$$C_{D_{uc}} = \delta_{\mu}\left(\frac{k_{uc}\left(m_{mto}g\right)^{0.785}}{S}\right) \tag{A-48}$$

where the coefficient, k_{uc}, is defined as a linear interpolation as a function of flap angle between the undercarriage drag coefficient with flaps retracted and that with flaps extended.

$$k_{uc} = k_{uc_{\delta_f=1}} + \left(\frac{k_{uc_{\delta_f=20}} - k_{uc_{\delta_f=1}}}{19}\right)\left(\delta_f - 1\right) \tag{A-49}$$

where $k_{uc_{\delta_{f=1}}} = 3.3\text{x}10^{-3}$ and $k_{uc_{\delta_{f=20}}} = 1.8\text{x}10^{-3}$ [61]. Undercarriage deflection, δ_{μ}, is defined in Chapter 3. The maximum take-off mass of the aircraft, $m_{mto} = 3909.4\,\text{lbs}$, and acceleration due to gravity, $g = 32.17417\,\text{ft/sec}^2$.

A.3 THRUST MODEL

The thrust model presented here has been extracted from Gautrey and Cook [55]. The engine intake pressure, P_{intake}, and intake temperature, T_{intake}, are defined by equations A.3-1 and A.3-2 respectively.

$$P_{intake} = \frac{P}{144}\left(1 + 0.2\text{M}^2\right)^{3.5} \tag{A.3-1}$$

$$T_{intake} = T\left(1 + 0.2\text{M}^2\right) \tag{A.3-2}$$

Atmospheric pressure, P, and temperature, T, are defined in section 3.4.1. Engine mass flow, $\dot{m}$, is defined as

$$\dot{m} = k_m k_h \frac{P_{intake}}{\sqrt{T_{intake}}} \tag{A.3-3}$$

where the altitude correction factor, k_h, is defined as a function of engine intake pressure, P_{intake}. The mass flow coefficient is defined, $k_{\dot{m}}$, is defined as a function of engine speed and intake temperature.

Engine intake drag is defined as

$$D_{\text{int}} = \frac{\dot{m} V_T}{g} \tag{A.3-4}$$

Pressure ratio, P_{ratio}, is defined as

$$P_{ratio} = \left(1 + 0.2\text{M}^2\right)^{3.5} \tag{A.3-5}$$

Equivalent non dimensional engine speed corrected for temperature, N_{nd}, is defined as

$$N_{nd} = \left(\frac{N1}{N1_{\max}} \right) \sqrt{\frac{288.2}{T_{intake}}} \qquad \text{(A.3-6)}$$

$N1$ is engine speed and $N1_{\max}$ is the maximum engine speed.

Engine pressure recovery, P_{rec}, is defined as a function of Mach number and engine pressure recovery factor $k_{P_{rec}}$.

Intake pressure ratio, $P_{int\,ratio}$, is defined as

$$P_{int\,ratio} = \frac{1}{\left(P_{rec} P_{ratio} \right)} \qquad \text{(A.3-7)}$$

Non dimensional gross thrust, $T_{G_{nd}}$, is a function of intake pressure ratio, $P_{int\,ratio}$, and non dimensional engine speed, N_{nd}.

Gross thrust, T_G, is defined as

$$T_G = k_{T_G} P \frac{\left(\frac{T_{G_{nd}}}{P_{\text{int}\,ratio}} - 1 \right)}{144} \qquad \text{(A.3-8)}$$

where k_{T_G} is the gross thrust factor.

Thrust, T_τ, is defined as

$$T_\tau = T_G - D_{\text{int}} \qquad \text{(A.3-9)}$$

A.4 AIRCRAFT INERTIA PROPERTIES

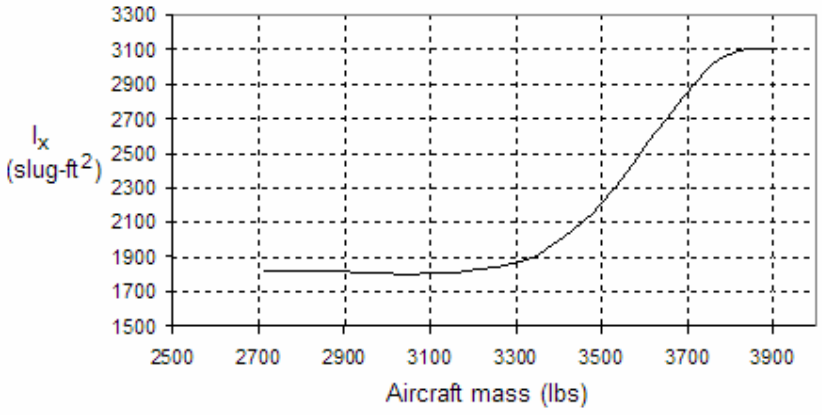

Figure A-12 I_x as a Function of Aircraft Mass [55]

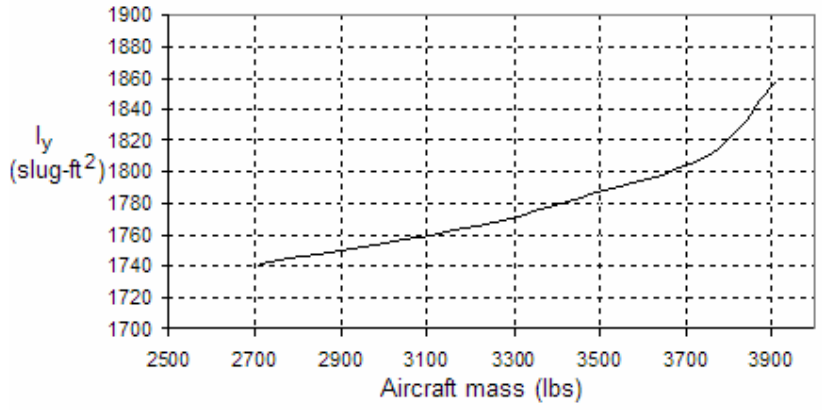

Figure A-13 I_y as a Function of Aircraft Mass [55]

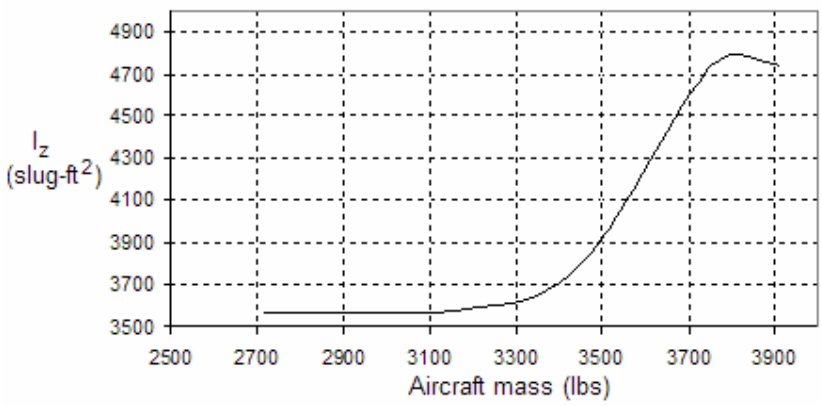

Figure A-14 I_z as a Function of Aircraft Mass [55]

A.5 FLIGHT CONTROL SYSTEM

A.5.1 SENSORS

A.5.1.1 ANGLE OF ATTACK PROBE

The probe quantity is calculated first by passing the angle of attack at the centre of gravity through a filter whose transfer function is presented in equation A-50 [71] which represents the probe dynamics. The probe dynamics are assumed constant through the operational envelope.

$$\frac{\alpha_{localprobe}(s)}{\alpha(s)} = \frac{1}{0.073s+1} \tag{A-50}$$

The local probe angle of attack is then adjusted as a function of airspeed and pitch rate to correct for the pitch rate induced upwash. Equation A-51 [71] defines the sensed angle of attack, α_s.

$$\alpha_s = \left(\alpha_{loacl\ probe} - \frac{l_p q}{V_T} \right) \tag{A-51}$$

Where the distance from the centre of gravity to the angle of attack probe, l_p, is defined as

$$l_p = 12.85 + h_{cg}\bar{c}\,(\text{ft}) \tag{A-52}$$

It should be noted that the angle of attack probe is assumed to be located at the tip of the boom extending from the nose of the aircraft.

The sensor output is limited in the range of +1 to -0.25 radians.

A.5.1.2 SIDESLIP VANE

The sideslip vane is modelled as a simple filter which represents the vane dynamics. This filter, the transfer function of which is presented in equation A-53, is based on that of the angle of attack probe presented in section A.5.1.1. Factors such as offset from the centre of gravity and local aerodynamic influences are not modelled. The output of the sideslip vane filter is limited to ±30 degrees.

$$\frac{\beta_s(s)}{\beta(s)} = \frac{1}{0.073s + 1} \tag{A-53}$$

It should be noted that the sideslip vane is assumed to be located at the tip of the boom extending from the nose of the aircraft. At this location it is assumed that the vane is not effected by the aerodynamic effects of the fuselage.

A.5.1.3 ACCELEROMETER

The inertial acceleration components of a point p(*x, y z*) in a rigid body can be calculated using equation A-8. In this case the point p(*x, y z*) is the location of the accelerometers on the aircraft relative to the centre of gravity. The accelerations are passed through a filter, the transfer function of which is presented in equation A-54 [71], which represents the accelerometer dynamics. The outputs of the accelerometer are limited to ±4g for lateral and axial accelerations and ±10g for normal accelerations.

$$\frac{a_{x_s}(s)}{a_x(s)} = \frac{a_{y_s}(s)}{a_y(s)} = \frac{a_{z_s}(s)}{a_z(s)} = \frac{34.557^2}{s^2 + 2(0.707)(34.557)s + 34.557^2} \tag{A-54}$$

In this case the accelerometer is located on the centreline of the aircraft, 7.43 feet forward of the leading edge of the wing and 1 foot below the body axes *x* axis.

A.5.1.4 RATE GYROS

Equations A-55 [71] and A-56 [71] represent the second order transfer functions of the filters applied to the body axes angular rates in units of degrees per second. The output of the roll rate filter is limited to ± 300 degrees per second while the output of the pitch rate and yaw rate filters are limited to ± 100 degrees per second

$$\frac{p_s(s)}{p(s)} = \frac{90^2}{s^2 + 2(0.8)(90)s + 90^2} \tag{A-55}$$

$$\frac{q_s(s)}{q(s)} = \frac{r_s(s)}{r(s)} = \frac{200^2}{s^2 + 2(0.89)(200)s + 200^2} \tag{A-56}$$

A.5.1.5 ATTITUDE GYROS

The attitude gyro is modelled as a simple first order filter the transfer function of which is presented in equation A-57. The output of the attitude gyros are limited to ±90° for pitch attitude, ±180° for roll and yaw attitudes.

$$\frac{\phi_s(s)}{\phi(s)} = \frac{\theta_s(s)}{\theta(s)} = \frac{\psi_s(s)}{\psi(s)} = \frac{1}{0.025s+1} \tag{A-57}$$

A.5.1.6 STATIC AND DYNAMIC PRESSURE

The static and dynamic pressure sensors are modelled as simple first order filter the transfer function of which is presented in equation A-58.

$$\frac{P_s(s)}{P(s)} = \frac{q_{dyn_s}(s)}{q_{dyn}(s)} = \frac{1}{0.025s+1} \tag{A-58}$$

A.5.1.7 MACH NUMBER

The Machmeter is modelled as a simple first order filter the transfer function of which is presented in equation A-59. The output of the Machmeter is not limited.

$$\frac{\mathrm{M}_s(s)}{\mathrm{M}(s)} = \frac{1}{0.025s+1} \tag{A-59}$$

A.5.1.8 ALTITUDE

The altimeter is modelled as a simple first order filter; the transfer function of which is presented in equation A-60. The output of the altimeter is not limited.

$$\frac{h_s(s)}{h(s)} = \frac{1}{0.025s+1} \tag{A-60}$$

where height, h, is defined as

$$h = -z_E \tag{A-61}$$

A.5.1.9 VELOCITY

As a result of both the static and dynamic pressure sensors having the first order characteristics presented in equation A-58 it follows that the velocity will have at best

the same characteristics. Hence equation A-62 represents the velocity channel characteristics of the air data computer. The output of the speedometer is not limited.

$$\frac{V_{T_S}(s)}{V_T(s)} = \frac{1}{0.03s+1} \tag{A-62}$$

A.5.2 ACTUATORS

A.5.2.1 ELEVATOR

The elevator actuator dynamics are represented by the transfer function presented as equation A-63 [71] . The elevator rate limit is defined as ± 40 deg/sec and the associated position limit is defined as ±45 degrees.

$$\frac{\delta_\eta(s)}{\eta_{actd}(s)} = \frac{30.74^2}{s^2+2(0.509)(30.74)s+30.74^2} \tag{A-63}$$

A.5.2.2 AILERON

The aileron actuator dynamics are represented by the transfer function presented as equation A-64 [71]. The aileron rate limit is defined as ±100 deg/sec and the associated position limit is defined as ±40 degrees.

$$\frac{\delta_\xi(s)}{\xi_{actd}(s)} = \frac{75^2}{s^2+2(0.59)(75)s+75^2} \tag{A-64}$$

A.5.2.3 RUDDER

The rudder actuator dynamics are represented by the transfer function presented as equation A-65 [71]. The rudder rate limit is defined as ±82 deg/sec and the associated position limit is defined as ±45 degrees.

$$\frac{\delta_\varsigma(s)}{\varsigma_{actd}(s)} = \frac{72.1^2}{s^2+2(0.69)(72.1)s+72.1^2} \tag{A-65}$$

A.5.2.4 TRAILING EDGE FLAP

The trailing edge flap actuator dynamics are represented by the transfer function presented as equation A-66 [71]. The trailing edge flap rate limit is defined as ±18 deg/sec and the associated position limit is defined as +1 degree to +35 degrees.

$$\frac{\delta_f(s)}{f_{actd}(s)} = \frac{35^2}{s^2 + 2(0.71)(35)s + 35^2} \tag{A-66}$$

A.5.2.5 SPOILER

The spoiler actuator dynamics are represented by the transfer function presented as equation A-67. In this case the spoiler actuator dynamics are the same as the aileron actuator dynamics. The spoiler rate limit is defined as ±100 deg/sec and the associated position limit is defined as +20 degrees.

$$\frac{\delta_s(s)}{s_{actd}(s)} = \frac{75^2}{s^2 + 2(0.59)(75)s + 75^2} \tag{A-67}$$

A.5.2.6 THRUST VECTORING PADDLES

Both the longitudinal and lateral thrust vectoring paddle actuators have the same dynamic properties as the elevator actuator; these dynamics are represented by the transfer function presented as equation A-68. The thrust vectoring paddles rate limit is defined as ±100 deg/sec and the associated position limit is defined as ±45 degrees.

$$\frac{\delta_{\theta_\tau}(s)}{\theta_{\tau actd}(s)} = \frac{\delta_{\phi_\tau}(s)}{\phi_{\tau actd}(s)} = \frac{30.74^2}{s^2 + 2(0.509)(30.74)s + 30.74^2} \tag{A-68}$$

A.5.2.7 UNDERCARRIAGE

The undercarriage actuator is modelled as a first order lag as represented by the transfer function presented as equation A-69. The position limits are 0 to +1, where 0 represents the undercarriage in the retracted position and +1 represents the undercarriage in the fully extended position. The undercarriage actuator dynamics dictate an extension time, or retraction time, of approximately 5.5 seconds.

$$\frac{\delta_\mu(s)}{\mu_{actd}(s)} = \frac{1}{0.75s + 1} \tag{A-69}$$

A.5.3 AUTOPILOTS

A.5.3.1 ALTITUDE ACQUIRE AND HOLD

The altitude acquire and hold autopilot architecture is presented in Figure A-15 and the associated control law is defined by equation A-70[56].

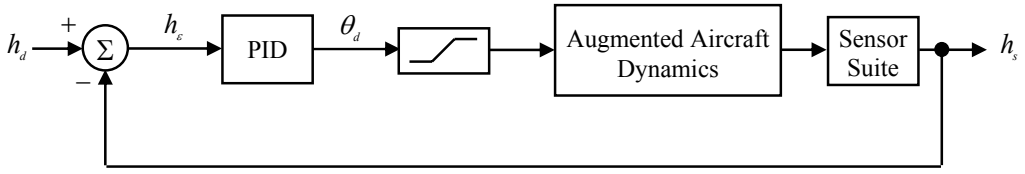

Figure A-15 Altitude Acquire and Hold Autopilot [56]

$$\theta_d = k_{hp} h_\varepsilon + k_{hi} \int h_\varepsilon + k_{hd} \frac{dh_\varepsilon}{dt} \tag{A-70}$$

The control system gains k_{hp}, k_{hi} and k_{hD} are selected as [56]

$$k_{hp} = 0.006 \text{ rad/ft}$$

$$k_{hi} = 0.000005 \text{ rad/ft} \tag{A-71}$$

$$k_{hd} = 0.0065 \text{ rad/ft}$$

The pitch attitude demand, θ_d, is nominally limited to +15 degrees and -10 degrees [56].

A.5.3.2 AUTOTHROTTLE

The autothrottle architecture is presented in Figure A-16 and the associated control law is defined by equation A-72[56].

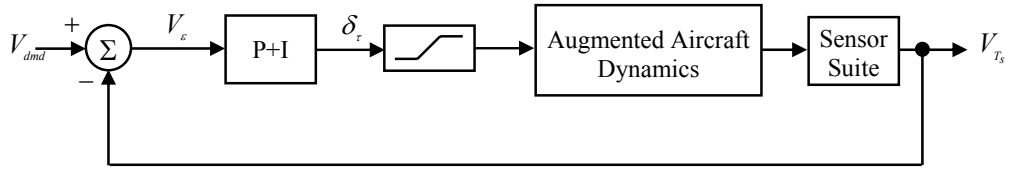

Figure A-16 Autothrottle[56]

$$\delta_\tau(s) = k_{Vp} V_\varepsilon + k_{Vi} \int V_\varepsilon \tag{A-72}$$

The control system gains, k_{vp} and k_{vi}, are selected as[56]

$$k_{vp} = 500 \text{ RPM/ft/sec}$$

$$k_{vi} = 5 \text{ RPM/ft/sec} \qquad \text{(A-73)}$$

A.5.3.3 HEADING ACQUIRE AND HOLD

The heading acquire and hold autopilot architecture is presented in Figure A-17 and the associated control law is defined by equation A-74 [56].

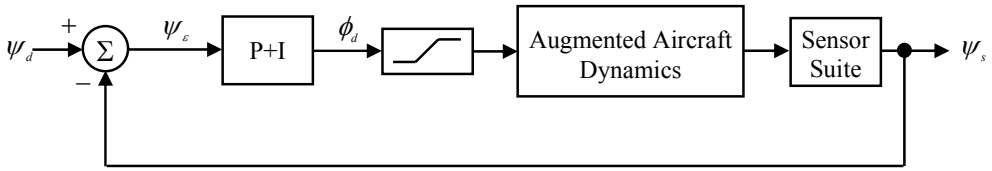

Figure A-17 Heading Acquire and Hold Autopilot[56]

$$\phi_d(s) = k_{\psi p}\psi_\varepsilon + k_{\psi i}\int \psi_\varepsilon \qquad \text{(A-74)}$$

The proportional control system gain, $k_{\psi p}$, is scheduled with airspeed while the integral control system gain, $k_{\psi i}$, has a single value. These are selected as[56]

$$\begin{aligned} k_{\psi p} &= 0.4 \text{ rad/rad} && \text{if } 0 < u \le 230 \text{ (ft/sec)} \\ k_{\psi p} &= 0.4 + \left(\frac{2.2-0.4}{720}\right)(u-230) \text{ rad/rad} && \text{if } 230 < u < 950 \text{ (ft/sec)} \\ k_{\psi p} &= 2.2 \text{ rad/rad} && \text{if } u \ge 950 \text{ (ft/sec)} \end{aligned} \qquad \text{(A-75)}$$

$$k_{\psi i} = 0.00005 \text{ rad/rad}$$

The roll attitude demand, ϕ_d, is nominally limited to ±45 degrees[56].

A.6 ATMOSPHERIC DISTURBANCE

The atmospheric disturbance model implemented in the simulation model is that presented in MIL-F-8785-C[63]. All data presented are from this source unless otherwise stated. It consists of a definition of a turbulence model, a gust model, a low level wind shear model and a carrier landing disturbance model. All disturbance velocity components are aligned with the earth axes system.

A.6.1 MEDIUM-HIGH ALTITUDE DISTURBANCE MODEL

The scales and intensities are based on the assumption that turbulence above 2,000 feet is isotropic, then

$$\sigma_u = \sigma_v = \sigma_w$$
$$L_u = L_v = L_w \tag{A-76}$$

A.6.1.1 TURBULENCE

The turbulence scale lengths when using the Dryden turbulence model are

$$L_u = L_v = L_w = 1,750\,\text{ft} \tag{A-77}$$

Root-mean-square turbulence intensities are presented in Figure A-18 as functions of altitude and probability of exceedance, χ,

A.6.1.2 GUSTS

Gust lengths, d_x, d_y, d_z, are user defined. It is usual to choose values of gust lengths so that the gust is tuned to the natural frequencies of the aircraft and its flight control system.

Gust magnitudes u_g, v_g, w_g are determined from Figure A-19 using values of d_x, d_y, d_z defined by the user, and the appropriate RMS turbulence intensities from Figure A-18.

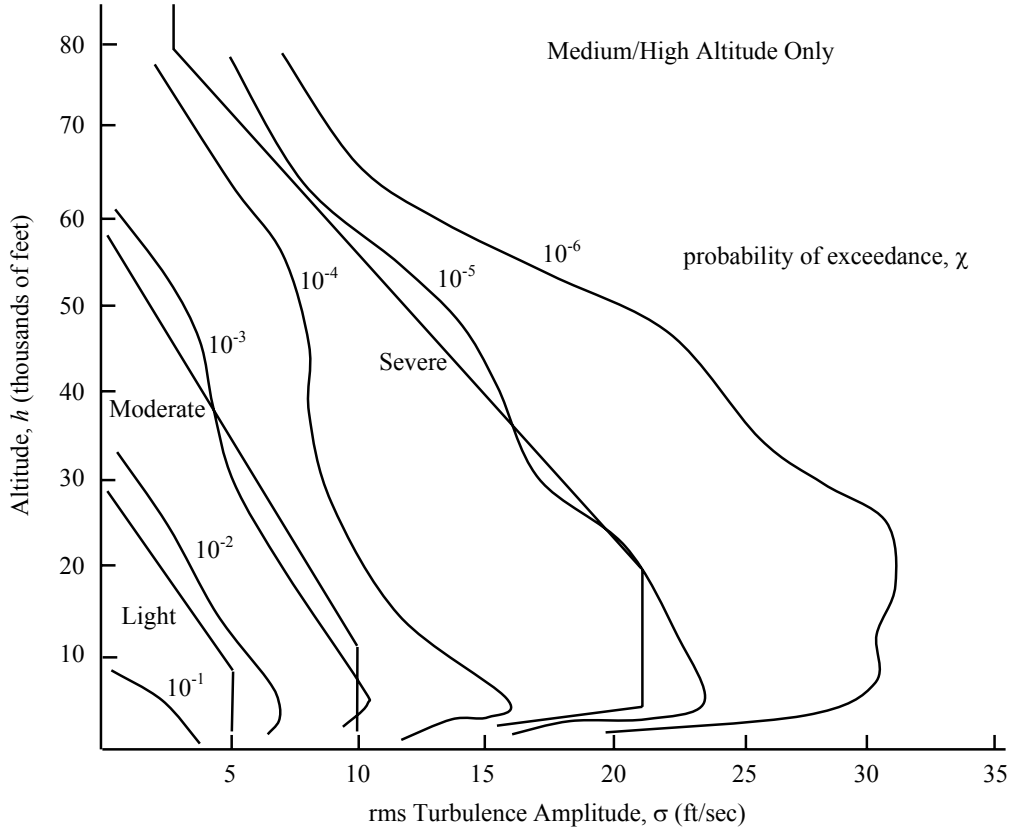

Figure A-18 Turbulence Exceedance Probability[63]

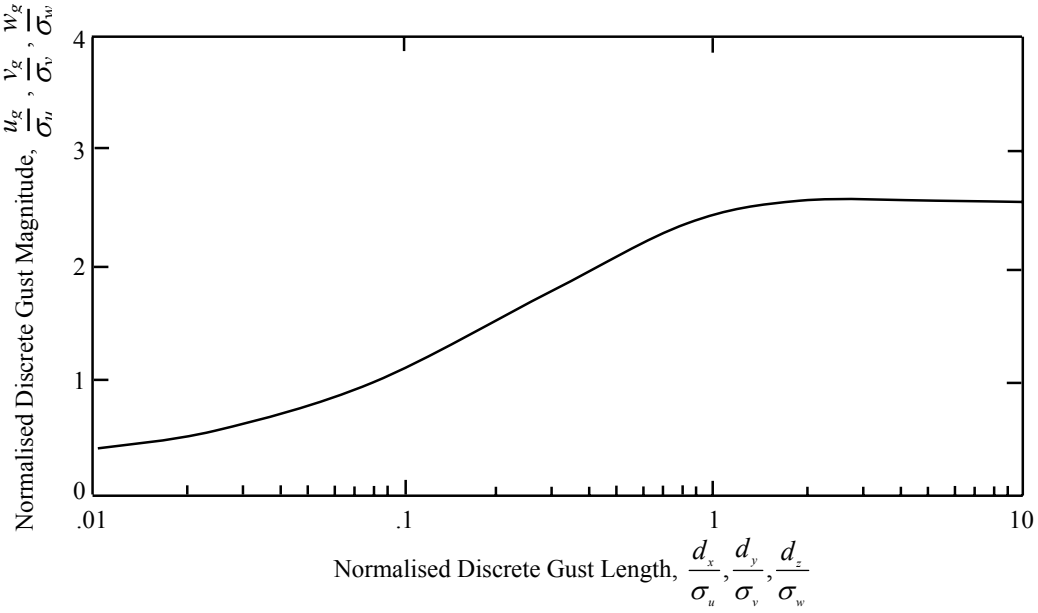

Figure A-19 Magnitude of Discrete Gusts[63]

A.6.2 LOW ALTITUDE DISTURBANCE MODEL

A.6.2.1 WIND SHEAR

The wind speed at 20 feet above the ground, u_{20}, is shown in Figure A-20 as a function of probability of occurrence, χ. The values to be used for the different intensities of atmospheric disturbance are indicated.

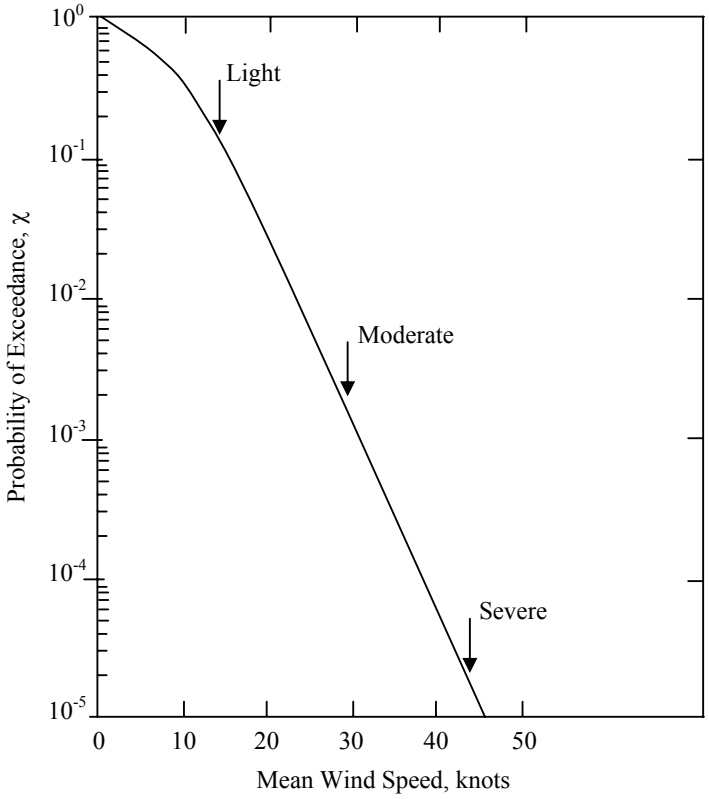

Figure A-20 Wind Speed at 20 Feet Above the Ground[63]

A.6.2.2 TURBULENCE

The appropriate scale lengths are presented in Figure A-21 as functions of altitude. The turbulence intensities to be used σ_u and σ_v are presented in Figure A-22 as functions of σ_w and altitude, h, where σ_w is defined as

$$\sigma_w = 0.1 u_{20} \tag{A-78}$$

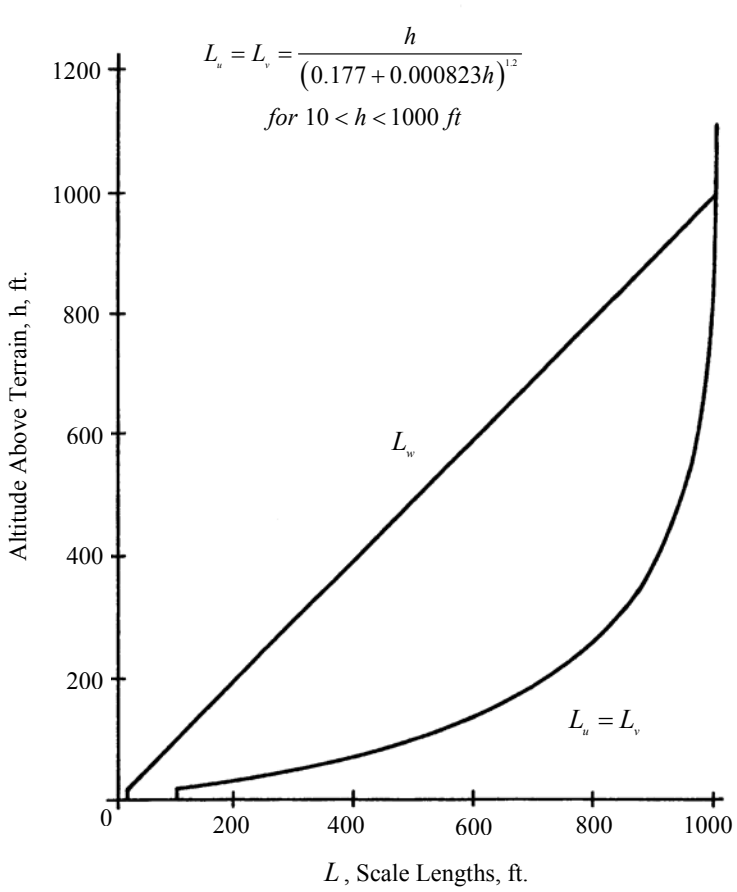

Figure A-21 Low Altitude Turbulence Integral Scales[63]

A.6.2.3 GUSTS

Gust lengths, d_x, d_y and d_z are user defined. It is usual to choose values of gust lengths so that the gust is tuned to the natural frequencies of the aircraft and its flight control system.

Gust magnitudes u_g, v_g, w_g are determined from Figure A-19 using values of d_x, d_y and d_z defined by the user and the appropriate values from Figures A-21 and A-22.

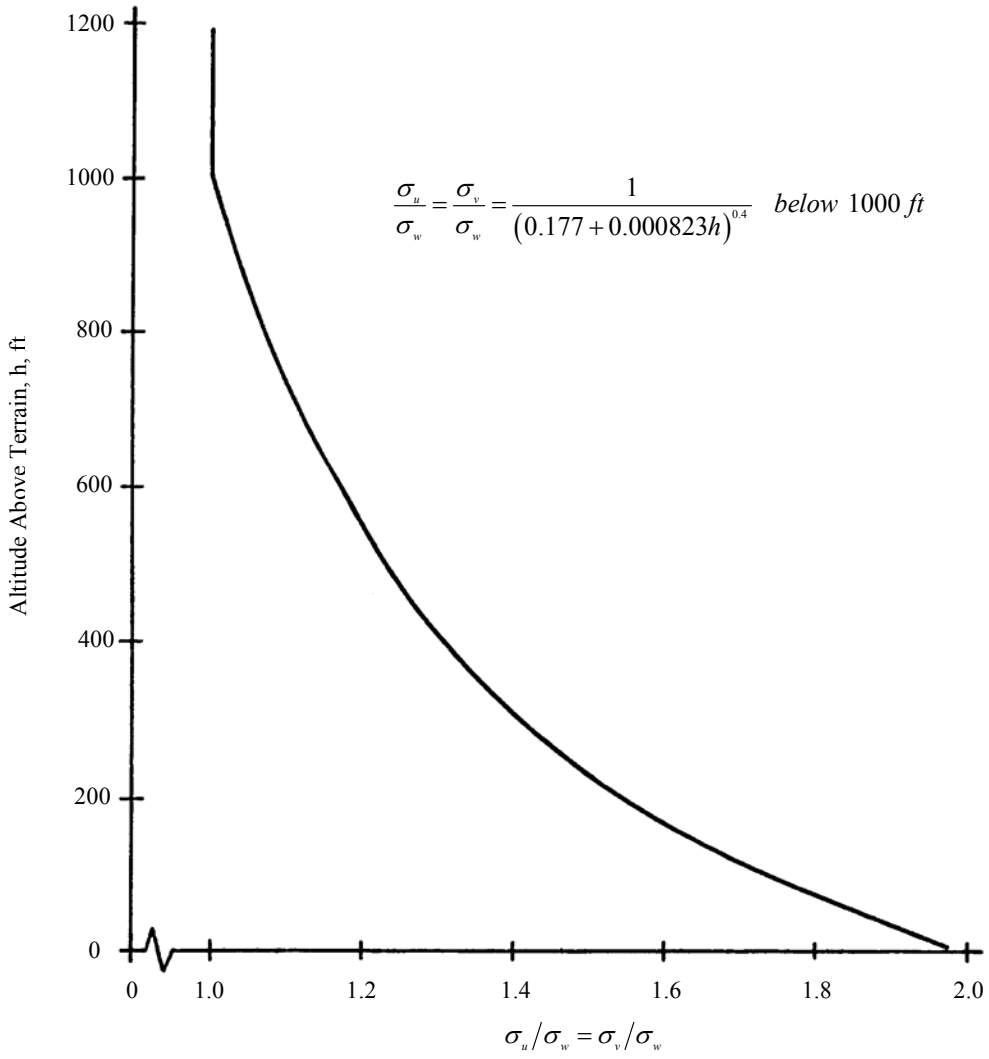

Figure A-22 Horizontal Turbulence RMS Intensities[63]

APPENDIX B APPROACH CONTROLLER STATISTICAL COMPARATIVE ANALYSIS DATA

B.1 INTRODUCTION

The data in the following Tables forms the basis for the discussion presented in section 7.5. Five approaches were simulated for each aircraft carrier motion case. Aircraft carrier motion is defined by aircraft carrier speed and wind speed. For each set of five approaches the performance metrics presented in section 7.2 were calculated. The mean and standard deviation of these metrics per aircraft carrier motion case are tabulated in Tables B-1 to B-32. The Tables are arranged in order of atmospheric disturbance case as presented in Table 7-5. The notation used in Tables B-1 to B-32 is defined in Table B-0.

# Successful Approach	The number of successful approaches
$\overline{h}_\varepsilon$ rms, σh_ε rms (ft)	Mean and standard deviation of approach glide path vertical deviation RMS of successful approaches
$\overline{\lambda}_\varepsilon$ rms, $\sigma\lambda_\varepsilon$ rms (ft)	Mean and standard deviation of approach track lateral deviation RMS of successful approaches
$\overline{u}_\varepsilon$ rms, σu_ε rms (kts)	Mean and standard deviation of approach speed deviation RMS of successful approaches
# Failed Approaches Vert	The number of approaches which were classified as a wave-off due to breaching the approach glide path vertical deviation limits
$\overline{t}_{td}$, σt_{td} (sec)	Mean and Standard deviation of Time to Touchdown at which the failed approaches breached the approach glide path vertical deviation limits
$\overline{h}_\varepsilon$ rms, σh_ε rms (ft)	Mean and standard deviation of approach glide path vertical deviation RMS of failed approaches up to the time of failure
$\overline{\lambda}_\varepsilon$ rms, $\sigma\lambda_\varepsilon$ rms (ft)	Mean and standard deviation of approach track lateral deviation RMS of failed approaches up to the time of failure
$\overline{u}_\varepsilon$ rms, σu_ε rms (kts)	Mean and standard deviation of approach speed deviation RMS of failed approaches up to the time of failure
# Failed Approaches Lat	The number of approaches which were classified as a wave-off due to breaching the approach track lateral deviation limits
$\overline{t}_{td}$, σt_{td} (sec)	Mean and Standard deviation of Time to Touchdown at which the failed approaches breached the approach glide path vertical deviation limits
$\overline{h}_\varepsilon$ rms, σh_ε rms (ft)	Mean and standard deviation of approach glide path vertical deviation RMS of failed approaches up to the time of failure
$\overline{\lambda}_\varepsilon$ rms, $\sigma\lambda_\varepsilon$ rms (ft)	Mean and standard deviation of approach track lateral deviation RMS of failed approaches up to the time of failure
$\overline{u}_\varepsilon$ rms, σu_ε rms (kts)	Mean and standard deviation of approach speed deviation RMS of failed approaches up to the time of failure
# Ramp Strikes	The number of Ramp Strikes
$\overline{h}_r$, σh_r (ft)	Mean and standard deviation of approach glide path vertical deviation at ramp crossing for successful approaches
$\overline{h}_{cr}$, σh_{cr} (ft)	Mean and standard deviation of ramp height at crossing for successful approaches
$\overline{\theta}_{cr}$, $\sigma\theta_{cr}$ (deg)	Mean and standard deviation of aircraft carrier pitch attitude at ramp crossing for successful approaches
# Bolters	The number of Bolters that occurred for successful approaches
$\overline{X}_d$, σX_d (ft)	Mean and standard deviation of longitudinal touchdown position for Bolters
$\overline{Y}_d$, σY_d (ft)	Mean and standard deviation of lateral touchdown position for Bolters
# Successful Touchdowns	The number of successful touchdown
$\overline{X}_d$, σX_d (ft)	Mean and standard deviation of longitudinal touchdown position for successful touchdowns
$\overline{Y}_d$, σY_d (ft)	Mean and standard deviation of lateral touchdown position for successful touchdowns
$\overline{\dot{h}}$, $\sigma\dot{h}$ (ft)	Mean and standard deviation of aircraft sink rate at touchdown for successful touchdowns
$\overline{\dot{h}}_C$, $\sigma\dot{h}_C$ (ft)	Mean and standard deviation of aircraft carrier height rate at touchdown for successful touchdowns

Table B-0 Appendix B Table Notation

		Wind Speed = 2 Knots No Turbulence					
		System 1		System 2		System 3	
Carrier Speed = 0 Knots	# Successful Approaches	5		5		5	
	$\bar{h}_e$ rms, σh_e rms (ft)	0.028409	9.39E-06	0.008057	1.30E-05	0.004522	4.06E-06
	$\bar{\lambda}_e$ rms, $\sigma\lambda_e$ rms (ft)	0	0	0	0	0	0
	$\bar{u}_e$ rms, σu_e rms (kts)	0.008707	0.00015	0.005211	0.000315	0.00113	8.81E-05
	# Failed Approaches Vert	0		0		0	
	$\bar{t}_{td}$, σt_{td} (sec)	-	-	-	-	-	-
	$\bar{h}_e$ rms, σh_e rms (ft)	-	-	-	-	-	-
	$\bar{\lambda}_e$ rms, $\sigma\lambda_e$ rms (ft)	-	-	-	-	-	-
	$\bar{u}_e$ rms, σu_e rms (kts)	-	-	-	-	-	-
	# Failed Approaches Lat	0		0		0	
	$\bar{t}_{td}$, σt_{td} (sec)	-	-	-	-	-	-
	$\bar{h}_e$ rms, σh_e rms (ft)	-	-	-	-	-	-
	$\bar{\lambda}_e$ rms, $\sigma\lambda_e$ rms (ft)	-	-	-	-	-	-
	$\bar{u}_e$ rms, σu_e rms (kts)	-	-	-	-	-	-
	# Ramp Strikes	0		0		0	
	$\bar{h}_t$, σh_t (ft)	8.4066	0.035197	8.3746	0.029444	8.368	0.029453
	$\bar{h}_{ac}$, σh_{ac} (ft)	0.045307	1.14E-05	0.014049	1.07E-05	0.007531	3.25E-06
	$\bar{\theta}_{ac}$, $\sigma\theta_{ac}$ (deg)	-0.00859	0.012605	-0.00886	0.010547	-0.00886	0.010547
	# Bolters	0		0		0	
	$\bar{X}_{td}$, σX_{td} (ft)	-	-	-	-	-	-
	$\bar{Y}_{td}$, σY_{td} (ft)	-	-	-	-	-	-
	# Successful Touchdowns	5		5		5	
	$\bar{X}_{td}$, σX_{td} (ft)	0.75763	0.14353	0.27021	0.009746	0.14297	0.041253
	$\bar{Y}_{td}$, σY_{td} (ft)	-0.00709	0.0058	-0.00029	0.000325	-0.0017	0.000328
	$\bar{h}_t$, σh_t (ft)	-12.1921	4.47E-05	-12.1911	5.48E-05	-12.1906	0
	h_t, σh_t (ft)	-0.013092	0.082476	-0.027981	0.046889	-0.02645	0.043779
Carrier Speed = 10Knots	# Successful Approaches	5		5		5	
	$\bar{h}_e$ rms, σh_e rms (ft)	0.028186	1.85E-05	0.009142	0.000101	0.006931	0.000301
	$\bar{\lambda}_e$ rms, $\sigma\lambda_e$ rms (ft)	0	0	0	0	0	0
	$\bar{u}_e$ rms, σu_e rms (kts)	0.008939	7.14E-05	0.009913	0.000484	0.005214	0.000253
	# Failed Approaches Vert	0		0		0	
	$\bar{t}_{td}$, σt_{td} (sec)	-	-	-	-	-	-
	$\bar{h}_e$ rms, σh_e rms (ft)	-	-	-	-	-	-
	$\bar{\lambda}_e$ rms, $\sigma\lambda_e$ rms (ft)	-	-	-	-	-	-
	$\bar{u}_e$ rms, σu_e rms (kts)	-	-	-	-	-	-
	# Failed Approaches Lat	0		0		0	
	$\bar{t}_{td}$, σt_{td} (sec)	-	-	-	-	-	-
	$\bar{h}_e$ rms, σh_e rms (ft)	-	-	-	-	-	-
	$\bar{\lambda}_e$ rms, $\sigma\lambda_e$ rms (ft)	-	-	-	-	-	-
	$\bar{u}_e$ rms, σu_e rms (kts)	-	-	-	-	-	-
	# Ramp Strikes	0		0		0	
	$\bar{h}_t$, σh_t (ft)	8.4518	0.042796	8.4163	0.029368	8.4117	0.029518
	$\bar{h}_{ac}$, σh_{ac} (ft)	0.044939	4.35E-05	0.015065	0.000328	0.010403	0.000389
	$\bar{\theta}_{ac}$, $\sigma\theta_{ac}$ (deg)	0.007746	0.015339	0.005727	0.01054	0.005754	0.010482
	# Bolters	0		0		0	
	$\bar{X}_{td}$, σX_{td} (ft)	-	-	-	-	-	-
	$\bar{Y}_{td}$, σY_{td} (ft)	-	-	-	-	-	-
	# Successful Touchdowns	5		5		5	
	$\bar{X}_{td}$, σX_{td} (ft)	0.62946	0.28139	0.30572	0.047802	0.22587	0.016638
	$\bar{Y}_{td}$, σY_{td} (ft)	-0.01639	0.000412	-0.00367	0.002685	-0.00178	0.000937
	$\bar{h}_t$, σh_t (ft)	-12.1914	4.47E-05	-12.1909	5.48E-05	-12.1898	4.47E-05
	h_t, σh_t (ft)	-0.06303	0.073729	0	0	0.038	0.057538
Carrier Speed = 33 Knots	# Successful Approaches	5		5		5	
	$\bar{h}_e$ rms, σh_e rms (ft)	0.025848	7.07E-05	0.030968	0.001557	0.034991	0.002413
	$\bar{\lambda}_e$ rms, $\sigma\lambda_e$ rms (ft)	0	0	0	0	0	0
	$\bar{u}_e$ rms, σu_e rms (kts)	0.008919	6.10E-05	0.027087	0.002977	0.02466	0.002599
	# Failed Approaches Vert	0		0		0	
	$\bar{t}_{td}$, σt_{td} (sec)	-	-	-	-	-	-
	$\bar{h}_e$ rms, σh_e rms (ft)	-	-	-	-	-	-
	$\bar{\lambda}_e$ rms, $\sigma\lambda_e$ rms (ft)	-	-	-	-	-	-
	$\bar{u}_e$ rms, σu_e rms (kts)	-	-	-	-	-	-
	# Failed Approaches Lat	0		0		0	
	$\bar{t}_{td}$, σt_{td} (sec)	-	-	-	-	-	-
	$\bar{h}_e$ rms, σh_e rms (ft)	-	-	-	-	-	-
	$\bar{\lambda}_e$ rms, $\sigma\lambda_e$ rms (ft)	-	-	-	-	-	-
	$\bar{u}_e$ rms, σu_e rms (kts)	-	-	-	-	-	-
	# Ramp Strikes	0		0		0	
	$\bar{h}_t$, σh_t (ft)	8.4182	0.01371	8.4255	0.008882	8.4295	0.006294
	$\bar{h}_{ac}$, σh_{ac} (ft)	0.041053	8.94E-05	0.048309	0.00163	0.052337	0.004345
	$\bar{\theta}_{ac}$, $\sigma\theta_{ac}$ (deg)	-0.00289	0.004941	-0.0029	0.002991	-0.00291	0.003001
	# Bolters	0		0		0	
	$\bar{X}_{td}$, σX_{td} (ft)	-	-	-	-	-	-
	$\bar{Y}_{td}$, σY_{td} (ft)	-	-	-	-	-	-
	# Successful Touchdowns	5		5		5	
	$\bar{X}_{td}$, σX_{td} (ft)	0.58313	0.060275	0.80373	0.26539	0.82307	0.23709
	$\bar{Y}_{td}$, σY_{td} (ft)	-0.00928	0.003292	-0.0107	0.005755	-0.00934	0.007422
	$\bar{h}_t$, σh_t (ft)	-12.1831	8.94E-05	-12.1882	0.033633	-12.1868	0.01189
	h_t, σh_t (ft)	-0.014516	0.041569	-0.004582	0.053127	-0.016358	0.064838

Table B-1 No Turbulence – Wind 2 Knots

		Wind Speed = 13.5 Knots No Turbulence					
		System 1		System 2		System 3	
Carrier Speed = 0 Knots	# Successful Approaches	5		5		5	
	$\bar{h}$, rms, σh, rms (ft)	0.036393	4.12E-05	0.007986	1.52E-05	0.004537	3.98E-06
	$\bar{\lambda}$, rms, $\sigma\lambda$, rms (ft)	0	0	0	0	0	0
	$\bar{u}$, rms, σu, rms (kts)	0.015332	3.21E-05	0.007018	0.000232	0.00212	0.000175
	# Failed Approaches Vert	0		0		0	
	$\bar{t}_{td}$, σt_{td} (sec)	-	-	-	-	-	-
	$\bar{h}$, rms, σh, rms (ft)	-	-	-	-	-	-
	$\bar{\lambda}$, rms, $\sigma\lambda$, rms (ft)	-	-	-	-	-	-
	$\bar{u}$, rms, σu, rms (kts)	-	-	-	-	-	-
	# Failed Approaches Lat	0		0		0	
	$\bar{t}_{td}$, σt_{td} (sec)	-	-	-	-	-	-
	$\bar{h}$, rms, σh, rms (ft)	-	-	-	-	-	-
	$\bar{\lambda}$, rms, $\sigma\lambda$, rms (ft)	-	-	-	-	-	-
	$\bar{u}$, rms, σu, rms (kts)	-	-	-	-	-	-
	# Ramp Strikes	0		0		0	
	$\bar{h}_{td}$, σh_{td} (ft)	8.4293	0.070835	8.4357	0.061915	8.4293	0.061932
	$\bar{h}_{sz}$, σh_{sz} (ft)	0.053467	1.61E-05	0.013974	1.30E-05	0.007546	3.38E-06
	$\bar{\theta}_{sz}$, $\sigma\theta_{sz}$ (deg)	-0.00337	0.025362	0.013059	0.022176	0.013059	0.022176
	# Bolters	0		0		0	
	$\bar{X}_{td}$, σX_{td} (ft)	-	-	-	-	-	-
	$\bar{Y}_{td}$, σY_{td} (ft)	-	-	-	-	-	-
	# Successful Touchdowns	5		5		5	
	$\bar{X}_{td}$, σX_{td} (ft)	0.92331	0.19877	0.24224	0.023018	0.14573	0.032211
	$\bar{Y}_{sz}$, σY_{sz} (ft)	-0.00972	0.004563	-0.00136	0.000875	-0.00136	0.000797
	$\bar{h}_{td}$, σh_{td} (ft)	-11.1839	0	-11.1744	0	-11.1738	7.07E-05
	$\bar{h}_{sz}$, σh_{sz} (ft)	-0.071307	0.25375	-0.029733	0.041366	-0.02953	0.042692
Carrier Speed = 10Knots	# Successful Approaches	5		5		5	
	$\bar{h}$, rms, σh, rms (ft)	0.035508	3.32E-05	0.00923	0.000289	0.00673	0.000528
	$\bar{\lambda}$, rms, $\sigma\lambda$, rms (ft)	0	0	0	0	0	0
	$\bar{u}$, rms, σu, rms (kts)	0.014714	1.05E-05	0.009692	0.000881	0.005219	0.000408
	# Failed Approaches Vert	0		0		0	
	$\bar{t}_{td}$, σt_{td} (sec)	-	-	-	-	-	-
	$\bar{h}$, rms, σh, rms (ft)	-	-	-	-	-	-
	$\bar{\lambda}$, rms, $\sigma\lambda$, rms (ft)	-	-	-	-	-	-
	$\bar{u}$, rms, σu, rms (kts)	-	-	-	-	-	-
	# Failed Approaches Lat	0		0		0	
	$\bar{t}_{td}$, σt_{td} (sec)	-	-	-	-	-	-
	$\bar{h}$, rms, σh, rms (ft)	-	-	-	-	-	-
	$\bar{\lambda}$, rms, $\sigma\lambda$, rms (ft)	-	-	-	-	-	-
	$\bar{u}$, rms, σu, rms (kts)	-	-	-	-	-	-
	# Ramp Strikes	0		0		0	
	$\bar{h}_{td}$, σh_{td} (ft)	8.4049	0.054107	8.411	0.04892	8.4066	0.048603
	$\bar{h}_{sz}$, σh_{sz} (ft)	0.052664	8.36E-05	0.015259	0.000551	0.010563	0.00071
	$\bar{\theta}_{sz}$, $\sigma\theta_{sz}$ (deg)	-0.01182	0.019398	0.003774	0.017575	0.003853	0.017463
	# Bolters	0		0		0	
	$\bar{X}_{td}$, σX_{td} (ft)	-	-	-	-	-	-
	$\bar{Y}_{td}$, σY_{td} (ft)	-	-	-	-	-	-
	# Successful Touchdowns	5		5		5	
	$\bar{X}_{td}$, σX_{td} (ft)	0.85493	0.040756	0.38969	0.059238	0.18058	0.059608
	$\bar{Y}_{sz}$, σY_{sz} (ft)	-0.00365	0.002187	-0.00206	0.002323	-0.00208	0.001317
	$\bar{h}_{td}$, σh_{td} (ft)	-11.1835	0.00011	-11.1741	0.000114	-11.173	5.48E-05
	$\bar{h}_{sz}$, σh_{sz} (ft)	0.13189	0.21523	0	0	0.32374	0.72421
Carrier Speed = 33 Knots	# Successful Approaches	5		5		5	
	$\bar{h}$, rms, σh, rms (ft)	0.032966	0.000137	0.039113	0.001828	0.049181	0.001518
	$\bar{\lambda}$, rms, $\sigma\lambda$, rms (ft)	0	0	0	0	0	0
	$\bar{u}$, rms, σu, rms (kts)	0.01545	5.66E-05	0.14773	0.00358	0.021093	0.003219
	# Failed Approaches Vert	0		0		0	
	$\bar{t}_{td}$, σt_{td} (sec)	-	-	-	-	-	-
	$\bar{h}$, rms, σh, rms (ft)	-	-	-	-	-	-
	$\bar{\lambda}$, rms, $\sigma\lambda$, rms (ft)	-	-	-	-	-	-
	$\bar{u}$, rms, σu, rms (kts)	-	-	-	-	-	-
	# Failed Approaches Lat	0		0		0	
	$\bar{t}_{td}$, σt_{td} (sec)	-	-	-	-	-	-
	$\bar{h}$, rms, σh, rms (ft)	-	-	-	-	-	-
	$\bar{\lambda}$, rms, $\sigma\lambda$, rms (ft)	-	-	-	-	-	-
	$\bar{u}$, rms, σu, rms (kts)	-	-	-	-	-	-
	# Ramp Strikes	0		0		0	
	$\bar{h}_{td}$, σh_{td} (ft)	8.4206	0.028313	8.4414	0.027234	8.4454	0.03003
	$\bar{h}_{sz}$, σh_{sz} (ft)	0.048456	0.000242	0.054373	0.002882	0.058994	0.004278
	$\bar{\theta}_{sz}$, $\sigma\theta_{sz}$ (deg)	-0.0047	0.010224	0.000634	0.010229	0.000405	0.010248
	# Bolters	0		0		0	
	$\bar{X}_{td}$, σX_{td} (ft)	-	-	-	-	-	-
	$\bar{Y}_{td}$, σY_{td} (ft)	-	-	-	-	-	-
	# Successful Touchdowns	5		5		5	
	$\bar{X}_{td}$, σX_{td} (ft)	0.96805	0.26038	1.1559	0.17487	1.0841	0.17596
	$\bar{Y}_{sz}$, σY_{sz} (ft)	-0.00515	0.002035	-0.00535	0.004311	-0.00457	0.00352
	$\bar{h}_{td}$, σh_{td} (ft)	-11.1737	0.00013	-11.1407	0.021387	-11.1665	0.008191
	$\bar{h}_{sz}$, σh_{sz} (ft)	-0.001455	0.058454	0.01461	0.055944	0.04585	0.058925

Table B-2 No Turbulence – Wind 13.5 Knots

		Wind Speed = 24 .5 Knots No Turbulence					
		System 1		System 2		System 3	
Carrier Speed = 0 Knots	# Successful Approaches	5		5		5	
	$\bar{h}_c$ rms, σh_c rms (ft)	0.045564	0.000186	0.007981	6.87E-05	0.00454	2.10E-05
	$\bar{\lambda}_c$ rms, $\sigma\lambda_c$ rms (ft)	0	0	0	0	0	0
	$\bar{u}_c$ rms, σu_c rms (kts)	0.047085	0.000201	0.007851	0.000842	0.002331	0.000562
	# Failed Approaches Vert	0		0		0	
	$\bar{t}_{td}$, σt_{td} (sec)	-	-	-	-	-	-
	$\bar{h}_c$ rms, σh_c rms (ft)	-	-	-	-	-	-
	$\bar{\lambda}_c$ rms, $\sigma\lambda_c$ rms (ft)	-	-	-	-	-	-
	$\bar{u}_c$ rms, σu_c rms (kts)	-	-	-	-	-	-
	# Failed Approaches Lat	0		0		0	
	$\bar{t}_{td}$, σt_{td} (sec)	-	-	-	-	-	-
	$\bar{h}_c$ rms, σh_c rms (ft)	-	-	-	-	-	-
	$\bar{\lambda}_c$ rms, $\sigma\lambda_c$ rms (ft)	-	-	-	-	-	-
	$\bar{u}_c$ rms, σu_c rms (kts)	-	-	-	-	-	-
	# Ramp Strikes	0		0		0	
	$\bar{h}_d$, σh_d (ft)	8.6055	0.29894	8.5275	0.19088	8.5208	0.191
	$\bar{h}_{cg}$, σh_{cg} (ft)	0.063133	0.000226	0.013957	4.67E-05	0.007548	1.76E-05
	$\bar{\theta}_{cg}$, $\sigma\theta_{cg}$ (deg)	0.056275	0.10713	0.045939	0.06837	0.045838	0.068391
	# Bolters	0		0		0	
	$\bar{X}_d$, σX_d (ft)	-	-	-	-	-	-
	$\bar{Y}_d$, σY_d (ft)	-	-	-	-	-	-
	# Successful Touchdowns	5		5		5	
	$\bar{X}_d$, σX_d (ft)	0.94063	0.048129	0.20897	0.026654	0.11173	0.021842
	$\bar{Y}_{cg}$, σY_{cg} (ft)	-0.01249	0.005207	-0.00239	0.001837	-0.0013	0.00082
	$\bar{h}_d$, σh_d (ft)	-10.2223	8.94E-05	-10.2018	8.37E-05	-10.2012	0.00011
	$\bar{h}_c$, σh_c (ft)	0.38925	0.85172	-0.080966	0.26178	-0.08515	0.2693
Carrier Speed = 10Knots	# Successful Approaches	5		5		5	
	$\bar{h}_c$ rms, σh_c rms (ft)	0.046741	0.000446	0.010208	0.001171	0.005465	0.001191
	$\bar{\lambda}_c$ rms, $\sigma\lambda_c$ rms (ft)	0	0	0	0	0	0
	$\bar{u}_c$ rms, σu_c rms (kts)	0.059174	0.000447	0.010318	0.001072	0.036848	0.000388
	# Failed Approaches Vert	0		0		0	
	$\bar{t}_{td}$, σt_{td} (sec)	-	-	-	-	-	-
	$\bar{h}_c$ rms, σh_c rms (ft)	-	-	-	-	-	-
	$\bar{\lambda}_c$ rms, $\sigma\lambda_c$ rms (ft)	-	-	-	-	-	-
	$\bar{u}_c$ rms, σu_c rms (kts)	-	-	-	-	-	-
	# Failed Approaches Lat	0		0		0	
	$\bar{t}_{td}$, σt_{td} (sec)	-	-	-	-	-	-
	$\bar{h}_c$ rms, σh_c rms (ft)	-	-	-	-	-	-
	$\bar{\lambda}_c$ rms, $\sigma\lambda_c$ rms (ft)	-	-	-	-	-	-
	$\bar{u}_c$ rms, σu_c rms (kts)	-	-	-	-	-	-
	# Ramp Strikes	0		0		0	
	$\bar{h}_d$, σh_d (ft)	8.5293	0.24215	8.3053	0.23035	8.2987	0.2307
	$\bar{h}_{cg}$, σh_{cg} (ft)	0.063813	0.000369	0.015968	0.001784	0.009371	0.002159
	$\bar{\theta}_{cg}$, $\sigma\theta_{cg}$ (deg)	0.028747	0.0868	-0.03434	0.081963	-0.03434	0.081963
	# Bolters	0		0		0	
	$\bar{X}_d$, σX_d (ft)	-	-	-	-	-	-
	$\bar{Y}_d$, σY_d (ft)	-	-	-	-	-	-
	# Successful Touchdowns	5		5		5	
	$\bar{X}_d$, σX_d (ft)	0.91155	0.2416	0.37872	0.069889	0.23658	0.10052
	$\bar{Y}_{cg}$, σY_{cg} (ft)	-0.01661	0.008479	-0.00404	0.00142	-0.00149	0.000893
	$\bar{h}_d$, σh_d (ft)	-10.2206	0.000451	-10.2017	0.000342	-10.2038	0.000308
	$\bar{h}_c$, σh_c (ft)	-0.035042	0.42994	0.01002	0.45875	-0.026605	0.48814
Carrier Speed = 33 Knots	# Successful Approaches	5		5		5	
	$\bar{h}_c$ rms, σh_c rms (ft)	0.040929	0.000432	0.041626	0.002074	0.04497	0.004565
	$\bar{\lambda}_c$ rms, $\sigma\lambda_c$ rms (ft)	0	0	0	0	0	0
	$\bar{u}_c$ rms, σu_c rms (kts)	0.044223	0.00166	0.13379	0.011875	0.028372	0.004836
	# Failed Approaches Vert	0		0		0	
	$\bar{t}_{td}$, σt_{td} (sec)	-	-	-	-	-	-
	$\bar{h}_c$ rms, σh_c rms (ft)	-	-	-	-	-	-
	$\bar{\lambda}_c$ rms, $\sigma\lambda_c$ rms (ft)	-	-	-	-	-	-
	$\bar{u}_c$ rms, σu_c rms (kts)	-	-	-	-	-	-
	# Failed Approaches Lat	0		0		0	
	$\bar{t}_{td}$, σt_{td} (sec)	-	-	-	-	-	-
	$\bar{h}_c$ rms, σh_c rms (ft)	-	-	-	-	-	-
	$\bar{\lambda}_c$ rms, $\sigma\lambda_c$ rms (ft)	-	-	-	-	-	-
	$\bar{u}_c$ rms, σu_c rms (kts)	-	-	-	-	-	-
	# Ramp Strikes	0		0		0	
	$\bar{h}_d$, σh_d (ft)	8.4765	0.082129	8.5318	0.15828	8.5269	0.16163
	$\bar{h}_{cg}$, σh_{cg} (ft)	0.056907	0.000734	0.059861	0.004123	0.057414	0.00267
	$\bar{\theta}_{cg}$, $\sigma\theta_{cg}$ (deg)	0.012295	0.029667	0.031052	0.056931	0.030165	0.057739
	# Bolters	0		0		0	
	$\bar{X}_d$, σX_d (ft)	-	-	-	-	-	-
	$\bar{Y}_d$, σY_d (ft)	-	-	-	-	-	-
	# Successful Touchdowns	5		5		5	
	$\bar{X}_d$, σX_d (ft)	0.90707	0.31038	1.0043	0.095595	0.97342	0.2217
	$\bar{Y}_{cg}$, σY_{cg} (ft)	-0.00969	0.009275	-0.00733	0.007043	-0.00401	0.003488
	$\bar{h}_d$, σh_d (ft)	-10.2109	0.000526	-10.1714	0.021448	-10.1839	0.01919
	$\bar{h}_c$, σh_c (ft)	-0.011555	0.2036	-0.15853	0.21742	-0.17262	0.17167

Table B-3 No Turbulence – Wind 24.5 Knots

		Wind Speed = 37 Knots No Turbulence					
		System 1		System 2		System 3	
Carrier Speed = 0 Knots	# Successful Approaches	5		5		5	
	$\bar{h}_r$ rms, σh_r rms (ft)	0.057883	0.000668	0.007814	4.57E-05	0.005017	0.000367
	$\bar{\lambda}_r$ rms, $\sigma\lambda_r$ rms (ft)	0	0	0	0	0	0
	$\bar{u}_r$ rms, σu_r rms (kts)	0.068555	0.00187	0.01734	0.00165	0.014406	0.003842
	# Failed Approaches Vert	0		0		0	
	$\bar{t}_{td}$, σt_{td} (sec)	-	-	-	-	-	-
	$\bar{h}_r$ rms, σh_r rms (ft)	-	-	-	-	-	-
	$\bar{\lambda}_r$ rms, $\sigma\lambda_r$ rms (ft)	-	-	-	-	-	-
	$\bar{u}_r$ rms, σu_r rms (kts)	-	-	-	-	-	-
	# Failed Approaches Lat	0		0		0	
	$\bar{t}_{td}$, σt_{td} (sec)	-	-	-	-	-	-
	$\bar{h}_r$ rms, σh_r rms (ft)	-	-	-	-	-	-
	$\bar{\lambda}_r$ rms, $\sigma\lambda_r$ rms (ft)	-	-	-	-	-	-
	$\bar{u}_r$ rms, σu_r rms (kts)	-	-	-	-	-	-
	# Ramp Strikes	0		0		0	
	$\bar{h}_d$, σh_d (ft)	8.5194	0.63918	7.8756	0.35989	7.8699	0.35898
	$\bar{h}_{dy}$, σh_{dy} (ft)	0.068783	0.001534	0.013701	3.88E-05	0.007942	0.000234
	$\bar{\theta}_{dy}$, $\sigma\theta_{dy}$ (deg)	0.023426	0.2294	-0.18742	0.12887	-0.18738	0.1285
	# Bolters	0		0		0	
	$\bar{X}_d$, σX_d (ft)	-	-	-	-	-	-
	$\bar{Y}_d$, σY_d (ft)	-	-	-	-	-	-
	# Successful Touchdowns	5		5		5	
	$\bar{X}_d$, σX_d (ft)	1.2354	0.36572	0.37598	0.084746	0.16692	0.12919
	$\bar{Y}_{dy}$, σY_{dy} (ft)	-0.01827	0.015763	-0.00594	0.004413	-0.00356	0.003921
	$\bar{h}_d$, σh_d (ft)	-9.1485	0.000812	-9.0975	0.000114	-9.0949	0.000374
	$\bar{h}_{dv}$, σh_{dv} (ft)	0.57805	1.4951	-0.10628	0.63458	-0.077666	0.62217
Carrier Speed = 10Knots	# Successful Approaches	5		5		5	
	$\bar{h}_r$ rms, σh_r rms (ft)	0.056979	0.001225	0.010896	0.001202	0.006861	0.001984
	$\bar{\lambda}_r$ rms, $\sigma\lambda_r$ rms (ft)	0	0	0	0	0	0
	$\bar{u}_r$ rms, σu_r rms (kts)	0.067851	0.001469	0.008401	0.003379	0.037544	0.000781
	# Failed Approaches Vert	0		0		0	
	$\bar{t}_{td}$, σt_{td} (sec)	-	-	-	-	-	-
	$\bar{h}_r$ rms, σh_r rms (ft)	-	-	-	-	-	-
	$\bar{\lambda}_r$ rms, $\sigma\lambda_r$ rms (ft)	-	-	-	-	-	-
	$\bar{u}_r$ rms, σu_r rms (kts)	-	-	-	-	-	-
	# Failed Approaches Lat	0		0		0	
	$\bar{t}_{td}$, σt_{td} (sec)	-	-	-	-	-	-
	$\bar{h}_r$ rms, σh_r rms (ft)	-	-	-	-	-	-
	$\bar{\lambda}_r$ rms, $\sigma\lambda_r$ rms (ft)	-	-	-	-	-	-
	$\bar{u}_r$ rms, σu_r rms (kts)	-	-	-	-	-	-
	# Ramp Strikes	0		0		0	
	$\bar{h}_d$, σh_d (ft)	8.511	0.50673	8.692	0.66493	8.6861	0.66613
	$\bar{h}_{dy}$, σh_{dy} (ft)	0.06876	0.001058	0.016963	0.002299	0.011151	0.003251
	$\bar{\theta}_{dy}$, $\sigma\theta_{dy}$ (deg)	0.020397	0.18174	0.10376	0.23739	0.10376	0.23739
	# Bolters	0		0		0	
	$\bar{X}_d$, σX_d (ft)	-	-	-	-	-	-
	$\bar{Y}_d$, σY_d (ft)	-	-	-	-	-	-
	# Successful Touchdowns	5		5		5	
	$\bar{X}_d$, σX_d (ft)	1.2087	0.38122	0.37212	0.048063	0.29354	0.052643
	$\bar{Y}_{dy}$, σY_{dy} (ft)	-0.01365	0.005874	-0.00561	0.004647	-0.00421	0.002079
	$\bar{h}_d$, σh_d (ft)	-9.1479	0.001488	-9.0961	0.000638	-9.0988	0.000472
	$\bar{h}_{dv}$, σh_{dv} (ft)	0.26626	1.3202	0.33093	0.65182	0.42974	0.71802
Carrier Speed = 33 Knots	# Successful Approaches	5		5		5	
	$\bar{h}_r$ rms, σh_r rms (ft)	0.35219	0.2612	0.09294	0.011975	0.059546	0.003461
	$\bar{\lambda}_r$ rms, $\sigma\lambda_r$ rms (ft)	0	0	0	0	0	0
	$\bar{u}_r$ rms, σu_r rms (kts)	0.20319	0.092745	0.52541	0.008633	0.3671	0.012988
	# Failed Approaches Vert	0		0		0	
	$\bar{t}_{td}$, σt_{td} (sec)	-	-	-	-	-	-
	$\bar{h}_r$ rms, σh_r rms (ft)	-	-	-	-	-	-
	$\bar{\lambda}_r$ rms, $\sigma\lambda_r$ rms (ft)	-	-	-	-	-	-
	$\bar{u}_r$ rms, σu_r rms (kts)	-	-	-	-	-	-
	# Failed Approaches Lat	0		0		0	
	$\bar{t}_{td}$, σt_{td} (sec)	-	-	-	-	-	-
	$\bar{h}_r$ rms, σh_r rms (ft)	-	-	-	-	-	-
	$\bar{\lambda}_r$ rms, $\sigma\lambda_r$ rms (ft)	-	-	-	-	-	-
	$\bar{u}_r$ rms, σu_r rms (kts)	-	-	-	-	-	-
	# Ramp Strikes	0		0		0	
	$\bar{h}_d$, σh_d (ft)	8.4365	0.62339	8.3742	0.49032	8.3687	0.46456
	$\bar{h}_{dy}$, σh_{dy} (ft)	0.074998	0.002991	0.074823	0.008505	0.057044	0.008578
	$\bar{\theta}_{dy}$, $\sigma\theta_{dy}$ (deg)	-0.00852	0.22258	-0.03076	0.17289	-0.02635	0.1638
	# Bolters	0		0		0	
	$\bar{X}_d$, σX_d (ft)	-	-	-	-	-	-
	$\bar{Y}_d$, σY_d (ft)	-	-	-	-	-	-
	# Successful Touchdowns	5		5		5	
	$\bar{X}_d$, σX_d (ft)	1.2341	0.41807	1.2579	0.16825	1.1191	0.35555
	$\bar{Y}_{dy}$, σY_{dy} (ft)	-0.01609	0.009862	-0.00846	0.007116	-0.00581	0.00357
	$\bar{h}_d$, σh_d (ft)	-9.1287	0.009639	-9.0643	0.016786	-9.0722	0.011995
	$\bar{h}_{dv}$, σh_{dv} (ft)	0.04177	1.0193	-0.31795	1.2319	-0.80744	1.0529

Table B-4 No Turbulence – Wind 37 Knots

		Wind Speed = 2 Knots Carrier Induced Turbulence Only					
		System 1		System 2		System 3	
Carrier Speed = 0 Knots	# Successful Approaches	5		5		5	
	$\bar{h}$, rms, σh, rms (ft)	0.1945	0.001919	0.23989	0.009191	0.10632	0.000659
	$\bar{\lambda}$, rms, $\sigma\lambda$, rms (ft)	0.00013	9.95E-06	0.000149	1.03E-05	0.000162	5.45E-06
	$\bar{u}$, rms, σu, rms (kts)	0.023896	0.00033	0.10868	0.005559	0.070318	0.000315
	# Failed Approaches Vert	0		0		0	
	$\bar{t}_{td}$, σt_{td} (sec)	-	-	-	-	-	-
	$\bar{h}$, rms, σh, rms (ft)	-	-	-	-	-	-
	$\bar{\lambda}$, rms, $\sigma\lambda$, rms (ft)	-	-	-	-	-	-
	$\bar{u}$, rms, σu, rms (kts)	-	-	-	-	-	-
	# Failed Approaches Lat	0		0		0	
	$\bar{t}_{td}$, σt_{td} (sec)	-	-	-	-	-	-
	$\bar{h}$, rms, σh, rms (ft)	-	-	-	-	-	-
	$\bar{\lambda}$, rms, $\sigma\lambda$, rms (ft)	-	-	-	-	-	-
	$\bar{u}$, rms, σu, rms (kts)	-	-	-	-	-	-
	# Ramp Strikes	0		0		0	
	$\bar{h}_{td}$, σh_{td} (ft)	7.9877	0.035765	8.1852	0.038558	8.2546	0.030201
	$\bar{h}_{td}$, σh_{td} (ft)	-0.37349	0.002191	-0.17528	0.01185	-0.10588	0.001106
	$\bar{\theta}_{td}$, $\sigma\theta_{td}$ (deg)	-0.00861	0.012671	-0.00886	0.010547	-0.00888	0.010471
	# Bolters	0		0		0	
	$\bar{X}_{td}$, σX_{td} (ft)	-	-	-	-	-	-
	$\bar{Y}_{td}$, σY_{td} (ft)	-	-	-	-	-	-
	# Successful Touchdowns	5		5		5	
	$\bar{X}_{td}$, σX_{td} (ft)	25.6301	1.1323	-2.1452	0.45314	-2.1164	0.028456
	$\bar{Y}_{td}$, σY_{td} (ft)	-0.05692	0.031232	0.015044	0.013196	0.039924	0.001542
	$\bar{h}_{td}$, σh_{td} (ft)	-14.328	0.018595	-10.2778	0.015422	-10.6301	0.002561
	$\bar{h}_{td}$, σh_{td} (ft)	-0.01789	0.085611	-0.029417	0.049724	-0.026228	0.053777
Carrier Speed = 10Knots	# Successful Approaches	5		5		5	
	$\bar{h}$, rms, σh, rms (ft)	0.15497	0.00114	0.17994	0.002473	0.11719	0.001761
	$\bar{\lambda}$, rms, $\sigma\lambda$, rms (ft)	0.000129	1.59E-05	0.000318	3.99E-05	0.000156	1.04E-05
	$\bar{u}$, rms, σu, rms (kts)	0.019467	0.000143	0.11466	0.001907	0.081241	0.000448
	# Failed Approaches Vert	0		0		0	
	$\bar{t}_{td}$, σt_{td} (sec)	-	-	-	-	-	-
	$\bar{h}$, rms, σh, rms (ft)	-	-	-	-	-	-
	$\bar{\lambda}$, rms, $\sigma\lambda$, rms (ft)	-	-	-	-	-	-
	$\bar{u}$, rms, σu, rms (kts)	-	-	-	-	-	-
	# Failed Approaches Lat	0		0		0	
	$\bar{t}_{td}$, σt_{td} (sec)	-	-	-	-	-	-
	$\bar{h}$, rms, σh, rms (ft)	-	-	-	-	-	-
	$\bar{\lambda}$, rms, $\sigma\lambda$, rms (ft)	-	-	-	-	-	-
	$\bar{u}$, rms, σu, rms (kts)	-	-	-	-	-	-
	# Ramp Strikes	0		0		0	
	$\bar{h}_{td}$, σh_{td} (ft)	7.761	0.044018	8.4366	0.028717	8.3797	0.029148
	$\bar{h}_{td}$, σh_{td} (ft)	-0.64575	0.001632	0.035274	0.010325	-0.02174	0.000627
	$\bar{\theta}_{td}$, $\sigma\theta_{td}$ (deg)	0.007691	0.015372	0.005753	0.010484	0.0058	0.010433
	# Bolters	0		0		0	
	$\bar{X}_{td}$, σX_{td} (ft)	-	-	-	-	-	-
	$\bar{Y}_{td}$, σY_{td} (ft)	-	-	-	-	-	-
	# Successful Touchdowns	5		5		5	
	$\bar{X}_{td}$, σX_{td} (ft)	22.0552	0.014662	-1.3544	0.79247	-1	3.75E-05
	$\bar{Y}_{td}$, σY_{td} (ft)	-0.01716	0.007566	-0.00244	0.001858	0.003578	0.00477
	$\bar{h}_{td}$, σh_{td} (ft)	-13.2771	0.001437	-11.4148	0.12116	-11.7935	0.006298
	$\bar{h}_{td}$, σh_{td} (ft)	0.05285	0.056681	0.02793	0.049749	0.0293	0.05549
Carrier Speed = 33 Knots	# Successful Approaches	5		5		5	
	$\bar{h}$, rms, σh, rms (ft)	0.12748	0.000562	0.30884	0.13761	0.14062	0.003517
	$\bar{\lambda}$, rms, $\sigma\lambda$, rms (ft)	0.000141	4.08E-06	0.004992	0.007221	0.000315	2.44E-05
	$\bar{u}$, rms, σu, rms (kts)	0.015854	5.68E-05	0.13687	0.043892	0.082871	0.002188
	# Failed Approaches Vert	0		0		0	
	$\bar{t}_{td}$, σt_{td} (sec)	-	-	-	-	-	-
	$\bar{h}$, rms, σh, rms (ft)	-	-	-	-	-	-
	$\bar{\lambda}$, rms, $\sigma\lambda$, rms (ft)	-	-	-	-	-	-
	$\bar{u}$, rms, σu, rms (kts)	-	-	-	-	-	-
	# Failed Approaches Lat	0		0		0	
	$\bar{t}_{td}$, σt_{td} (sec)	-	-	-	-	-	-
	$\bar{h}$, rms, σh, rms (ft)	-	-	-	-	-	-
	$\bar{\lambda}$, rms, $\sigma\lambda$, rms (ft)	-	-	-	-	-	-
	$\bar{u}$, rms, σu, rms (kts)	-	-	-	-	-	-
	# Ramp Strikes	0		0		0	
	$\bar{h}_{td}$, σh_{td} (ft)	7.8357	0.014423	9.1916	0.9861	8.3917	0.010323
	$\bar{h}_{td}$, σh_{td} (ft)	-0.54142	0.000689	0.81438	0.98982	0.014601	0.003171
	$\bar{\theta}_{td}$, $\sigma\theta_{td}$ (deg)	-0.0029	0.004956	-0.00288	0.002949	-0.00292	0.002908
	# Bolters	0		0		0	
	$\bar{X}_{td}$, σX_{td} (ft)	-	-	-	-	-	-
	$\bar{Y}_{td}$, σY_{td} (ft)	-	-	-	-	-	-
	# Successful Touchdowns	5		5		5	
	$\bar{X}_{td}$, σX_{td} (ft)	18.434	0.7859	-5.8229	6.9457	1.2761	0.16149
	$\bar{Y}_{td}$, σY_{td} (ft)	0.057657	0.002691	0.12159	0.20171	0.009309	0.001747
	$\bar{h}_{td}$, σh_{td} (ft)	-14.018	0.01303	-12.8227	1.9436	-11.5766	0.01045
	$\bar{h}_{td}$, σh_{td} (ft)	-0.00844	0.020511	-0.007451	0.034216	-0.009741	0.041485

Table B-5 Carrier Induced Turbulence Only – Wind 2 Knots

		Wind Speed = 13.5 Knots Carrier Induced Turbulence Only					
		System 1		System 2		System 3	
Carrier Speed = 0 Knots	# Successful Approaches	5		5		5	
	$\bar{h}_r$ rms, σh_r rms (ft)	0.34304	0.010357	0.2484	0.011407	0.10934	0.001008
	$\bar{\lambda}_r$ rms, $\sigma\lambda_r$ rms (ft)	0.002262	6.42E-05	0.00218	5.10E-05	0.002173	2.76E-05
	$\bar{u}_r$ rms, σu_r rms (kts)	0.066409	0.001931	0.11115	0.003879	0.079494	0.000554
	# Failed Approaches Vert	0		0		0	
	$\bar{t}_{td}$, σt_{td} (sec)	-	-	-	-	-	-
	$\bar{h}_r$ rms, σh_r rms (ft)	-	-	-	-	-	-
	$\bar{\lambda}_r$ rms, $\sigma\lambda_r$ rms (ft)	-	-	-	-	-	-
	$\bar{u}_r$ rms, σu_r rms (kts)	-	-	-	-	-	-
	# Failed Approaches Lat	0		0		0	
	$\bar{t}_{td}$, σt_{td} (sec)	-	-	-	-	-	-
	$\bar{h}_r$ rms, σh_r rms (ft)	-	-	-	-	-	-
	$\bar{\lambda}_r$ rms, $\sigma\lambda_r$ rms (ft)	-	-	-	-	-	-
	$\bar{u}_r$ rms, σu_r rms (kts)	-	-	-	-	-	-
	# Ramp Strikes	0		0		0	
	$\bar{h}_d$, σh_d (ft)	9.8892	0.064668	8.3396	0.055143	8.3554	0.062863
	$\bar{h}_{dy}$, σh_{dy} (ft)	1.5153	0.01247	-0.08049	0.011026	-0.06443	0.001599
	$\bar{\theta}_{dy}$, $\sigma\theta_{dy}$ (deg)	-0.00406	0.02685	0.012483	0.021979	0.012398	0.021948
	# Bolters	0		0		0	
	$\bar{X}_d$, σX_d (ft)	-	-	-	-	-	-
	$\bar{Y}_d$, σY_d (ft)	-	-	-	-	-	-
	# Successful Touchdowns	5		5		5	
	$\bar{X}_d$, σX_d (ft)	-15.438	0.62888	-2.4385	0.93097	-2.0022	1.2899
	$\bar{Y}_{dy}$, σY_{dy} (ft)	0.025459	0.008815	0.015964	0.019951	0.04576	0.013289
	$\bar{h}_d$, σh_d (ft)	-11.2679	0.021826	-9.6737	0.080543	-10.1311	0.062807
	$\bar{h}_{dy}$, σh_{dy} (ft)	-0.076482	0.27288	-0.045674	0.064583	-0.042107	0.04083
Carrier Speed = 10Knots	# Successful Approaches	5		5		5	
	$\bar{h}_r$ rms, σh_r rms (ft)	0.30391	0.003405	0.23138	0.005191	0.12011	0.002679
	$\bar{\lambda}_r$ rms, $\sigma\lambda_r$ rms (ft)	0.002799	4.86E-05	0.002525	0.000214	0.002146	8.45E-05
	$\bar{u}_r$ rms, σu_r rms (kts)	0.057753	0.000713	0.13175	0.007922	0.088679	0.000916
	# Failed Approaches Vert	0		0		0	
	$\bar{t}_{td}$, σt_{td} (sec)	-	-	-	-	-	-
	$\bar{h}_r$ rms, σh_r rms (ft)	-	-	-	-	-	-
	$\bar{\lambda}_r$ rms, $\sigma\lambda_r$ rms (ft)	-	-	-	-	-	-
	$\bar{u}_r$ rms, σu_r rms (kts)	-	-	-	-	-	-
	# Failed Approaches Lat	0		0		0	
	$\bar{t}_{td}$, σt_{td} (sec)	-	-	-	-	-	-
	$\bar{h}_r$ rms, σh_r rms (ft)	-	-	-	-	-	-
	$\bar{\lambda}_r$ rms, $\sigma\lambda_r$ rms (ft)	-	-	-	-	-	-
	$\bar{u}_r$ rms, σu_r rms (kts)	-	-	-	-	-	-
	# Ramp Strikes	0		0		0	
	$\bar{h}_d$, σh_d (ft)	8.3374	0.055238	8.6426	0.071152	8.5288	0.045631
	$\bar{h}_{dy}$, σh_{dy} (ft)	-0.01736	0.001332	0.24504	0.055743	0.13089	0.016942
	$\bar{\theta}_{dy}$, $\sigma\theta_{dy}$ (deg)	-0.01091	0.019577	0.004403	0.016723	0.004526	0.016579
	# Bolters	0		0		0	
	$\bar{X}_d$, σX_d (ft)	-	-	-	-	-	-
	$\bar{Y}_d$, σY_d (ft)	-	-	-	-	-	-
	# Successful Touchdowns	5		5		5	
	$\bar{X}_d$, σX_d (ft)	-17.4775	1.0984	-2.8078	0.55722	-1.1337	0.29873
	$\bar{Y}_{dy}$, σY_{dy} (ft)	0.049808	0.020492	0.04659	0.017996	0.014435	0.007456
	$\bar{h}_d$, σh_d (ft)	-7.7044	0.01885	-10.488	0.069987	-10.8214	0.051295
	$\bar{h}_{dy}$, σh_{dy} (ft)	0.07922	0.10927	0.07585	0.17294	0.06947	0.1674
Carrier Speed = 33 Knots	# Successful Approaches	5		5		5	
	$\bar{h}_r$ rms, σh_r rms (ft)	0.3343	0.00088	0.21818	0.035596	0.10974	0.001511
	$\bar{\lambda}_r$ rms, $\sigma\lambda_r$ rms (ft)	0.002419	0.000114	0.004354	0.000799	0.002339	9.51E-05
	$\bar{u}_r$ rms, σu_r rms (kts)	0.056647	0.000165	0.24492	0.003692	0.086965	0.002281
	# Failed Approaches Vert	0		0		0	
	$\bar{t}_{td}$, σt_{td} (sec)	-	-	-	-	-	-
	$\bar{h}_r$ rms, σh_r rms (ft)	-	-	-	-	-	-
	$\bar{\lambda}_r$ rms, $\sigma\lambda_r$ rms (ft)	-	-	-	-	-	-
	$\bar{u}_r$ rms, σu_r rms (kts)	-	-	-	-	-	-
	# Failed Approaches Lat	0		0		0	
	$\bar{t}_{td}$, σt_{td} (sec)	-	-	-	-	-	-
	$\bar{h}_r$ rms, σh_r rms (ft)	-	-	-	-	-	-
	$\bar{\lambda}_r$ rms, $\sigma\lambda_r$ rms (ft)	-	-	-	-	-	-
	$\bar{u}_r$ rms, σu_r rms (kts)	-	-	-	-	-	-
	# Ramp Strikes	0		0		0	
	$\bar{h}_d$, σh_d (ft)	9.0149	0.029771	8.5585	0.4267	8.5765	0.032022
	$\bar{h}_{dy}$, σh_{dy} (ft)	0.64236	0.00507	0.17046	0.41772	0.18893	0.004733
	$\bar{\theta}_{dy}$, $\sigma\theta_{dy}$ (deg)	-0.00456	0.010312	0.000994	0.010185	0.000831	0.010202
	# Bolters	0		0		0	
	$\bar{X}_d$, σX_d (ft)	-	-	-	-	-	-
	$\bar{Y}_d$, σY_d (ft)	-	-	-	-	-	-
	# Successful Touchdowns	5		5		5	
	$\bar{X}_d$, σX_d (ft)	-2.537	0.015861	-5.7731	4.9082	-0.42088	0.41538
	$\bar{Y}_{dy}$, σY_{dy} (ft)	0.01071	0.003901	-0.01488	0.030072	-0.01337	0.008323
	$\bar{h}_d$, σh_d (ft)	-14.0211	0.00363	-10.0384	1.4218	-10.4567	0.024722
	$\bar{h}_{dy}$, σh_{dy} (ft)	0.00123	0.037962	0.03007	0.041307	0.02851	0.040394

Table B-6 Carrier Induced Turbulence Only – Wind 13.5 Knots

		Wind Speed = 24.5 Knots Carrier Induced Turbulence Only					
		System 1		System 2		System 3	
Carrier Speed = 0 Knots	# Successful Approaches	5		5		5	
	$\bar{h}_{rms}$, σh_{rms} (ft)	0.55418	0.013288	0.31879	0.082763	0.13139	0.01474
	$\bar{\lambda}_{rms}$, $\sigma\lambda_{rms}$ (ft)	0.005018	0.000639	0.003807	0.000639	0.00339	8.92E-05
	$\bar{u}_{rms}$, σu_{rms} (kts)	0.12218	0.002964	0.14247	0.026063	0.10289	0.008646
	# Failed Approaches Vert	0		0		0	
	$\bar{t}_{td}$, σt_{td} (sec)	-	-	-	-	-	-
	$\bar{h}_{rms}$, σh_{rms} (ft)	-	-	-	-	-	-
	$\bar{\lambda}_{rms}$, $\sigma\lambda_{rms}$ (ft)	-	-	-	-	-	-
	$\bar{u}_{rms}$, σu_{rms} (kts)	-	-	-	-	-	-
	# Failed Approaches Lat	0		0		0	
	$\bar{t}_{td}$, σt_{td} (sec)	-	-	-	-	-	-
	$\bar{h}_{rms}$, σh_{rms} (ft)	-	-	-	-	-	-
	$\bar{\lambda}_{rms}$, $\sigma\lambda_{rms}$ (ft)	-	-	-	-	-	-
	$\bar{u}_{rms}$, σu_{rms} (kts)	-	-	-	-	-	-
	# Ramp Strikes	0		0		0	
	$\bar{h}_{td}$, σh_{td} (ft)	10.2757	0.29291	8.595	0.27965	8.49	0.19995
	$\bar{h}_{sp}$, σh_{sp} (ft)	1.7325	0.012897	0.089036	0.15672	-0.01481	0.043782
	$\bar{\theta}_{sp}$, $\sigma\theta_{sp}$ (deg)	0.056556	0.10878	0.043241	0.069432	0.042816	0.069518
	# Bolters	0		0		0	
	$\bar{X}_{td}$, σX_{td} (ft)	-	-	-	-	-	-
	$\bar{Y}_{td}$, σY_{td} (ft)	-	-	-	-	-	-
	# Successful Touchdowns	5		5		5	
	$\bar{X}_{td}$, σX_{td} (ft)	0.34965	0.19131	0.007619	10.0356	-2.5369	1.0741
	$\bar{Y}_{sp}$, σY_{sp} (ft)	0.004714	0.003564	0.065553	0.060329	0.030273	0.017505
	$\bar{h}_{td}$, σh_{td} (ft)	-11.6157	0.003776	-10.0932	2.0339	-9.297	0.16443
	$\bar{h}_{sp}$, σh_{sp} (ft)	0.16976	0.37913	-0.1108	0.26945	-0.11389	0.26785
Carrier Speed = 10Knots	# Successful Approaches	5		5		5	
	$\bar{h}_{rms}$, σh_{rms} (ft)	0.5815	0.020658	0.29665	0.1506	0.14591	0.007176
	$\bar{\lambda}_{rms}$, $\sigma\lambda_{rms}$ (ft)	0.004429	0.000548	0.003956	0.000903	0.003611	0.000138
	$\bar{u}_{rms}$, σu_{rms} (kts)	0.13288	0.003376	0.15159	0.041409	0.10218	0.004735
	# Failed Approaches Vert	0		0		0	
	$\bar{t}_{td}$, σt_{td} (sec)	-	-	-	-	-	-
	$\bar{h}_{rms}$, σh_{rms} (ft)	-	-	-	-	-	-
	$\bar{\lambda}_{rms}$, $\sigma\lambda_{rms}$ (ft)	-	-	-	-	-	-
	$\bar{u}_{rms}$, σu_{rms} (kts)	-	-	-	-	-	-
	# Failed Approaches Lat	0		0		0	
	$\bar{t}_{td}$, σt_{td} (sec)	-	-	-	-	-	-
	$\bar{h}_{rms}$, σh_{rms} (ft)	-	-	-	-	-	-
	$\bar{\lambda}_{rms}$, $\sigma\lambda_{rms}$ (ft)	-	-	-	-	-	-
	$\bar{u}_{rms}$, σu_{rms} (kts)	-	-	-	-	-	-
	# Ramp Strikes	0		0		0	
	$\bar{h}_{td}$, σh_{td} (ft)	10.0071	0.23465	8.6508	0.20679	8.5062	0.31243
	$\bar{h}_{sp}$, σh_{sp} (ft)	1.5487	0.026868	0.35575	0.19713	0.21091	0.085926
	$\bar{\theta}_{sp}$, $\sigma\theta_{sp}$ (deg)	0.026191	0.088465	-0.03229	0.087543	-0.03223	0.087906
	# Bolters	0		0		0	
	$\bar{X}_{td}$, σX_{td} (ft)	-	-	-	-	-	-
	$\bar{Y}_{td}$, σY_{td} (ft)	-	-	-	-	-	-
	# Successful Touchdowns	5		5		5	
	$\bar{X}_{td}$, σX_{td} (ft)	27.794	2.5592	-4.5517	4.3672	-3.6838	2.469
	$\bar{Y}_{sp}$, σY_{sp} (ft)	0.12825	0.092587	0.026091	0.058567	0.029049	0.018478
	$\bar{h}_{td}$, σh_{td} (ft)	-13.831	0.059201	-9.6319	1.5996	-10.2644	0.30168
	$\bar{h}_{sp}$, σh_{sp} (ft)	-0.037711	0.44374	0.06555	0.45883	0.01732	0.53484
Carrier Speed = 33 Knots	# Successful Approaches	5		5		5	
	$\bar{h}_{rms}$, σh_{rms} (ft)	0.53397	0.002546	0.2459	0.11468	0.12469	0.003935
	$\bar{\lambda}_{rms}$, $\sigma\lambda_{rms}$ (ft)	0.005042	0.001507	0.004399	0.000705	0.003496	0.000186
	$\bar{u}_{rms}$, σu_{rms} (kts)	0.12069	0.000429	0.23798	0.025627	0.094549	0.001301
	# Failed Approaches Vert	0		0		0	
	$\bar{t}_{td}$, σt_{td} (sec)	-	-	-	-	-	-
	$\bar{h}_{rms}$, σh_{rms} (ft)	-	-	-	-	-	-
	$\bar{\lambda}_{rms}$, $\sigma\lambda_{rms}$ (ft)	-	-	-	-	-	-
	$\bar{u}_{rms}$, σu_{rms} (kts)	-	-	-	-	-	-
	# Failed Approaches Lat	0		0		0	
	$\bar{t}_{td}$, σt_{td} (sec)	-	-	-	-	-	-
	$\bar{h}_{rms}$, σh_{rms} (ft)	-	-	-	-	-	-
	$\bar{\lambda}_{rms}$, $\sigma\lambda_{rms}$ (ft)	-	-	-	-	-	-
	$\bar{u}_{rms}$, σu_{rms} (kts)	-	-	-	-	-	-
	# Ramp Strikes	0		0		0	
	$\bar{h}_{td}$, σh_{td} (ft)	10.067	0.088658	9.1694	1.2575	8.7015	0.15917
	$\bar{h}_{sp}$, σh_{sp} (ft)	1.6548	0.02132	0.69089	1.3405	0.2244	0.012433
	$\bar{\theta}_{sp}$, $\sigma\theta_{sp}$ (deg)	0.009681	0.028621	0.033399	0.054136	0.032899	0.054665
	# Bolters	0		0		0	
	$\bar{X}_{td}$, σX_{td} (ft)	-	-	-	-	-	-
	$\bar{Y}_{td}$, σY_{td} (ft)	-	-	-	-	-	-
	# Successful Touchdowns	5		5		5	
	$\bar{X}_{td}$, σX_{td} (ft)	-11.1448	0.81794	0.070082	3.9375	0.33815	1.0228
	$\bar{Y}_{sp}$, σY_{sp} (ft)	-0.04418	0.02053	0.027107	0.055471	-0.01405	0.002716
	$\bar{h}_{td}$, σh_{td} (ft)	-11.5737	0.004109	-11.5744	3.4642	-10.0911	0.19688
	$\bar{h}_{sp}$, σh_{sp} (ft)	-0.038446	0.1784	0.14449	0.15462	0.11481	0.15541

Table B-7 Carrier Induced Turbulence Only – Wind 24.5 Knots

		Wind Speed = 37 Knots Carrier Induced Turbulence Only					
		System 1		System 2		System 3	
Carrier Speed = 0 Knots	# Successful Approaches	5		5		5	
	$\bar{h}$ rms, σh rms (ft)	0.8021	0.011113	0.59526	0.17189	0.26752	0.075124
	$\bar{\lambda}$ rms, $\sigma\lambda$ rms (ft)	0.041742	0.004173	0.021073	0.028556	0.006846	0.00082
	$\bar{u}$ rms, σu rms (kts)	0.21671	0.002944	0.21545	0.032942	0.16893	0.017557
	# Failed Approaches Vert	0		0		0	
	$\bar{t}_{td}$, σt_{td} (sec)	-	-	-	-	-	-
	$\bar{h}$ rms, σh rms (ft)	-	-	-	-	-	-
	$\bar{\lambda}$ rms, $\sigma\lambda$ rms (ft)	-	-	-	-	-	-
	$\bar{u}$ rms, σu rms (kts)	-	-	-	-	-	-
	# Failed Approaches Lat	0		0		0	
	$\bar{t}_{td}$, σt_{td} (sec)	-	-	-	-	-	-
	$\bar{h}$ rms, σh rms (ft)	-	-	-	-	-	-
	$\bar{\lambda}$ rms, $\sigma\lambda$ rms (ft)	-	-	-	-	-	-
	$\bar{u}$ rms, σu rms (kts)	-	-	-	-	-	-
	# Ramp Strikes	0		0		0	
	$\bar{h}_{td}$, σh_{td} (ft)	11.2605	0.63156	9.6187	2.7945	7.5611	0.70053
	$\bar{h}_{td}$, σh_{td} (ft)	2.7556	0.13402	1.7456	2.6425	-0.31266	0.43669
	$\bar{\theta}_{td}$, $\sigma\theta_{td}$ (deg)	0.042844	0.26311	-0.18339	0.124	-0.18314	0.12336
	# Bolters	0		1		0	
	$\bar{X}_{td}$, σX_{td} (ft)	-	-	84.831	0	-	-
	$\bar{Y}_{td}$, σY_{td} (ft)	-	-	-0.52769	0	-	-
	# Successful Touchdowns	5		4		5	
	$\bar{X}_{td}$, σX_{td} (ft)	-3.7371	0.38899	0.47227	34.1129	6.5494	11.0921
	$\bar{Y}_{td}$, σY_{td} (ft)	0.031143	0.084192	-0.45694	0.73352	0.1239	0.33719
	$\bar{h}_{t}$, σh_{t} (ft)	-10.8258	0.07717	-11.7977	4.4986	-8.1876	1.1315
	$\bar{h}_{td}$, σh_{td} (ft)	0.51808	1.4332	0.13189	0.69645	-0.040168	0.65713
Carrier Speed = 10Knots	# Successful Approaches	5		5		5	
	$\bar{h}$ rms, σh rms (ft)	0.86331	0.031991	0.64317	0.15944	0.30674	0.080391
	$\bar{\lambda}$ rms, $\sigma\lambda$ rms (ft)	0.035828	0.007854	0.020887	0.012994	0.005483	0.001074
	$\bar{u}$ rms, σu rms (kts)	0.23411	0.004054	0.22752	0.02363	0.1534	0.017171
	# Failed Approaches Vert	0		0		0	
	$\bar{t}_{td}$, σt_{td} (sec)	-	-	-	-	-	-
	$\bar{h}$ rms, σh rms (ft)	-	-	-	-	-	-
	$\bar{\lambda}$ rms, $\sigma\lambda$ rms (ft)	-	-	-	-	-	-
	$\bar{u}$ rms, σu rms (kts)	-	-	-	-	-	-
	# Failed Approaches Lat	0		0		0	
	$\bar{t}_{td}$, σt_{td} (sec)	-	-	-	-	-	-
	$\bar{h}$ rms, σh rms (ft)	-	-	-	-	-	-
	$\bar{\lambda}$ rms, $\sigma\lambda$ rms (ft)	-	-	-	-	-	-
	$\bar{u}$ rms, σu rms (kts)	-	-	-	-	-	-
	# Ramp Strikes	0		0		0	
	$\bar{h}_{td}$, σh_{td} (ft)	10.5679	0.50765	9.0955	1.2402	9.0363	0.8391
	$\bar{h}_{td}$, σh_{td} (ft)	2.1454	0.14801	0.40808	0.6808	0.34834	0.16378
	$\bar{\theta}_{td}$, $\sigma\theta_{td}$ (deg)	0.013363	0.21783	0.10822	0.24509	0.1084	0.24537
	# Bolters	0		0		0	
	$\bar{X}_{t}$, σX_{t} (ft)	-	-	-	-	-	-
	$\bar{Y}_{t}$, σY_{t} (ft)	-	-	-	-	-	-
	# Successful Touchdowns	5		5		5	
	$\bar{X}_{td}$, σX_{td} (ft)	-9.2699	1.4327	-1.7816	9.2599	-8.2642	6.1037
	$\bar{Y}_{td}$, σY_{td} (ft)	-0.00641	0.10115	-0.03546	0.48289	0.10909	0.14589
	$\bar{h}_{t}$, σh_{t} (ft)	-9.9869	0.086303	-9.7509	3.1143	-9.3331	0.73204
	$\bar{h}_{td}$, σh_{td} (ft)	-0.079632	1.2336	0.32912	0.64985	0.29827	0.62384
Carrier Speed = 33 Knots	# Successful Approaches	5		5		5	
	$\bar{h}$ rms, σh rms (ft)	1.1084	0.15042	0.68057	0.033945	0.32695	0.047624
	$\bar{\lambda}$ rms, $\sigma\lambda$ rms (ft)	0.069231	0.049594	0.040817	0.036528	0.007352	0.001225
	$\bar{u}$ rms, σu rms (kts)	0.31911	0.049932	0.66333	0.027901	0.47614	0.016945
	# Failed Approaches Vert	0		0		0	
	$\bar{t}_{td}$, σt_{td} (sec)	-	-	-	-	-	-
	$\bar{h}$ rms, σh rms (ft)	-	-	-	-	-	-
	$\bar{\lambda}$ rms, $\sigma\lambda$ rms (ft)	-	-	-	-	-	-
	$\bar{u}$ rms, σu rms (kts)	-	-	-	-	-	-
	# Failed Approaches Lat	0		0		0	
	$\bar{t}_{td}$, σt_{td} (sec)	-	-	-	-	-	-
	$\bar{h}$ rms, σh rms (ft)	-	-	-	-	-	-
	$\bar{\lambda}$ rms, $\sigma\lambda$ rms (ft)	-	-	-	-	-	-
	$\bar{u}$ rms, σu rms (kts)	-	-	-	-	-	-
	# Ramp Strikes	0		0		0	
	$\bar{h}_{td}$, σh_{td} (ft)	10.6205	0.73007	10.9472	1.6885	8.8781	0.6766
	$\bar{h}_{td}$, σh_{td} (ft)	2.1981	0.08422	2.6889	2.0602	0.61047	0.45987
	$\bar{\theta}_{td}$, $\sigma\theta_{td}$ (deg)	0.013314	0.28655	-0.04547	0.20335	-0.04212	0.19548
	# Bolters	0		0		0	
	$\bar{X}_{t}$, σX_{t} (ft)	-	-	-	-	-	-
	$\bar{Y}_{t}$, σY_{t} (ft)	-	-	-	-	-	-
	# Successful Touchdowns	5		5		5	
	$\bar{X}_{td}$, σX_{td} (ft)	-3.6408	0.9683	-3.2073	14.191	1.9962	2.9142
	$\bar{Y}_{td}$, σY_{td} (ft)	-0.05896	0.089616	0.48743	0.82319	-0.011	0.045825
	$\bar{h}_{t}$, σh_{t} (ft)	-13.7123	0.1244	-13.3899	2.3664	-10.9055	0.65771
	$\bar{h}_{td}$, σh_{td} (ft)	0.2103	0.96318	-0.35934	1.0874	-0.27486	0.95104

Table B-8 Carrier Induced Turbulence Only – Wind 37 Knots

		Wind Speed = 2 Knots Light Three Dimensional Turbulence and Carrier Induced Turbulence					
		System 1		System 2		System 3	
Carrier Speed = 0 Knots	# Successful Approaches	5		5		5	
	$\bar{h}$ rms, σh rms (ft)	0.75299	0.000633	0.53813	0.006489	0.28713	0.000484
	$\bar{\lambda}$ rms, $\sigma\lambda$ rms (ft)	0.095701	9.23E-05	0.47806	0.005048	0.22706	0.00061
	$\bar{u}$ rms, σu rms (kts)	0.15212	8.96E-05	0.23225	0.000718	0.21555	0.000116
	# Failed Approaches Vert	0		0		0	
	$\bar{t}_{td}$, σt_{td} (sec)	-	-	-	-	-	-
	$\bar{h}$ rms, σh rms (ft)	-	-	-	-	-	-
	$\bar{\lambda}$ rms, $\sigma\lambda$ rms (ft)	-	-	-	-	-	-
	$\bar{u}$ rms, σu rms (kts)	-	-	-	-	-	-
	# Failed Approaches Lat	0		0		0	
	$\bar{t}_{td}$, σt_{td} (sec)	-	-	-	-	-	-
	$\bar{h}$ rms, σh rms (ft)	-	-	-	-	-	-
	$\bar{\lambda}$ rms, $\sigma\lambda$ rms (ft)	-	-	-	-	-	-
	$\bar{u}$ rms, σu rms (kts)	-	-	-	-	-	-
	# Ramp Strikes	0		0		0	
	$\bar{h}_{td}$, σh_{td} (ft)	9.1767	0.036176	8.6401	0.15476	8.6184	0.031164
	$\bar{h}_{td}$, σh_{td} (ft)	0.81553	0.001788	0.27946	0.13868	0.25777	0.001308
	$\bar{\theta}_{td}$, $\sigma\theta_{td}$ (deg)	-0.00864	0.012803	-0.00881	0.010775	-0.00883	0.0107
	# Bolters	0		0		0	
	$\bar{X}_{td}$, σX_{td} (ft)	-	-	-	-	-	-
	$\bar{Y}_{td}$, σY_{td} (ft)	-	-	-	-	-	-
	# Successful Touchdowns	5		5		5	
	$\bar{X}_{td}$, σX_{td} (ft)	29.4622	0.83952	-7.9893	1.0274	-1	3.25E-05
	$\bar{Y}_{td}$, σY_{td} (ft)	0.41102	0.0021	3.944	0.055349	0.93575	0.000927
	$\bar{h}_{td}$, σh_{td} (ft)	-17.0079	0.011907	-9.9881	0.12231	-11.3559	0.003622
	$\bar{h}_{td}$, σh_{td} (ft)	-0.018104	0.085896	-0.028903	0.046459	-0.030378	0.047237
Carrier Speed = 10Knots	# Successful Approaches	5		5		5	
	$\bar{h}$ rms, σh rms (ft)	0.74338	0.000697	0.41633	0.007932	0.2851	0.001614
	$\bar{\lambda}$ rms, $\sigma\lambda$ rms (ft)	0.097437	4.39E-05	0.32705	0.007066	0.23107	0.000323
	$\bar{u}$ rms, σu rms (kts)	0.14928	0.000149	0.20719	0.000186	0.22074	0.000672
	# Failed Approaches Vert	0		0		0	
	$\bar{t}_{td}$, σt_{td} (sec)	-	-	-	-	-	-
	$\bar{h}$ rms, σh rms (ft)	-	-	-	-	-	-
	$\bar{\lambda}$ rms, $\sigma\lambda$ rms (ft)	-	-	-	-	-	-
	$\bar{u}$ rms, σu rms (kts)	-	-	-	-	-	-
	# Failed Approaches Lat	0		0		0	
	$\bar{t}_{td}$, σt_{td} (sec)	-	-	-	-	-	-
	$\bar{h}$ rms, σh rms (ft)	-	-	-	-	-	-
	$\bar{\lambda}$ rms, $\sigma\lambda$ rms (ft)	-	-	-	-	-	-
	$\bar{u}$ rms, σu rms (kts)	-	-	-	-	-	-
	# Ramp Strikes	0		0		0	
	$\bar{h}_{td}$, σh_{td} (ft)	8.3207	0.044232	8.2275	0.033068	8.289	0.029236
	$\bar{h}_{td}$, σh_{td} (ft)	-0.08573	0.00177	-0.17358	0.005877	-0.11212	0.001015
	$\bar{\theta}_{td}$, $\sigma\theta_{td}$ (deg)	0.007575	0.015431	0.005673	0.010657	0.005673	0.010657
	# Bolters	0		0		0	
	$\bar{X}_{td}$, σX_{td} (ft)	-	-	-	-	-	-
	$\bar{Y}_{td}$, σY_{td} (ft)	-	-	-	-	-	-
	# Successful Touchdowns	5		5		5	
	$\bar{X}_{td}$, σX_{td} (ft)	37.8586	0.94603	1.2384	0.10584	4.738	0.070506
	$\bar{Y}_{td}$, σY_{td} (ft)	0.34815	0.010769	1.2287	0.025061	0.90144	0.002004
	$\bar{h}_{td}$, σh_{td} (ft)	-16.4626	0.030914	-12.159	0.022386	-12.3154	0.005308
	$\bar{h}_{td}$, σh_{td} (ft)	0.05318	0.057053	0.04035	0.071309	0.0402	0.071561
Carrier Speed = 33 Knots	# Successful Approaches	5		5		5	
	$\bar{h}$ rms, σh rms (ft)	0.74033	0.001176	0.32418	0.011444	0.2661	0.005313
	$\bar{\lambda}$ rms, $\sigma\lambda$ rms (ft)	0.10049	0.000226	0.17351	0.012257	0.21449	0.002898
	$\bar{u}$ rms, σu rms (kts)	0.14947	0.000113	0.17989	0.003567	0.19216	0.006645
	# Failed Approaches Vert	0		0		0	
	$\bar{t}_{td}$, σt_{td} (sec)	-	-	-	-	-	-
	$\bar{h}$ rms, σh rms (ft)	-	-	-	-	-	-
	$\bar{\lambda}$ rms, $\sigma\lambda$ rms (ft)	-	-	-	-	-	-
	$\bar{u}$ rms, σu rms (kts)	-	-	-	-	-	-
	# Failed Approaches Lat	0		0		0	
	$\bar{t}_{td}$, σt_{td} (sec)	-	-	-	-	-	-
	$\bar{h}$ rms, σh rms (ft)	-	-	-	-	-	-
	$\bar{\lambda}$ rms, $\sigma\lambda$ rms (ft)	-	-	-	-	-	-
	$\bar{u}$ rms, σu rms (kts)	-	-	-	-	-	-
	# Ramp Strikes	0		0		0	
	$\bar{h}_{td}$, σh_{td} (ft)	8.3224	0.014372	8.0356	0.058858	8.1445	0.012864
	$\bar{h}_{td}$, σh_{td} (ft)	-0.05467	0.000526	-0.34158	0.058947	-0.23254	0.006178
	$\bar{\theta}_{td}$, $\sigma\theta_{td}$ (deg)	-0.00291	0.00498	-0.00289	0.002964	-0.00293	0.002993
	# Bolters	0		0		0	
	$\bar{X}_{td}$, σX_{td} (ft)	-	-	-	-	-	-
	$\bar{Y}_{td}$, σY_{td} (ft)	-	-	-	-	-	-
	# Successful Touchdowns	5		5		5	
	$\bar{X}_{td}$, σX_{td} (ft)	23.9838	0.009645	4.9859	0.46637	5.8395	0.27807
	$\bar{Y}_{td}$, σY_{td} (ft)	0.3876	0.000294	0.90582	0.013625	0.8875	0.00235
	$\bar{h}_{td}$, σh_{td} (ft)	-16.7362	0.005049	-12.6603	0.073121	-12.4196	0.02608
	$\bar{h}_{td}$, σh_{td} (ft)	-0.009052	0.020977	-0.008312	0.036101	-0.007884	0.036725

Table B-9 Light Turbulence 3D and Carrier Induced Turbulence – Wind 2 Knots

		Wind Speed = 13.5 Knots Light Three Dimensional Turbulence and Carrier Induced Turbulence					
		System 1		System 2		System 3	
Carrier Speed = 0 Knots	# Successful Approaches	5		5		5	
	$\bar{h}_w$ rms, σh_w rms (ft)	0.93892	0.004821	0.54081	0.034488	0.28676	0.000959
	$\bar{\lambda}_w$ rms, $\sigma\lambda_w$ rms (ft)	0.049725	0.000608	0.25202	0.002993	0.22	0.001788
	$\bar{u}_w$ rms, σu_w rms (kts)	0.2228	0.001604	0.24582	0.000769	0.21781	0.000417
	# Failed Approaches Vert	0		0		0	
	$\bar{t}_{td}$, σt_{td} (sec)	-	-	-	-	-	-
	$\bar{h}_w$ rms, σh_w rms (ft)	-	-	-	-	-	-
	$\bar{\lambda}_w$ rms, $\sigma\lambda_w$ rms (ft)	-	-	-	-	-	-
	$\bar{u}_w$ rms, σu_w rms (kts)	-	-	-	-	-	-
	# Failed Approaches Lat	0		0		0	
	$\bar{t}_{td}$, σt_{td} (sec)	-	-	-	-	-	-
	$\bar{h}_w$ rms, σh_w rms (ft)	-	-	-	-	-	-
	$\bar{\lambda}_w$ rms, $\sigma\lambda_w$ rms (ft)	-	-	-	-	-	-
	$\bar{u}_w$ rms, σu_w rms (kts)	-	-	-	-	-	-
	# Ramp Strikes	0		0		0	
	$\bar{h}_d$, σh_d (ft)	9.0277	0.061403	9.3935	0.29713	8.5316	0.069463
	$\bar{h}_{dz}$, σh_{dz} (ft)	0.65195	0.011233	0.97269	0.24686	0.11099	0.008713
	$\bar{\theta}_{dz}$, $\sigma\theta_{dz}$ (deg)	-0.00339	0.025352	0.012734	0.022068	0.012651	0.022039
	# Bolters	0		0		0	
	$\bar{X}_d$, σX_d (ft)	-	-	-	-	-	-
	$\bar{Y}_d$, σY_d (ft)	-	-	-	-	-	-
	# Successful Touchdowns	5		5		5	
	$\bar{X}_d$, σX_d (ft)	-29.5646	1.4282	-2.3286	1.6252	3.3538	0.38395
	$\bar{Y}_{dz}$, σY_{dz} (ft)	0.51071	0.002732	1.3303	0.17894	0.93643	0.005322
	$\bar{h}_d$, σh_d (ft)	-9.2736	0.091993	-9.3702	0.19064	-11.2143	0.037638
	$\bar{h}_{dz}$, σh_{dz} (ft)	-0.076416	0.27208	-0.032597	0.04627	-0.020831	0.029861
Carrier Speed = 10Knots	# Successful Approaches	5		5		5	
	$\bar{h}_w$ rms, σh_w rms (ft)	0.95265	0.004647	0.42854	0.031929	0.29036	0.00271
	$\bar{\lambda}_w$ rms, $\sigma\lambda_w$ rms (ft)	0.051039	0.000901	0.32962	0.081708	0.22081	0.004408
	$\bar{u}_w$ rms, σu_w rms (kts)	0.22306	0.000502	0.21734	0.017458	0.22636	0.000776
	# Failed Approaches Vert	0		0		0	
	$\bar{t}_{td}$, σt_{td} (sec)	-	-	-	-	-	-
	$\bar{h}_w$ rms, σh_w rms (ft)	-	-	-	-	-	-
	$\bar{\lambda}_w$ rms, $\sigma\lambda_w$ rms (ft)	-	-	-	-	-	-
	$\bar{u}_w$ rms, σu_w rms (kts)	-	-	-	-	-	-
	# Failed Approaches Lat	0		0		0	
	$\bar{t}_{td}$, σt_{td} (sec)	-	-	-	-	-	-
	$\bar{h}_w$ rms, σh_w rms (ft)	-	-	-	-	-	-
	$\bar{\lambda}_w$ rms, $\sigma\lambda_w$ rms (ft)	-	-	-	-	-	-
	$\bar{u}_w$ rms, σu_w rms (kts)	-	-	-	-	-	-
	# Ramp Strikes	0		0		0	
	$\bar{h}_d$, σh_d (ft)	7.2294	0.054826	8.3926	0.066171	8.3834	0.054988
	$\bar{h}_{dz}$, σh_{dz} (ft)	-1.1234	0.001718	-0.00428	0.028566	-0.01382	0.012504
	$\bar{\theta}_{dz}$, $\sigma\theta_{dz}$ (deg)	-0.0116	0.01944	0.004172	0.016909	0.004283	0.016748
	# Bolters	5		0		0	
	$\bar{X}_d$, σX_d (ft)	97.7432	5.1377	-	-	-	-
	$\bar{Y}_d$, σY_d (ft)	0.54321	0.026737	-	-	-	-
	# Successful Touchdowns	0		5		5	
	$\bar{X}_d$, σX_d (ft)	-	-	1.9417	2.9355	6.2805	0.60443
	$\bar{Y}_{dz}$, σY_{dz} (ft)	-	-	1.3779	0.4197	0.88805	0.010179
	$\bar{h}_d$, σh_d (ft)	-	-	-11.2131	0.33282	-11.5404	0.020256
	$\bar{h}_{dz}$, σh_{dz} (ft)	-	-	0.07946	0.15468	0.06908	0.16754
Carrier Speed = 33 Knots	# Successful Approaches	5		5		5	
	$\bar{h}_w$ rms, σh_w rms (ft)	1.0453	0.001444	0.62804	0.038807	0.28089	0.004364
	$\bar{\lambda}_w$ rms, $\sigma\lambda_w$ rms (ft)	0.067737	0.000995	0.39542	0.090221	0.29092	0.005242
	$\bar{u}_w$ rms, σu_w rms (kts)	0.20656	0.000304	0.33728	0.009391	0.18235	0.001962
	# Failed Approaches Vert	0		0		0	
	$\bar{t}_{td}$, σt_{td} (sec)	-	-	-	-	-	-
	$\bar{h}_w$ rms, σh_w rms (ft)	-	-	-	-	-	-
	$\bar{\lambda}_w$ rms, $\sigma\lambda_w$ rms (ft)	-	-	-	-	-	-
	$\bar{u}_w$ rms, σu_w rms (kts)	-	-	-	-	-	-
	# Failed Approaches Lat	0		0		0	
	$\bar{t}_{td}$, σt_{td} (sec)	-	-	-	-	-	-
	$\bar{h}_w$ rms, σh_w rms (ft)	-	-	-	-	-	-
	$\bar{\lambda}_w$ rms, $\sigma\lambda_w$ rms (ft)	-	-	-	-	-	-
	$\bar{u}_w$ rms, σu_w rms (kts)	-	-	-	-	-	-
	# Ramp Strikes	0		0		0	
	$\bar{h}_d$, σh_d (ft)	8.5804	0.029117	8.4782	0.85199	7.7383	0.02992
	$\bar{h}_{dz}$, σh_{dz} (ft)	0.20814	0.003687	0.090439	0.86081	-0.64898	0.007628
	$\bar{\theta}_{dz}$, $\sigma\theta_{dz}$ (deg)	-0.00464	0.010269	0.000909	0.01017	0.000714	0.0102
	# Bolters	0		0		0	
	$\bar{X}_d$, σX_d (ft)	-	-	-	-	-	-
	$\bar{Y}_d$, σY_d (ft)	-	-	-	-	-	-
	# Successful Touchdowns	5		5		5	
	$\bar{X}_d$, σX_d (ft)	-31.8684	0.039636	4.644	10.0829	-2.7107	0.33528
	$\bar{Y}_{dz}$, σY_{dz} (ft)	0.34676	0.003095	1.7692	1.2264	1.8633	0.015725
	$\bar{h}_d$, σh_d (ft)	-17.4238	0.008921	-10.6792	1.7873	-8.7437	0.025338
	$\bar{h}_{dz}$, σh_{dz} (ft)	0.00199	0.034707	0.04615	0.054412	0.03071	0.043428

Table B-10 Light Turbulence 3D and Carrier Induced Turbulence – Wind 13.5 Knots

		Wind Speed = 24.5 Knots Light Three Dimensional Turbulence and Carrier Induced Turbulence					
		System 1		System 2		System 3	
Carrier Speed = 0 Knots	# Successful Approaches	5		5		5	
	$\bar{h}_{ac}$ rms, σh_{ac} rms (ft)	1.4143	0.006273	0.55588	0.045056	0.29331	0.005423
	$\bar{\lambda}_{ac}$ rms, $\sigma\lambda_{ac}$ rms (ft)	0.20498	0.009597	0.21522	0.024996	0.19663	0.007426
	$\bar{u}_{ac}$ rms, σu_{ac} rms (kts)	0.30098	0.001957	0.26312	0.007925	0.22418	0.002717
	# Failed Approaches Vert	0		0		0	
	$\bar{t}_{td}$, σt_{td} (sec)	-	-	-	-	-	-
	$\bar{h}_{ac}$ rms, σh_{ac} rms (ft)	-	-	-	-	-	-
	$\bar{\lambda}_{ac}$ rms, $\sigma\lambda_{ac}$ rms (ft)	-	-	-	-	-	-
	$\bar{u}_{ac}$ rms, σu_{ac} rms (kts)	-	-	-	-	-	-
	# Failed Approaches Lat	0		0		0	
	$\bar{t}_{td}$, σt_{td} (sec)	-	-	-	-	-	-
	$\bar{h}_{ac}$ rms, σh_{ac} rms (ft)	-	-	-	-	-	-
	$\bar{\lambda}_{ac}$ rms, $\sigma\lambda_{ac}$ rms (ft)	-	-	-	-	-	-
	$\bar{u}_{ac}$ rms, σu_{ac} rms (kts)	-	-	-	-	-	-
	# Ramp Strikes	0		0		0	
	$\bar{h}_{td}$, σh_{td} (ft)	8.6486	0.28492	10.5568	0.43641	8.5493	0.22112
	$\bar{h}_{ac}$, σh_{ac} (ft)	0.10549	0.026	2.0491	0.43673	0.042782	0.034691
	$\bar{\theta}_{ac}$, $\sigma\theta_{ac}$ (deg)	0.056542	0.1087	0.043846	0.069116	0.043412	0.069347
	# Bolters	0		0		0	
	$\bar{X}_{td}$, σX_{td} (ft)	-	-	-	-	-	-
	$\bar{Y}_{td}$, σY_{td} (ft)	-	-	-	-	-	-
	# Successful Touchdowns	5		5		5	
	$\bar{X}_{td}$, σX_{td} (ft)	-33.6716	3.5848	0.60598	1.2817	4.2681	0.70009
	$\bar{Y}_{td}$, σY_{td} (ft)	1.913	0.063792	0.86257	0.42579	0.9492	0.034925
	$\bar{h}_{td}$, σh_{td} (ft)	-12.0607	0.067105	-9.3434	0.67426	-10.0018	0.34228
	$\bar{h}_{ac}$, σh_{ac} (ft)	0.15023	0.41121	0.037447	0.064157	-0.11357	0.33444
Carrier Speed = 10Knots	# Successful Approaches	0		5		5	
	$\bar{h}_{ac}$ rms, σh_{ac} rms (ft)	-	-	0.6165	0.12496	0.3342	0.011278
	$\bar{\lambda}_{ac}$ rms, $\sigma\lambda_{ac}$ rms (ft)	-	-	0.76066	0.077646	0.52903	0.008338
	$\bar{u}_{ac}$ rms, σu_{ac} rms (kts)	-	-	0.2396	0.016106	0.1987	0.0056
	# Failed Approaches Vert	5		0		0	
	$\bar{t}_{td}$, σt_{td} (sec)	6.1343	0.039347	-	-	-	-
	$\bar{h}_{ac}$ rms, σh_{ac} rms (ft)	1.2891	0.008184	-	-	-	-
	$\bar{\lambda}_{ac}$ rms, $\sigma\lambda_{ac}$ rms (ft)	0.087176	0.006666	-	-	-	-
	$\bar{u}_{ac}$ rms, σu_{ac} rms (kts)	0.30198	0.005602	-	-	-	-
	# Failed Approaches Lat	0		0		0	
	$\bar{t}_{td}$, σt_{td} (sec)	-	-	-	-	-	-
	$\bar{h}_{ac}$ rms, σh_{ac} rms (ft)	-	-	-	-	-	-
	$\bar{\lambda}_{ac}$ rms, $\sigma\lambda_{ac}$ rms (ft)	-	-	-	-	-	-
	$\bar{u}_{ac}$ rms, σu_{ac} rms (kts)	-	-	-	-	-	-
	# Ramp Strikes	0		0		0	
	$\bar{h}_{td}$, σh_{td} (ft)	-	-	9.6153	0.77388	8.8357	0.34041
	$\bar{h}_{ac}$, σh_{ac} (ft)	-	-	1.3209	0.86261	0.54174	0.1119
	$\bar{\theta}_{ac}$, $\sigma\theta_{ac}$ (deg)	-	-	-0.03254	0.08687	-0.0327	0.086955
	# Bolters	0		0		0	
	$\bar{X}_{td}$, σX_{td} (ft)	-	-	-	-	-	-
	$\bar{Y}_{td}$, σY_{td} (ft)	-	-	-	-	-	-
	# Successful Touchdowns	0		5		5	
	$\bar{X}_{td}$, σX_{td} (ft)	-	-	2.2391	16.1087	-9.5521	1.4894
	$\bar{Y}_{td}$, σY_{td} (ft)	-	-	3.192	1.9239	0.17427	0.053642
	$\bar{h}_{td}$, σh_{td} (ft)	-	-	-15.8075	1.493	-10.7064	0.16136
	$\bar{h}_{ac}$, σh_{ac} (ft)	-	-	0.03108	0.57377	0.0321	0.52944
Carrier Speed = 33 Knots	# Successful Approaches	5		5		5	
	$\bar{h}_{ac}$ rms, σh_{ac} rms (ft)	1.476	0.004965	0.63298	0.021327	0.28434	0.013287
	$\bar{\lambda}_{ac}$ rms, $\sigma\lambda_{ac}$ rms (ft)	0.2572	0.002286	0.37337	0.035684	0.27662	0.005571
	$\bar{u}_{ac}$ rms, σu_{ac} rms (kts)	0.30219	0.002482	0.32404	0.014637	0.18204	0.00401
	# Failed Approaches Vert	0		0		0	
	$\bar{t}_{td}$, σt_{td} (sec)	-	-	-	-	-	-
	$\bar{h}_{ac}$ rms, σh_{ac} rms (ft)	-	-	-	-	-	-
	$\bar{\lambda}_{ac}$ rms, $\sigma\lambda_{ac}$ rms (ft)	-	-	-	-	-	-
	$\bar{u}_{ac}$ rms, σu_{ac} rms (kts)	-	-	-	-	-	-
	# Failed Approaches Lat	0		0		0	
	$\bar{t}_{td}$, σt_{td} (sec)	-	-	-	-	-	-
	$\bar{h}_{ac}$ rms, σh_{ac} rms (ft)	-	-	-	-	-	-
	$\bar{\lambda}_{ac}$ rms, $\sigma\lambda_{ac}$ rms (ft)	-	-	-	-	-	-
	$\bar{u}_{ac}$ rms, σu_{ac} rms (kts)	-	-	-	-	-	-
	# Ramp Strikes	0		0		0	
	$\bar{h}_{td}$, σh_{td} (ft)	9.4625	0.087802	8.7153	0.49949	8.013	0.23527
	$\bar{h}_{ac}$, σh_{ac} (ft)	1.0495	0.008827	0.23723	0.62907	-0.4632	0.080958
	$\bar{\theta}_{ac}$, $\sigma\theta_{ac}$ (deg)	0.009912	0.02867	0.033256	0.054257	0.032564	0.055278
	# Bolters	0		0		0	
	$\bar{X}_{td}$, σX_{td} (ft)	-	-	-	-	-	-
	$\bar{Y}_{td}$, σY_{td} (ft)	-	-	-	-	-	-
	# Successful Touchdowns	5		5		5	
	$\bar{X}_{td}$, σX_{td} (ft)	-37.4475	0.94437	-1.2803	1.7172	-4.1928	1.4879
	$\bar{Y}_{td}$, σY_{td} (ft)	1.9571	0.019262	3.2859	0.67953	1.8235	0.035436
	$\bar{h}_{td}$, σh_{td} (ft)	-12.4017	0.029948	-10.5456	1.1009	-9.2665	0.43663
	$\bar{h}_{ac}$, σh_{ac} (ft)	-0.039169	0.19303	0.08573	0.15908	0.15038	0.17196

Table B-11 Light Turbulence 3D and Carrier Induced Turbulence – Wind 24.5 Knots

		Wind Speed = 37 Knots Light Three Dimensional Turbulence and Carrier Induced Turbulence					
		System 1		System 2		System 3	
Carrier Speed = 0 Knots	# Successful Approaches	5		5		5	
	$\bar{h}$, rms, σh, rms (ft)	1.7447	0.023923	0.73648	0.12313	0.46406	0.018419
	$\bar{\lambda}$, rms, $\sigma\lambda$, rms (ft)	2.2156	0.28796	0.26634	0.092103	0.20119	0.046091
	$\bar{u}$, rms, σu, rms (kts)	0.38894	0.00798	0.26986	0.012828	0.2518	0.005207
	# Failed Approaches Vert	0		0		0	
	$\bar{t}_{td}$, σt_{td} (sec)	-	-	-	-	-	-
	$\bar{h}$, rms, σh, rms (ft)	-	-	-	-	-	-
	$\bar{\lambda}$, rms, $\sigma\lambda$, rms (ft)	-	-	-	-	-	-
	$\bar{u}$, rms, σu, rms (kts)	-	-	-	-	-	-
	# Failed Approaches Lat	0		0		0	
	$\bar{t}_{td}$, σt_{td} (sec)	-	-	-	-	-	-
	$\bar{h}$, rms, σh, rms (ft)	-	-	-	-	-	-
	$\bar{\lambda}$, rms, $\sigma\lambda$, rms (ft)	-	-	-	-	-	-
	$\bar{u}$, rms, σu, rms (kts)	-	-	-	-	-	-
	# Ramp Strikes	0		0		0	
	$\bar{h}_d$, σh_d (ft)	6.3937	0.71996	8.9805	1.9337	7.9724	0.68446
	$\bar{h}_{ac}$, σh_{ac} (ft)	-2.1345	0.077304	1.1091	1.748	0.099058	0.39711
	$\bar{\theta}_{ac}$, $\sigma\theta_{ac}$ (deg)	0.051219	0.2783	-0.18401	0.12437	-0.18332	0.12404
	# Bolters	0		1		0	
	$\bar{X}_d$, σX_d (ft)	-	-	97.5187	0	-	-
	$\bar{Y}_d$, σY_d (ft)	-	-	1.2586	0	-	-
	# Successful Touchdowns	5		4		5	
	$\bar{X}_d$, σX_d (ft)	-77.2127	17.294	1.0548	43.4578	-4.8024	18.605
	$\bar{Y}_{td}$, σY_d (ft)	0.95637	0.51573	1.4731	1.2829	0.55944	0.43015
	$\bar{h}_d$, σh (ft)	-12.2668	0.88136	-11.6752	2.6364	-7.5894	0.46166
	$\bar{h}_{ac}$, σh_{ac} (ft)	0.56021	1.2624	0.19992	0.77282	0.05762	0.74408
Carrier Speed = 10Knots	# Successful Approaches	0		3		5	
	$\bar{h}$, rms, σh, rms (ft)	-	-	0.76645	0.11623	0.87974	0.26831
	$\bar{\lambda}$, rms, $\sigma\lambda$, rms (ft)	-	-	1.5178	0.56168	1.5719	0.44252
	$\bar{u}_s$, rms, σu_s, rms (kts)	-	-	0.42754	0.032511	0.57214	0.10992
	# Failed Approaches Vert	0		0		0	
	$\bar{t}_{td}$, σt_{td} (sec)	-	-	-	-	-	-
	$\bar{h}$, rms, σh, rms (ft)	-	-	-	-	-	-
	$\bar{\lambda}$, rms, $\sigma\lambda$, rms (ft)	-	-	-	-	-	-
	$\bar{u}_s$, rms, σu_s, rms (kts)	-	-	-	-	-	-
	# Failed Approaches Lat	5		2		0	
	$\bar{t}_{td}$, σt_{td} (sec)	9.5547	0.1837	6.9715	0.28503	-	-
	$\bar{h}$, rms, σh, rms (ft)	1.5916	0.01186	0.6146	0.086161	-	-
	$\bar{\lambda}$, rms, $\sigma\lambda$, rms (ft)	2.0373	0.013287	1.3866	0.1171	-	-
	$\bar{u}_s$, rms, σu_s, rms (kts)	0.38649	0.009394	0.40982	0.009432	-	-
	# Ramp Strikes	0		0		0	
	$\bar{h}_d$, σh_d (ft)	-	-	8.4398	0.14439	8.0611	0.70966
	$\bar{h}_{ac}$, σh_{ac} (ft)	-	-	0.37472	0.59573	-0.47658	0.58547
	$\bar{\theta}_{ac}$, $\sigma\theta_{ac}$ (deg)	-	-	-0.11466	0.21963	0.054572	0.28374
	# Bolters	0		0		0	
	$\bar{X}_d$, σX_d (ft)	-	-	-	-	-	-
	$\bar{Y}_d$, σY_d (ft)	-	-	-	-	-	-
	# Successful Touchdowns	0		3		5	
	$\bar{X}_d$, σX_d (ft)	-	-	24.6896	20.9166	9.4889	3.0967
	$\bar{Y}_{td}$, σY_d (ft)	-	-	-0.58994	0.79492	-0.6567	0.84053
	$\bar{h}_d$, σh (ft)	-	-	-8.7543	3.43	-8.9542	1.218
	$\bar{h}_{ac}$, σh_{ac} (ft)	-	-	-0.49169	1.46	-0.75949	1.3929
Carrier Speed = 33 Knots	# Successful Approaches	0		5		5	
	$\bar{h}$, rms, σh, rms (ft)	-	-	1.0123	0.26398	0.39639	0.031626
	$\bar{\lambda}$, rms, $\sigma\lambda$, rms (ft)	-	-	0.33879	0.11641	0.30723	0.011874
	$\bar{u}_s$, rms, σu_s, rms (kts)	-	-	0.71805	0.057495	0.51986	0.03313
	# Failed Approaches Vert	0		0		0	
	$\bar{t}_{td}$, σt_{td} (sec)	-	-	-	-	-	-
	$\bar{h}$, rms, σh, rms (ft)	-	-	-	-	-	-
	$\bar{\lambda}$, rms, $\sigma\lambda$, rms (ft)	-	-	-	-	-	-
	$\bar{u}_s$, rms, σu_s, rms (kts)	-	-	-	-	-	-
	# Failed Approaches Lat	5		0		0	
	$\bar{t}_{td}$, σt_{td} (sec)	7.7895	0.065863	-	-	-	-
	$\bar{h}$, rms, σh, rms (ft)	1.7751	0.041954	-	-	-	-
	$\bar{\lambda}$, rms, $\sigma\lambda$, rms (ft)	1.6395	0.079805	-	-	-	-
	$\bar{u}_s$, rms, σu_s, rms (kts)	0.42678	0.021603	-	-	-	-
	# Ramp Strikes	0		0		0	
	$\bar{h}_d$, σh_d (ft)	-	-	11.3726	2.5473	9.467	0.32262
	$\bar{h}_{ac}$, σh_{ac} (ft)	-	-	3.1126	2.1599	1.1979	0.25901
	$\bar{\theta}_{ac}$, $\sigma\theta_{ac}$ (deg)	-	-	-0.04482	0.20207	-0.04158	0.19502
	# Bolters	0		0		0	
	$\bar{X}_d$, σX_d (ft)	-	-	-	-	-	-
	$\bar{Y}_d$, σY_d (ft)	-	-	-	-	-	-
	# Successful Touchdowns	0		5		5	
	$\bar{X}_d$, σX_d (ft)	-	-	5.3734	29.3842	3.3941	2.1108
	$\bar{Y}_{td}$, σY_d (ft)	-	-	-1.5181	1.0626	-0.10393	0.059159
	$\bar{h}_d$, σh (ft)	-	-	-12.3413	3.2081	-9.3433	0.25602
	$\bar{h}_{ac}$, σh_{ac} (ft)	-	-	-0.32452	0.98357	-0.2554	0.93223

Table B-12 Light Turbulence 3D and Carrier Induced Turbulence – Wind 37 Knots

		Wind Speed = 2 Knots Light Two Dimensional Turbulence and Carrier Induced Turbulence					
		System 1		System 2		System 3	
Carrier Speed = 0 Knots	# Successful Approaches	5		5		5	
	$\bar{h}_w$ rms, σh_w rms (ft)	0.76093	0.00049	0.536	0.006043	0.28956	0.000584
	$\bar{\lambda}_w$ rms, $\sigma\lambda_w$ rms (ft)	0.000114	1.40E-05	0.000597	0.000381	0.000156	5.66E-06
	$\bar{u}_w$ rms, σu_w rms (kts)	0.15357	9.98E-05	0.23266	0.000376	0.21666	0.000143
	# Failed Approaches Vert	0		0		0	
	$\bar{t}_{td}$, σt_{td} (sec)	-	-	-	-	-	-
	$\bar{h}_w$ rms, σh_w rms (ft)	-	-	-	-	-	-
	$\bar{\lambda}_w$ rms, $\sigma\lambda_w$ rms (ft)	-	-	-	-	-	-
	$\bar{u}_w$ rms, σu_w rms (kts)	-	-	-	-	-	-
	# Failed Approaches Lat	0		0		0	
	$\bar{t}_{td}$, σt_{td} (sec)	-	-	-	-	-	-
	$\bar{h}_w$ rms, σh_w rms (ft)	-	-	-	-	-	-
	$\bar{\lambda}_w$ rms, $\sigma\lambda_w$ rms (ft)	-	-	-	-	-	-
	$\bar{u}_w$ rms, σu_w rms (kts)	-	-	-	-	-	-
	# Ramp Strikes	0		0		0	
	$\bar{h}_d$, σh_d (ft)	9.2215	0.036026	8.4745	0.11249	8.6336	0.031171
	$\bar{h}_{dy}$, σh_{dy} (ft)	0.86041	0.001859	0.11382	0.092451	0.27305	0.00135
	$\bar{\theta}_{dy}$, $\sigma\theta_{dy}$ (deg)	-0.00864	0.012803	-0.00881	0.010775	-0.00883	0.0107
	# Bolters	0		0		0	
	$\bar{X}_d$, σX_d (ft)	-	-	-	-	-	-
	$\bar{Y}_d$, σY_d (ft)	-	-	-	-	-	-
	# Successful Touchdowns	5		5		5	
	$\bar{X}_d$, σX_d (ft)	30.0683	0.31814	-7.6874	0.041976	-1	2.46E-05
	$\bar{Y}_{dy}$, σY_d (ft)	0.032666	0.021505	0.021781	0.010876	0.003876	0.000484
	$\bar{h}_d$, σh_d (ft)	-17.0526	0.002568	-9.7378	0.059312	-11.3818	0.003964
	$\bar{h}_{dy}$, σh_{dy} (ft)	-0.019481	0.083089	-0.029872	0.048141	-0.030103	0.046166
Carrier Speed = 10Knots	# Successful Approaches	5		5		5	
	$\bar{h}_w$ rms, σh_w rms (ft)	0.75096	0.00036	0.41744	0.007495	0.28737	0.002062
	$\bar{\lambda}_w$ rms, $\sigma\lambda_w$ rms (ft)	0.000174	2.22E-06	0.000425	4.78E-05	0.000166	7.16E-06
	$\bar{u}_w$ rms, σu_w rms (kts)	0.15073	0.000139	0.2071	0.000329	0.22166	0.000472
	# Failed Approaches Vert	0		0		0	
	$\bar{t}_{td}$, σt_{td} (sec)	-	-	-	-	-	-
	$\bar{h}_w$ rms, σh_w rms (ft)	-	-	-	-	-	-
	$\bar{\lambda}_w$ rms, $\sigma\lambda_w$ rms (ft)	-	-	-	-	-	-
	$\bar{u}_w$ rms, σu_w rms (kts)	-	-	-	-	-	-
	# Failed Approaches Lat	0		0		0	
	$\bar{t}_{td}$, σt_{td} (sec)	-	-	-	-	-	-
	$\bar{h}_w$ rms, σh_w rms (ft)	-	-	-	-	-	-
	$\bar{\lambda}_w$ rms, $\sigma\lambda_w$ rms (ft)	-	-	-	-	-	-
	$\bar{u}_w$ rms, σu_w rms (kts)	-	-	-	-	-	-
	# Ramp Strikes	0		0		0	
	$\bar{h}_d$, σh_d (ft)	8.3789	0.044651	8.2282	0.033224	8.2848	0.029684
	$\bar{h}_{dy}$, σh_{dy} (ft)	-0.02753	0.002122	-0.17289	0.006444	-0.1163	0.000847
	$\bar{\theta}_{dy}$, $\sigma\theta_{dy}$ (deg)	0.007575	0.015431	0.005673	0.010657	0.005673	0.010657
	# Bolters	0		0		0	
	$\bar{X}_d$, σX_d (ft)	-	-	-	-	-	-
	$\bar{Y}_d$, σY_d (ft)	-	-	-	-	-	-
	# Successful Touchdowns	5		5		5	
	$\bar{X}_d$, σX_d (ft)	38.1067	1.1677	1.8712	0.05245	5.3021	1.1549
	$\bar{Y}_{dy}$, σY_d (ft)	0.065648	0.013443	0.01259	0.003504	0.065126	0.00996
	$\bar{h}_d$, σh_d (ft)	-16.5129	0.037739	-12.1596	0.019823	-12.371	0.020644
	$\bar{h}_{dy}$, σh_{dy} (ft)	0.05338	0.057332	0.03991	0.053861	0.03323	0.065371
Carrier Speed = 33 Knots	# Successful Approaches	5		5		5	
	$\bar{h}_w$ rms, σh_w rms (ft)	0.74877	0.000377	0.33125	0.041145	0.27174	0.007949
	$\bar{\lambda}_w$ rms, $\sigma\lambda_w$ rms (ft)	0.000177	1.03E-06	0.000219	2.96E-05	0.000203	1.64E-05
	$\bar{u}_w$ rms, σu_w rms (kts)	0.15061	0.000201	0.18202	0.008634	0.19361	0.004028
	# Failed Approaches Vert	0		0		0	
	$\bar{t}_{td}$, σt_{td} (sec)	-	-	-	-	-	-
	$\bar{h}_w$ rms, σh_w rms (ft)	-	-	-	-	-	-
	$\bar{\lambda}_w$ rms, $\sigma\lambda_w$ rms (ft)	-	-	-	-	-	-
	$\bar{u}_w$ rms, σu_w rms (kts)	-	-	-	-	-	-
	# Failed Approaches Lat	0		0		0	
	$\bar{t}_{td}$, σt_{td} (sec)	-	-	-	-	-	-
	$\bar{h}_w$ rms, σh_w rms (ft)	-	-	-	-	-	-
	$\bar{\lambda}_w$ rms, $\sigma\lambda_w$ rms (ft)	-	-	-	-	-	-
	$\bar{u}_w$ rms, σu_w rms (kts)	-	-	-	-	-	-
	# Ramp Strikes	0		0		0	
	$\bar{h}_d$, σh_d (ft)	8.3591	0.014812	8.0351	0.097079	8.1329	0.010004
	$\bar{h}_{dy}$, σh_{dy} (ft)	-0.01802	0.001983	-0.342	0.094059	-0.24417	0.00501
	$\bar{\theta}_{dy}$, $\sigma\theta_{dy}$ (deg)	-0.00291	0.00498	-0.00293	0.002998	-0.00291	0.003001
	# Bolters	0		0		0	
	$\bar{X}_d$, σX_d (ft)	-	-	-	-	-	-
	$\bar{Y}_d$, σY_d (ft)	-	-	-	-	-	-
	# Successful Touchdowns	5		5		5	
	$\bar{X}_d$, σX_d (ft)	23.818	0.006299	4.6928	0.58465	6.3659	0.48465
	$\bar{Y}_{dy}$, σY_d (ft)	-0.04942	0.002973	0.013069	0.01034	0.01707	0.007618
	$\bar{h}_d$, σh_d (ft)	-16.7684	0.002565	-12.6363	0.069451	-12.37	0.010753
	$\bar{h}_{dy}$, σh_{dy} (ft)	-0.008898	0.020589	-0.009072	0.032887	-0.008231	0.036274

Table B-13 Light Turbulence 2D and Carrier Induced Turbulence – Wind 2 Knots

		Wind Speed = 13.5 Knots Light Two Dimensional Turbulence and Carrier Induced Turbulence					
		System 1		System 2		System 3	
Carrier Speed = 0 Knots	# Successful Approaches	5		5		5	
	$\bar{h}_r$ rms, σh_r rms (ft)	0.9486	0.004894	0.52089	0.025578	0.29016	0.001014
	$\bar{\lambda}_r$ rms, $\sigma\lambda_r$ rms (ft)	0.002382	0.000143	0.003988	0.002008	0.00226	6.41E-05
	$\bar{u}_r$ rms, σu_r rms (kts)	0.22519	0.001631	0.24545	0.001373	0.21892	0.000553
	# Failed Approaches Vert	0		0		0	
	$\bar{t}_{td}$, σt_{td} (sec)	-	-	-	-	-	-
	$\bar{h}_r$ rms, σh_r rms (ft)	-	-	-	-	-	-
	$\bar{\lambda}_r$ rms, $\sigma\lambda_r$ rms (ft)	-	-	-	-	-	-
	$\bar{u}_r$ rms, σu_r rms (kts)	-	-	-	-	-	-
	# Failed Approaches Lat	0		0		0	
	$\bar{t}_{td}$, σt_{td} (sec)	-	-	-	-	-	-
	$\bar{h}_r$ rms, σh_r rms (ft)	-	-	-	-	-	-
	$\bar{\lambda}_r$ rms, $\sigma\lambda_r$ rms (ft)	-	-	-	-	-	-
	$\bar{u}_r$ rms, σu_r rms (kts)	-	-	-	-	-	-
	# Ramp Strikes	0		0		0	
	$\bar{h}_d$, σh_d (ft)	8.9521	0.062133	9.6166	0.32743	8.5408	0.069327
	$\bar{h}_{dy}$, σh_{dy} (ft)	0.5763	0.010526	1.1957	0.27623	0.12019	0.008496
	$\bar{\theta}_{dy}$, $\sigma\theta_{dy}$ (deg)	-0.00339	0.025352	0.012763	0.022047	0.012651	0.022039
	# Bolters	0		0		0	
	$\bar{X}_d$, σX_d (ft)	-	-	-	-	-	-
	$\bar{Y}_d$, σY_d (ft)	-	-	-	-	-	-
	# Successful Touchdowns	5		5		5	
	$\bar{X}_d$, σX_d (ft)	-29.9237	1.2997	-0.3744	1.2762	3.5572	0.15641
	$\bar{Y}_{dy}$, σY_d (ft)	0.022183	0.047188	0.019333	0.059365	-0.0141	0.006533
	$\bar{h}_d$, σh_d (ft)	-9.1586	0.082909	-9.4136	0.26564	-11.2275	0.033594
	$\bar{h}_{dy}$, σh_{dy} (ft)	-0.080747	0.27775	-0.025148	0.048544	-0.032732	0.048196
Carrier Speed = 10Knots	# Successful Approaches	5		5		5	
	$\bar{h}_r$ rms, σh_r rms (ft)	0.96839	0.004578	0.4251	0.023401	0.2917	0.002432
	$\bar{\lambda}_r$ rms, $\sigma\lambda_r$ rms (ft)	0.002603	9.14E-05	0.002417	0.000376	0.002178	0.000131
	$\bar{u}_r$ rms, σu_r rms (kts)	0.22541	0.000509	0.21688	0.015599	0.22707	0.000698
	# Failed Approaches Vert	0		0		0	
	$\bar{t}_{td}$, σt_{td} (sec)	-	-	-	-	-	-
	$\bar{h}_r$ rms, σh_r rms (ft)	-	-	-	-	-	-
	$\bar{\lambda}_r$ rms, $\sigma\lambda_r$ rms (ft)	-	-	-	-	-	-
	$\bar{u}_r$ rms, σu_r rms (kts)	-	-	-	-	-	-
	# Failed Approaches Lat	0		0		0	
	$\bar{t}_{td}$, σt_{td} (sec)	-	-	-	-	-	-
	$\bar{h}_r$ rms, σh_r rms (ft)	-	-	-	-	-	-
	$\bar{\lambda}_r$ rms, $\sigma\lambda_r$ rms (ft)	-	-	-	-	-	-
	$\bar{u}_r$ rms, σu_r rms (kts)	-	-	-	-	-	-
	# Ramp Strikes	0		0		0	
	$\bar{h}_d$, σh_d (ft)	7.1999	0.058724	8.6085	0.48622	8.3866	0.054394
	$\bar{h}_{dy}$, σh_{dy} (ft)	-1.1526	0.005688	0.21164	0.47777	-0.0107	0.011736
	$\bar{\theta}_{dy}$, $\sigma\theta_{dy}$ (deg)	-0.01171	0.019418	0.004172	0.016909	0.004325	0.016823
	# Bolters	5		0		0	
	$\bar{X}_d$, σX_d (ft)	103.1492	5.1404	-	-	-	-
	$\bar{Y}_d$, σY_d (ft)	0.10952	0.18605	-	-	-	-
	# Successful Touchdowns	0		5		5	
	$\bar{X}_d$, σX_d (ft)	-	-	3.3552	1.5538	6.6981	0.43512
	$\bar{Y}_{dy}$, σY_d (ft)	-	-	-0.00399	0.029081	-0.01318	0.005988
	$\bar{h}_d$, σh_d (ft)	-	-	-11.3975	0.25195	-11.5426	0.019323
	$\bar{h}_{dy}$, σh_{dy} (ft)	-	-	0.0109	0.074166	0.06606	0.15688
Carrier Speed = 33 Knots	# Successful Approaches	5		5		5	
	$\bar{h}_r$ rms, σh_r rms (ft)	1.0537	0.001242	0.59601	0.033964	0.28194	0.004705
	$\bar{\lambda}_r$ rms, $\sigma\lambda_r$ rms (ft)	0.002536	6.61E-05	0.006246	0.003392	0.002256	5.81E-05
	$\bar{u}_r$ rms, σu_r rms (kts)	0.20918	0.000158	0.3323	0.004391	0.18232	0.002614
	# Failed Approaches Vert	0		0		0	
	$\bar{t}_{td}$, σt_{td} (sec)	-	-	-	-	-	-
	$\bar{h}_r$ rms, σh_r rms (ft)	-	-	-	-	-	-
	$\bar{\lambda}_r$ rms, $\sigma\lambda_r$ rms (ft)	-	-	-	-	-	-
	$\bar{u}_r$ rms, σu_r rms (kts)	-	-	-	-	-	-
	# Failed Approaches Lat	0		0		0	
	$\bar{t}_{td}$, σt_{td} (sec)	-	-	-	-	-	-
	$\bar{h}_r$ rms, σh_r rms (ft)	-	-	-	-	-	-
	$\bar{\lambda}_r$ rms, $\sigma\lambda_r$ rms (ft)	-	-	-	-	-	-
	$\bar{u}_r$ rms, σu_r rms (kts)	-	-	-	-	-	-
	# Ramp Strikes	0		0		0	
	$\bar{h}_d$, σh_d (ft)	8.6261	0.0345	9.006	0.069454	7.6869	0.031316
	$\bar{h}_{dy}$, σh_{dy} (ft)	0.25381	0.007087	0.61824	0.0685	-0.70033	0.011822
	$\bar{\theta}_{dy}$, $\sigma\theta_{dy}$ (deg)	-0.00462	0.010276	0.000895	0.010189	0.000703	0.010221
	# Bolters	0		0		0	
	$\bar{X}_d$, σX_d (ft)	-	-	-	-	-	-
	$\bar{Y}_d$, σY_d (ft)	-	-	-	-	-	-
	# Successful Touchdowns	5		5		5	
	$\bar{X}_d$, σX_d (ft)	-32.207	0.014616	-3.0562	3.02	-3.0656	0.29784
	$\bar{Y}_{dy}$, σY_d (ft)	0.040912	0.005981	0.084558	0.079881	-0.02272	0.007397
	$\bar{h}_d$, σh_d (ft)	-17.4963	0.004948	-10.3817	0.15128	-8.7346	0.02303
	$\bar{h}_{dy}$, σh_{dy} (ft)	0.00205	0.035133	0.03275	0.043887	0.0335	0.046387

Table B-14 Light Turbulence 2D and Carrier Induced Turbulence – Wind 13.5 Knots

		Wind Speed = 24.5 Knots Light Two Dimensional Turbulence and Carrier Induced Turbulence					
		System 1		System 2		System 3	
Carrier Speed = 0 Knots	# Successful Approaches	5		5		5	
	$\bar{h}_{ss}$ rms, σh_{ss} rms (ft)	1.4518	0.00673	0.55672	0.037917	0.29532	0.006545
	$\bar{\lambda}_{ss}$ rms, $\sigma\lambda_{ss}$ rms (ft)	0.022798	0.00405	0.006704	0.003593	0.003332	0.000112
	$\bar{u}_{ss}$ rms, σu_{ss} rms (kts)	0.29898	0.001952	0.26342	0.0055	0.22492	0.002563
	# Failed Approaches Vert	0		0		0	
	$\bar{t}_{fd}$, σt_{fd} (sec)	-	-	-	-	-	-
	$\bar{h}_{ss}$ rms, σh_{ss} rms (ft)	-	-	-	-	-	-
	$\bar{\lambda}_{ss}$ rms, $\sigma\lambda_{ss}$ rms (ft)	-	-	-	-	-	-
	$\bar{u}_{ss}$ rms, σu_{ss} rms (kts)	-	-	-	-	-	-
	# Failed Approaches Lat	0		0		0	
	$\bar{t}_{fd}$, σt_{fd} (sec)	-	-	-	-	-	-
	$\bar{h}_{ss}$ rms, σh_{ss} rms (ft)	-	-	-	-	-	-
	$\bar{\lambda}_{ss}$ rms, $\sigma\lambda_{ss}$ rms (ft)	-	-	-	-	-	-
	$\bar{u}_{ss}$ rms, σu_{ss} rms (kts)	-	-	-	-	-	-
	# Ramp Strikes	0		0		0	
	$\bar{h}_{fd}$, σh_{fd} (ft)	8.785	0.29461	10.7405	0.3873	8.5676	0.20559
	$\bar{h}_{ss}$, σh_{ss} (ft)	0.24176	0.009738	2.2329	0.42289	0.061167	0.027712
	$\bar{\theta}_{ss}$, $\sigma\theta_{ss}$ (deg)	0.056565	0.1086	0.043799	0.069106	0.043412	0.069347
	# Bolters	0		0		0	
	$\bar{X}_{fd}$, σX_{fd} (ft)	-	-	-	-	-	-
	$\bar{Y}_{fd}$, σY_{fd} (ft)	-	-	-	-	-	-
	# Successful Touchdowns	5		5		5	
	$\bar{X}_{td}$, σX_{td} (ft)	-28.6812	3.47	1.4846	0.96511	4.0643	0.72537
	$\bar{Y}_{td}$, σY_{td} (ft)	0.004059	0.20249	-0.04911	0.14303	-0.01833	0.046382
	$\bar{h}_{fd}$, σh_{fd} (ft)	-11.8408	0.080814	-9.5057	0.54908	-9.9529	0.28664
	$\bar{h}_{ss}$, σh_{ss} (ft)	0.16486	0.4154	-0.13167	0.1483	-0.081196	0.31374
Carrier Speed = 10Knots	# Successful Approaches	0		5		5	
	$\bar{h}_{ss}$ rms, σh_{ss} rms (ft)	-	-	0.58151	0.14693	0.33633	0.012159
	$\bar{\lambda}_{ss}$ rms, $\sigma\lambda_{ss}$ rms (ft)	-	-	0.004544	0.000842	0.003756	0.000249
	$\bar{u}_{ss}$ rms, σu_{ss} rms (kts)	-	-	0.2294	0.027103	0.19713	0.005579
	# Failed Approaches Vert	5		0		0	
	$\bar{t}_{fd}$, σt_{fd} (sec)	6.2815	0.0331	-	-	-	-
	$\bar{h}_{ss}$ rms, σh_{ss} rms (ft)	1.2875	0.008181	-	-	-	-
	$\bar{\lambda}_{ss}$ rms, $\sigma\lambda_{ss}$ rms (ft)	0.007313	0.002478	-	-	-	-
	$\bar{u}_{ss}$ rms, σu_{ss} rms (kts)	0.30119	0.005382	-	-	-	-
	# Failed Approaches Lat	0		0		0	
	$\bar{t}_{fd}$, σt_{fd} (sec)	-	-	-	-	-	-
	$\bar{h}_{ss}$ rms, σh_{ss} rms (ft)	-	-	-	-	-	-
	$\bar{\lambda}_{ss}$ rms, $\sigma\lambda_{ss}$ rms (ft)	-	-	-	-	-	-
	$\bar{u}_{ss}$ rms, σu_{ss} rms (kts)	-	-	-	-	-	-
	# Ramp Strikes	0		0		0	
	$\bar{h}_{fd}$, σh_{fd} (ft)	-	-	9.1027	0.3593	8.8277	0.34338
	$\bar{h}_{ss}$, σh_{ss} (ft)	-	-	0.80893	0.20387	0.53341	0.11475
	$\bar{\theta}_{ss}$, $\sigma\theta_{ss}$ (deg)	-	-	-0.03276	0.08676	-0.03258	0.086934
	# Bolters	0		0		0	
	$\bar{X}_{fd}$, σX_{fd} (ft)	-	-	-	-	-	-
	$\bar{Y}_{fd}$, σY_{fd} (ft)	-	-	-	-	-	-
	# Successful Touchdowns	0		5		5	
	$\bar{X}_{td}$, σX_{td} (ft)	-	-	-0.72552	15.0519	-10.2436	1.5157
	$\bar{Y}_{td}$, σY_{td} (ft)	-	-	0.039871	0.1042	0.060116	0.044715
	$\bar{h}_{fd}$, σh_{fd} (ft)	-	-	-14.5834	2.2762	-10.7206	0.16141
	$\bar{h}_{ss}$, σh_{ss} (ft)	-	-	-0.008508	0.50086	0.04416	0.54934
Carrier Speed = 33 Knots	# Successful Approaches	5		5		5	
	$\bar{h}_{ss}$ rms, σh_{ss} rms (ft)	1.5248	0.003125	0.55079	0.067278	0.28647	0.008295
	$\bar{\lambda}_{ss}$ rms, $\sigma\lambda_{ss}$ rms (ft)	0.019165	0.006013	0.006466	0.003112	0.00352	0.000221
	$\bar{u}_{ss}$ rms, σu_{ss} rms (kts)	0.295	0.002295	0.3226	0.017709	0.18365	0.006003
	# Failed Approaches Vert	0		0		0	
	$\bar{t}_{fd}$, σt_{fd} (sec)	-	-	-	-	-	-
	$\bar{h}_{ss}$ rms, σh_{ss} rms (ft)	-	-	-	-	-	-
	$\bar{\lambda}_{ss}$ rms, $\sigma\lambda_{ss}$ rms (ft)	-	-	-	-	-	-
	$\bar{u}_{ss}$ rms, σu_{ss} rms (kts)	-	-	-	-	-	-
	# Failed Approaches Lat	0		0		0	
	$\bar{t}_{fd}$, σt_{fd} (sec)	-	-	-	-	-	-
	$\bar{h}_{ss}$ rms, σh_{ss} rms (ft)	-	-	-	-	-	-
	$\bar{\lambda}_{ss}$ rms, $\sigma\lambda_{ss}$ rms (ft)	-	-	-	-	-	-
	$\bar{u}_{ss}$ rms, σu_{ss} rms (kts)	-	-	-	-	-	-
	# Ramp Strikes	0		0		0	
	$\bar{h}_{fd}$, σh_{fd} (ft)	9.4963	0.081797	8.8516	0.7102	7.9715	0.22798
	$\bar{h}_{ss}$, σh_{ss} (ft)	1.0829	0.0197	0.37362	0.74801	-0.5048	0.075418
	$\bar{\theta}_{ss}$, $\sigma\theta_{ss}$ (deg)	0.010099	0.028778	0.033219	0.054389	0.03259	0.055303
	# Bolters	0		0		0	
	$\bar{X}_{fd}$, σX_{fd} (ft)	-	-	-	-	-	-
	$\bar{Y}_{fd}$, σY_{fd} (ft)	-	-	-	-	-	-
	# Successful Touchdowns	5		5		5	
	$\bar{X}_{td}$, σX_{td} (ft)	-35.4799	1.0276	-3.4408	5.8132	-4.3257	1.735
	$\bar{Y}_{td}$, σY_{td} (ft)	-0.06942	0.027797	0.026699	0.029348	-0.02787	0.0144
	$\bar{h}_{fd}$, σh_{fd} (ft)	-12.1199	0.034149	-9.2671	1.2698	-9.1454	0.37614
	$\bar{h}_{ss}$, σh_{ss} (ft)	-0.040407	0.18786	0.14912	0.17005	0.1425	0.16833

Table B-15 Light Turbulence 2D and Carrier Induced Turbulence – Wind 24.5 Knots

		Wind Speed = 37 Knots Light Two Dimensional Turbulence and Carrier Induced Turbulence					
		System 1		System 2		System 3	
Carrier Speed = 0 Knots	# Successful Approaches	5		5		5	
	$\bar{h}_{rms}$, σh_{rms} rms (ft)	1.7083	0.02044	0.73537	0.1127	0.46712	0.019287
	$\bar{\lambda}_{rms}$, $\sigma\lambda_{rms}$ rms (ft)	0.057778	0.019851	0.009533	0.003234	0.006866	0.000988
	$\bar{u}_{rms}$, σu_{rms} rms (kts)	0.31841	0.001936	0.26969	0.013804	0.25229	0.00471
	# Failed Approaches Vert	0		0		0	
	$\bar{t}_{td}$, σt_{td} (sec)	-	-	-	-	-	-
	$\bar{h}_{rms}$ rms, σh_{rms} rms (ft)	-	-	-	-	-	-
	$\bar{\lambda}_{rms}$ rms, $\sigma\lambda_{rms}$ rms (ft)	-	-	-	-	-	-
	$\bar{u}_{rms}$ rms, σu_{rms} rms (kts)	-	-	-	-	-	-
	# Failed Approaches Lat	0		0		0	
	$\bar{t}_{td}$, σt_{td} (sec)	-	-	-	-	-	-
	$\bar{h}_{rms}$ rms, σh_{rms} rms (ft)	-	-	-	-	-	-
	$\bar{\lambda}_{rms}$ rms, $\sigma\lambda_{rms}$ rms (ft)	-	-	-	-	-	-
	$\bar{u}_{rms}$ rms, σu_{rms} rms (kts)	-	-	-	-	-	-
	# Ramp Strikes	0		0		0	
	$\bar{h}_{td}$, σh_{td} (ft)	6.8567	0.64303	8.9378	2.1812	7.967	0.69942
	$\bar{h}_{rms}$, σh_{rms} (ft)	-1.6547	0.15011	1.0657	2.0095	0.094296	0.39984
	$\bar{\theta}_{rms}$, $\sigma\theta_{rms}$ (deg)	0.045164	0.26662	-0.18373	0.12456	-0.18353	0.12389
	# Bolters	0		1		0	
	$\bar{X}_{td}$, σX_{td} (ft)	-	-	132.8435	0	-	-
	$\bar{Y}_{td}$, σY_{td} (ft)	-	-	3.5863	0	-	-
	# Successful Touchdowns	5		4		5	
	$\bar{X}_{td}$, σX_{td} (ft)	-69.1491	15.3286	25.2529	19.9773	-5.4916	20.0865
	$\bar{Y}_{td}$, σY_{td} (ft)	-0.19891	0.77033	-0.14958	0.16933	-0.24371	0.5113
	$\bar{h}_{td}$, σh_{td} (ft)	-11.0674	0.59006	-11.5039	2.9082	-7.4605	0.49997
	$\bar{h}_{rms}$, σh_{rms} (ft)	0.55376	1.2966	-0.069147	0.826	-0.00293	0.75493
Carrier Speed = 10Knots	# Successful Approaches	5		5		5	
	$\bar{h}_{rms}$ rms, σh_{rms} rms (ft)	1.8329	0.007996	0.5973	0.12911	0.39254	0.038043
	$\bar{\lambda}_{rms}$ rms, $\sigma\lambda_{rms}$ rms (ft)	0.049708	0.014021	0.010677	0.005055	0.008194	0.003658
	$\bar{u}_{rms}$ rms, σu_{rms} rms (kts)	0.33448	0.000527	0.24113	0.027946	0.20963	0.010869
	# Failed Approaches Vert	0		0		0	
	$\bar{t}_{td}$, σt_{td} (sec)	-	-	-	-	-	-
	$\bar{h}_{rms}$ rms, σh_{rms} rms (ft)	-	-	-	-	-	-
	$\bar{\lambda}_{rms}$ rms, $\sigma\lambda_{rms}$ rms (ft)	-	-	-	-	-	-
	$\bar{u}_{rms}$ rms, σu_{rms} rms (kts)	-	-	-	-	-	-
	# Failed Approaches Lat	0		0		0	
	$\bar{t}_{td}$, σt_{td} (sec)	-	-	-	-	-	-
	$\bar{h}_{rms}$ rms, σh_{rms} rms (ft)	-	-	-	-	-	-
	$\bar{\lambda}_{rms}$ rms, $\sigma\lambda_{rms}$ rms (ft)	-	-	-	-	-	-
	$\bar{u}_{rms}$ rms, σu_{rms} rms (kts)	-	-	-	-	-	-
	# Ramp Strikes	0		0		0	
	$\bar{h}_{td}$, σh_{td} (ft)	5.9888	0.5171	9.527	1.9043	9.5857	1.2456
	$\bar{h}_{rms}$, σh_{rms} (ft)	-2.4314	0.1579	0.84054	2.2011	0.89893	0.70882
	$\bar{\theta}_{rms}$, $\sigma\theta_{rms}$ (deg)	0.012518	0.2225	0.10786	0.24464	0.10797	0.24454
	# Bolters	0		0		0	
	$\bar{X}_{td}$, σX_{td} (ft)	-	-	-	-	-	-
	$\bar{Y}_{td}$, σY_{td} (ft)	-	-	-	-	-	-
	# Successful Touchdowns	5		5		5	
	$\bar{X}_{td}$, σX_{td} (ft)	-73.0662	23.3334	-9.9502	10.2276	-8.6081	8.3878
	$\bar{Y}_{td}$, σY_{td} (ft)	0.069564	1.1091	0.013846	0.34596	-0.08767	0.18111
	$\bar{h}_{td}$, σh_{td} (ft)	-9.5394	0.87824	-11.143	3.8942	-10.4897	1.117
	$\bar{h}_{rms}$, σh_{rms} (ft)	-0.086717	1.1877	0.30682	0.65584	0.34659	0.56212
Carrier Speed = 33 Knots	# Successful Approaches	5		5		5	
	$\bar{h}_{rms}$ rms, σh_{rms} rms (ft)	2.2474	0.03002	1.0656	0.30125	0.40473	0.025564
	$\bar{\lambda}_{rms}$ rms, $\sigma\lambda_{rms}$ rms (ft)	0.079825	0.022	0.034024	0.013285	0.021941	0.012162
	$\bar{u}_{rms}$ rms, σu_{rms} rms (kts)	0.43545	0.021005	0.72668	0.056698	0.52093	0.030597
	# Failed Approaches Vert	0		0		0	
	$\bar{t}_{td}$, σt_{td} (sec)	-	-	-	-	-	-
	$\bar{h}_{rms}$ rms, σh_{rms} rms (ft)	-	-	-	-	-	-
	$\bar{\lambda}_{rms}$ rms, $\sigma\lambda_{rms}$ rms (ft)	-	-	-	-	-	-
	$\bar{u}_{rms}$ rms, σu_{rms} rms (kts)	-	-	-	-	-	-
	# Failed Approaches Lat	0		0		0	
	$\bar{t}_{td}$, σt_{td} (sec)	-	-	-	-	-	-
	$\bar{h}_{rms}$ rms, σh_{rms} rms (ft)	-	-	-	-	-	-
	$\bar{\lambda}_{rms}$ rms, $\sigma\lambda_{rms}$ rms (ft)	-	-	-	-	-	-
	$\bar{u}_{rms}$ rms, σu_{rms} rms (kts)	-	-	-	-	-	-
	# Ramp Strikes	0		0		0	
	$\bar{h}_{td}$, σh_{td} (ft)	13.4789	0.79918	11.3505	2.6015	9.4153	0.3145
	$\bar{h}_{rms}$, σh_{rms} (ft)	5.0523	0.043937	3.0906	2.5951	1.1438	0.24858
	$\bar{\theta}_{rms}$, $\sigma\theta_{rms}$ (deg)	0.014804	0.29152	-0.04485	0.20184	-0.04075	0.194
	# Bolters	0		0		0	
	$\bar{X}_{td}$, σX_{td} (ft)	-	-	-	-	-	-
	$\bar{Y}_{td}$, σY_{td} (ft)	-	-	-	-	-	-
	# Successful Touchdowns	5		5		5	
	$\bar{X}_{td}$, σX_{td} (ft)	-6.4213	2.3914	10.3955	30.9484	3.6782	2.4769
	$\bar{Y}_{td}$, σY_{td} (ft)	0.059219	0.088959	0.018837	0.69255	0.021891	0.052142
	$\bar{h}_{td}$, σh_{td} (ft)	-17.5133	0.10875	-14.5886	1.6062	-9.2533	0.24618
	$\bar{h}_{rms}$, σh_{rms} (ft)	0.22368	0.97868	-0.33138	1.035	-0.28386	0.96248

Table B-16 Light Turbulence 2D and Carrier Induced Turbulence – Wind 37 Knots

		Wind Speed = 2 Knots Moderate Three Dimensional Turbulence and Carrier Induced Turbulence					
		System 1		System 2		System 3	
Carrier Speed = 0 Knots	# Successful Approaches	5		5		5	
	$\bar{h}_{ac}$ rms, σh_{ac} rms (ft)	1.4116	0.000419	1.224	0.001659	0.63518	0.00249
	$\bar{\lambda}_{ac}$ rms, $\sigma\lambda_{ac}$ rms (ft)	0.26203	0.002342	1.0673	0.00699	0.94408	0.00081
	$\bar{u}_{ac}$ rms, σu_{ac} rms (kts)	0.3186	0.000218	0.43924	0.000845	0.44337	0.001308
	# Failed Approaches Vert	0		0		0	
	$\bar{t}_{td}$, σt_{td} (sec)	-	-	-	-	-	-
	$\bar{h}_{ac}$ rms, σh_{ac} rms (ft)	-	-	-	-	-	-
	$\bar{\lambda}_{ac}$ rms, $\sigma\lambda_{ac}$ rms (ft)	-	-	-	-	-	-
	$\bar{u}_{ac}$ rms, σu_{ac} rms (kts)	-	-	-	-	-	-
	# Failed Approaches Lat	0		0		0	
	$\bar{t}_{td}$, σt_{td} (sec)	-	-	-	-	-	-
	$\bar{h}_{ac}$ rms, σh_{ac} rms (ft)	-	-	-	-	-	-
	$\bar{\lambda}_{ac}$ rms, $\sigma\lambda_{ac}$ rms (ft)	-	-	-	-	-	-
	$\bar{u}_{ac}$ rms, σu_{ac} rms (kts)	-	-	-	-	-	-
	# Ramp Strikes	0		0		0	
	$\bar{h}_{td}$, σh_{td} (ft)	10.4399	0.036404	11.0816	0.027248	8.7796	0.03191
	$\bar{h}_{ac}$, σh_{ac} (ft)	2.0789	0.001274	2.7209	0.010869	0.41891	0.001404
	$\bar{\theta}_{ac}$, $\sigma\theta_{ac}$ (deg)	-0.00866	0.01297	-0.00878	0.010926	-0.00878	0.010926
	# Bolters	0		0		0	
	$\bar{X}_{td}$, σX_{td} (ft)	-	-	-	-	-	-
	$\bar{Y}_{td}$, σY_{td} (ft)	-	-	-	-	-	-
	# Successful Touchdowns	5		5		5	
	$\bar{X}_{td}$, σX_{td} (ft)	29.4796	0.42861	12.8225	0.46214	1.5023	0.028241
	$\bar{Y}_{td}$, σY_{td} (ft)	0.85715	0.001798	8.134	0.044402	3.0167	0.023315
	$\bar{h}_{ac}$, σh_{ac} (ft)	-19.3793	0.00811	-10.8754	0.062383	-11.0681	0.004828
	$\bar{h}_{td}$, σh_{td} (ft)	-0.02102	0.08069	-0.03561	0.041535	-0.048634	0.064227
Carrier Speed = 10Knots	# Successful Approaches	5		5		5	
	$\bar{h}_{ac}$ rms, σh_{ac} rms (ft)	1.4105	0.000616	1.1692	0.004254	0.66472	0.000669
	$\bar{\lambda}_{ac}$ rms, $\sigma\lambda_{ac}$ rms (ft)	0.31015	0.001363	0.91751	0.003737	0.93586	0.00225
	$\bar{u}_{ac}$ rms, σu_{ac} rms (kts)	0.31521	0.000293	0.40718	0.001662	0.44951	0.000865
	# Failed Approaches Vert	0		0		0	
	$\bar{t}_{td}$, σt_{td} (sec)	-	-	-	-	-	-
	$\bar{h}_{ac}$ rms, σh_{ac} rms (ft)	-	-	-	-	-	-
	$\bar{\lambda}_{ac}$ rms, $\sigma\lambda_{ac}$ rms (ft)	-	-	-	-	-	-
	$\bar{u}_{ac}$ rms, σu_{ac} rms (kts)	-	-	-	-	-	-
	# Failed Approaches Lat	0		0		0	
	$\bar{t}_{td}$, σt_{td} (sec)	-	-	-	-	-	-
	$\bar{h}_{ac}$ rms, σh_{ac} rms (ft)	-	-	-	-	-	-
	$\bar{\lambda}_{ac}$ rms, $\sigma\lambda_{ac}$ rms (ft)	-	-	-	-	-	-
	$\bar{u}_{ac}$ rms, σu_{ac} rms (kts)	-	-	-	-	-	-
	# Ramp Strikes	0		0		0	
	$\bar{h}_{td}$, σh_{td} (ft)	8.9835	0.044136	8.0331	0.032672	8.3951	0.029808
	$\bar{h}_{ac}$, σh_{ac} (ft)	0.57759	0.001789	-0.36772	0.007601	-0.00573	0.000726
	$\bar{\theta}_{ac}$, $\sigma\theta_{ac}$ (deg)	0.007419	0.015488	0.005591	0.010833	0.005591	0.010833
	# Bolters	0		0		0	
	$\bar{X}_{td}$, σX_{td} (ft)	-	-	-	-	-	-
	$\bar{Y}_{td}$, σY_{td} (ft)	-	-	-	-	-	-
	# Successful Touchdowns	5		5		5	
	$\bar{X}_{td}$, σX_{td} (ft)	42.4438	0.95868	8.1619	0.95958	6.7688	0.56081
	$\bar{Y}_{td}$, σY_{td} (ft)	0.83079	0.00606	5.1491	0.077239	3.2135	0.024557
	$\bar{h}_{ac}$, σh_{ac} (ft)	-19.033	0.016165	-12.7747	0.3209	-11.7983	0.011244
	$\bar{h}_{td}$, σh_{td} (ft)	0.05428	0.059027	0.04119	0.06889	0.03074	0.051167
Carrier Speed = 33 Knots	# Successful Approaches	5		5		5	
	$\bar{h}_{ac}$ rms, σh_{ac} rms (ft)	1.4272	0.000261	1.0867	0.033337	0.68136	0.007701
	$\bar{\lambda}_{ac}$ rms, $\sigma\lambda_{ac}$ rms (ft)	0.28392	0.000856	0.99454	0.025072	0.94963	0.009367
	$\bar{u}_{ac}$ rms, σu_{ac} rms (kts)	0.31768	0.000166	0.39533	0.008688	0.42497	0.004202
	# Failed Approaches Vert	0		0		0	
	$\bar{t}_{td}$, σt_{td} (sec)	-	-	-	-	-	-
	$\bar{h}_{ac}$ rms, σh_{ac} rms (ft)	-	-	-	-	-	-
	$\bar{\lambda}_{ac}$ rms, $\sigma\lambda_{ac}$ rms (ft)	-	-	-	-	-	-
	$\bar{u}_{ac}$ rms, σu_{ac} rms (kts)	-	-	-	-	-	-
	# Failed Approaches Lat	0		0		0	
	$\bar{t}_{td}$, σt_{td} (sec)	-	-	-	-	-	-
	$\bar{h}_{ac}$ rms, σh_{ac} rms (ft)	-	-	-	-	-	-
	$\bar{\lambda}_{ac}$ rms, $\sigma\lambda_{ac}$ rms (ft)	-	-	-	-	-	-
	$\bar{u}_{ac}$ rms, σu_{ac} rms (kts)	-	-	-	-	-	-
	# Ramp Strikes	0		0		0	
	$\bar{h}_{td}$, σh_{td} (ft)	8.905	0.015113	7.0347	0.54844	8.0815	0.013095
	$\bar{h}_{ac}$, σh_{ac} (ft)	0.52789	0.001418	-1.3424	0.54192	-0.29567	0.014042
	$\bar{\theta}_{ac}$, $\sigma\theta_{ac}$ (deg)	-0.00291	0.004996	-0.00292	0.003059	-0.0029	0.003075
	# Bolters	0		0		0	
	$\bar{X}_{td}$, σX_{td} (ft)	-	-	-	-	-	-
	$\bar{Y}_{td}$, σY_{td} (ft)	-	-	-	-	-	-
	# Successful Touchdowns	5		5		5	
	$\bar{X}_{td}$, σX_{td} (ft)	25.7483	0.003745	16.8581	23.4431	5.5165	0.48089
	$\bar{Y}_{td}$, σY_{td} (ft)	0.81188	0.000246	4.2982	0.82503	2.2467	0.14446
	$\bar{h}_{ac}$, σh_{ac} (ft)	-19.2092	0.001369	-12.9866	1.2869	-11.9066	0.014592
	$\bar{h}_{td}$, σh_{td} (ft)	-0.008702	0.019972	-0.006599	0.028794	-0.008002	0.035493

Table B-17 Moderate Turbulence 3D and Carrier Induced Turbulence – Wind 2 Knots

		Wind Speed = 13.5 Knots Moderate Three Dimensional Turbulence and Carrier Induced Turbulence					
		System 1		System 2		System 3	
Carrier Speed = 0 Knots	# Successful Approaches	0		5		5	
	$\bar{h}_{ac}$ rms, σh_{ac} rms (ft)	-	-	1.1276	0.050714	0.65134	0.000701
	$\bar{\lambda}_{ac}$ rms, $\sigma\lambda_{ac}$ rms (ft)	-	-	0.90977	0.061951	0.85449	0.002553
	$\bar{u}_{ac}$ rms, σu_{ac} rms (kts)	-	-	0.41556	0.01859	0.44705	0.000571
	# Failed Approaches Vert	5		0		0	
	$\bar{t}_{td}$, σt_{td} (sec)	6.1627	0.014483	-	-	-	-
	$\bar{h}_{ac}$ rms, σh_{ac} rms (ft)	1.4185	0.001461	-	-	-	-
	$\bar{\lambda}_{ac}$ rms, $\sigma\lambda_{ac}$ rms (ft)	0.11306	0.00153	-	-	-	-
	$\bar{u}_{ac}$ rms, σu_{ac} rms (kts)	0.37872	0.002102	-	-	-	-
	# Failed Approaches Lat	0		0		0	
	$\bar{t}_{td}$, σt_{td} (sec)	-	-	-	-	-	-
	$\bar{h}_{ac}$ rms, σh_{ac} rms (ft)	-	-	-	-	-	-
	$\bar{\lambda}_{ac}$ rms, $\sigma\lambda_{ac}$ rms (ft)	-	-	-	-	-	-
	$\bar{u}_{ac}$ rms, σu_{ac} rms (kts)	-	-	-	-	-	-
	# Ramp Strikes	0		0		0	
	$\bar{h}_{td}$, σh_{td} (ft)	-	-	10.1472	0.40733	8.9089	0.059448
	$\bar{h}_{ac}$, σh_{ac} (ft)	-	-	1.7258	0.46667	0.48759	0.002758
	$\bar{\theta}_{ac}$, $\sigma\theta_{ac}$ (deg)	-	-	0.012944	0.022082	0.012898	0.022124
	# Bolters	0		0		0	
	$\bar{X}_{td}$, σX_{td} (ft)	-	-	-	-	-	-
	$\bar{Y}_{td}$, σY_{td} (ft)	-	-	-	-	-	-
	# Successful Touchdowns	0		5		5	
	$\bar{X}_{td}$, σX_{td} (ft)	-	-	12.3045	0.57808	9.2123	0.40026
	$\bar{Y}_{td}$, σY_{td} (ft)	-	-	5.5398	1.3268	4.4173	0.044846
	$\bar{h}_{td}$, σh_{td} (ft)	-	-	-9.7038	0.3999	-12.1006	0.063868
	$\bar{h}_{ac}$, σh_{ac} (ft)	-	-	-0.026725	0.049619	-0.021796	0.043628
Carrier Speed = 10Knots	# Successful Approaches	5		5		5	
	$\bar{h}_{ac}$ rms, σh_{ac} rms (ft)	1.973	0.005813	1.0824	0.025416	0.69468	0.001542
	$\bar{\lambda}_{ac}$ rms, $\sigma\lambda_{ac}$ rms (ft)	0.33034	0.006465	1.0009	0.044862	0.89317	0.006428
	$\bar{u}_{ac}$ rms, σu_{ac} rms (kts)	0.44357	0.001477	0.40712	0.005311	0.45363	0.001252
	# Failed Approaches Vert	0		0		0	
	$\bar{t}_{td}$, σt_{td} (sec)	-	-	-	-	-	-
	$\bar{h}_{ac}$ rms, σh_{ac} rms (ft)	-	-	-	-	-	-
	$\bar{\lambda}_{ac}$ rms, $\sigma\lambda_{ac}$ rms (ft)	-	-	-	-	-	-
	$\bar{u}_{ac}$ rms, σu_{ac} rms (kts)	-	-	-	-	-	-
	# Failed Approaches Lat	0		0		0	
	$\bar{t}_{td}$, σt_{td} (sec)	-	-	-	-	-	-
	$\bar{h}_{ac}$ rms, σh_{ac} rms (ft)	-	-	-	-	-	-
	$\bar{\lambda}_{ac}$ rms, $\sigma\lambda_{ac}$ rms (ft)	-	-	-	-	-	-
	$\bar{u}_{ac}$ rms, σu_{ac} rms (kts)	-	-	-	-	-	-
	# Ramp Strikes	0		0		0	
	$\bar{h}_{td}$, σh_{td} (ft)	6.6071	0.053972	8.0904	0.29198	8.5571	0.049926
	$\bar{h}_{ac}$, σh_{ac} (ft)	-1.7442	0.00281	-0.30631	0.33232	0.16064	0.006621
	$\bar{\theta}_{ac}$, $\sigma\theta_{ac}$ (deg)	-0.01216	0.019335	0.00409	0.017136	0.004011	0.017243
	# Bolters	5		0		0	
	$\bar{X}_{td}$, σX_{td} (ft)	210.3439	3.8004	-	-	-	-
	$\bar{Y}_{td}$, σY_{td} (ft)	6.2814	0.07198	-	-	-	-
	# Successful Touchdowns	0		5		5	
	$\bar{X}_{td}$, σX_{td} (ft)	-	-	27.113	29.0534	11.328	0.1106
	$\bar{Y}_{td}$, σY_{td} (ft)	-	-	4.3475	1.0184	3.5638	0.10409
	$\bar{h}_{td}$, σh_{td} (ft)	-	-	-12.9831	3.162	-11.323	0.030423
	$\bar{h}_{ac}$, σh_{ac} (ft)	-	-	0.07257	0.13012	0.07615	0.17497
Carrier Speed = 33 Knots	# Successful Approaches	5		5		5	
	$\bar{h}_{ac}$ rms, σh_{ac} rms (ft)	1.8545	0.001411	1.117	0.059137	0.70389	0.012338
	$\bar{\lambda}_{ac}$ rms, $\sigma\lambda_{ac}$ rms (ft)	0.15364	0.001758	4.0571	0.51982	4.3664	0.14084
	$\bar{u}_{ac}$ rms, σu_{ac} rms (kts)	0.38798	0.000847	0.50517	0.021977	0.45901	0.012332
	# Failed Approaches Vert	0		0		0	
	$\bar{t}_{td}$, σt_{td} (sec)	-	-	-	-	-	-
	$\bar{h}_{ac}$ rms, σh_{ac} rms (ft)	-	-	-	-	-	-
	$\bar{\lambda}_{ac}$ rms, $\sigma\lambda_{ac}$ rms (ft)	-	-	-	-	-	-
	$\bar{u}_{ac}$ rms, σu_{ac} rms (kts)	-	-	-	-	-	-
	# Failed Approaches Lat	0		0		0	
	$\bar{t}_{td}$, σt_{td} (sec)	-	-	-	-	-	-
	$\bar{h}_{ac}$ rms, σh_{ac} rms (ft)	-	-	-	-	-	-
	$\bar{\lambda}_{ac}$ rms, $\sigma\lambda_{ac}$ rms (ft)	-	-	-	-	-	-
	$\bar{u}_{ac}$ rms, σu_{ac} rms (kts)	-	-	-	-	-	-
	# Ramp Strikes	0		0		0	
	$\bar{h}_{td}$, σh_{td} (ft)	7.9181	0.028454	9.9004	0.082792	7.9195	0.044561
	$\bar{h}_{ac}$, σh_{ac} (ft)	-0.45403	0.003067	1.5129	0.090994	-0.46741	0.033869
	$\bar{\theta}_{ac}$, $\sigma\theta_{ac}$ (deg)	-0.0047	0.010224	0.000816	0.010222	0.000606	0.010232
	# Bolters	0		0		0	
	$\bar{X}_{td}$, σX_{td} (ft)	-	-	-	-	-	-
	$\bar{Y}_{td}$, σY_{td} (ft)	-	-	-	-	-	-
	# Successful Touchdowns	5		5		5	
	$\bar{X}_{td}$, σX_{td} (ft)	-55.7027	0.24317	-7.899	0.97894	-5.4207	0.66652
	$\bar{Y}_{td}$, σY_{td} (ft)	0.36522	0.008476	3.8845	1.0709	3.214	0.21941
	$\bar{h}_{td}$, σh_{td} (ft)	-20.6363	0.00305	-8.6984	0.10957	-7.2207	0.02193
	$\bar{h}_{ac}$, σh_{ac} (ft)	0.00332	0.034259	0.03078	0.04247	-0.03163	0.044051

Table B-18 Moderate Turbulence 3D and Carrier Induced Turbulence – Wind 13.5 Knots

		Wind Speed = 24.5 Knots Moderate Three Dimensional Turbulence and Carrier Induced Turbulence					
		System 1		System 2		System 3	
Carrier Speed = 0 Knots	# Successful Approaches	0		5		5	
	$\bar{h}_{ac}$ rms, σh_{ac} rms (ft)	-	-	1.1327	0.06157	0.65129	0.008289
	$\bar{\lambda}_{ac}$ rms, $\sigma\lambda_{ac}$ rms (ft)	-	-	0.91301	0.077869	0.76492	0.011679
	$\bar{u}_{ac}$ rms, σu_{ac} rms (kts)	-	-	0.41959	0.014501	0.45404	0.001999
	# Failed Approaches Vert	5		0		0	
	$\bar{t}_{td}$, σt_{td} (sec)	8.667	0.009772	-	-	-	-
	$\bar{h}_{ac}$ rms, σh_{ac} rms (ft)	1.7484	0.005338	-	-	-	-
	$\bar{\lambda}_{ac}$ rms, $\sigma\lambda_{ac}$ rms (ft)	0.18263	0.007399	-	-	-	-
	$\bar{u}_{ac}$ rms, σu_{ac} rms (kts)	0.38366	0.001397	-	-	-	-
	# Failed Approaches Lat	0		0		0	
	$\bar{t}_{td}$, σt_{td} (sec)	-	-	-	-	-	-
	$\bar{h}_{ac}$ rms, σh_{ac} rms (ft)	-	-	-	-	-	-
	$\bar{\lambda}_{ac}$ rms, $\sigma\lambda_{ac}$ rms (ft)	-	-	-	-	-	-
	$\bar{u}_{ac}$ rms, σu_{ac} rms (kts)	-	-	-	-	-	-
	# Ramp Strikes	0		0		0	
	$\bar{h}_{td}$, σh_{td} (ft)	-	-	11.0766	1.2706	8.9399	0.22217
	$\bar{h}_{ac}$, σh_{ac} (ft)	-	-	2.5676	1.2568	0.43114	0.048549
	$\bar{\theta}_{ac}$, $\sigma\theta_{ac}$ (deg)	-	-	0.044324	0.069043	0.044229	0.069092
	# Bolters	0		0		0	
	$\bar{X}_{td}$, σX_{td} (ft)	-	-	-	-	-	-
	$\bar{Y}_{td}$, σY_{td} (ft)	-	-	-	-	-	-
	# Successful Touchdowns	0		5		5	
	$\bar{X}_{td}$, σX_{td} (ft)	-	-	16.9847	7.2355	14.9927	0.70426
	$\bar{Y}_{td}$, σY_{td} (ft)	-	-	6.7417	1.2426	4.3971	0.21071
	$\bar{h}_{td}$, σh_{td} (ft)	-	-	-10.1941	2.8379	-12.0199	0.35037
	$\bar{h}_{ac}$, σh_{ac} (ft)	-	-	-0.11682	0.31738	-0.10313	0.28592
Carrier Speed = 10Knots	# Successful Approaches	0		5		5	
	$\bar{h}_{ac}$ rms, σh_{ac} rms (ft)	-	-	1.0911	0.014488	0.71918	0.019114
	$\bar{\lambda}_{ac}$ rms, $\sigma\lambda_{ac}$ rms (ft)	-	-	1.7087	0.08697	1.9085	0.072968
	$\bar{u}_{ac}$ rms, σu_{ac} rms (kts)	-	-	0.37627	0.004256	0.4224	0.005502
	# Failed Approaches Vert	5		0		0	
	$\bar{t}_{td}$, σt_{td} (sec)	6.9348	0.008124	-	-	-	-
	$\bar{h}_{ac}$ rms, σh_{ac} rms (ft)	2.0417	0.008971	-	-	-	-
	$\bar{\lambda}_{ac}$ rms, $\sigma\lambda_{ac}$ rms (ft)	0.22844	0.044531	-	-	-	-
	$\bar{u}_{ac}$ rms, σu_{ac} rms (kts)	0.42024	0.004881	-	-	-	-
	# Failed Approaches Lat	0		0		0	
	$\bar{t}_{td}$, σt_{td} (sec)	-	-	-	-	-	-
	$\bar{h}_{ac}$ rms, σh_{ac} rms (ft)	-	-	-	-	-	-
	$\bar{\lambda}_{ac}$ rms, $\sigma\lambda_{ac}$ rms (ft)	-	-	-	-	-	-
	$\bar{u}_{ac}$ rms, σu_{ac} rms (kts)	-	-	-	-	-	-
	# Ramp Strikes	0		0		0	
	$\bar{h}_{td}$, σh_{td} (ft)	-	-	7.5585	0.55549	9.7694	0.25806
	$\bar{h}_{ac}$, σh_{ac} (ft)	-	-	-0.73561	0.67732	1.4763	0.12225
	$\bar{\theta}_{ac}$, $\sigma\theta_{ac}$ (deg)	-	-	-0.03264	0.086322	-0.03301	0.085867
	# Bolters	0		0		0	
	$\bar{X}_{td}$, σX_{td} (ft)	-	-	-	-	-	-
	$\bar{Y}_{td}$, σY_{td} (ft)	-	-	-	-	-	-
	# Successful Touchdowns	0		5		5	
	$\bar{X}_{td}$, σX_{td} (ft)	-	-	10.2946	5.0883	7.9568	3.3752
	$\bar{Y}_{td}$, σY_{td} (ft)	-	-	6.2421	0.4436	6.8157	0.26929
	$\bar{h}_{td}$, σh_{td} (ft)	-	-	-11.219	1.6866	-13.5318	0.48374
	$\bar{h}_{ac}$, σh_{ac} (ft)	-	-	-0.041616	0.44895	0.05663	0.59353
Carrier Speed = 33 Knots	# Successful Approaches	0		5		5	
	$\bar{h}_{ac}$ rms, σh_{ac} rms (ft)	-	-	1.1499	0.059972	0.73104	0.019478
	$\bar{\lambda}_{ac}$ rms, $\sigma\lambda_{ac}$ rms (ft)	-	-	3.2607	1.0521	4.4552	0.068244
	$\bar{u}_{ac}$ rms, σu_{ac} rms (kts)	-	-	0.48402	0.012979	0.45339	0.019072
	# Failed Approaches Vert	5		0		0	
	$\bar{t}_{td}$, σt_{td} (sec)	8.538	0.011606	-	-	-	-
	$\bar{h}_{ac}$ rms, σh_{ac} rms (ft)	1.9666	0.001293	-	-	-	-
	$\bar{\lambda}_{ac}$ rms, $\sigma\lambda_{ac}$ rms (ft)	0.36591	0.091321	-	-	-	-
	$\bar{u}_{ac}$ rms, σu_{ac} rms (kts)	0.39677	0.003412	-	-	-	-
	# Failed Approaches Lat	0		0		0	
	$\bar{t}_{td}$, σt_{td} (sec)	-	-	-	-	-	-
	$\bar{h}_{ac}$ rms, σh_{ac} rms (ft)	-	-	-	-	-	-
	$\bar{\lambda}_{ac}$ rms, $\sigma\lambda_{ac}$ rms (ft)	-	-	-	-	-	-
	$\bar{u}_{ac}$ rms, σu_{ac} rms (kts)	-	-	-	-	-	-
	# Ramp Strikes	0		0		0	
	$\bar{h}_{td}$, σh_{td} (ft)	-	-	10.6883	0.84831	8.4006	0.16967
	$\bar{h}_{ac}$, σh_{ac} (ft)	-	-	2.2113	0.83899	-0.07437	0.13087
	$\bar{\theta}_{ac}$, $\sigma\theta_{ac}$ (deg)	-	-	0.032853	0.054854	0.032119	0.055783
	# Bolters	0		0		0	
	$\bar{X}_{td}$, σX_{td} (ft)	-	-	-	-	-	-
	$\bar{Y}_{td}$, σY_{td} (ft)	-	-	-	-	-	-
	# Successful Touchdowns	0		5		5	
	$\bar{X}_{td}$, σX_{td} (ft)	-	-	-18.0064	5.7611	-10.6544	0.84334
	$\bar{Y}_{td}$, σY_{td} (ft)	-	-	2.6671	1.524	2.9649	0.56393
	$\bar{h}_{td}$, σh_{td} (ft)	-	-	-12.9907	1.511	-8.2468	0.16172
	$\bar{h}_{ac}$, σh_{ac} (ft)	-	-	0.13269	0.1668	-0.14352	0.16343

Table B-19 Moderate Turbulence 3D and Carrier Induced Turbulence – Wind 24.5 Knots

		Wind Speed = 37 Knots Moderate Three Dimensional Turbulence and Carrier Induced Turbulence					
		System 1		System 2		System 3	
Carrier Speed = 0 Knots	# Successful Approaches	0		0		0	
	$\bar{h}_r$ rms, σh_r rms (ft)	-	-	-	-	-	-
	$\bar{\lambda}_r$ rms, $\sigma\lambda_r$ rms (ft)	-	-	-	-	-	-
	$\bar{u}_r$ rms, σu_r rms (kts)	-	-	-	-	-	-
	# Failed Approaches Vert	0		1		0	
	$\bar{t}_{td}$, σt_{td} (sec)	-	-	5.7566	0	-	-
	$\bar{h}_r$ rms, σh_r rms (ft)	-	-	1.5856	0	-	-
	$\bar{\lambda}_r$ rms, $\sigma\lambda_r$ rms (ft)	-	-	2.7508	0	-	-
	$\bar{u}_r$ rms, σu_r rms (kts)	-	-	0.52483	0	-	-
	# Failed Approaches Lat	5		4		5	
	$\bar{t}_{td}$, σt_{td} (sec)	13.9873	0.096764	6.5151	0.4055	7.1675	0.25936
	$\bar{h}_r$ rms, σh_r rms (ft)	2.7839	0.055737	1.4065	0.10211	1.175	0.19751
	$\bar{\lambda}_r$ rms, $\sigma\lambda_r$ rms (ft)	2.1388	0.018996	2.5338	0.13213	2.721	0.26334
	$\bar{u}_r$ rms, σu_r rms (kts)	0.47129	0.025308	0.54191	0.011774	0.66178	0.026378
	# Ramp Strikes	0		0		0	
	$\bar{h}_{td}$, σh_{td} (ft)	-	-	-	-	-	-
	$\bar{h}_{td}$, σh_{td} (ft)	-	-	-	-	0	
	$\bar{\theta}_{td}$, $\sigma\theta_{td}$ (deg)	-	-	-	-	-	-
	# Bolters	0		0		-	-
	$\bar{X}_{td}$, σX_{td} (ft)	-	-	-	-	0	
	$\bar{Y}_{td}$, σY_{td} (ft)	-	-	-	-	-	-
	# Successful Touchdowns	0		0		0	
	$\bar{X}_{td}$, σX_{td} (ft)	-	-	-	-	-	-
	$\bar{Y}_{td}$, σY_{td} (ft)	-	-	-	-	-	-
	$\bar{h}_r$, σh_r (ft)	-	-	-	-	-	-
	$\bar{h}_{td}$, σh_{td} (ft)	-	-	-	-	-	-
Carrier Speed = 10Knots	# Successful Approaches	0		1		1	
	$\bar{h}_r$ rms, σh_r rms (ft)	-	-	1.6371	0	2.0073	0
	$\bar{\lambda}_r$ rms, $\sigma\lambda_r$ rms (ft)	-	-	3.0316	0	3.0107	0
	$\bar{u}_r$ rms, σu_r rms (kts)	-	-	0.56028	0	0.77395	0
	# Failed Approaches Vert	0		0		0	
	$\bar{t}_{td}$, σt_{td} (sec)	-	-	-	-	-	-
	$\bar{h}_r$ rms, σh_r rms (ft)	-	-	-	-	-	-
	$\bar{\lambda}_r$ rms, $\sigma\lambda_r$ rms (ft)	-	-	-	-	-	-
	$\bar{u}_r$ rms, σu_r rms (kts)	-	-	-	-	-	-
	# Failed Approaches Lat	5		4		4	
	$\bar{t}_{td}$, σt_{td} (sec)	14.1493	0.012482	7.278	1.9237	7.6036	0.37635
	$\bar{h}_r$ rms, σh_r rms (ft)	2.8986	0.042638	1.3498	0.070349	1.2268	0.037327
	$\bar{\lambda}_r$ rms, $\sigma\lambda_r$ rms (ft)	2.1355	0.058306	2.7701	0.24284	3.1033	0.47411
	$\bar{u}_r$ rms, σu_r rms (kts)	0.5404	0.010429	0.52435	0.028811	0.70372	0.07059
	# Ramp Strikes	0		0		0	
	$\bar{h}_{td}$, σh_{td} (ft)	-	-	9.0362	0	10.8696	0
	$\bar{h}_{td}$, σh_{td} (ft)	-	-	0.3215	0	1.3546	0
	$\bar{\theta}_{td}$, $\sigma\theta_{td}$ (deg)	-	-	0.11796	0	0.40455	0
	# Bolters	0		0		0	
	$\bar{X}_{td}$, σX_{td} (ft)	-	-	-	-	-	-
	$\bar{Y}_{td}$, σY_{td} (ft)	-	-	-	-	-	-
	# Successful Touchdowns	0		1		1	
	$\bar{X}_{td}$, σX_{td} (ft)	-	-	-13.0357	0	-22.452	0
	$\bar{Y}_{td}$, σY_{td} (ft)	-	-	-0.58265	0	-1.8912	0
	$\bar{h}_r$, σh_r (ft)	-	-	-7.6695	0	-4.8772	0
	$\bar{h}_{td}$, σh_{td} (ft)	-	-	1.4266	0	1.138	0
Carrier Speed = 33 Knots	# Successful Approaches	0		4		5	
	$\bar{h}_r$ rms, σh_r rms (ft)	-	-	3.5316	1.2165	2.5934	0.44206
	$\bar{\lambda}_r$ rms, $\sigma\lambda_r$ rms (ft)	-	-	4.7269	0.77742	2.1733	0.079865
	$\bar{u}_r$ rms, σu_r rms (kts)	-	-	0.81385	0.047396	0.96051	0.072892
	# Failed Approaches Vert	0		0		0	
	$\bar{t}_{td}$, σt_{td} (sec)	-	-	-	-	-	-
	$\bar{h}_r$ rms, σh_r rms (ft)	-	-	-	-	-	-
	$\bar{\lambda}_r$ rms, $\sigma\lambda_r$ rms (ft)	-	-	-	-	-	-
	$\bar{u}_r$ rms, σu_r rms (kts)	-	-	-	-	-	-
	# Failed Approaches Lat	5		1		0	
	$\bar{t}_{td}$, σt_{td} (sec)	11.2553	0.054584	8.0955	0	-	-
	$\bar{h}_r$ rms, σh_r rms (ft)	3.1813	0.016788	2.1356	0	-	-
	$\bar{\lambda}_r$ rms, $\sigma\lambda_r$ rms (ft)	1.5775	0.027839	1.8105	0	-	-
	$\bar{u}_r$ rms, σu_r rms (kts)	0.47471	0.032634	0.66913	0	-	-
	# Ramp Strikes	0		0		0	
	$\bar{h}_{td}$, σh_{td} (ft)	-	-	11.4173	1.3098	11.109	2.141
	$\bar{h}_{td}$, σh_{td} (ft)	-	-	2.6912	0.99847	2.7282	1.336
	$\bar{\theta}_{td}$, $\sigma\theta_{td}$ (deg)	-	-	0.12205	0.23286	-0.00158	0.30437
	# Bolters	0		0		0	
	$\bar{X}_{td}$, σX_{td} (ft)	-	-	-	-	-	-
	$\bar{Y}_{td}$, σY_{td} (ft)	-	-	-	-	-	-
	# Successful Touchdowns	0		4		5	
	$\bar{X}_{td}$, σX_{td} (ft)	-	-	-9.6356	3.3229	-4.0993	4.0638
	$\bar{Y}_{td}$, σY_{td} (ft)	-	-	7.884	9.1468	-3.565	0.72817
	$\bar{h}_r$, σh_r (ft)	-	-	-12.2345	1.9236	-12.9691	1.631
	$\bar{h}_{td}$, σh_{td} (ft)	-	-	0.47669	0.83051	-1.4544	3.7625

Table B-20 Moderate Turbulence 3D and Carrier Induced Turbulence – Wind 37 Knots

		Wind Speed = 2 Knots Moderate Two Dimensional Turbulence and Carrier Induced Turbulence					
		System 1		System 2		System 3	
Carrier Speed = 0 Knots	# Successful Approaches	5		5		5	
	$\bar{h}_w$ rms, σh_w rms (ft)	1.4454	0.000362	1.1879	0.002291	0.64668	0.001027
	$\bar{\lambda}_w$ rms, $\sigma\lambda_w$ rms (ft)	0.000117	6.48E-06	0.00047	4.11E-05	0.000209	1.50E-05
	$\bar{u}_w$ rms, σu_w rms (kts)	0.32557	0.000185	0.43801	0.001024	0.44648	0.000391
	# Failed Approaches Vert	0		0		0	
	$\bar{t}_{td}$, σt_{td} (sec)	-	-	-	-	-	-
	$\bar{h}_w$ rms, σh_w rms (ft)	-	-	-	-	-	-
	$\bar{\lambda}_w$ rms, $\sigma\lambda_w$ rms (ft)	-	-	-	-	-	-
	$\bar{u}_w$ rms, σu_w rms (kts)	-	-	-	-	-	-
	# Failed Approaches Lat	0		0		0	
	$\bar{t}_{td}$, σt_{td} (sec)	-	-	-	-	-	-
	$\bar{h}_w$ rms, σh_w rms (ft)	-	-	-	-	-	-
	$\bar{\lambda}_w$ rms, $\sigma\lambda_w$ rms (ft)	-	-	-	-	-	-
	$\bar{u}_w$ rms, σu_w rms (kts)	-	-	-	-	-	-
	# Ramp Strikes	0		0		0	
	$\bar{h}_d$, σh_d (ft)	10.662	0.036142	10.6173	0.13681	8.9544	0.032673
	$\bar{h}_{dy}$, σh_{dy} (ft)	2.3009	0.000942	2.2565	0.13048	0.59366	0.002311
	$\bar{\theta}_{dy}$, $\sigma\theta_{dy}$ (deg)	-0.00866	0.01297	-0.00874	0.010971	-0.00878	0.010926
	# Bolters	0		0		0	
	$\bar{X}_d$, σX_d (ft)	-	-	-	-	-	-
	$\bar{Y}_d$, σY_d (ft)	-	-	-	-	-	-
	# Successful Touchdowns	5		5		5	
	$\bar{X}_d$, σX_d (ft)	30.3163	1.2504	11.3541	0.96694	4.3496	0.33367
	$\bar{Y}_{dy}$, σY_{dy} (ft)	0.098371	0.021878	-0.02275	0.014258	0.018901	0.004358
	$\bar{h}_d$, σh_d (ft)	-19.5454	0.007735	-10.2966	0.12575	-11.3751	0.029743
	$\bar{h}_{dv}$, σh_{dv} (ft)	-0.021606	0.090693	-0.036398	0.04069	-0.031078	0.039326
Carrier Speed = 10Knots	# Successful Approaches	5		5		5	
	$\bar{h}_w$ rms, σh_w rms (ft)	1.4456	0.000172	1.158	0.001265	0.67109	0.00092
	$\bar{\lambda}_w$ rms, $\sigma\lambda_w$ rms (ft)	0.000187	1.47E-06	0.000919	0.000178	0.000252	2.85E-05
	$\bar{u}_w$ rms, σu_w rms (kts)	0.32246	0.000162	0.41206	0.001177	0.45208	0.000975
	# Failed Approaches Vert	0		0		0	
	$\bar{t}_{td}$, σt_{td} (sec)	-	-	-	-	-	-
	$\bar{h}_w$ rms, σh_w rms (ft)	-	-	-	-	-	-
	$\bar{\lambda}_w$ rms, $\sigma\lambda_w$ rms (ft)	-	-	-	-	-	-
	$\bar{u}_w$ rms, σu_w rms (kts)	-	-	-	-	-	-
	# Failed Approaches Lat	0		0		0	
	$\bar{t}_{td}$, σt_{td} (sec)	-	-	-	-	-	-
	$\bar{h}_w$ rms, σh_w rms (ft)	-	-	-	-	-	-
	$\bar{\lambda}_w$ rms, $\sigma\lambda_w$ rms (ft)	-	-	-	-	-	-
	$\bar{u}_w$ rms, σu_w rms (kts)	-	-	-	-	-	-
	# Ramp Strikes	0		0		0	
	$\bar{h}_d$, σh_d (ft)	9.253	0.044505	8.5459	0.037454	8.4276	0.029801
	$\bar{h}_{dy}$, σh_{dy} (ft)	0.84718	0.001791	0.14511	0.038653	0.026828	0.001369
	$\bar{\theta}_{dy}$, $\sigma\theta_{dy}$ (deg)	0.007386	0.015497	0.005564	0.010892	0.005564	0.010892
	# Bolters	0		0		0	
	$\bar{X}_d$, σX_d (ft)	-	-	-	-	-	-
	$\bar{Y}_d$, σY_d (ft)	-	-	-	-	-	-
	# Successful Touchdowns	5		5		5	
	$\bar{X}_d$, σX_d (ft)	43.4008	0.010286	2.7559	0.27031	11.4168	0.060027
	$\bar{Y}_{dy}$, σY_{dy} (ft)	-0.0146	0.009857	-0.02082	0.005294	0.008315	0.003448
	$\bar{h}_d$, σh_d (ft)	-19.2354	0.000598	-10.6121	0.022457	-12.4586	0.008377
	$\bar{h}_{dv}$, σh_{dv} (ft)	0.05491	0.059621	0.04594	0.079649	0.03487	0.057219
Carrier Speed = 33 Knots	# Successful Approaches	5		5		5	
	$\bar{h}_w$ rms, σh_w rms (ft)	1.4625	0.000525	1.1006	0.023522	0.68288	0.003618
	$\bar{\lambda}_w$ rms, $\sigma\lambda_w$ rms (ft)	0.000151	8.33E-07	0.001184	0.000556	0.00018	1.77E-05
	$\bar{u}_w$ rms, σu_w rms (kts)	0.32453	0.000192	0.3889	0.014224	0.43266	0.003688
	# Failed Approaches Vert	0		0		0	
	$\bar{t}_{td}$, σt_{td} (sec)	-	-	-	-	-	-
	$\bar{h}_w$ rms, σh_w rms (ft)	-	-	-	-	-	-
	$\bar{\lambda}_w$ rms, $\sigma\lambda_w$ rms (ft)	-	-	-	-	-	-
	$\bar{u}_w$ rms, σu_w rms (kts)	-	-	-	-	-	-
	# Failed Approaches Lat	0		0		0	
	$\bar{t}_{td}$, σt_{td} (sec)	-	-	-	-	-	-
	$\bar{h}_w$ rms, σh_w rms (ft)	-	-	-	-	-	-
	$\bar{\lambda}_w$ rms, $\sigma\lambda_w$ rms (ft)	-	-	-	-	-	-
	$\bar{u}_w$ rms, σu_w rms (kts)	-	-	-	-	-	-
	# Ramp Strikes	0		0		0	
	$\bar{h}_d$, σh_d (ft)	9.1721	0.015753	6.2633	0.30119	8.0985	0.009056
	$\bar{h}_{dy}$, σh_{dy} (ft)	0.79501	0.00236	-2.1138	0.30478	-0.27863	0.004038
	$\bar{\theta}_{dy}$, $\sigma\theta_{dy}$ (deg)	-0.00291	0.004998	-0.00291	0.003049	-0.0029	0.003079
	# Bolters	0		0		0	
	$\bar{X}_d$, σX_d (ft)	-	-	-	-	-	-
	$\bar{Y}_d$, σY_d (ft)	-	-	-	-	-	-
	# Successful Touchdowns	5		5		5	
	$\bar{X}_d$, σX_d (ft)	25.3036	0.15152	44.8088	21.8786	8.2311	0.56932
	$\bar{Y}_{dy}$, σY_{dy} (ft)	0.009494	0.002125	-0.03746	0.060327	0.048351	0.008183
	$\bar{h}_d$, σh_d (ft)	-19.3962	0.003216	-14.0632	1.0955	-11.9206	0.008937
	$\bar{h}_{dv}$, σh_{dv} (ft)	-0.009432	0.020894	-0.009235	0.027731	-0.008513	0.032666

Table B-21 Moderate Turbulence 2D and Carrier Induced Turbulence – Wind 2 Knots

		Wind Speed = 13.5 Knots Moderate Two Dimensional Turbulence and Carrier Induced Turbulence					
		System 1		System 2		System 3	
Carrier Speed = 0 Knots	# Successful Approaches	0		5		5	
	$\bar{h}_w$ rms, σh_w rms (ft)	-	-	1.1923	0.009455	0.6582	0.002287
	$\bar{\lambda}_w$ rms, $\sigma\lambda_w$ rms (ft)	-	-	0.002217	0.000118	0.002203	0.000144
	$\bar{u}_w$ rms, σu_w rms (kts)	-	-	0.43345	0.002134	0.45014	0.000614
	# Failed Approaches Vert	5		0		0	
	$\bar{t}_{td}$, σt_{td} (sec)	6.1476	0.016712	-	-	-	-
	$\bar{h}_w$ rms, σh_w rms (ft)	1.4683	0.001895	-	-	-	-
	$\bar{\lambda}_w$ rms, $\sigma\lambda_w$ rms (ft)	0.003804	0.000449	-	-	-	-
	$\bar{u}_w$ rms, σu_w rms (kts)	0.38499	0.001742	-	-	-	-
	# Failed Approaches Lat	0		0		0	
	$\bar{t}_{td}$, σt_{td} (sec)	-	-	-	-	-	-
	$\bar{h}_w$ rms, σh_w rms (ft)	-	-	-	-	-	-
	$\bar{\lambda}_w$ rms, $\sigma\lambda_w$ rms (ft)	-	-	-	-	-	-
	$\bar{u}_w$ rms, σu_w rms (kts)	-	-	-	-	-	-
	# Ramp Strikes	0		0		0	
	$\bar{h}_d$, σh_d (ft)	-	-	10.5547	0.46279	8.9278	0.03457
	$\bar{h}_{dc}$, σh_{dc} (ft)	-	-	2.1332	0.5181	0.50641	0.032871
	$\bar{\theta}_{dc}$, $\sigma\theta_{dc}$ (deg)	-	-	0.012979	0.02215	0.012938	0.022185
	# Bolters	0		0		0	
	$\bar{X}_d$, σX_d (ft)	-	-	-	-	-	-
	$\bar{Y}_d$, σY_d (ft)	-	-	-	-	-	-
	# Successful Touchdowns	0		5		5	
	$\bar{X}_d$, σX_d (ft)	-	-	15.1632	1.3207	12.4493	0.070998
	$\bar{Y}_{td}$, σY_d (ft)	-	-	-0.01793	0.037549	0.0182	0.010096
	$\bar{h}_d$, σh_d (ft)	-	-	-9.9164	0.3883	-12.6941	0.061868
	$\bar{h}_{dc}$, σh_{dc} (ft)	-	-	-0.024443	0.051198	-0.021446	0.071488
Carrier Speed = 10Knots	# Successful Approaches	5		5		5	
	$\bar{h}_w$ rms, σh_w rms (ft)	2.0833	0.006283	1.0903	0.02289	0.7029	0.002279
	$\bar{\lambda}_w$ rms, $\sigma\lambda_w$ rms (ft)	0.009009	0.001244	0.003525	0.000974	0.002738	4.45E-05
	$\bar{u}_w$ rms, σu_w rms (kts)	0.44403	0.000932	0.40994	0.002422	0.45592	0.002559
	# Failed Approaches Vert	0		0		0	
	$\bar{t}_{td}$, σt_{td} (sec)	-	-	-	-	-	-
	$\bar{h}_w$ rms, σh_w rms (ft)	-	-	-	-	-	-
	$\bar{\lambda}_w$ rms, $\sigma\lambda_w$ rms (ft)	-	-	-	-	-	-
	$\bar{u}_w$ rms, σu_w rms (kts)	-	-	-	-	-	-
	# Failed Approaches Lat	0		0		0	
	$\bar{t}_{td}$, σt_{td} (sec)	-	-	-	-	-	-
	$\bar{h}_w$ rms, σh_w rms (ft)	-	-	-	-	-	-
	$\bar{\lambda}_w$ rms, $\sigma\lambda_w$ rms (ft)	-	-	-	-	-	-
	$\bar{u}_w$ rms, σu_w rms (kts)	-	-	-	-	-	-
	# Ramp Strikes	0		0		0	
	$\bar{h}_d$, σh_d (ft)	6.4649	0.048943	8.1644	0.24421	8.5032	0.051498
	$\bar{h}_{dc}$, σh_{dc} (ft)	-1.886	0.005307	-0.23202	0.27671	0.10675	0.006967
	$\bar{\theta}_{dc}$, $\sigma\theta_{dc}$ (deg)	-0.01228	0.019314	0.004011	0.017243	0.004011	0.017243
	# Bolters	5		1		0	
	$\bar{X}_d$, σX_d (ft)	225.5366	3.7892	61.084	0	-	-
	$\bar{Y}_d$, σY_d (ft)	-0.52947	0.14448	0.18612	0	-	-
	# Successful Touchdowns	0		4		5	
	$\bar{X}_d$, σX_d (ft)	-	-	39.3256	21.6101	16.8619	1.0309
	$\bar{Y}_{td}$, σY_d (ft)	-	-	-0.12774	0.042394	0.025757	0.018941
	$\bar{h}_d$, σh_d (ft)	-	-	-14.7133	2.8283	-11.3066	0.044334
	$\bar{h}_{dc}$, σh_{dc} (ft)	-	-	0.09572	0.12708	0.06934	0.15844
Carrier Speed = 33 Knots	# Successful Approaches	5		5		5	
	$\bar{h}_w$ rms, σh_w rms (ft)	1.8919	0.002569	1.1544	0.046715	0.69395	0.009443
	$\bar{\lambda}_w$ rms, $\sigma\lambda_w$ rms (ft)	0.003544	0.000853	0.003616	0.000615	0.002974	0.000267
	$\bar{u}_w$ rms, σu_w rms (kts)	0.39465	0.00024	0.49425	0.014589	0.45233	0.005253
	# Failed Approaches Vert	0		0		0	
	$\bar{t}_{td}$, σt_{td} (sec)	-	-	-	-	-	-
	$\bar{h}_w$ rms, σh_w rms (ft)	-	-	-	-	-	-
	$\bar{\lambda}_w$ rms, $\sigma\lambda_w$ rms (ft)	-	-	-	-	-	-
	$\bar{u}_w$ rms, σu_w rms (kts)	-	-	-	-	-	-
	# Failed Approaches Lat	0		0		0	
	$\bar{t}_{td}$, σt_{td} (sec)	-	-	-	-	-	-
	$\bar{h}_w$ rms, σh_w rms (ft)	-	-	-	-	-	-
	$\bar{\lambda}_w$ rms, $\sigma\lambda_w$ rms (ft)	-	-	-	-	-	-
	$\bar{u}_w$ rms, σu_w rms (kts)	-	-	-	-	-	-
	# Ramp Strikes	0		0		0	
	$\bar{h}_d$, σh_d (ft)	7.8912	0.029966	9.7596	0.13888	7.7719	0.036318
	$\bar{h}_{dc}$, σh_{dc} (ft)	-0.48088	0.002133	1.3722	0.15907	-0.61489	0.030917
	$\bar{\theta}_{dc}$, $\sigma\theta_{dc}$ (deg)	-0.00471	0.010216	0.000773	0.010211	0.00055	0.010256
	# Bolters	0		0		0	
	$\bar{X}_d$, σX_d (ft)	-	-	-	-	-	-
	$\bar{Y}_d$, σY_d (ft)	-	-	-	-	-	-
	# Successful Touchdowns	5		5		5	
	$\bar{X}_d$, σX_d (ft)	-56.3178	0.67466	-11.1526	1.5716	-6.8971	0.32971
	$\bar{Y}_{td}$, σY_d (ft)	0.025237	0.048231	-0.02232	0.013777	-0.01622	0.012543
	$\bar{h}_d$, σh_d (ft)	-20.7958	0.00951	-8.673	0.31491	-7.1491	0.032031
	$\bar{h}_{dc}$, σh_{dc} (ft)	-0.00267	0.033649	0.02857	0.040621	-0.03078	0.044047

Table B-22 Moderate Turbulence 2D and Carrier Induced Turbulence – Wind 13.5 Knots

		Wind Speed = 24.5 Knots Moderate Two Dimensional Turbulence and Carrier Induced Turbulence					
		System 1		System 2		System 3	
Carrier Speed = 0 Knots	# Successful Approaches	0		5		5	
	$\bar{h}_{ss}$ rms, σh_{ss} rms (ft)	-	-	1.2099	0.078052	0.66409	0.006814
	$\bar{\lambda}_{ss}$ rms, $\sigma\lambda_{ss}$ rms (ft)	-	-	0.005755	0.001303	0.00424	0.000224
	$\bar{u}_{ss}$ rms, σu_{ss} rms (kts)	-	-	0.44532	0.02441	0.45702	0.00167
	# Failed Approaches Vert	5		0		0	
	$\bar{t}_{fail}$, σt_{fail} (sec)	8.7289	0.009437	-	-	-	-
	$\bar{h}_{ss}$ rms, σh_{ss} rms (ft)	1.7936	0.005858	-	-	-	-
	$\bar{\lambda}_{ss}$ rms, $\sigma\lambda_{ss}$ rms (ft)	0.021345	0.004297	-	-	-	-
	$\bar{u}_{ss}$ rms, σu_{ss} rms (kts)	0.38071	0.000772	-	-	-	-
	# Failed Approaches Lat	0		0		0	
	$\bar{t}_{fail}$, σt_{fail} (sec)	-	-	-	-	-	-
	$\bar{h}_{ss}$ rms, σh_{ss} rms (ft)	-	-	-	-	-	-
	$\bar{\lambda}_{ss}$ rms, $\sigma\lambda_{ss}$ rms (ft)	-	-	-	-	-	-
	$\bar{u}_{ss}$ rms, σu_{ss} rms (kts)	-	-	-	-	-	-
	# Ramp Strikes	0		0		0	
	$\bar{h}_{ss}$, σh_{ss} (ft)	-	-	12.4763	1.6759	9.008	0.27053
	$\bar{h}_{ss}$, σh_{ss} (ft)	-	-	3.9674	1.8081	0.49921	0.081208
	$\bar{\theta}_{ss}$, $\sigma\theta_{ss}$ (deg)	-	-	0.044289	0.06883	0.044231	0.069141
	# Bolters	0		0		0	
	$\bar{X}_{td}$, σX_{td} (ft)	-	-	-	-	-	-
	$\bar{Y}_{td}$, σY_{td} (ft)	-	-	-	-	-	-
	# Successful Touchdowns	0		5		5	
	$\bar{X}_{td}$, σX_{td} (ft)	-	-	22.9182	9.5725	20.1463	1.6832
	$\bar{Y}_{td}$, σY_{td} (ft)	-	-	-0.0747	0.12768	0.087574	0.064429
	$\bar{h}_{c}$, σh_{c} (ft)	-	-	-12.2507	1.8325	-12.5293	0.47137
	$\bar{h}_{c}$, σh_{c} (ft)	-	-	0.08705	0.30159	-0.086886	0.28366
Carrier Speed = 10Knots	# Successful Approaches	0		5		5	
	$\bar{h}_{ss}$ rms, σh_{ss} rms (ft)	-	-	1.1281	0.067406	0.71772	0.023146
	$\bar{\lambda}_{ss}$ rms, $\sigma\lambda_{ss}$ rms (ft)	-	-	0.004394	0.000623	0.005642	0.000687
	$\bar{u}_{ss}$ rms, σu_{ss} rms (kts)	-	-	0.3862	0.015368	0.41696	0.004133
	# Failed Approaches Vert	5		0		0	
	$\bar{t}_{fail}$, σt_{fail} (sec)	6.9875	0.009219	-	-	-	-
	$\bar{h}_{ss}$ rms, σh_{ss} rms (ft)	2.0843	0.008795	-	-	-	-
	$\bar{\lambda}_{ss}$ rms, $\sigma\lambda_{ss}$ rms (ft)	0.028031	0.014838	-	-	-	-
	$\bar{u}_{ss}$ rms, σu_{ss} rms (kts)	0.41677	0.003773	-	-	-	-
	# Failed Approaches Lat	0		0		0	
	$\bar{t}_{fail}$, σt_{fail} (sec)	-	-	-	-	-	-
	$\bar{h}_{ss}$ rms, σh_{ss} rms (ft)	-	-	-	-	-	-
	$\bar{\lambda}_{ss}$ rms, $\sigma\lambda_{ss}$ rms (ft)	-	-	-	-	-	-
	$\bar{u}_{ss}$ rms, σu_{ss} rms (kts)	-	-	-	-	-	-
	# Ramp Strikes	0		0		0	
	$\bar{h}_{ss}$, σh_{ss} (ft)	-	-	7.3586	0.7368	9.6821	0.30121
	$\bar{h}_{ss}$, σh_{ss} (ft)	-	-	-0.93447	0.80953	1.3889	0.15415
	$\bar{\theta}_{ss}$, $\sigma\theta_{ss}$ (deg)	-	-	-0.03301	0.085867	-0.03297	0.0858
	# Bolters	0		0		0	
	$\bar{X}_{td}$, σX_{td} (ft)	-	-	-	-	-	-
	$\bar{Y}_{td}$, σY_{td} (ft)	-	-	-	-	-	-
	# Successful Touchdowns	0		5		5	
	$\bar{X}_{td}$, σX_{td} (ft)	-	-	1.2012	5.3648	-0.57532	3.6339
	$\bar{Y}_{td}$, σY_{td} (ft)	-	-	0.009379	0.045299	0.07333	0.019508
	$\bar{h}_{c}$, σh_{c} (ft)	-	-	-11.0365	1.5103	-13.6305	0.46838
	$\bar{h}_{c}$, σh_{c} (ft)	-	-	5.94E-05	0.53298	-0.009531	0.51445
Carrier Speed = 33 Knots	# Successful Approaches	0		5		5	
	$\bar{h}_{ss}$ rms, σh_{ss} rms (ft)	-	-	1.1601	0.058404	0.7314	0.021851
	$\bar{\lambda}_{ss}$ rms, $\sigma\lambda_{ss}$ rms (ft)	-	-	0.012213	0.005814	0.006385	0.00095
	$\bar{u}_{ss}$ rms, σu_{ss} rms (kts)	-	-	0.47868	0.010423	0.44602	0.005767
	# Failed Approaches Vert	5		0		0	
	$\bar{t}_{fail}$, σt_{fail} (sec)	8.6142	0.006833	-	-	-	-
	$\bar{h}_{ss}$ rms, σh_{ss} rms (ft)	2.0454	0.003238	-	-	-	-
	$\bar{\lambda}_{ss}$ rms, $\sigma\lambda_{ss}$ rms (ft)	0.037099	0.005938	-	-	-	-
	$\bar{u}_{ss}$ rms, σu_{ss} rms (kts)	0.39749	0.000824	-	-	-	-
	# Failed Approaches Lat	0		0		0	
	$\bar{t}_{fail}$, σt_{fail} (sec)	-	-	-	-	-	-
	$\bar{h}_{ss}$ rms, σh_{ss} rms (ft)	-	-	-	-	-	-
	$\bar{\lambda}_{ss}$ rms, $\sigma\lambda_{ss}$ rms (ft)	-	-	-	-	-	-
	$\bar{u}_{ss}$ rms, σu_{ss} rms (kts)	-	-	-	-	-	-
	# Ramp Strikes	0		0		0	
	$\bar{h}_{ss}$, σh_{ss} (ft)	-	-	11.0982	0.63842	8.3053	0.13237
	$\bar{h}_{ss}$, σh_{ss} (ft)	-	-	2.6212	0.48708	-0.16923	0.075827
	$\bar{\theta}_{ss}$, $\sigma\theta_{ss}$ (deg)	-	-	0.032847	0.054821	0.031985	0.055917
	# Bolters	0		0		0	
	$\bar{X}_{td}$, σX_{td} (ft)	-	-	-	-	-	-
	$\bar{Y}_{td}$, σY_{td} (ft)	-	-	-	-	-	-
	# Successful Touchdowns	0		5		5	
	$\bar{X}_{td}$, σX_{td} (ft)	-	-	-18.9955	1.7946	-12.231	0.75391
	$\bar{Y}_{td}$, σY_{td} (ft)	-	-	-0.19048	0.16738	-0.04771	0.033543
	$\bar{h}_{c}$, σh_{c} (ft)	-	-	-13.7642	1.538	-8.1851	0.060968
	$\bar{h}_{c}$, σh_{c} (ft)	-	-	0.13758	0.16727	-0.14648	0.17134

Table B-23 Moderate Turbulence 2D and Carrier Induced Turbulence – Wind 24.5 Knots

		Wind Speed = 37 Knots Moderate Two Dimensional Turbulence and Carrier Induced Turbulence					
		System 1		System 2		System 3	
Carrier Speed = 0 Knots	# Successful Approaches	0		5		5	
	$\bar{h}_w$ rms, σh_w rms (ft)	-	-	1.3147	0.1108	0.77881	0.042037
	$\bar{\lambda}_w$ rms, $\sigma\lambda_w$ rms (ft)	-	-	0.008013	0.00257	0.007614	0.001255
	$\bar{u}_w$ rms, σu_w rms (kts)	-	-	0.42882	0.020846	0.46482	0.003325
	# Failed Approaches Vert	5		0		0	
	$\bar{t}_{td}$, σt_{td} (sec)	6.189	0.097167	-	-	-	-
	$\bar{h}_w$ rms, σh_w rms (ft)	3.0197	0.041803	-	-	-	-
	$\bar{\lambda}_w$ rms, $\sigma\lambda_w$ rms (ft)	0.061284	0.006996	-	-	-	-
	$\bar{u}_w$ rms, σu_w rms (kts)	0.36683	0.001343	-	-	-	-
	# Failed Approaches Lat	0		0		0	
	$\bar{t}_{td}$, σt_{td} (sec)	-	-	-	-	-	-
	$\bar{h}_w$ rms, σh_w rms (ft)	-	-	-	-	-	-
	$\bar{\lambda}_w$ rms, $\sigma\lambda_w$ rms (ft)	-	-	-	-	-	-
	$\bar{u}_w$ rms, σu_w rms (kts)	-	-	-	-	-	-
	# Ramp Strikes	0		0		0	
	$\bar{h}_d$, σh_d (ft)	-	-	7.0487	1.2632	8.7782	0.38932
	$\bar{h}_{dv}$, σh_{dv} (ft)	-	-	-0.82273	0.95635	0.90774	0.48973
	$\bar{\theta}_{dv}$, $\sigma\theta_{dv}$ (deg)	-	-	-0.18399	0.12471	-0.18433	0.12497
	# Bolters	0		2		0	
	$\bar{X}_d$, σX_d (ft)	-	-	109.8193	62.2663	-	-
	$\bar{Y}_d$, σY_d (ft)	-	-	1.7596	3.1854	-	-
	# Successful Touchdowns	0		3		5	
	$\bar{X}_d$, σX_d (ft)	-	-	20.7396	24.9111	9.5161	2.6203
	$\bar{Y}_{dv}$, σY_d (ft)	-	-	-0.08365	0.12093	-0.13245	0.11706
	$\bar{h}_c$, σh_c (ft)	-	-	-7.5893	4.136	-6.8462	0.74185
	$\bar{h}_{cv}$, σh_{cv} (ft)	-	-	0.0833	0.87806	-0.034178	0.72732
Carrier Speed = 10Knots	# Successful Approaches	0		5		5	
	$\bar{h}_w$ rms, σh_w rms (ft)	-	-	1.2641	0.13424	0.76414	0.042965
	$\bar{\lambda}_w$ rms, $\sigma\lambda_w$ rms (ft)	-	-	0.019943	0.017196	0.0097	0.004019
	$\bar{u}_w$ rms, σu_w rms (kts)	-	-	0.42961	0.0311	0.42494	0.00607
	# Failed Approaches Vert	5		0		0	
	$\bar{t}_{td}$, σt_{td} (sec)	6.5042	0.059259	-	-	-	-
	$\bar{h}_w$ rms, σh_w rms (ft)	3.1126	0.032815	-	-	-	-
	$\bar{\lambda}_w$ rms, $\sigma\lambda_w$ rms (ft)	0.094112	0.053802	-	-	-	-
	$\bar{u}_w$ rms, σu_w rms (kts)	0.37153	0.000613	-	-	-	-
	# Failed Approaches Lat	0		0		0	
	$\bar{t}_{td}$, σt_{td} (sec)	-	-	-	-	-	-
	$\bar{h}_w$ rms, σh_w rms (ft)	-	-	-	-	-	-
	$\bar{\lambda}_w$ rms, $\sigma\lambda_w$ rms (ft)	-	-	-	-	-	-
	$\bar{u}_w$ rms, σu_w rms (kts)	-	-	-	-	-	-
	# Ramp Strikes	0		0		0	
	$\bar{h}_d$, σh_d (ft)	-	-	7.9604	1.0321	10.0073	0.75317
	$\bar{h}_{dv}$, σh_{dv} (ft)	-	-	-0.72365	0.72129	1.3225	0.19314
	$\bar{\theta}_{dv}$, $\sigma\theta_{dv}$ (deg)	-	-	0.10701	0.24322	0.10729	0.24339
	# Bolters	0		0		0	
	$\bar{X}_d$, σX_d (ft)	-	-	-	-	-	-
	$\bar{Y}_d$, σY_d (ft)	-	-	-	-	-	-
	# Successful Touchdowns	0		5		5	
	$\bar{X}_d$, σX_d (ft)	-	-	12.4695	17.0776	8.0962	4.969
	$\bar{Y}_{dv}$, σY_d (ft)	-	-	-0.23091	0.38156	-0.12178	0.12122
	$\bar{h}_c$, σh_c (ft)	-	-	-11.2777	2.4248	-12.7923	1.4241
	$\bar{h}_{cv}$, σh_{cv} (ft)	-	-	0.27777	0.71369	0.36674	0.71478
Carrier Speed = 33 Knots	# Successful Approaches	0		5		5	
	$\bar{h}_w$ rms, σh_w rms (ft)	-	-	1.6445	0.34927	0.87419	0.09192
	$\bar{\lambda}_w$ rms, $\sigma\lambda_w$ rms (ft)	-	-	0.052291	0.036661	0.055405	0.036109
	$\bar{u}_w$ rms, σu_w rms (kts)	-	-	0.82733	0.040499	0.76317	0.06844
	# Failed Approaches Vert	5		0		0	
	$\bar{t}_{td}$, σt_{td} (sec)	5.46	0.012604	-	-	-	-
	$\bar{h}_w$ rms, σh_w rms (ft)	3.3175	0.0173	-	-	-	-
	$\bar{\lambda}_w$ rms, $\sigma\lambda_w$ rms (ft)	0.095495	0.031144	-	-	-	-
	$\bar{u}_w$ rms, σu_w rms (kts)	0.43086	0.023632	-	-	-	-
	# Failed Approaches Lat	0		0		0	
	$\bar{t}_{td}$, σt_{td} (sec)	-	-	-	-	-	-
	$\bar{h}_w$ rms, σh_w rms (ft)	-	-	-	-	-	-
	$\bar{\lambda}_w$ rms, $\sigma\lambda_w$ rms (ft)	-	-	-	-	-	-
	$\bar{u}_w$ rms, σu_w rms (kts)	-	-	-	-	-	-
	# Ramp Strikes	0		0		0	
	$\bar{h}_d$, σh_d (ft)	-	-	12.7317	1.786	9.619	0.74335
	$\bar{h}_{dv}$, σh_{dv} (ft)	-	-	4.4678	2.087	1.343	0.26987
	$\bar{\theta}_{dv}$, $\sigma\theta_{dv}$ (deg)	-	-	-0.04344	0.19947	-0.03913	0.18837
	# Bolters	0		0		0	
	$\bar{X}_d$, σX_d (ft)	-	-	-	-	-	-
	$\bar{Y}_d$, σY_d (ft)	-	-	-	-	-	-
	# Successful Touchdowns	0		5		5	
	$\bar{X}_d$, σX_d (ft)	-	-	19.1967	22.8168	5.1574	12.0345
	$\bar{Y}_{dv}$, σY_d (ft)	-	-	-0.31569	0.47797	-0.32616	0.64181
	$\bar{h}_c$, σh_c (ft)	-	-	-11.1073	3.0162	-9.343	1.6439
	$\bar{h}_{cv}$, σh_{cv} (ft)	-	-	-0.36755	1.0278	-0.41102	1.0115

Table B-24 Moderate Turbulence 2D and Carrier Induced Turbulence – Wind 37 Knots

		Wind Speed = 2 Knots Severe Three Dimensional Turbulence and Carrier Induced Turbulence					
		System 1		System 2		System 3	
Carrier Speed = 0 Knots	# Successful Approaches	5		5		5	
	$\bar{h}$ rms, σh rms (ft)	1.7171	0.00087	1.4028	0.003104	0.84755	0.002065
	$\bar{\lambda}$ rms, $\sigma\lambda$ rms (ft)	0.33261	0.000265	1.5552	0.008372	1.3125	0.000331
	$\bar{u}$ rms, σu rms (kts)	0.40087	0.00066	0.56589	0.001362	0.58902	0.002661
	# Failed Approaches Vert	0		0		0	
	$\bar{t}_{td}$, σt_{td} (sec)	-	-	-	-	-	-
	$\bar{h}$ rms, σh rms (ft)	-	-	-	-	-	-
	$\bar{\lambda}$ rms, $\sigma\lambda$ rms (ft)	-	-	-	-	-	-
	$\bar{u}$ rms, σu rms (kts)	-	-	-	-	-	-
	# Failed Approaches Lat	0		0		0	
	$\bar{t}_{td}$, σt_{td} (sec)	-	-	-	-	-	-
	$\bar{h}$ rms, σh rms (ft)	-	-	-	-	-	-
	$\bar{\lambda}$ rms, $\sigma\lambda$ rms (ft)	-	-	-	-	-	-
	$\bar{u}$ rms, σu rms (kts)	-	-	-	-	-	-
	# Ramp Strikes	0		0		0	
	$\bar{h}_{td}$, σh_{td} (ft)	11.0157	0.036463	10.2663	0.095672	8.7433	0.031347
	$\bar{h}_{ac}$, σh_{ac} (ft)	2.6546	0.000727	1.9054	0.10991	0.38257	0.001976
	$\bar{\theta}_{ac}$, $\sigma\theta_{ac}$ (deg)	-0.00867	0.013037	-0.00874	0.011075	-0.00876	0.011001
	# Bolters	0		0		0	
	$\bar{X}_{td}$, σX_{td} (ft)	-	-	-	-	-	-
	$\bar{Y}_{td}$, σY_{td} (ft)	-	-	-	-	-	-
	# Successful Touchdowns	5		5		5	
	$\bar{X}_{td}$, σX_{td} (ft)	28.5322	1.2487	17.2834	3.1262	0.99222	0.014493
	$\bar{Y}_{td}$, σY_{td} (ft)	1.3041	0.004944	9.022	0.11903	5.5252	0.019771
	$\bar{h}_{td}$, σh_{td} (ft)	-20.3691	0.012915	-9.4399	1.0738	-10.6674	0.002858
	$\bar{h}_{ac}$, σh_{ac} (ft)	-0.021519	0.084403	-0.036687	0.036554	0	0
Carrier Speed = 10Knots	# Successful Approaches	5		5		5	
	$\bar{h}$ rms, σh rms (ft)	1.7201	0.000683	1.4774	0.009953	0.89364	0.0019
	$\bar{\lambda}$ rms, $\sigma\lambda$ rms (ft)	0.35172	0.001775	1.4309	0.009715	1.3565	0.007863
	$\bar{u}$ rms, σu rms (kts)	0.39677	0.000526	0.56083	0.001807	0.60114	0.002209
	# Failed Approaches Vert	0		0		0	
	$\bar{t}_{td}$, σt_{td} (sec)	-	-	-	-	-	-
	$\bar{h}$ rms, σh rms (ft)	-	-	-	-	-	-
	$\bar{\lambda}$ rms, $\sigma\lambda$ rms (ft)	-	-	-	-	-	-
	$\bar{u}$ rms, σu rms (kts)	-	-	-	-	-	-
	# Failed Approaches Lat	0		0		0	
	$\bar{t}_{td}$, σt_{td} (sec)	-	-	-	-	-	-
	$\bar{h}$ rms, σh rms (ft)	-	-	-	-	-	-
	$\bar{\lambda}$ rms, $\sigma\lambda$ rms (ft)	-	-	-	-	-	-
	$\bar{u}$ rms, σu rms (kts)	-	-	-	-	-	-
	# Ramp Strikes	0		0		0	
	$\bar{h}_{td}$, σh_{td} (ft)	9.3321	0.044556	8.5033	0.21564	8.4097	0.031076
	$\bar{h}_{ac}$, σh_{ac} (ft)	0.9263	0.001726	0.10264	0.22467	0.008913	0.000691
	$\bar{\theta}_{ac}$, $\sigma\theta_{ac}$ (deg)	0.007353	0.015505	0.005536	0.010951	0.005564	0.010892
	# Bolters	0		4		0	
	$\bar{X}_{td}$, σX_{td} (ft)	-	-	65.3239	3.0025	-	-
	$\bar{Y}_{td}$, σY_{td} (ft)	-	-	8.841	0.056725	-	-
	# Successful Touchdowns	5		1		5	
	$\bar{X}_{td}$, σX_{td} (ft)	42.8033	1.1756	56.4408	0	6.3516	0.042447
	$\bar{Y}_{td}$, σY_{td} (ft)	1.3469	0.003754	8.74	0	3.4937	0.029595
	$\bar{h}_{td}$, σh_{td} (ft)	-20.1112	0.02069	-17.6786	0	-11.3115	0.008045
	$\bar{h}_{ac}$, σh_{ac} (ft)	0.05512	0.059961	-0.025572	0	0.03251	0.053518
Carrier Speed = 33 Knots	# Successful Approaches	5		5		5	
	$\bar{h}$ rms, σh rms (ft)	1.7465	0.001565	1.4642	0.027571	1.0159	0.00342
	$\bar{\lambda}$ rms, $\sigma\lambda$ rms (ft)	0.33431	0.000303	1.4495	0.11734	1.1361	0.012149
	$\bar{u}$ rms, σu rms (kts)	0.40052	0.000355	0.55755	0.012023	0.68711	0.00618
	# Failed Approaches Vert	0		0		0	
	$\bar{t}_{td}$, σt_{td} (sec)	-	-	-	-	-	-
	$\bar{h}$ rms, σh rms (ft)	-	-	-	-	-	-
	$\bar{\lambda}$ rms, $\sigma\lambda$ rms (ft)	-	-	-	-	-	-
	$\bar{u}$ rms, σu rms (kts)	-	-	-	-	-	-
	# Failed Approaches Lat	0		0		0	
	$\bar{t}_{td}$, σt_{td} (sec)	-	-	-	-	-	-
	$\bar{h}$ rms, σh rms (ft)	-	-	-	-	-	-
	$\bar{\lambda}$ rms, $\sigma\lambda$ rms (ft)	-	-	-	-	-	-
	$\bar{u}$ rms, σu rms (kts)	-	-	-	-	-	-
	# Ramp Strikes	0		0		0	
	$\bar{h}_{td}$, σh_{td} (ft)	9.2656	0.014496	6.7675	0.45507	7.8851	0.013691
	$\bar{h}_{ac}$, σh_{ac} (ft)	0.88848	0.001657	-1.6097	0.4496	-0.49203	0.012515
	$\bar{\theta}_{ac}$, $\sigma\theta_{ac}$ (deg)	-0.00291	0.005003	-0.0029	0.003107	-0.0029	0.003149
	# Bolters	0		1		0	
	$\bar{X}_{td}$, σX_{td} (ft)	-	-	67.8612	0	-	-
	$\bar{Y}_{td}$, σY_{td} (ft)	-	-	7.3189	0	-	-
	# Successful Touchdowns	5		4		5	
	$\bar{X}_{td}$, σX_{td} (ft)	24.7651	0.11038	42.0625	6.4956	6.1546	0.14824
	$\bar{Y}_{td}$, σY_{td} (ft)	1.224	0.001502	7.6687	0.26476	7.018	0.2525
	$\bar{h}_{td}$, σh_{td} (ft)	-20.2676	0.001482	-13.9537	0.61091	-10.9896	0.029493
	$\bar{h}_{ac}$, σh_{ac} (ft)	-0.009981	0.021587	-0.017258	0.029595	0.008424	0.026864

Table B-25 Severe Turbulence 3D and Carrier Induced Turbulence – Wind 2 Knots

		Wind Speed = 13.5 Knots Severe Three Dimensional Turbulence and Carrier Induced Turbulence					
		System 1		System 2		System 3	
Carrier Speed = 0 Knots	# Successful Approaches	0		5		5	
	$\bar{h}_{ss}$ rms, σh_{ss} rms (ft)	-	-	1.4398	0.007445	0.83004	0.001967
	$\bar{\lambda}_{ss}$ rms, $\sigma\lambda_{ss}$ rms (ft)	-	-	1.4359	0.013757	1.2846	0.010891
	$\bar{u}_{ss}$ rms, σu_{ss} rms (kts)	-	-	0.54317	0.002362	0.59059	0.002709
	# Failed Approaches Vert	5		0		0	
	$\bar{t}_{td}$, σt_{td} (sec)	6.3924	0.006403	-	-	-	-
	$\bar{h}_{ss}$ rms, σh_{ss} rms (ft)	1.6749	0.000959	-	-	-	-
	$\bar{\lambda}_{ss}$ rms, $\sigma\lambda_{ss}$ rms (ft)	0.20667	0.003685	-	-	-	-
	$\bar{u}_{ss}$ rms, σu_{ss} rms (kts)	0.44407	0.0019	-	-	-	-
	# Failed Approaches Lat	0		0		0	
	$\bar{t}_{td}$, σt_{td} (sec)	-	-	-	-	-	-
	$\bar{h}_{ss}$ rms, σh_{ss} rms (ft)	-	-	-	-	-	-
	$\bar{\lambda}_{ss}$ rms, $\sigma\lambda_{ss}$ rms (ft)	-	-	-	-	-	-
	$\bar{u}_{ss}$ rms, σu_{ss} rms (kts)	-	-	-	-	-	-
	# Ramp Strikes	0		0		0	
	$\bar{h}_{td}$, σh_{td} (ft)	-	-	10.5907	0.10572	8.8041	0.058789
	$\bar{h}_{ss}$, σh_{ss} (ft)	-	-	2.169	0.16418	0.38259	0.005283
	$\bar{\theta}_{ss}$, $\sigma\theta_{ss}$ (deg)	-	-	0.013059	0.022176	0.012979	0.02215
	# Bolters	0		0		0	
	$\bar{X}_{td}$, σX_{td} (ft)	-	-	-	-	-	-
	$\bar{Y}_{td}$, σY_{td} (ft)	-	-	-	-	-	-
	# Successful Touchdowns	0		5		5	
	$\bar{X}_{td}$, σX_{td} (ft)	-	-	27.513	6.2128	6.4372	0.12122
	$\bar{Y}_{td}$, σY_{td} (ft)	-	-	8.1264	0.30005	5.1633	0.10629
	$\bar{h}_{td}$, σh_{td} (ft)	-	-	-14.1278	1.3171	-11.6053	0.072834
	$\bar{h}_{ss}$, σh_{ss} (ft)	-	-	-0.01869	0.051844	-0.019761	0.035881
Carrier Speed = 10Knots	# Successful Approaches	0		5		5	
	$\bar{h}_{ss}$ rms, σh_{ss} rms (ft)	-	-	1.4809	0.029249	0.92735	0.004768
	$\bar{\lambda}_{ss}$ rms, $\sigma\lambda_{ss}$ rms (ft)	-	-	1.4519	0.011864	1.582	0.016803
	$\bar{u}_{ss}$ rms, σu_{ss} rms (kts)	-	-	0.56347	0.007933	0.60792	0.00332
	# Failed Approaches Vert	5		0		0	
	$\bar{t}_{td}$, σt_{td} (sec)	6.9125	0.005307	-	-	-	-
	$\bar{h}_{ss}$ rms, σh_{ss} rms (ft)	1.6811	0.001923	-	-	-	-
	$\bar{\lambda}_{ss}$ rms, $\sigma\lambda_{ss}$ rms (ft)	0.172	0.00118	-	-	-	-
	$\bar{u}_{ss}$ rms, σu_{ss} rms (kts)	0.4316	0.000571	-	-	-	-
	# Failed Approaches Lat	0		0		0	
	$\bar{t}_{td}$, σt_{td} (sec)	-	-	-	-	-	-
	$\bar{h}_{ss}$ rms, σh_{ss} rms (ft)	-	-	-	-	-	-
	$\bar{\lambda}_{ss}$ rms, $\sigma\lambda_{ss}$ rms (ft)	-	-	-	-	-	-
	$\bar{u}_{ss}$ rms, σu_{ss} rms (kts)	-	-	-	-	-	-
	# Ramp Strikes	0		0		0	
	$\bar{h}_{td}$, σh_{td} (ft)	-	-	8.1841	0.49485	8.4336	0.051806
	$\bar{h}_{ss}$, σh_{ss} (ft)	-	-	-0.21204	0.45607	0.037075	0.025089
	$\bar{\theta}_{ss}$, $\sigma\theta_{ss}$ (deg)	-	-	0.003894	0.017538	0.00405	0.017318
	# Bolters	0		4		0	
	$\bar{X}_{td}$, σX_{td} (ft)	-	-	73.4125	1.1803	-	-
	$\bar{Y}_{td}$, σY_{td} (ft)	-	-	8.5822	0.25752	-	-
	# Successful Touchdowns	0		1		5	
	$\bar{X}_{td}$, σX_{td} (ft)	-	-	32.611	0	7.6969	0.13472
	$\bar{Y}_{td}$, σY_{td} (ft)	-	-	8.3652	0	3.1292	0.034786
	$\bar{h}_{td}$, σh_{td} (ft)	-	-	-14.0488	0	-10.6313	0.017617
	$\bar{h}_{ss}$, σh_{ss} (ft)	-	-	-0.081385	0	0.05682	0.13361
Carrier Speed = 33 Knots	# Successful Approaches	5		4		5	
	$\bar{h}_{ss}$ rms, σh_{ss} rms (ft)	2.2233	0.005267	1.5687	0.053046	1.0079	0.023244
	$\bar{\lambda}_{ss}$ rms, $\sigma\lambda_{ss}$ rms (ft)	0.28153	0.009517	6.1273	1.2769	7.5636	0.19628
	$\bar{u}_{ss}$ rms, σu_{ss} rms (kts)	0.46637	0.000915	0.6228	0.004387	0.61541	0.010123
	# Failed Approaches Vert	0		0		0	
	$\bar{t}_{td}$, σt_{td} (sec)	-	-	-	-	-	-
	$\bar{h}_{ss}$ rms, σh_{ss} rms (ft)	-	-	-	-	-	-
	$\bar{\lambda}_{ss}$ rms, $\sigma\lambda_{ss}$ rms (ft)	-	-	-	-	-	-
	$\bar{u}_{ss}$ rms, σu_{ss} rms (kts)	-	-	-	-	-	-
	# Failed Approaches Lat	0		1		0	
	$\bar{t}_{td}$, σt_{td} (sec)	-	-	23.7178	0	-	-
	$\bar{h}_{ss}$ rms, σh_{ss} rms (ft)	-	-	0.66845	0	-	-
	$\bar{\lambda}_{ss}$ rms, $\sigma\lambda_{ss}$ rms (ft)	-	-	6.6148	0	-	-
	$\bar{u}_{ss}$ rms, σu_{ss} rms (kts)	-	-	0.3025	0	-	-
	# Ramp Strikes	0		0		0	
	$\bar{h}_{td}$, σh_{td} (ft)	7.5162	0.048597	8.4605	0.15101	7.4395	0.049601
	$\bar{h}_{ss}$, σh_{ss} (ft)	-0.8559	0.022435	0.073339	0.13977	-0.94732	0.038717
	$\bar{\theta}_{ss}$, $\sigma\theta_{ss}$ (deg)	-0.00471	0.010211	0.000691	0.011782	0.000557	0.010217
	# Bolters	0		0		0	
	$\bar{X}_{td}$, σX_{td} (ft)	-	-	-	-	-	-
	$\bar{Y}_{td}$, σY_{td} (ft)	-	-	-	-	-	-
	# Successful Touchdowns	5		4		5	
	$\bar{X}_{td}$, σX_{td} (ft)	-65.2116	0.70027	-29.9151	4.4578	-14.3743	0.31907
	$\bar{Y}_{td}$, σY_{td} (ft)	0.10067	0.041727	3.4066	2.6376	1.9858	0.20466
	$\bar{h}_{td}$, σh_{td} (ft)	-21.8785	0.024216	-10.7727	0.68056	-7.146	0.048247
	$\bar{h}_{ss}$, σh_{ss} (ft)	0.00383	0.034027	0.02235	0.040343	0.02956	0.04109

Table B-26 Severe Turbulence 3D and Carrier Induced Turbulence – Wind 13.5 Knots

		Wind Speed = 24.5 Knots Severe Three Dimensional Turbulence and Carrier Induced Turbulence					
		System 1		System 2		System 3	
Carrier Speed = 0 Knots	# Successful Approaches	0		5		5	
	$\bar{h}_{ac}$ rms, σh_{ac} rms (ft)	-	-	1.4321	0.004723	0.8275	0.010077
	$\bar{\lambda}_{ac}$ rms, $\sigma\lambda_{ac}$ rms (ft)	-	-	1.4228	0.06183	1.2419	0.007602
	$\bar{u}_{ac}$ rms, σu_{ac} rms (kts)	-	-	0.53213	0.002668	0.59074	0.002275
	# Failed Approaches Vert	5		0		0	
	$\bar{t}_{td}$, σt_{td} (sec)	8.7985	0.005458	-	-	-	-
	$\bar{h}_{ac}$ rms, σh_{ac} rms (ft)	2.0932	0.003352	-	-	-	-
	$\bar{\lambda}_{ac}$ rms, $\sigma\lambda_{ac}$ rms (ft)	0.35532	0.023845	-	-	-	-
	$\bar{u}_{ac}$ rms, σu_{ac} rms (kts)	0.43781	0.00104	-	-	-	-
	# Failed Approaches Lat	0		0		0	
	$\bar{t}_{td}$, σt_{td} (sec)	-	-	-	-	-	-
	$\bar{h}_{ac}$ rms, σh_{ac} rms (ft)	-	-	-	-	-	-
	$\bar{\lambda}_{ac}$ rms, $\sigma\lambda_{ac}$ rms (ft)	-	-	-	-	-	-
	$\bar{u}_{ac}$ rms, σu_{ac} rms (kts)	-	-	-	-	-	-
	# Ramp Strikes	0		0		0	
	$\bar{h}_{td}$, σh_{td} (ft)	-	-	10.1376	1.0934	8.9801	0.18018
	$\bar{h}_{ac}$, σh_{ac} (ft)	-	-	1.6281	0.91151	0.47132	0.037155
	$\bar{\theta}_{ac}$, $\sigma\theta_{ac}$ (deg)	-	-	0.04449	0.068952	0.044222	0.069
	# Bolters	0		0		0	
	$\bar{X}_{td}$, σX_{td} (ft)	-	-	-	-	-	-
	$\bar{Y}_{td}$, σY_{td} (ft)	-	-	-	-	-	-
	# Successful Touchdowns	0		5		5	
	$\bar{X}_{td}$, σX_{td} (ft)	-	-	21.9741	4.3811	12.534	1.2804
	$\bar{Y}_{td}$, σY_{td} (ft)	-	-	6.6085	0.67583	7.6363	0.081734
	$\bar{h}_{td}$, σh_{td} (ft)	-	-	-10.7821	1.6627	-11.0273	0.50662
	$\bar{h}_{ac}$, σh_{ac} (ft)	-	-	-0.063812	0.33761	-0.089055	0.26701
Carrier Speed = 10Knots	# Successful Approaches	0		5		5	
	$\bar{h}_{ac}$ rms, σh_{ac} rms (ft)	-	-	1.4348	0.011097	0.9522	0.023452
	$\bar{\lambda}_{ac}$ rms, $\sigma\lambda_{ac}$ rms (ft)	-	-	4.2913	0.083329	4.1216	0.080179
	$\bar{u}_{ac}$ rms, σu_{ac} rms (kts)	-	-	0.53387	0.01211	0.57761	0.002576
	# Failed Approaches Vert	5		0		0	
	$\bar{t}_{td}$, σt_{td} (sec)	7.0403	0.008114	-	-	-	-
	$\bar{h}_{ac}$ rms, σh_{ac} rms (ft)	2.4528	0.012731	-	-	-	-
	$\bar{\lambda}_{ac}$ rms, $\sigma\lambda_{ac}$ rms (ft)	0.31584	0.054501	-	-	-	-
	$\bar{u}_{ac}$ rms, σu_{ac} rms (kts)	0.46901	0.005736	-	-	-	-
	# Failed Approaches Lat	0		0		0	
	$\bar{t}_{td}$, σt_{td} (sec)	-	-	-	-	-	-
	$\bar{h}_{ac}$ rms, σh_{ac} rms (ft)	-	-	-	-	-	-
	$\bar{\lambda}_{ac}$ rms, $\sigma\lambda_{ac}$ rms (ft)	-	-	-	-	-	-
	$\bar{u}_{ac}$ rms, σu_{ac} rms (kts)	-	-	-	-	-	-
	# Ramp Strikes	0		0		0	
	$\bar{h}_{td}$, σh_{td} (ft)	-	-	6.9283	0.55089	9.7336	0.12894
	$\bar{h}_{ac}$, σh_{ac} (ft)	-	-	-1.3645	0.68031	1.4406	0.22207
	$\bar{\theta}_{ac}$, $\sigma\theta_{ac}$ (deg)	-	-	-0.03309	0.08545	-0.03304	0.085391
	# Bolters	0		0		0	
	$\bar{X}_{td}$, σX_{td} (ft)	-	-	-	-	-	-
	$\bar{Y}_{td}$, σY_{td} (ft)	-	-	-	-	-	-
	# Successful Touchdowns	0		5		5	
	$\bar{X}_{td}$, σX_{td} (ft)	-	-	5.9704	13.0015	16.2611	4.787
	$\bar{Y}_{td}$, σY_{td} (ft)	-	-	7.3863	0.45957	8.7006	0.90874
	$\bar{h}_{td}$, σh_{td} (ft)	-	-	-10.7059	2.5363	-14.4594	0.4433
	$\bar{h}_{ac}$, σh_{ac} (ft)	-	-	0.01097	0.56783	0.01869	0.59357
Carrier Speed = 33 Knots	# Successful Approaches	0		5		3	
	$\bar{h}_{ac}$ rms, σh_{ac} rms (ft)	-	-	1.5728	0.056703	1.1075	0.073815
	$\bar{\lambda}_{ac}$ rms, $\sigma\lambda_{ac}$ rms (ft)	-	-	5.7805	1.1688	7.7291	0.081132
	$\bar{u}_{ac}$ rms, σu_{ac} rms (kts)	-	-	0.60693	0.005064	0.65767	0.044116
	# Failed Approaches Vert	5		0		0	
	$\bar{t}_{td}$, σt_{td} (sec)	8.6645	0.010244	-	-	-	-
	$\bar{h}_{ac}$ rms, σh_{ac} rms (ft)	2.3138	0.003465	-	-	-	-
	$\bar{\lambda}_{ac}$ rms, $\sigma\lambda_{ac}$ rms (ft)	0.42552	0.096943	-	-	-	-
	$\bar{u}_{ac}$ rms, σu_{ac} rms (kts)	0.44914	0.001036	-	-	-	-
	# Failed Approaches Lat	0		0		2	
	$\bar{t}_{td}$, σt_{td} (sec)	-	-	-	-	23.7808	0.12813
	$\bar{h}_{ac}$ rms, σh_{ac} rms (ft)	-	-	-	-	0.46279	0.001226
	$\bar{\lambda}_{ac}$ rms, $\sigma\lambda_{ac}$ rms (ft)	-	-	-	-	6.6958	0.12206
	$\bar{u}_{ac}$ rms, σu_{ac} rms (kts)	-	-	-	-	0.24098	0.00414
	# Ramp Strikes	0		0		0	
	$\bar{h}_{td}$, σh_{td} (ft)	-	-	9.181	0.23509	8.0132	0.16377
	$\bar{h}_{ac}$, σh_{ac} (ft)	-	-	0.70413	0.11581	-0.50345	0.034386
	$\bar{\theta}_{ac}$, $\sigma\theta_{ac}$ (deg)	-	-	0.032818	0.054794	0.047044	0.057998
	# Bolters	0		0		0	
	$\bar{X}_{td}$, σX_{td} (ft)	-	-	-	-	-	-
	$\bar{Y}_{td}$, σY_{td} (ft)	-	-	-	-	-	-
	# Successful Touchdowns	0		5		3	
	$\bar{X}_{td}$, σX_{td} (ft)	-	-	-29.0933	1.2472	-18.4705	1.013
	$\bar{Y}_{td}$, σY_{td} (ft)	-	-	4.1856	1.3028	3.0859	1.7495
	$\bar{h}_{td}$, σh_{td} (ft)	-	-	-12.1282	0.29961	-8.6801	0.25491
	$\bar{h}_{ac}$, σh_{ac} (ft)	-	-	0.13254	0.17005	0.0642	0.17081

Table B-27 Severe Turbulence 3D and Carrier Induced Turbulence – Wind 24.5 Knots

		Wind Speed = 37 Knots Severe Three Dimensional Turbulence and Carrier Induced Turbulence					
		System 1		System 2		System 3	
Carrier Speed = 0 Knots	# Successful Approaches	0		0		0	
	$\bar{h}_{ac}$ rms, σh_{ac} rms (ft)	-	-	-	-	-	-
	$\bar{\lambda}_{ac}$ rms, $\sigma\lambda_{ac}$ rms (ft)	-	-	-	-	-	-
	$\bar{u}_{ac}$ rms, σu_{ac} rms (kts)	-	-	-	-	-	-
	# Failed Approaches Vert	0		0		0	
	$\bar{t}_{td}$, σt_{td} (sec)	-	-	-	-	-	-
	$\bar{h}_{td}$ rms, σh_{td} rms (ft)	-	-	-	-	-	-
	$\bar{\lambda}_{td}$ rms, $\sigma\lambda_{td}$ rms (ft)	-	-	-	-	-	-
	$\bar{u}_{td}$ rms, σu_{td} rms (kts)	-	-	-	-	-	-
	# Failed Approaches Lat	5		5		5	
	$\bar{t}_{td}$, σt_{td} (sec)	12.9132	0.071991	6.9221	0.29336	7.3324	0.27889
	$\bar{h}_{td}$ rms, σh_{td} rms (ft)	3.7328	0.003964	2.0806	0.17706	1.5725	0.11607
	$\bar{\lambda}_{td}$ rms, $\sigma\lambda_{td}$ rms (ft)	2.6053	0.006966	2.5626	0.16892	3.1065	0.70725
	$\bar{u}_{td}$ rms, σu_{td} rms (kts)	0.66632	0.017298	0.59793	0.028908	0.71548	0.011001
	# Ramp Strikes	0		0		0	
	$\bar{h}_{tg}$, σh_{tg} (ft)	-	-	-	-	-	-
	$\bar{h}_{tg}$, σh_{tg} (ft)	-	-	-	-	-	-
	$\bar{\theta}_{tg}$, $\sigma\theta_{tg}$ (deg)	-	-	-	-	-	-
	# Bolters	0		0		0	
	$\bar{X}_{td}$, σX_{td} (ft)	-	-	-	-	-	-
	$\bar{Y}_{td}$, σY_{td} (ft)	-	-	-	-	-	-
	# Successful Touchdowns	0		0		0	
	$\bar{X}_{td}$, σX_{td} (ft)	-	-	-	-	-	-
	$\bar{Y}_{td}$, σY_{td} (ft)	-	-	-	-	-	-
	$\bar{h}_{td}$, σh_{td} (ft)	-	-	-	-	-	-
	$\bar{h}_{td}$, σh_{td} (ft)	-	-	-	-	-	-
Carrier Speed = 10Knots	# Successful Approaches	0		1		0	
	$\bar{h}_{ac}$ rms, σh_{ac} rms (ft)	-	-	2.2308	0	-	-
	$\bar{\lambda}_{ac}$ rms, $\sigma\lambda_{ac}$ rms (ft)	-	-	4.4194	0	-	-
	$\bar{u}_{ac}$ rms, σu_{ac} rms (kts)	-	-	0.62602	0	-	-
	# Failed Approaches Vert	0		0		0	
	$\bar{t}_{td}$, σt_{td} (sec)	-	-	-	-	-	-
	$\bar{h}_{td}$ rms, σh_{td} rms (ft)	-	-	-	-	-	-
	$\bar{\lambda}_{td}$ rms, $\sigma\lambda_{td}$ rms (ft)	-	-	-	-	-	-
	$\bar{u}_{td}$ rms, σu_{td} rms (kts)	-	-	-	-	-	-
	# Failed Approaches Lat	5		4		5	
	$\bar{t}_{td}$, σt_{td} (sec)	13.0678	0.11172	7.0195	0.22352	7.5712	0.17578
	$\bar{h}_{td}$ rms, σh_{td} rms (ft)	3.7787	0.008635	1.9351	0.10738	1.7784	0.4635
	$\bar{\lambda}_{td}$ rms, $\sigma\lambda_{td}$ rms (ft)	2.6352	0.031912	3.0731	0.65002	2.9965	0.55411
	$\bar{u}_{td}$ rms, σu_{td} rms (kts)	0.70834	0.016119	0.58537	0.031248	0.76709	0.11161
	# Ramp Strikes	0		0		0	
	$\bar{h}_{tg}$, σh_{tg} (ft)	-	-	10.4082	0	-	-
	$\bar{h}_{tg}$, σh_{tg} (ft)	-	-	1.6809	0	-	-
	$\bar{\theta}_{tg}$, $\sigma\theta_{tg}$ (deg)	-	-	0.12248	0	-	-
	# Bolters	0		0		0	
	$\bar{X}_{td}$, σX_{td} (ft)	-	-	-	-	-	-
	$\bar{Y}_{td}$, σY_{td} (ft)	-	-	-	-	-	-
	# Successful Touchdowns	0		1		0	
	$\bar{X}_{td}$, σX_{td} (ft)	-	-	4.6965	0	-	-
	$\bar{Y}_{td}$, σY_{td} (ft)	-	-	-1.0653	0	-	-
	$\bar{h}_{td}$, σh_{td} (ft)	-	-	-7.2475	0	-	-
	$\bar{h}_{td}$, σh_{td} (ft)	-	-	1.2733	0	-	-
Carrier Speed = 33 Knots	# Successful Approaches	0		3		5	
	$\bar{h}_{ac}$ rms, σh_{ac} rms (ft)	-	-	5.2302	1.6148	2.9719	0.42417
	$\bar{\lambda}_{ac}$ rms, $\sigma\lambda_{ac}$ rms (ft)	-	-	5.481	0.94179	3.5966	0.82746
	$\bar{u}_{ac}$ rms, σu_{ac} rms (kts)	-	-	0.85157	0.061454	0.94676	0.090705
	# Failed Approaches Vert	0		0		0	
	$\bar{t}_{td}$, σt_{td} (sec)	-	-	-	-	-	-
	$\bar{h}_{td}$ rms, σh_{td} rms (ft)	-	-	-	-	-	-
	$\bar{\lambda}_{td}$ rms, $\sigma\lambda_{td}$ rms (ft)	-	-	-	-	-	-
	$\bar{u}_{td}$ rms, σu_{td} rms (kts)	-	-	-	-	-	-
	# Failed Approaches Lat	5		2		0	
	$\bar{t}_{td}$, σt_{td} (sec)	10.8122	0.029963	12.7035	7.2034	-	-
	$\bar{h}_{td}$ rms, σh_{td} rms (ft)	2.5936	0.025914	3.7281	0.028903	-	-
	$\bar{\lambda}_{td}$ rms, $\sigma\lambda_{td}$ rms (ft)	1.1308	0.069127	3.1111	0.29748	-	-
	$\bar{u}_{td}$ rms, σu_{td} rms (kts)	0.35769	0.032646	0.7634	0.05307	-	-
	# Ramp Strikes	0		0		0	
	$\bar{h}_{tg}$, σh_{tg} (ft)	-	-	11.7072	0.93344	11.1303	0.91769
	$\bar{h}_{tg}$, σh_{tg} (ft)	-	-	2.9242	0.14682	2.757	0.77455
	$\bar{\theta}_{tg}$, $\sigma\theta_{tg}$ (deg)	-	-	0.14243	0.28601	-0.00426	0.3125
	# Bolters	0		0		0	
	$\bar{X}_{td}$, σX_{td} (ft)	-	-	-	-	-	-
	$\bar{Y}_{td}$, σY_{td} (ft)	-	-	-	-	-	-
	# Successful Touchdowns	0		3		5	
	$\bar{X}_{td}$, σX_{td} (ft)	-	-	-7.5676	7.2499	6.081	10.8936
	$\bar{Y}_{td}$, σY_{td} (ft)	-	-	12.7818	12.429	3.1534	4.582
	$\bar{h}_{td}$, σh_{td} (ft)	-	-	-11.8266	0.87027	-13.7989	2.2766
	$\bar{h}_{td}$, σh_{td} (ft)	-	-	0.36137	0.95696	-0.37574	1.2965

Table B-28 Severe Turbulence 3D and Carrier Induced Turbulence – Wind 37 Knots

		Wind Speed = 2 Knots Severe Two Dimensional Turbulence and Carrier Induced Turbulence					
		System 1		System 2		System 3	
Carrier Speed = 0 Knots	# Successful Approaches	5		5		5	
	$\bar{h}_r$ rms, σh_r rms (ft)	1.7695	0.000647	1.4197	0.004313	0.86231	0.000479
	$\bar{\lambda}_r$ rms, $\sigma\lambda_r$ rms (ft)	0.000135	2.65E-06	0.000242	4.53E-05	0.000267	1.31E-05
	$\bar{u}_r$ rms, σu_r rms (kts)	0.40995	0.000182	0.56004	0.001783	0.59325	0.00173
	# Failed Approaches Vert	0		0		0	
	$\bar{t}_{td}$, σt_{td} (sec)	-	-	-	-	-	-
	$\bar{h}_r$ rms, σh_r rms (ft)	-	-	-	-	-	-
	$\bar{\lambda}_r$ rms, $\sigma\lambda_r$ rms (ft)	-	-	-	-	-	-
	$\bar{u}_r$ rms, σu_r rms (kts)	-	-	-	-	-	-
	# Failed Approaches Lat	0		0		0	
	$\bar{t}_{td}$, σt_{td} (sec)	-	-	-	-	-	-
	$\bar{h}_r$ rms, σh_r rms (ft)	-	-	-	-	-	-
	$\bar{\lambda}_r$ rms, $\sigma\lambda_r$ rms (ft)	-	-	-	-	-	-
	$\bar{u}_r$ rms, σu_r rms (kts)	-	-	-	-	-	-
	# Ramp Strikes	0		0		0	
	$\bar{h}_d$, σh_d (ft)	11.3721	0.036452	9.1096	0.27483	9.1241	0.033
	$\bar{h}_{ar}$, σh_{ar} (ft)	3.0111	0.000686	0.74872	0.25472	0.76326	0.003458
	$\bar{\theta}_{ar}$, $\sigma\theta_{ar}$ (deg)	-0.00867	0.013037	-0.00872	0.011095	-0.00874	0.011075
	# Bolters	0		0		0	
	$\bar{X}_d$, σX_d (ft)	-	-	-	-	-	-
	$\bar{Y}_d$, σY_d (ft)	-	-	-	-	-	-
	# Successful Touchdowns	5		5		5	
	$\bar{X}_d$, σX_d (ft)	29.2925	1.2643	12.8167	2.3264	9.7065	0.024105
	$\bar{Y}_{td}$, σY_d (ft)	0.10101	0.02981	0.030914	0.010021	0.004071	0.001692
	$\bar{h}_d$, σh_d (ft)	-20.6219	0.017342	-9.6301	0.33898	-11.6262	0.010882
	$\bar{h}_{dr}$, σh_{dr} (ft)	-0.021177	0.087265	-0.033885	0.036616	-0.03998	0.045575
Carrier Speed = 10Knots	# Successful Approaches	5		5		5	
	$\bar{h}_r$ rms, σh_r rms (ft)	1.7732	0.00061	1.4965	0.013482	0.90365	0.00096
	$\bar{\lambda}_r$ rms, $\sigma\lambda_r$ rms (ft)	0.000156	2.76E-06	0.000443	0.000149	0.000183	1.93E-05
	$\bar{u}_r$ rms, σu_r rms (kts)	0.40655	0.000345	0.5547	0.00044	0.6046	0.001026
	# Failed Approaches Vert	0		0		0	
	$\bar{t}_{td}$, σt_{td} (sec)	-	-	-	-	-	-
	$\bar{h}_r$ rms, σh_r rms (ft)	-	-	-	-	-	-
	$\bar{\lambda}_r$ rms, $\sigma\lambda_r$ rms (ft)	-	-	-	-	-	-
	$\bar{u}_r$ rms, σu_r rms (kts)	-	-	-	-	-	-
	# Failed Approaches Lat	0		0		0	
	$\bar{t}_{td}$, σt_{td} (sec)	-	-	-	-	-	-
	$\bar{h}_r$ rms, σh_r rms (ft)	-	-	-	-	-	-
	$\bar{\lambda}_r$ rms, $\sigma\lambda_r$ rms (ft)	-	-	-	-	-	-
	$\bar{u}_r$ rms, σu_r rms (kts)	-	-	-	-	-	-
	# Ramp Strikes	0		0		0	
	$\bar{h}_d$, σh_d (ft)	9.7337	0.04443	8.7256	0.21413	8.4714	0.030361
	$\bar{h}_{ar}$, σh_{ar} (ft)	1.328	0.001657	0.325	0.21478	0.070824	0.004005
	$\bar{\theta}_{ar}$, $\sigma\theta_{ar}$ (deg)	0.00732	0.015514	0.005508	0.01101	0.005508	0.01101
	# Bolters	0		4		0	
	$\bar{X}_d$, σX_d (ft)	-	-	65.8897	2.117	-	-
	$\bar{Y}_d$, σY_d (ft)	-	-	0.11878	0.066859	-	-
	# Successful Touchdowns	5		1		5	
	$\bar{X}_d$, σX_d (ft)	44.6747	0.009012	48.7605	0	17.0451	1.1701
	$\bar{Y}_{td}$, σY_d (ft)	-0.02406	0.013557	0.013769	0	-0.01321	0.065118
	$\bar{h}_d$, σh_d (ft)	-20.4617	0.002197	-17.1335	0	-13.0176	0.078024
	$\bar{h}_{dr}$, σh_{dr} (ft)	0.05489	0.0608	0.03432	0	-.03496	0.05373
Carrier Speed = 33 Knots	# Successful Approaches	5		5		5	
	$\bar{h}_r$ rms, σh_r rms (ft)	1.8002	0.000294	1.4479	0.015116	0.99353	0.00567
	$\bar{\lambda}_r$ rms, $\sigma\lambda_r$ rms (ft)	0.00013	8.27E-07	0.000271	3.32E-05	0.000206	1.63E-05
	$\bar{u}_r$ rms, σu_r rms (kts)	0.40979	0.00019	0.55673	0.009143	0.68011	0.00511
	# Failed Approaches Vert	0		0		0	
	$\bar{t}_{td}$, σt_{td} (sec)	-	-	-	-	-	-
	$\bar{h}_r$ rms, σh_r rms (ft)	-	-	-	-	-	-
	$\bar{\lambda}_r$ rms, $\sigma\lambda_r$ rms (ft)	-	-	-	-	-	-
	$\bar{u}_r$ rms, σu_r rms (kts)	-	-	-	-	-	-
	# Failed Approaches Lat	0		0		0	
	$\bar{t}_{td}$, σt_{td} (sec)	-	-	-	-	-	-
	$\bar{h}_r$ rms, σh_r rms (ft)	-	-	-	-	-	-
	$\bar{\lambda}_r$ rms, $\sigma\lambda_r$ rms (ft)	-	-	-	-	-	-
	$\bar{u}_r$ rms, σu_r rms (kts)	-	-	-	-	-	-
	# Ramp Strikes	0		0		0	
	$\bar{h}_d$, σh_d (ft)	9.6554	0.011626	8.0512	0.50362	8.2405	0.011145
	$\bar{h}_{ar}$, σh_{ar} (ft)	1.2783	0.00238	-0.32599	0.50695	-0.13667	0.004119
	$\bar{\theta}_{ar}$, $\sigma\theta_{ar}$ (deg)	-0.00291	0.005005	-0.0029	0.003177	-0.00289	0.003191
	# Bolters	0		0		0	
	$\bar{X}_d$, σX_d (ft)	-	-	-	-	-	-
	$\bar{Y}_d$, σY_d (ft)	-	-	-	-	-	-
	# Successful Touchdowns	5		5		5	
	$\bar{X}_d$, σX_d (ft)	25.4762	0.011859	19.7994	9.0646	12.925	0.36689
	$\bar{Y}_{td}$, σY_d (ft)	0.069144	0.006052	0.026625	0.050475	0.01647	0.0181
	$\bar{h}_d$, σh_d (ft)	-20.5265	0.003427	-12.177	1.2619	-11.2606	0.025945
	$\bar{h}_{dr}$, σh_{dr} (ft)	-0.010112	0.023159	-0.008286	0.029385	-0.007689	0.02754

Table B-29 Severe Turbulence 2D and Carrier Induced Turbulence – Wind 2 Knots

		Wind Speed = 13.5 Knots Severe Two Dimensional Turbulence and Carrier Induced Turbulence					
		System 1		System 2		System 3	
Carrier Speed = 0 Knots	# Successful Approaches	0		5		5	
	$\bar{h}_{ss}$ rms, σh_{ss} rms (ft)	-	-	1.4473	0.005962	0.83946	0.000952
	$\bar{\lambda}_{ss}$ rms, $\sigma\lambda_{ss}$ rms (ft)	-	-	0.003108	0.000113	0.002408	3.91E-05
	$\bar{u}_{ss}$ rms, σu_{ss} rms (kts)	-	-	0.54123	0.002131	0.59376	0.003393
	# Failed Approaches Vert	5		0		0	
	$\bar{t}_{fd}$, σt_{fd} (sec)	6.3829	0.006324	-	-	-	-
	$\bar{h}_{ss}$ rms, σh_{ss} rms (ft)	1.7539	0.001123	-	-	-	-
	$\bar{\lambda}_{ss}$ rms, $\sigma\lambda_{ss}$ rms (ft)	0.003721	8.98E-05	-	-	-	-
	$\bar{u}_{ss}$ rms, σu_{ss} rms (kts)	0.45281	0.001338	-	-	-	-
	# Failed Approaches Lat	0		0		0	
	$\bar{t}_{fd}$, σt_{fd} (sec)	-	-	-	-	-	-
	$\bar{h}_{ss}$ rms, σh_{ss} rms (ft)	-	-	-	-	-	-
	$\bar{\lambda}_{ss}$ rms, $\sigma\lambda_{ss}$ rms (ft)	-	-	-	-	-	-
	$\bar{u}_{ss}$ rms, σu_{ss} rms (kts)	-	-	-	-	-	-
	# Ramp Strikes	0		0		0	
	$\bar{h}_{rs}$, σh_{rs} (ft)	-	-	10.0738	0.37789	9.1904	0.060877
	$\bar{h}_{ss}$, σh_{ss} (ft)	-	-	1.6519	0.42985	0.76845	0.004522
	$\bar{\theta}_{ss}$, $\sigma\theta_{ss}$ (deg)	-	-	0.013139	0.022201	0.013139	0.022201
	# Bolters	0		0		0	
	$\bar{X}_{fd}$, σX_{fd} (ft)	-	-	-	-	-	-
	$\bar{Y}_{fd}$, σY_{fd} (ft)	-	-	-	-	-	-
	# Successful Touchdowns	0		5		5	
	$\bar{X}_{td}$, σX_{td} (ft)	-	-	15.5047	2.3189	15.5474	0.15851
	$\bar{Y}_{td}$, σY_{td} (ft)	-	-	0.05354	0.014635	-0.02301	0.006845
	$\bar{h}_{rs}$, σh_{rs} (ft)	-	-	-10.2339	0.19085	-13.212	0.061564
	$\bar{h}_{ss}$, σh_{ss} (ft)	-	-	-0.027054	0.048913	-0.022168	0.053049
Carrier Speed = 10Knots	# Successful Approaches	0		5		5	
	$\bar{h}_{ss}$ rms, σh_{ss} rms (ft)	-	-	1.4863	0.029025	0.93681	0.004337
	$\bar{\lambda}_{ss}$ rms, $\sigma\lambda_{ss}$ rms (ft)	-	-	0.00374	0.000292	0.002616	0.00022
	$\bar{u}_{ss}$ rms, σu_{ss} rms (kts)	-	-	0.56253	0.007199	0.61048	0.004383
	# Failed Approaches Vert	5		0		0	
	$\bar{t}_{fd}$, σt_{fd} (sec)	6.9011	0.006246	-	-	-	-
	$\bar{h}_{ss}$ rms, σh_{ss} rms (ft)	1.76	0.001823	-	-	-	-
	$\bar{\lambda}_{ss}$ rms, $\sigma\lambda_{ss}$ rms (ft)	0.008487	0.000329	-	-	-	-
	$\bar{u}_{ss}$ rms, σu_{ss} rms (kts)	0.44092	0.000728	-	-	-	-
	# Failed Approaches Lat	0		0		0	
	$\bar{t}_{fd}$, σt_{fd} (sec)	-	-	-	-	-	-
	$\bar{h}_{ss}$ rms, σh_{ss} rms (ft)	-	-	-	-	-	-
	$\bar{\lambda}_{ss}$ rms, $\sigma\lambda_{ss}$ rms (ft)	-	-	-	-	-	-
	$\bar{u}_{ss}$ rms, σu_{ss} rms (kts)	-	-	-	-	-	-
	# Ramp Strikes	0		0		0	
	$\bar{h}_{rs}$, σh_{rs} (ft)	-	-	8.9286	0.69601	8.5982	0.059492
	$\bar{h}_{ss}$, σh_{ss} (ft)	-	-	0.53261	0.65386	0.20221	0.022686
	$\bar{\theta}_{ss}$, $\sigma\theta_{ss}$ (deg)	-	-	0.003858	0.017604	0.003853	0.017463
	# Bolters	0		2		0	
	$\bar{X}_{fd}$, σX_{fd} (ft)	-	-	70.6807	2.2493	-	-
	$\bar{Y}_{fd}$, σY_{fd} (ft)	-	-	-0.17582	0.016614	-	-
	# Successful Touchdowns	0		3		5	
	$\bar{X}_{td}$, σX_{td} (ft)	-	-	40.4921	12.5542	18.884	0.96098
	$\bar{Y}_{td}$, σY_{td} (ft)	-	-	-0.09248	0.049684	-0.04609	0.019535
	$\bar{h}_{rs}$, σh_{rs} (ft)	-	-	-14.404	2.2692	-11.4315	0.04728
	$\bar{h}_{ss}$, σh_{ss} (ft)	-	-	-0.027869	0.057038	0.06528	0.14895
Carrier Speed = 33 Knots	# Successful Approaches	5		5		5	
	$\bar{h}_{ss}$ rms, σh_{ss} rms (ft)	2.2838	0.002481	1.6017	0.066628	0.98461	0.011836
	$\bar{\lambda}_{ss}$ rms, $\sigma\lambda_{ss}$ rms (ft)	0.002587	0.000161	0.002711	0.000194	0.003267	0.000154
	$\bar{u}_{ss}$ rms, σu_{ss} rms (kts)	0.4738	0.000529	0.61412	0.006353	0.57631	0.004883
	# Failed Approaches Vert	0		0		0	
	$\bar{t}_{fd}$, σt_{fd} (sec)	-	-	-	-	-	-
	$\bar{h}_{ss}$ rms, σh_{ss} rms (ft)	-	-	-	-	-	-
	$\bar{\lambda}_{ss}$ rms, $\sigma\lambda_{ss}$ rms (ft)	-	-	-	-	-	-
	$\bar{u}_{ss}$ rms, σu_{ss} rms (kts)	-	-	-	-	-	-
	# Failed Approaches Lat	0		0		0	
	$\bar{t}_{fd}$, σt_{fd} (sec)	-	-	-	-	-	-
	$\bar{h}_{ss}$ rms, σh_{ss} rms (ft)	-	-	-	-	-	-
	$\bar{\lambda}_{ss}$ rms, $\sigma\lambda_{ss}$ rms (ft)	-	-	-	-	-	-
	$\bar{u}_{ss}$ rms, σu_{ss} rms (kts)	-	-	-	-	-	-
	# Ramp Strikes	0		0		0	
	$\bar{h}_{rs}$, σh_{rs} (ft)	7.6014	0.033216	8.2854	0.021815	7.6264	0.039284
	$\bar{h}_{ss}$, σh_{ss} (ft)	-0.77064	0.008174	-0.10184	0.014578	-0.76023	0.013474
	$\bar{\theta}_{ss}$, $\sigma\theta_{ss}$ (deg)	-0.00472	0.010208	0.000703	0.010221	0.000495	0.010261
	# Bolters	0		0		0	
	$\bar{X}_{fd}$, σX_{fd} (ft)	-	-	-	-	-	-
	$\bar{Y}_{fd}$, σY_{fd} (ft)	-	-	-	-	-	-
	# Successful Touchdowns	5		5		5	
	$\bar{X}_{td}$, σX_{td} (ft)	-65.7448	0.58705	-29.5199	0.74079	-11.6388	0.73921
	$\bar{Y}_{td}$, σY_{td} (ft)	-0.05262	0.050731	-0.02762	0.039332	-0.02595	0.007347
	$\bar{h}_{rs}$, σh_{rs} (ft)	-22.1557	0.015261	-9.8064	0.16039	-6.6947	0.054359
	$\bar{h}_{ss}$, σh_{ss} (ft)	0.00358	0.032787	0.03087	0.041065	0.03421	0.048771

Table B-30 Severe Turbulence 2D and Carrier Induced Turbulence – Wind 13.5 Knots

		Wind Speed = 24.5 Knots Severe Two Dimensional Turbulence and Carrier Induced Turbulence					
		System 1		System 2		System 3	
Carrier Speed = 0 Knots	# Successful Approaches	0		5		5	
	$\bar{h}_{ss}$ rms, σh_{ss} rms (ft)	-	-	1.4648	0.017657	0.84416	0.009436
	$\bar{\lambda}_{ss}$ rms, $\sigma\lambda_{ss}$ rms (ft)	-	-	0.004168	0.000149	0.003828	0.000188
	$\bar{u}_{ss}$ rms, σu_{ss} rms (kts)	-	-	0.53408	0.004674	0.59298	0.003771
	# Failed Approaches Vert	5		0		0	
	$\bar{t}_{fd}$, σt_{fd} (sec)	8.8644	0.005817	-	-	-	-
	$\bar{h}_{ss}$ rms, σh_{ss} rms (ft)	2.1936	0.00612	-	-	-	-
	$\bar{\lambda}_{ss}$ rms, $\sigma\lambda_{ss}$ rms (ft)	0.05164	0.006287	-	-	-	-
	$\bar{u}_{ss}$ rms, σu_{ss} rms (kts)	0.43854	0.001071	-	-	-	-
	# Failed Approaches Lat	0		0		0	
	$\bar{t}_{fd}$, σt_{fd} (sec)	-	-	-	-	-	-
	$\bar{h}_{ss}$ rms, σh_{ss} rms (ft)	-	-	-	-	-	-
	$\bar{\lambda}_{ss}$ rms, $\sigma\lambda_{ss}$ rms (ft)	-	-	-	-	-	-
	$\bar{u}_{ss}$ rms, σu_{ss} rms (kts)	-	-	-	-	-	-
	# Ramp Strikes	0		0		0	
	$\bar{h}_{rs}$, σh_{rs} (ft)	-	-	10.5087	0.51441	9.3199	0.18108
	$\bar{h}_{ss}$, σh_{ss} (ft)	-	-	1.9983	0.32305	0.8106	0.04603
	$\bar{\theta}_{ss}$, $\sigma\theta_{ss}$ (deg)	-	-	0.044815	0.068985	0.044434	0.069037
	# Bolters	0		0		0	
	$\bar{X}_{fd}$, σX_{fd} (ft)	-	-	-	-	-	-
	$\bar{Y}_{fd}$, σY_{fd} (ft)	-	-	-	-	-	-
	# Successful Touchdowns	0		5		5	
	$\bar{X}_{td}$, σX_{td} (ft)	-	-	23.2159	5.6033	22.5882	1.3808
	$\bar{Y}_{td}$, σY_{td} (ft)	-	-	0.10643	0.076802	0.13845	0.065327
	$\bar{h}_{td}$, σh_{td} (ft)	-	-	-10.429	1.9378	-13.0391	0.36473
	$\bar{h}_{rs}$, σh_{rs} (ft)	-	-	-0.062745	0.29903	-0.091653	0.3061
Carrier Speed = 10Knots	# Successful Approaches	0		5		5	
	$\bar{h}_{ss}$ rms, σh_{ss} rms (ft)	-	-	1.4091	0.022008	0.94129	0.025824
	$\bar{\lambda}_{ss}$ rms, $\sigma\lambda_{ss}$ rms (ft)	-	-	0.006551	0.001035	0.004306	0.000321
	$\bar{u}_{ss}$ rms, σu_{ss} rms (kts)	-	-	0.51676	0.008661	0.55245	0.004074
	# Failed Approaches Vert	5		0		0	
	$\bar{t}_{fd}$, σt_{fd} (sec)	7.0919	0.004732	-	-	-	-
	$\bar{h}_{ss}$ rms, σh_{ss} rms (ft)	2.5195	0.01318	-	-	-	-
	$\bar{\lambda}_{ss}$ rms, $\sigma\lambda_{ss}$ rms (ft)	0.043587	0.012992	-	-	-	-
	$\bar{u}_{ss}$ rms, σu_{ss} rms (kts)	0.47358	0.00473	-	-	-	-
	# Failed Approaches Lat	0		0		0	
	$\bar{t}_{fd}$, σt_{fd} (sec)	-	-	-	-	-	-
	$\bar{h}_{ss}$ rms, σh_{ss} rms (ft)	-	-	-	-	-	-
	$\bar{\lambda}_{ss}$ rms, $\sigma\lambda_{ss}$ rms (ft)	-	-	-	-	-	-
	$\bar{u}_{ss}$ rms, σu_{ss} rms (kts)	-	-	-	-	-	-
	# Ramp Strikes	0		0		0	
	$\bar{h}_{rs}$, σh_{rs} (ft)	-	-	6.8524	0.55731	9.5948	0.14733
	$\bar{h}_{ss}$, σh_{ss} (ft)	-	-	-1.4409	0.7001	1.3026	0.21029
	$\bar{\theta}_{ss}$, $\sigma\theta_{ss}$ (deg)	-	-	-0.03293	0.085218	-0.03331	0.084755
	# Bolters	0		0		0	
	$\bar{X}_{fd}$, σX_{fd} (ft)	-	-	-	-	-	-
	$\bar{Y}_{fd}$, σY_{fd} (ft)	-	-	-	-	-	-
	# Successful Touchdowns	0		5		5	
	$\bar{X}_{td}$, σX_{td} (ft)	-	-	-4.5159	10.3618	-0.37963	4.052
	$\bar{Y}_{td}$, σY_{td} (ft)	-	-	0.072425	0.024347	0.04279	0.025549
	$\bar{h}_{td}$, σh_{td} (ft)	-	-	-10.9494	2.0265	-14.0163	0.096672
	$\bar{h}_{rs}$, σh_{rs} (ft)	-	-	0.03852	0.52576	0.01651	0.56512
Carrier Speed = 33 Knots	# Successful Approaches	0		5		5	
	$\bar{h}_{ss}$ rms, σh_{ss} rms (ft)	-	-	1.6114	0.047239	1.0639	0.063339
	$\bar{\lambda}_{ss}$ rms, $\sigma\lambda_{ss}$ rms (ft)	-	-	0.009806	0.003	0.01114	0.002268
	$\bar{u}_{ss}$ rms, σu_{ss} rms (kts)	-	-	0.59761	0.009678	0.60945	0.031947
	# Failed Approaches Vert	5		0		0	
	$\bar{t}_{fd}$, σt_{fd} (sec)	8.7528	0.008923	-	-	-	-
	$\bar{h}_{ss}$ rms, σh_{ss} rms (ft)	2.4647	0.003802	-	-	-	-
	$\bar{\lambda}_{ss}$ rms, $\sigma\lambda_{ss}$ rms (ft)	0.035709	0.02002	-	-	-	-
	$\bar{u}_{ss}$ rms, σu_{ss} rms (kts)	0.45469	0.000831	-	-	-	-
	# Failed Approaches Lat	0		0		0	
	$\bar{t}_{fd}$, σt_{fd} (sec)	-	-	-	-	-	-
	$\bar{h}_{ss}$ rms, σh_{ss} rms (ft)	-	-	-	-	-	-
	$\bar{\lambda}_{ss}$ rms, $\sigma\lambda_{ss}$ rms (ft)	-	-	-	-	-	-
	$\bar{u}_{ss}$ rms, σu_{ss} rms (kts)	-	-	-	-	-	-
	# Ramp Strikes	0		0		0	
	$\bar{h}_{rs}$, σh_{rs} (ft)	-	-	9.0391	0.22949	8.0219	0.10734
	$\bar{h}_{ss}$, σh_{ss} (ft)	-	-	0.56273	0.12511	-0.45204	0.11772
	$\bar{\theta}_{ss}$, $\sigma\theta_{ss}$ (deg)	-	-	0.03263	0.055093	0.031777	0.056169
	# Bolters	0		0		0	
	$\bar{X}_{fd}$, σX_{fd} (ft)	-	-	-	-	-	-
	$\bar{Y}_{fd}$, σY_{fd} (ft)	-	-	-	-	-	-
	# Successful Touchdowns	0		5		5	
	$\bar{X}_{td}$, σX_{td} (ft)	-	-	-32.5634	1.6419	-17.5908	0.68359
	$\bar{Y}_{td}$, σY_{td} (ft)	-	-	0.089464	0.066068	-0.03914	0.07629
	$\bar{h}_{td}$, σh_{td} (ft)	-	-	-12.1186	0.40346	-8.0392	0.27836
	$\bar{h}_{rs}$, σh_{rs} (ft)	-	-	0.13574	0.17038	0.13771	0.16539

Table B-31 Severe Turbulence 2D and Carrier Induced Turbulence – Wind 24.5 Knots

		Wind Speed = 37 Knots Severe Two Dimensional Turbulence and Carrier Induced Turbulence					
		System 1		System 2		System 3	
Carrier Speed = 0 Knots	# Successful Approaches	0		5		5	
	$\bar{h}_{ss}$ rms, σh_{ss} rms (ft)	-	-	1.5794	0.027938	1.0335	0.029613
	$\bar{\lambda}_{ss}$ rms, $\sigma\lambda_{ss}$ rms (ft)	-	-	0.007694	0.002668	0.007537	0.001256
	$\bar{u}_{ss}$ rms, σu_{ss} rms (kts)	-	-	0.54667	0.030161	0.60958	0.008464
	# Failed Approaches Vert	5		0		0	
	$\bar{t}_{td}$, σt_{td} (sec)	9.3798	5.9505	-	-	-	-
	$\bar{h}_{ss}$ rms, σh_{ss} rms (ft)	3.6983	0.28403	-	-	-	-
	$\bar{\lambda}_{ss}$ rms, $\sigma\lambda_{ss}$ rms (ft)	0.081177	0.066278	-	-	-	-
	$\bar{u}_{ss}$ rms, σu_{ss} rms (kts)	0.35448	0.041865	-	-	-	-
	# Failed Approaches Lat	0		0		0	
	$\bar{t}_{td}$, σt_{td} (sec)	-	-	-	-	-	-
	$\bar{h}_{ss}$ rms, σh_{ss} rms (ft)	-	-	-	-	-	-
	$\bar{\lambda}_{ss}$ rms, $\sigma\lambda_{ss}$ rms (ft)	-	-	-	-	-	-
	$\bar{u}_{ss}$ rms, σu_{ss} rms (kts)	-	-	-	-	-	-
	# Ramp Strikes	0		0		0	
	$\bar{h}_{td}$, σh_{td} (ft)	-	-	6.3987	0.93279	8.6287	0.23038
	$\bar{h}_{ss}$, σh_{ss} (ft)	-	-	-1.4705	0.63339	0.75925	0.39917
	$\bar{\theta}_{ss}$, $\sigma\theta_{ss}$ (deg)	-	-	-0.1848	0.12544	-0.18471	0.12551
	# Bolters	0		3		0	
	$\bar{X}_{td}$, σX_{td} (ft)	-	-	105.8593	50.0656	-	-
	$\bar{Y}_{td}$, σY_{td} (ft)	-	-	-2.006	1.9946	-	-
	# Successful Touchdowns	0		2		5	
	$\bar{X}_{td}$, σX_{td} (ft)	-	-	52.1065	4.5682	10.7715	1.9485
	$\bar{Y}_{td}$, σY_{td} (ft)	-	-	-0.36966	0.009008	-0.13564	0.14007
	$\bar{h}_{td}$, σh_{td} (ft)	-	-	-9.0983	2.889	-6.8634	0.12376
	$\bar{h}_{ss}$, σh_{ss} (ft)	-	-	-0.43788	0.31836	-0.078391	0.76975
Carrier Speed = 10Knots	# Successful Approaches	0		3		5	
	$\bar{h}_{ss}$ rms, σh_{ss} rms (ft)	-	-	1.5141	0.11677	0.99761	0.033346
	$\bar{\lambda}_{ss}$ rms, $\sigma\lambda_{ss}$ rms (ft)	-	-	0.013288	0.001881	0.008679	0.004146
	$\bar{u}_{ss}$ rms, σu_{ss} rms (kts)	-	-	0.56369	0.040642	0.57508	0.013705
	# Failed Approaches Vert	5		2		0	
	$\bar{t}_{td}$, σt_{td} (sec)	7.0197	0.029028	8.2747	0.15726	-	-
	$\bar{h}_{ss}$ rms, σh_{ss} rms (ft)	3.8979	0.042344	1.3779	0.042282	-	-
	$\bar{\lambda}_{ss}$ rms, $\sigma\lambda_{ss}$ rms (ft)	0.082066	0.041047	0.008119	0.002138	-	-
	$\bar{u}_{ss}$ rms, σu_{ss} rms (kts)	0.37243	0.004108	0.52839	0.011879	-	-
	# Failed Approaches Lat	0		0		0	
	$\bar{t}_{td}$, σt_{td} (sec)	-	-	-	-	-	-
	$\bar{h}_{ss}$ rms, σh_{ss} rms (ft)	-	-	-	-	-	-
	$\bar{\lambda}_{ss}$ rms, $\sigma\lambda_{ss}$ rms (ft)	-	-	-	-	-	-
	$\bar{u}_{ss}$ rms, σu_{ss} rms (kts)	-	-	-	-	-	-
	# Ramp Strikes	0		0		0	
	$\bar{h}_{td}$, σh_{td} (ft)	-	-	7.5174	0.99556	10.0082	1.1041
	$\bar{h}_{ss}$, σh_{ss} (ft)	-	-	-1.2716	0.35178	1.3251	0.48362
	$\bar{\theta}_{ss}$, $\sigma\theta_{ss}$ (deg)	-	-	0.14455	0.24043	0.10668	0.24257
	# Bolters	0		0		0	
	$\bar{X}_{td}$, σX_{td} (ft)	-	-	-	-	-	-
	$\bar{Y}_{td}$, σY_{td} (ft)	-	-	-	-	-	-
	# Successful Touchdowns	0		3		5	
	$\bar{X}_{td}$, σX_{td} (ft)	-	-	-2.9884	6.7467	6.9643	7.9152
	$\bar{Y}_{td}$, σY_{td} (ft)	-	-	0.008445	0.1159	-0.14849	0.14315
	$\bar{h}_{td}$, σh_{td} (ft)	-	-	-9.4401	1.8281	-13.0983	1.0812
	$\bar{h}_{ss}$, σh_{ss} (ft)	-	-	0.23577	0.52485	0.35528	0.66922
Carrier Speed = 33 Knots	# Successful Approaches	0		3		5	
	$\bar{h}_{ss}$ rms, σh_{ss} rms (ft)	-	-	1.6778	0.14334	1.1635	0.13067
	$\bar{\lambda}_{ss}$ rms, $\sigma\lambda_{ss}$ rms (ft)	-	-	0.061327	0.02565	0.067916	0.035222
	$\bar{u}_{ss}$ rms, σu_{ss} rms (kts)	-	-	0.87229	0.013792	0.83694	0.017262
	# Failed Approaches Vert	5		2		0	
	$\bar{t}_{td}$, σt_{td} (sec)	18.5238	0.15814	9.0416	0.55402	-	-
	$\bar{h}_{ss}$ rms, σh_{ss} rms (ft)	3.0219	0.030594	1.6486	0.12066	-	-
	$\bar{\lambda}_{ss}$ rms, $\sigma\lambda_{ss}$ rms (ft)	0.043537	0.012731	0.005435	0.002019	-	-
	$\bar{u}_{ss}$ rms, σu_{ss} rms (kts)	0.33133	0.041371	0.72939	0.005119	-	-
	# Failed Approaches Lat	0		0		0	
	$\bar{t}_{td}$, σt_{td} (sec)	-	-	-	-	-	-
	$\bar{h}_{ss}$ rms, σh_{ss} rms (ft)	-	-	-	-	-	-
	$\bar{\lambda}_{ss}$ rms, $\sigma\lambda_{ss}$ rms (ft)	-	-	-	-	-	-
	$\bar{u}_{ss}$ rms, σu_{ss} rms (kts)	-	-	-	-	-	-
	# Ramp Strikes	0		0		0	
	$\bar{h}_{td}$, σh_{td} (ft)	-	-	11.4239	1.1993	9.9274	0.63839
	$\bar{h}_{ss}$, σh_{ss} (ft)	-	-	2.9775	0.50061	1.6482	0.17491
	$\bar{\theta}_{ss}$, $\sigma\theta_{ss}$ (deg)	-	-	0.021889	0.25019	-0.03798	0.18772
	# Bolters	0		0		0	
	$\bar{X}_{td}$, σX_{td} (ft)	-	-	-	-	-	-
	$\bar{Y}_{td}$, σY_{td} (ft)	-	-	-	-	-	-
	# Successful Touchdowns	0		3		5	
	$\bar{X}_{td}$, σX_{td} (ft)	-	-	13.3203	3.6109	4.5349	20.0613
	$\bar{Y}_{td}$, σY_{td} (ft)	-	-	0.37966	0.52377	0.31943	0.55029
	$\bar{h}_{td}$, σh_{td} (ft)	-	-	-8.9011	0.44596	-8.4915	1.6583
	$\bar{h}_{ss}$, σh_{ss} (ft)	-	-	0.08378	1.2161	-0.31257	1.0459

Table B-32 Severe Turbulence 2D and Carrier Induced Turbulence – Wind 37 Knots